frontiers | Research Topics

Water and ecological system: Response, management, and restoration

Edited by
Chunhui Li, Qiang Liu and Celso Santos

Published in
Frontiers in Earth Science
Frontiers in Ecology and Evolution
Frontiers in Environmental Science

ISSN 1664-8714
ISBN 978-2-83251-941-7
DOI 10.3389/978-2-83251-941-7

About Frontiers

Frontiers is more than just an open access publisher of scholarly articles: it is a pioneering approach to the world of academia, radically improving the way scholarly research is managed. The grand vision of Frontiers is a world where all people have an equal opportunity to seek, share and generate knowledge. Frontiers provides immediate and permanent online open access to all its publications, but this alone is not enough to realize our grand goals.

Frontiers journal series

The Frontiers journal series is a multi-tier and interdisciplinary set of open-access, online journals, promising a paradigm shift from the current review, selection and dissemination processes in academic publishing. All Frontiers journals are driven by researchers for researchers; therefore, they constitute a service to the scholarly community. At the same time, the *Frontiers journal series* operates on a revolutionary invention, the tiered publishing system, initially addressing specific communities of scholars, and gradually climbing up to broader public understanding, thus serving the interests of the lay society, too.

Dedication to quality

Each Frontiers article is a landmark of the highest quality, thanks to genuinely collaborative interactions between authors and review editors, who include some of the world's best academicians. Research must be certified by peers before entering a stream of knowledge that may eventually reach the public - and shape society; therefore, Frontiers only applies the most rigorous and unbiased reviews. Frontiers revolutionizes research publishing by freely delivering the most outstanding research, evaluated with no bias from both the academic and social point of view. By applying the most advanced information technologies, Frontiers is catapulting scholarly publishing into a new generation.

What are Frontiers Research Topics?

Frontiers Research Topics are very popular trademarks of the *Frontiers journals series*: they are collections of at least ten articles, all centered on a particular subject. With their unique mix of varied contributions from Original Research to Review Articles, Frontiers Research Topics unify the most influential researchers, the latest key findings and historical advances in a hot research area.

Find out more on how to host your own Frontiers Research Topic or contribute to one as an author by contacting the Frontiers editorial office: frontiersin.org/about/contact

Water and ecological system: Response, management, and restoration

Topic editors

Chunhui Li — Beijing Normal University, China

Qiang Liu — Beijing Normal University, China

Celso Santos — Federal University of Paraíba, Brazil

Citation

Li, C., Liu, Q., Santos, C., eds. (2023). *Water and ecological system: Response, management, and restoration*. Lausanne: Frontiers Media SA.

doi: 10.3389/978-2-83251-941-7

Table of contents

frontiers | Frontiers in Earth Science

TYPE Editorial
PUBLISHED 02 March 2023
DOI 10.3389/feart.2023.1133154

OPEN ACCESS

EDITED AND REVIEWED BY
Wouter Buytaert,
Imperial College London,
United Kingdom

*CORRESPONDENCE
Celso Augusto Guimarães Santos,
celso@ct.ufpb.br

SPECIALTY SECTION
This article was submitted to Hydrosphere, a section of the journal Frontiers in Earth Science

RECEIVED 28 December 2022
ACCEPTED 20 February 2023
PUBLISHED 02 March 2023

CITATION
Santos CAG, Li C and Liu Q (2023), Editorial: Water and ecological systems: Response, management, and restoration. *Front. Earth Sci.* 11:1133154. doi: 10.3389/feart.2023.1133154

Editorial: Water and ecological systems: Response, management, and restoration

Celso Augusto Guimarães Santos [1]*, Chunhui Li [2] and Qiang Liu [3]

[1]Department of Civil and Environmental Engineering, Federal University of Paraíba, João Pessoa, Brazil, [2]School of Environment, Beijing Normal University, Beijing, China, [3]Beijing Normal University, Beijing, China

KEYWORDS

spatiotemporal time series analysis, ecological footprint, food web, eDNA, drought

Editorial on the Research Topic
Water and Ecological Systems: Response, Management, and Restoration

Climate change and human activities have induced significant alterations in global hydrological and ecological systems, leading to different hydrological responses and water demands in different regions. In order to better manage water resources and restore ecological systems, it is important to understand how these responses are affected by global change. The articles in this Research Topic explore various aspects of the hydrological and ecological response to global change and their implications for water resources management and ecological restoration. This Research Topic features 14 articles that cover a wide range of topics in the field of water resources and ecology. The main themes of the issue include water supply, ecological impact, vegetation responses, industrial structure, hydrological drought, water consumption patterns, bibliometric analysis, allocation of water resources, river temperature analysis, effects of total dissolved gas, food web structure and function, coal ash loaded nano iron, spatial patterns of macrobenthos taxonomic and functional diversity, and response relationships between environmental DNA and biomass. Some of the specific studies that address these themes include "A new method for estimating multi-source water supply considering joint probability distributions under uncertainty" which explores a new method for water supply estimation, "Analysis on the ecological impact of the Xiaolangdi Reservoir on the Yellow River Delta wetland and coastal areas" which examines the impact of a reservoir on the environment, and "Study on the propagation probability characteristics and prediction model of meteorological drought to hydrological drought in the basin based on copula function" which investigates the relationship between meteorological drought and hydrological drought. These studies demonstrate the breadth and depth of research in the field of water resources and ecology and provide valuable insights for further exploration and understanding and can be divided into four categories (i) water supply and distribution, (ii) environmental impacts and evaluation, (iii) water quality and drought analysis, (iv) biodiversity and food web analysis, and (v) bibliometric analysis and water treatment and technology.

Water supply and distribution

Four articles address various aspects of water management and distribution. For instance, efficient water management strategies are crucial for addressing water scarcity, which is a significant challenge for many countries, as highlighted by the extensive analysis of Kuwait's water resources and management strategies (Tariq et al., 2022). Therefore, the findings from Wei et al. and the Kuwait study can inform practical suggestions for water-resource planning and management not only in China and Kuwait but also in other regions facing similar challenges. By applying the new method for estimating multi-source water supply in Xiong'an New Area, China, Wei et al. demonstrate the potential of innovative approaches to improve water management and increase the availability of water resources. Such methods can contribute to the sustainable management of water resources and the promotion of economic and social development in regions facing water scarcity. Sun and Li explore the classification of water consumption patterns in 110 cities in the Yangtze River Economic Belt and provide targeted water-saving policies based on these patterns. Understanding water consumption patterns and identifying effective policies to promote water conservation are critical for sustainable urban development, as shown by the declining water consumption in some of the major Spanish cities, which is attributed to a combination of economic, technological, and behavioural factors, as well as the impact of contingent events such as droughts and economic crises (Sauri, 2019). Meanwhile, Zhang et al. focus on the optimization of water resource allocation in the lower Yellow River area, considering the uncertainty of water resources, water demand, and water requirements of different users. This highlights the need to balance economic development with environmental sustainability, which is also addressed in the article on the stochastic convergence of ecological footprints within BRICS countries (Wu, 2022). The findings from both articles suggest that achieving sustainable development requires considering ecological factors in decision-making processes, to ensure the availability of water resources for future generations and address public health concerns. Those articles illustrate the diverse topics covered in this Journal Research Topic and highlight the importance of addressing the challenges in water supply and distribution for sustainable water management.

Environmental impacts and evaluation

In three articles, the authors are concerned with the environmental impacts and evaluations of human activities on the environment. Shang et al. focus on the impact of the Xiaolangdi Reservoir on the deltaic coastal wetland ecosystem and propose a method for quantitative analysis. The results show that the Xiaolangdi Reservoir has had a positive effect on the ecosystem by reducing drying up days, increasing the assurance rate of ecological base flow, and increasing the volume of water flowing into the sea. This study shares similarities with recent research conducted by Mishra et al. (2021b), Mishra et al. (2021c), Mishra et al. (2021d) in the field of shoreline changes, which also aims to understand the impact of large-scale projects on the natural environment. Zhou et al. evaluate the relationship between vegetation dynamics and meteorological drought in the Pearl River Basin, using NDVI and SIF to assess changes in vegetation cover and photosynthetic capacity. The authors also explore the teleconnection factors that may impact the relationship between drought and vegetation, such as climate patterns and solar activity. This research is significant, as drought is a global concern that affects various ecosystems and has been recently discussed in several articles, including Oliveira et al. (2022), de Oliveira et al. (2022), Santos et al. (2017, Santos et al. (2019), Santos et al. (2021), Silva et al. (2021), and Zerouali et al. (2021), which highlights the need to understand the impact of drought on vegetation and explore the factors that influence this relationship. The insights from this research can inform the development of policies and strategies that promote ecosystem resilience and address the challenges of water scarcity and climate change. Bu et al. focused on improving water environment capacity (WEC) by adjusting the industrial structure and analysing economic changes. The authors estimate economic efficiency, water use efficiency, and water treatment efficiency and divide the industry into three types based on their environmental risk. The results show that adjusting the industrial structure has a positive impact on the WECs of various pollutants. This study is significant, as it highlights the importance of industrial structure adjustment for improving water environment capacity and reducing environmental risk, which is consistent with recent research on the mechanisms of industrial structure optimization and population agglomeration on carbon emissions, such as the article on carbon emissions in China (Liang et al., 2022), which shows the direct and indirect effects of industrial structure optimization and population agglomeration on carbon emissions and highlights the double threshold effect of population agglomeration on the carbon emission reduction effect of industrial structure optimization.

Water quality and drought analysis

The main theme of water quality and drought analysis is the study of various factors that affect water quality and drought conditions. In this context, several studies have been conducted to understand and mitigate the impact of such conditions. For example, Wang et al. studied the probability characteristics of meteorological drought transmission to hydrological drought by using Standardized Precipitation Index (SPI) and Standardized Streamflow Index (SSI) and proposed a hydrological drought prediction model based on the SPI-P(SSI|SPI) relation curve. This research is particularly relevant, as drought and SPI have been a recent topic of discussion in research worldwide, as demonstrated by the recent research of Brasil Neto et al. (2020), Brasil Neto R et al. (2021), Brasil Neto R M et al. (2021), 2022), Brito et al. (2021), da Silva et al. (2020), and Dantas et al. (2020). These studies have made significant contributions to the understanding of drought and SPI, which can inform the development of policies and strategies that promote water resource management and ecosystem resilience in the face of climate change. Seyedhashemi et al. (2021) investigated the thermal signatures of dams and ponds and their impact on stream temperature at the regional scale, shedding light on an important factor affecting water temperature dynamics. Moulin et al., on the other hand, utilized Independent

Component Analysis (ICA) to identify the primary factors influencing water temperature and improve the accuracy of water temperature forecasting, providing a complementary approach to understanding the complex dynamics of water temperature. Broadhurst et al. (2021) investigated the use of environmental DNA (eDNA) in mapping mammalian distributions and diversity in rivers. Similarly, Govindarajan et al. (2021) explored the potential of eDNA to detect animal taxa in the mesopelagic zone. In contrast, Huang et al. evaluated the persistence of eDNA under different flow conditions in aquatic ecosystems with high dams, providing important insights into the applicability of eDNA in such environments and complementing the findings of the other two studies. These studies demonstrate the importance of understanding various factors that impact water quality and drought conditions and the role of innovative techniques in improving our understanding of these factors.

Biodiversity and food web analysis

Articles Yang et al., Fu et al., and Zhang et al. all focus on the study of biodiversity and food web analysis, each exploring different aspects of the topic. Yang et al. focus on the analysis of the food web dynamics of Lake Baiyangdian in northern China over five representative years (1958, 1980, 1993, 2009, and 2019) by using a Bayesian isotope mixing model combined with a food web energetics model. The article argues that combining unweighted and weighted indicators is important for understanding the responses of highly aggregated food webs to changing hydrological regimes and water quality, and for improving the management and restoration of shallow lake ecosystems (Lynam et al., 2017; Bartley et al., 2019). Fu et al. study the macrobenthos biodiversity patterns in the river-lake ecotones along the Fu River-Baiyangdian Lake gradient in northern China (Wang et al., 2019; Mishra et al., 2022b). The article found that water depth, water transparency, TN, and TP were the main drivers of macrobenthos taxonomic and functional diversity, while sediment Cd, Cr, Cu, Pb, and Zn contents also had an impact on macrobenthos diversity (Li et al., 2019; Mosbahi et al., 2019). The article suggests that functional diversity approaches based on biological traits can complement taxonomic approaches in river-lake ecotones. Zhang et al. focus on the relationship between environmental DNA (eDNA) concentration and biomass in a typical fish species of rivers in southwest China. The article found that water pH and temperature had a great influence on eDNA concentration and that environmental factors need to be considered when using eDNA concentration to estimate biomass.

Bibliometric analysis and water treatment and technology

Finally, Yang et al. and Zhang et al. address topics related to water treatment and technology. Yang et al. focus on the bibliometric analysis of Water Resources Carrying Capacity, demonstrating the power of bibliometric analysis as a tool for understanding the current state and progress of research in this area. Recent studies have increasingly used bibliometric analysis as a powerful tool to assess trends and impacts in research, as exemplified by the works of Mishra et al. (2020), Mishra et al. (2021a), Mishra et al. (2022a). In their study, the authors propose a four-staged bibliometric analysis method and conduct a comprehensive analysis of 271 records. Their findings reveal that China is a major contributor to research in this area, with a focus on modelling and system dynamics, linked to population carrying capacity, groundwater resources, urbanization, and water shortage. The authors divide the research progress into five stages and suggest that the method proposed can serve as a reference for future bibliometric studies. On the other hand, Zhang et al. focus on the use of ceramsite composite made from coal ash and modified by nano-iron to remove phosphorus in the water. Maamoun et al. (2018) also seek to improve the removal efficiency of phosphorus, an important pollutant in water. However, the results of the study of this Research Topic show that the modified ceramsite has a good removal effect on phosphorus, with a removal rate of over 99%. This study provides a new method for utilizing coal ash as a resource and a novel approach for improving filler in bioretention facilities.

Thus, the articles in this collection are expected to provide valuable information and insights for communities, basins, and government agencies involved in water and ecosystem management and to support the development of strategies for adapting to the changing world. In conclusion, the articles present a comprehensive and multidisciplinary approach to understanding the hydrological and ecological response to global change and its implications for water resources management and ecological restoration. By drawing on a wide range of sources and methodologies, the articles offer new insights into the challenges and opportunities associated with water and ecosystem management in the context of global change. They offer practical guidance and support to communities, basins, and government agencies in their efforts to develop strategies for adapting to the changing world. These articles are an important contribution to the field of hydrology, ecology, and water resources management and will be of interest to researchers, policymakers, and practitioners in these fields.

Author contributions

CG: Writing—original draft preparation. CG, CL, and QL: Writing—reviewing and editing.

Conflict of interest

The authors declare that the research was conducted in the absence of any commercial or financial relationships that could be construed as a potential conflict of interest.

Publisher's note

References

Bartley, T. J., McCann, K. S., Bieg, C., Cazelles, K., Granados, M., Guzzo, M. M., et al. (2019). Food web rewiring in a changing world. *Nat. Ecol. Evol.* 3, 345–354. doi:10.1038/s41559-018-0772-3

Brasil Neto, R. M., Santos, C. A. G., Nascimento, T. V. M. D., Silva, R. M. D., and dos Santos, C. A. C. (2020). Evaluation of the trmm product for monitoring drought over paraíba state, northeastern Brazil: A statistical analysis. *Remote Sens.* 12 (14), 2184. doi:10.3390/rs12142184

Brasil Neto, R. M., Santos, C. A. G., Silva, J. F. C. B. d. C., da Silva, R. M., dos Santos, C. A. C., and Mishra, M. (2021). Evaluation of the TRMM product for monitoring drought over paraíba state, northeastern Brazil: A trend analysis. *Sci. Rep.* 11, 1097. doi:10.1038/s41598-020-80026-5

Brasil Neto, R. M., Santos, C. A. G., Silva, R. M. D., Santos, C. A. C. D., Liu, Z., and Quinn, N. W. (2021). Geospatial cluster analysis of the state, duration and severity of drought over Paraíba State, northeastern Brazil. *Sci. Total Environ.* 799, 149492. doi:10.1016/j.scitotenv.2021.149492

Brito, C. S. D., Silva, R. M. D., Santos, C. A. G., Neto, B., and Coelho, V. H. R. (2021). Monitoring meteorological drought in a semiarid region using two long-term satellite-estimated rainfall datasets: A case study of the piranhas River Basin, northeastern Brazil. *Atmos. Res.* 250, 105380. doi:10.1016/j.atmosres.2020.105380

Broadhurst, H. A., Gregory, L. M., Bleakley, E. K., Perkins, J. C., Lavin, J. V., Bolton, P., et al. (2021). Mapping differences in mammalian distributions and diversity using environmental DNA from rivers. *Sci. Total Environ.* 801, 149724. doi:10.1016/j.scitotenv.2021.149724

da Silva, G. J. F., de Oliveira, N. M., Santos, C. A. G., and da Silva, R. M. (2020). Spatiotemporal variability of vegetation due to drought dynamics (2012–2017): A case study of the upper paraíba River Basin, Brazil. *Braz. Nat. Hazards* 102, 939–964. doi:10.1007/s11069-020-03940-x

Dantas, J. C., da Silva, R. M., and Santos, C. A. G. (2020). Drought impacts, social organization, and public policies in northeastern Brazil: A case study of the upper paraíba River Basin. *Environ. Monit. Assess.* 192, 317. doi:10.1007/s10661-020-8219-0

de Oliveira, M. L., de Oliveira, G., Silva, M. T., da Silva, B. B., Cunha, J. E. d. B., et al. (2022). Remote sensing-based assessment of land degradation and drought impacts over terrestrial ecosystems in Northeastern Brazil. *Sci. Total Environ.* 835, 155490. doi:10.1016/j.scitotenv.2022.155490

Govindarajan, A. F., Francolini, R. D., Jech, J. M., Lavery, A. C., Llopiz, J. K., Wiebe, P. H., et al. (2021). Exploring the use of environmental DNA (eDNA) to detect animal taxa in the mesopelagic zone. *Front. Ecol. Evol.* 9, 574877. doi:10.3389/fevo.2021.574877

Li, X. X., Yang, W., Sun, T., and Su, L. Y. (2019). Framework of multidimensional macrobenthos biodiversity to evaluate ecological restoration in wetlands. *Environ. Res. Lett.* 14, 054003. doi:10.1088/1748-9326/ab142c

Liang, L., Huang, C., and Hu, Z. (2022). Industrial structure optimization, population agglomeration and carbon emissions–Empirical evidence from 30 provinces in China. *Front. Environ. Sci., Sec. Environ. Citiz. Sci.* 10. doi:10.3389/fenvs.2022.1078319

Lynam, C. P., Llope, M., Möllmann, C., Helaouët, P., Bayliss-Brown, G. A., and Stenseth, N. C. (2017). Interaction between top-down and bottom-up control in marine food webs. *S. A* 114, 1952–1957. doi:10.1073/pnas.1621037114

Maamoun, I., Eljamal, O., Khalil, A. M. E., Sugihara, Y., and Matsunaga, N. (2018). Phosphate removal through nano-zero-valent iron permeable reactive barrier; column experiment and reactive solute transport modeling. *Transp. Porous Media* 125, 395–412. doi:10.1007/s11242-018-1124-0

Mishra, M., Acharyya, T., Chand, P., Santos, C. A. G., Kar, D., Das, P. P., et al. (2021b). Analyzing shoreline dynamicity and the associated socioecological risk along the Southern Odisha Coast of India using remote sensing-based and statistical approaches. *Geocarto Int.* 37, 3991–4027. doi:10.1080/10106049.2021.1882005

Mishra, M., Acharyya, T., Chand, P., Santos, C. A. G., Silva, R. M. D., Santos, C. A. C. D., et al. (2022b). Response of long-to short-term tidal inlet morphodynamics on the ecological ramification of Chilika lake, the tropical Ramsar wetland in India. *Sci. Total Environ.* 807, 150769. doi:10.1016/j.scitotenv.2021.150769

Mishra, M., Acharyya, T., Kar, D., Debanath, M., Santos, C. A. G., Silva, R. M. D., et al. (2021d). Geo-ecological cues for mass nesting synchronization of Olive Ridley turtles along Rushikulya estuary in Odisha, East Coast of India. *Mar. Pollut. Bull.* 172, 112881. doi:10.1016/j.marpolbul.2021.112881

Mishra, M., Acharyya, T., Santos, C. A. G., Silva, R. M. D., Kar, D., Kamal, M., et al. (2021c). Geo-ecological impact assessment of severe cyclonic storm Amphan on Sundarban mangrove forest using geospatial technology. *Coast. Shelf Sci.* 260, 107486. doi:10.1016/j.ecss.2021.107486

Mishra, M., Dash, M. K., Sudarsan, D., Santos, C. A. G., Mishra, S. K., Kar, D., et al. (2022a). Assessment of trend and current pattern of open educational resources: A bibliometric analysis. *J. Acad. Librariansh.* 48 (3), 102520. doi:10.1016/j.acalib.2022.102520

Mishra, M., Sudarsan, D., Kar, D., Naik, A. K., Das, P. P., Santos, C. A. G., et al. (2020). The development and research trend of using dsas tool for shoreline change analysis: A scientometric analysis. *J. Urban Environ. Eng.* 14 (1), 69–77. doi:10.4090/juee.2020.v14n1.069077

Mishra, M., Sudarsan, D., Santos, C. A. G., Mishra, S. K., Kar, D., Baral, K., et al. (2021a). An overview of research on natural resources and indigenous communities: A bibliometric analysis based on scopus database (1979–2020). *Environ. Monit. Assess.* 193, 59. doi:10.1007/s10661-020-08793-2

Mosbahi, N., Serbaji, M. M., Pezy, J. P., Neifar, L., and Dauvin, J. C. (2019). Response of benthic macrofauna to multiple anthropogenic pressures in the shallow coastal zone south of Sfax (Tunisia, central Mediterranean Sea). *Environ. Pollut.* 253, 474–487. doi:10.1016/j.envpol.2019.06.080

Neto, B., Santos, R. M., Silva, C. A. G., dos, R. M., and Santos, C. A. C. (2022). Evaluation of TRMM satellite dataset for monitoring meteorological drought in northeastern Brazil. *Hydrological Sci. J.* 67, 2100–2120. doi:10.1080/02626667.2022.2130333

Oliveira, N. M., Silva, R. M., Brasil Neto, R. M., Santos, C. A. G., and Vianna, P. C. G. (2022). Spatiotemporal patterns of agricultural and meteorological droughts using SPI and MODIS-based estimates over a Brazilian semiarid region: Study case of upper paraíba River Basin. *Geocarto Int.*, 1–24. doi:10.1080/10106049.2022.2060315

Santos, C. A. G., Brasil Neto, R. M., da Silva, R. M., and dos Santos, D. C. (2019). Innovative approach for geospatial drought severity classification: A case study of paraíba state, Brazil. *Braz. Stoch. Environ. Res. Risk Assess.* 33, 545–562. doi:10.1007/s00477-018-1619-9

Santos, C. A. G., Brasil Neto, R. M., Passos, J. S. d. A., and da Silva, R. M. (2017). Drought assessment using a TRMM-derived standardized precipitation index for the upper São Francisco River basin, Brazil. *Braz. Environ. Monit. Assess.* 189, 250. doi:10.1007/s10661-017-5948-9

Santos, C. A. G., Neto, B., Nascimento, T. V. M. D., Silva, R. M. D., Mishra, M., and Frade, T. G. (2021). Geospatial drought severity analysis based on PERSIANN-CDR-estimated rainfall data for Odisha state in India (1983–2018). *Sci. Total Environ.* 750, 141258. doi:10.1016/j.scitotenv.2020.141258

Sauri, D. (2019). The decline of water consumption in Spanish cities: Structural and contingent factors. *D.* 36, 909–925. doi:10.1080/07900627.2019.1634999

Seyedhashemi, H., Moatar, F., Vidal, J.-P., Diamond, J. S., Beaufort, A., Chandesris, A., et al. (2021). Thermal signatures identify the influence of dams and ponds on stream temperature at the regional scale. *Sci. Total Environ.* 766, 142667. doi:10.1016/j.scitotenv.2020.142667

Silva, J. F. C. B. d., da Silva, R. M., Santos, C. A. G., and Vianna, P. C. G. (2021). Analysis of the response of the Epitácio Pessoa reservoir (Brazilian semiarid region) to potential future drought, water transfer and LULC scenarios. *Nat. Hazards* 108, 1347–1371. doi:10.1007/s11069-021-04736-3

Tariq, M. A., Alotaibi, R., Weththasinghe, K. K., and Rajabi, Z. (2022). A detailed perspective of water resource management in a dry and water scarce country: The case in Kuwait. *Front. Environ. Sci.* 10. doi:10.3389/fenvs.2022.1073834

Wang, C., Li, X., Yu, H., and Wang, Y. (2019). Tracing the spatial variation and value change of ecosystem services in Yellow River Delta, China. *Indic* 96, 270–277. doi:10.1016/j.ecolind.2018.09.015

Wu, J. (2022). Testing the stochastic convergence of ecological indicators in BRICS in the perspective of public health. *Front. Public Health* 10, 897459. doi:10.3389/fpubh.2022.897459

Zerouali, B., Chettih, M., Abda, Z., Mesbah, M., Santos, C. A. G., Brasil Neto, R. M., et al. (2021). Spatiotemporal meteorological drought assessment in a humid mediterranean region: Case study of the oued sebaou basin (northern central Algeria). *Nat. Hazards* 108, 689–709. doi:10.1007/s11069-021-04701-0

frontiers | Frontiers in Ecology and Evolution

TYPE Original Research
PUBLISHED 29 July 2022
DOI 10.3389/fevo.2022.972680

OPEN ACCESS

EDITED BY
Chunhui Li,
Beijing Normal University, China

REVIEWED BY
Wei Huang,
China Institute of Water Resources and Hydropower Research, China
Yusong Li,
University of Nebraska-Lincoln, United States
Zhe Li,
Chinese Academy of Sciences (CAS), China

*CORRESPONDENCE
Yurong Wang
wangyurong@scu.edu.cn

SPECIALTY SECTION
This article was submitted to Conservation and Restoration Ecology, a section of the journal Frontiers in Ecology and Evolution

RECEIVED 18 June 2022
ACCEPTED 12 July 2022
PUBLISHED 29 July 2022

CITATION
Zhang J, Ding R, Wang Y and Wen J (2022) Experimental study on the response relationship between environmental DNA concentration and biomass of *Schizothorax prenanti* in still water.
Front. Ecol. Evol. 10:972680.
doi: 10.3389/fevo.2022.972680

Experimental study on the response relationship between environmental DNA concentration and biomass of *Schizothorax prenanti* in still water

Jianmin Zhang, Ruiyu Ding, Yurong Wang* and Jiating Wen

State Key Laboratory of Hydraulics and Mountain River Engineering, Sichuan University, Chengdu, China

The superiority of the environmental DNA (eDNA) method for estimating the biomass of aquatic species has been demonstrated. However, the relationship between eDNA concentration and biomass is difficult to clarify under the influence of complex water flow and habitat conditions. It seriously restricts the popularization and application of the eDNA method in estimating aquatic biomass. In this paper, a typical fish species of rivers in southwest China, *Schizothorax prenanti*, was selected as the target species. Under standardized laboratory hydrostatic conditions, two environmental factors, water pH and water temperature were firstly determined through pre-experiments. Then we investigated the correlation between eDNA concentration and biomass under different body sizes and different body size compositions. The experimental results showed that water pH and the water temperature had a great influence on eDNA concentration. Therefore, the effects of these environmental factors need to be considered simultaneously when using eDNA concentration to estimate biomass. Under the premise of consistent environmental conditions, the biomass of *Schizothorax prenanti* was positively correlated with the eDNA concentration when the individual body size was the same. For each 1% increase in biomass of the fish, the eDNA concentration of adult (larger size) fish increased by 0.98%, while the eDNA concentration of juvenile (smaller size) fish increased by 1.38%. The smaller the size of individual fish, the greater the increase of eDNA concentration with biomass, and the increase of juvenile fish was about 1.4 times that the adult fish. When the biomass was the same but the body size composition was different, the higher the proportion of small body size individuals in the population, the higher the eDNA concentration. Special attention needs to be paid to the body size composition of the population to avoid the biomass estimation being

lower than the actual value when the smaller size fish are dominant. The experimental results provide a strong basis for a more accurate estimation of aquatic biomass in reservoirs, lakes, and other still water areas by using the eDNA method.

KEYWORDS

eDNA, biomass, body size, water pH, water temperature

Introduction

Environmental DNA (eDNA) refers to DNA noninvasively extracted from any environmental sample, such as water (Ficetola et al., 2008), sediments (Willerslev et al., 2003), or air (Longhi et al., 2009). It is thought to be derived from mixtures of feces (Martellini et al., 2005), skin cells (Ficetola et al., 2008), mucus (Merkes et al., 2014), and secretions (Bylemans et al., 2018) of organisms. As an innovative method, environmental DNA is increasingly used to investigate and monitor macroorganisms, especially aquatic species (Minamoto et al., 2011; Taberlet et al., 2012; Takahara et al., 2012; Ushio et al., 2017; Tsuji et al., 2019; Govindarajan et al., 2021). Traditional survey methods, such as electrofishing, netting, and snorkeling, are time-consuming and costly. The detection rate is low and may cause harm to the target species (Bohmann et al., 2014; Deiner et al., 2017; Kirtane et al., 2021). Studies have demonstrated that the eDNA method has a higher detection sensitivity than traditional aquatic species investigation methods (Dejean et al., 2012; Thomsen et al., 2012; Mahon et al., 2013; Krol et al., 2019; Afzali et al., 2020). It is less invasive and is especially useful for rare and endangered species (Fukumoto et al., 2015; Sigsgaard et al., 2015; Pfleger et al., 2016; Doi et al., 2017; Sakata et al., 2017; Mizumoto et al., 2020). The technique works even when animals are at low densities in the wild (Goldberg et al., 2011). It has been applied extensively for the detection of invasive and endangered species and for the estimation of biodiversity (Goldberg et al., 2013; Pilliod et al., 2014; Jane et al., 2015; Muha et al., 2017; Suarez-Menendez et al., 2020).

The study on estimation of abundance and biomass by the eDNA method is an important frontier of eDNA research (Spear et al., 2020). Previous studies have reported a positive correlation between eDNA concentration and species abundance/biomass (Takahara et al., 2012; Thomsen et al., 2012; Goldberg et al., 2013; Pilliod et al., 2013; Pont et al., 2018). In still water, Takahara et al. found that the concentration of eDNA was positively correlated with carp biomass in both aquaria and experimental ponds (Takahara et al., 2012). Under flowing water conditions, Pilliod et al. compared sampling results from traditional field methods with eDNA methods for two amphibians in 13 streams in central Idaho, United States. They found that eDNA concentration was positively related to field-measured density and biomass (Pilliod et al., 2013). A significant, positive relationship between snorkel-survey counts of the stream-dwelling fish Plecoglossus altivelis and eDNA concentration in the Saba River, Japan. was detected (Doi et al., 2017). Previous studies have shown that flowing water complicates the relationship between eDNA production, transport, and clearance. Nevertheless, a weak but positive relationship was still found between eDNA concentration, zebra mussels, and biophysical parameters (Shogren et al., 2019). The results of these and other recent studies (e.g., Tillotson et al., 2018; Itakura et al., 2019; McElroy et al., 2020) suggest that it is indeed possible to estimate the abundance of aquatic organisms using the eDNA method.

The positive relationships between eDNA concentration and fish biomass may be affected by the shedding and degradation rate of eDNA (Pilliod et al., 2013; Eichmiller et al., 2014; Lacoursiere-Roussel et al., 2016; Yamamoto et al., 2016; Jo et al., 2017). There are still many uncertainties regarding the shedding and degradation of DNA in the aquatic environment (Barnes and Turner, 2015; Civade et al., 2016; Jerde et al., 2016; Sassoubre et al., 2016; Shogren et al., 2016; Andruszkiewicz et al., 2017; Mathieu et al., 2020). Existing studies have shown that the degradation rate of eDNA may vary with water temperature (Tsuji et al., 2016; Jo et al., 2019) and water pH (Barnes et al., 2014; Tsuji et al., 2016) and other environmental factors. Therefore, before using the eDNA method to evaluate biomass, preliminary experiments were firstly conducted to explore how these environmental factors altered eDNA concentration, providing a reliable basis for subsequent experimental condition settings. Furthermore, the shedding rate of eDNA may change with the age and body size of organisms (Maruyama et al., 2014; Thalinger et al., 2021). However, few studies have systematically studied the relationship between biomass and eDNA concentration from the perspective of fish body size and body size composition of the fish population.

In this paper, two experiments were first conducted to clarify the effects of two environmental factors, water pH and water temperature, on eDNA concentration. Then, on the premise of consistent environmental conditions, we systematically studied the relationship between eDNA concentration and biomass in still water by changing the body size and body size composition

of *Schizothorax prenanti*. It provides a scientific reference for improving the ability to accurately estimate biomass using the eDNA method in still water such as reservoirs and lakes.

Materials and methods

In this study, we take the *Schizothorax prenanti* as a typical fish representative, which is mainly distributed in the Jinsha River, Min River, and other rivers of the upper reaches of the Yangtze River in China. It is an important economic fish species in southwest China. Therefore, it is of great significance to monitor the biomass of this target fish species. However, it is difficult to investigate the biomass of *Schizothorax prenanti* in the wild, so it is necessary to explore the eDNA method to estimate the biomass of aquatic species in the river ecosystem.

The fish used in this experiment were obtained from an aquaculture institution in Chengdu, China. They were reared in laboratory aquariums. The aquariums were thoroughly rinsed and disinfected before the fish were placed. To avoid the introduction of target species DNA from pathways outside the aquarium water environment, no feeding was performed during the experiment. All experiments were approved by the ethics committee prior and performed in accordance with relevant institutional and national guidelines and regulations.

Experimental design and sampling

Effect of environmental conditions on environmental DNA

We conducted two experiments to explore the effect of water temperature and water pH on eDNA concentration. For the experimental treatment group with water temperature as an environmental variable, six equal volume water samples were collected from the aquarium in which the *Schizothorax prenanti* were reared. The water pH of these samples was set to six levels: pH 5, pH 6, pH 7, pH 7.6, pH 8, and pH 9. The water of all treatments was neutral when the experiment began; therefore, the treatment of water pH 7 was not manipulated. Acidic and alkaline treatments were achieved using sterile 1 M HCl or 0.5 M NaOH, respectively. We monitored pH levels to make sure they were stable throughout the experiment. For the experimental treatment group with water temperature as the environmental variable, six equal volume water samples were collected in the same way. The water temperature of these samples was set to six levels: 12°C, 23°C, 26°C, 29°C, 32°C, and 35°C. Each treatment temperature level was held in a separate growth chamber automated to maintain a constant temperature. For each experimental treatment, we collected 100 ml water samples at 0 h, 12 h, 24 h, 36 h, 48 h, and 60 h after the setting of environmental variables reached stability.

Relationship between biomass and environmental DNA

The experimental fish were reared in several aquariums with the same volume of water storage, and each aquarium was one experimental treatment. All experimental treatments were exposed to the same environmental conditions, where the water temperature was 23°C ± 0.2 and the water pH level was pH7.

To evaluate the correlation between eDNA concentration and fish biomass, we implemented four experiments. Experiments I and II investigated the correlation between biomass and eDNA concentration when fish were of the same body size in each treatment; Experiments III and IV investigated the variation of eDNA concentration under different body size compositions when biomass was the same in each treatment.

Four experimental treatments were set up in Experiment I, in which 1, 2, 3, and 4 adult fish with an individual weight of about 500 g were reared in four experimental aquariums, respectively. In Experiment II, six experimental treatments were set up, and 3, 4, 6, 8, 9, and 12 juvenile fish with an individual weight of about 20 g were reared in 6 experimental aquariums. In Experiment III, three experimental treatments were set, and the biomass of each experimental treatment was about 2,000 g/m^3. There was one fish with an individual weight of about 1,000 g in Treatment 1; two fish with an individual weight of about 500 g in Treatment 2, and 46 fish with an individual weight of about 20 g in Treatment 3. In Experiment IV, three experimental treatments were also set, and the biomass of each treatment was about 4,000 g/m^3. There were two fish with an individual weight of about 1,000 g in Treatment 1; two fish with an individual weight of about 500 g and one fish with an individual weight of about 1,000 g in Treatment 2. For Treatment 3, there was one fish with an individual weight of about 1,000 g, one fish with an individual weight of about 500 g, and 50 juvenile fish with an individual weight of about 20 g. The specific experimental conditions of each experimental treatment were presented in **Table 1**.

For each treatment, the fish were reared in the aquarium to adapt to the environment for 24 h before the experiment began. For all experimental treatments, 100 ml of water samples were collected at 48 h, 72 h, and 96 h since the start of the experiment.

DNA extraction and qPCR

All water samples were collected in the same way and filtered within half an hour after sampling using glass fiber filters with a pore size of 0.45 μm (Xingya Purification Materials Company, Shanghai, China). Deionized water was used as negative control. All filtration equipment (i.e., filter funnels and forceps) was sterilized using sodium hypochlorite and rinsed with deionized water Contaminants were strictly controlled. The filters were

TABLE 1 Experimental conditions for each experimental treatment.

Experiment number	Experimental treatment number	Fish abundance	Individual fish weight	Fish biomass (g/m^3)
I	1	1	500 ± 67 g	945
	2	2		1,681
	3	3		2,576
	4	4		3,353
II	1	3	20 ± 6.8 g	330
	2	4		530
	3	6		685
	4	8		925
	5	9		1,050
	6	12		1,405
III	1	1	1214 g	2,023
	2	2	685g、534 g	2,032
	3	46	20 ± 3.2 g	1,700
IV	1	2	1218g、1182 g	4,000
	2	3	818g、891g、864 g	4,288
	3	52	1100g、585g、20 ± 3.2 g(50 fish)	4,635

stored in sterile 2 ml tubes at −80°C until DNA extraction with the DNeasy Blood and Tissue Kit (Qiagen, Hilden, Germany).

The quantification of eDNA was performed using real-time quantitative PCR. Through design and screening, we identified the primers and probe for *Schizothorax prenanti* as follows: forward primer (5′-GAGTGCGGATTTGACCCAC-3′), reverse primer (5′-TAACCCCCCCTATTCTGCTCATTC-3′), and probe (5′- TCCGCCCGCCTACCATTTTCTCTCTA -3′). The primers are highly specific to the target species. Real-time quantitative PCR was performed in a 20 μl reaction for each sample. QuantiNova Probe PCR Master Mix (Qiagen, Hilden, Germany) was used following the manufacturer's protocol. The mixture of the reagents was as follows: 10 μl of 2 × PCR master mix, 6 μl of RNase-free water, 0.8 μl of each primer, 0.4 μl probe, and 2 μl of extracted DNA solution. The qPCR thermal conditions were as follows: 2 min at 95°C, and 39 cycles of 5 s at 95°C and 10 s at 56°C. Quantitative real-time PCR (qPCR) was performed in triplicate, and the mean value was used during assays. PCR products of the target sequences were cloned into the plasmid, and a dilution series of the plasmid were amplified as standards in triplicate in all qPCR assays. Three wells of a no-template negative control were included in each qPCR plate and showed no amplification. The R^2 values for the standard curves were ≥0.99 for all qPCR reactions. which met the requirements of the standard curve required for fluorescence absolute quantitative PCR. All samples were assayed in triplicate. Figure 1 outlines the experimental procedure from water sample collection to the eDNA concentration detection.

Results

Experimental treatments of water pH and temperature

The eDNA concentration detected in the water samples decreased over time in all experimental treatments. The relative eDNA concentration (C/C_0) of the water samples was obtained by dividing the eDNA concentration C at each time point t with their corresponding initial eDNA concentration C_0 (at time t = 0). The trends of relative eDNA concentration over time for each water pH treatment were shown in Figure 2; the trends of relative eDNA concentration over time for each water temperature treatment were shown in Figure 3. The results showed that both water pH and water temperature had a significant influence on the change of eDNA concentration. Therefore, when conducting subsequent experimental studies on the correlation between biomass and environmental DNA, we must ensure that all experimental treatments were conducted under the same environmental conditions such as water pH and water temperature. The water pH and water temperature were monitored for each experimental treatment to eliminate the effects of environmental variables.

Experimental treatments of the same fish body size

According to the detected eDNA concentration of water samples in each treatment of Experiment I, we obtained the relationship between the biomass and eDNA concentration of adult *Schizothorax prenanti* at different sampling times, as shown in Figure 4A. According to Experiment II, the relationship between the biomass and eDNA concentration of juvenile fish at different sampling time can be seen in Figure 4B.

As shown in Figures 4A,B, at the same sampling time, there was a linear correlation between the biomass and eDNA concentration of *Schizothorax prenanti* in both adult and juvenile experimental groups. The larger the biomass (the number of individuals of fish), the higher the eDNA concentration, which presents a linear growth trend.

The biomass and corresponding eDNA concentration data for each of the above six experimental treatments were collected and further analyze. The biomass of each experimental treatment was linearly fitted to its corresponding eDNA concentration at different sampling time points, and the expression of the first-order function was as follows:

$$C = aM + b$$

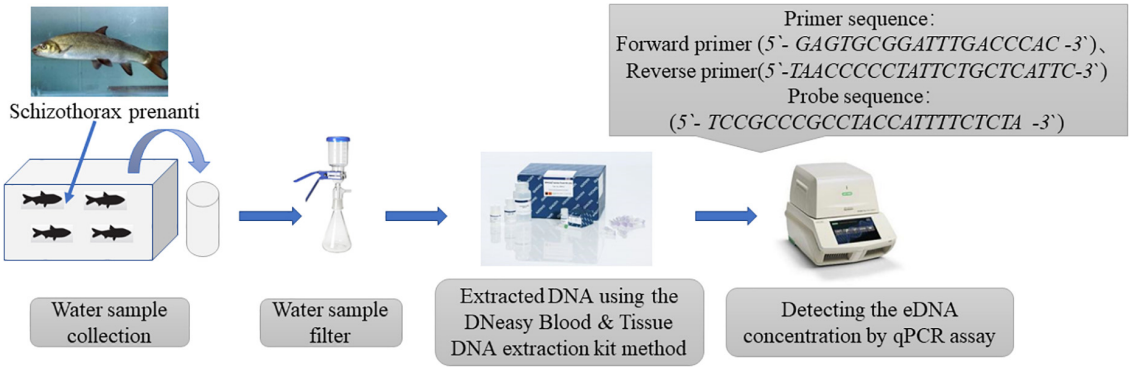

FIGURE 1
Flow chart of experimental operation.

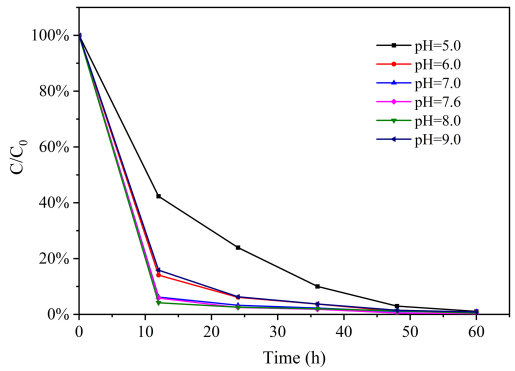

FIGURE 2
The variation trend of relative eDNA concentration under different water pH.

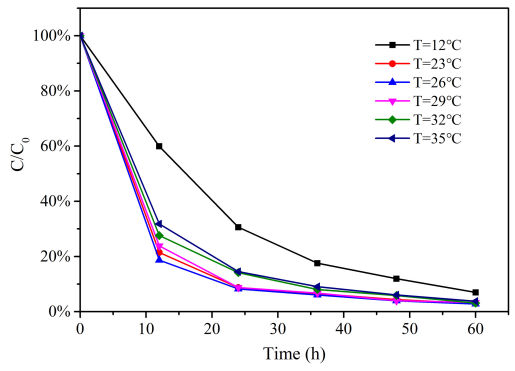

FIGURE 3
The variation trend of relative eDNA concentration under different water temperature.

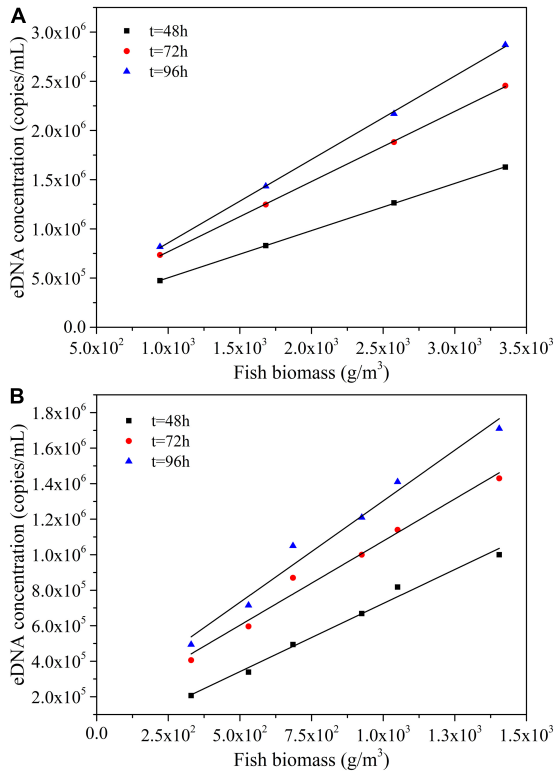

FIGURE 4
Relationship between biomass and eDNA concentration at different sampling time: **(A)** Adult fish experimental group. **(B)** Juvenile fish experimental group.

where C is the eDNA concentration; M is the biomass of each experimental treatment; a is the slope of the fitting line, i.e., $\triangle C/\triangle M$; b is the intercept. The coefficients a and b of the fitted first-order function are summarized in Table 2. As can be seen from Table 2, the later the sampling time is, the higher the slope of the fitting line is, regardless of the adult fish experimental group or the juvenile fish experimental group. That is, the greater the cumulative increase of eDNA concentration with biomass. This may be due to the increasing adaptation of

Schizothorax prenanti to the aquarium environment over time. Therefore, their metabolic rate increases, and the rate of shedding eDNA into the water increases.

Experimental treatments of the same fish biomass

The biomass of each experimental treatment in Experiment III was about 2,000 g/m^3, and the eDNA concentration detected in each experimental treatment in Experiment III at different sampling times were compared, as shown in **Figure 5A**. The eDNA concentration corresponding to per unit biomass (1 g/m^3) of *Schizothorax prenanti* in each experimental treatment was calculated. Then the comparison of eDNA concentration corresponding to per unit biomass (1 g/m^3) of *Schizothorax prenanti* was drawn, as shown in **Figure 5B**. The biomass of each experimental treatment in Experiment IV was about 4,000 g/m^3. Similarly, the eDNA concentration detected in each experimental treatment in Experiment IV at different sampling times are shown in **Figure 6A**, and the corresponding eDNA concentration per unit biomass (1 g/m^3) are plotted for comparison, see **Figure 6B**.

Discussion

Experimental treatments of water pH and temperature

The concentration of environmental DNA decreased over time for all experimental treatments. This is due to the process of continuous degradation of eDNA in parallel with the fact that no more organisms continue to shed eDNA into the water after the water samples are collected from the aquarium. Based on our experimental data, it can be observed that the degradation of environmental DNA is very sharp in the initial stages. The consistency of degradation patterns across a range of environmental covariates provides evidence that the initial sharp decline in eDNA is common across a variety of systems and environmental conditions (Dejean et al., 2011; Thomsen et al., 2012; Barnes et al., 2014).

Figure 2 showed that the water pH level had a great influence on the eDNA degradation. The degradation rate was faster when the water pH is between 7.0 and 8.0. The reason for this phenomenon may be that the suitable water pH for the survival and reproduction of most microorganisms in the experimental water body and the suitable water pH for the extracellular enzyme to degrade eDNA were neutral and weakly alkaline; Strong acidic and strong alkaline conditions would inhibit the activities of microorganisms and enzymes, thus reducing the degradation rate of eDNA.

In this experiment, water temperature also had a great influence on the degradation of *Schizothorax prenanti* eDNA. According to **Figure 3**, it can be seen that the degradation rate is highest when water temperature is between 23°C and 29°C. The degradation rate at 12°C was much lower than that at 26°C, which was consistent with previous studies (Strickler et al., 2015). The reason for this phenomenon may be that the optimum temperature for the growth and reproduction of microorganisms in the experimental water and the suitable temperature for enzyme activities is between 23°C and 29°C. In the case of lower water temperature or higher water temperature, the activities of microorganisms and enzymes in the water are inhibited, thus reducing the eDNA degradation rate. That is, water temperature affects the degradation rate of eDNA by affecting the activities of microorganisms and enzymes.

In general, water pH and water temperature significantly affect the concentration of eDNA in an aquatic environment, mainly by altering the activity of microorganisms and enzymes that affect the degradation rate of eDNA. Therefore, when using eDNA methods to predict the biomass of aquatic species, the effects of environmental factors need to be considered simultaneously. For example, changes in water temperature in different seasons or differences in water pH in different watersheds may lead to different prediction results. The trends of environmental DNA of target species under different environmental conditions such as water pH and water temperature can be obtained in the laboratory before fieldwork, which facilitates comparisons between different rivers under different environmental conditions.

Experimental treatments of the same fish body size

The eDNA concentration of the juvenile fish experimental group and adult fish experimental group under different experimental conditions was compared and analyzed, as shown in **Figure 7A**. The dashed line is a linear fit of the mean eDNA concentration for each experimental treatment under different biomass conditions. It can be observed from the fitting line that the eDNA concentration of the juvenile fish group is higher than that of the corresponding adult fish experimental group under the same biomass level. Previous studies have pointed out that the shedding rate of environmental DNA may change with the age and body size of organisms (Maruyama et al., 2014). Therefore, we analyzed that this may be due to the higher activity intensity, higher metabolic rate, and greater rate of eDNA shedding in juvenile fish than in adult fish. Therefore, we analyzed that this may be due to the higher activity intensity and metabolic rate of juvenile fish than adult fish, with a larger eDNA shedding rate.

TABLE 2 Linear fitting function coefficients of biomass and eDNA concentration.

Coefficient	Adult fish treatments			Juvenile fish treatments		
	t = 48h	t = 48h	t = 48h	t = 48h	t = 72h	t = 96h
A	479.40	713.33	847.98	767.08	948.45	1,142.24
b	23,685.02	54,278.62	9,703.46	42,051.09	128,477.34	160,576.23
R^2	0.99991	0.99974	0.99939	0.98581	0.97781	0.97299

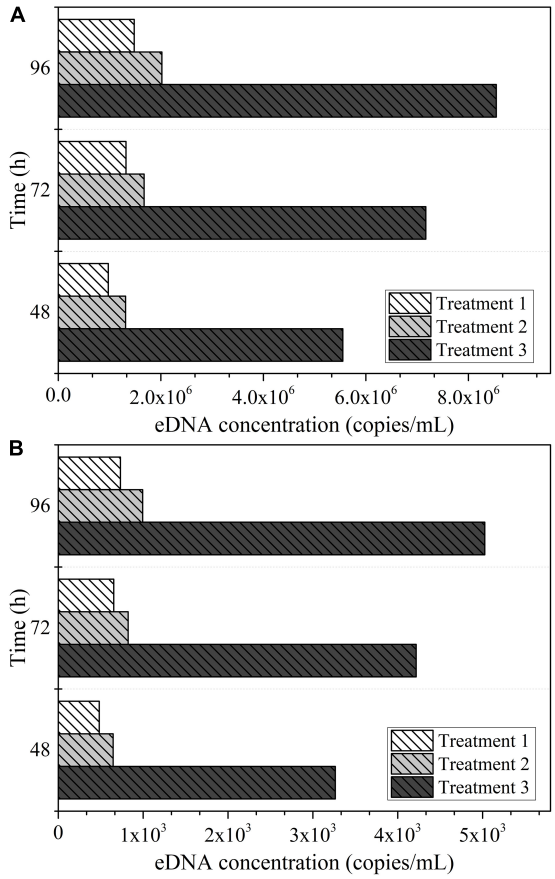

FIGURE 5
The eDNA concentration detected at different sampling times for each experimental treatment in Experiment III: **(A)** eDNA concentration corresponding to total biomass. **(B)** eDNA concentration corresponding to per unit biomass.

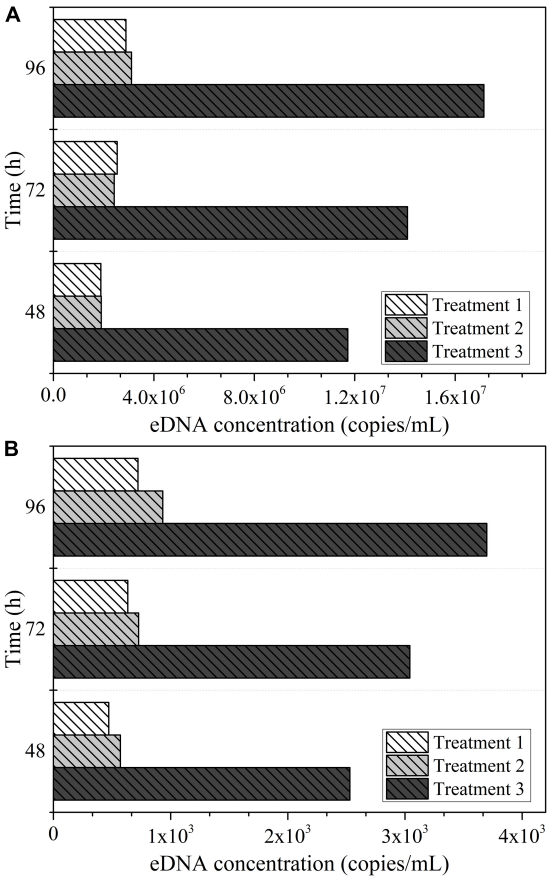

FIGURE 6
The eDNA concentration detected at different sampling times for each experimental treatment in Experiment IV: **(A)** eDNA concentration corresponding to total biomass. **(B)** eDNA concentration corresponding to per unit biomass.

In the adult fish experimental group, for each increase of per unit biomass (1 g/m^3), the eDNA concentration increased by about 680 copies/ml. In the juvenile fish experimental group, for each increase of 1 unit of biomass (1 g/m^3), the corresponding eDNA concentration increased by about 953 copies/ml. In other words, the increase in eDNA concentration with biomass in the juvenile group was about 1.4 times higher than that in the adult group.

The two variables depicted in Figure 7A, biomass and eDNA concentration, were dimensionless and the results were shown in Figure 7B. M_{Max} is the maximum biomass corresponding to all experimental treatments of Experiment I and II, and C_{Max} is the mean value of eDNA concentration corresponding to M_{Max}. From Figure 7B, we can obtain that for each 1% increase in biomass of the juvenile fish experimental group, the eDNA concentration increased by 1.38% accordingly; For each 1% increase in biomass in the adult fish experimental group, the

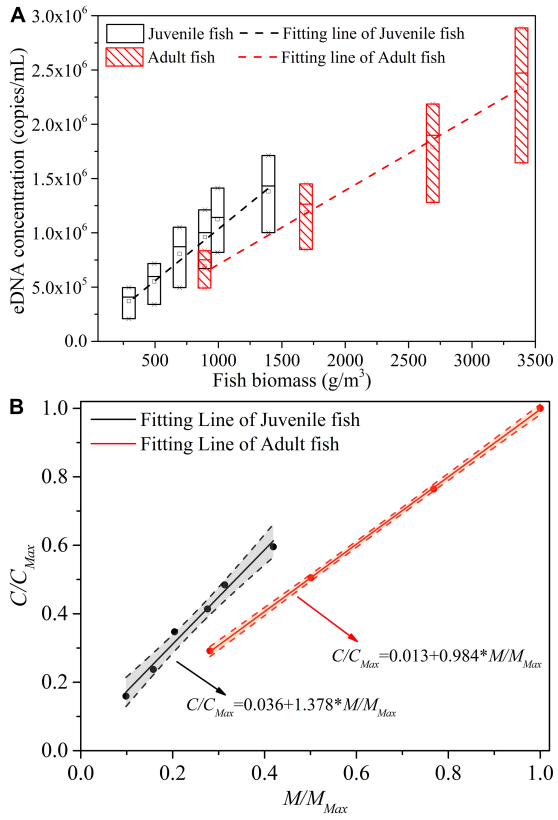

FIGURE 7
Comparison of the relationship between biomass and eDNA concentration in the adult and juvenile fish experimental groups: **(A)** Raw data; **(B)** Normalized data.

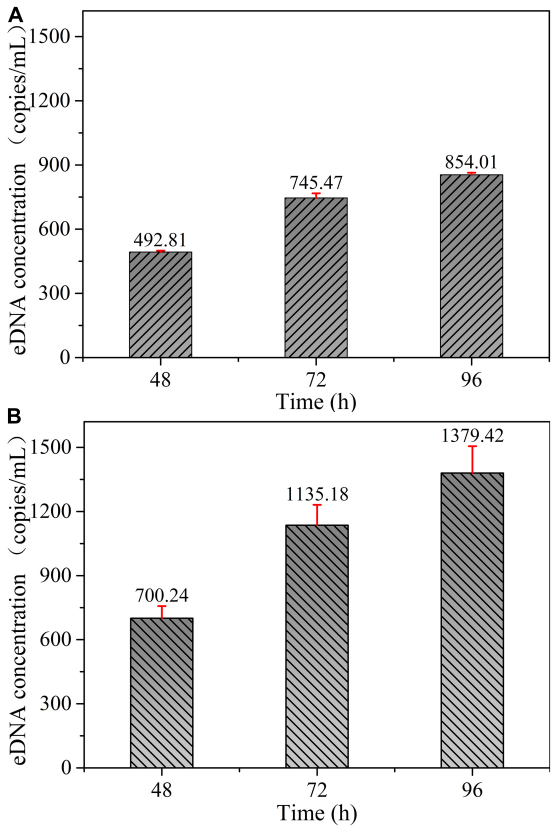

FIGURE 8
eDNA concentration corresponding to per unit biomass at different sampling times: **(A)** Adult fish experimental group. **(B)** Juvenile fish experimental group.

eDNA concentration increased by 0.98% accordingly, i.e., the growth rate of the juvenile fish group is 0.4% higher than that in the adult fish group.

For the adult fish experimental group, the growth rate of biomass and the corresponding growth rate of eDNA concentration was almost equal. However, for the juvenile fish experimental group, the growth rate of biomass was slightly higher than the corresponding growth rate of eDNA concentration. Therefore, when we use the eDNA method to evaluate the change of biomass in still water, we can predict it according to the change rate of environmental DNA concentration, However, the effect of age/body size composition of biological populations on the predicted results cannot be ignored. If the proportion of juvenile fish in the population is greater, the rate of change in population biomass will be higher than the rate of change in eDNA concentration.

eDNA concentration corresponding to per unit biomass (1 g/m^3) was calculated for all experimental samples of adult fish collected in Experiment I, and then statistical analysis was performed to obtain the bar graphs shown in **Figure 8A**. Each bar depicts the mean quantification value (with accompanying standard deviation) of the eDNA concentration corresponding to per unit biomass (1 g/m^3) for the four experimental treatments at different sampling times. The eDNA concentration corresponding to per unit biomass (1 g/m^3) was calculated for all juvenile fish experimental group samples collected in Experiment II, and the same statistical analysis of data was performed to obtain **Figure 8B**.

As can be seen in **Figure 8**, under the same sampling time conditions, the eDNA concentration released per unit of biomass was basically the same among different experimental treatments for both the adult and juvenile fish groups. The dispersion of the data was slightly higher in the juvenile group than in the adult group. The results showed that the eDNA release rate per unit of biomass was almost the same between the two experiments under the same body size condition. The number of individual fish had almost no effect on the eDNA release rate per unit of biomass.

Through the above two groups of experiments with the same individual body size of fish but different total biomass, we proved that when ignoring the complexity of the

individual body size composition of fish populations in natural basins, the eDNA concentration increases with the increase of biomass. However, the environmental DNA concentration was influenced by the body size of the individuals. The smaller the body size of the individual fish, the greater the increase in eDNA concentration with increasing biomass. For the adult fish group, the growth rate of biomass is approximately equal to the corresponding growth rate of eDNA, while the juvenile fish group is slightly greater than the growth rate of eDNA. Therefore, when using the eDNA method to assess biomass changes in still waters, the influence of the body size composition of the biological population on the predictions cannot be ignored. If the proportion of fish with small body size in the population is larger, the rate of change in population biomass will be higher than the rate of change in eDNA concentration.

Experimental treatments of the same fish biomass

According to the experimental design of Experiment III, the proportion of juvenile fish (small body size fish) reared in Treatment 3 to the total population was much higher than that in the other two treatments. The setup between the three treatments in Experiment IV was the same as in Experiment III. As can be seen from **Figures 5**, **6**, both for Experiment III and IV, the eDNA concentration and the eDNA concentration per unit biomass (1 g/m^3) were significantly higher in Treatment 3 than in Treatments 1 and 2. It implies that under the same biomass conditions, the treatment with a larger proportion of juvenile fish to the total population, the higher the corresponding eDNA concentration. The patterns obtained from these two experiments were consistent, so the effect of accidental factors could be excluded.

The above two experiments compared the effect of different fish body size composition on eDNA concentration under the same total biomass condition. The experimental group with a higher proportion of small body size individuals proved to have greater eDNA concentrations than the experimental group with a higher proportion of large body size individuals. The reason may be that the metabolic rate and activity of small body size fish are significantly higher than those of large body size fish, resulting in a higher eDNA release rate and higher eDNA concentration in the same condition of biomass. Therefore, in actual natural river surveys, when assessing biomass by the eDNA method, it is advisable to investigate the population structure characteristics of the target fish in advance, and when the population is dominated by juveniles, quantitative eDNA concentration data should be carefully interpreted to avoid underestimation of biomass.

Conclusion

In this paper, we took *Schizothorax prenanti* as the target species. Firstly, the influence of water pH and water temperature on environmental DNA concentration was determined by pre-experiments. Under the premise of consistent experimental environmental conditions, we investigated the correlation between eDNA concentration and biomass under different conditions of body size and body size composition. The main results and conclusions are as follows.

(1). Water pH and water temperature significantly affect the concentration of environmental DNA in fish in aquatic environments, mainly by altering the activity of microorganisms and enzymes that affect the degradation rate of environmental DNA. Therefore, when using environmental DNA methods to predict the biomass of aquatic species, the effects of environmental factors need to be considered simultaneously. For example, changes in water temperature in different seasons or differences in water pH in different watersheds may lead to different prediction results.

(2). Under the same environmental conditions, there is a positive correlation between biomass and eDNA concentration when the body size of individual *Schizothorax prenanti* is uniform. The smaller the individual body size, the greater the increase of eDNA concentration with biomass. For the juvenile environmental group, the increase of eDNA concentration with biomass was about 1.4 times higher than that for the adult environmental group.

(3). The growth rate of biomass and the corresponding growth rate of eDNA concentration was approximately equal for the adult fish group. For each 1% increase in biomass, the corresponding growth rate of eDNA concentration for the juvenile fish group is 0.4% higher than that in the adult fish group. Therefore, when using the eDNA method to assess biomass changes in still water, the influence of the fish body size on the predicted results cannot be ignored. If the proportion of juvenile fish in the population is larger, the rate of change in population biomass will be higher than the rate of change in eDNA concentration.

(4). When the total biomass of *Schizothorax prenanti* was the same but with different body size compositions, the higher the proportion of small-sized individuals in the overall population, the greater the environmental DNA concentration. Therefore, the structural characteristics of the population should not be ignored when assessing biomass by environmental DNA methods.

In summary, when using environmental DNA methods to estimate the biomass of aquatic species in reservoirs, lakes, and other still water in actual river sections, the effects of factors such

as water pH, water temperature, organism body size, and body size composition on eDNA concentration should be taken into account. If the proportion of small body size individuals in the population is high, it is important to avoid biomass assessment lower than the actual value. A model for estimating biomass through eDNA concentration should be established under the premise of combining environmental conditions and population characteristics, so that biomass estimation can be more accurate.

Data availability statement

The original contributions presented in this study are included in the article/supplementary material, further inquiries can be directed to the corresponding author/s.

Ethics statement

The animal study was reviewed and approved by Ethics Committee, College of Life Sciences, Sichuan University.

Author contributions

JZ and YW conceived and designed the experiments. RD and JW performed the experiments. JZ, YW, RD, and JW designed the methodology and conducted data analyses. RD and JW led the writing of the manuscript. All authors contributed to data interpretation, structuring of the manuscript, reviewed and edited the manuscript, and approved the final version for submission.

Funding

This research was supported by the National Natural Science Foundation of China (No. 52079082) and the Open Research Fund of State Key Laboratory of Simulation and Regulation of Water Cycle in River Basin, China Institute of Water Resources and Hydropower Research (No. IWHR-SKL-KF202107).

Conflict of interest

The authors declare that the research was conducted in the absence of any commercial or financial relationships that could be construed as a potential conflict of interest.

Publisher's note

All claims expressed in this article are solely those of the authors and do not necessarily represent those of their affiliated organizations, or those of the publisher, the editors and the reviewers. Any product that may be evaluated in this article, or claim that may be made by its manufacturer, is not guaranteed or endorsed by the publisher.

References

Afzali, S. F., Bourdages, H., Laporte, M., Mérot, C., Normandeau, E., Audet, C., et al. (2020). Comparing environmental metabarcoding and trawling survey of demersal fish communities in the Gulf of St. Lawrence, Canada. *Environ. DNA* 3, 22–42. doi: 10.1002/edn3.111

Andruszkiewicz, E. A., Sassoubre, L. M., and Boehm, A. B. (2017). Persistence of marine fish environmental DNA and the influence of sunlight. *PLoS One* 12:e0185043. doi: 10.1371/journal.pone.0185043

Barnes, M. A., and Turner, C. R. (2015). The ecology of environmental DNA and implications for conservation genetics. *Conservat. Genetics* 17, 1–17. doi: 10.1007/s10592-015-0775-4

Barnes, M. A., Turner, C. R., Jerde, C. L., Renshaw, M. A., Chadderton, W. L., and Lodge, D. M. (2014). Environmental conditions influence eDNA persistence in aquatic systems. *Environ. Sci. Technol.* 48, 1819–1827. doi: 10.1021/es404734p

Bohmann, K., Evans, A., Gilbert, M. T. P., Carvalho, G. R., Creer, S., Knapp, M., et al. (2014). Erratum: environmental DNA for wildlife biology and biodiversity monitoring. *Trends Ecol. Evol.* 29, 358–367. doi: 10.1016/j.tree.2014.05.012

Bylemans, J., Furlan, E. M., Gleeson, D. M., Hardy, C. M., and Duncan, R. P. (2018). Does Size Matter? An experimental evaluation of the relative abundance and decay rates of aquatic environmental DNA. *Environ. Sci. Technol.* 52, 6408–6416. doi: 10.1021/acs.est.8b01071

Civade, R., Dejean, T., Valentini, A., Roset, N., Raymond, J. C., Bonin, A., et al. (2016). Spatial representativeness of environmental DNA metabarcoding signal for fish biodiversity assessment in a natural freshwater system. *PLoS One* 11:e0157366. doi: 10.1371/journal.pone.0157366

Deiner, K., Bik, H. M., Machler, E., Seymour, M., Lacoursiere-Roussel, A., Altermatt, F., et al. (2017). Environmental DNA metabarcoding: transforming how we survey animal and plant communities. *Mol. Ecol.* 26, 5872–5895. doi: 10.1111/mec.14350

Dejean, T., Valentini, A., Duparc, A., Pellier-Cuit, S., Pompanon, F., Taberlet, P., et al. (2011). Persistence of environmental DNA in freshwater ecosystems. *PLoS One*. 6:e23398. doi: 10.1371/journal.pone.0023398

Dejean, T., Valentini, A., Miquel, C., Taberlet, P., Bellemain, E., and Miaud, C. (2012). Improved detection of an alien invasive species through environmental DNA barcoding: the example of the American bullfrog *Lithobates catesbeianus*. *J. Appl. Ecol.* 49, 953–959. doi: 10.1111/j.1365-2664.2012.02171.x

Doi, H., Katano, I., Sakata, Y., Souma, R., Kosuge, T., Nagano, M., et al. (2017). Detection of an endangered aquatic heteropteran using environmental DNA in a wetland ecosystem. *R. Soc. Open Sci.* 4:170568. doi: 10.1098/rsos.170568

Eichmiller, J. J., Bajer, P. G., and Sorensen, P. W. (2014). The relationship between the distribution of common carp and their environmental DNA in a small lake. *PLoS One* 9:e112611. doi: 10.1371/journal.pone.0112611

Ficetola, G. F., Miaud, C., Pompanon, F., and Taberlet, P. (2008). Species detection using environmental DNA from water samples. *Biol. Lett.* 4, 423–425. doi: 10.1098/rsbl.2008.0118

Fukumoto, S., Ushimaru, A., Minamoto, T., and Crispo, E. (2015). A basin-scale application of environmental DNA assessment for rare endemic species and closely related exotic species in rivers: a case study of giant salamanders in Japan. *J. Appl. Ecol.* 52, 358–365. doi: 10.1111/1365-2664.12392

Goldberg, C. S., Pilliod, D. S., Arkle, R. S., and Waits, L. P. (2011). Molecular detection of vertebrates in stream water: a demonstration using Rocky Mountain tailed frogs and Idaho giant salamanders. *PLoS One* 6:e22746. doi: 10.1371/journal.pone.0022746

Goldberg, C. S., Sepulveda, A., Ray, A., Baumgardt, J., and Waits, L. P. (2013). Environmental DNA as a new method for early detection of New Zealand mudsnails (*Potamopyrgus antipodarum*). *Freshw. Sci.* 32, 792–800. doi: 10.1899/13-046.1

Govindarajan, A. F., Francolini, R. D., Jech, J. M., Lavery, A. C., Llopiz, J. K., Wiebe, P. H., et al. (2021). Exploring the use of environmental DNA (eDNA) to detect animal taxa in the mesopelagic zone. *Front. Ecol. Evol.* 9:574877. doi: 10.3389/fevo.2021.574877

Itakura, H., Wakiya, R., Yamamoto, S., Kaifu, K., Sato, T., and Minamoto, T. (2019). Environmental DNA analysis reveals the spatial distribution, abundance, and biomass of Japanese eels at the river-basin scale. *Aquat. Conserv. Ecosyst.* 29, 361–373. doi: 10.1002/aqc.3058

Jane, S. F., Wilcox, T. M., McKelvey, K. S., Young, M. K., Schwartz, M. K., Lowe, W. H., et al. (2015). Distance, flow and PCR inhibition: eDNA dynamics in two headwater streams. *Mol. Ecol. Resour.* 15, 216–227. doi: 10.1111/1755-0998.12285

Jerde, C. L., Olds, B. P., Shogren, A. J., Andruszkiewicz, E. A., Mahon, A. R., Bolster, D., et al. (2016). Influence of stream bottom substrate on retention and transport of vertebrate environmental DNA. *Environ. Sci. Technol.* 50, 8770–8779. doi: 10.1021/acs.est.6b01761

Jo, T., Murakami, H., Masuda, R., Sakata, M. K., Yamamoto, S., and Minamoto, T. (2017). Rapid degradation of longer DNA fragments enables the improved estimation of distribution and biomass using environmental DNA. *Mol. Ecol. Resour.* 17, e25–e33. doi: 10.1111/1755-0998.12685

Jo, T., Murakami, H., Yamamoto, S., Masuda, R., and Minamoto, T. (2019). Effect of water temperature and fish biomass on environmental DNA shedding, degradation, and size distribution. *Ecol. Evol.* 9, 1135–1146. doi: 10.1002/ece3.4802

Kirtane, A., Wieczorek, D., Noji, T., Baskin, L., Ober, C., Plosica, R., et al. (2021). Quantification of Environmental DNA (eDNA) shedding and decay rates for three commercially harvested fish species and comparison between eDNA detection and trawl catches. *Environ. DNA* 3, 1142–1155. doi: 10.1002/edn3.236

Krol, L., Van der Hoorn, B., Gorsich, E. E., Trimbos, K., Bodegom, P. M. V., and Schrama, M. (2019). How Does eDNA compare to traditional trapping? Detecting mosquito communities in south-african freshwater ponds. *Front. Ecol. Evol.* 7:260. doi: 10.3389/fevo.2019.00260

Lacoursiere-Roussel, A., Rosabal, M., and Bernatchez, L. (2016). Estimating fish abundance and biomass from eDNA concentrations: variability among capture methods and environmental conditions. *Mol. Ecol. Resour.* 16, 1401–1414. doi: 10.1111/1755-0998.12522

Longhi, S., Cristofori, A., Gatto, P., Cristofolini, F., Grando, M. S., and Gottardini, E. (2009). Biomolecular identification of allergenic pollen: a new perspective for aerobiological monitoring? *Ann. Allergy Asthma Immunol.* 103, 508–514. doi: 10.1016/s1081-1206(10)60268-2

Mahon, A. R., Jerde, C. L., Galaska, M., Bergner, J. L., Chadderton, W. L., Lodge, D. M., et al. (2013). Validation of eDNA surveillance sensitivity for detection of Asian carps in controlled and field experiments. *PLoS One* 8:e58316. doi: 10.1371/journal.pone.0058316

Martellini, A., Payment, P., and Villemur, R. (2005). Use of eukaryotic mitochondrial DNA to differentiate human, bovine, porcine and ovine sources in fecally contaminated surface water. *Water Res.* 39, 541–548. doi: 10.1016/j.watres.2004.11.012

Maruyama, A., Nakamura, K., Yamanaka, H., Kondoh, M., and Minamoto, T. (2014). The release rate of environmental DNA from juvenile and adult fish. *PLoS One* 9:e114639. doi: 10.1371/journal.pone.0114639

Mathieu, C., Hermans, S. M., Lear, G., Buckley, T. R., Lee, K. C., and Buckley, H. L. (2020). A systematic review of sources of variability and uncertainty in eDNA data for environmental monitoring. *Front. Ecol. Evol.* 8:135. doi: 10.3389/fevo.2020.00135

McElroy, M. E., Dressler, T. L., Titcomb, G. C., Wilson, E. A., Deiner, K., Dudley, T. L., et al. (2020). Calibrating environmental DNA metabarcoding to conventional surveys for measuring fish species richness. *Front. Ecol. Evol.* 8:276. doi: 10.3389/fevo.2020.00276

Merkes, C. M., McCalla, S. G., Jensen, N. R., Gaikowski, M. P., and Amberg, J. J. (2014). Persistence of DNA in carcasses, slime and avian feces may affect interpretation of environmental DNA data. *PLoS One* 9:e113346. doi: 10.1371/journal.pone.0113346

Minamoto, T., Yamanaka, H., Takahara, T., Honjo, M. N., and Kawabata, Z. I (2011). Surveillance of fish species composition using environmental DNA. *Limnology* 13, 193–197. doi: 10.1007/s10201-011-0362-4

Mizumoto, H., Mitsuzuka, T., and Araki, H. (2020). An environmental DNA survey on distribution of an endangered salmonid species, *Parahucho perryi*, in Hokkaido, Japan. *Front. Ecol. Evol.* 8:569425. doi: 10.3389/fevo.2020.569425

Muha, T. P., Rodríguez-Rey, M., Rolla, M., and Tricarico, E. (2017). Using environmental DNA to improve species distribution models for freshwater invaders. *Front. Ecol. Evol.* 5:158. doi: 10.3389/fevo.2017.00158

Pfleger, M. O., Rider, S. J., Johnston, C. E., and Janosik, A. M. (2016). Saving the doomed: using eDNA to aid in detection of rare sturgeon for conservation (Acipenseridae). *Glob. Ecol. Conserv.* 8, 99–107. doi: 10.1016/j.gecco.2016.08.008

Pilliod, D. S., Goldberg, C. S., Arkle, R. S., and Waits, L. P. (2013). Estimating occupancy and abundance of stream amphibians using environmental DNA from filtered water samples. *Can. J. Fish. Aquat. Sci.* 70, 1123–1130. doi: 10.1139/cjfas-2013-0047

Pilliod, D. S., Goldberg, C. S., Arkle, R. S., and Waits, L. P. (2014). Factors influencing detection of eDNA from a stream-dwelling amphibian. *Mol. Ecol. Resour.* 14, 109–116. doi: 10.1111/1755-0998.12159

Pont, D., Rocle, M., Valentini, A., Civade, R., Jean, P., Maire, A., et al. (2018). Environmental DNA reveals quantitative patterns of fish biodiversity in large rivers despite its downstream transportation. *Sci. Rep.* 8:10361. doi: 10.1038/s41598-018-28424-8

Sakata, M. K., Maki, N., Sugiyama, H., and Minamoto, T. (2017). Identifying a breeding habitat of a critically endangered fish, *Acheilognathus typus*, in a natural river in Japan. *Naturwissenschaften* 104:100. doi: 10.1007/s00114-017-1521-1

Sassoubre, L. M., Yamahara, K. M., Gardner, L. D., Block, B. A., and Boehm, A. B. (2016). Quantification of environmental DNA (eDNA) shedding and decay rates for three marine fish. *Environ. Sci. Technol.* 50, 10456–10464. doi: 10.1021/acs.est.6b03114

Shogren, A. J., Tank, J. L., Andruszkiewicz, E. A., Olds, B., Jerde, C., and Bolster, D. (2016). Modelling the transport of environmental DNA through a porous substrate using continuous flow-through column experiments. *J. R. Soc. Interface* 13:20160290. doi: 10.1098/rsif.2016.0290

Shogren, A. J., Tank, J. L., Egan, S. P., Bolster, D., and Riis, T. (2019). Riverine distribution of mussel environmental DNA reflects a balance among density, transport, and removal processes. *Freshw. Biol.* 64, 1467–1479. doi: 10.1111/fwb.13319

Sigsgaard, E. E., Carl, H., Møller, P. R., and Thomsen, P. F. (2015). Monitoring the near-extinct European weather loach in Denmark based on environmental DNA from water samples. *Biol. Conserv.* 183, 46–52. doi: 10.1016/j.biocon.2014.11.023

Spear, M. J., Embke, H. S., Krysan, P. J., and Vander Zanden, M. J. (2020). Application of eDNA as a tool for assessing fish population abundance. *Environ. DNA* 3, 83–91. doi: 10.1002/edn3.94

Strickler, K. M., Fremier, A. K., and Goldberg, C. S. (2015). Quantifying effects of UV-B, temperature, and pH on eDNA degradation in aquatic microcosms. *Biol. Conserv.* 183, 85–92. doi: 10.1016/j.biocon.2014.11.038

Suarez-Menendez, M., Planes, S., Garcia-Vazquez, E., and Ardura, A. (2020). Early alert of biological risk in a coastal lagoon through eDNA metabarcoding. *Front. Ecol. Evol.* 8:9. doi: 10.3389/fevo.2020.00009

Taberlet, P., Coissac, E., Pompanon, F., Brochmann, C., and Willerslev, E. (2012). Towards next-generation biodiversity assessment using DNA metabarcoding. *Mol. Ecol.* 21, 2045–2050. doi: 10.1111/j.1365-294X.2012.05470.x

Takahara, T., Minamoto, T., Yamanaka, H., Doi, H., and Kawabata, Z. (2012). Estimation of fish biomass using environmental DNA. *PLoS One* 7:e35868. doi: 10.1371/journal.pone.0035868

Thalinger, B., Rieder, A., Teuffenbach, A., Pütz, Y., Schwerte, T., Wanzenböck, J., et al. (2021). The effect of activity, energy use, and species identity on environmental DNA shedding of freshwater fish. *Front. Ecol. Evol.* 9:623718. doi: 10.3389/fevo.2021.623718

Thomsen, P. F., Kielgast, J., Iversen, L. L., Wiuf, C., Rasmussen, M., Gilbert, M. T., et al. (2012). Monitoring endangered freshwater biodiversity using environmental DNA. *Mol. Ecol.* 21, 2565–2573. doi: 10.1111/j.1365-294X.2011.05418.x

Tillotson, M. D., Kelly, R. P., Duda, J. J., Hoy, M., Kralj, J., and Quinn, T. P. (2018). Concentrations of environmental DNA (eDNA) reflect spawning salmon abundance at fine spatial and temporal scales. *Biol. Conserv.* 220, 1–11. doi: 10.1016/j.biocon.2018.01.030

Tsuji, S., Takahara, T., Doi, H., Shibata, N., and Yamanaka, H. (2019). The detection of aquatic macroorganisms using environmental DNA analysis—A review of methods for collection, extraction, and detection. *Environ. DNA* 1, 99–108. doi: 10.1002/edn3.21

Tsuji, S., Yamanaka, H., and Minamoto, T. (2016). Effects of water pH and proteinase K treatment on the yield of environmental DNA from water samples. *Limnology* 18, 1–7. doi: 10.1007/s10201-016-0483-x

Ushio, M., Murakami, H., Masuda, R., Sado, T., Miya, M., Sakurai, S., et al. (2017). *Quantitative Monitoring of Multispecies Fish Environmental DNA using High-Throughput Sequencing*. Cold Spring Harbor, NY: Cold Spring Harbor Laboratory, doi: 10.1101/113472

Willerslev, E., Hansen, A. J., Binladen, J., Brand, T. B., Gilbert, M. T., Shapiro, B., et al. (2003). Diverse plant and animal genetic records from Holocene and Pleistocene sediments. *Science* 300, 791–795. doi: 10.1126/science.1084114

Yamamoto, S., Minami, K., Fukaya, K., Takahashi, K., Sawada, H., Murakami, H., et al. (2016). Environmental DNA as a 'Snapshot' of fish distribution: a case study of Japanese jack mackerel in Maizuru Bay, Sea of Japan. *PLoS One* 11:e0149786. doi: 10.1371/journal.pone.0149786

frontiers | Frontiers in Environmental Science

TYPE Original Research
PUBLISHED 05 August 2022
DOI 10.3389/fenvs.2022.952414

OPEN ACCESS

EDITED BY
Chunhui Li,
Beijing Normal University, China

REVIEWED BY
Wei Huang,
China Institute of Water Resources and Hydropower Research, China
Yusong Li,
University of Nebraska-Lincoln, United States
Dan Xu,
Shanghai Ocean University, China
Zhe Li,
Chinese Academy of Sciences (CAS), China

*CORRESPONDENCE
Yurong Wang,
wangyurong@scu.edu.cn

SPECIALTY SECTION
This article was submitted to Conservation and Restoration Ecology, a section of the journal Frontiers in Environmental Science

RECEIVED 25 May 2022
ACCEPTED 08 July 2022
PUBLISHED 05 August 2022

CITATION
Huang L, Zhang J and Wang Y (2022), Effects of total dissolved gas supersaturation and sediment on environmental DNA persistence of grass carp (Ctenopharyngodon idella) in water.
Front. Environ. Sci. 10:952414.
doi: 10.3389/fenvs.2022.952414

Effects of total dissolved gas supersaturation and sediment on environmental DNA persistence of grass carp (*Ctenopharyngodon idella*) in water

Lei Huang, Jianmin Zhang and Yurong Wang*

State Key Laboratory of Hydraulics and Mountain River Engineering, Sichuan University, Chengdu, Sichuan, China

Environmental DNA (eDNA) technology has become an alternative tool for monitoring aquatic communities due to its sensitive, economical, and non-invasive properties. However, the application of this technique is often limited by the complexity of environmental conditions, which often poses a barrier to the transmission of biological information. Here, we conducted a series of experiments with grass carp as the target species to evaluate the effects of total dissolved gas (TDG) supersaturation and sediment on the persistence of eDNA under different flow conditions. The results showed TDG supersaturation promoted eDNA decay in still water but with no significant effect in flowing water for rapid dissipation of TDG. For sediment, its presence accelerated the decay of eDNA no matter the flow conditions. The grass carp eDNA showed an exponential decay pattern in water and the decay rate constant decreased gradually with time. Our study highlights the importance of integrating experimental results with the natural environment and provides an important reference for species monitoring using eDNA technology in aquatic ecosystems with high dams built.

KEYWORDS

decay, environmental DNA, sediment, supersaturation, total dissolved gas

Introduction

The widespread environmental DNA (eDNA) technology utilizes DNA molecules that organisms continuously release into the environment (Li et al., 2018), which consist predominately of genetic materials in the form of cell-free DNA (Lydolph et al., 2005), mucus, feces (Merkes et al., 2014) and cells (Turner et al., 2014). As an emerging method, eDNA technology combines molecular biology with species monitoring and improves the ability of species detection by eliminating the effects of morphological characteristics (Sansom and Sassoubre, 2017). Additionally, it has higher temporal and spatial sampling

resolution and could improve sampling accuracy compared to traditional biomonitoring methods (Seymour et al., 2018). Thus, eDNA technology is gradually complementing or even replacing the application of traditional methods (Czeglédi et al., 2021). Nowadays, eDNA technology is used frequently for invasive species detection (Crane et al., 2021; Whitaker et al., 2021), endangered species monitoring (Budd et al., 2021), species biomass estimation (Tillotson et al., 2018), and biodiversity evaluation (Port et al., 2016; Vašutová et al., 2021). Among many ecosystems, aquatic ecosystems are especially appropriate for eDNA analysis because water is a highly efficient medium for transport and deposition, and eDNA can be easily sampled and detected in all water bodies (Bylemans et al., 2019; Lawson Handley et al., 2019; Djurhuus et al., 2020; Broadhurst et al., 2021). Since eDNA technology was first applied to investigate invasive species in French (Ficetola et al., 2008), it has been common in research work on aquatic organisms from a range of different ecological communities, such as fish (Dully et al., 2021; Sales et al., 2021), crustaceans (Johnsen et al., 2020; Crane et al., 2021), amphibians (Valentini et al., 2016), and mollusks (Sansom and Sassoubre, 2017).

Although eDNA technology is currently being increasingly used in aquatic ecosystems, the biological information conveyed by eDNA is often ambiguous at a given sampling time and site (Jo and Minamoto, 2021). Available study shows that the removal of eDNA in aquatic ecosystems mainly includes three processes: degradation, sedimentation, and transport (Harrison et al., 2019). The degradation of eDNA in water is affected by various factors, such as temperature (Eichmiller et al., 2016), pH (Seymour et al., 2018), and UV(Machler et al., 2018), and bacteria (Wei et al., 2018). These biotic and abiotic elements increase eDNA degradation by disrupting DNA structure directly and altering microbial metabolism and enzyme kinetics indirectly (Barnes et al., 2014; Strickler et al., 2015). For sedimentation and transport, different flow conditions may cause their contribution to eDNA persistence differently. First in the lentic environment (lakes and reservoirs), when eDNA molecules are released into the water column, they will spread around in a short time and some larger eDNA molecules will settle down over time, which leads to a decrease in eDNA concentration. However, additional removal processes occur in a lotic environment (rivers and streams) because the eDNA molecules might be transported downstream with the flow before settling down. eDNA of organisms might decay more rapidly in flowing water and could not even be detectable for a short time (Stoeckle et al., 2017).

Although different flow conditions determine the difference in the removal process of eDNA, sediment might be an important influencing factor in two different aquatic ecosystems. Because both in the lentic and lotic environment, eDNA could be removed from the water by falling into sediment interstices and being adsorbed on the surface of the sediment. Additionally, after a period of preservation in sediment, eDNA molecules could be resuspended into the water, which always leads to a problem of false-positive eDNA detection (Stoeckle et al., 2017). Therefore, the presence of sediment may increase the complexity of eDNA technology application and its impact on eDNA persistence in aquatic ecosystems still needs further validation. For the complex, open and dynamic ecosystem of rivers, in addition to their flow characteristics, artificial structures such as dams can also have an impact on aquatic species by altering river structures and creating a range of environmental problems (Consuegra et al., 2021). When high dams release water during flood season, a large amount of air below the dams could be swept into rivers and dissolves in water under very high pressure, leading to the supersaturation of total dissolved gas (TDG) in water and gas bubble disease (GBD) in aquatic organisms (Weitkamp and Katz, 1980; Wang et al., 2017). These problems significantly affect the survival of aquatic species (especially farmed fish) and are harmful to the maintenance of biodiversity in rivers and reservoirs. Existing studies have focused questions on the effects of river fragmentation and GBD on aquatic organisms caused by high dam construction (Weitkamp and Katz, 1980; Consuegra et al., 2021), while the effect of TDG supersaturation on eDNA persistence is still unknown, which leads to uncertainty in the application of eDNA technology in affected water bodies and thus hinders the transfer of biological information.

Here, we conducted a series of experiments to investigate the effects of total dissolved gas supersaturation and sediment on the persistence of eDNA in water. The grass carp (*Ctenopharyngodon Idella*), an important freshwater farmed fish in China, is used as the target species. The results are intended to provide theoretical support for applications of eDNA technology in rivers and reservoirs downstream of high dams.

Materials and methods

Experimental design and sampling

A total of six grass carp used in this study were kept in 100 L tanks after being purchased from the aquaculture section of Baijia Agricultural Products Wholesale Market in Chengdu, China. To ensure the stability of eDNA concentration in water, the grass carp were not fed during the experiment. We used the TDG supersaturation generation device invented by Sichuan University to prepare supersaturated total dissolved gas water (Li et al., 2010). The principle of the device is to mix the high-speed circulating water flow (experimental water, without grass carp eDNA) with the high-pressure gas generated by air compressor to create the conditions for supersaturated TDG water. TDG saturation was controlled in the experiment by adjusting the amount of water pumped into the reactor vessel. Previous study has shown that the TDG saturations in rivers downstream of high dams range from 122 to 140% (Feng et al.,

TABLE 1 Abbreviations of the treatments and the corresponding influencing factor settings. NF/F means no water flow/flowing water, NS/S means no sediment/sediment, and NTDGS/TDGS means total dissolved gas not supersaturated/total dissolved gas supersaturated.

Treatment	Flow conditions	Sediment conditions	Total dissolved gas
NF-S-TDGS	no water flow	sediment	supersaturated
NF-NS-TDGS	no water flow	no sediment	supersaturated
NF-S-NTDGS	no water flow	sediment	not supersaturated
NF-NS-NTDGS	no water flow	no sediment	not supersaturated
F-S-TDGS	flowing water	sediment	supersaturated
F-NS-TDGS	flowing water	no sediment	supersaturated
F-S-NTDGS	flowing water	sediment	not supersaturated
F-NS-NTDGS	flowing water	no sediment	not supersaturated

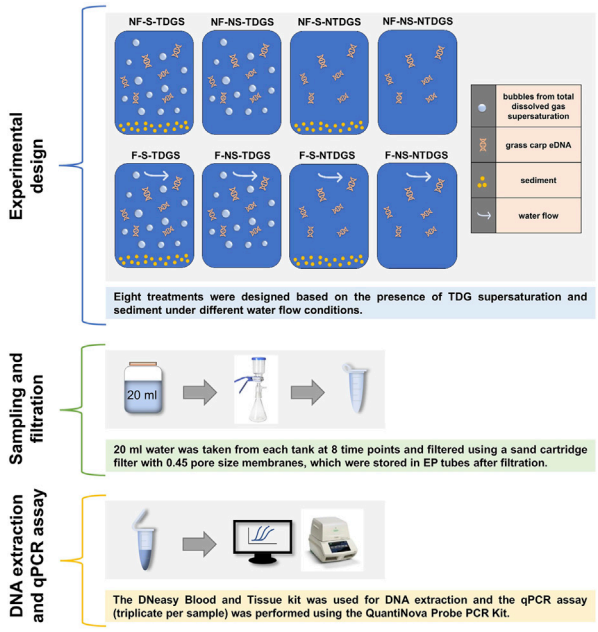

FIGURE 1
Overall flowchart for the tank experiments. Eight treatments were carried out based on flow conditions, whether the total dissolved gas was supersaturated, and whether the sediment was present. 20 ml water was collected at 8 time points and filtered with 0.45 pore size membranes. After extracting eDNA, the copy numbers of DNA were estimated by qPCR.

2014). To keep the initial TDG saturation in water at a high level and to maintain TDG supersaturation over a long time, the TDG saturation of water used in the experiment was set to about 145%. Homogeneous river sand with a particle size of 1 mm was selected as sediment in this study, which was purchased from a river sand manufacturer in Chengdu, China. Before the experiment, the sediment was sifted, cleaned and dried to remove impurities.

To investigate the effects of total dissolved gas supersaturation and sediment, eight treatments were designed based on flow conditions, whether the total dissolved gas was supersaturated, and whether the sediment was present (Table 1; Figure 1). The effect of a single factor and the combined effect of multiple factors on the persistence of eDNA was investigated through a controlled variables approach.

The eight treatments were carried out in water tanks of the same size, which were 50 cm in length, 10 cm in width, and 20 cm in height and made of polyethylene plastic. Four tanks of the flowing water condition were equipped with external short pipes (2 cm in length and 25 cm in diameter) on both sides, and two soft PVC rubber pipes (1 m in length and 25 cm in diameter) were externally connected. The other end of the PVC rubber pipes was connected with water pumps with the same power of 55W, and water in tanks was driven to circulate by water pumps to achieve the same flow conditions. We set the sediment thickness to 2 cm and the sediment gravel was evenly distributed at the bottom of the tanks. We added the water uniformly and slowly to achieve a homogeneous mixture of grass carp eDNA water and supersaturated TDG water or pure water in tanks. The volume of the total water in one tank was 4 L and the ratio of two different water is controlled at 1:1. To detect changes in eDNA concentration over time, we collected 20 ml water from each tank at the initial time and then at 1, 3, 6, 11, 23, 35, and 48 h elapsed time.

An additional experiment was conducted to investigate the changes in TDG saturation for those TDGS treatments to eliminate the interference of TDG saturation measurement on eDNA concentration. The supersaturated TDG water was added with the same dissolved gas saturation (TDG saturation changed to about 120% after mixing the two kinds of water). Other experimental settings were consistent with the eDNA experiment mentioned above. The TDG saturation level was recorded with a portable TGP meter (OxyGuard, Denmark) at eight time points: Pre, 0, 0.5, 1, 3, 6, 18, and 24 h.

TABLE 2 The primers and probes for the targeted DNA designed in the experiment.

No.	Primer	Primer sequence 5`→3′	Probe sequence
1	CO1-F (forward)	AGCCTCTTCTG GTGTTGAGG	ACAGTTTACCCACCA
	CO1-R (reverse)	GGTATTGGGAG ATGGCTGGT	CTCGCAGGCA
2	cytb-F (forward)	AACACGATTTTT CGCATTCCA	CCTATTACCATTCT
	cytb-R (reverse)	TGGGGTGAAGT TTTCTGGGT	CGTCGCCGCC

Filtration and DNA extraction

The collected water samples were filtered using a sand cartridge filter with 0.45 pore size membranes. After filtration, filter membranes were stored in numbered 1.5 ml centrifugal tubes and immediately followed by DNA extraction.

The DNeasy Blood & Tissue kit (Qiagen, Hilden, Germany) was used for DNA extraction. We added 180 µl of DNA lysate Buffer ATL and 20 µl of Proteinase K to the centrifugal tube and incubated it in a thermostatic metal bath at 56°C for 12 min. We then added 200 µl of Buffer AL to the tube and vortexed it for 15s and incubated it again at 56°C for 12 min. After short centrifugation at 8,000 rpm, we transferred 400 µl supernatant to a new centrifugal column and centrifuged for 1 min (8,000 rpm) to ensure all liquid entered the collection tube of the centrifuge column. We then added 500 µl of Buffer AW1 to the column and centrifuged it at 8,000 rpm for 1 min. After replacing the collection tube with a new column, we added 500 µl of Buffer AW2 to the column and centrifuged it for 1 min (8,000 rpm). Finally, we added 100 µl of Buffer AE to the column and centrifuged it again for 1 min (8,000 rpm), the solution retained in the tube was the desired eDNA sample solution. All eDNA samples obtained were stored at −20°C for subsequent qPCR assay.

Primer-probe design and specificity testing

To detect and quantify the DNA of grass carp using qPCR, primers and probe were designed with Primer3 version 4.0.0 based on the full-length sequence of grass carp mtDNA, which is available from the National Center of Biotechnology Information (NCBI) (GenBank, https://www.ncbi.nlm.nih.gov). To improve the amplification efficiency of the designed primer-probe, we selected two primer-probes for the specificity test (Table 2).

We used the DNeasy blood tissue kit (Qiagen, Hilden, Germany) to extract DNA from grass carp tissues and made the extracted solution as a positive DNA sample. We then PCR-amplified the DNA sample using two designed primer-probes and subjected the products to electrophoresis and sequencing. Analysis of the electrophoresis results showed the length and sequence of the product obtained from the No.2 primer-probe matched the expected product better. Accordingly, the No. 2 primer-probe was selected for subsequent experiments in this study.

qPCR assay

qPCR assay was performed using the QuantiNova Probe PCR Kit (Qiagen, Hilden, Germany). Individual qPCR reactions (in triplicate) consisted of 20 µl of Probe PCR Master Mix, 6 µl of RNase-Free Water, 1.6 µl of forward and reverse primers (0.8 µl each), 0.4 µl of probe, and 2 µl of eDNA sample. The reactions were performed with the following steps: a PCR initial activation of 95°C for 2 min, 39 cycles with 95°C for 5 s (denaturation), and 60°C for 5 s (combined annealing/extension). The standard curve of this experiment was determined by a series of standard samples of the target gene with known concentration gradients. The regression equation was $y = -3.4706x+42.582$ with correlation coefficient (r^2) of 0.9997 and amplification efficiency of 94% (Supplementary Material). The eDNA concentration at each time point was calculated by the Ct value and sampled water volume (i.e.,20 ml) combined with the standard curve. Samples were considered as not detected if there was no exponential growth during the 39cycles, or if only 1 amplification was detected in triplicate qPCR assays.

Data analysis

The decay of aquatic organisms' eDNA mostly showed an exponential pattern in water. Accordingly, we evaluated the decay of grass carp eDNA by a Single First-Order rate model (SFO) in this study. The equation of the SFO model is as follows:

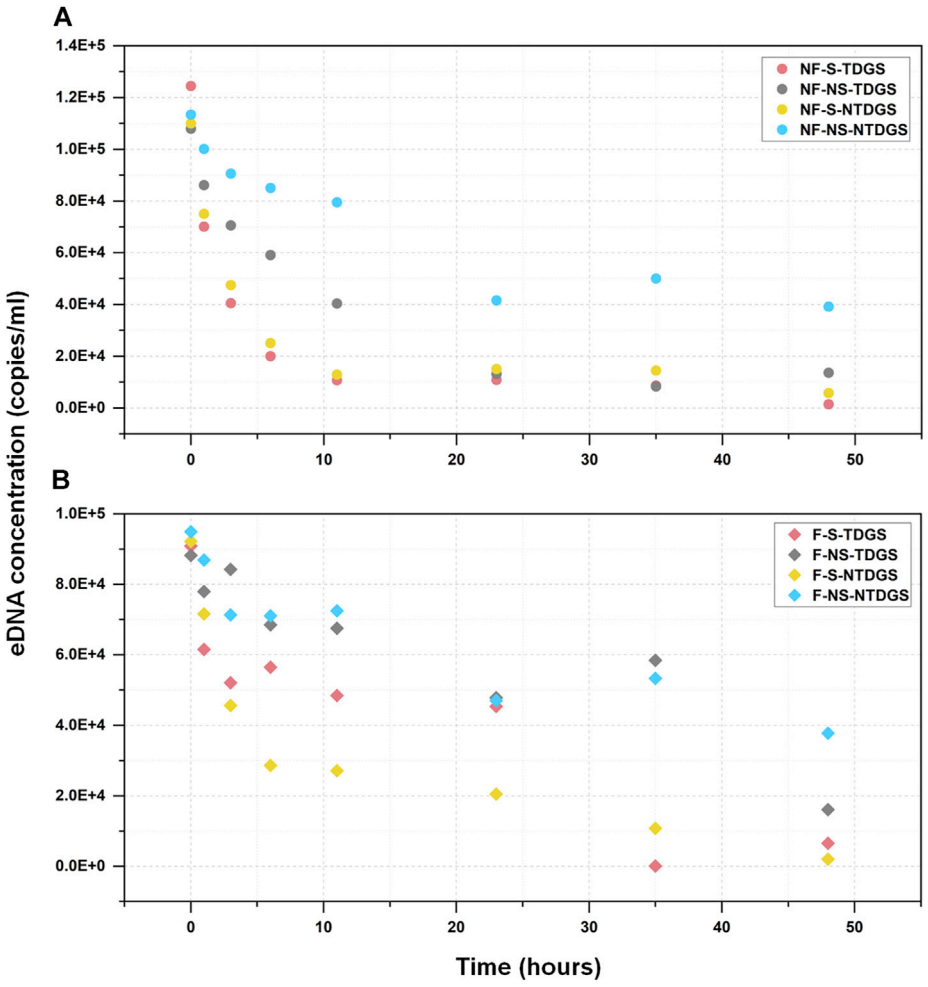

FIGURE 2
The relationship between the grass carp eDNA concentration (mean value) and sampling time. The circular and prismatic dots represent the eDNA concentration at each time point in still water **(A)** and flowing water **(B)** respectively. The colors represent different treatments: red, NF-S-TDGS/F-S-TDGS; gray, NF-NS-TDGS/F-NS-TDGS; yellow, NF-S-NTDGS/F-S-NTDGS; blue, NF-NS-NTDGS/F-NS-NTDGS.

$$C(t) = C_0 e^{-kt} \quad (1)$$

where $C(t)$ is the eDNA concentration at time t, copies/ml; C_0 is the eDNA concentration at the initial time, copies/ml; t is the sampling time, h; k is the decay rate constant per hour.

The decay of aquatic organisms' eDNA is also a multiphase process, and different forms of DNA may decay at different rates in water. When DNA molecules that decay more easily are removed from water, eDNA concentration might decrease and the decay rate constant might change in the absence of new eDNA sources, which could make the application of the SFO model inappropriate. Therefore, a Weibull decay model was fitted to the data to verify whether the grass carp eDNA decay rate constant would change with time in this study. The Weibull decay model equation is as follows:

$$C(t) = C_0 e^{-kt^{\beta}} \quad (2)$$

Where β is the Weibull parameter, allowing the decay rate constant to vary with time, $\beta < 1$ means the decay rate constant decreases with time; $\beta > 1$ means the decay rate constant increases with time, when $\beta = 1$, the model is simplified to the SFO model. The goodness of fit of the two models was compared by calculating the determinate coefficient R^2.

Multi-factor analysis of variance was used to test whether TDG supersaturation and sediment under different flow conditions had a significant effect on decay rate constant. A significant effect was determined by comparing the p-value to the significance level ($\alpha = 0.05$), with $p < 0.05$ indicating a significant effect and $p > 0.05$ indicating a non-significant effect.

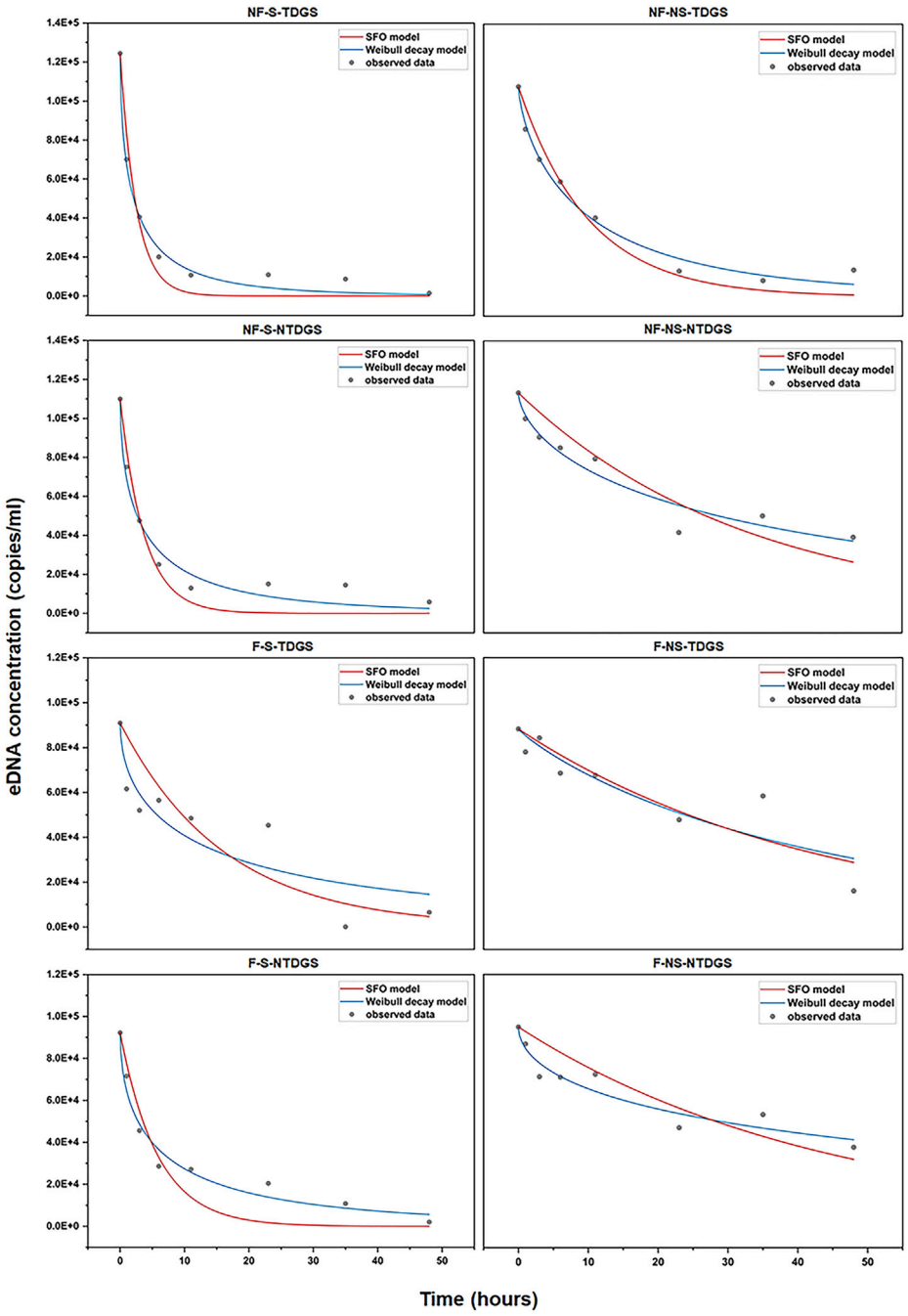

FIGURE 3
Fit of the SFO model (red curve) and the Weibull decay model (blue curve) for each treatment, the grey dots represent the grass carp eDNA concentration detected at each time point.

Results

eDNA concentration detection

We quantified the changes in grass carp eDNA concentration over time in still and flowing water and found that eDNA concentration decreased with time in all eight treatments (Figure 2). In still water, grass carp eDNA concentration of NF-S-TDGS and NF-S-NTDGS decreased more rapidly within the first 11 h and tended to be 0 copies/ml at 48 h. For NF-NS-TDGS, although the rate of decline in eDNA concentration was slower than NF-S-TDGS and NF-S-NTDGS in the first 11 h, the

TABLE 3 The Weibull parameter (β ± SE) and determination coefficient (R^2) of the Weibull decay model and the SFO model.

Treatment	Model	β ± SE	R^2
NF-S-TDG	SFO	-	0.95632
	Weibull	0.54456 ± 0.06172	0.99006
NF-NS-TDG	SFO	-	0.95479
	Weibull	0.69197 ± 0.0617	0.98649
NF-S-NTDG	SFO	-	0.93631
	Weibull	0.54036 ± 0.08793	0.96989
NF-NS-NTDG	SFO	-	0.84408
	Weibull	0.60718 ± 0.09317	0.94659
F-S-TDG	SFO	-	0.69909
	Weibull	0.52535 ± 0.17016	0.81983
F-NS-TDG	SFO	-	0.81903
	Weibull	0.8859 ± 0.28045	0.82267
F-S-NTDG	SFO	-	0.88217
	Weibull	0.53296 ± 0.07249	0.97238
F-NS-NTDG	SFO	-	0.73736
	Weibull	0.51579 ± 0.09661	0.92102

eDNA concentration was similarly close to 0 copies/ml in the last detection. As expected, NF-NS-NTDGS had higher eDNA concentration than the other three treatments at all time points and the slowest rate of decline. Thus, it can be easily found that TDG supersaturation and sediment contributed to grass carp eDNA decay and eDNA decayed fastest when both were present in still water.

The variation pattern of grass carp eDNA concentration in flowing water was more chaotic. But in the same way, the decline rate was faster for F-S-TDGS and F-S-NTDGS where sediment was present in flowing water, which indicated the presence of sediment accelerated the decline of eDNA concentration no matter what the flow conditions were. However, for F-NS-TDGS and F-NS-NTDGS, the eDNA concentration of both treatments was basically at the same level during the experimental period, and TDG supersaturation did not promote the decrease of eDNA concentration, which showed the effects of TDG supersaturation varied with flow conditions in this study.

Simulation of eDNA decay models

By comparing the fitting curves and determination coefficient (R^2) of the two models (Figure 3; Table 3), it can be found that the Weibull decay model had better goodness of fit and can better describe the removal process of grass carp eDNA in water. Additionally, the parameter β for each treatment was less than 1, which indicated the decay rate constant of grass carp eDNA gradually decreased with time.

Although the Weibull decay model indicated the decay rate constant varied with time, we chose to further analyze the decay rate constant (mean value) calculated by the Weibull decay model as it was more applicable than the SFO model. The results (Figure 4) showed the k value increased due to the existence of TDG supersaturation or sediment and reached a maximum when both factors were present (NF-S-TDGS, k ± SE = 0.61229 ± 0.05838) in still water. But in flowing water, only the presence of sediment increased the decay rate constant, and TDG supersaturation did not accelerate the decay of grass carp eDNA. It can be seen that the effects of sediment in still and flowing water were consistent, but TDG supersaturation showed different effects with different flow conditions.

Multi-factor analysis of variance

The effects of TDG supersaturation, sediment and flow conditions on the decay rate constant (k, the Weibull decay model) were variable (Table 4). The main effect of TDG supersaturation on the decay rate constant was not significant ($p = 0.569$), but the main effect of sediment and flow conditions was significant ($p < 0.001$). The interaction effect of TDG supersaturation with sediment was not significant ($p = 0.275$), but the interaction effect of TDG supersaturation with flow conditions was significant ($p = 0.001$). There was also a significant interaction effect between sediment and flow conditions ($p = 0.011$), but the interaction effect between TDG supersaturation, sediment, and flow conditions was not significant ($p = 0.364$).

On the premise of significant interaction, we conducted a simple effect test to analyze the different effects of TDG supersaturation and sediment on decay rate constant under different flow conditions. The results (Table 5) showed that the decay rate constant of eDNA in still water was significantly higher than that in flowing water when dissolved gas was supersaturated and sediment existed in water (mean difference (I-J) = −0.263, $p < 0.001$; mean difference (I-J) = −0.233, $p < 0.001$).

Taken together, TDG supersaturation had a significant contribution to eDNA decay in still water but not in flowing water. The effect of sediment, although slightly different depending on the flow conditions, showed a significant effect on grass carp eDNA decay in general.

Discussion

Effect of total dissolved gas supersaturation

TDG is a gas mixture with the same composition as the atmosphere (Weitkamp and Katz, 1980), in which the partial

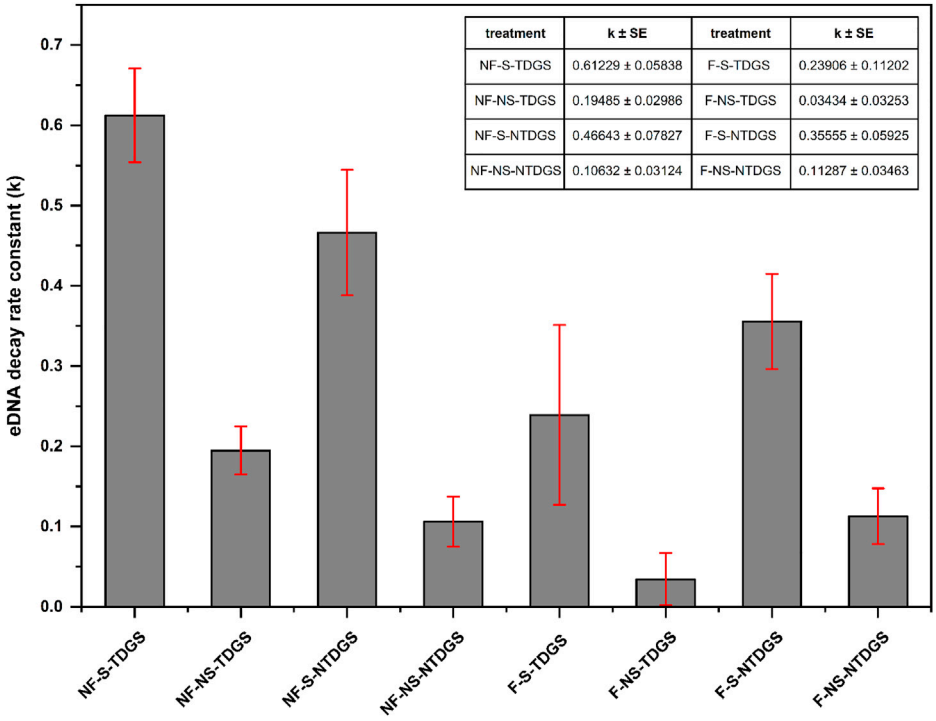

FIGURE 4
The decay rate constant (k) estimated from the Weibull decay model for each treatment, the error bars represent standard error (SE).

TABLE 4 Results of multi-factor analysis of variance. Analysis of the main effect and interaction effect of TDG supersaturation, sediment and flow conditions on the decay rate constant (k). Significant *p*-values are indicated in bold.

Variables	Dependent variable	*p*-value
TDG supersaturation	decay rate constant (k)	0.569
sediment		**<0.001**
flow conditions		**<0.001**
TDG supersaturation*sediment		0.275
TDG supersaturation*flow conditions		**0.001**
sediment*flow conditions		**0.011**
TDG supersaturation*sediment*flow conditions		0.364

*Interaction between variables.

TABLE 5 Results of simple effect test. Analysis of the different effects of TDG supersaturation and sediment on decay rate constant under different flow conditions. Significant *p*-values are indicated in bold.

Variables	Flow conditions(I)	Flow conditions(J)	Mean difference (I-J)	Std Error	*p*-value
TDG supersaturation	flowing water	no water flow	−0.263[a]	0.035	**<0.001**
	no water flow	Flowing water	0.263[a]	0.035	**<0.001**
sediment	Flowing water	no water flow	−0.233[a]	0.035	**<0.001**
	no water flow	flowing water	0.233[a]	0.035	**<0.001**

[a]The mean difference is significant at the 0.05 level.

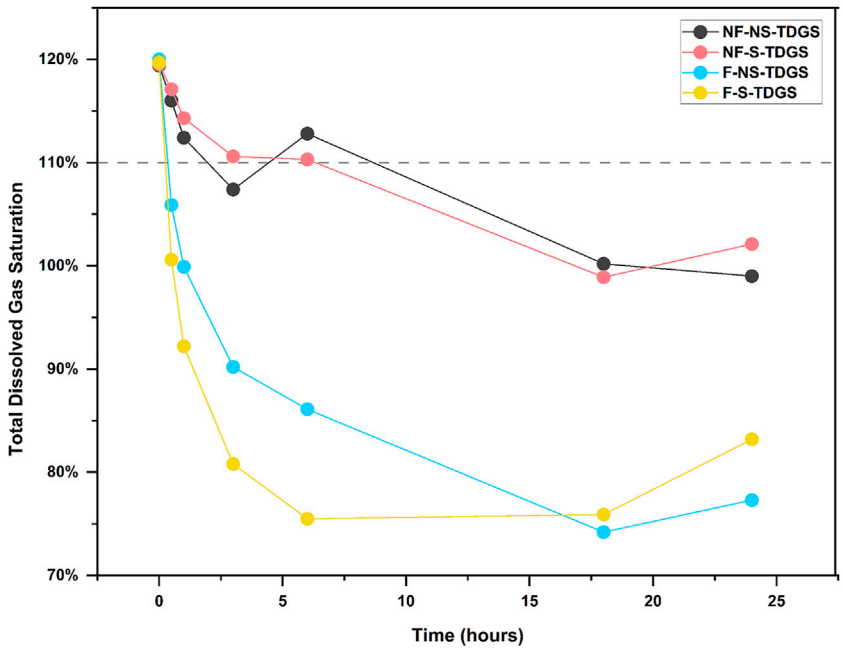

FIGURE 5
Variation of TDG saturation in TDGS treatments during the experiment period. The dots indicate the TDG saturation at each time point for different treatments: black, NF-NS-TDGS; red, NF-S-TDGS; blue, F-NS-TDGS, yellow, F-S-TDGS. The gray dashed line represents the minimum standard limit of 110% for TDG supersaturation.

pressure of oxygen is about 21%. As a biologically active gas, a change in oxygen content affects microbial metabolism in water (Barnes et al., 2014). Existing studies have shown DNA can be rapidly degraded in the aquatic environment due to oxidation and microbial activity (Lindahl, 1993; Torti et al., 2015). However, when oxygen content and microbial action are reduced or absent, these genetic materials can last for a long time (Seymour et al., 2018). Accordingly, for this study, the effect of TDG supersaturation which accelerated the decay of eDNA in still water was likely to alter the oxygen content of water and thus ultimately enhanced the microbial metabolism. However, in flowing water, TDG supersaturation did not have the same effect. Combined with the results of dissolved gas saturation monitoring (Figure 5), it can be found that the rate of TDG dissipation in flowing water was faster than in still water, and the gas dissolved saturation was already below the standard limit of TDG supersaturation (110%) (Engineers, 2005) within half an hour. This suggested that water flow affected the rate of total dissolved supersaturated gas dissipation, which was consistent with the previous study (Li et al., 2013). If the turbulence intensity of the flow increases, the TDG dissipation rate will increase. Consequently, it can be hypothesized that TDG supersaturation in flowing water did not significantly affect the decay of eDNA can be attributed to the rapid dissipation of TDG caused by flow turbulence, eventually failing to significantly affect microbial metabolic activities as in still water.

Effect of sediment

Unlike the effect of TDG supersaturation, sediment played a crucial role in the persistence of grass carp eDNA both in still and flowing water, which is in line with previous research (Stoeckle et al., 2017). When biological DNA molecules and cells are released into the water column, in addition to their gradual decay, they will settle under the force of gravity and eventually attach to the sediment surface or fall into the sediment interstices. When these eDNA molecules come into contact with sediment particles, they will bind to gravel particles due to electrostatic interactions and other forces (Hou et al., 2014) and adhere to biofilms on the sediment surface. eDNA from organisms will be degraded by components such as heterotrophic microorganisms in biofilm as a carbon source (Jerde et al., 2016), eventually reducing the detectable eDNA concentration in the water column. Therefore, even though a small fraction of eDNA molecules in this study will be resuspended into water under the disturbance of water flow (Turner et al., 2015), the presence of sediment still significantly reduced the concentration of eDNA in water.

Weibull decay model better reflects the eDNA decay pattern

The SFO model suggests the decay processes for intracellular DNA and extracellular free DNA fragments occur on similar time scales, and the rate of cell decomposition and DNA decay in water is the same (Saito and Doi, 2021). Therefore, researchers can use different combinations of experiments to quantify the decay rate constant under different conditions and compare their difference (Bylemans et al., 2018). However, in this study, the Weibull decay model was proved to have a better description of the decay pattern of grass carp eDNA, with a rapid decay period at the initial time and then the decay rate constant decreasing with time. Previous studies have also shown that the decay rate decreases with time in a model that better reflects the decay process of biological DNA in water (Bylemans et al., 2018; Eichmiller et al., 2016; Shogren et al., 2018). Thus, it can be inferred that eDNA does exist in water with different decay rates (e.g., nuclear and mitochondrial DNA, long fragments and short fragments of DNA). Some eDNA fragments decay at a faster rate, and the DNA concentration in water decreases gradually with time, ultimately resulting in a decrease in the total decay rate constant. Therefore, when considering the persistence of eDNA in natural environments, the use of the Weibull decay model can more accurately predict the residence time of biological eDNA in water or more accurately predict the initial eDNA concentration in this area based on the concentration of eDNA detected at a certain moment. This allows researchers to better apply eDNA analysis methods and more accurately understand the basic information of eDNA in the natural environment.

Relationship between experimental results and natural environment

Experimental variables in this study, including total dissolved gas supersaturation, sediment, and flow conditions, had measurable effects on the eDNA persistence of grass carp. However, all the results were obtained under controlled experimental conditions, which did not fully reflect the patterns in the natural environment. Because in aquatic ecosystems, these factors may play a more complex role in biological eDNA. For TDG supersaturation, the experiment was conducted to explore its effect on eDNA persistence by adding dissolved gas supersaturated water. Rapid dissipation of TDG resulted in almost no effect on eDNA decay in flowing water. But in the natural environment, TDG supersaturation continues to occur in rivers downstream of high dams, and it is difficult to release quickly into the atmosphere and could be transported over long distances (Yuan et al., 2020). Accordingly, in natural rivers, the effect of TDG supersaturation on biological eDNA might be similar to that in still water of this study. Secondly, this study demonstrated the presence of sediment can improve the removal of eDNA from water through adsorption and biofilms. But at the same time, sediment can also protect eDNA molecules from nuclease degradation and chemical damage (Romanowski et al., 1991; Hou et al., 2014) and protect cell and tissue fragments from shear forces and microbial degradation (Bradford et al., 2013). These effects tend to make the persistence of eDNA much higher in sediment (Troth et al., 2021), thus creating an opportunity for resuspension of eDNA and blurring the inference of spatial and temporal scales of eDNA in water columns (Turner et al., 2015). Finally, the flow conditions in this study are fundamentally designed to simulate the turbulence of natural rivers, where the dynamic processes of DNA molecules in water are dominated by dilution, degradation, sedimentation, retention, and resuspension. However, eDNA in rivers could also be affected by long-distance transportation along with water flow (Shogren et al., 2017), which tends to reduce the detectable concentration of eDNA at the original location and increases the uncertainty of eDNA technology application. Given the above, results based on controlled experiments must be carefully interpreted and analyzed in close relation to factors in the natural environment, only in this way can eDNA technology be applied to species monitoring properly.

Conclusion

This study investigated the effects of TDG supersaturation and sediment on the persistence of grass carp eDNA in still and flowing water, and the results showed:

1) the effect of TDG supersaturation varied with flow conditions, with TDG supersaturation promoting eDNA decay in still water, but with no significant effect in flowing water due to rapid dissipation of TDG.
2) The effect of sediment on eDNA persistence is consistent in different flow conditions. The presence of sediment accelerated the decay of grass carp eDNA in water.
3) The Weibull decay model with decay rate constant varies with time can better describe the decay process of eDNA than the Single First-Order rate model (SFO model), which suggested grass carp eDNA decayed rapidly during the initial period, and then the decay rate constant decreased with time.

In conclusion, TDG supersaturation and sediment can affect the persistence of aquatic eDNA in different ways under still and flowing water conditions, and all factors interact with each other and act together. Meanwhile, it is

worth noting that results based on controlled experiments might deviate from the true patterns in the natural environment. Therefore, in practical applications, the interpretation of sampling results should always be integrated with the prevailing environmental conditions to get the most accurate species information.

Data availability statement

The datasets presented in this study can be found in online repositories. The names of the repository/repositories and accession number(s) can be found in the article/ Supplementary Material.

Ethics statement

The animal study was reviewed and approved by Ethics Committee, College of Life Sciences, Sichuan University.

Author contributions

All authors conceived and planned the experiments. LH performed the experiment, analyzed the data, interpreted the results, wrote the manuscript, and designed the figures. JZ helped perform the analysis and edited the manuscript with constructive discussions. YW acquired funding, participated in data analysis, and revised it critically for important intellectual content. All authors approved of the final draft.

Funding

This work was supported by the National Natural Science Foundation of China (Grant NO. 52079082) and the Open Research Fund of State Key Laboratory of Simulation and Regulation of Water Cycle in River Basin, China Institute of Water Resources and Hydropower Research (Grant NO. IWHR-SKL-KF202107).

Conflict of interest

The authors declare that the research was conducted in the absence of any commercial or financial relationships that could be construed as a potential conflict of interest.

Publisher's note

All claims expressed in this article are solely those of the authors and do not necessarily represent those of their affiliated organizations, or those of the publisher, the editors and the reviewers. Any product that may be evaluated in this article, or claim that may be made by its manufacturer, is not guaranteed or endorsed by the publisher.

Supplementary material

The Supplementary Material for this article can be found online at: https://www.frontiersin.org/articles/10.3389/fenvs.2022.952414/full#supplementary-material

References

Barnes, M. A., Turner, C. R., Jerde, C. L., Renshaw, M. A., Chadderton, W. L., Lodge, D. M., et al. (2014). Environmental conditions influence eDNA persistence in aquatic systems. *Environ. Sci. Technol.* 48, 1819–1827. doi:10.1021/es404734p

Bradford, S. A., Morales, V. L., Zhang, W., Harvey, R. W., Packman, A. I., Mohanram, A., et al. (2013). Transport and fate of microbial pathogens in agricultural settings. *Crit. Rev. Environ. Sci. Technol.* 43, 775–893. doi:10.1080/10643389.2012.710449

Broadhurst, H. A., Gregory, L. M., Bleakley, E. K., Perkins, J. C., Lavin, J. V., Bolton, P., et al. (2021). Mapping differences in mammalian distributions and diversity using environmental DNA from rivers. *Sci. Total Environ.* 801, 149724. doi:10.1016/j.scitotenv.2021.149724

Budd, A. M., Cooper, M. K., Port, A. L., Schils, T., Mills, M. S., Deinhart, M. E., et al. (2021). First detection of critically endangered scalloped hammerhead sharks (*Sphyrna lewini*) in Guam, Micronesia, in five decades using environmental DNA. *Ecol. Indic.* 127, 107649. doi:10.1016/j.ecolind.2021.107649

Bylemans, J., Furlan, E. M., Gleeson, D. M., Hardy, C. M., and Duncan, R. P. (2018). Does size matter? An experimental evaluation of the relative abundance and decay rates of aquatic environmental DNA. *Environ. Sci. Technol.* 52, 6408–6416. doi:10.1021/acs.est.8b01071

Bylemans, J., Gleeson, D. M., Duncan, R. P., Hardy, C. M., and Furlan, E. M. (2019). A performance evaluation of targeted eDNA and eDNA metabarcoding analyses for freshwater fishes. *Environ. DNA* 1, 402–414. doi:10.1002/edn3.41

Consuegra, S., O'Rorke, R., Rodriguez-Barreto, D., Fernandez, S., Jones, J., Garcia de Leaniz, C., et al. (2021). Impacts of large and small barriers on fish assemblage composition assessed using environmental DNA metabarcoding. *Sci. Total Environ.* 790, 148054. doi:10.1016/j.scitotenv.2021.148054

Crane, L. C., Goldstein, J. S., Thomas, D. W., Rexroth, K. S., and Watts, A. W. (2021). Effects of life stage on eDNA detection of the invasive European green crab (*Carcinus maenas*) in estuarine systems. *Ecol. Indic.* 124, 107412. doi:10.1016/j.ecolind.2021.107412

Czeglédi, I., Sály, P., Specziár, A., Preiszner, B., Szalóky, Z., Maroda, Á., et al. (2021). Congruency between two traditional and eDNA-based sampling methods in characterising taxonomic and trait-based structure of fish communities and community-environment relationships in lentic environment. *Ecol. Indic.* 129, 107952. doi:10.1016/j.ecolind.2021.107952

Djurhuus, A., Closek, C. J., Kelly, R. P., Pitz, K. J., Michisaki, R. P., Starks, H. A., et al. (2020). Environmental DNA reveals seasonal shifts and potential interactions in a marine community. *Nat. Commun.* 11, 254. doi:10.1038/s41467-019-14105-1

Dully, V., Balliet, H., Frühe, L., Däumer, M., Thielen, A., Gallie, S., et al. (2021). Robustness, sensitivity and reproducibility of eDNA metabarcoding as an environmental biomonitoring tool in coastal salmon aquaculture – an inter-laboratory study. *Ecol. Indic.* 121, 107049. doi:10.1016/j.ecolind.2020.107049

Eichmiller, J. J., Best, S. E., and Sorensen, P. W. (2016). Effects of temperature and trophic state on degradation of environmental DNA in lake water. *Environ. Sci. Technol.* 50, 1859–1867. doi:10.1021/acs.est.5b05672

Engineers, U. A. C. o. (2005). *Technical analysis of TDG processes*. Portland: US Army Corps of Engineers-Northwest Division, Environmental Resources and Fish Planning Offices.

Feng, J., Li, R., Ma, Q., and Wang, L. (2014). Experimental and field study on dissipation coefficient of supersaturated total dissolved gas. *J. Central South Univ.* 21, 1995–2003. doi:10.1007/s11771-014-2148-4

Ficetola, G. F., Miaud, C., Pompanon, F., and Taberlet, P. (2008). Species detection using environmental DNA from water samples. *Biol. Lett.* 4, 423–425. doi:10.1098/rsbl.2008.0118

Harrison, J. B., Sunday, J. M., and Rogers, S. M. (2019). Predicting the fate of eDNA in the environment and implications for studying biodiversity. *Proc. R. Soc. B* 286, 20191409. doi:10.1098/rspb.2019.1409

Hou, Y., Wu, P., and Zhu, N. (2014). The protective effect of clay minerals against damage to adsorbed DNA induced by cadmium and mercury. *Chemosphere* 95, 206–212. doi:10.1016/j.chemosphere.2013.08.069

Jerde, C. L., Olds, B. P., Shogren, A. J., Andruszkiewicz, E. A., Mahon, A. R., Bolster, D., et al. (2016). Influence of stream bottom substrate on retention and transport of vertebrate environmental DNA. *Environ. Sci. Technol.* 50, 8770–8779. doi:10.1021/acs.est.6b01761

Jo, T., and Minamoto, T. (2021). Complex interactions between environmental DNA (eDNA) state and water chemistries on eDNA persistence suggested by meta-analyses. *Mol. Ecol. Resour.* 21, 1490–1503. doi:10.1111/1755-0998.13354

Johnsen, S. I., Strand, D. A., Rusch, J. C., and Vrålstad, T. (2020). Environmental DNA (eDNA) monitoring of noble crayfish *Astacus astacus* in lentic environments offers reliable presence-absence surveillance – but fails to predict population density. *Front. Environ. Sci.* 8. doi:10.3389/fenvs.2020.612253

Lawson Handley, L., Read, D. S., Winfield, I. J., Kimbell, H., Johnson, H., Li, J., et al. (2019). Temporal and spatial variation in distribution of fish environmental DNA in England's largest lake. *Environ. DNA* 1, 26–39. doi:10.1002/edn3.5

Li, F., Peng, Y., Fang, W., Altermatt, F., Xie, Y., Yang, J., et al. (2018). Application of environmental DNA metabarcoding for predicting anthropogenic pollution in rivers. *Environ. Sci. Technol.* 52, 11708–11719. doi:10.1021/acs.est.8b03869

Li, R., Hodges, B. R., Feng, J., and Yong, X. (2013). Comparison of supersaturated total dissolved gas dissipation with dissolved oxygen dissipation and reaeration. *J. Environ. Eng. New. York.* 139, 385–390. doi:10.1061/(ASCE)EE.1943-7870.0000598

Li, R., Huang, X., Li, K., Yi, W., and Li, J. (2010). *Device for generation of total dissolved gas supersaturation in water body and research on influence of total dissolved gas supersaturation on fish*. CN 201479739 U. Chengdu.

Lindahl, T. (1993). Instability and decay of the primary structure of DNA. *Nature* 362, 709–715. doi:10.1038/362709a0

Lydolph, M. C., Jacobsen, J., Arctander, P., Gilbert, M. T. P., Gilichinsky, D. A., Hansen, A. J., et al. (2005). Beringian paleoecology inferred from permafrost-preserved fungal DNA. *Appl. Environ. Microbiol.* 71, 1012–1017. doi:10.1128/AEM.71.2.1012-1017.2005

Machler, E., Osathanunkul, M., and Altermatt, F. (2018). Shedding light on eDNA: Neither natural levels of UV radiation nor the presence of a filter feeder affect eDNA-based detection of aquatic organisms. *Plos One* 13, e0195529. doi:10.1371/journal.pone.0195529

Merkes, C. M., McCalla, S. G., Jensen, N. R., Gaikowski, M. P., and Amberg, J. J. (2014). Persistence of DNA in carcasses, slime and avian feces may affect interpretation of environmental DNA data. *Plos One* 9, e113346. doi:10.1371/journal.pone.0113346

Port, J. A., O'Donnell, J. L., Romero-Maraccini, O. C., Leary, P. R., Litvin, S. Y., Nickols, K. J., et al. (2016). Assessing vertebrate biodiversity in a kelp forest ecosystem using environmental DNA. *Mol. Ecol.* 25, 527–541. doi:10.1111/mec.13481

Romanowski, G., Lorenz, M. G., and Wackernagel, W. (1991). Adsorption of plasmid DNA to mineral surfaces and protection against DNase I. *Appl. Environ. Microbiol.* 57, 1057–1061. doi:10.1128/aem.57.4.1057-1061.1991

Saito, T., and Doi, H. (2021). Degradation modeling of water environmental DNA: Experiments on multiple DNA sources in pond and seawater. *Environ. DNA* 3, 850–860. doi:10.1002/edn3.192

Sales, N. G., Wangensteen, O. S., Carvalho, D. C., Deiner, K., Praebel, K., Coscia, I., et al. (2021). Space-time dynamics in monitoring neotropical fish communities using eDNA metabarcoding. *Sci. Total Environ.* 754, 142096. doi:10.1016/j.scitotenv.2020.142096

Sansom, B. J., and Sassoubre, L. M. (2017). Environmental DNA (eDNA) shedding and decay rates to model freshwater mussel eDNA transport in a river. *Environ. Sci. Technol.* 51, 14244–14253. doi:10.1021/acs.est.7b05199

Seymour, M., Durance, I., Cosby, B. J., Ransom-Jones, E., Deiner, K., Ormerod, S. J., et al. (2018). Acidity promotes degradation of multi-species environmental DNA in lotic mesocosms. *Commun. Biol.* 1, 4. doi:10.1038/s42003-017-0005-3

Shogren, A. J., Tank, J. L., Egan, S. P., August, O., Rosi, E. J., Hanrahan, B. R., et al. (2018). Water flow and biofilm cover influence environmental DNA detection in recirculating streams. *Environ. Sci. Technol.* 52, 8530–8537. doi:10.1021/acs.est.8b01822

Shogren, A. J., Tank, J. L., Andruszkiewicz, E., Olds, B., Mahon, A. R., Jerde, C. L., et al. (2017). Controls on eDNA movement in streams: Transport, retention, and resuspension. *Sci. Rep.* 7, 5065. doi:10.1038/s41598-017-05223-1

Stoeckle, B. C., Beggel, S., Cerwenka, A. F., Motivans, E., Kuehn, R., Geist, J., et al. (2017). A systematic approach to evaluate the influence of environmental conditions on eDNA detection success in aquatic ecosystems. *Plos One* 12, e0189119. doi:10.1371/journal.pone.0189119

Strickler, K. M., Fremier, A. K., and Goldberg, C. S. (2015). Quantifying effects of UV-B, temperature, and pH on eDNA degradation in aquatic microcosms. *Biol. Conserv.* 183, 85–92. doi:10.1016/j.biocon.2014.11.038

Tillotson, M. D., Kelly, R. P., Duda, J. J., Hoy, M., Kralj, J., Quinn, T. P., et al. (2018). Concentrations of environmental DNA (eDNA) reflect spawning salmon abundance at fine spatial and temporal scales. *Biol. Conserv.* 220, 1–11. doi:10.1016/j.biocon.2018.01.030

Torti, A., Lever, M. A., and Jorgensen, B. B. (2015). Origin, dynamics, and implications of extracellular DNA pools in marine sediments. *Mar. Genomics* 24 Pt 3, 185–196. doi:10.1016/j.margen.2015.08.007

Troth, C. R., Sweet, M. J., Nightingale, J., and Burian, A. (2021). Seasonality, DNA degradation and spatial heterogeneity as drivers of eDNA detection dynamics. *Sci. Total Environ.* 768, 144466. doi:10.1016/j.scitotenv.2020.144466

Turner, C. R., Barnes, M. A., Xu, C. C. Y., Jones, S. E., Jerde, C. L., Lodge, D. M., et al. (2014). Particle size distribution and optimal capture of aqueous macrobialeDNA. *Methods Ecol. Evol.* 5, 676–684. doi:10.1111/2041-210x.12206

Turner, C. R., Uy, K. L., and Everhart, R. C. (2015). Fish environmental DNA is more concentrated in aquatic sediments than surface water. *Biol. Conserv.* 183, 93–102. doi:10.1016/j.biocon.2014.11.017

Valentini, A., Taberlet, P., Miaud, C., Civade, R., Herder, J., Thomsen, P. F., et al. (2016). Next-generation monitoring of aquatic biodiversity using environmental DNA metabarcoding. *Mol. Ecol.* 25, 929–942. doi:10.1111/mec.13428

Vašutová, M., Jiroušek, M., and Hájek, M. (2021). High fungal substrate specificity limits the utility of environmental DNA to detect fungal diversity in bogs. *Ecol. Indic.* 121, 107009. doi:10.1016/j.ecolind.2020.107009

Wang, Y., An, R., Li, Y., and Li, K. (2017). Swimming performance of rock carp *Procypris rabaudi* and prenant's schizothoracin *Schizothorax prenanti* acclimated to total dissolved gas supersaturated water. *North Am. J. Fish. Manag.* 37, 1183–1190. doi:10.1080/02755947.2017.1353558

Wei, N., Nakajima, F., and Tobino, T. (2018). A microcosm study of surface sediment environmental DNA: Decay observation, abundance estimation, and fragment length comparison. *Environ. Sci. Technol.* 52, 12428–12435. doi:10.1021/acs.est.8b04956

Weitkamp, D. E., and Katz, M. (1980). A review of dissolved gas supersaturation literature. *Trans. Am. Fish. Soc.* 109, 659–702. doi:10.1577/1548-8659(1980)109<659:arodgs>2.0.co;2

Whitaker, J. M., Brower, A. L., and Janosik, A. M. (2021). Invasive lionfish detected in estuaries in the northern Gulf of Mexico using environmental DNA. *Environ. Biol. Fishes* 104, 1475–1485. doi:10.1007/s10641-021-01177-6

Yuan, Y., Huang, J., Wang, Z., Gu, Y., Li, R., Li, K., et al. (2020). Experimental investigations on the dissipation process of supersaturated total dissolved gas: Focus on the adsorption effect of solid walls. *Water Res.* 183, 116087. doi:10.1016/j.watres.2020.116087

frontiers | Frontiers in Ecology and Evolution

TYPE Original Research
PUBLISHED 10 August 2022
DOI 10.3389/fevo.2022.922539

OPEN ACCESS

EDITED BY
Celso Santos,
Federal University of Paraíba, Brazil

REVIEWED BY
Augustine Ovie Edegbene,
Federal University of Health Sciences, Nigeria
Linlin Zhao,
Ministry of Natural Resources, China

*CORRESPONDENCE
Wei Yang
yangwei@bnu.edu.cn

SPECIALTY SECTION
This article was submitted to Conservation and Restoration Ecology, a section of the journal Frontiers in Ecology and Evolution

RECEIVED 18 April 2022
ACCEPTED 22 July 2022
PUBLISHED 10 August 2022

CITATION
Fu X, Yang W, Zheng L, Liu D and Li X (2022) Spatial patterns of macrobenthos taxonomic and functional diversity throughout the ecotones from river to lake: A case study in Northern China. *Front. Ecol. Evol.* 10:922539. doi: 10.3389/fevo.2022.922539

Spatial patterns of macrobenthos taxonomic and functional diversity throughout the ecotones from river to lake: A case study in Northern China

Xianting Fu[1], Wei Yang[1]*, Lei Zheng[2], Dan Liu[1] and Xiaoxiao Li[1,3]

[1]State Key Laboratory of Water Environment Simulation, School of Environment, Beijing Normal University, Beijing, China, [2]College of Water Sciences, Beijing Normal University, Beijing, China, [3]Guangdong Provincial Key Laboratory of Water Quality Improvement and Ecological Restoration for Watersheds, School of Ecology, Environment and Resources, Guangdong University of Technology, Guangzhou, China

Macrobenthos taxonomic and functional diversity are key indicators of ecosystem health. River–lake ecotones are key macrobenthos habitats. However, we don't fully understand macrobenthos biodiversity patterns in these ecotones. We studied water environment, sediment heavy metal contents, and macrobenthos community, which we sampled simultaneously from 29 sampling sites along the Fu River–Baiyangdian Lake gradient in Northern China with five field surveys from 2018 to 2019. Six trait classes resolved into 25 categories were allocated to macrobenthos through a binary coding system. We used the RLQ framework (R, environmental variables; L, species of taxa; Q, traits) and fourth-corner analyses to evaluate the relationship between environmental variables and macrobenthos traits. Finally, we carried out variance partitioning to assess the contributions of environmental variables to variation of macrobenthos diversities. As the results, *TN* and *TP* contents in the river and lake mouths were lower than those in the adjacent river and lake, indicating that the river–lake ecotones played a role in purifying the water and buffering pollution. High taxonomic diversity of macrobenthos in the lake mouth and the presence of unique taxa in the two ecotones revealed edge effects, but the macrobenthos abundance and biomass were extremely low compared with those in the adjacent river and lake. We found no significant correlation between the taxonomic and functional diversity indices in the river and lake mouths. Water depth, water transparency, *TN*, and *TP* were the main water environmental drivers of macrobenthos taxonomic and functional diversity, explaining up to 45.5% and 56.2% of the variation, respectively. Sediment Cd, Cr, Cu, Pb, and Zn contents explained 15.1% and 32.8%, respectively, of macrobenthos taxonomic and functional diversity. Our results suggest that functional diversity approaches based on biological traits can complement taxonomic approaches in river–lake ecotones. Furthermore, improving water

depth, transparency, eutrophication, and heavy metal pollution will improve macrobenthos diversity in these ecotones and maintain ecosystem health.

KEYWORDS

taxonomic diversity, functional diversity, macrobenthos, environmental factors, river-lake ecotone, Baiyangdian lake-river system

Introduction

River–lake systems (i.e., rivers flowing through or into the lakes) can be regarded as continuous aquatic ecosystem, and are affected by the hydraulic exchanges and hydrological connectivity (Hillbricht-Ilkowska, 1999). As a result, they provide multiple ecological functions, such as material cycling, energy flows, and biotic exchanges (Zhang et al., 2020). Ecotones are zones of transition between rivers and lakes, and are key parts of a river–lake system (Holland, 1988; Gosz, 1993; Kolasa and Zalewski, 1995). They can exhibit edge effects (Odum, 1971; Murcia, 1995), with elevated species abundance and biodiversity in some parts of the ecotone (Winterbourn, 1971; Willis and Magnuson, 2000) and the presence of taxa specific to different parts of the ecotones (Poznańska et al., 2010). In addition, ecotones are sensitive to environmental variations (Risser, 1995; Allen and Breshears, 1998), which play important role in purifying water and buffering pollution (Risser, 1995; Ward and Tockner, 2001).

The macrobenthos community show a range of life history characteristics (e.g., relatively long lifespans, sedentary existence), and play a central role in energy flows and material circulation in aquatic ecosystems (Li et al., 2019a; Mosbahi et al., 2019). In general, the macrobenthos have been regarded as key biological indicators of freshwater ecosystem health because these organisms are in direct contact with the sediment and are highly sensitive to changes in physiochemistry of the environment (Soldner et al., 2004; O'Brien et al., 2016; Piló et al., 2016; Eriksen et al., 2021). Most recent studies that documented the macrobenthos biodiversity have focused solely on rivers (Azrina et al., 2006; Gonzalo and Camargo, 2013; Li Z. F. et al., 2020; Buffagni, 2021) or on lakes (Van De Meutter et al., 2006; Li et al., 2016; Cai et al., 2017; Zhang et al., 2019). Only few studies have accounted for both the river and lake components of these systems (Obolewski et al., 2014; Jakubik et al., 2015). However, to date, limited work has been conducted on the macrobenthos community structure and diversity in river–lake ecotones (Szkokan-Emilson et al., 2011; Patrick, 2014). These results have suggested that the environmental characteristics and macroinvertebrate assemblages of ecotones differ from those in adjacent lakes and tributaries (Krebs et al., 2018; Salvo et al., 2020).

Previous studies on macrobenthos biodiversity typically focused on species richness and taxonomic diversity (Li et al., 2016; Wu et al., 2019; Lento et al., 2020), but such a focus conceals ecological differences among species and ignores specific roles they play in the ecosystem (Heino et al., 2007). As a result, they cannot effectively guide biodiversity conservation (Cadotte et al., 2011; Gagic et al., 2015). Each species of macrobenthos is a collection of individuals with multiple functional traits (including phenotypic and behavioral traits) that determine their performance and fitness (Steneck and Dethier, 1994; Violle et al., 2007). More generally, these characteristics determine the compatibility of species with the characteristics of their environment (Martello et al., 2018; Brumm et al., 2021). Recent studies have considered the role of species functional diversity based on biological traits (e.g., body morphology, physiology, trophic habits, and life-history strategies) in a community (Schmera et al., 2017; Espinoza-Toledo et al., 2021; Paz et al., 2022), which may provide a more mechanistic perspective on the community–environment relationships than is possible with approaches based purely on taxonomic diversity (Violle et al., 2007; Cadotte et al., 2011). More importantly, some studies have shown that macrobenthos taxonomic and functional diversity indices respond differently to the same environmental gradients (Heino and Tolonen, 2017; Li et al., 2019b,c; Baker et al., 2021). This suggests that functional diversity metrics complement the information provided by classical taxonomic diversity metrics (England and Wilkes, 2018; Zhang et al., 2021).

Baiyangdian Lake is the largest shallow lake in Northern China. Most previous studies of the lake's macrobenthos communities focused on the lake, with few studies in the tributaries. These studies showed that the macrobenthos richness and biodiversity in Baiyangdian Lake and its rivers have decreased significantly since the 1960s (Zhang et al., 2018; Yang et al., 2020). In the present study, we selected China's Baiyangdian Lake–Fu River system as a case study, with the goals being to (1) compare the spatial distributions of the macrobenthos community structure among the river, river-lake ecotones, and lake; (2) explore the spatial patterns and differences of multiple aspects of macrobenthos biodiversity (including taxonomic and functional diversity) in different ecosystem types (the river, river and lake mouths, and lake); and (3) determine which functional traits respond to specific environmental factors and quantify the effects of the water environment and sediment heavy metal contents on the macrobenthos taxonomic and functional diversity in the river–lake system. We hypothesized that macrobenthos

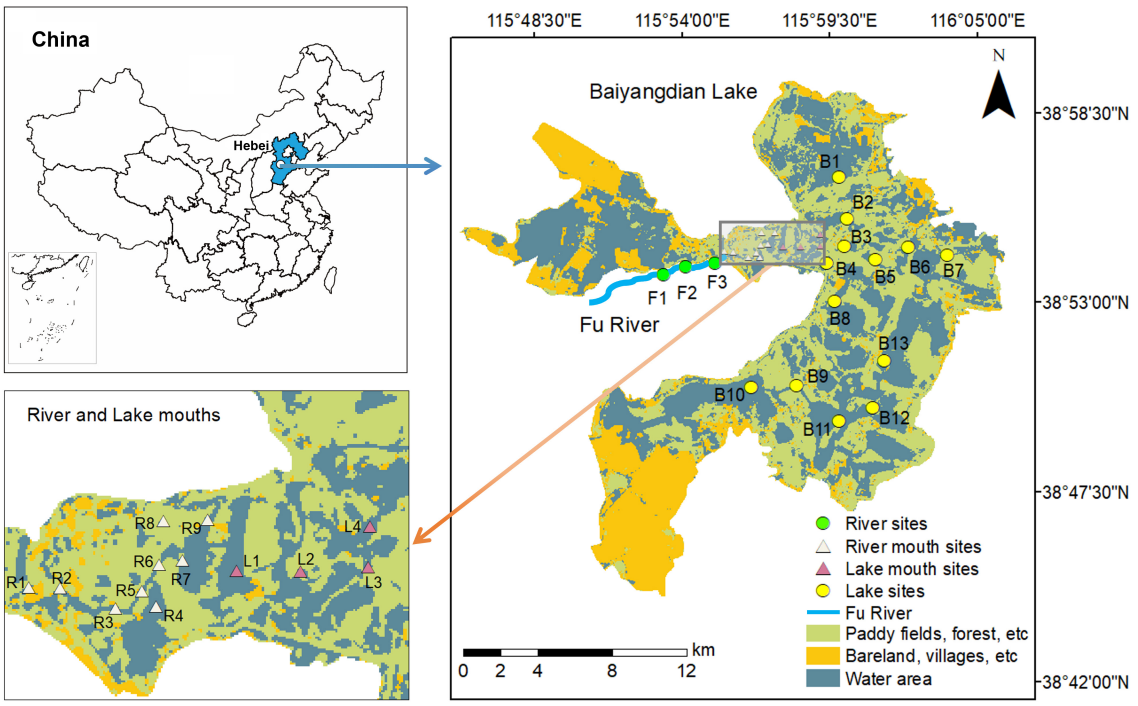

FIGURE 1
Location of Baiyangdian Lake in China and distribution of sampling sites in the study area.

community characteristics would differ significantly along gradients in the above mentioned environmental factors.

Materials and methods

Study area

Baiyangdian Lake (38°43′N to 39°02′N, 115°45′E to 116°07′E) is the largest shallow lake in the North China Plain (Figure 1). The region has a typical warm-temperate monsoon climate, with monthly mean water temperatures of 2–29°C; the average annual precipitation and pan evaporation are approximately 550 and 1,637 mm, respectively. The lake plays an important role in providing habitats for native plants and animals, in water purification, as well as in protecting against floods. Historically, nine upstream rivers flowed into Baiyangdian Lake. Prior to 1960, the lake was dominated by natural flows. However, upstream dams and reservoirs have greatly reduced inflows to the lake, and left insufficient water to sustain the lake's environmental flows. In recent years, the inflows of Baiyangdian Lake have come from three main rivers: Fu River, Xiaoyi River, and Baigouyin River. The Fu River is the main source of inflows, and includes water from upstream rivers, reclaimed city water, and storm runoff.

Our study focused on quantifying the spatial differences of macrobenthos diversity among the lake, the lake–river ecotones, and the main tributary (the Fu River). Based on our preliminary field investigations, combined with measurements of the distribution of the water area in Baiyangdian Lake, we chose 13 sample sites (B1 to B13) that covered the entire lake. We chose three representative sampling sites (F1 to F3) in the downstream of the Fu River. In addition, we chose nine (R1 to R9) and four (L1 to L4) sampling sites from the river mouth and lake mouth zones, respectively (Figure 1), with the category defined by using the hydrologic boundaries of the ecotone between the Fu River and Baiyangdian lake (Tian et al., 2020). We performed five field surveys: in July and November 2018, and in April, June, and September 2019. We simultaneously collected samples of the water, sediments, and macrobenthos from the 29 sampling sites for each field survey in the river–lake system.

Samples for environmental factors

Water environmental factors

Water depth (*H*) and water transparency (the Secchi depth, *SD*) were measured on-site using a plumb-line (measured in centimeter) and a Secchi disk, respectively. We also measured the water temperature (*Tw*), dissolved oxygen (*DO*), and pH *in situ* with a multiparameter handheld probe (YSI Professional Plus; YSI, Yellow Springs, OH, United States). Moreover, we collected 2-L water samples for physicochemical analysis

from the surface water (50 cm below the water surface) and then preserved the samples in pre-cleaned polyethylene bottles according to standard protocols (China Bureau of Environmental Protection [CBEP], 2002). These samples were transported in a portable refrigerator, and were carried back to the laboratory for further analysis. We measured total suspended solids (*TSS*), chemical demand oxygen (*COD*), total nitrogen (*TN*), total phosphorus (*TP*), phosphate (PO_4^{3-}) and ammonium nitrogen (NH_4^+) in the laboratory. Total suspended solids (*TSS*) were measured by gravimetric methods. Chemical oxygen demand (*COD*), total nitrogen (*TN*) and ammonium nitrogen (NH_4^+) were determined using the potassium dichromate method, the alkaline potassium persulfate digestion UV spectrophotometric method and the Nessler's reagent spectrophotometry, respectively. Total phosphorus (*TP*) and phosphate (PO_4^{3-}) were both measured by means of ammonium molybdate tetrahydrate spectrophotometry.

Heavy metals in sediments

We collected three random sediments samples (to a depth of 10 cm) at each sampling site using a Van Veen grab sampler, and composited them into a single bulk sample. The composited samples were sealed in pre-labeled polyethylene zipper bags and stored in a portable refrigerator, and then brought back to the laboratory to determine the concentrations of As, Cd, Cr, Pb, Cu, and Zn. The sediment samples were air-dried and ground to a fine powder in the laboratory. We digested about 50 mg subsample of sediment samples using $HCl–HNO_3$ solution (v/v, 3:1) to determine the total As content using reduction gasification–atomic fluorescence spectroscopy method according to standard protocol (HJ 680-2013). To determine the Cd, Cr, Pb, Cu, and Zn contents, we completely digested sediment subsamples (approximately 100 mg) with a 1:2:1:1 mixed acid solution ($HCl–HNO_3–HF–HClO_4$) in closed Teflon bombs, evaporated to near dryness (*Digi*Prep HotBlock; SCP Science, Baie d'Urfé, QC, Canada), and then diluted to 50 mL with Milli-Q water for further analysis. We determined the heavy metal contents (Cd, Cr, Pb, Cu, and Zn) in the diluted extracts using inductively coupled plasma mass spectrometry (X Series; Thermo Electron, Waltham, MA, United States) according to standard protocol (DB37/T 4435-2021).

Macrobenthos samples

We collected three random subsamples of the macrobenthos at each sampling site using a Van Veen grab sampler with a mouth area of 1/16 m^2 following the general protocol by Chiasson and Williams (1999). Three subsamples were grouped into one composite sample to describe the macrobenthos community of each sampling site. Samples were sieved through a 0.425-mm mesh, and we manually removed impurities such as aquatic plants and gravel in the field. The sieve contents were then placed in white trays to let us manually remove the organisms. All macrobenthos were preserved in 75% ethanol. The organisms were identified to the lowest possible taxonomic level (i.e., species or genus) in the laboratory using a stereomicroscope (Nikon SM2, Nikon Ltd., Japan) based on appropriate identification guides (e.g., Liu et al., 1979; Morse et al., 1984; Tong, 1996; Wang, 2002; Tang, 2006), and were then counted and weighed to determine the fresh weight.

Taxonomic and functional diversity indices

Taxonomic diversity

To describe the taxonomic diversity of the macrobenthos community, we used the Shannon–Weiner diversity (*H'*), Simpson diversity (*D*), Pielou evenness (*E*), and Margalef richness (*d*) indices. The four indices were calculated as follows:

$$H' = \sum_{1}^{s} P_i ln P_i \quad (1)$$

$$D = 1 - \sum_{1}^{S} P_i^2 \quad (2)$$

$$E = H'/ln\,(S) \quad (3)$$

$$d = (S-1)/ln(N) \quad (4)$$

where P_i is the probability of occurrence of the i^{th} species in a community; *S* is the total number of species in a community; and *N* is the total number of individuals in a community.

Functional diversity

We considered six functional trait classes to characterize macrobenthos, consisting of adult body size, longevity, voltinism, swimming ability, locomotion, and feeding habit (**Supplementary Table 1**), which have been widely used to characterize functional diversity (Coccia et al., 2021; Edegbene et al., 2021; Akamagwuna et al., 2022). For each trait, a set of attributes were used to categorize the macrobenthos species (**Supplementary Table 1**). These trait classes and their associated attributes are related to morphology, life history, and behavior of macrobenthos (Usseglio-Polatera et al., 2000; Akamagwuna et al., 2022), and showed sensitively response to various environmental stress (Li et al., 2019c; Li Z. F. et al., 2020; Juvigny-Khenafou et al., 2021). Additionally, they reflect the macrobenthos-related ecological functions, such as secondary production, energetic transference, and the nutrients cycle (Hébert et al., 2016; Braghin et al., 2018). We further used a binary coding approach (i.e., 1 if a species displays a trait attribute, 0 if not) to encode trait attributes of the macrobenthos collected in the river–lake system (**Supplementary Table 2**; Li et al., 2019a,c; Li S. H. et al., 2020; Juvigny-Khenafou et al., 2021). Information regarding the functional traits of macrobenthos

was mainly obtained from the published literature on freshwater ecosystem (Li et al., 2019a; Zhang et al., 2019; Li Z. F. et al., 2020; Dolédec et al., 2021; Juvigny-Khenafou et al., 2021; Peng et al., 2021). Where the trait attributes of a given species were not available, we used information from other species within the same genus or family (Sivadas et al., 2021; Paz et al., 2022).

We used the following functional diversity indices: functional richness (*FRic*), functional evenness (*FEve*), functional divergence (*FDiv*), and Rao's quadratic entropy index (*RaoQ*). *FRic* indicates the functional niche space occupied by a given community, and in general, a lower value implies low utilization of the ecological space (Villéger et al., 2008; Liu et al., 2021). *FEve* corresponds to the evenness of the distribution of species abundance within the functional trait space, and higher *FEve* indicates high utilization efficiency of the niche space (Mason et al., 2005; Villéger et al., 2008). *FDiv* (the functional divergence) describes the distribution of species abundance across the niche space, which reflects the degrees of niche differentiation and resource competition within the community. High *FDiv* entails a high degree of species niche complementarity and low resource competition (Villéger et al., 2008). *RaoQ* measures pairwise differences in trait composition between taxa weighted by their relative abundance (Botta-Dukát, 2005). It combines both *FRic* and *FDiv*, and therefore considers potential redundancy or complementarity between these diversity indices (Péru and Dolédec, 2010).

RLQ and fourth-corner analysis methods

We combined the RLQ method (Dolédec et al., 1996), which uses environmental variables (R), species of taxa (L), and traits (Q), with the fourth-corner method (Kleyer et al., 2012; Dray et al., 2014) to assess the responses of macrobenthos traits to environmental gradients. The RLQ method is a three-table ordination analysis that accounts for environmental variables in the **R** table (environment × site), for species abundance in the **L** table (species × site), and for functional traits in the **Q** table (trait × species). First, we conducted correspondence analysis (function *dudi.coa*) on the L table, and principal-components analysis (function *dudi.pca*) on the R and Q tables. We then combined these separate analyses using RLQ analysis (function *rlq* in R package *ade4*, Dolédec et al., 1996). We assessed the overall significance of this relationship using a global Monte Carlo test with 49,999 random permutations of both model 2 (H1: assuming no relationship between R and L) and model 4 (H2: assuming no relationship between L and Q). Since the global test could not test the bivariate relationship between individual environmental variables and functional traits, we used fourth-corner analysis with an adjusted p value (i.e., p-values were corrected using the false discovery rate adjustment method to limit bias due to multiple-test comparisons) to test their relationships (function *fourthcorner* in R package *ade4*, Benjamini and Hochberg, 1995; Dong et al., 2021). Furthermore, we used a combination of RLQ and fourth-corner analyses to evaluate the significance of the associations between environmental variables (or functional traits) and the RLQ axes (Dray et al., 2014).

Data analysis

We calculated the taxonomic and functional diversity indices of the macrobenthos community in each of the four ecosystem types (river, river mouth, lake mouth, lake) using version 2.5–7 of the "vegan" package[1] and version 1.0–12 of the "FD" package[2] for the R software (version 4.1.2[3]), respectively. We used version 1.7–18 of the "ade4" package[4] for the RLQ and fourth-corner analysis. In addition, to evaluate the contributions of the water environmental variables and sediment heavy metals to variation of the taxonomic and functional diversities, we carried out variance partitioning analysis using the "vegan" package.

Our primary goal was to detect relationships between environmental factors and macrobenthos diversity; because of this goal and limitations on our budget, we did not collect large enough samples on different dates to robustly test for changes in macrobenthos communities between sample dates. We used one-way ANOVA to test whether there were significant spatial differences in environmental variables, taxonomic diversity indices, and functional diversity indices. If the result was significant, we used a *post hoc* test (the least-significant-difference test) for pairwise comparisons of variables between pairs of ecosystem types. To identify relationships between the taxonomic and functional diversity metrics, we calculated Pearson's correlation coefficient (r) for each ecosystem type. These statistical analyses were conducted using version 26.0 of the SPSS software[5].

Results

Spatial variations of water environmental variables and sediment heavy metals

Table 1 shows the values (mean ± SE) of the water environmental variables and sediment heavy metals in the

1 https://cran.r-project.org/web/packages/vegan/index.html
2 https://cran.r-project.org/web/packages/FD/index.html
3 http://www.r-project.org/
4 https://cran.r-project.org/web/packages/ade4/index.html
5 https://www.ibm.com/analytics/spss-statistics-software

four ecosystem types. There were significant differences among the four ecosystem types in *SD* ($F = 4.681$, $p < 0.05$), *TSS* ($F = 7.872$, $p < 0.05$), *DO* ($F = 3.095$, $p < 0.05$), *TN* ($F = 11.428$, $p < 0.05$), and *TP* ($F = 7.617$, $p < 0.05$). Water transparency (*SD*) increased moving downstream from the river (with an average depth of 0.63 ± 0.06 m) to the lake (with an average depth of 0.88 ± 0.03 m), but was only significantly lower in the river than in the other sites. Mean *DO* was much greater in the lake mouth (8.39 ± 1.20 mg/L) and river mouth (8.39 ± 0.85 mg/L) than in the river (5.29 ± 0.61 mg/L) and lake (6.87 ± 0.43 mg/L), and the differences were significant. The highest and lowest values of *TSS*, *TN*, and *TP* were observed in the river and lake mouth, respectively, and the differences were significant. In addition, *TN* concentrations exceeded the fourth grade (IV) in the environmental quality standards for surface water of China (i.e., had water quality sufficiently bad that it was only suitable for industrial water supply and recreation in which there is no direct human contact with the water) at 80.0%, 55.6%, 54.6%, and 53.8% of sampling sites in the river, river mouth, lake mouth, and lake, respectively. The average *TP* ranged from 0.05 mg/L to 0.21 mg/L, and the concentrations of 88.2%, 75.9%, 66.7%, and 67.3% of the sampling sites along the river–lake gradient, respectively, exceeded grade IV.

The values of Cd ($F = 9.473$, $p < 0.05$), Cr ($F = 4.941$, $p < 0.05$), Cu ($F = 12.539$, $p < 0.05$), Pb ($F = 13.205$, $p < 0.05$), and Zn ($F = 29.733$, $p < 0.05$) differed significantly among the four ecosystem types. The average Cd, Cr, Cu, Pb, and Zn concentrations were significantly higher in the river and river mouth than in the lake mouth and lake.

Macrobenthos community structure

Macrobenthos abundance and biomass

We identified a total of 30 macrobenthos taxa across all sampled areas (**Supplementary Table 3**): 12 Insecta (40.0%), 11 Gastropoda (36.7%), three Oligochaeta (10%), two Bivalvia (6.7%), one Crustacea (3.3%), and one Hirudinea (3.3%). The numbers of species in the different ecosystems were 13, 17, 12, and 25 in the river, river mouth, lake mouth, and lake, respectively. Among these taxa, only eight species (*Limnodrilus hoffmeisteri*, *Bellamya aeruginosa*, *Bellamya purificata*, *Bithynia fuchsiana*, *Bithynia misella*, *Einfeldia dissidens*, *Propsilocerus kamusi*, and *Orthocladius* sp.) appeared in all the four ecosystem types. *Tubifex tubifex* was only observed in the river. Seven species (*Cipangopaludina cahayensis*, *Parafossarulus eximius*, *Semisulcospira cancellate*, *Stenothyra glabra*, *Unio dongtasiae*, *Glyptotendipes tokunagai*, *Microchironomus tener*) were found only in the lake, but not in the other three study areas. *Glossiphonia* sp. and *Polypedilum* sp. were found only in the river mouth, and *Dicrotendipes nervosus* and *Hyale changi* were found only in the lake mouth.

Figure 2A shows that the total of the average abundance of all macrobenthos taxa in the lake (373.91 ± 77.79

TABLE 1 Mean and standard error (mean ± SE) of the water environmental variables and sediment heavy metals in the four ecosystem types.

Variables	Ecosystem types			
	River	River mouth	Lake mouth	Lake
Water environmental variables				
Water depth (*H*, m)	1.87 ± 0.22^{a}	2.19 ± 0.08^{a}	2.41 ± 0.21^{a}	2.36 ± 0.09^{a}
pH	8.13 ± 0.11^{a}	8.32 ± 0.04^{a}	8.35 ± 0.06^{a}	8.26 ± 0.05^{a}
Water temperature (*Tw*, °C)	21.00 ± 1.98^{a}	24.09 ± 1.00^{a}	25.10 ± 1.45^{a}	22.69 ± 0.94^{a}
Secchi depth (*SD*, m)	0.63 ± 0.06^{b}	0.77 ± 0.04^{b}	0.79 ± 0.05^{ab}	0.88 ± 0.03^{a}
Total suspended solids (*TSS*, mg/L)	15.13 ± 1.80^{a}	6.54 ± 0.81^{b}	6.47 ± 1.23^{b}	7.18 ± 1.02^{b}
Dissolved oxygen (*DO*, mg/L)	5.29 ± 0.61^{b}	8.39 ± 0.85^{a}	8.39 ± 1.20^{a}	6.87 ± 0.43^{ab}
Total nitrogen (*TN*, mg/L)	5.96 ± 0.81^{a}	2.48 ± 0.41^{b}	2.14 ± 0.35^{b}	2.46 ± 0.28^{b}
Total phosphorus (*TP*, mg/L)	0.21 ± 0.05^{a}	0.08 ± 0.02^{b}	0.05 ± 0.01^{b}	0.07 ± 0.01^{b}
Ammonium nitrogen (NH_4^+, mg/L)	0.82 ± 0.29^{a}	0.36 ± 0.09^{a}	0.45 ± 0.11^{a}	0.43 ± 0.06^{a}
Phosphate (PO_4^{3-}, mg/L)	0.07 ± 0.02^{a}	0.06 ± 0.01^{a}	0.04 ± 0.01^{a}	0.04 ± 0.01^{a}
Chemical oxygen demand (*COD*, mg/L)	30.63 ± 4.99^{a}	20.71 ± 2.21^{a}	27.15 ± 7.30^{a}	27.50 ± 2.71^{a}
Heavy metals in sediments				
As (mg/kg)	9.40 ± 0.58^{a}	10.16 ± 0.54^{a}	9.75 ± 0.90^{a}	10.72 ± 0.55^{a}
Cd (mg/kg)	1.67 ± 0.13^{a}	1.95 ± 0.35^{a}	0.68 ± 0.13^{b}	0.56 ± 0.10^{b}
Cr (mg/kg)	104.76 ± 15.36^{a}	82.42 ± 4.40^{b}	60.85 ± 2.93^{c}	73.03 ± 4.47^{bc}
Cu (mg/kg)	62.63 ± 2.10^{a}	53.40 ± 2.42^{a}	37.19 ± 2.60^{b}	38.59 ± 2.41^{b}
Pb (mg/kg)	50.35 ± 2.12^{a}	47.41 ± 2.97^{a}	34.25 ± 2.60^{b}	31.83 ± 1.59^{b}
Zn (mg/kg)	311.00 ± 14.89^{a}	269.65 ± 20.64^{a}	122.83 ± 11.87^{b}	113.95 ± 10.68^{b}

Values of a variable labeled with different letters differed significantly (ANOVA followed by least-significant-difference test, $p < 0.05$).

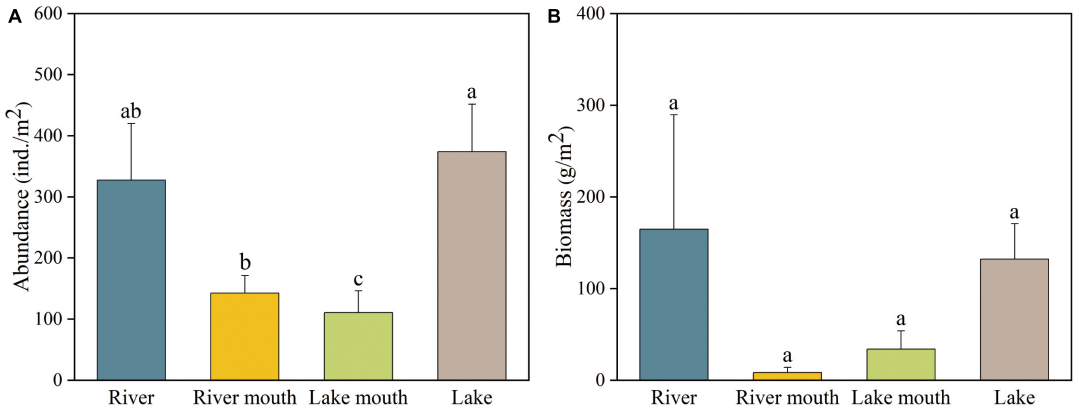

FIGURE 2
(A) Abundance and **(B)** biomass of macrobenthos communities in the four study areas. Values are mean ± SE. Values of a variable labeled with different letters differed significantly (ANOVA followed by least-significant-difference test, $p < 0.05$).

ind./m^2, mean ± SE) was significantly greater than that in the river mouth (142.48 ± 28.68 ind./m^2) and lake mouth (110.55 ± 35.74 ind./m^2), but not significantly different from the abundance in the river (327.38 ± 92.56 ind./m^2). *Limnodrilus hoffmeisteri* was the most abundant species in the river (153.85 ± 54.91 ind./m^2) and river mouth (64.00 ± 16.49 ind./m^2), whereas *Propsilocerus kamusi* and *Bithynia misella* were the most abundant taxa in the lake mouth (37.82 ± 23.26 ind./m^2) and lake (155.13 ± 44.15 ind./m^2), respectively (**Supplementary Table 4**). The highest average macrobenthos biomass occurred in the river (164.64 ± 124.78 g/m^2), followed by the lake (132.06 ± 38.58 g/m^2), with the lowest biomass in the river mouth (8.41 ± 5.52 g/m^2, **Figure 2B**); however, due to high variation, these differences were not significant. *Bellamya aeruginosa* was the species with the highest biomass both in the river and lake mouths (4.98 ± 3.89 g/m^2 and 23.44 ± 16.09 g/m^2, respectively), whereas *Anodonta woodiana* and *Bithynia misella* were the species with the highest biomass in the river (75.23 ± 75.23 g/m^2) and lake (58.29 ± 23.89 g/m^2), respectively (**Supplementary Table 5**). In addition, **Supplementary Figure 1** shows the temporal changes in the species richness of macrobenthos in Baiyangdian Lake.

Macrobenthos biological traits

Figure 3 shows the proportions of the macrobenthos communities in the four study areas. The macrobenthos functional traits in the river–lake system was mainly characterized by very small body size (≤ 10 mm, BS1). The proportions of short-lived taxa (AL1) were higher than those of long-lived taxa (AL2) in the river, river mouth, and the lake, but equal in the lake mouth. The proportions of taxa with a univoltine life cycle (V2) were much higher than those of bi- or multivoltine (V3) and semivoltine (V1) taxa, and the proportion of univoltine taxa increased along the gradient from the river to the lake, with proportions of 61.5%, 64.7%, 66.7%, and 68.0%, respectively. More taxa were characterized as having no mobility (SA1) and weak mobility (SA2) in all four ecosystem types, but a few taxa with strong mobility (SA3) occurred in the lake mouth. Higher proportions of burrowers (H1, > 50%) appeared in the river and river mouth ecosystems, whereas climbers (H2) dominated the lake mouth. We found the same proportions (48%) of burrowers (H1) and climbers (H2) in the lake. Most taxa were scrapers (FH3) and collector-filterers (FH2) in all four ecosystem types. Among the 25 biological trait categories, we observed no semivoltine taxa (V1), swimming taxa (H5), and parasitic taxa (FH6) in the four ecosystem types.

Macrobenthos taxonomic and functional diversity

Taxonomic diversity

We found significant differences among the four ecosystem types in the Pielou evenness ($F = 4.149$, $p < 0.05$, **Figure 4C**). The peak and minimum values of the Pielou evenness were recorded at the lake mouth (0.99 ± 0.01, mean ± SE) and the river mouth (0.67 ± 0.07), respectively, and this difference was significant. The highest values of the Shannon–Wiener diversity and Simpson diversity both occurred at the lake mouth, followed by the lake, with the lowest values in the river mouth (**Figures 4A,B**); however, these differences were not significant. The average value of the Margalef richness was higher in the lake and river than that of in the river mouth and lake mouth (**Figure 4D**); however, these differences were not significant.

Functional diversity

FRic differed significantly among the four studied ecosystem types ($F = 10.381$, $p < 0.05$), with significantly higher values

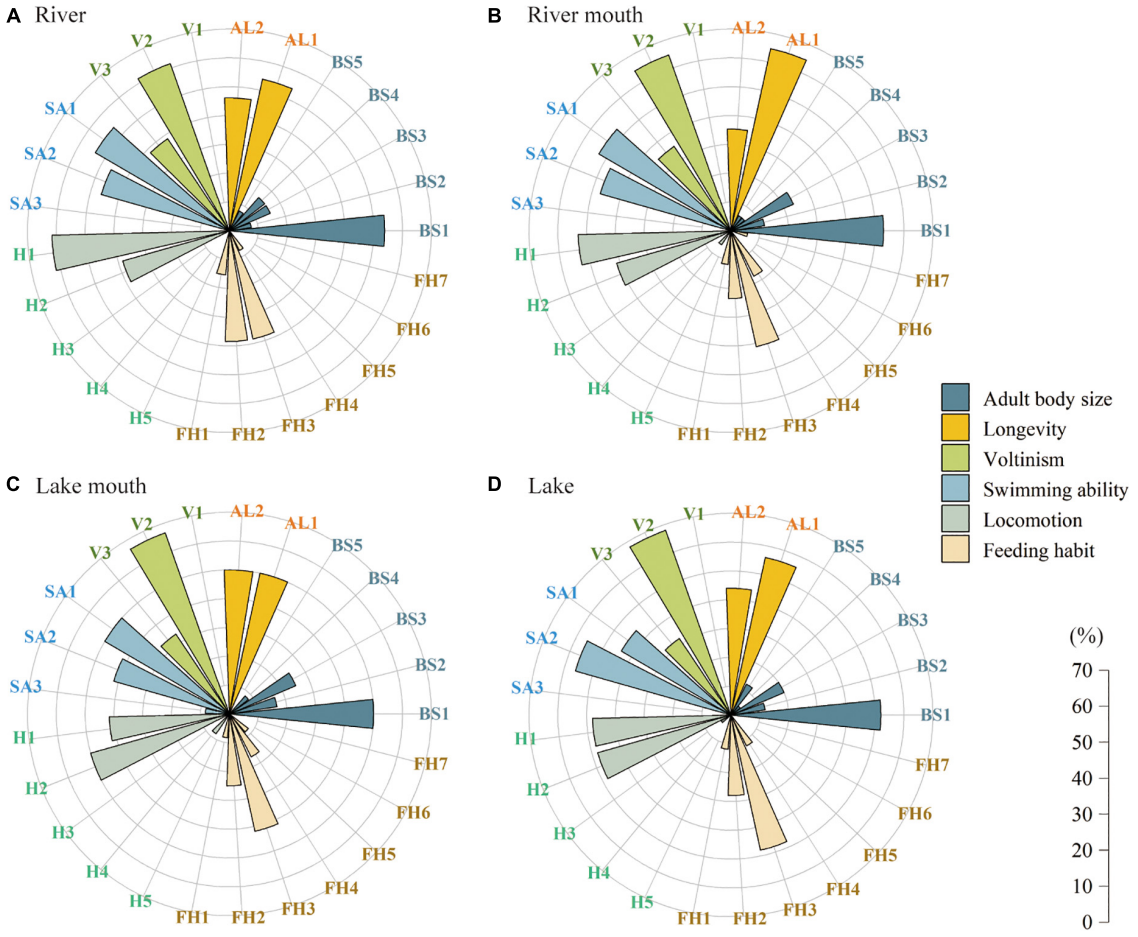

FIGURE 3
Proportion of the trait values for the macrobenthos communities in the four ecosystem types: **(A)** River, **(B)** River mouth, **(C)** Lake mouth, and **(D)** Lake. Trait values are defined in **Supplementary Table 1**.

in the river (3.13 ± 0.54, mean ± SE) than in the lake mouth (0.94 ± 0.46) or the lake (0.87 ± 0.17, **Figure 5A**). *FEve* in the lake mouth and river mouth (0.68 and 0.71, respectively) were slightly greater than those in the river and lake (both about 0.62), but did not differ significantly among the locations (**Figure 5B**). *FDiv* showed the opposite pattern compared with *FEve*, and the differences were not significant (**Figure 5C**). For *RaoQ*, the greatest value (1.15 ± 0.23) was observed in the river, and the lowest value (0.61 ± 0.18) was in the river mouth (**Figure 5D**), but the differences were not significant.

Correlation between taxonomic and functional diversity indices

Figure 6 shows the significant correlations between each pair of biodiversity indices for the four ecosystem types. Overall, the taxonomic diversity indices had stronger correlations with each other than with the functional diversity indices. There were significant positive relationships between the Shannon–Wiener diversity and the other three taxonomic diversity indices in the river, river mouth, and lake, whereas Simpson diversity was significantly positively correlated with the Shannon–Wiener diversity and Margalef richness in the lake mouth. In addition, the Simpson diversity was positively correlated with all other taxonomic diversity indices in the river and lake. Among the functional diversity indices, *RaoQ* was significantly positively correlated with *FEve* in the river, *FDiv* was significantly positively correlated with *FRic* and *RaoQ* in the river mouth, and *FRic* was significantly negatively correlated with *FEve* in the lake. There was no significant relationship between pairs of functional diversity indices in the lake mouth. *RaoQ* was significantly positively correlated with all taxonomic diversity indices in the river. Pielou evenness and *FDiv* were significantly negatively and positively correlated in the river and lake, respectively. Among the taxonomic diversity indices, Simpson diversity and Pielou evenness were significantly positively correlated with *FEve* in the river but not in the lake, whereas Pielou evenness and Margalef richness were significantly positively and negatively correlated (respectively) with *FEve* in the lake. We found no

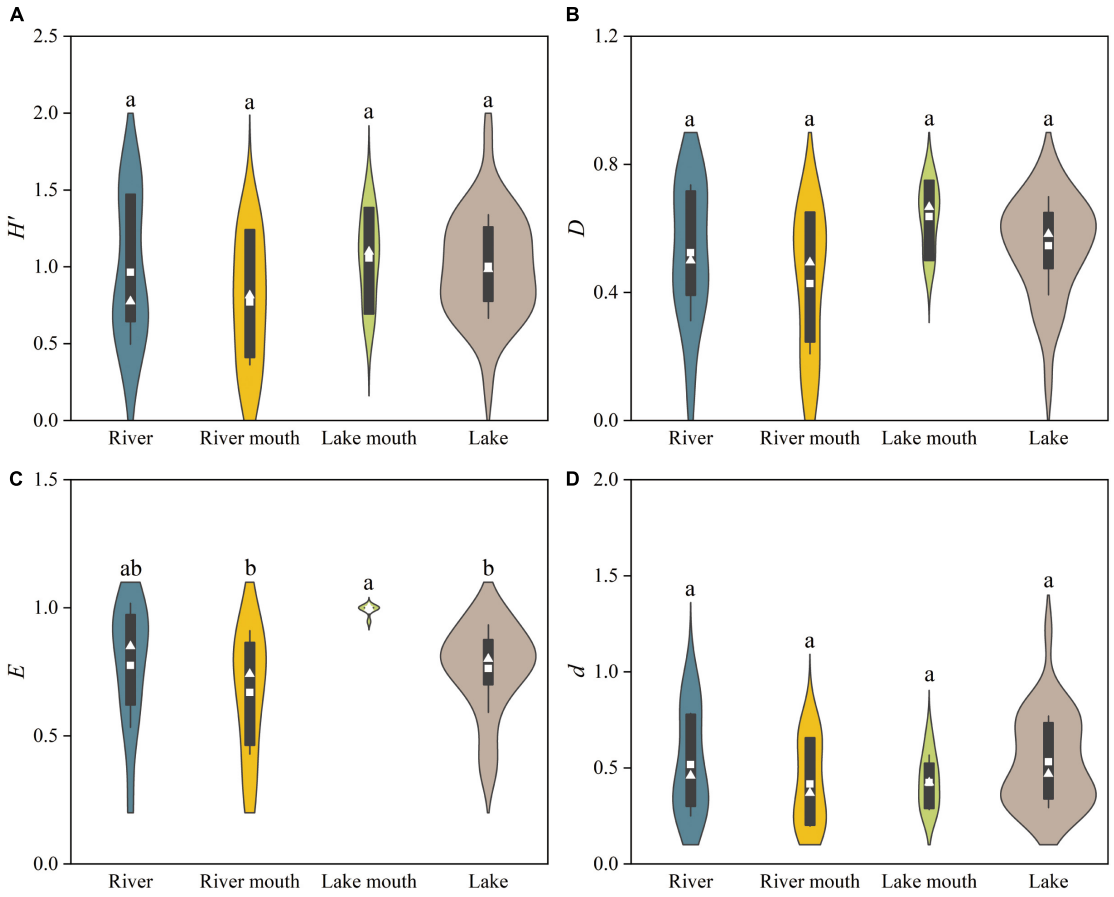

FIGURE 4
Taxonomic diversity indices for the macrobenthos communities in the four ecosystem types: **(A)** Shannon–Wiener diversity (*H'*), **(B)** Simpson diversity (*D*), **(C)** Pielou evenness (*E*), and **(D)** Margalef richness (*d*). Values are: Mean, white squares; standard deviation, vertical black bars; median, white triangles. The shaded areas correspond to the kernel density shapes. Distributions labeled with different letters differ significantly (ANOVA followed by least-significant-difference test, $p < 0.05$).

significant correlation between the taxonomic and functional diversity indices in the river mouth and lake mouth.

Relationships between macrobenthos traits and environmental variables

Figure 7 and Supplementary Table 10 show the relationships between the macrobenthos traits and the environmental variables. Overall, these were significant (Model 2, $p < 0.01$; Model 4, $p < 0.01$). The first two axes of the RLQ multivariate analysis explained 98.9% of the total inertia of the three tables, with the first and second RLQ axes explaining 93.4% and 5.5% of the total variance, respectively.

The left (negative) part of the first RLQ axis (Figure 7A) included Oligochaeta species (i.e., *Limnodrilus hoffmeisteri*, *Branchiura sowerbyi*, and *Tubifex tubifex*), which were with characteristics of large body size and collector-gatherers (Figure 7B). These taxa were mostly found in the river (Figure 7D), with higher *TN*, *TP*, and Cr concentrations (Figure 7C). The left (negative) part of the first RLQ axis also showed that the trait states (e.g., burrower, no mobility) largely matched the characteristics of the Insecta species (e.g., *Tanypus villipennis*, *Chironomus plumosus*, *Polypedilum* sp.), which was related to the increasing heavy metal concentrations for Pb, Zn, Cu, and Cd, and tended to emerge in the river mouth. The right (positive) part of the first RLQ axis indicated trait states (e.g., univoltine life cycle, climber, weak mobility) were associated with the physical variables *H* and *SD*. The most representative species were Gastropoda (e.g., *Semisulcospira cancellata*, *Stenothyra glabra*, *Gyraulus convexiusculus*) and tended to emerge in the lake. The positive (top) part of the second RLQ axis showed trait states (e.g., medium body size and long life) associated with higher concentrations of NH_4^+, *TSS*, *COD*, and As. These trait states largely matched the characteristics of the Gastropoda and Bivalvia. Furthermore, the negative (bottom) part of the second RLQ axis illustrated that Hirudinea

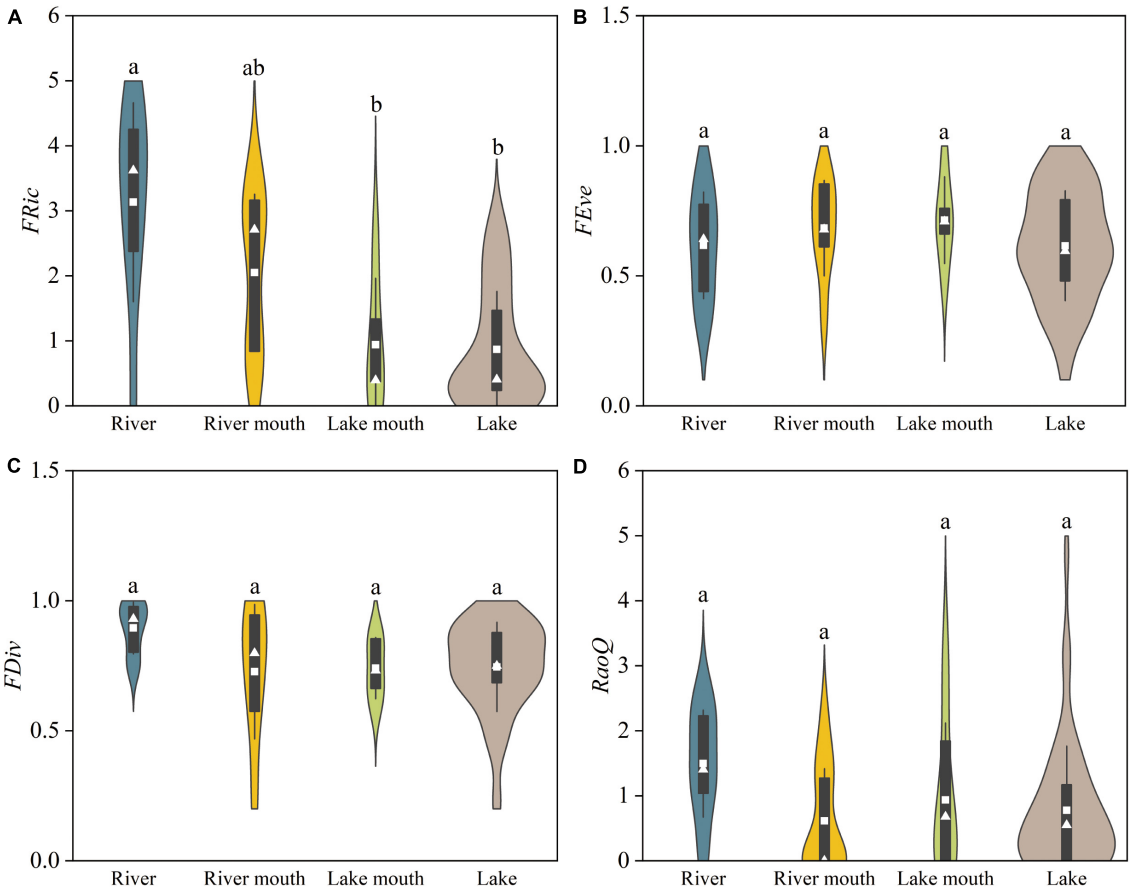

FIGURE 5
Functional diversity indices for macrobenthos communities in the four ecosystem types: **(A)** *FRic*, functional richness; **(B)** *FEve*, functional evenness; **(C)** *FDiv*, functional divergence; **(D)** *RaoQ*, Rao's quadratic entropy. Values are: Mean, white squares; standard deviation, vertical black bars; median, white triangles. The shaded areas correspond to the kernel density shapes. Distributions labeled with different letters differ significantly (ANOVA followed by least-significant-difference test, $p < 0.05$).

(*Glossiphonia* sp.) and Insecta (e.g., *Propsilocerus kamusi*, *Procladius* sp., *Dicrotendipes nervosus*) with a short life and a scraper feeding mode were more susceptible to PO_4^{3-}, *T*w, *DO*, and pH, and tended to emerge in the river mouth and lake mouth areas.

The fourth corner analysis showed no significant bivariate associations between a single trait state and a single environmental factor (p-adjusted < 0.05). Therefore, we further examined the relationships between individual trait states and the two RLQ environmental axes, as well as those between individual environmental variables and the two RLQ trait axes (**Supplementary Figure 2**). The first RLQ trait axis (AxcQ1) was significantly positively correlated with two physical variables (*H* and *SD*, p-adjusted < 0.05) and significantly negatively correlated with *TN* and *TP* (p-adjusted < 0.05). In addition, all heavy metals except As were significantly negatively correlated with the first RLQ trait axis (p-adjusted < 0.05). We found no other significant relationships between the two RLQ environmental axes and individual trait states.

Partitioning of the influences of environmental variables on macrobenthos diversities

Variance partitioning revealed that the water environmental variables and sediment heavy metals both played important roles in the macrobenthos taxonomic and functional diversity in the river–lake system (**Supplementary Figure 3**). Water environmental variables accounted for a larger proportion of the variation than sediment heavy metals for both taxonomic and functional diversity. The combination of both variable categories explained the taxonomic diversity well (66.8% of the variance; **Supplementary Figure 3A**), which was higher than the sum for the individual environmental variables (60.5%). The variability of taxonomic diversity explained by the interaction between water environmental variables and sediment heavy metals was 6.2%. For functional diversity (**Supplementary Figure 3B**), the sum of the individual environmental variables (89.0%) explained more

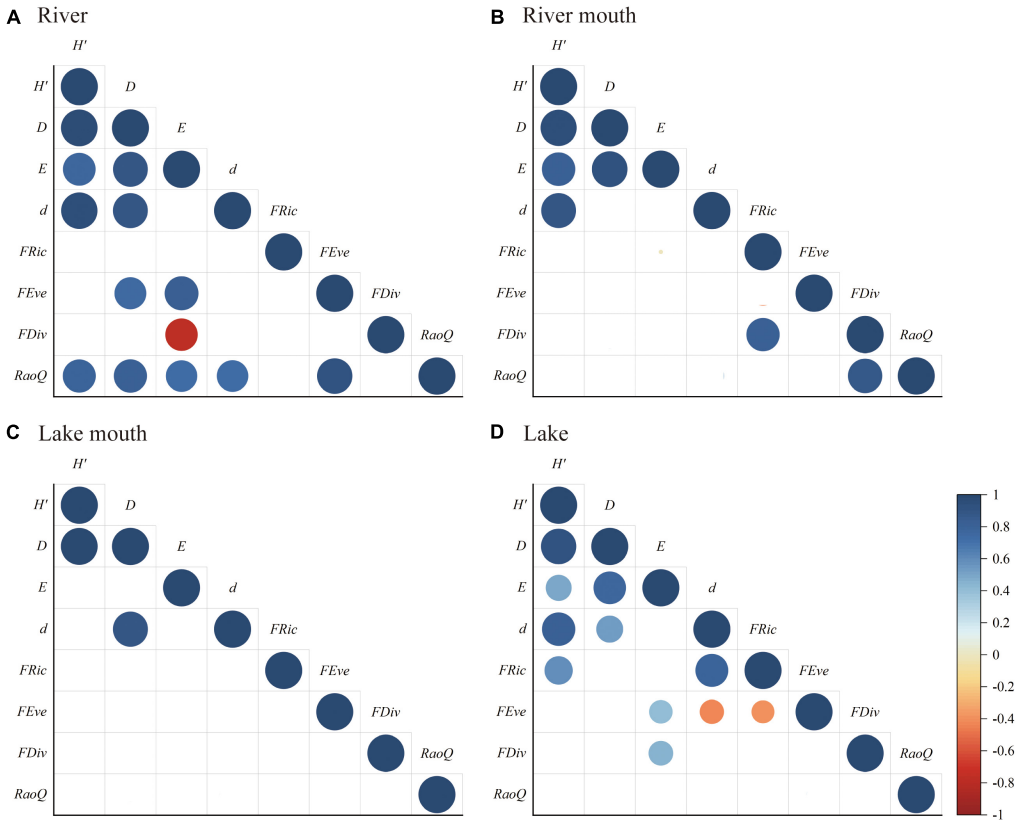

FIGURE 6
Pearson's correlation coefficients (*r*) for the relationships between pairs of macrobenthos taxonomic and functional diversities in the **(A)** River, **(B)** River mouth, **(C)** Lake mouth, **(D)** Lake: *H′*, Shannon–Wiener diversity; *D*, Simpson diversity; *E*, Pielou evenness; *d*, Margalef richness; *FRic*, functional richness; *FEve*, functional evenness; *FDiv*, functional divergence; *RaoQ*, Rao's quadratic entropy. The actual r values are presented in **Supplementary Tables 6–9**. Lower blank cells indicate insignificant correlation ($p > 0.05$).

than the combination of water environmental variables and sediment heavy metals (77.6%). The variability of functional diversity explained by the interaction between water environmental variables and sediment heavy metals was −11.4%. Remarkably, the amount of the variation explained by water environmental variables and sediment heavy metals were both higher for functional diversity than for taxonomic diversity.

Discussion

Spatial patterns of macrobenthos taxonomic and functional diversity

Functional diversity measures are increasingly being incorporated into making better conservation and restoration decisions for freshwater ecosystems (Cadotte et al., 2011; Schmera et al., 2017; Coccia et al., 2021). Using several functional trait indices is likely to provide more insight into functional attributes of the ecosystem than relying only on species-based indices (Gagic et al., 2015; Sotomayor et al., 2021). In the present study, we investigated the spatial patterns of macrobenthos taxonomic and functional diversity along the gradient from the Fu River to Baiyangdian Lake. Our results support our hypothesis that macrobenthos community characteristics would differ significantly along gradients in the environmental factors. The average abundance of all macrobenthos taxa was significantly greater in the lake than that in the river and lake mouths. Pielou evenness was significantly higher in the lake mouth than in the river mouth and lake. Similarly, Poznańska et al. (2010) found that the higher taxonomic diversity (e.g., Pielou eveness) but extremely lower abundance of macrobenthos in a transition zone (i.e., the sandy substrata) compared with that found at the adjacent reservoir ecosystem. Functional richness was significantly higher in the river than in the lake mouth and lake, which can be interpreted as a sign of functional redundancy in the lake mouth and lake (Arenas-Sánchez et al., 2021). In addition, greater functional evenness in the river and lake mouths indicated

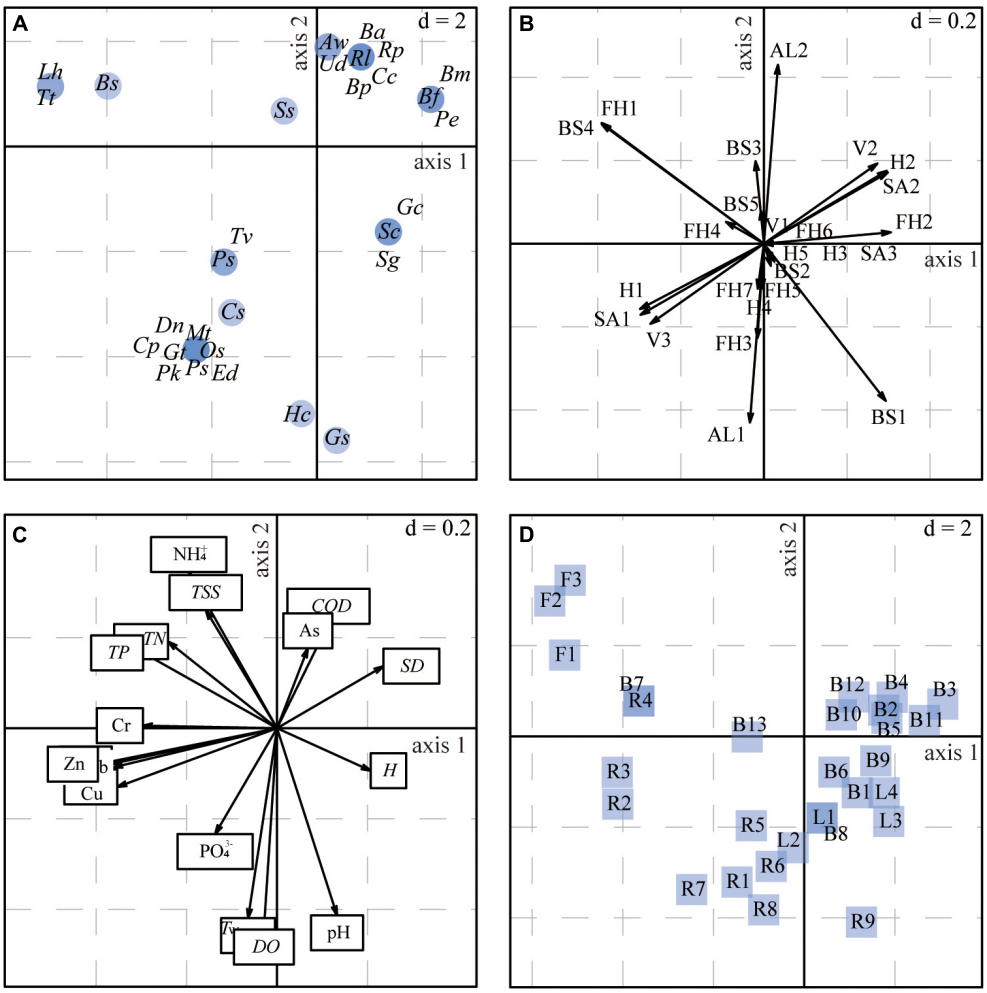

FIGURE 7
Results of the RLQ analysis represented by the first and second axes based on data for the four ecosystem types combined: **(A)** species scores, **(B)** trait states, **(C)** coefficients for the environmental variables, **(D)** projection of sampling sites. The *d* value represents the grid size of the graph. Species codes in panel **(A)** are defined in **Supplementary Table 3**; trait codes in panel **(B)** are defined in **Supplementary Table 1**.

that functional traits were distributed more evenly across the trait space than that in the river and lake, which was associated with greater response diversity and resilience in aquatic ecosystems (Gagic et al., 2015; Schriever et al., 2015; England and Wilkes, 2018). Differences other three taxonomic diversity indices (i.e., Shannon–Weiner diversity, Simpson diversity, and Margalef richness) were not significant among the four ecosystem types. These can be related to the fact that the collected communities were dominated by few taxa with high abundances in each ecosystem type (**Supplementary Table 4**; Arenas-Sánchez et al., 2021).

We found significant positive correlations among the taxonomic diversity indices in our study area, which was consistent with previous studies (Heino et al., 2007; Gascón et al., 2009; Tolonen et al., 2017). Moreover, there was significant positive relationship between the Rao's quadratic entropy and functional evenness in the river, whereas Rao's quadratic entropy was significantly positively correlated with functional divergence in the river mouth. In contrast, De Castro-Català et al. (2020) indicated that Rao's quadratic entropy was negatively correlated with functional evenness and functional divergence of macrobenthos in European river basins. In addition, the relationships between the taxonomic and functional diversity indices were complex and differed among the four ecosystem types. In the river, Rao's quadratic entropy was significantly positively correlated with the four taxonomic diversity indices, which corresponded with findings of De Castro-Català et al. (2020). Similarly, Feld et al. (2014) revealed a strong positive relationship between Rao's quadratic entropy and three taxonomic diversity indices

(Shannon–Weiner diversity, Simpson diversity, and Pielou evenness) of benthic macroinvertebrates along a gradient of hydromorphological alteration across 65 lowland river sites. In the lake, Pielou evenness was significantly positively correlated with functional divergence and functional evenness. Similar results have been reported for macroinvertebrate communities in a large lake undergoing eutrophication, where Pielou evenness was found to be significantly positively correlated with functional divergence and functional evenness (Tolonen et al., 2017).

Some studies on the relationships between taxonomic and functional diversity indices of freshwater macrobenthos suggest that even if some taxonomic and functional diversity indices are correlated, the correlation is not sufficient to guarantee that they can replace each other (Heino et al., 2008; Cadotte et al., 2011; Gallardo et al., 2011; Feld et al., 2014). In particular, despite these significant correlations between macrobenthos taxonomic and functional diversity indices, this trend is not universally supported. We found no significant correlation between taxonomic and functional diversity indices in the river mouth and lake mouth ecosystems. Some studies on macrobenthos also indicated that functional diversity fluctuates independently from taxonomic diversity (Cadotte et al., 2011; Reynaga and Dos Santos, 2013). These results highlight and support the importance of functional diversity as complementary to, rather than a replacement for, taxonomic biodiversity in river–lake ecotones. The different indices quantify different and unique aspects of biodiversity, so using complementary and uncorrelated diversity indices can provide a more thorough understanding of the multiple facets of biodiversity (Wilsey et al., 2005; Gallardo et al., 2011).

Effects of water environmental variables and sediment heavy metals on the macrobenthos community

In the present study, ecotones are transitional areas between a river (a lotic environment) and a lake (a lentic environment). In such river–lake systems, ecotones can function as water purification areas and pollution buffers. Nutrient concentrations (i.e., *TN* and *TP*) in the river mouth and lake mouth were both lower than those in the adjacent river, and the lake mouth values were lower than those in the adjacent lake. The sediment Cr, Cu, Pb, and Zn concentrations in the river mouth were generally lower than those in the adjacent river but higher than those in the adjacent lake mouth. The RLQ and fourth-corner results clarified the relationships between environmental factors and functional traits in the four ecosystem types. They not only indicated that the functional traits of macrobenthos communities can respond to different environmental variables, but also support previous research, in which the functional traits of these communities are not randomly spatially distributed (Piló et al., 2016; Kuzmanovic et al., 2017; Hu et al., 2019).

The effects of water environmental variables on macrobenthos community might be complex and indirect, which might work by the alterations in their water habitat conditions. Even so we still tried to explore the statistical relationship between water environmental variables and macrobenthos community from the field survey. We found that physical conditions (*H* and *SD*) strongly correlated with the abundance and traits of many of the macrobenthos in Baiyangdian Lake, which confirms previous studies in this region (Yi et al., 2018; Yang et al., 2020). In addition, the RLQ analysis showed that with increasing eutrophication as a result of high *TN* and *TP*, a community dominated by macrobenthos with climber, scraper, and weak mobility functional traits changed to a community dominated by burrowers, collector-gatherers, and organisms with no mobility. These results support the hypothesis that spatial variation of the macrobenthos community structure can be largely attributed to a gradient from eutrophic to oligotrophic conditions in a freshwater ecosystem (Birk et al., 2020; Faghihinia et al., 2021). In addition, semivoltine and univoltine species were more common in Baiyangdian Lake than in the ecotones and the Fu River, which were lotic environments and were constantly disturbed by hydraulic exchanges. The semivoltine and univoltine macrobenthos require a longer period with a stable water environment to reach maturity and reproduce, whereas bi- or multivoltine species can reach maturity faster and maintain their populations despite constant disturbance (Weiher, 2011; Saito et al., 2015; Dolédec et al., 2021).

Our variance partitioning analysis results revealed that sediment heavy metals contributed more to the variation of functional diversity than to the variation of taxonomic diversity, which suggests that the functional diversity can serve as a good indicator for monitoring heavy metal pollution. In particular, the dominant trait modalities (burrower, no swimming ability, bi- or multivoltine life cycles) may be indicators of the effects of heavy metal pollution. Our results therefore provide information on the responses of functional traits to heavy metal pollution in river–lake ecotones. In addition, adult body size has been proven to be important in previous studies of the effects of heavy metal pollution on changes in macrobenthos functional traits (Gusmao et al., 2016; Odume, 2020; Dong et al., 2021). Adult body size is a direct and intuitive trait of macrobenthos (Edegbene et al., 2020; Odume, 2020) and is usually associated with environmental gradients. The present results indicated that a large adult body size (BS4) was a dominant trait state in areas with high sediment heavy metal contents (e.g., Cr, Pb, Zn, Cu, and Cd). These results support the common hypothesis that large adult body size

is a more prevalent functional trait than small or very small adult sizes in areas contaminated with heavy metals (Gusmao et al., 2016; Dong et al., 2021). This may be because of a higher content of organic matter with high concentrations of heavy metals (Zhang et al., 2014). Areas rich in organic matter may represent a large food resource and, therefore, may increase the potential for certain organisms that feed on organic detritus to grow and attain greater body size, despite any toxic effects from heavy metals (Ryu et al., 2011; Hu et al., 2019).

Management insights

Eutrophication and heavy metal contamination have attracted much attention in Baiyangdian Lake (Zhao et al., 2011; Ji et al., 2019a,b). Although ecotones between the Fu River and Baiyangdian Lake functioned as a water purification and pollution buffer, the contents of nutrients (i.e., *TN* and *TP*) and heavy metals in the ecotones were still high. In addition, the macrobenthos abundance and biomass in the two ecotones were extremely low compared with those in the adjacent river and lake. A current dredging project aims to reduce the load of endogenous pollution (heavy metals and nutrients) in the sediments and thereby improve water quality in Baiyangdian Lake (Li et al., 2021; Zhou et al., 2021). However, previous studies of other shallow lakes (Dąbkowski et al., 2016; Meng et al., 2018, 2020; Zou et al., 2019) showed that dredging can cause a significant reduction in the macrobenthos species richness, abundance, biomass, and taxonomic and functional diversity indices. These negative consequences could be due to the direct removal of macrobenthos in the sediment (Meng et al., 2018, 2021; Piló et al., 2019) combined with alterations of physical environmental conditions (e.g., water depth and turbidity), thereby making the environment less suitable for these organisms (Robinson et al., 2005; Meng et al., 2018). We therefore recommend that dredging be stopped until studies can be conducted to confirm that this activity will not adversely affect the macrobenthos community in the long term.

Our results show that macrobenthos taxonomic and functional diversity responded strongly to water depth, water transparency, *TN*, *TP*, and sediment heavy metals in the river–lake system. Therefore, we recommend that if dredging continues, managers define an appropriate dredging depth to protect the macrobenthos and maintain high water transparency, thereby mitigating the consequences for the macrobenthos community composition. Furthermore, most studies indicated that macrobenthos species richness, abundance, and taxonomic diversity can eventually recover after dredging, and may even surpass the pre-dredging levels during the recovery period (Aldridge, 2000; Dąbkowski et al., 2016; Zawal et al., 2016; Piló et al., 2019; Meng et al., 2021). Thus, it will be necessary to provide a recovery period to promote restoration of the macrobenthos taxonomic and functional diversity.

Conclusion

In this study, we investigated the spatial patterns of macrobenthos taxonomic and functional diversity along a river–lake gradient for a shallow lake in Northern China. We found that nutrient concentrations (i.e., *TN* and *TP*) in the river mouth and lake mouth were both lower than those in the adjacent river and lake. Cr, Cu, Pb, and Zn contents in the river mouth and lake mouth were generally lower than those in the river. These results indicated that the river–lake ecotones functioned as a water purification and pollution buffer. The macrobenthos abundance and biomass in the two ecotones (river mouth and lake mouth) were both lower than those in the river and lake. The highest values of three macrobenthos taxonomic diversity indices (Shannon–Wiener diversity, Simpson diversity, and Pielou evenness) occurred in the lake mouth, with the lowest in the river mouth; however, the differences between ecosystem types were only significant for Pielou evenness. Moreover, the highest macrobenthos functional evenness occurred in the lake mouth, whereas the lowest values of functional divergence and Rao's quadratic entropy index occurred in the river mouth. We also found that the first RLQ trait axis was significantly positively correlated with two physical variables (*H* and *SD*) and significantly negatively correlated with *TN* and *TP*. All heavy metals except for As were significantly negatively correlated with the first RLQ trait axis. Furthermore, the proportions of variation explained by the taxonomic and functional diversity were 66.8% and 77.6%, respectively, which reflect the combined effects of water environmental variables and sediment heavy metals. Overall, our results suggest that studies of macrobenthos functional diversity in ecotones will complement the information provided by classical taxonomic diversity indices, and can therefore provide useful data to support the management of river–lake systems. Because we combined samples from multiple dates in our analysis, it was not possible to test whether the environmental values and macrobenthos community varied over time. Improving our understanding of these variations will be an important area of future research. In addition, the macrobenthos are only one component of biodiversity. In future research, it will be important to sample other components of biodiversity, such as the plant and fish communities.

Data availability statement

The original contributions presented in this study are included in the article/**Supplementary material**, further inquiries can be directed to the corresponding author/s.

Author contributions

XF, DL, and LZ conducted the field sampling. XF and DL processed samples in the laboratory. XF and LZ analyzed and visualized the data. WY and XF wrote the first draft of this manuscript. WY obtained the funding. XL and LZ revised the manuscript. All authors conceived and designed the study.

Funding

This study was supported by the National Natural Science Foundation of China (no. 52079006), the National Key R&D Program of China (no. 2017YFC0404505), and the Beijing Advanced Innovation Program for Land Surface Science.

Acknowledgments

We would like to thank Geoffrey Hart for providing language help during the writing of this manuscript.

Conflict of interest

The authors declare that the research was conducted in the absence of any commercial or financial relationships that could be construed as a potential conflict of interest.

Publisher's note

Supplementary material

The Supplementary Material for this article can be found online at: https://www.frontiersin.org/articles/10.3389/fevo.2022.922539/full#supplementary-material

References

Akamagwuna, F. C., Odume, O. N., and Richoux, N. B. (2022). Exploring the community structure of Afrotropical macroinvertebrate traits and ecological preferences along an agricultural pollution gradient in the Kat River, Eastern Cape, South Africa. *Ecol. Indic.* 135:108570. doi: 10.1016/j.ecolind.2022.108570

Aldridge, D. C. (2000). The impacts of dredging and weed cutting on a population of freshwater mussels (Bivalvia: Unionidae). *Biol. Conserv.* 95, 247–257. doi: 10.1016/S0006-3207(00)00045-8

Allen, C. D., and Breshears, D. D. (1998). Drought-induced shift of a forest–woodland ecotone: Rapid landscape response to climate variation. *Proc. Natl. Acad. Sci. U.S.A.* 95, 14839–14842. doi: 10.1073/pnas.95.25.14839

Arenas-Sánchez, A., Dolédec, S., Vighi, M., and Rico, A. (2021). Effects of anthropogenic pollution and hydrological variation on macroinvertebrates in Mediterranean rivers: A case-study in the upper Tagus river basin (Spain). *Sci. Total Environ.* 766:144044. doi: 10.1016/j.scitotenv.2020.144044

Azrina, M. Z., Yap, C. K., Rahim Ismail, A., Ismail, A., and Tan, S. G. (2006). Anthropogenic impacts on the distribution and biodiversity of benthic macroinvertebrates and water quality of the Langat River, Peninsular Malaysia. *Ecotoxicol. Environ. Saf.* 64, 337–347. doi: 10.1016/j.ecoenv.2005.04.003

Baker, N. J., Pilotto, F., Haubrock, P. J., Beudert, B., and Haase, P. (2021). Multidecadal changes in functional diversity lag behind the recovery of taxonomic diversity. *Ecol. Evol.* 11, 17471–17484. doi: 10.1002/ece3.8381

Benjamini, Y., and Hochberg, Y. (1995). Controlling the false discovery rate: A practical and powerful approach to multiple testing. *J. R. Stat. Soc. Ser. B* 57, 289–300. doi: 10.1111/j.2517-6161.1995.tb02031.x

Birk, S., Chapman, D., Carvalho, L., Spears, B. M., Andersen, H. E., Argillier, C., et al. (2020). Impacts of multiple stressors on freshwater biota across spatial scales and ecosystems. *Nat. Ecol. Evol.* 4, 1060–1068. doi: 10.1038/s41559-020-1216-4

Botta-Dukát, Z. (2005). Rao's quadratic entropy as a measure of functional diversity based on multiple traits. *J. Veg. Sci.* 16, 533–540. doi: 10.1111/j.1654-1103.2005.tb02393.x

Braghin, L. S. M., Almeida, B. A., Amaral, D. C., Canella, T. F., Gimenez, B. C. G., and Bonecker, C. C. (2018). Effects of dams decrease zooplankton functional β−diversity in river-associated lakes. *Freshw. Biol.* 63, 721–730. doi: 10.1111/fwb.13117

Brumm, K. J., Daniel Hanks, R., Baldwin, R. F., and Peoples, B. K. (2021). Accounting for multiple dimensions of biodiversity to assess surrogate performance in a freshwater conservation prioritization. *Ecol. Indic.* 122:107320. doi: 10.1016/j.ecolind.2020.107320

Buffagni, A. (2021). The lentic and lotic characteristics of habitats determine the distribution of benthic macroinvertebrates in Mediterranean rivers. *Freshw. Biol.* 66, 13–34. doi: 10.1111/fwb.13596

Cadotte, M. W., Carscadden, K., and Mirotchnick, N. (2011). Beyond species: Functional diversity and the maintenance of ecological processes and services. *J. Appl. Ecol.* 48, 1079–1087. doi: 10.1111/j.1365-2664.2011.02048.x

Cai, Y. J., Zhang, Y., Wu, Z. S., Chen, Y. W., Xu, J., and Gong, Z. J. (2017). Composition, diversity, and environmental correlates of benthic macroinvertebrate communities in the five largest freshwater lakes of China. *Hydrobiologia* 788, 85–98. doi: 10.1007/s10750-016-2989-y

Chiasson, A., and Williams, C. (1999). *Protocols for assessing water quality and aquatic biodiversity using macroinvertebrates*. Lower Cove: Fundy Model Forest.

China Bureau of Environmental Protection [CBEP] (2002). *Methods for monitoring and analysis of water and wastewater*, 4th Edn. Beijing: China Environmental Science Press.

Coccia, C., Almeida, B. A., Green, A. J., Gutiérrez, A. B., and Carbonell, J. A. (2021). Functional diversity of macroinvertebrates as a tool to evaluate wetland restoration. *J. Appl. Ecol.* 58, 2999–3011. doi: 10.1111/1365-2664.14038

Dąbkowski, P., Buczyński, P., Zawal, A., Stêpień, E., Buczyńska, E., Stryjecki, R., et al. (2016). The impact of dredging of a small lowland river on water beetle fauna (Coleoptera). *J. Limnol.* 75, 472–487. doi: 10.4081/jlimnol.2016.1270

De Castro-Català, N., Dolédec, S., Kalogianni, E., Skoulikidis, N. T., Paunovic, M., Vasiljeviæ, B., et al. (2020). Unravelling the effects of multiple stressors on diatom and macroinvertebrate communities in European river basins using

structural and functional approaches. *Sci. Total Environ.* 742:140543. doi: 10.1016/j.scitotenv.2020.140543

Dolédec, S., Chessel, D., ter Braak, C. J. F., and Champely, S. (1996). Matching species traits to en- vironmental variables: A new three-table ordination method. *Environ. Ecol. Stat.* 3, 143–166. doi: 10.1007/BF02427859

Dolédec, S., Simon, L., Blemus, J., Rigal, A., Robin, J., and Mermillod-Blondin, F. (2021). Multiple stressors shape invertebrate assemblages and reduce their trophic niche: A case study in a regulated stream. *Sci. Total Environ.* 773:145061. doi: 10.1016/j.scitotenv.2021.145061

Dong, J. Y., Zhao, L., Sun, X., Hu, C., Wang, Y., Li, W. T., et al. (2021). Response of macrobenthic communities to heavy metal pollution in Laoshan Bay, China: A trait-based method. *Mar. Pollut. Bull.* 167:112292. doi: 10.1016/j.marpolbul.2021.112292

Dray, S., Choler, P., Dolédec, S., Peres-Neto, P. R., Thuiller, W., Pavoine, S., et al. (2014). Combining the fourth-corner and the RLQ methods for assessing trait responses to environmental variation. *Ecology* 95, 14–21. doi: 10.1890/13-0196.1

Edegbene, A. O., Arimoro, F. O., and Odume, O. N. (2020). Exploring the distribution patterns of macroinvertebrate signature traits and ecological preferences and their responses to urban and agricultural pollution in selected rivers in the Niger Delta ecoregion, Nigeria. *Aquat. Ecol.* 54, 553–573. doi: 10.1007/s10452-020-09759-9

Edegbene, A. O., Odume, O. N., Arimoro, F. O., and Keke, U. N. (2021). Identifying and classifying macroinvertebrate indicator signature traits and ecological preferences along urban pollution gradient in the Niger Delta. *Environ. Pollut.* 281:117076. doi: 10.1016/j.envpol.2021.117076

England, J., and Wilkes, M. A. (2018). Does river restoration work? Taxonomic and functional trajectories at two restoration schemes. *Sci. Total Environ.* 618, 961–970. doi: 10.1016/j.scitotenv.2017.09.014

Eriksen, T. E., Brittain, J. E., Søli, G., Jacobsen, D., Goethals, P., and Friberg, N. (2021). A global perspective on the application of riverine macroinvertebrates as biological indicators in Africa, South-Central America, Mexico and Southern Asia. *Ecol. Indic.* 126:107609. doi: 10.1016/j.ecolind.2021.107609

Espinoza-Toledo, A., Mendoza-Carranza, M., Castillo, M. M., Barba-Macías, E., and Capps, K. A. (2021). Taxonomic and functional responses of macroinvertebrates to riparian forest conversion in tropical streams. *Sci. Total Environ.* 757:143972. doi: 10.1016/j.scitotenv.2020.143972

Faghihinia, M., Xu, Y., Liu, D., and Wu, N. (2021). Freshwater biodiversity at different habitats: Research hotspots with persistent and emerging themes. *Ecol. Indic.* 129:107926. doi: 10.1016/j.ecolind.2021.107926

Feld, C. K., de Bello, F., and Dolédec, S. (2014). Biodiversity of traits and species both show weak responses to hydromorphological alteration in lowland river macroinvertebrates. *Freshw. Biol.* 59, 233–248. doi: 10.1111/fwb.12260

Gagic, V., Bartomeus, I., Jonsson, T., Taylor, A., Winqvist, C., Fischer, C., et al. (2015). Functional identity and diversity of animals predict ecosystem functioning better than species-based indices. *Proc. R. Soc. B Biol. Sci.* 282:20142620. doi: 10.1098/rspb.2014.2620

Gallardo, B., Gascón, S., Quintana, X., and Comín, F. A. (2011). How to choose a biodiversity indicator—redundancy and complementarity of biodiversity metrics in a freshwater ecosystem. *Ecol. Indic.* 11, 1177–1184. doi: 10.1016/j.ecolind.2010.12.019

Gascón, S., Boix, D., and Sala, J. (2009). Are different biodiversity metrics related to the same factors? A case study from Mediterranean wetlands. *Biol. Conserv.* 142, 2602–2612. doi: 10.1016/j.biocon.2009.06.008

Gonzalo, C., and Camargo, J. A. (2013). The impact of an industrial effluent on the water quality, submersed macrophytes and benthic macroinvertebrates in a dammed river of central Spain. *Chemosphere* 93, 1117–1124. doi: 10.1016/j.chemosphere.2013.06.032

Gosz, J. R. (1993). Ecotone hierarchies. *Ecol. Appl.* 3, 369–376. doi: 10.2307/1941905

Gusmao, J. B., Brauko, K. M., Eriksson, B. K., and Lana, P. C. (2016). Functional diversity of macrobenthic assemblages decreases in response to sewage discharges. *Ecol. Indic.* 66, 65–75. doi: 10.1016/j.ecolind.2016.01.003

Hébert, M. P., Beisner, B. E., and Maranger, R. (2016). A meta-analysis of zooplankton functional traits influencing ecosystem function. *Ecology* 97, 1069–1080. doi: 10.1890/15-1084.1

Heino, J., Mykrä, H., Hämäläinen, H., Aroviita, J., and Muotka, T. (2007). Responses of taxonomic distinctness and species diversity indices to anthropogenic impacts and natural environmental gradients in stream macroinvertebrates. *Freshw. Biol.* 52, 1846–1861. doi: 10.1111/j.1365-2427.2007.01801.x

Heino, J., Mykrä, H., and Kotanen, J. (2008). Weak relationships between landscape characteristics and multiple facets of stream macroinvertebrate biodiversity in a boreal drainage basin. *Landsc. Ecol.* 23, 417–426. doi: 10.1007/s10980-008-9199-6

Heino, J., and Tolonen, K. T. (2017). Ecological drivers of multiple facets of beta diversity in a lentic macroinvertebrate metacommunity. *Limnol. Oceanogr.* 62, 2431–2444. doi: 10.1002/lno.10577

Hillbricht-Ilkowska, A. (1999). Shallow lakes in lowland river systems: Role in transport and transformations of nutrients and in biological diversity. *Hydrobiologia* 408, 349–358. doi: 10.1007/978-94-017-2986-4_39

Holland, M. M. (1988). "SCOPE/MAB technical consultations on landscape boundaries. Report of a SCOPE/MAB workshop on ecotones," in *A new look at ecotones: Emerging international projects on landscape boundaries*, Vol. 17, eds F. di Castri, A. J. Hansen, and M. M. Holland (Paris: International Union of Biological Sciences), 47–106.

Hu, C. Y., Dong, J. Y., Gao, L. J., Yang, X. L., Wang, Z., and Zhang, X. M. (2019). Macrobenthos functional trait responses to heavy metal pollution gradients in a temperate lagoon. *Environ. Pollut.* 253, 1107–1116. doi: 10.1016/j.envpol.2019.06.117

Jakubik, B., Koperski, P., and Lewandowski, K. (2015). Diversity of mollusca in lowland river–lake system: Lentic versus lotic patches. *Pol. J. Ecol.* 62, 335–348. doi: 10.3161/104.062.0212

Ji, Z. H., Zhang, H., Zhang, Y., Chen, T., Long, Z. W., Li, M., et al. (2019a). Distribution, ecological risk and source identification of heavy metals in sediments from the Baiyangdian Lake, Northern China. *Chemosphere* 237:124425. doi: 10.1016/j.chemosphere.2019.124425

Ji, Z. H., Zhang, Y., Zhang, H., Huang, C. X., and Pei, Y. S. (2019b). Fraction spatial distributions and ecological risk assessment of heavy metals in the sediments of Baiyangdian Lake. *Ecotoxicol. Environ. Saf.* 174, 417–428. doi: 10.1016/j.ecoenv.2019.02.062

Juvigny-Khenafou, N. P. D., Piggott, J. J., Atkinson, D., Zhang, Y., Macaulay, S. J., Wu, N., et al. (2021). Impacts of multiple anthropogenic stressors on stream macroinvertebrate community composition and functional diversity. *Ecol. Evol.* 11, 133–152. doi: 10.1002/ece3.6979

Kleyer, M., Dray, S., Bello, F., Lepš, J., Pakeman, R. J., Strauss, B., et al. (2012). Assessing species and community functional responses to environmental gradients: Which multivariate methods? *J. Veg. Sci.* 23, 805–821. doi: 10.1111/j.1654-1103.2012.01402.x

Kolasa, J., and Zalewski, M. (1995). Notes on ecotone attributes and functions. *Hydrobiologia*. 303, 1–7. doi: 10.1007/BF00034039

Krebs, R. A., Prescott, T. J., Clapham, W. B., and Klarer, D. M. (2018). Freshwater mussel assemblages at the lotic-lentic interface along Lake Erie. *Am. Malacol. Bull.* 36, 31–41. doi: 10.4003/006.036.0104

Kuzmanovic, M., Dolédec, S., de Castro-Catala, N., Ginebreda, A., Sabater, S., Muñoz, I., et al. (2017). Environmental stressors as a driver of the trait composition of benthic macroinvertebrate assemblages in polluted Iberian rivers. *Environ. Res.* 156, 485–493. doi: 10.1016/j.envres.2017.03.054

Lento, J., Laske, S. M., Lavoie, I., Bogan, D., Brua, R. B., Campeau, S., et al. (2020). Diversity of diatoms, benthic macroinvertebrates, and fish varies in response to different environmental correlates in Arctic rivers across North America. *Freshw. Biol.* 67, 95–115. doi: 10.1111/fwb.13600

Li, D., Erickson, R. A., Tang, S., Zhang, Y., Niu, Z., Liu, H., et al. (2016). Structure and spatial patterns of macrobenthic community in Tai Lake, a large shallow lake, China. *Ecol. Indic.* 61, 179–187. doi: 10.1016/j.ecolind.2015.08.043

Li, X. X., Yang, W., Sun, T., and Su, L. Y. (2019a). Framework of multidimensional macrobenthos biodiversity to evaluate ecological restoration in wetlands. *Environ. Res. Lett.* 14:054003. doi: 10.1088/1748-9326/ab142c

Li, Z. F., Jiang, X. M., Wang, J., Meng, X. L., Heino, J., and Xie, Z. C. (2019b). Multiple facets of stream macroinvertebrate alpha diversity are driven by different ecological factors across an extensive altitudinal gradient. *Ecol. Evol.* 9, 1306–1322. doi: 10.1002/ece3.4841

Li, Z. F., Wang, J., Liu, Z. Y., Meng, X. L., Heino, J., Jiang, X. K., et al. (2019c). Different responses of taxonomic and functional structures of stream macroinvertebrate communities to local stressors and regional factors in a subtropical biodiversity hotspot. *Sci. Total Environ.* 655, 1288–1300. doi: 10.1016/j.scitotenv.2018.11.222

Li, Y. L., Lv, J. X., and Li, L. J. (2021). Coordinated development of water environment protection and water ecological carbon sink in Baiyangdian Lake. *Processes* 9:2066. doi: 10.3390/pr9112066

Li, Z. F., Liu, Z. Y., Heino, J., Jiang, X. M., Wang, J., Tang, T., et al. (2020). Discriminating the effects of local stressors from climatic factors and dispersal processes on multiple biodiversity dimensions of macroinvertebrate communities

across subtropical drainage basins. *Sci. Total Environ*. 711:134750. doi: 10.1016/j.scitotenv.2019.134750

Li, S. H., Sun, T., Yang, W., Cui, B. S., and Yin, X. A. (2020). A biodiversity evaluation framework for restoration of aquatic macrophyte communities in shallow lakes driven by hydrological process management. *Hydrol. Process.* 35:e13983. doi: 10.1002/hyp.13983

Liu, Y., Zhang, M., Peng, W. Q., Qu, X. D., Zhang, Y. H., Du, L. F., et al. (2021). Phylogenetic and functional diversity could be better indicators of macroinvertebrate community stability. *Ecol. Indic.* 129:107892. doi: 10.1016/j.ecolind.2021.107892

Liu, Y. Y., Zhang, W. Z., and Wang, Y. X. (1979). *China economic animal: Freshwater mollusks*. Beijing: Science Press.

Martello, F., De Bello, F., De Castro Morini, M. S., Silva, R. R., De Souza-Campana, D. R., Ribeiro, M. C., et al. (2018). Homogenization and impoverishment of taxonomic and functional diversity of ants in *Eucalyptus* plantations. *Sci. Rep*. 8:3266. doi: 10.1038/s41598-018-20823-1

Mason, N. W. H., Mouillot, D., Lee, W. G., and Wilson, J. B. (2005). Functional richness, functional evenness and functional divergence: The primary components of functional diversity. *Oikos* 111, 112–118. doi: 10.1111/j.0030-1299.2005.13886.x

Meng, X. L., Chen, J. J., Li, Z. F., Liu, Z. Y., Jiang, X. K., Ge, Y. H., et al. (2020). Degraded functional structure of macroinvertebrates caused by commercial sand dredging practices in a flood plain lake. *Environ. Pollut*. 263:114415. doi: 10.1016/j.envpol.2020.114415

Meng, X. L., Cooper, K. M., Liu, Z., Li, Z. Y., Chen, J. J., Jiang, X. K., et al. (2021). Integration of α, β and γ components of macroinvertebrate taxonomic and functional diversity to measure of impacts of commercial sand dredging. *Environ. Pollut.* 269:116059. doi: 10.1016/j.envpol.2020.116059

Meng, X. L., Jiang, X. M., Li, Z. F., Wang, J., Cooper, K. M., and Xie, Z. C. (2018). Responses of macroinvertebrates and local environment to short-term commercial sand dredging practices in a flood-plain lake. *Sci. Total Environ.* 631-632, 1350–1359. doi: 10.1016/j.scitotenv.2018.03.086

Morse, J. C., Yang, L., and Tian, L. (1984). *Aquatic insects of China useful for monitoring water quality*. Nanjing: Hohai University Press.

Mosbahi, N., Serbaji, M. M., Pezy, J. P., Neifar, L., and Dauvin, J. C. (2019). Response of benthic macrofauna to multiple anthropogenic pressures in the shallow coastal zone south of Sfax (Tunisia, central Mediterranean Sea). *Environ. Pollut.* 253, 474–487. doi: 10.1016/j.envpol.2019.06.080

Murcia, C. (1995). Edge effects in fragmented forests: Implications for conservation. *Trends Ecol. Evol.* 10, 58–62. doi: 10.1016/S0169-5347(00)88977-6

Obolewski, K., Glińska-Lewczuk, K., Jarząb, N., Burandt, P., Kobus, S., Kujawa, R., et al. (2014). Benthic invertebrates in floodplain lakes of a Polish River: Structure and biodiversity analyses in relation to hydrological conditions. *Pol. J. Environ. Stud*. 23, 1679–1689.

O'Brien, A., Townsend, K., Hale, R., Sharley, D., and Pettigrove, V. (2016). How is ecosystem health defined and measured? A critical review of freshwater and estuarine studies. *Ecol. Indic.* 69, 722–729. doi: 10.1016/j.ecolind.2016.05.004

Odum, E. P. (1971). *Fundamentals of ecology*, 3rd Edn. Philadelphie, PA: W.B. Saunders Company.

Odume, O. N. (2020). Searching for urban pollution signature and sensitive macroinvertebrate traits and ecological preferences in a river in the Eastern Cape of South Africa. *Ecol. Indic.* 108:105759. doi: 10.1016/j.ecolind.2019.105759

Patrick, C. J. (2014). Macroinvertebrate communities of ecotones between the boundaries of streams, wetlands, and lakes. *Fundam. Appl. Limnol.* 185, 223–233. doi: 10.1127/fal/2014/0645

Paz, L. E., Rodriguez, M., Gullo, B., and Rodrigues Capítulo, A. (2022). Impacts of urban and industrial pollution on functional traits of benthic macroinvertebrates: Are some traits advantageous for survival? *Sci. Total Environ*. 807:150650. doi: 10.1016/j.scitotenv.2021.150650

Peng, F. J., ter Braak, C. J. F., Rico, A., and Van den Brink, P. J. (2021). Double constrained ordination for assessing biological trait responses to multiple stressors: A case study with benthic macroinvertebrate communities. *Sci. Total Environ.* 754:142171. doi: 10.1016/j.scitotenv.2020.142171

Péru, N., and Dolédec, S. (2010). From compositional to functional biodiversity metrics in bioassessment: A case study using stream macroinvertebrate communities. *Ecol. Indic.* 10, 1025–1036. doi: 10.1016/j.ecolind.2010.02.011

Piló, D., Ben-Hamadou, R., Pereira, F., Carriço, A., Pereira, P., Corzo, A., et al. (2016). How functional traits of estuarine macrobenthic assemblages respond to metal contamination? *Ecol. Indic*. 71, 645–659. doi: 10.1016/j.ecolind.2016.07.019

Piló, D., Carvalho, A. N., Pereira, F., Coelho, H. E., and Gaspar, M. B. (2019). Evaluation of macrobenthic community responses to dredging through a multimetric approach: Effective or apparent recovery? *Ecol. Indic.* 96, 656–668. doi: 10.1016/j.ecolind.2018.08.064

Poznańska, M., Kobak, J., Wolnomiejski, N., and Kakareko, T. (2010). Macrozoobenthos communities from two types of land-water transition zones in a European lowland dam reservoir. *Fundam. Appl. Limnol.* 176, 115–126. doi: 10.1127/1863-9135/2010/0176-0115

Reynaga, M. C., and Dos Santos, D. A. (2013). Contrasting taxonomical and functional responses of stream invertebrates across space and time in a Neotropical basin. *Fundam. Appl. Limnol*. 183, 121–133. doi: 10.1127/1863-9135/2013/0501

Risser, P. G. (1995). The status of the science examining ecotones. *Bioscience* 45, 318–325. doi: 10.2307/1312492

Robinson, J. E., Newell, R. C., Seiderer, L. J., and Simpson, N. M. (2005). Impacts of aggregate dredging on sediment composition and associated benthic fauna at an offshore dredge site in the southern North Sea. *Mar. Environ. Res.* 60, 51–68. doi: 10.1016/j.marenvres.2004.09.001

Ryu, J., Khim, J. S., Kang, S. G., Kang, D., Lee, C. H., and Koh, C. H. (2011). The impact of heavy metal pollution gradients in sediments on benthic macrofauna at population and community levels. *Environ. Pollut*. 159, 2622–2629. doi: 10.1016/j.envpol.2011.05.034

Saito, V. S., Siqueira, T., and Fonseca-Gessner, A. A. (2015). Should phylogenetic and functional diversity metrics compose macroinvertebrate multimetric indices for stream biomonitoring? *Hydrobiologia* 745, 167–179. doi: 10.1007/s10750-014-2102-3

Salvo, J., Valdovinos, C., and Fierro, P. (2020). Benthic macroinvertebrate assemblages of a stream-lake network in the upper zone of the trans-Andean basin of the Valdivia River (Chile). *N. Z. J. Mar. Freshw. Res.* 55, 375–392. doi: 10.1080/00288330.2020.1784239

Schmera, D., Heino, J., Podani, J., Erõs, T., and Dolédec, S. (2017). Functional diversity: A review of methodology and current knowledge in freshwater macroinvertebrate research. *Hydrobiologia* 787, 27–44. doi: 10.1007/s10750-016-2974-5

Schriever, T. A., Bogan, M. T., Boersma, K. S., Cañedo-Argüelles, M., Jaeger, K. L., Olden, J. D., et al. (2015). Hydrology shapes taxonomic and functional structure of desert stream invertebrate communities. *Freshw. Sci.* 34, 399–409. doi: 10.1086/680518

Sivadas, S. K., Gupta, G. V. M., Kumar, S., and Ingole, B. S. (2021). Trait-based and taxonomic macrofauna community patterns in the upwelling ecosystem of the southeastern Arabian sea. *Mar. Environ. Res.* 170:105431. doi: 10.1016/j.marenvres.2021.105431

Soldner, M., Stephen, I., Ramos, L., Angus, R., Wells, N. C., Grosso, A., et al. (2004). Relationship between macroinvertebrate fauna and environmental variables in small streams of the Dominican Republic. *Water Res.* 38, 863–874. doi: 10.1016/S0043-1354(03)00406-8

Sotomayor, G., Hampel, H., Vázquez, R. F., Forio, M. A. E., and Goethals, P. L. M. (2021). Implications of macroinvertebrate taxonomic resolution for freshwater assessments using functional traits: The Paute River Basin (Ecuador) case. *Divers. Distrib*. 28, 1735–1747. doi: 10.1111/ddi.13418

Steneck, R. S., and Dethier, M. N. (1994). A functional group approach to the structure of algal-dominated communities. *Oikos* 69, 476–498. doi: 10.2307/3545860

Szkokan-Emilson, E. J., Wesolek, B. E., and Gunn, J. M. (2011). Terrestrial organic matter as subsidies that aid in the recovery of macroinvertebrates in industrially damaged lakes. *Ecol. Appl.* 21, 2082–2093. doi: 10.1890/10-1967.1

Tang, H. Q. (2006). *Biosystematic study on the chironomid larvae in China (Diptera: Chironomidae)*. TianJing: Nankai University, 945.

Tian, K., Yang, W., Zhao, Y. W., Yin, X. A., Cui, B. S., and Yang, Z. F. (2020). Development of a hydrological boundary method for the river–lake transition zone based on flow velocity gradients, and case study of Baiyangdian Lake transition zones, China. *Water* 12:674. doi: 10.3390/w12030674

Tolonen, K. T., Vilmi, A., Karjalainen, S. M., Hellsten, S., and Heino, J. (2017). Do different facets of littoral macroinvertebrate diversity show congruent patterns in a large lake system? *Commun. Ecol.* 18, 109–116. doi: 10.1556/168.2017.18.1.12

Tong, Y. (1996). *Fauna sinica: Hirudinea*. Beijing: Science Press.

Usseglio-Polatera, P., Bournaud, M., Richoux, P., and Tachet, H. (2000). Biological and ecological traits of benthic freshwater macroinvertebrates relationships and definition of groups with similar traits. *Freshw. Biol*. 43, 175–205. doi: 10.1046/j.1365-2427.2000.00535.x

Van De Meutter, F., Stoks, R., and De Meester, L. (2006). Rapid response of macroinvertebrates to drainage management of shallow connected lakes. *J. Appl. Ecol.* 43, 51–60. doi: 10.1111/j.1365-2664.2005.01115.x

Villéger, S., Mason, N. W. H., and Mouillot, D. (2008). New multidimensional functional diversity indices for a multifaceted framework in functional ecology. *Ecology* 89, 2290–2301. doi: 10.1890/07-1206.1

Violle, C., Navas, M.-L., Vile, D., Kazakou, E., Fortunel, C., Hummel, I., et al. (2007). Let the concept of trait be functional! *Oikos* 116, 882–892. doi: 10.1111/j.2007.0030-1299.15559.x

Wang, H. Z. (2002). *Studies on taxonomy, distribution and ecology of microdrile oligochaetes of China, with descriptions of two new species from the vicinity of the great wall station of China, Antarctica*. Beijing: Higher Education Press.

Ward, J. V., and Tockner, K. (2001). Biodiversity: Towards a unifying theme for river ecology. *Freshw. Biol.* 46, 807–819. doi: 10.1046/j.1365-2427.2001.00713.x

Weiher, E. (2011). "A primer of trait and functional diversity," in *Biological diversity: Frontiers in measurement and assessment*, eds A. E. Magurran and B. J. McGill (Oxford: Oxford University Press), 175–193.

Willis, T. V., and Magnuson, J. J. (2000). Patterns in fish species composition across the interface between streams and lakes. *Can. J. Fish. Aquat. Sci.* 57, 1042–1052. doi: 10.1139/cjfas-57-5-1042

Wilsey, B. J., Chalcraft, D. R., Bowles, C. M., and Willig, M. R. (2005). Relationships among indices suggest that richness is an incomplete surrogate for grassland biodiversity. *Ecology* 86, 1178–1184. doi: 10.1890/04-0394

Winterbourn, M. J. (1971). The life histories and trophic relationships of the trichoptera of Marion Lake, British Columbia. *Can. J. Zool.* 49, 623–635. doi: 10.1139/z71-100

Wu, H. P., Chen, J., Xu, J. J., Zeng, G. M., Sang, L. H., Liu, Q., et al. (2019). Effects of dam construction on biodiversity: A review. *J. Clean. Prod.* 221, 480–489. doi: 10.1016/j.jclepro.2019.03.001

Yang, Y. F., Yi, Y. J., Zhou, Y., Wang, X., Zhang, S. H., and Yang, Z. F. (2020). Spatio-temporal variations of benthic macroinvertebrates and the driving environmental variables in a shallow lake. *Ecol. Indic.* 110:105948. doi: 10.1016/j.ecolind.2019.105948

Yi, Y. J., Sun, J., Yang, Y. F., Zhou, Y., Tang, C. H., Wang, X., et al. (2018). Habitat suitability evaluation of a benthic macroinvertebrate community in a shallow lake. *Ecol. Indic.* 90, 451–459. doi: 10.1016/j.ecolind.2018.03.039

Zawal, A., Czachorowski, S., Stępień, E., Buczyńska, E., Szlauer-Łukaszewska, A., Buczyński, P., et al. (2016). Early post-dredging recolonization of caddisflies (Insecta: Trichoptera) in a small lowland river (NW Poland). *Limnology* 17, 71–85. doi: 10.1007/s10201-015-0466-3

Zhang, C., Shan, B. Q., Zhao, Y., Song, Z. X., and Tang, W. Z. (2018). Spatial distribution, fractionation, toxicity and risk assessment of surface sediments from the Baiyangdian Lake in Northern China. *Ecol. Indic.* 90, 633–642. doi: 10.1016/j.ecolind.2018.03.078

Zhang, C., Yu, Z. G., Zeng, G. M., Jiang, M., Yang, Z. Z., Cui, F., et al. (2014). Effects of sediment geochemical properties on heavy metal bioavailability. *Environ. Int.* 73, 270–281. doi: 10.1016/j.envint.2014.08.010

Zhang, C., Zhu, R., Sui, X. Y., Li, X. Q., and Chen, Y. F. (2021). Understanding patterns of taxonomic diversity, functional diversity, and ecological drivers of fish fauna in the Mekong River. *Glob. Ecol. Conserv.* 28:e01711. doi: 10.1016/j.gecco.2021.e01711

Zhang, W. L., Zhu, M. J., Li, Y., Wang, C., Qian, B., Niu, L. H., et al. (2020). How fluvial inputs directly and indirectly affect the ecological status of different lake regions: A bio-assessment framework. *J. Hydrol.* 582:124502. doi: 10.1016/j.jhydrol.2019.124502

Zhang, Y., Cheng, L., Li, K. Y., Zhang, L., Cai, Y. J., Wang, X. L., et al. (2019). Nutrient enrichment homogenizes taxonomic and functional diversity of benthic macroinvertebrate assemblages in shallow lakes. *Limnol. Oceanogr.* 64, 1047–1058. doi: 10.1002/lno.11096

Zhao, Y., Xia, X. H., Yang, Z. F., and Xia, N. (2011). Temporal and spatial variations of nutrients in Baiyangdian Lake, North China. *J. Environ. Inf.* 17, 102–108. doi: 10.3808/jei.201100192

Zhou, H., Zhang, W. J., Li, L. Q., Zhang, M. Y., and Wang, D. S. (2021). Environmental impact and optimization of lake dredged-sludge treatment and disposal technologies based on life cycle assessment (LCA) analysis. *Sci. Total Environ.* 787:147703. doi: 10.1016/j.scitotenv.2021.147703

Zou, W., Tolonen, K. T., Zhu, G. W., Qin, B. Q., Zhang, Y. N., Cao, Z. G., et al. (2019). Catastrophic effects of sand mining on macroinvertebrates in a large shallow lake with implications for management. *Sci. Total Environ.* 695:133706. doi: 10.1016/j.scitotenv.2019.133706

frontiers | Frontiers in Earth Science

TYPE Original Research
PUBLISHED 11 August 2022
DOI 10.3389/feart.2022.953805

OPEN ACCESS

EDITED BY
Qiang Liu,
Beijing Normal University, China

REVIEWED BY
Pengnian Huang,
Nanjing University of Information Science and Technology, China
Baoqing Zhang,
Lanzhou University, China

*CORRESPONDENCE
Haiyun Shi,
shihy@sustech.edu.cn

SPECIALTY SECTION
This article was submitted to Hydrosphere, a section of the journal Frontiers in Earth Science

RECEIVED 26 May 2022
ACCEPTED 11 July 2022
PUBLISHED 11 August 2022

CITATION
Zhou Z, Ding Y, Fu Q, Wang C, Wang Y, Cai H, Liu S and Shi H (2022), Comprehensive evaluation of vegetation responses to meteorological drought from both linear and nonlinear perspectives.
Front. Earth Sci. 10:953805.
doi: 10.3389/feart.2022.953805

Comprehensive evaluation of vegetation responses to meteorological drought from both linear and nonlinear perspectives

Zhaoqiang Zhou[1,2], Yibo Ding[3], Qiang Fu[4], Can Wang[1,2], Yao Wang[1,2], Hejiang Cai[1,2,5], Suning Liu[6] and Haiyun Shi[1,2]*

[1]State Environmental Protection Key Laboratory of Integrated Surface Water-Groundwater Pollution Control, School of Environmental Science and Engineering, Southern University of Science and Technology, Shenzhen, Guangdong, China, [2]Guangdong Provincial Key Laboratory of Soil and Groundwater Pollution Control, School of Environmental Science and Engineering, Southern University of Science and Technology, Shenzhen, Guangdong, China, [3]Yellow River Engineering Consulting Co., Ltd., Zhengzhou, China, [4]School of Water Conservancy and Civil Engineering, Northeast Agricultural University, Harbin, China, [5]Department of Civil and Environmental Engineering, National University of Singapore, Singapore, Singapore, [6]Center for Climate Physics, Institute for Basic Science, Daejeon, South Korea

The frequent occurrence of drought events in recent years has caused significant changes in plant biodiversity. Understanding vegetation dynamics and their responses to climate change is of great significance to reveal the behaviour mechanism of terrestrial ecosystems. In this study, NDVI and SIF were used to evaluate the dynamic changes of vegetation in the Pearl River Basin (PRB). The relationship between vegetation and meteorological drought in the PRB was evaluated from both linear and nonlinear perspectives, and the difference of vegetation response to meteorological drought in different land types was revealed. Cross wavelet analysis was used to explore the teleconnection factors (e.g., large-scale climate patterns and solar activity) that may affect the relationship between meteorological drought and vegetation dynamics. The results show that 1) from 2001 to 2019, the vegetation cover and photosynthetic capacity of the PRB both showed increasing trends, with changing rates of 0.055/10a and 0.036/10a, respectively; 2) compared with NDVI, the relationship between SIF and meteorological drought was closer; 3) the vegetation response time (VRT) obtained based on NDVI was mainly 4–5 months, which was slightly longer than that based on SIF (mainly 3–4 months); 4) the VRT of woody vegetation (mainly 3–4 months) was longer than that of herbaceous vegetation (mainly 4–5 months); and 5) vegetation had significant positive correlations with the El Niño Southern Oscillation (ENSO) and sunspots but a significant negative correlation with the Pacific Decadal Oscillation (PDO). Compared with sunspots, the ENSO and the PDO were more closely related to the response relationship between meteorological drought and vegetation. The outcomes of this study can help reveal the relationship between vegetation dynamics and climate change under the background of global warming and provide a new perspective for studying the relationship between drought and vegetation.

KEYWORDS

meteorological drought, normalized difference vegetation index, solar-induced chlorophyll fluorescence, vegetation response time, linear, nonlinear

1 Introduction

In the context of global warming, the frequency and intensity of droughts will increase (Wang et al., 2021). In many parts of an increasingly globalized world, drought can have devastating agricultural, environmental, and socio-economic impacts (Shi H.Y. et al., 2018; Zhou et al., 2020a; Xu et al., 2020). Therefore, monitoring the impacts of drought on vegetation health will be increasingly important for agricultural production, ecological restoration and water resource planning and management.

Drought is very difficult to observe, and the definition of drought is inconsistent due to different application needs. In general, drought can be divided into four types, i.e., meteorological drought, hydrological drought, agricultural drought, and socio-economic drought (Zhou et al., 2021a). Meteorological drought is usually defined as a long-term shortage of precipitation in an area. Since it is difficult to monitor the onset and termination of drought, many scholars have developed drought indices to evaluate drought characteristics. For example, Shahabfar and Eitzinger (2013) evaluated the temporal and spatial changes in meteorological drought in Iran by using six meteorological drought indices. Rahmat et al. (2015) evaluated meteorological drought characteristics in Australia by using the standardized precipitation index (SPI) and the reconnaissance drought index (RDI). Fu et al. (2018) evaluated the spatiotemporal variation characteristics of meteorological drought in Northeast China by using the SPI. Zhou et al. (2020a) used the standardized precipitation evapotranspiration index (SPEI) to evaluate the relationship between meteorological drought characteristics and maize yield in Northeast China.

Understanding how vegetation responds to drought is a challenge because the effects of drought on vegetation growth are not immediate and linear. Normally, the time required for vegetation to respond to drought is called the vegetation response time (VRT). Previous studies have shown that there is a lag in the response between vegetation and drought (Jiao et al., 2019; Zhao et al., 2020; Zhong et al., 2021). In addition, many studies have demonstrated that there is a nonlinear relationship between drought and vegetation. For instance, Hu et al. (2021) studied the nonlinear changes in climate change, vegetation growth and the coupling between vegetation growth and precipitation during 1982–2015 and showed that the nonlinear response between vegetation and drought became more obvious with the aggravation of drought. Xu et al. (2021) found that differences in vegetation types and their adaptation and vulnerability to drought led to nonlinear responses of vegetation to drought. Ji et al. (2021) found that there was an obvious nonlinear response between the vegetation growing season and drought. Although previous studies on drought have shown the effectiveness of satellite data, they still have inherent limitations in drought monitoring and assessment. Reflectance-based vegetation indices, e.g., the normalized difference vegetation index (NDVI) and the enhanced vegetation index (EVI), have been widely used in dynamic vegetation monitoring (Zhao et al., 2020; Zhou et al., 2020b; De Souza et al., 2022; Li et al., 2022; Yang et al., 2022). When water stress occurs, the spectral characteristics of the vegetation canopy do not change immediately, so the response of vegetation to drought is obviously delayed (Dobrowski et al., 2005). Solar-induced chlorophyll fluorescence (SIF) is different from the traditional vegetation reflectance index and provides an alternative method for global vegetation spatial monitoring. SIF is directly related to photosynthesis of vegetation and may reflect the rapid change in canopy water stress. Recent studies have successfully extracted high-precision global time series of SIF from satellite observations (Li and Xiao, 2019).

The Pearl River Basin (PRB), which is of great significance for socio-economic development of China, has become the major source of carbon dioxide emissions in China (Zhang et al., 2015). As the PRB is located in a humid area, it has a complex vegetation ecosystem, which is of great significance for local biological carbon sequestration to partially offset fossil fuel emissions (Zhou and Zhou, 2021). However, Deng et al. (2018) showed that both drought frequency and severity increased in the PRB, which might weaken the absorption of carbon by vegetation. Therefore, this study evaluated the vegetation changes in the PRB based on NDVI and SIF and assessed the responses of vegetation to meteorological drought from both linear and nonlinear perspectives. The differences in the two indices (NDVI and SIF) in evaluating the relationship between drought and vegetation were compared. Moreover, this study analysed the teleconnection factors that might influence the response relationship between meteorological drought and vegetation. The objectives of this study are to 1) evaluate the dynamic changes in vegetation in the PRB, 2) evaluate the VRT of different vegetation types from both linear and nonlinear perspectives, 3) explore the differences between SIF and NDVI responses to meteorological drought and 4) explore the factors that may influence the relationship between vegetation and drought. The outcomes of this study can help reveal the relationship between vegetation dynamics and climate change under the background of global warming and provide a new perspective for studying the relationship between drought and vegetation. In addition, studying the responses of vegetation to drought at different time scales can aid in identifying ecosystems that are vulnerable to meteorological drought, which can provide a basis for drought mitigation and land planning.

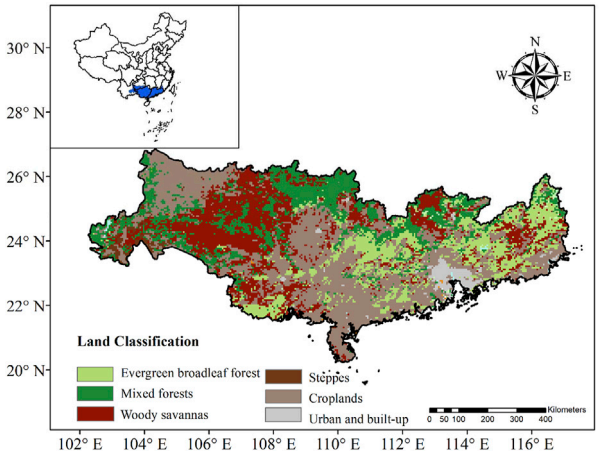

FIGURE 1
The land cover types of the Pearl River Basin (PRB) in China.

2 Study area and data sources

2.1 Study area

The PRB is located in the tropical and subtropical climate zone of South China (Figure 1). The PRB is the third largest river basin in terms of drainage area and the second largest river in terms of streamflow in China. Water resources in the PRB are relatively abundant. However, precipitation is unevenly distributed in both space and time, which is mainly distributed in the wet season (i.e., from April to September) and accounts for about 80% of the annual total. Therefore, drought and flood events occur frequently in the PRB. The land cover types in the PRB mainly include evergreen broadleaf forest (EBF), mixed forest (MF), cropland (CP) and woody savannas (WS) (see Figure 1).

2.2 Data sources

The precipitation data (2001–2019) used to calculate the SPI are derived from the ERA-5 Land Reanalysis Dataset provided by the European Center for Medium Range Weather Forecasts (ECMWF), with a spatial resolution of 0.1° and a temporal resolution of 1°month. Several studies have evaluated the applicability of ERA-5 Land Reanalysis precipitation data in China. Jiang et al. (2021) compared the ERA-5 reanalysis precipitation data and the precipitation data of satellites and observation stations in mainland China. They found that the spatial patterns of annual precipitation were consistent with the gauge observations, and ERA-5 reanalysis precipitation data performs better than other satellites products (e.g., Tropical Rainfall Measurement Mission and Climate Prediction Center Morphing technique bias-corrected product). Xu et al. (2022) showed that the spatial patterns of annual precipitation of ERA-5-Land and ERA-5 in mainland China were similar, but their statistical indicators (e.g., correlation coefficient, root mean square error, probability of detection, and false alarm ratio) of ERA-5-Land reanalysis precipitation data were superior to ERA-5. Xin et al. (2021) explored the applicability of ERA-5-Land reanalysis data in the Greater Bay Area based on precipitation, and the results showed that ERA-5-Land reanalysis precipitation data could better describe the spatial distribution and temporal variation trend of monthly precipitation. Zhang et al. (2021) showed that although ERA-5 reanalysis precipitation data overestimated precipitation, it had high simulation accuracy in the monitoring of drought and heat wave events in South China. Zhou et al. (2021a) showed that the meteorological drought events based on ERA-5-Land reanalysis precipitation data were basically consistent with the historical observed drought events, and could well represent the drought events in the PRB. Therefore, ERA-5-Land reanalysis precipitation data was selected in this study.

Both the NDVI and land use data were derived from the Model Resolution Imaging Spectroradiometer (MODIS). The NDVI product (MOD13C2) has a spatial resolution of 0.05° and a temporal resolution of 1 month, while the land cover type product (MCD12C1) has a spatial resolution of 0.05°. In this study, the MCD12C1 product in 2019 was selected to classify different land use types without considering the land cover change during the study period. Combining the Orbiting Carbon Observatory (OCO-2) SIF with machine learning and other higher resolution data, Li and Xiao (2019) constructed the global OCO-2 SIF (GOSIF) dataset. For this dataset, the spatial resolution is 0.05°, and the time resolution is 1 month. To match data with different spatial resolutions, this study resampled both the NDVI and SIF to 0.1°. The 0.1° land cover data were derived from the 0.05° land cover map based on the main land cover types in the 0.05° pixels in each 0.1° grid cell (Zhou et al., 2022). Moreover, this study analysed the effects of large-scale circulation patterns and solar activity on vegetation in the PRB. The monthly El Niño Southern Oscillation (ENSO) and the Pacific Decadal Oscillation (PDO) data are provided by the National Oceanic and Atmospheric Administration. The monthly sunspot data are provided by the International Council of Scientific Unions (ICSU) world data system (WDS).

3 Methodology

3.1 Drought indices

In recent decades, an increasing number of drought indicators have been developed to meet different application needs. This study chose the SPI to represent meteorological drought. The SPI is a widely used drought index

recommended by the World Meteorological Organization. It is widely used in drought monitoring and impact assessment (Fu et al., 2018; Fang et al., 2020; Shi et al., 2022). The main advantages of SPI include low data requirements, simple calculation, time and space comparability and multi scalar characteristics, which can study the impacts of drought at different time scales (Patel et al., 2007; Fang et al., 2019, 2020; Zhou et al., 2021a). The main purpose of this study is to explore the relationship between meteorological drought and vegetation. Drought indices at multiple time scales are useful for evaluating vegetation responses to short-, medium-, and long-term drought. Therefore, the SPI was chosen to represent meteorological drought in this study. The SPI series over cumulation periods varying from 1 to 12°months were calculated to access the vegetation responses to meteorological drought. For the specific calculation process, please refer to McKee et al. (1993) and Fu et al. (2018).

3.2 Trend analysis method

In this study, Mann-Kendall trend analysis method and Sen's slope method were used to analyze the changes of vegetation. These two methods are usually used together to evaluate the variation characteristics of hydrometeorological time series (Fu et al., 2018; Zhou et al., 2020a; Zhou et al., 2021a). Mann-Kendall trend analysis method can be used to evaluate the change trend and significance of time series, and Sen's slope method is usually used to evaluate the change magnitude of time series. The specific calculation process of SPI can be found in the studies of Fu et al. (2018).

3.3 Pearson correlation coefficient(PCC)

The PCC has been widely used to test the linear correlation between two random variables. The use of the PCC requires the basic assumption that the random variables under investigation are linearly dependent. In this study, the PCC was used to calculate the correlation coefficients between meteorological drought (SPI1-SPI12) and vegetation (NDVI and SIF). The specific calculation process is shown as follows:

$$R_{N,i} = corr\left(NDVI, SPI_i\right),\ i = 1,\ 2,\ \ldots,\ 12 \tag{1}$$

$$R_{S,i} = corr\left(SIF, SPI_i\right),\ i = 1,\ 2,\ \ldots,\ 12 \tag{2}$$

where $R_{N,i}$ and $R_{S,i}$ represent the PCC between NDVI/SIF and SPI, i is the accumulated time from one-month to twelve-month SPI (SPI1-SPI12). The time scale of meteorological drought (e.g., i) corresponding to the maximum PCC (MPCC) was considered as the VRT.

$$MPCC_N = \max\left\{R_{N,i}\right\},\ i = 1,\ 2,\ \ldots,\ 12 \tag{3}$$

$$MPCC_S = \max\left\{R_{S,i}\right\},\ i = 1,\ 2,\ \ldots,\ 12 \tag{4}$$

3.4 Directed information transfer index

The assumption of linear correlation is often challenged in hydrological systems. Due to the effects of climate change and human activities, there is not only a linear relationship but also a nonlinear relationship between vegetation and meteorological drought (Papagiannopoulou et al., 2017; Hu et al., 2021). Ignoring the nonlinear relationship between meteorological drought and vegetation may not obtain the accurate VRT. The limitations of linear correlation analysis have driven the development of another dependency measure. Mutual information is an important method in information theory and is commonly used to test the nonlinear relationship between two sequences (Shi B. et al., 2018; Fang et al., 2020). The DITI is used to represent the directional information transfer quantity of a specific information source by information entropy based on mutual information and is used to characterize the relationship between the information source and information function points (Zhou et al., 2021b). In this study, meteorological drought and vegetation change were taken as the information source and the information function point, respectively. The accumulation period of the SPI corresponding to the maximum value of the DITI is taken as the VRT from a nonlinear perspective.

For two time series X and Y, their domain of definition is S. The information entropy of X and Y can be defined as follows:

$$H\left(X\right) = -\sum_{i=1}^{n} f_X\left(x\right)\log f_X\left(x\right) \tag{5}$$

$$H\left(Y\right) = -\sum_{i=1}^{n} f_Y\left(y\right)\log f_Y\left(y\right) \tag{6}$$

where $f_X(x)$ and $f_Y(y)$ are the marginal distributions of X and Y, respectively.

Mutual information (MI) can be defined as follows:

$$I\left(X;Y\right) = \int\int_S f_{X,Y}\left(x,y\right)\log\frac{f_{X,Y}\left(x,y\right)}{f_X\left(x\right)f_Y\left(y\right)}dxdy \tag{7}$$

where $f_{X,Y}\ (x,\ y)$ is the joint distribution of X and Y.

Therefore, the DITI from information source X to information function point Y can be defined as follows:

$$DITI\left(X;Y\right) = \frac{I\left(X;Y\right)}{H\left(Y\right)} \tag{8}$$

3.5 Cross wavelet transform

XWT is an effective tool to study the correlation between two correlation time series. It combines wavelet transform and cross spectrum analysis, which can show the correlation between two time series in the time domain (Han et al., 2019; Zhou et al., 2021a). In this study, XWT is used to analyse the relationship

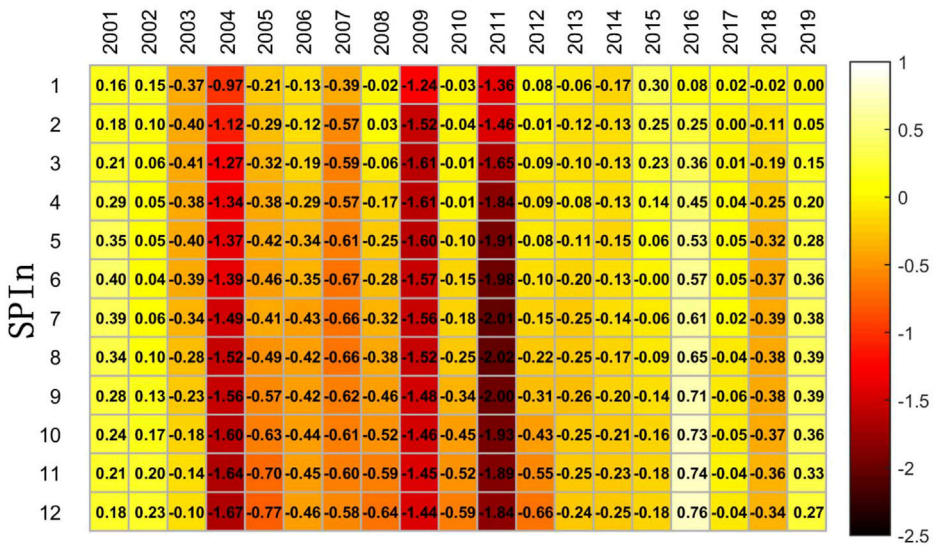

FIGURE 2
The changing characteristics of meteorological drought (SPI1-SPI12) in the PRB.

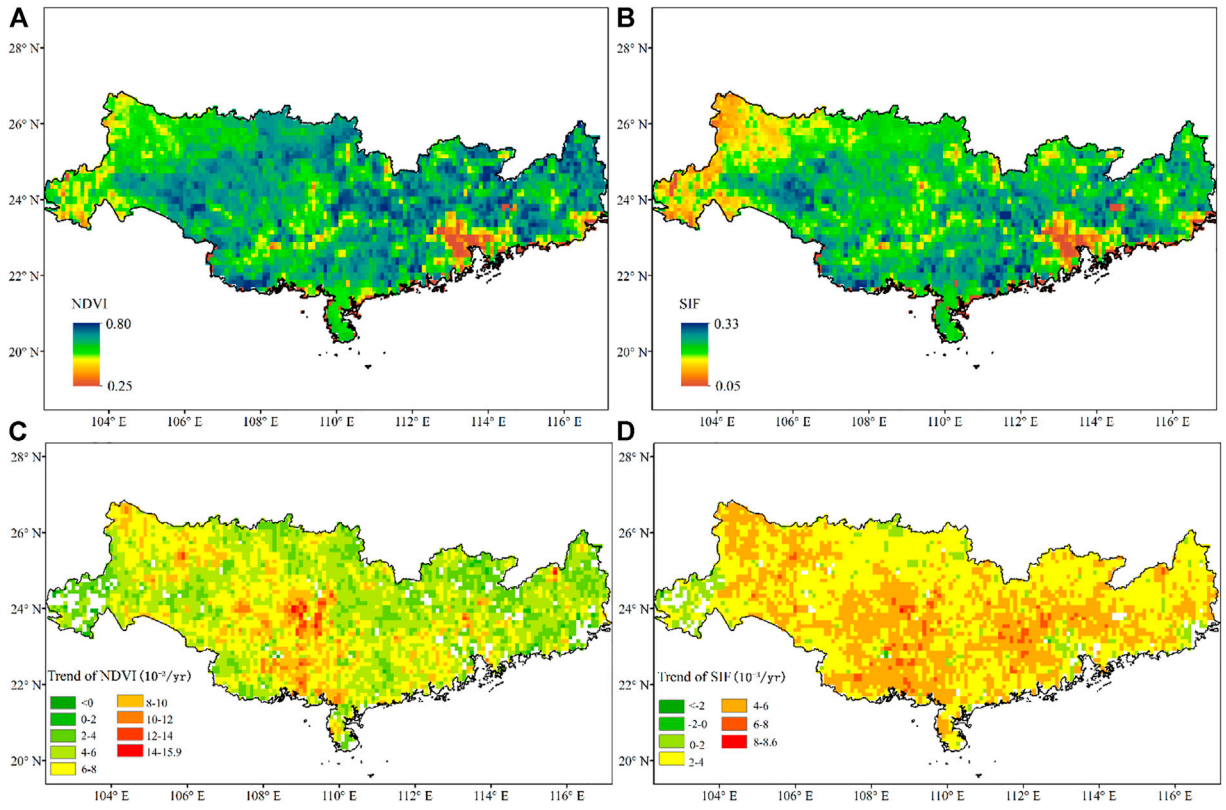

FIGURE 3
Spatial distributions of annual mean **(A)** NDVI and **(B)** SIF and trend in **(C)** NDVI and **(D)** SIF in the PRB from 2001 to 2019.

between vegetation and drought. Moreover, XWT is also used to explore the relationship between large-scale climatic patterns (ENSO and PDO) and solar activity (sunspot) and vegetation. For two time series x(t) and y(t), the cross wavelet power spectrum can be defined as follows:

$$W_{XY}(a,\tau) = C_X(a,\tau)C_Y^*(a,\tau) \quad (9)$$

where $C_X(a,\tau)$ is the wavelet transform coefficient of $x(t)$ and $C_Y^*(a,\tau)$ is the complex conjugate of the wavelet transform coefficient of $y(t)$. The codes are available at https://noc.ac.uk/using-science/crosswaveletwavelet-coherence.

4 Results

4.1 Spatiotemporal variations in meteorological drought and vegetation

Figure 2 shows the variation characteristics of meteorological drought at different time scales. Known from Figure 2, severe drought events occurred in 2004, 2007, 2009, and 2011. Drought statistics of the Pearl River Water Resources Commission (https://www.pearlwater.gov.cn/xxcx/szygg) showed that, in 2003, 2004, 2007, 2009, and 2010, severe drought events occurred in the PRB, and our research results are basically consistent with them.

Figures 3A,B shows the spatial distributions of the annual mean NDVI and SIF in the PRB from 2001 to 2019. The spatial distribution characteristics of vegetation cover and photosynthetic capacity in the PRB were similar, with low spatial characteristics in the west and high spatial characteristics in the east. The western PRB has a higher elevation and is dominated by karst topography. Compared with the central and eastern plain regions, the vegetation coverage and photosynthetic capacity were lower. In particular, compared with the vegetation coverage and photosynthetic capacity in the western PRB, the vegetation coverage and photosynthetic capacity in the Guangdong-Hong Kong-Macao Greater Bay Area were lower, which may be due to the rapid economic development, rapid urbanization and human activities affecting the change in vegetation. Figures 3C,D shows the spatial distributions of the trend of NDVI and SIF in the PRB from 2001 to 2019 after performing a 95% significance test. Known from Figure 3A that the change trend of NDVI in the middle of the PRB was relatively large, and only 4.6% of the regions do not exceed the significance test. In the regions exceeding the significance test, the NDVI of 99.87% of the PRB showed an increasing trend, and that of 0.13% of the PRB showed a decreasing trend. The maximum and minimum trends were $15.9*10^{-3}$/yr and $-4.8*10^{-3}$/yr, respectively. For the trend of SIF, only 2.2% of the regions do not exceed the significance test. In the regions exceeding the significance test, the SIF of 99.85% of the PRB showed an increasing trend, and that of 0.15% of the PRB showed a decreasing trend. The maximum and minimum trends were $8.6*10^{-3}$/yr and $-2.7*10^{-3}$/yr, respectively.

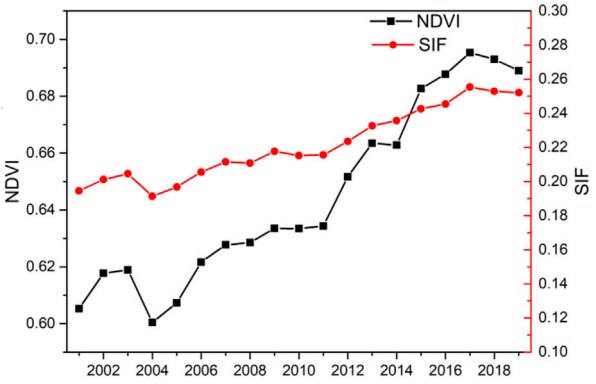

FIGURE 4
Trends in annual vegetation cover and photosynthetic capacity in the PRB from 2001 to 2019.

Figure 4 shows the trends of annual vegetation cover and photosynthetic capacity in the PRB from 2001 to 2019. As shown in Figure 4, the NDVI showed a slow increasing trend from 2001 to 2019, with a change rate of 0.055/10a. The maximum NDVI value (0.69) appeared in 2017, the minimum NDVI value (0.60) appeared in 2004, and the annual average value of NDVI was 0.64. The SIF also showed a slow increasing trend from 2001 to 2019, with a change rate of 0.036/10a. The maximum SIF value (0.26) appeared in 2017, the minimum SIF value (0.19) appeared in 2004, and the annual average value of SIF was 0.22. In general, the vegetation cover and photosynthetic capacity of the PRB showed an increasing trend from 2001 to 2019.

It is worth noting that both NDVI and SIF have shown increasing trends since 2011. Due to the severe drought events in 2009 and 2011, the annual precipitation was less than 1,200 mm, so the continuous recovery of precipitation since 2011 led to the rapid growth of vegetation. However, the increase of NDVI was much larger than that of SIF, which might be caused by the seasonal characteristics of NDVI and SIF. Solar radiation has obvious seasonal characteristics, increasing in spring and summer and decreasing in autumn and winter. SIF represents the photosynthetic capacity of vegetation, and thus, is closely related to solar radiation (Ma et al., 2020) and also has similar seasonal characteristics (Liu et al., 2019; Wu et al., 2021). The study of Jeong et al. (2017) showed that the phenological time determined based on NDVI was longer than that based on SIF, and the change of vegetation greenness may be decoupled from seasonality. Xie et al. (2016) showed that the air temperature in the PRB showed an increasing trend. The increase of temperature in winter and spring will lead to an earlier onset of greenness, while the increase of temperature in autumn will delay the decrease of greenness (Jeong et al., 2011). This may result in a

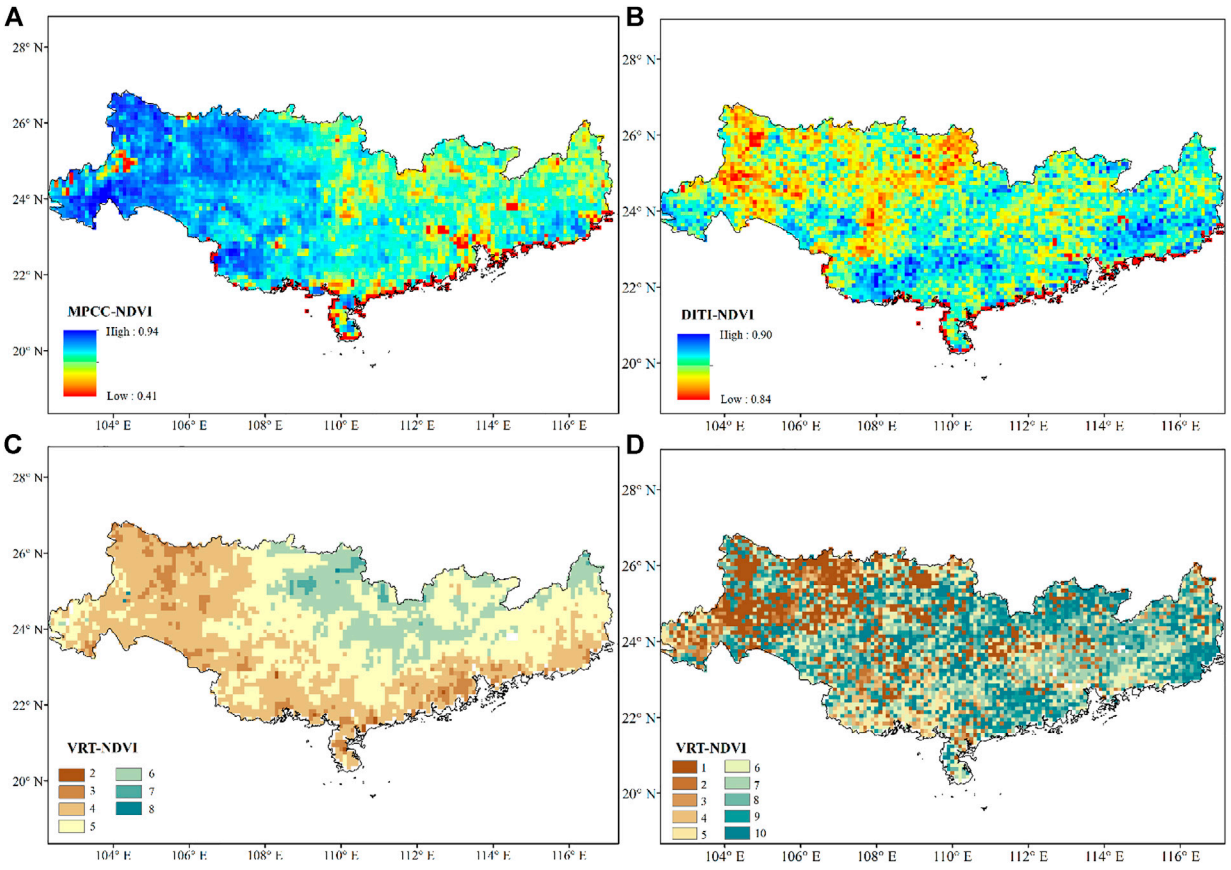

FIGURE 5
Spatial distributions of the MPCC **(A)** and the DITI **(B)** and corresponding VRT **(C,D)** are based on the NDVI.

high level of vegetation greenness variation in the inter-annual variation. Therefore, the increase of NDVI was greater than that of SIF.

4.2 Spatial distribution of the meteorological drought-vegetation correlation

To explore the response of vegetation dynamic changes to meteorological drought, the PCC and the DITI were used to determine the response relationship and VRT from linear and nonlinear perspectives, respectively. The values of the PCC and the DITI between the NDVI or SIF and the SPI at different scales were calculated. The time scale corresponding to the maximum SPI-NDVI and SPI-SIF relationship characteristics was defined as the VRT. Figure 5 shows the spatial distribution of the MPCC and DITI and the corresponding VRT based on the NDVI.

As shown in Figure 5A, there was a close relationship between meteorological drought and the NDVI in the PRB, with the MPCC ranging from 0.41 to 0.94 and passing the significance test at 95%. The MPCC was larger in the western PRB. The spatial distribution characteristics of VRT were similar from the linear perspective (Figure 5C). The VRT was larger in the middle of the PRB and decreased from the middle of the PRB to other directions. The VRT based on the NDVI from linear perspectives ranged from 2 to 8 months, and the VRT in most (93.2%) areas ranged from 4 to 6 months, accounting for 36.5% (4 months), 40.4% (5 months) and 16.3% (6 months), respectively. As shown in Figure 5B, there was also a close nonlinear relationship between meteorological drought and the NDVI in the PRB, with the DITI ranging from 0.83–0.90. Figure 5D shows that the VRT determined from nonlinear perspectives was relatively discrete, among which the VRT at 1 month accounted for the largest proportion (17.17%).

Figure 6 shows the spatial distribution of the MPCC and the DITI and the corresponding VRT based on SIF. Compared with the NDVI, there was a closer relationship between meteorological drought and SIF, with the MPCC ranging from 0.41 to 0.94 and passing the significance test at 95%. The MPCC was also larger in the western PRB (Figure 6A). The VRT based on SIF from linear perspectives (ranging from 2 to 6 months) was shorter than that

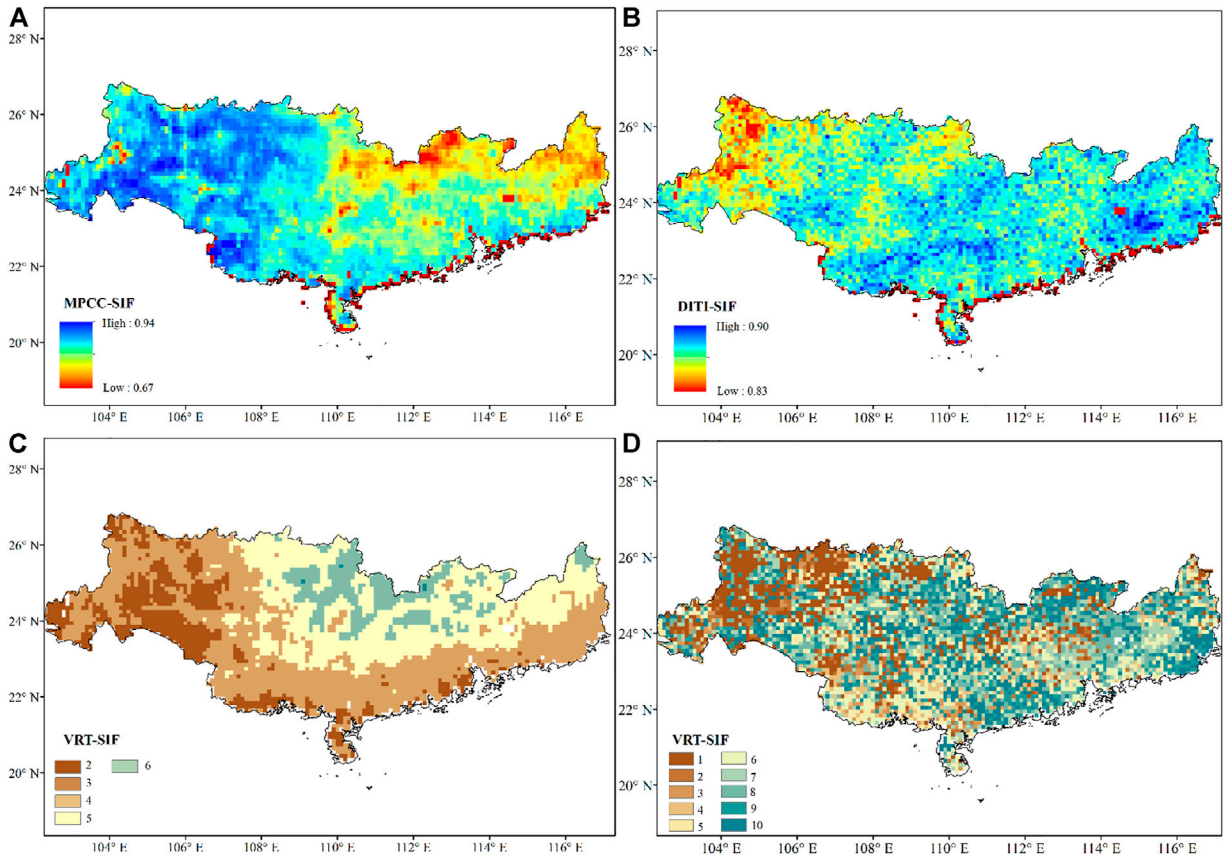

FIGURE 6
Spatial distributions of the MPCC **(A)** and the DITI **(B)** and corresponding VRT **(C,D)** are based on SIF.

based on the NDVI, and the VRT in most areas (89.4%) ranged from 2 to 4 months (Figure 6C), accounting for 15.3% (2 months), 42% (3 months) and 32.1% (4 months), respectively. As shown in Figure 6B, there was also a close nonlinear relationship between meteorological drought and SIF in the PRB, with the DITI ranging from 0.82–0.90. Figure 6D shows that the VRT determined from nonlinear perspectives was also relatively discrete, among which the VRT at 1 month accounted for the largest proportion (16.57%).

4.3 Spatial distribution of the final vegetation response time

The SPI-SRI correlation quantified above represents the dependence of runoff anomalies on precipitation anomalies. Two candidate VRT can be obtained from linear and nonlinear perspectives. To determine the VRT more reasonably, the water deficit of meteorological drought corresponding to the linear and nonlinear VRT of each grid was calculated. In general, a precipitation deficit is an important factor that causes vegetation dynamic changes (Khosravi et al., 2017; Fang et al., 2019; Wu et al., 2019). Therefore, this study takes the accumulation period corresponding to meteorological drought with a greater deficit as the VRT of this grid. Figure 7 shows the spatial distributions of the final VRT based on the NDVI and SIF. As shown in Figure 7, the VRT based on the NDVI in most areas ranged from 4 to 5 months, accounting for 36.41% (4 months) and 39.95% (5 months), respectively. The VRT based on SIF in most areas ranged from 3 to 4 months, accounting for 36.58% (3 months) and 30.75% (4 months), respectively.

To reveal the link between vegetation and meteorological drought, XWT was used to analyse the relationship between meteorological drought and vegetation. According to the results of subsection 4.2, the VRT with the largest proportion of grids (5 months for the NDVI and 3 months for SIF) was selected to analyse the relationship between meteorological drought and vegetation (Figure 8). The darker and lighter colours indicate higher and lower energy densities, respectively. The solid black line represents the wavelet influence cone, and the area within the cone line represents more than 95% in the significance test. The

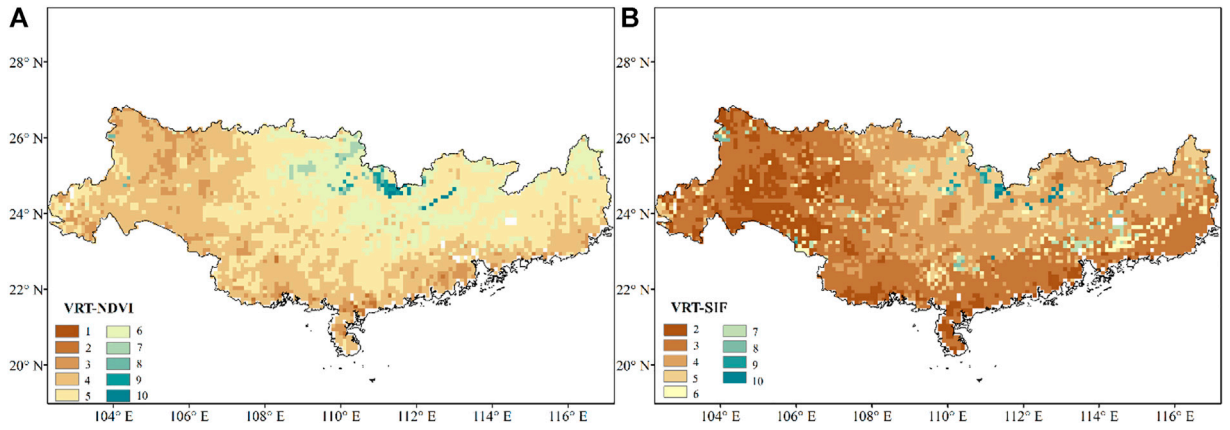

FIGURE 7
Spatial distributions of the final VRT based on **(A)** the NDVI and **(B)** SIF.

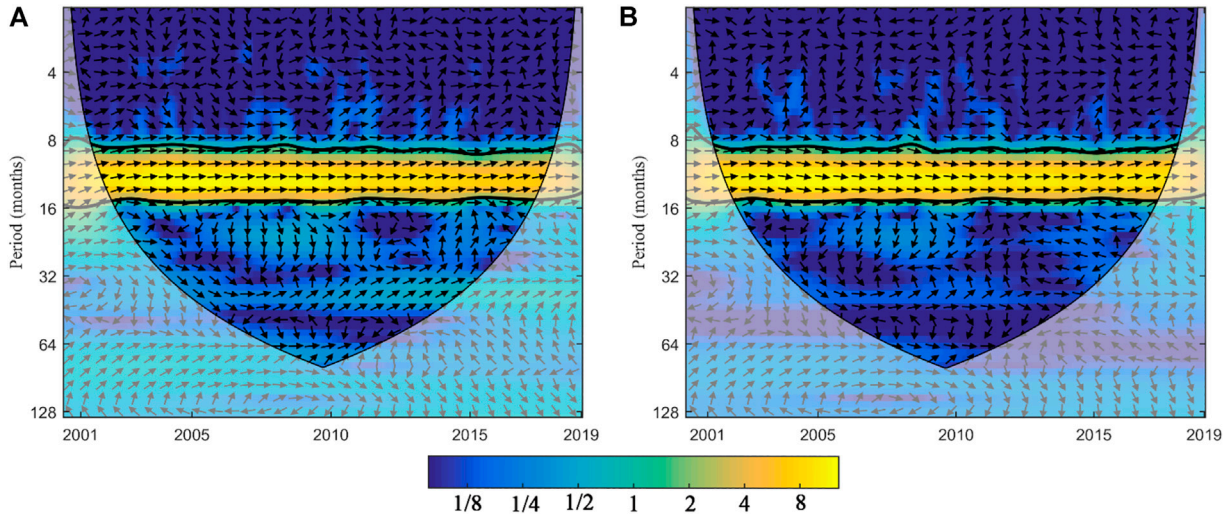

FIGURE 8
The cross wavelet transforms between meteorological and vegetation factors in the PRB: **(A)** NDVI and SPI5; **(B)** SIF and SPI3.

direction of the arrow represents the phase change in the two variables. The arrow to the right indicates that the two variables show a positive correlation, and the arrow to the left indicates that the two variables show a negative correlation. The arrow pointing up indicates that the change in variable 1 lags variable 2, and the arrow pointing down indicates that the change in variable 1 leads variable 2 (Chang et al., 2017). Figure 8A shows that the SPI5 and the NDVI had an obvious positive phase relationship in the 8–16 months resonance period from 2001 to 2019. Similarly, Figure 8B shows that SPI3 and SIF had an obvious positive phase relationship during 8–16 months of the resonance period from 2001 to 2019. In general, there was a stable relationship between meteorological drought and vegetation in the PRB. In addition, the phase angle is almost 0°, the arrow direction points horizontally to the right, the two variables are in the same phase, and there is no lag phenomenon; thus, the VRT determined in this study is reasonable.

To further study the response of vegetation dynamic changes to meteorological drought, the VRT corresponding to different vegetation types was counted. For the VRT-NDVI, the VRT of different vegetation types decreased from MF (5.25 ± 1.21 months), EBF (5.11 ± 0.76 months), WS (4.51 ±

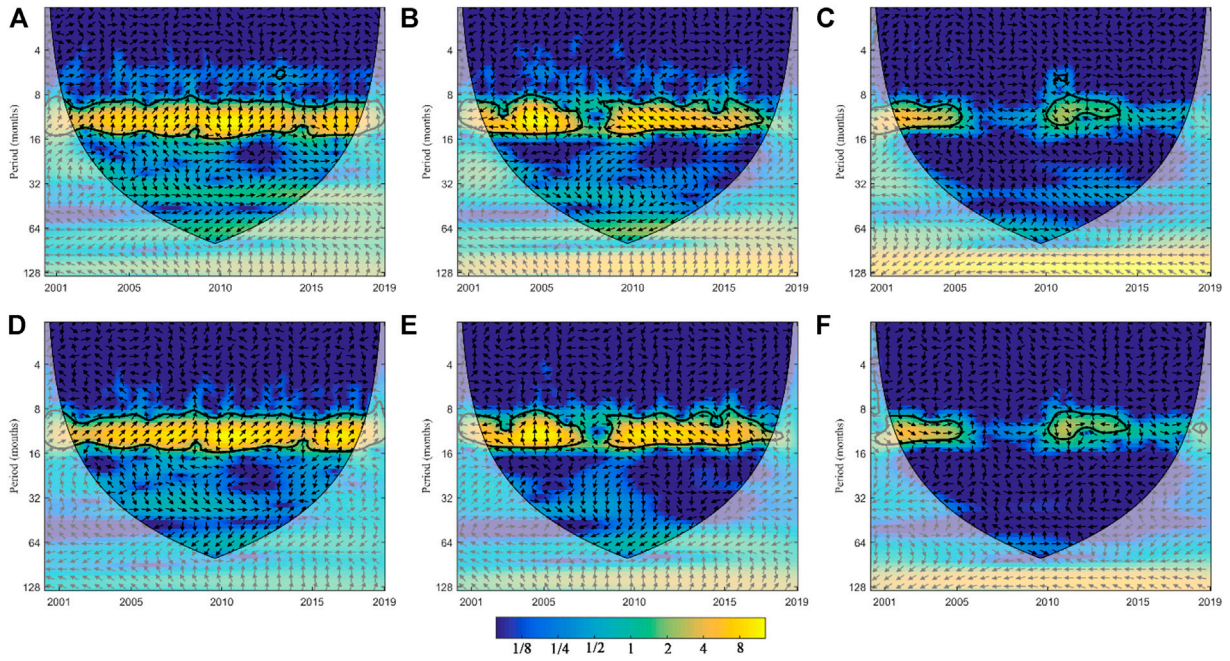

FIGURE 9
The XWT between monthly NDVI series **(A–C)**/SIF series **(D–F)** and large-scale climate patterns and solar activity in the PRB.

0.75 months), and CP (4.47 ± 0.95 months). For VRT-SIF, the VRT of different vegetation types decreased from MF (4.13 ± 1.42 months), EBF (4.05 ± 1.07 months), WS (3.44 ± 1.13 months), and CP (3.58 ± 1.18 months). Xu et al. (2020) showed that herbaceous plants had a shorter response time to drought than woody plants, and our results were consistent with those results. In general, SIF was more responsive to meteorological drought than the NDVI. In practical applications, according to the different responses of SIF and the NDVI to meteorological drought, SIF is more suitable for early drought monitoring and vegetation management, while the NDVI is more suitable for regional long-term disaster prevention and vegetation management.

4.4 The influences of teleconnection factors on the response relationship

The XWT was used to investigate the impacts of large-scale climate patterns and solar activity on vegetation. Figures 8A–C shows the influences of the ENSO, PDO and sunspots on the NDVI, and Figures 8D–F shows the influences of the ENSO, PDO and sunspots on SIF. As shown in Figure 9A, there was a significant positive correlation between the NDVI and ENSO in the period of 8–16 months during the whole study period. During 2001–2007 and 2008–2017, there was a significant negative correlation between the NDVI and PDO in the period of 8–16 months (Figure 9B). There was a significant positive correlation between the NDVI and sunspots in the period of 8–16 months during 2001–2005 and 2010–2014 (Figure 9C). The influences of the ENSO, PDO and sunspots on SIF were similar to those of the NDVI. SIF had a significant positive correlation with the ENSO and sunspots and a significant negative correlation with the PDO.

According to the VRT determined by the NDVI and SIF in subsection 4.3, the VRT with the largest proportion of grids (5 months for the NDVI and 3 months for SIF) was selected. Figure 10 shows the XWT between the monthly SPI5 (a-c)/SPI3 series (d-f) and large-scale climate patterns and solar activity in the PRB. As shown in Figure 10, meteorological drought had a significant positive correlation with the ENSO and sunspots and a significant negative correlation with the PDO. Therefore, large-scale climate patterns and solar activity can affect vegetation growth in the PRB by influencing meteorological drought. In addition, the ENSO and PDO were more closely related to meteorological drought and vegetation growth in the PRB.

5 Discussion

5.1 Possible reason for the difference in the response relationship

From subsections 4.2, it is found that the linear relationship was larger in the western part of the PRB and smaller in the eastern

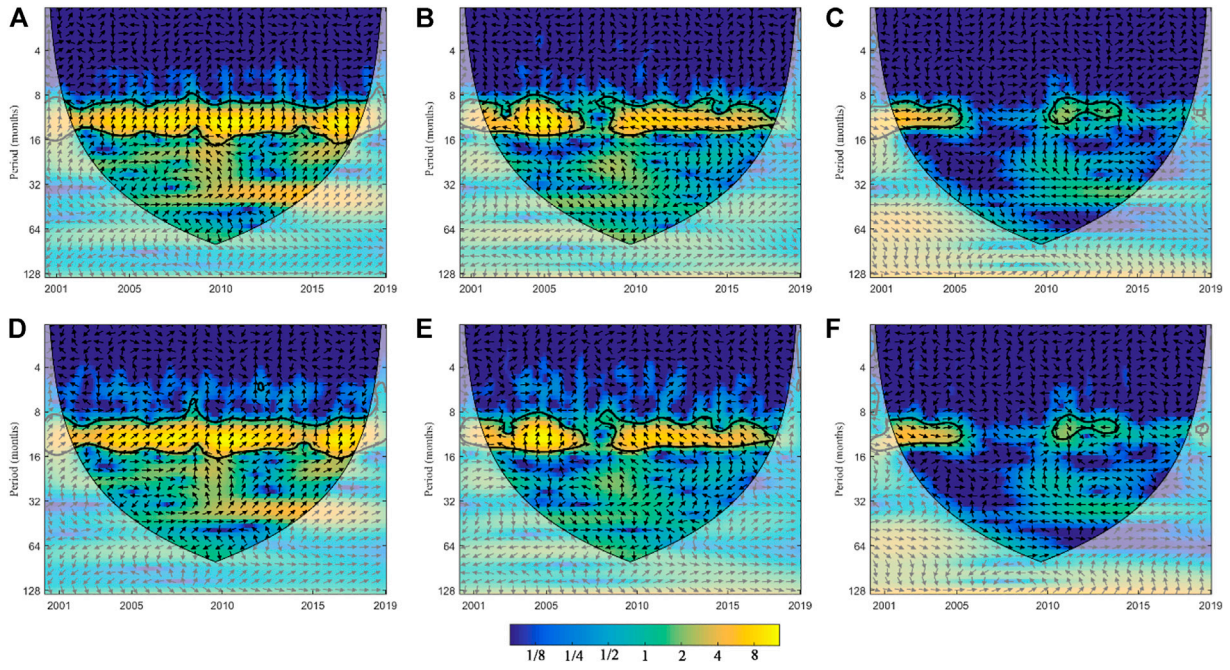

FIGURE 10
The XWT between the monthly SPI5 **(A–C)**/SPI3 series **(D–F)** and large-scale climate patterns and solar activity in the PRB.

part of the PRB; on the contrary, the nonlinear relationship was smaller in the western part of the PRB and larger in the eastern part of the PRB. Some studies have proved that the spatial distribution characteristics of linear relationship between meteorological drought and vegetation are mainly related to land cover types. Zhou et al. (2022) showed that the response relationship between meteorological drought and vegetation was larger on WS and CP than on EBF and MF. Xu et al. (2020) showed that herbaceous plants responded faster to drought than woody plants. Known from Figure 1, WS and CP are the main land use types in the western part of the PRB, so the MPCC was relatively larger in the western part of the PRB. The EBF and MF have complex vertical structures (mainly in the eastern part of the PRB), and EBF and MF have deeper roots and stronger water storage capacity (Wang et al., 2014; Tania and Irma, 2020; Kilic, 2021), so the nonlinear relationship was relatively larger in the eastern part of the PRB. In addition, some studies have proved that climate change (such as changes in precipitation and temperature) and human activities (such as irrigation) are also important factors affecting the relationship between meteorological drought and vegetation response (Fang et al., 2005; Hennekam et al., 2016; Papagiannopoulou et al., 2017; Ding et al., 2021), which can be further explored in future studies.

From subsections 4.2, and 4.3, the VRTs that were determined based on the NDVI and SIF were different, and the VRT determined based on SIF was shorter than that based on the NDVI, which might be caused by the different monitoring principles of the NDVI and SIF. The NDVI and SIF monitor vegetation based on the reflectance of vegetation leaves to radiation and the intensity of vegetation photosynthesis, respectively. Drought can affect vegetation photosynthesis and leaf area (Xie et al., 2020). When a short-term drought occurs, the NDVI can still maintain a high level, while SIF is directly related to vegetation photosynthesis and can reflect the rapid change in canopy water stress (Wang et al., 2016). When a long-term drought occurs, the water deficit makes the stomata of vegetation leaves close, leading to water loss and contraction of vegetation leaves. The photosynthetic capacity of leaves is also weakened, which leads to the contraction of leaves due to water shortage. Leaf atrophy of vegetation will lead to a decrease in the vertical projection area of vegetation, so the NDVI will also decrease (Gitelson et al., 2021). Therefore, different VRTs may reflect the physiological performance of leaves during a drought event, and the change in photosynthetic capacity occurs earlier than the change in leaf area, so the VRT based on the NDVI is larger than that based on SIF. In practical applications, according to the different responses of SIF and the NDVI to meteorological drought, SIF is more suitable for early drought monitoring and vegetation management, while the NDVI is more suitable for regional long-term disaster prevention and vegetation management.

As shown in subsection 4.3, there were differences in the VRT among the different vegetation types. In general, when a drought event occurs, vegetation can absorb water from the soil to help it grow. The reason why the VRT of woody vegetation was

longer than that of herbaceous vegetation might be due to the higher drought tolerance of woody vegetation. The ability of trees to resist drought comes from their deep root and xylem systems for water storage and long life (McDowell et al., 2008). The roots and stems of woody vegetation can utilize more soil water content (Xu et al., 2020). Due to the complex vertical structure, the performance of MFs in water and soil conservation was better than that of pure forests (Kilic, 2021), and their drought resistance may be stronger. Therefore, the VRT in the MF was greater than that in the evergreen broad-leaved forest.

5.2 Possible physical mechanisms for the correlation between vegetation and teleconnection factors

ENSO was closely correlated with precipitation, temperature, and meteorological drought in the PRB (Huang et al., 2017; Li et al., 2019). In general, large-scale climatic patterns influence vegetation growth by influencing water vapour and heat conditions. The ENSO can influence vegetation growth by redistributing water vapour and heat (Yeh et al., 2014). The PDO is also an important factor affecting drought in the PRB, and different types of droughts in the PRB are closely related to large-scale climate patterns (Han et al., 2019). The phase change in the PDO (cold and warm) was closely related to regional temperature and precipitation changes and significantly affected the interannual and seasonal changes in vegetation growth by controlling the regional climate (Zhang et al., 2017).

Vegetation cannot grow without the Sun, and the activity of sunspots has periodic characteristics and will change the solar radiation intensity (Balasubramaniam and Henry, 2016). Solar radiation also provides necessary energy for evapotranspiration, and the change in evapotranspiration intensity can affect precipitation by influencing the content of water vapour in the atmosphere and then indirectly affecting the growth of vegetation (Dong et al., 2017). Zhou et al. (2013) showed that solar energy can influence regional climate (such as precipitation and temperature) and then affect vegetation growth by influencing circulation movement.

In general, ENSO and PDO affect vegetation dynamics by influencing regional climate characteristics. The process of solar activity affecting vegetation dynamics is indirect. Solar activity first affects circulation, then affects regional climate characteristics, and finally affects vegetation. The process is more indirect, which may be the reason why the ENSO and PDO are more closely related to drought and vegetation in the PRB.

5.3 Limitations and extensions

In general, different definitions of drought will lead to different drought characteristics. Previous studies have shown that when calculating the drought index, if more variables are considered, such as temperature, evaporation and soil moisture, the trend in drought will change (Sohrabi et al., 2015; Liu et al., 2021). In this study, the SPI, with multiple time scales and easy calculation, was selected to represent meteorological drought. In future studies, meteorological drought indices with multiple factors could be selected to evaluate the relationship between meteorological drought and vegetation. The effect of drought on vegetation is a complex process. This paper only studied the response between meteorological drought and vegetation. Agricultural drought is closely related to soil moisture, and hydrological drought is closely related to watershed hydrological conditions and may also affect the dynamic change in vegetation. Previous studies have shown that vegetation growth is closely related to soil water content and runoff (Peel, 2009; Zhang et al., 2016). Therefore, future studies on the relationship between drought and vegetation should fully consider the impact of different types of droughts on vegetation. Notably, the feedback between different types of droughts and vegetation would be an interesting study. Causal analysis has been applied in environmental science in recent years. Wei et al. (2022) used the Granger causality test to analyse the feedback relationship between vegetation and soil moisture on the Loess Plateau. Shi et al. (2022) used convergent cross mapping to study the causal relationship between meteorological drought and hydrological drought. Wang et al. (2018) used convergent cross mapping to study the feedback relationship between precipitation and soil moisture. Therefore, future studies on the feedback relationship between vegetation and drought based on causal analysis can be carried out. In addition, due to the impacts of climate change and human activities, more people have begun to pay attention to the nonlinear impacts caused by climate change. This study introduces the DITI in information theory to study the relationship between meteorological drought and vegetation. Some studies have explored the effects of drought on vegetation using machine learning methods (Ribeiro et al., 2019; Lees et al., 2022). However, these methods are used to explore the relationship between drought and vegetation from the perspective of statistical algorithms. The impacts of drought on vegetation can be further explored based on plant physical models in the future.

6 Conclusion

In this study, the relationship between meteorological drought and the dynamics of vegetation was evaluated from both linear and nonlinear perspectives in the PRB, and the differences between the VRT based on the NDVI and SIF were compared. Moreover, the influences of teleconnection factors on the response relationship were analysed. The results can aid in understanding the mechanism of vegetation dynamic

response to meteorological drought and provide a good reference for regional drought prevention. The main conclusions are summarized as follows:

(1) The spatial distribution characteristics of vegetation cover and photosynthetic capacity in the PRB were similar, with low spatial characteristics in the west and high spatial characteristics in the east. The vegetation cover and photosynthetic capacity in the PRB showed an increasing trend from 2001 to 2019.
(2) Compared with the NDVI, SIF was more closely related to meteorological drought. The VRT based on the NDVI was typically 4–5 months, accounting for 36.41% (4 months) and 39.95% (5 months), respectively. The VRT based on the NDVI was typically 3–4 months, accounting for 36.58% (3 months) and 30.75% (4 months), respectively. The VRT on woody vegetation was longer than that on herbaceous vegetation.
(3) Large-scale climatic patterns and solar activity can affect vegetation growth by influencing meteorological drought in the PRB. Compared with sunspots, the ENSO and PDO were more closely related to the response relationship between meteorological drought and vegetation in the PRB.

Data availability statement

The original contributions presented in the study are included in the article/supplementary material, further inquiries can be directed to the corresponding author.

Author contributions

Conceptualization: HS. Data curation: ZZ. Formal analysis: ZZ. Funding acquisition: HS. Methodology: ZZ, HS. Supervision: HS, QF, and SL. Validation: ZZ, YD, CW, YW, and HC. Writing—original draft: ZZ. Writing—Reviewing and Editing: HS, SL.

Funding

This study was supported by the National Natural Science Foundation of China funded projects (51909117 and 51825901), Natural Science Foundation of Shenzhen funded project (JCYJ20210324105014039), Heilongjiang Provincial Science Fund for Distinguished Young Scholars (YQ 2020E002), Guangdong Provincial Key Laboratory of Soil and Groundwater Pollution Control (2017B030301012), and State Environmental Protection Key Laboratory of Integrated Surface Water-Groundwater Pollution Control.

Conflicts of interest

Author YD is employed by Yellow River Engineering Consulting Co., Ltd.

The remaining authors declare that the research was conducted in the absence of any commercial or financial relationships that could be construed as a potential conflict of interest.

Publisher's note

All claims expressed in this article are solely those of the authors and do not necessarily represent those of their affiliated organizations, or those of the publisher, the editors and the reviewers. Any product that may be evaluated in this article, or claim that may be made by its manufacturer, is not guaranteed or endorsed by the publisher.

References

Balasubramaniam, K. S., and Henry, T. W. (2016). Sunspot numbers from ISOON: A ten-year data analysis. *Sol. Phys.* 291 (9–10), 3123–3138. doi:10.1007/s11207-016-0874-5

Chang, T. P., Liu, F. J., Ko, H. H., and Huang, M. C. (2017). Oscillation characteristic study of wind speed, global solar radiation and air temperature using wavelet analysis. *Appl. Energy* 190, 650–657. doi:10.1016/j.apenergy.2016.12.149

De Souza, R. D., Moura, V., Paloschi, R. A., Aguiar, R. G., Webler, A. D., Borma, L. D., et al. (2022). Assessing drought response in the Southwestern Amazon Forest by remote sensing and *in situ* measurements. *Remote Sens.* 14 (7), 1733. doi:10.3390/rs14071733

Deng, S. L., Chen, T., Yang, N., Qiu, L., Li, M. C., Chen, D., et al. (2018). Spatial and temporal distribution of rainfall and drought characteristics across the Pearl River Basin. *Sci. Total Environ.* 619, 28–41. doi:10.1016/j.scitotenv.2017.10.339

Ding, Y. B., Wang, F. Z., Mu, Q., Sun, Y., Cai, H. J., Xu, J. T., et al. (2021). Estimating land use/land cover change impacts on vegetation response to drought under 'Grain for Green' in the Loess plateau. *Land Degrad. Dev.* 32 (17), 5083–5098. doi:10.1002/ldr.4093

Dobrowski, S., Pushnik, J., Zarcotejada, P., and Ustin, S. (2005). Simple reflectance indices track heat and water stress-induced changes in steady-state chlorophyll fluorescence at the canopy scale. *Remote Sens. Environ.* 97, 403–414. doi:10.1016/j.rse.2005.05.006

Dong, L., Zhang, P., Liu, J., Tong, X., and Xie, H. (2017). Combined influence of solar activity and ENSO on hydrological processes in Yoshino River basin, Japan. *Adv. Water Sci.* 28 (5), 671–680.

Fang, J. Y., Piao, S. L., Zhou, L. M., He, J. S., Wei, F. Y., Myneni, R. B., et al. (2005). Precipitation patterns alter growth of temperate vegetation. *Geophys. Res. Lett.* 32 (21), L21411. doi:10.1029/2005gl024231

Fang, W., Huang, S. Z., Huang, Q., Huang, G. H., Wang, H., Leng, G. Y., et al. (2019). Probabilistic assessment of remote sensing-based terrestrial vegetation vulnerability to drought stress of the Loess Plateau in China. *Remote Sens. Environ.* 232, 111290. doi:10.1016/j.rse.2019.111290

Fang, W., Huang, S. Z., Huang, Q., Huang, G. H., Wang, H., Leng, G. Y., et al. (2020). Identifying drought propagation by simultaneously considering linear and nonlinear dependence in the Wei River basin of the Loess Plateau, China. *J. Hydrology* 591, 125287. doi:10.1016/j.jhydrol.2020.125287

Fu, Q., Zhou, Z. Q., Li, T. X., Liu, D., Hou, R. J., Cui, S., et al. (2018). Spatiotemporal characteristics of droughts and floods in northeastern China and their impacts on agriculture. *Stoch. Environ. Res. Risk Assess.* 30 (10), 2913–2931. doi:10.1007/s00477-018-1543-z

Gitelson, A., Arkebauer, T., Viña, A., Skakun, S., and Inoue, Y. (2021). Evaluating plant photosynthetic traits via absorption coefficient in the photosynthetically active radiation region. *Remote Sens. Environ.* 258, 112401. doi:10.1016/j.rse.2021.112401

Han, Z. M., Huang, S. Z., Huang, Q., Leng, G. Y., Wang, H., Bai, Q. J., et al. (2019). Propagation dynamics from meteorological to groundwater drought and their possible influence factors. *J. Hydrology* 578, 124102. doi:10.1016/j.jhydrol.2019.124102

Hennekam, R., Donders, T. H., Zwiep, K., and de Lange, G. J. (2016). Integral view of Holocene precipitation and vegetation changes in the Nile catchment area as inferred from its delta sediments. *Quat. Sci. Rev.* 130 (SI), 189–199. doi:10.1016/j.quascirev.2015.05.031

Hu, X., Jiang, L. B., Shi, F. Z., Li, X. Y., Zhang, S. L., Zhao, Y. D., et al. (2021). Intensified drought enhances coupling between vegetation growth and pregrowing season precipitation in the drylands of the Silk Road Economic Belt. *JGR. Biogeosciences* 126 (3), e2020JG005914. doi:10.1029/2020jg005914

Huang, C., Zhang, Q., Singh, V. P., Gu, X. H., and Shi, P. J. (2017). Spatio-temporal variation of dryness/wetness across the Pearl River basin, China, and relation to climate indices. *Int. J. Climatol.* 37, 318–332. doi:10.1002/joc.5005

Jeong, S. J., Ho, C. H., Gim, H. J., and Brown, M. E. (2011). Phenology shifts at start vs. end of growing season in temperate vegetation over the Northern Hemisphere for the period 1982–2008. *Glob. Change Biol.* 17, 2385–2399. doi:10.1111/j.1365-2486.2011.02397.x

Jeong, S. J., Schimel, D., Frankenberg, C., Drewry, D. T., Fisher, J. B., Verma, M., et al. (2017). Application of satellite solar-induced chlorophyll fluorescence to understanding large-scale variations in vegetation phenology and function over northern high latitude forests. *Remote Sens. Environ.* 190, 178–187. doi:10.1016/j.rse.2016.11.021

Ji, S. P., Ren, S. L., Li, Y. R., Dong, Y. J., Wang, L. F., Quan, Q., et al. (2021). Diverse responses of spring phenology to preseason drought and warming under different biomes in the North China Plain. *Sci. Total Environ.* 706, 144437. doi:10.1016/j.scitotenv.2020.144437

Jiang, Q., Li, W. Y., Fan, Z. D., He, X. G., Sun, W. W., Chen, S., et al. (2021). Evaluation of the ERA5 reanalysis precipitation dataset over Chinese Mainland. *J. Hydrology* 595, 125660. doi:10.1016/j.jhydrol.2020.125660

Jiao, W. Z., Chang, Q., and Wang, L. Q. (2019). The sensitivity of satellite solar-induced chlorophyll fluorescence to meteorological drought. *Earth's. Future* 7, 558–573. doi:10.1029/2018ef001087

Khosravi, I., Haydari, E., Shekoohizadegan, S., and Zareie, S. (2017). Assessment the effect of drought on vegetation in desert area using Landsat data. *Egypt. J. Remote Sens. Space Sci.* 20, S3–S12. doi:10.1016/j.ejrs.2016.11.007

Kilic, O. M. (2021). Effects of land use and land cover changes on soil erosion in semi-arid regions of Turkey; A case study in Almus lake watershed. *Carpath. J. Earth Environ. Sci.* 16 (1), 129–138. Tokat Gaziosmanpasa University, Arts and Science Faculty, Department of Geography, Tokat, Turkey. doi:10.26471/cjees/2021/016/161

Lees, T., Tseng, T., Atzberger, C., Reece, S., and Dadson, S. (2022). Deep learning for vegetation health forecasting: A case study in Kenya. *Remote Sens.* 14 (3), 698. doi:10.3390/rs14030698

Li, J. C., Pang, G. J., Wang, X. J., Liu, F., and Zhang, Y. T. (2022). Spatiotemporal dynamics of land surface albedo and its influencing factors in the Qilian Mountains, Northeastern Tibetan Plateau. *Remote Sens.* 14 (8), 1922. doi:10.3390/rs14081922

Li, X., and Xiao, J. F. (2019). A global 0.05-degree product of solar-induced chlorophyll fluorescence derived from OCO-2, MODIS, and Reanalysis Data. *Remote Sens.* 11 (5), 517. doi:10.3390/rs11050517

Li, Y., Ma, B. S., and Yang, X. (2019). Impact of two types of ENSO events on the extreme precipitation in Eastern China. *Resour. Environ. Yangtze Basin* 28 (2), 469–482. (in Chinese). doi:10.11870/cjlyzyyhj201902023

Liu, L. Y., Yang, X. Q., Gong, F. X., Su, Y. X., Huang, G. Q., Chen, X. Z., et al. (2021). The novel microwave temperature vegetation drought index (MTVDI) captures canopy seasonality across Amazonian tropical evergreen forests. *Remote Sens.* 13 (3), 339. doi:10.3390/rs13030339

Liu, L. Z., Zhao, W. H., Wu, J. J., Liu, S. S., Teng, Y. G., Yang, J. H., et al. (2019). The impacts of growth and environmental parameters on solar-induced chlorophyll fluorescence at seasonal and diurnal scales. *Remote Sens.* 11, 2002. doi:10.3390/rs11172002

Ma, Y., Liu, L. Y., Chen, R. N., Du, S. S., and Liu, X. J. (2020). Generation of a global spatially continuous TanSat solar-induced chlorophyll fluorescence product by considering the impact of the solar radiation intensity. *Remote Sens.* 12, 2167. doi:10.3390/rs12132167

McDowell, N., Pockman, W. T., Allen, C. D., Breshears, D. D., Cobb, N., Kolb, T., et al. (2008). Mechanisms of plant survival and mortality during drought: Why do some plants survive while others succumb to drought? *New Phytol.* 178, 719–739. doi:10.1111/j.1469-8137.2008.02436.x

McKee, T. B., Doesken, N. J., and Kleist, J. (1993). "The relationship of drought frequency and duration to time scales. No. 22," in Proceedings of the 8th Conference on Applied Climatology (Boston, MA: American Meteorological Society), 179–183.

Papagiannopoulou, C., Miralles, D. G., Dorigo, W. A., Verhoest, N. E. C., Depoorter, M., Waegeman, W., et al. (2017). Vegetation anomalies caused by antecedent precipitation in most of the world. *Environ. Res. Lett.* 12 (7), 074016. doi:10.1088/1748-9326/aa7145

Patel, N. R., Chopra, P., and Dadhwal, V. K. (2007). Analyzing spatial patterns of meteorological drought using standardized precipitation index. *Met. Apps.* 14 (4), 329–336. doi:10.1002/met.33

Peel, M. C. (2009). Hydrology: Catchment vegetation and runoff. *Prog. Phys. Geogr. Earth Environ.* 33 (6), 837–844. doi:10.1177/0309133309350122

Rahmat, S. N., Jayasuriya, N., and Bhuiyan, M. (2015). Assessing droughts using meteorological drought indices in Victoria, Australia. *Hydrology Res.* 46 (3), 463–476. doi:10.2166/nh.2014.105

Ribeiro, A. F. S., Russo, A., Gouveia, C. M., and Pascoa, P. (2019). Modelling drought-related yield losses in Iberia using remote sensing and multiscalar indices. *Theor. Appl. Climatol.* 136 (1-2), 203–220. doi:10.1007/s00704-018-2478-5

Shahabfar, A., and Eitzinger, J. (2013). Spatio-temporal analysis of droughts in semi-arid regions by using meteorological drought indices. *Atmosphere* 4 (2), 94–112. doi:10.3390/atmos4020094

Shi, B., Jiang, J. P., Sivakumar, B., Zheng, Y., and Wang, P. (2018). Quantitative design of emergency monitoring network for river chemical spills based on discrete entropy theory. *Water Res.* 134, 140–152. doi:10.1016/j.watres.2018.01.057

Shi, H. Y., Chen, J., Wang, K. Y., and Niu, J. (2018). A new method and a new index for identifying socioeconomic drought events under climate change: A case study of the east river Basin in China. *Sci. Total Environ.* 616-617, 363–375. doi:10.1016/j.scitotenv.2017.10.321

Shi, H. Y., Zhao, Y. Y., Liu, S. N., Cai, H. J., and Zhou, Z. Q. (2022). A new perspective on drought propagation: Causality. *Geophys. Res. Lett.* 49, e2021GL096758. doi:10.1029/2021gl096758

Sohrabi, M. M., Ryu, J. H., Abatzoglou, J., and Tracy, J. (2015). Development of soil moisture drought index to characterize droughts. *J. Hydrol. Eng.* 20 (11), 04015025. doi:10.1061/(asce)he.1943-5584.0001213

Tania, F., and Irma, T. (2020). Rainfall interception based on indirect methods: A case study in temperate forests in oaxaca, Mexico. *J. Am. Water Resour. Assoc.* 56 (4), 712–723. doi:10.1111/1752-1688.12844

Wang, B., Zhang, G. H., Shi, Y. Y., and Zhang, X. C. (2014). Soil detachment by overland flow under different vegetation restoration models in the Loess Plateau of China. *Catena* 116, 51–59. doi:10.1016/j.catena.2013.12.010

Wang, S. H., Huang, C. P., Zhang, L. F., Lin, Y., Cen, Y., Wu, T. X., et al. (2016). Monitoring and assessing the 2012 drought in the great plains: Analyzing satellite-retrieved solar-induced chlorophyll fluorescence, drought indices, and gross primary production. *Remote Sens.* 8 (2), 61. doi:10.3390/rs8020061

Wang, T., Tu, X. J., Singh, V. P., Chen, X. H., and Lin, K. R. (2021). Global data assessment and analysis of drought characteristics based on CMIP6. *J. Hydrology* 596, 126091. doi:10.1016/j.jhydrol.2021.126091

Wang, Y. Q., Yang, J., Chen, Y. N., Maeyer, P. D., Li, Z., Duan, W. L., et al. (2018). Detecting the causal effect of soil moisture on precipitation using convergent cross mapping. *Sci. Rep.* 8, 12171. doi:10.1038/s41598-018-30669-2

Wei, X. T., Huang, Q., Huang, S. Z., Leng, G. Y., Qu, Y. P., Deng, M. J., et al. (2022). Assessing the feedback relationship between vegetation and soil moisture over the Loess Plateau, China. *Ecol. Indic.* 134, 108493. doi:10.1016/j.ecolind.2021.108493

Wu, J. P., Liu, L. Y., Sun, C. H., Su, Y. X., Wang, C. J., Yang, J., et al. (2019). Estimating rainfall interception of vegetation canopy from MODIS imageries in Southern China. *Remote Sens.* 11 (21), 2468. doi:10.3390/rs11212468

Wu, J. P., Su, Y., Chen, X., Liu, L., Yang, X., Gong, F., et al. (2021). Leaf shedding of Pan-Asian tropical evergreen forests depends on the synchrony of seasonal variations of rainfall and incoming solar radiation. *Agric. For. Meteorology* 311, 108691. doi:10.1016/j.agrformet.2021.108691

Xie, X. Y., Li, A. N., Tan, J. B., Lei, G. B., and Zhang, Z. J. (2020). Uncertainty analysis of multiple global GPP datasets in characterizing the lagged effect of drought on photosynthesis. *Ecol. Indic.* 113, 106224. doi:10.1016/j.ecolind.2020.106224

Xie, Y. W., Li, J., Chen, W. R., and Luo, S. H. (2016). Spatio-temporal variation of average temperature over the Pearl River basin during 1959-2013. *ACTA Sci. Nat. Univ. SunYatseni* 55 (3), 31–38.

Xin, Y., Lu, N., Jiang, H., Liu, Y. X. Y., and Yao, L. (2021). Performance of ERA5 reanalysis precipitation products in the Guangdong-Hong Kong-Macao greater Bay Area, China. *J. Hydrology* 602, 126791. doi:10.1016/j.jhydrol.2021.126791

Xu, H. J., Wang, X. P., and Zhao, C. Y. (2021). Drought sensitivity of vegetation photosynthesis along the aridity gradient in northern China. *Int. J. Appl. Earth Observation Geoinformation* 102, 102418. doi:10.1016/j.jag.2021.102418

Xu, H. J., Wang, X. P., Zhao, C. Y., and Yang, X. M. (2020). Assessing the response of vegetation photosynthesis to meteorological drought across northern China. *Land Degrad. Dev.* 32 (1), 20–34. doi:10.1002/ldr.3701

Xu, J. T., Ma, Z. Q., Yan, S. K., and Peng, J. (2022). Do ERA5 and ERA5-land precipitation estimates outperform satellite-based precipitation products? A comprehensive comparison between state-of-the-art model-based and satellite-based precipitation products over mainland China. *J. Hydrology* 605, 127353. doi:10.1016/j.jhydrol.2021.127353

Yang, Z., Shen, Y. Y., Li, J., Jiang, H. W., and Zhao, L. K. (2022). Unsupervised monitoring of vegetation in a surface coal mining region based on NDVI time series. *Environ. Sci. Pollut. Res.* 29 (18), 26539–26548. doi:10.1007/s11356-021-17696-9

Yeh, S. W., Kug, J. S., Dewitte, B., Kwon, M. H., and Jin, F. F. (2014). El Niño in a changing climate. *Nature* 461, 511–514. doi:10.1038/nature08316

Zhang, L. K., Qiu, X. Q., Liu, P. Y., Huang, Q. B., Lan, F. N., Li, H. B., et al. (2015). Estimation of carbon sink fluxes in the Pearl River basin (China) based on a water–rock–gas–organism interaction model. *Environ. Earth Sci.* 74, 945–952. doi:10.1007/s12665-014-3788-2

Zhang, W., Zhou, T., and Zhang, L. (2017). Wetting and greening Tibetan plateau in early summer in recent decades: Wetting and greening Tibetan plateau. *J. Geophys. Res. Atmos.* 122 (11), 5808–5822. doi:10.1002/2017jd026468

Zhang, Y. Q., Mao, G. X., Chen, C. C., Shen, L. C., and Xiao, B. Y. (2021). Population exposure to compound droughts and heatwaves in the observations and ERA5 Reanalysis Data in the Gan River Basin, China. *Land* 10, 1021. doi:10.3390/land10101021

Zhang, Y. W., Deng, L., Yan, W. M., and Shangguan, Z. P. (2016). Interaction of soil water storage dynamics and long-term natural vegetation succession on the Loess Plateau, China. *Catena* 137, 52–60. doi:10.1016/j.catena.2015.08.016

Zhao, A. Z., Yu, Q. Y., Feng, L. L., Zhang, A. B., and Pei, T. (2020a). Evaluating the cumulative and time-lag effects of drought on grassland vegetation: A case study in the Chinese loess plateau. *J. Environ. Manag.* 261, 110214. doi:10.1016/j.jenvman.2020.110214

Zhao, J., Huang, S. Z., Huang, Q., Wang, H., Leng, G. Y., Fang, W., et al. (2020b). Time-lagged response of vegetation dynamics to climatic and teleconnection Factors. *Catena* 189, 104474. doi:10.1016/j.catena.2020.104474

Zhong, S. B., Sun, Z. H., and Di, L. P. (2021). Characteristics of vegetation response to drought in the CONUS based on long-term remote sensing and meteorological data. *Ecol. Indic.* 127, 107767. doi:10.1016/j.ecolind.2021.107767

Zhou, Q., Chen, W., and Zhou, W. (2013). Solar cycle modulation of the ENSO impact on the winter climate of East Asia. *J. Geophys. Res. Atmos.* 118, 5111–5119. doi:10.1002/jgrd.50453

Zhou, Y. L., and Zhou, P. (2021). Decline in net primary productivity caused by severe droughts: Evidence from the Pearl River basin in China. *Hydrology Res.* 52 (6), 1559–1576. doi:10.2166/nh.2021.061

Zhou, Z. Q., Ding, Y. B., Shi, H. Y., Cai, H. J., Fu, Q., Liu, S. N., et al. (2020b). Analysis and prediction of vegetation dynamic changes in China: Past, present and future. *Ecol. Indic.* 117, 106642. doi:10.1016/j.ecolind.2020.106642

Zhou, Z. Q., Liu, S. N., Ding, Y. B., Fu, Q., Wang, Y., Cai, H. J., et al. (2022). Assessing the responses of vegetation to meteorological drought and its influencing factors with partial wavelet coherence analysis. *J. Environ. Manag.* 311, 114879. doi:10.1016/j.jenvman.2022.114879

Zhou, Z. Q., Shi, H. Y., Fu, Q., Ding, Y. B., Li, T. X., Liu, S. N., et al. (2021b). Investigating the propagation from meteorological to hydrological drought by introducing the nonlinear dependence with directed information transfer index. *Water Resour. Res.* 57, e2021WR030028. doi:10.1029/2021wr030028

Zhou, Z. Q., Shi, H. Y., Fu, Q., Ding, Y. B., Li, T. X., Wang, Y., et al. (2021a). Characteristics of propagation from meteorological drought to hydrological drought in the Pearl River Basin. *JGR. Atmos.* 126, e2020JD033959. doi:10.1029/2020jd033959

Zhou, Z. Q., Shi, H. Y., Fu, Q., Li, T. X., Gan, T. Y., Liu, S. N., et al. (2020a). Assessing spatiotemporal characteristics of drought and its effects on climate-induced yield of maize in Northeast China. *J. Hydrology* 588, 125097. doi:10.1016/j.jhydrol.2020.125097

frontiers | Frontiers in Earth Science

TYPE Original Research
PUBLISHED 24 August 2022
DOI 10.3389/feart.2022.969991

OPEN ACCESS

EDITED BY
Chunhui Li,
Beijing Normal University, China

REVIEWED BY
Liu Liu,
China Agricultural University, China
Xingcai Liu,
Institute of Geographic Sciences and Natural Resources Research (CAS), China

*CORRESPONDENCE
Boyang Sun,
sunboyang@aliyun.com

SPECIALTY SECTION
This article was submitted to Hydrosphere, a section of the journal Frontiers in Earth Science

RECEIVED 15 June 2022
ACCEPTED 29 July 2022
PUBLISHED 24 August 2022

CITATION
Sun B and Li F (2022), Water consumption patterns of 110 cities in the Yangtze River Economic Belt in 2015.
Front. Earth Sci. 10:969991.
doi: 10.3389/feart.2022.969991

Water consumption patterns of 110 cities in the Yangtze River Economic Belt in 2015

Boyang Sun* and Fapeng Li

Development Research Center of the Ministry of Water Resources of P.R. China, Beijing, China

How to formulate scientific and effective water-saving policies is of great significance for the sustainable water consumption. As a country with the largest water consumption in the world, China has been committed to formulating scientific and effective water-saving policies. However, due to geospatial variations of water consumption in different regions, how to formulate targeted and efficient water-saving policies which suit for different local characteristics has always been a key issue to be solved. In a quest to understand the water consumption patterns, this study first adopted a dual evaluation index system combining Gini coefficient and Global Moran's Index to classify different types of water consumption. Taking 110 cities in the Yangtze River Economic Belt as research objects, the water consumption of 110 cities was divided into nine types. According to each type, a targeted water-saving policy is given. This study provides important theoretical support for the efficient management of water resources in the Yangtze River Economic Belt, and provides reference for water resources management in other regions at the same time.

KEYWORDS

water consumption, Yangtze River Economic Belt, Global Moran I, Gini coefficient, water resources management

Introduction

Research background

China is a country with severe drought and water shortage. China's per capita water resources is only one quarter of the world average. It has been listed by the United Nations as one of the 13 countries with the most water stress. However, China is also a country with the largest water consumption in the world, accounting for about 13% of the world's annual consumption (UN-water, 2018). China's water resources situation is severe, therefore effective water resources management is of great significance to China's sustainable development.

In response to the current problems of over-exploitation of water resources, China strictly controls the excessive growth of total water consumption. To address the current problems of over-exploitation of water resources, China proposed to limit its total water consumption to 700 billion cubic meters by 2030 (CPGPRC (The Central People's

Government of the People's Republic of China), 2010). The situation of water resource consumption reduction is severe. It is important to carry out refined management of water resources and formulate appropriate policies to efficiently and effectively reduce water consumption.

The Yangtze River Economic Belt is one of China's most developed regions with an area of about 2.05 million square kilometers. Its population and GDP are more than 40% of the total (EPMC (Environmental Protection Ministry of China), 2017). Working out effective policies to reduce water consumption in the Yangtze River Economic Belt is critical to China achieving its stated goal of controlling total water consumption to 700 billion cubic meters per year by 2030. In addition, the Yangtze River Economic Belt is an important water-out area in China's South-to-North Water Diversion Project. The research on the patterns of water resource consumption in the Yangtze River Economic Belt is conducive to the formulation and implementation of more effective water-saving policies in this region, which is of great significance for ensuring China's water security and improving the spatial equilibrium of water resource in China.

Literature review and research gap

In academia, water resources management has always been a research hotspot, and has received widespread attention from scholars worldwide (Bian et al., 2022a). According to the existing literature, research on water resources management mainly focuses on the following four aspects: 1) water resources development and protection, 2) optimal allocation of water resources, 3) watershed non-point source pollution control, and 4) water carrying capacity. Comparatively, there is relatively little research on water consumption. This is because research on water consumption requires a large amount of data on a small scale, which is often difficult to obtain. However, research on water consumption is very important and can provide important support for the development of more targeted water resources management policies.

When it comes to water consumption, there is a large degree of confusion between these concepts: water consumption, water use, water withdrawal and water demand. One has to be careful when using these concepts (Bian et al., 2022b). The contents of these concepts are slightly different. Water use refers to the actual amount of water resources used at a certain period of time or in a region or for a specific production activity. Water withdrawal generally refers to the amount of water extracted from a water source within a certain period of time or in an area for a specific production activity. Water demand refers to the amount of water resources required for a specific time or in a region for a specific production activity (Gleick, 2003).

Water consumption has two separated meanings: 1) The relatively narrow understanding, which refers to the amount of water resources that evaporate and infiltrate in an irreparable loss. 2) The widely understood concept of water consumption which refers to the actual water usage at a certain period of time for a specific production activity. The concept of water consumption used in this study refers to the later one.

In order to find out the factors that affect water consumption, some researches in recent years have focused on the driving factors of water consumption. Jaramillo and Destouni (2015) studied the relationship between the extensive use of dam construction and irrigation facilities and the consumption of water resources based on the hydrological and climatic observations of 100 large hydrological basins around the world. Compared with the years from 1901 to 1954, the per capita consumption of fresh water resources increased significantly from 1955 to 2008. Long et al. (2019) used the logarithmic mean Divisia index to decompose the driving factors of water consumption in China's provinces from 2000 to 2015. The results are as follows: 1) In the agricultural field, technological progress and population mobility are the main reasons for the decline in water consumption. 2) In the industrial sector, advances in industrial technology have contributed to the decline in water consumption. 3) In the residential sector, technological advances in household appliances have contributed to the decline in water consumption. At the same time, per capita income is a major factor that affects water consumption. Studies have also shown that water consumption is strongly related to the level of economic development (Fercovic et al., 2019). Sauri (2019) has studied the driving factors of the significant decline in water consumption in some major Spanish cities between 2003 and 2016. The study believes that the driving factors that caused the decline in water consumption are multifaceted. The study also discussed the different degrees of economic, technological, and behavioral aspects driving the decline in water consumption.

Another research area of water consumption is water use efficiency. For example, Hu et al. (2006) applied data envelopment analysis to study the efficiency of water resources use in China from 1997 to 2002, taking the provincial level as the research scale. They found that water efficiency in central areas of China is the worst. In central China, more efficient production processes and advanced technologies are needed to improve water efficiency. Deng et al. (2016) evaluated water efficiency of 31 provinces in China from 2004 to 2013 by using slack based measure-data development analysis. Wang et al. (2015) studied the relationship between the water efficiency of China's regional industrial systems and the emission reduction costs of related pollutants based on the relaxation variable method.

Other studies have focused on two parts. On one hand, water consumption research is concentrated in some special industries, such as water consumption in aquaculture (Lebel et al., 2019), rice planting (Silalertruksa et al., 2017), and power generation (Chang et al., 2015). On the other hand, water consumption

research focuses on water consumption and other related fields, such as virtual water (Zhang et al., 2019), water use efficiency (Freire-González, 2019), sewage treatment (Risch et al., 2014), water footprints (Hoekstra and Chapagain, 2006; Boulay et al., 2018), spatial imbalance (Cole et al., 2018), and other studies.

However, research on water consumption is very limited. The only few studies on water consumption focused on households and studied the water consumption in various parts of the household (such as showers, toilets, washing machines, and garden irrigation). Keshavarzi et al. (2006) collected water consumption from 653 households in 33 villages from 1999 to 2004 through a questionnaire survey. They found that household water consumption was significantly related to the number of households and the age of the head of household. The study also found that in rural households, water consumption is related to the area of the garden and the greenhouse, and the frequency of watering. Jethoo and Poonia (2011) used a questionnaire method to investigate the relationship between household water consumption and household income in Jaipur City, India. The study found that these two aspects are highly correlated. Willis et al. (2013) used a combination of both actual monitoring and questionnaires to study the different performances of water consumption in households located in different socioeconomic states and those with different number of users of facilities such as the kitchen, toilet, washing machine, shower etc., and gave out a number of water conservation recommendations.

Even though, research on water consumption is very limited, based on the analysis of the existing literature above, we find that research on water consumption has attracted more attention in recent years. Furthermore, research on water consumption is mostly focused on the study of driving factors, water efficiency, water consumption in some special industries, water consumption and other research in related fields, and very little research on the patterns of water consumption. From the view of research scale and data acquisition methods, the research on water consumption driving factors and water efficiency are mainly concentrated on the provincial scale or industry scale. The data is generally obtained through national statistical yearbooks, while for research on water consumption patterns concentrated on the household scale, the data is obtained by questionnaires or combined with actual monitoring.

However, research on water consumption at the provincial and industry scales is generally difficult to formulate water resources management policies for different regions due to the large research scale. The research on water consumption on a household scale does not take into account other aspects such as agricultural water use, industrial water use, and eco-environment water use. It also has no reference value when formulating water management policies for different regions. Therefore, because studying the consumption of water resources at the city scale takes into account all the water consumption channels in the city, it can provide a reliable basis for effective water resources management, help to formulate targeted policies, and be more targeted, thus can reduce water consumption.

Because the characteristics of water consumption in different cities vary, it is very necessary to figure out the key differences in water consumption in different cities and clarify the water consumption patterns, so that more effective localized policies can be formulated and implemented. When studying water consumption patterns in different cities, it is necessary to take the differences in water consumption in different areas of the city into account, in order to formulate water resources management policies for the main water consumption areas. And in order to formulate water resources management policies with different regional characteristic, it is also necessary to take full account of the spatial distribution characteristics of regional water consumption. In other words, both the quantitative and spatial differences in water consumption in different areas of the city should be fully considered.

The main work and innovations

This study evaluates the water consumption patterns of 110 cities in the Yangtze River Economic Belt and compares the difference in the amount of water resources as well as the spatial variations in water use within the cities. We used Gini coefficient to characterize the amount of water resources in different areas of the city and Global Moran's I (index) to characterize the regional differences in water consumption in different regions of the city. Based on the calculation results of Gini coefficient and Global Moran's I, the water consumption patterns of 110 cities in the Yangtze River Economic Belt are divided. For different types, more specific water resource management recommendations are given, which will provide important support for minimizing water consumption in the Yangtze River Economic Belt. At the same time, this study can provide reference for water resources management and control in other regions.

Materials and methods

Study area

The research area in this study is the Yangtze River Economic Belt. The Yangtze River Economic Belt is one of the most developed regions in China. It is a strategic water source for China's water resources allocation, an important

strategic base for clean energy, and a natural treasure house of rare aquatic life (EPMC (Environmental Protection Ministry of China), 2017). It has a very important strategic position in environmental protection. The Yangtze River Economic Belt covers 11 provincial-level administrative regions including Shanghai, Jiangsu, Zhejiang, Anhui, Jiangxi, Hubei, Hunan, Chongqing, Sichuan, Yunnan and Guizhou, including the Yangtze River Delta urban agglomeration, urban agglomeration in the middle reaches of the Yangtze River, and the Chengdu-Chongqing urban agglomeration. The eastern region of the Yangtze River Economic Belt includes Shanghai, Jiangsu, and Zhejiang. It is the core component of the Yangtze River Delta and the most economically developed region in the Yangtze River Economic Belt. The central region includes Hubei, Hunan, Jiangxi, and Anhui. The region has abundant natural resources and convenient transportation. The central region has obvious advantages in grain production, strong industrial foundation, and good conditions for accelerating economic and social development. Western region includes Chongqing, Sichuan, Yunnan, Guizhou, and is rich in hydropower, minerals, and biological resource. The Yangtze River Economic Belt plays an extremely important role in China's economic and social development and ecological environment protection.

The Yangtze River Economic Belt covers 11 provincial-level administrative regions including 130 prefecture level cities. Considering the accuracy of Global Moran's I, a city needs to have at least 4 second-tier cities. In this study, we chose 110 of 130 cities in the Yangtze River Economic Belt as research objects as presented in Table 1.

Data collection

Data on water resources planning and management normally comes from Statistical Yearbooks or Water Resources Bulletins. However, the data in the Statistical Yearbook and Water Resources Bulletin is on city scale, but in order to formulate more targeted and localized policies, smaller level, like sub-cities level data has been required. But this data is usually not available in Statistical Yearbooks and Water Resources Bulletins. Data in the study is the water consumption data of all sub-cities of the 110 cities in the Yangtze River Economic Belt in 2015. This data has been obtained by an investigation among the water resources planning and management department of the local government of these 110 cities. After we obtained the water consumption data of all the sub-cities of the 110 cities in the Yangtze River Economic Belt in 2015, we obtained water consumption data of the 110 cities at the same time. And then, a comparison between water consumption data of the 110 cities in 2015 that we obtained and water consumption data of these 110 cities that in the Water Resources Bulletin have been carried out. If they are not equal, we reinvestigated. The amount of water collected included agricultural water, industrial water, domestic water, and ecological water.

TABLE 1 110 selected cities and 20 unselected cities in the Yangtze River Economic Belt.

Provinces	Cities selected	Unselected cities
Zhejiang (10/11)	Hangzhou, Huzhou, Jiaxing, Jinhua, Lishui, Ningbo, Quzhou, Shaoxing, Taizhou (Z), Wenzhou	Zhoushan
Jiangxi (8/11)	Fuzhou, Ganzhou, Ji'an, Jiujiang, Nanchang, Pingxiang, Shangrao, Yichun	Jingdezhen, Xinyu, Yingtan
Hubei (10/16)	Enshi, Huanggang, Jingmen, Jingzhou, Shiyan, Wuhan, Xianning, Xiangyang, Xiaogan, Yichang	Huangshi, Suizhou, Xiantao, Qianjiang, Tianmen, Shennongjia
Guizhou (9/9)	Anshun, Bijie, Guiyang, Liupanshui, Qiandongnan, Qiannan, Qianxinan, Tongren, Zunyi	—
Sichuan (18/21)	Abazhou, Bazhong, Chengdu, Dazhou, Deyang, Garze, Guang'an, Guangyuan, Leshan, Liangshan, Luzhou, Meishan, Mianyang, Nanchong, Neijiang, Ya'an, Yibin, Ziyang	Zigong, Suining, Panzhihua
Shanghai (1/1)	Shanghai	—
Chongqing (1/1)	Chongqing	—
Yunnan (14/16)	Baoshan, Chuxiong, Dali, Dehong, Honghe, Kunming, Lijiang, Lincang, Nujiang, Puer, Qujing, Wenshan, Yuxi, Zhaotong	Diqing, Xishuangbanna
Jiangsu (13/13)	Changzhou, Huaian, Lianyungang, Nnanjing, Nantong, Suzhou (J), Taizhou (J), Wuxi, Suqian, Xuzhou, Yancheng, Yangzhou, Zhenjiang	—
Anhui (13/17)	Anqing, Bengbu, Chizhou, Chuzhou, Fuyang, Bozhou, Hefei, Huangshan, Lu'an, Maanshan, Wuhu, Suzhou (A), Xuancheng	Huaibei, Huainan, Tongling, Chaohu
Hunan (13/14)	Changde, Chenzhou, Hengyang, Huaihua, Loudi, Shaoyang, Xiangtan, Xiangxizhou, Yiyang, Yongxing, Yueyang, Changsha, Zhuzhou	Zhangjiajie

1) Shanghai and Chongqing are municipalities directly under the Central Government. 2) In the brackets of the first column, there are two numbers. The first number is the number of cities selected from this province and the latter number is the total number of cities in this province.

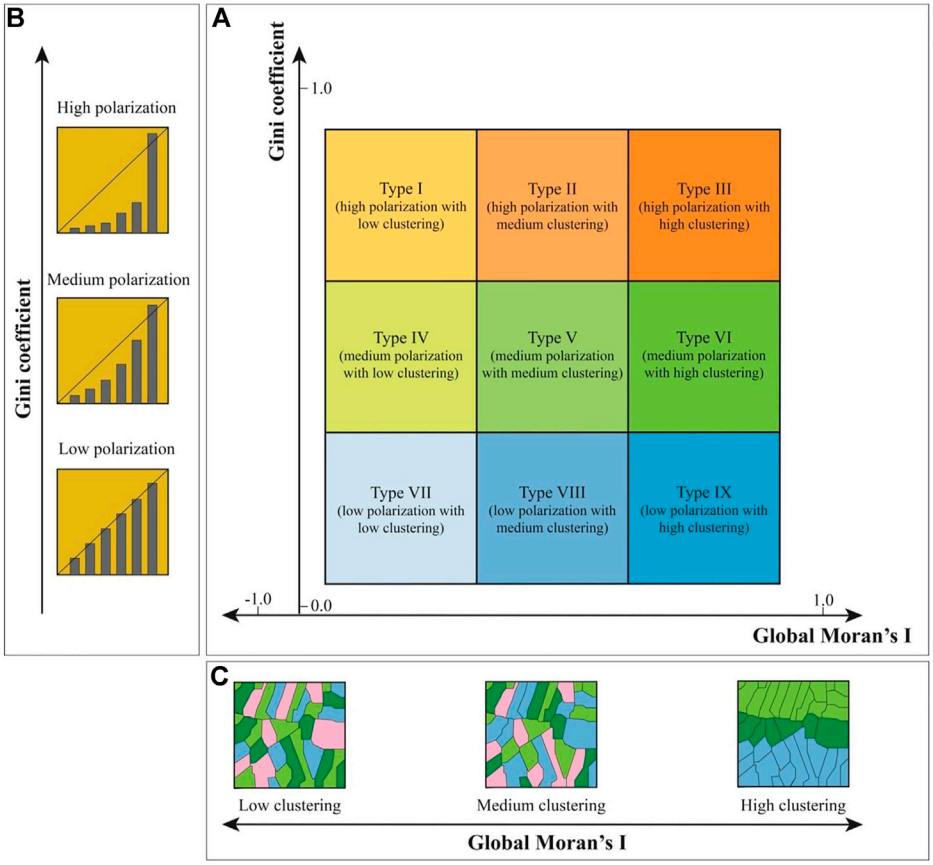

FIGURE 1
Classification method for water consumption patterns.

Patterns classification of water consumption by adopting two statistics

In order to achieve better management of water resources, the common way is to evaluate water carrying capacity or water efficiency. The core of water resources carrying capacity evaluation is to find the population or economic scale of the largest amount of water that can be carried by the water resources in a certain area. The core of water efficiency is to find the way to obtain the maximum output with the least water resources input. When evaluate water resources carrying capacity, both the consumption and the supply of water resources have been taken into consideration comprehensively. While assess water efficiency, the relationship between the consumption of water resources and the output (generally economic benefits) has been comprehensively considered.

Both water carry capacity and water efficiency provide a solid foundation and theoretical basis for water resources management. The research focus on water resources carrying capacity is to pay attention to whether the overall state of the city exceeds the threshold that the regional water resources can bear. Although the unevenness of the spatial distribution of water resources has been considered by water carrying capacity evaluation, the quantitative dimensions have not been researched. Water efficiency focuses on the relationship between water consumption and the output (generally refers to economic benefits). It takes the quantitative unevenness of water consumption into account without considering the spatial imbalance of water consumption. Neither water carrying capacity nor water efficiency has taken full account of water consumption patterns. However, water consumption patterns in different regions are not the same. Only by fully researching water consumption patterns in different regions, can more effective comprehensive water resources management and control strategies be formulated.

Therefore, we adopt the method proposed by Liu et al. (2019) when studying the carbon dioxide emission patterns. Two indicators have been selected in their research. The two indicators are Gini coefficient and Global Moran's I. Gini coefficient is used to represent the unevenness in quantity; Global Moran's I is used to represent the special unevenness.

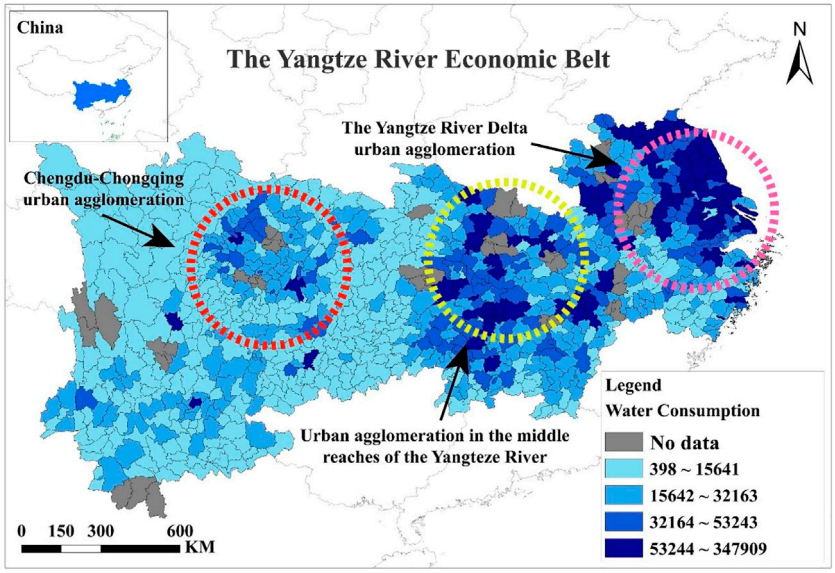

FIGURE 2
Water consumption of sub-cities in the Yangtze River Economic Belt (2015). Unit: 10,000 cubic meters.

Based on these two indicators, it is possible to study the water consumption patterns of 110 cities in the Yangtze River Economic Belt. By classifying different urban water consumption patterns, targeted measures are given for each category.

Gini coefficient

Gini coefficient is a term of economics, which refers to a common indicator used internationally to measure the income gap of residents in a country or region. The

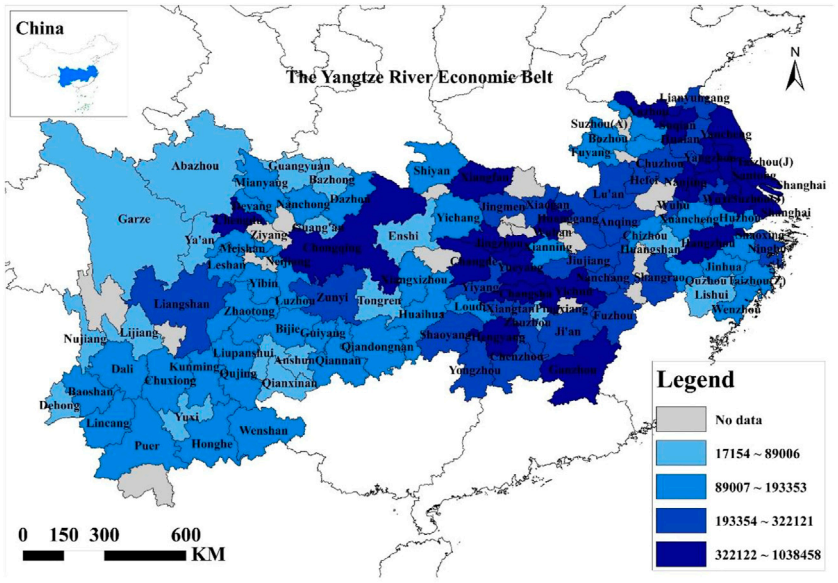

FIGURE 3
Consumption of water resources at the city scale in the Yangtze River Economic Belt (2015) Unit: 10,000 cubic meters.

maximum Gini coefficient is "1" and the minimum is equal to "0". In economics: the closer Gini coefficient is to 0, the more equal the wealth distribution is; when Gini coefficient is larger, the gap between the rich and the poor is larger. Gini coefficient has been introduced in other research fields, such as carbon dioxide emissions, water resources and other fields, to study the quantitative distribution characteristics. The larger Gini coefficient, the more uneven the distribution, and vice versa. We also use water consumption of sub-cities to fit the Lorentz curve, assuming that the area enclosed by the Lorentz curve and the two axes is S_B. And assuming that the area enclosed by diagonal and the two axes is S_{A+B}. Since the range of the coordinate axis is 0–1, the area of S_{A+B} is 0.5. Gini coefficient is defined as $(S_{A+B}-S_B)/S_{A+B}$. In this study, it is assumed that the Lorentz curve satisfies $LC = \alpha P^{\beta}$. Then, regression analysis is performed through water consumption data to obtain the values of α and β. Suppose the values of α and β are x and y, respectively. Then, S_B can be calculated by the following formula:

$$S_B = \int_0^1 mp^n dp = \frac{x}{y+1} \tag{1}$$

Gini coefficient can then be expressed as:

$$\text{Gini coefficient} = \frac{S_{A+B} - S_B}{S_{A+B}} = 1 - \frac{2x}{y+1} \tag{2}$$

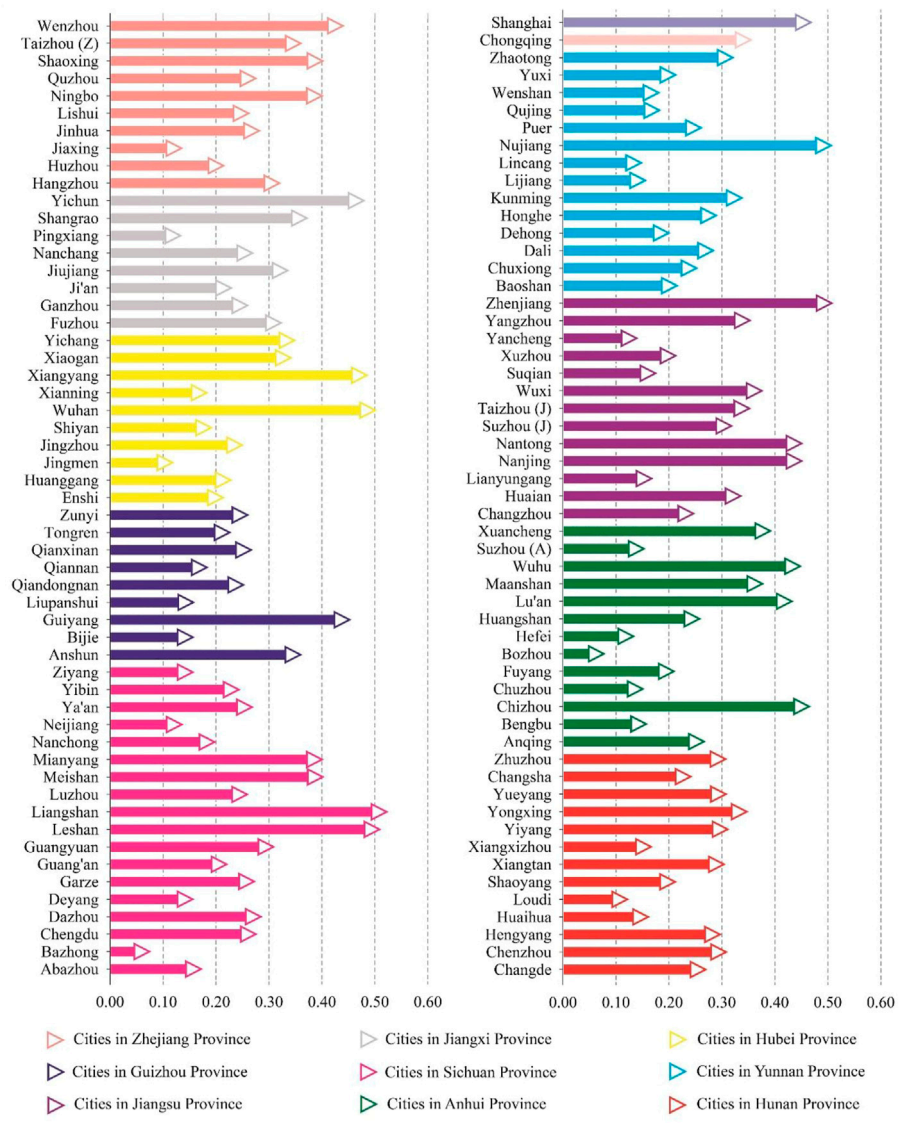

FIGURE 4
Gini coefficient of 110 cities (2015).

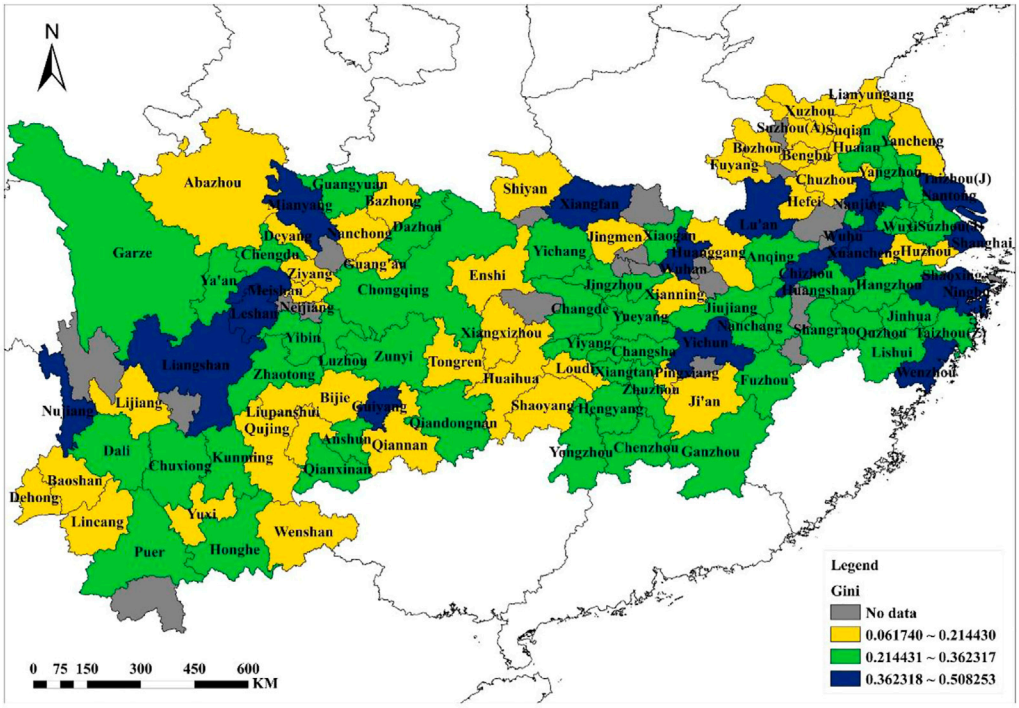

FIGURE 5
The spatial distribution of Gini coefficient of 110 cities (2015).

From the formula above, Gini coefficient of water consumption in each city is calculated by a python program. In general, the larger Gini coefficient, the more polarized the quantity of water consumption.

Global Moran's I

Global Moran's I is an index that reflects spatial autocorrelation, and it has been widely used. Global Moran's I is a maximum of "1" and a minimum of "−1". If Global Moran's I is greater than 0, indicating a positive spatial correlation. The larger the value is, the more obvious the spatial correlation. When Global Moran's I is less than 0, it indicates a negative spatial correlation. And the smaller the value is, the greater the spatial difference is. If Global Moran's I is equal to 0, it means that the spatial distribution of data is random. Global Moran's I has been calculated by spatial autocorrelation analysis in the ArcGis software toolbox.

The method for classification

In order to classify water consumption patterns of 110 cities in the Yangtze River Economic Belt, both Gini coefficient and Global Moran's I of the water consumption of 110 cities in the Yangtze River Economic Belt have been calculated, by adopting Natural Breaks, Gini coefficient and Global Moran's I has been divided into 3°. Then, based on a two-dimensional Cartesian coordinate system, we have obtained nine types of water consumption patterns (see Figure 1). Natural Breaks is a grading and classification method according to the statistical distribution of numerical statistics. It can maximize the difference between classes. It is worth noting that among these 9 types, there is none that is better than the others.

Results and discussion

Water consumption of 110 cities in the Yangtze River Economic Belt in 2015

Figure 2 shows the location of the three major urban agglomerations of the Yangtze River Economic Belt and the water consumption of the 877 sub-cities in the Yangtze River Economic Belt in 2015. It can be seen that water consumption is related to the distribution of urban agglomerations.

Figure 3 shows the water consumption of 110 cities in the Yangtze River Economic Belt in 2015.

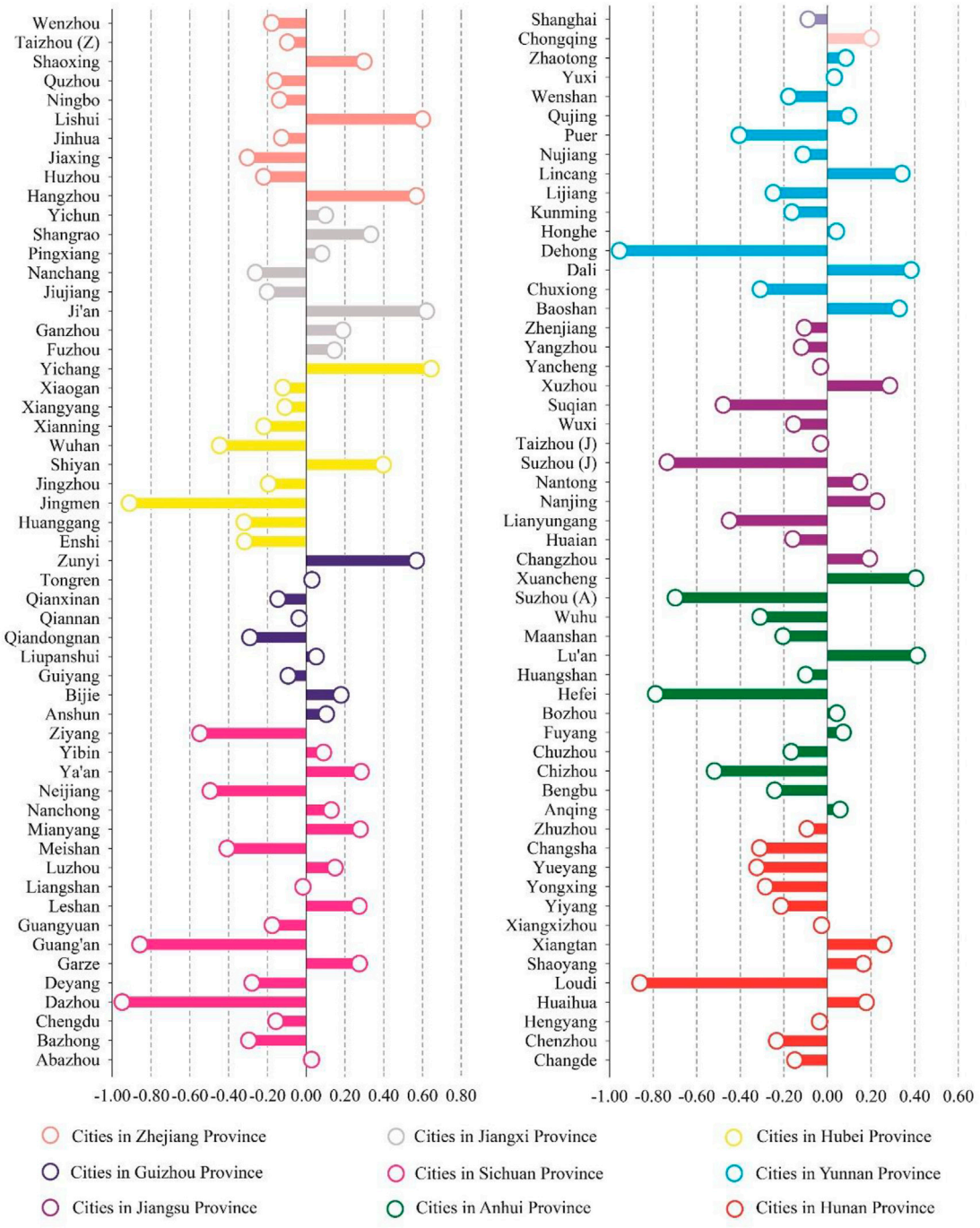

FIGURE 6
Global Moran's I of 110 cities (2015).

The quantitative pattern of water consumption

The calculation results of Gini coefficients of 110 cities in the Yangtze River Economic Belt are shown in Figure 4. On the whole, Gini coefficients of 110 cities are almost all less than 0.5. From this result, we can draw two conclusions. Firstly, because Gini coefficient varies from 0 to 1, and Gini coefficients of 110 cities are almost in the range of 0–0.5, indicating that Gini coefficients of water consumption in 110 cities are not

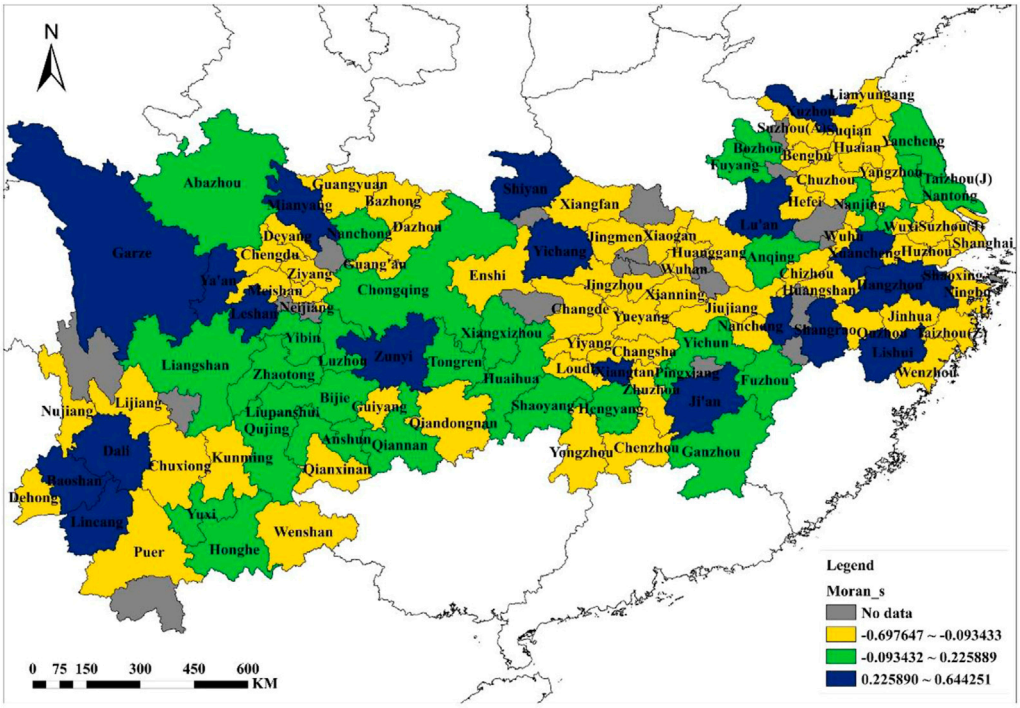

FIGURE 7
Spatial distribution of Global Moran's I of 110 cities (2015).

much different. Secondly, it can be seen that the water consumption of each region in each of the 110 cities does not vary greatly in quantity, and there is no one area or several areas that consume the entire city plays a decisive role, so we cannot reduce the overall water consumption of the city by controlling the water consumption of certain areas in the city.

Although Gini coefficients of the 110 cities are not much different, Gini coefficients of water consumption in different cities still have the following differences. For example, Gini coefficient of water consumption in Liangshan is the largest, slightly exceeding 0.5, and is 0.5082, indicating that the water consumption in various areas within the city of Liangshan has the largest difference in quantity. In 110 cities, with the exception of Liangshan, Gini coefficient of water consumption in other cities are all less than 0.5. The top 10 cities with the highest Gini coefficients are Liangshan, Leshan, Zhenjiang, Nujiang, Wuhan, Xiangyang, Yichun, Shanghai, and Chizhou. For the two municipalities Shanghai and Chongqing, Gini coefficients of water consumption are 0.4545 and 0.3420 respectively. Gini coefficients of water consumption of 13 cities in Hunan Province are almost in the range of 0.1–0.3.

From the perspective of the spatial distribution of water consumption in 110 cities, the regions with severely polarized water consumption in 110 cities in the Yangtze River Economic Belt are concentrated in the east and west of the Yangtze River Economic Belt, as shown in Figure 5. The highly polarized areas are almost all concentrated within the three major urban agglomerations of the Yangtze River Economic Belt (the locations of the three major urban agglomerations in the Yangtze River Economic Belt are shown in Figure 2). Such distribution characteristics may be one of the effects of the implementation of the Yangtze River Economic Belt strategy by the Chinese central government in 2014. In addition, it can be seen from Figure 5 and Figure 2 that the polarization phenomenon and water consumption have a great correlation with the location of the three major urban agglomerations in the Yangtze River Economic Belt. In 2018, General Secretary of China Xi Jinping pointed out, "the Yangtze River has a unique ecosystem and is an important ecological treasure trove of our country. For a long period of time now and in the future, we must put the restoration of the Yangtze River ecological environment in an overwhelming position." This shows the Chinese government's determination to improve the restoration of the ecological environment of the Yangtze River.

The spatial pattern of water consumption

Judging from the results of Global Moran's I on the water consumption of 110 cities in the Yangtze River Economic Belt, Global Moran's I is between 0–1 and 0–1. The city with the

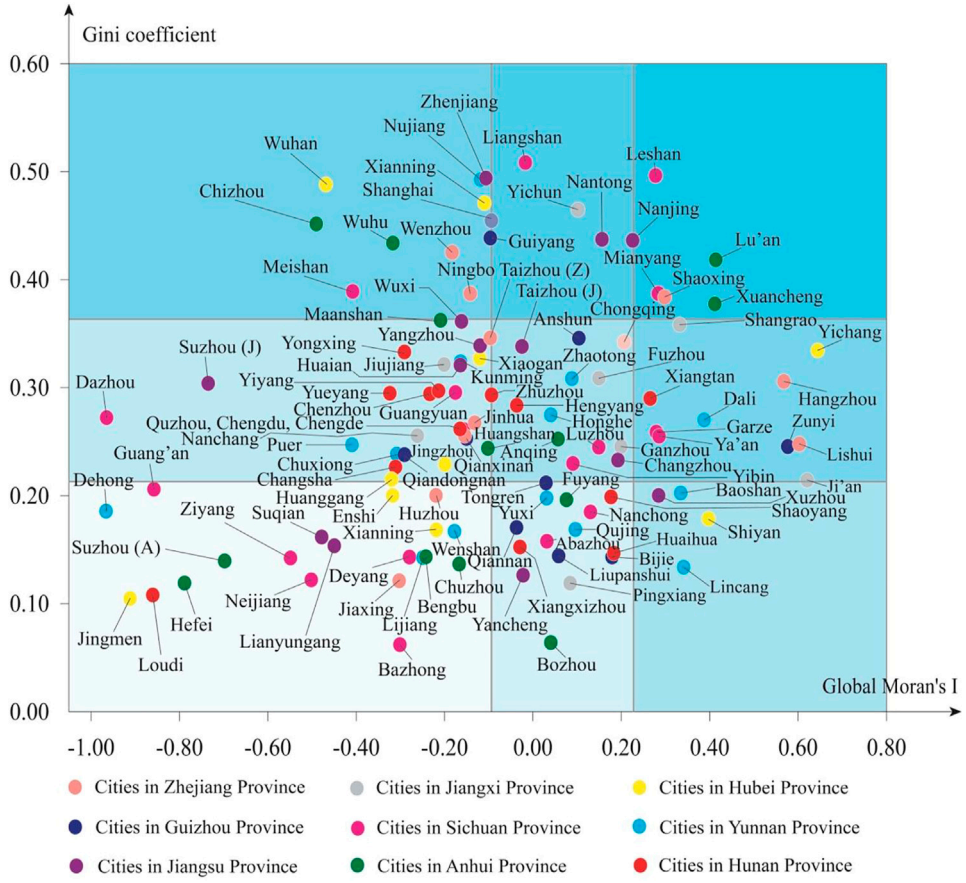

FIGURE 8
Classification of 110 cities in the Yangtze River Economic Belt based on water consumption in 2015.

largest Global Moran's I is Yichang, it is 0.6443; the second is Ji'an, it is 0.6205; and the third is Lishui, it is 0.6028. There are 44 cities with a positive Global Moran's I. The larger Global Moran's I indicates that the city's water consumption is agglomerated the city's water consumption. In other words, as the spatial distribution of the location is gathered, the correlation of water consumption is more significant. There are 66 cities with negative Global Moran's I, the smallest are Dazhou, Dehong, Jingmen, and their Global Moran's I are −0.969401, −0.96612, −0.91164, which are all close to −1.0, indicating that the water consumption situation shows a discrete phenomenon meaning as the spatial distribution location is discrete, the correlation of water consumption becomes significant. Because Global Moran's I of 110 cities in the Yangtze River Economic Belt is distributed in the range of 0–1 and 0–1, we can draw the conclusion that the water consumption of these 110 cities in terms of water consumption spatial autocorrelation is different, but this different trend of spatial autocorrelation is temporarily uncertain (Figure 6). To determine this trend, one needs to obtain water consumption data on the sub-cities scale of these 110 cities over a long period of time.

The spatial distribution of Global Moran's I of water consumption in 110 cities in the Yangtze River Economic Belt is shown in Figure 7. As can be seen from Figure 7, the regions with high, medium, and low global Moran indices are scattered. The areas with high Global Moran's I and low areas are distributed in the east, middle and west of the Yangtze River Economic Belt, while the areas with medium Global Moran's I are mainly distributed in the central and western regions of the Yangtze River Economic Belt. The distribution of Global Moran's I is not significantly related to the distribution of the three major urban agglomerations in the Yangtze River Economic Belt.

City type and policy implications

Based on the classification method given in Part 2, we divided Gini coefficient and Global Moran's I of the 110 cities

TABLE 2 City types and corresponding policy recommendations.

Type	Cities	Policy recommendations
I	Zhenjiang, Nujiang, Xianning, Shanghai, Wuhan, Chizhou, Wuhu, Wenzhou, Guiyang, Meishan, Ningbo	To develop water-saving policies for large water users in all regions
II	Liangshan, Yichun, Nantong, Nanjing	To develop water-saving policies for large water users in some regions
III	Leshan, Lu'an, Mianyang, Shanxing, Xuancheng	To develop water-saving policies for major water users in several key locations
IV	Dazhou, Suzhou(J), Mananshan, Wuxi, Yangzhou, Yongxing, Jiujiang, Yiyang, Xiaogan, Kunming, Taizhou(Z), Zhuzhou, Huaian, Yueyang, Chenzhou, Guangyuan, Jinhua, Huangshan, Jingzhou, Qianxinan, Qiandongnan, Huanggang, Changsha, Chuxiong, Puer, Nanchang, Quzhou, Chengdu, Chengde	To develop water-saving policies for key water users in all regions
V	Taizhou(J), Anshun, Chongqing, Zhaotong, Fuzhou, Hengyang, Honghe, Luzhou, Anqing, Ganzhou, Changzhou, Yibin	To develop water-saving policies for major water users in some regions
VI	Shangrao, Yichang, Xiangtan, Dali, Hangzhou, Garze, Ya'an, Zunyi, Lishui, Ji'an	To develop water-saving policies for key water users in several key locations
VII	Dehong, Guang'an, Ziyang, Suqian, Enshi, Huzhou, Xianning, Suzhou(A), Jingmen, Loudi, Hefei, Neijiang, Lianyungang, Deyang, Wenshan, Chuzhou, Jiaxing, Bengbu, Lijiang, Bazhong	To develop water-saving policies for all water users in all regions
VIII	Tongren, Fuyang, Nanchong, Qujing, Abazhou, Yuxi, Qiannan, Yancheng, Bozhou, Xiangxizhou, Pingxiang, Liupanshui, Bijie, Huaihua, Shaoyang	To develop water-saving policies for all water users in some regions
IX	Baoshan, Xuzhou, Shiyan, Lincang	To develop water-saving policies for all water users in several key locations

in the Yangtze River Economic Belt into three levels by adopting Natural Breaks. Then, in the two-dimensional Cartesian coordinate system composed of Gini coefficient and Global Moran's I, water consumption patterns of 110 cities in the Yangtze River Economic Belt are divided into nine types, and the classification results are shown in Figure 8. In the image below, each rectangle represents one type. Each pie shape in Figure 8 represents a city, and the colors of the different pie shapes represent the provinces to which the city belongs. The names of the provinces corresponding to each color are shown in Figure 8.

As can be seen from Figure 8, each type contains at least one city. Cities tend to be located in the middle of the rectangular coordinate system. The distribution of 110 cities in the Yangtze River Economic Belt in nine types is shown in Table 2. 11 cities belong to type I, four cities belong to type II, five cities belong to type III, and there are 29 cities belong to type IV. Twelve cities belong to type V, 10 cities belong to type VI, 20 cities belong to type VII, 15 cities belong to type VIII, and four cities belonging to type IX.

It is important to note that when formulating effective policies to reduce water consumption according to different types of consumption patterns, the following principles need to be followed:

1) When Gini coefficient of the city's water consumption is high, it indicates that the polarization of water consumption in the city is more obvious. In order to effectively reduce water consumption, effective water saving policies needs to be formulated for large water users.
2) When Gini coefficient of the city's water consumption is low, it indicates that the polarization of water consumption in the city is not obvious. To effectively reduce water consumption, it is necessary to formulate effective water saving policies for all water users.
3) When the city's water consumption is in a medium Gini coefficient, it indicates that the polarization of water consumption in the city is between obvious and inconspicuous. In order to effectively reduce water consumption, develop effective water-saving policies for major water users (broader users than large water users).
4) When Global Moran's I of the city's water consumption is at a high level, it indicates that the city's water consumption has a significant autocorrelation in space meaning, with the accumulation of spatial distribution locations of the water consumption, the correlation becomes more significant. Therefore, in order to effectively reduce the consumption of water resources, effective water conservation policies should be formulated in several key positions as a priority.
5) When Global Moran's I of the city's water consumption is low, it indicates that the city's water consumption is in a discrete form in space, that is, as the spatial distribution location is discrete, the correlation of water consumption is more significant. In order to effectively reduce the consumption of water resources, priority should be given to effective water conservation policies in some regions.
6) When Global Moran's I of the city's water consumption is in a medium state, it indicates that the city's water consumption is randomly distributed in space. Therefore, in order to effectively

reduce water consumption, it should be formulated in all regions. This is targeted water-saving policy.

Based on the principles above, we provide policies that can effectively reduce water consumption for nine different urban water consumption modes, as shown in Table 2. For example, in the cities of type I, water consumption is the most polarized in terms of quantity and the spatial autocorrelation is the worst. Therefore, in order to reduce water consumption to the greatest extent, it is necessary to formulate water conservation for large water users in all regions. When a city is located in type II, water consumption is highly polarized in quantity, and the spatial autocorrelation is in a medium state. It is necessary to formulate water-saving policies for large water users in some areas.

From the perspective of the provinces, the cities of Hunan Province are mainly distributed in Type IV, indicating that the polarization of water consumption in various cities in Hunan Province is at a medium level. Cities need to prioritize water conservation policies for key water users in all regions. However, the distribution of cities in other provinces in the two-dimensional rectangular coordinate system does not show obvious distribution rules.

Conclusion

Water consumption patterns of different regions are not the same. Only by fully researching water consumption patterns in different regions can more effective comprehensive water resources management and control strategies be formulated. According to the characteristics of different regions, it is necessary to formulate different and more effective water—saving policies.

Consequently, this study introduced Gini coefficient and Global Moran's I, and divided each index into three levels by adopting Natural Breaks. In this way, all cities in the two-dimensional Cartesian coordinate system composed of Gini coefficient and Global Moran's I. The water consumption patterns can be divided into nine types. On the one hand, from the perspective of Gini coefficient: cities with high Gini coefficients indicate that there is a significant polarization in the amount of water consumed. Therefore, by effectively managing large water users, it is possible to achieve overall reductions in water consumption. For cities with lower Gini coefficients, it means that the water consumption in those cities is less quantitative in quantity, because in order to effectively reduce water consumption, it is necessary to formulate water conservation policies for all water users. On the other hand, from the perspective of Global Moran's I: cities with a high Global Moran's I indicate that there is a clear spatial autocorrelation phenomenon in water consumption, and therefore effective water conservation policies need to be formulated in several key locations and for cities where Global Moran's I is low, it shows that the city's water consumption is spatially discrete. In order to effectively reduce water consumption, priority should be given to effective water conservation policies in some areas. This study uses the above methods to divide the water consumption patterns of 110 cities in the Yangtze River Economic Belt into nine types in 2015. Based on the above principles, targeted water conservation is given to cities that belong to each type of water consumption pattern.

At the same time, through the visualization of nine types of water consumption patterns of 110 cities in the Yangtze River Economic Belt, it was found that 110 cities belonged to the largest number of types IV, VII, and VIII. A large number of cities are located in the lower left corner of the two-dimensional Cartesian coordinate system, indicating that these cities belong to a state where the polarization phenomenon is not obvious and the spatial distribution is discrete. For this type of city, it is necessary to formulate sections for all water users in all regions.

This study provides important technical and theoretical support for effectively reducing water consumption in cities in the Yangtze River Economic Belt. At the same time, this research can provide reference significance for the formulation of policies on water consumption in other regions or cities. It is hoped that the methods used in this research can be widely applied in future research.

Data availability statement

The original contributions presented in the study are included in the article/supplementary material, further inquiries can be directed to the corresponding author.

Author contributions

BS contributed to conception and design of the study, analysis and interpretation of data, drafting the manuscript. FL wrote sections of the manuscript, acquisition of data. All authors contributed to manuscript revision, read, and approved the submitted version.

Conflict of interest

The authors declare that the research was conducted in the absence of any commercial or financial relationships that could be construed as a potential conflict of interest.

Publisher's note

References

Bian, D., Yang, X., Wu, F., Babuna, P., Luo, Y., Wang, B., et al. (2022a). A three-stage hybrid model investigating regional evaluation, pattern analysis and obstruction factor analysis for water resource spatial equilibrium in China. *J. Clean. Prod.* 331, 129940. doi:10.1016/j.jclepro.2021.129940

Bian, D., Yang, X., Xiang, W., Sun, B., Chen, Y., Babuna, P., et al. (2022b). A new model to evaluate water resource spatial equilibrium based on the game theory coupling weight method and the coupling coordination degree. *J. Clean. Prod.* 366, 132907. doi:10.1016/j.jclepro.2022.132907

Boulay, A., Bare, J., Benini, L., Berger, M., Lathuillière, M. J., Manzardo, A., et al. (2018). The WULCA consensus characterization model for water scarcity footprints: assessing impacts of water consumption based on available water remaining (AWARE). *Int. J. Life Cycle Assess.* 23 (2), 368–378. doi:10.1007/s11367-017-1333-8

Chang, Y., Huang, R., Ries, R. J., and Masanet, E. (2015). Life-cycle comparison of greenhouse gas emissions and water consumption for coal and shale gas fired power generation in China. *Energy* 86, 335–343. doi:10.1016/j.energy.2015.04.034

Cole, M. J., Bailey, R. M., Cullis, J. D. S., and New, M. G. (2018). Spatial inequality in water access and water use in South Africa. *Water Policy* 20 (1), 37–52. doi:10.2166/wp.2017.111

CPGPRC (The Central People's Government of the People's Republic of China) (2010). National comprehensive water resources plan. [in Chinese] Available at: http://www.gov.cn/gzdt/2010-11/25/content_1753339.htm (Accessed December 25, 2010).

Deng, G., Li, L., and Song, Y. (2016). Provincial water use efficiency measurement and factor analysis in China: based on SBM-DEA model. *Ecol. Indic.* 69, 12–18. doi:10.1016/j.ecolind.2016.03.052

EPMC (Environmental Protection Ministry of China) (2017). Ecological environment protection plan of the Yangtze river economic belt. [in Chinese] Available at: http://www.mee.gov.cn/gkml/hbb/bwj/201707/t20170718_418053.htm (Accessed July 17, 2017).

Fercovic, J., Foster, W., and Melo, O. (2019). Economic development and residential water consumption in Chile. *Environ. Dev. Econ.* 24 (1), 23–46. doi:10.1017/s1355770x18000463

Freire-González, J. (2019). Does water efficiency reduce water consumption? The economy-wide water rebound effect. *Water Resour. Manage.* 33 (6), 2191–2202. doi:10.1007/s11269-019-02249-0

Gleick, P. H. (2003). Water use. *Annu. Rev. Environ. Resour.* 28 (1), 275–314. doi:10.1146/annurev.energy.28.040202.122849

Hoekstra, A. Y., and Chapagain, A. K. (2006). Water footprints of nations: water use by people as a function of their consumption pattern. *Water Resour. Manage.* 21 (1), 35–48. doi:10.1007/s11269-006-9039-x

Hu, J., Wang, S., and Yeh, F. (2006). Total-factor water efficiency of regions in China. *Resour. Policy* 31 (4), 217–230. doi:10.1016/j.resourpol.2007.02.001

Jaramillo, F., and Destouni, G. (2015). Local flow regulation and irrigation raise global human water consumption and footprint. *Science* 350 (6265), 1248–1251. doi:10.1126/science.aad1010

Jethoo, A. S., and Poonia, M. P. (2011). Water consumption pattern of Jaipur city (India). *Int. J. Env. Sci. Dev.* 2 (2), 152–155. doi:10.7763/ijesd.2011.v2.114

Keshavarzi, A. R., Sharifzadeh, M., Kamgar Haghighi, A. A., Amin, S., Keshtkar, S., and Bamdad, A. (2006). Rural domestic water consumption behavior: a case study in ramjerd area, fars province, I.R. Iran. *Water Res.* 40 (6), 1173–1178. doi:10.1016/j.watres.2006.01.021

Lebel, L., Lebel, P., and Chuah, C. J. (2019). Governance of aquaculture water use. *Int. J. Water Resour. Dev.* 35 (4), 659–681. doi:10.1080/07900627.2018.1457513

Liu, H., Nie, J., Cai, B., Cao, L., and Wang, X. (2019). CO2 emissions patterns of 26 cities in the Yangtze River Delta in 2015: Evidence and implications. *Environ. Pollut.* 252, 1678–1686. doi:10.1016/j.envpol.2019.06.102

Long, H., Lin, B., Ou, Y., and Chen, Q. (2019). Spatio-temporal analysis of driving factors of water resources consumption in China. *Sci. Total Environ.* 690, 1321–1330. doi:10.1016/j.scitotenv.2019.06.311

Risch, E., Loubet, P., Núñez, M., and Roux, P. (2014). How environmentally significant is water consumption during wastewater treatment?: application of recent developments in LCA to WWT technologies used at 3 contrasted geographical locations. *Water Res.* 57, 20–30. doi:10.1016/j.watres.2014.03.023

Sauri, D. (2019). The decline of water consumption in Spanish cities: structural and contingent factors. *Int. J. Water Resour. D.* 36, 909–925. doi:10.1080/07900627.2019.1634999

Silalertruksa, T., Gheewala, S., Mungkung, R., Nilsalab, P., Lecksiwilai, N., and Sawaengsak, W. (2017). Implications of water use and water scarcity footprint for sustainable rice cultivation. *Sustainability* 9 (12), 2283. doi:10.3390/su9122283

UN-water (2018). World water development report 2018. Available at: https://www.unwater.org/publications/world-water-development-report-2018/(Accessed March 19, 2018).

Wang, Y., Bian, Y., and Xu, H. (2015). Water use efficiency and related pollutants' abatement costs of regional industrial systems in China: a slacks-based measure approach. *J. Clean. Prod.* 101, 301–310. doi:10.1016/j.jclepro.2015.03.092

Willis, R. M., Stewart, R. A., Giurco, D. P., Talebpour, M. R., and Mousavinejad, A. (2013). End use water consumption in households: impact of socio-demographic factors and efficient devices. *J. Clean. Prod.* 60, 107–115. doi:10.1016/j.jclepro.2011.08.006

Zhang, X., Liu, J., Zhao, X., Yang, H., Deng, X., Jiang, X., et al. (2019). Linking physical water consumption with virtual water consumption: methodology, application and implications. *J. Clean. Prod.* 228, 1206–1217. doi:10.1016/j.jclepro.2019.04.297

frontiers | Frontiers in Earth Science

TYPE Review
PUBLISHED 25 August 2022
DOI 10.3389/feart.2022.970582

OPEN ACCESS

EDITED BY
Chunhui Li,
Beijing Normal University, China

REVIEWED BY
Ying Zhu,
Xi'an University of Architecture and Technology, China
Yongyong Zhang,
Institute of Geographic Sciences and Natural Resources (CAS), China
Baohui Men,
North China Electric Power University, China
Liu Liu,
China Agricultural University, China

*CORRESPONDENCE
Boyang Sun,
sunboyang@aliyun.com

SPECIALTY SECTION
This article was submitted to Hydrosphere, a section of the journal Frontiers in Earth Science

RECEIVED 16 June 2022
ACCEPTED 25 July 2022
PUBLISHED 25 August 2022

CITATION
Yang X, Sun B, Lei S, Li F and Qu Y (2022), A bibliometric analysis and review of water resources carrying capacity using rené descartes's discourse theory. *Front. Earth Sci.* 10:970582. doi: 10.3389/feart.2022.970582

A bibliometric analysis and review of water resources carrying capacity using rené descartes's discourse theory

Xiaojing Yang[1], Boyang Sun[2]*, Sheng Lei[3], Fapeng Li[2] and Yanping Qu[1]

[1]Research Center on Flood and Drought Disaster Reduction, China Institute of Water Resources and Hydropower Research, Beijing, China, [2]Development Research Center of the Ministry of Water Resources of P.R.China, Beijing, China, [3]Jiangxi Academy of Water Science and Engineering, Nanchang, China

Water Resources Carrying Capacity is an important indicator of water sustainable and economic development, yet few studies investigated a bibliometric analysis of Water Resources Carrying Capacity research. In this research, we proposed a four-staged bibliometric analysis method for Water Resources Carrying Capacity studies following the René Descartes's *Discourse on the Method* guidelines which makes the bibliometric analysis process more systematic. Our four-staged bibliometric analysis method contains a refined screening process of the records, which can successfully delete poorly correlated data from tens of thousands of data within a short period of time and determined the subject-related data. The screening results shortlisted 271 records from an initial 16,769. We further conducted a complete bibliometric, statistical and meta-analysis of the 271 records. The results showed that China is the major country that conducts research on Water Resources Carrying Capacity. Modeling in various forms and system dynamics are the mainstream methods of Water Resources Carrying Capacity research. Water Resources Carrying Capacity is intrinsically linked to population carrying capacity, groundwater resources, urbanization and water shortage. Based on a comprehensive analysis of the research of Water Resources Carrying Capacity, we divided the research progress into five stages lastly. The method proposed in this research can provide reference for future bibliometric studies.

KEYWORDS

water resources carrying capacity, screening method, bibliometric analysis, water carrying state, VOSviewer

1 Introduction

1.1 Research backgound

Water resources are an important part of the natural environment and guarantee the development of the human society and economy. However, the distribution of water resources in space and time is often uneven. Rapidly developing and densely populated areas need more water resources but due to their uneven distribution, water resources in some areas cannot satisfy the local human population and economic demand for water (Yu et al., 2017). In this regard, it is important to pay attention to the relationship between the supply and consumption of water resources to be able to balance interaction between the two. Studying the relationship between water supply and consumption, that is, focusing on the water resources carrying capacity, is of great significance for the sustainable use of water resources within a certain region. Concern on sustainable use of water resources has increased due to the unprecedented growth and expansion of global economies within the last 3 decades that has placed an insatiable demand on water resources (Wu et al., 2020; Bian et al., 2022a). Hence, it important to comprehensively study Water Resources Carrying Capacity (WRCC) to be able to achieve an efficient water related sustainable management.

1.2 Literature review and research gap

The concept of carrying capacity began in the study of physics and refers to the maximum load that an object can bear before any irreversible deformation occurs (Dhondt, 1988). Carrying capacity was however introduced from biology where it was applied in the study of wild animals (Young, 1998; Malthus, 1798). In 1921, Park and Burgess (Park and Burgess, 1921) re-invented the idea to calculate the maximum population that can be carried by a specific area from an ecological perspective based on the supply of objects and the state of natural and social resources in a specific period. From hence, carrying capacity has been applied in the field of ecology (Mcnaughton and Wolf, 1970; Kessler, 1994).

From early 1970, population and economic expansion, which sustained for 30 years, created a contradiction between social development and environmental sustainability and this triggered a worldwide exploration of the issue of Resources and Environmental Carrying Capacity (RECC). Afterwards, other concepts such as Land Carrying Capacity (Shi et al., 2013), Environmental Carrying Capacity (Li et al., 2019), and Resource Carrying Capacity (Wang et al., 2020) emerged, peaking research on carrying capacity.

In 1985, the United Nations Educational, Scientific and Cultural Organization (UNESCO) (UNESCO&FAO, 1985) proposed the definition of Resources Carrying Capacity. Onwards, from then, carrying capacity has become one of the main contents of the concept of sustainable development (Bolis et al., 2017). In 1995, Arrow, the Nobel laureate in economics, and other well-known economists and ecologists (Arrow et al., 1995) published an article "Economic Growth, Carrying Capacity and Environment" in "Science", which greatly improved the sustainable development and cataloged carrying capacity research in the scientific community.

WRCC is an extension of the concept of carrying capacity in the field of water resources, and belongs to a research aspect of Resources Carrying Capacity. WRCC research mainly originated in China. Though studied in other parts of the world at the time, scholars elsewhere regarded WRCC as part of the contents of sustainable development research and described it with terms such as available water and limits of river development (Falkemark and Lundqvist, 1998; Jonathan, 1999; Rijisberman and Frans, 2000; Gleick and Palaniappan, 2010; Zhu et al., 2010). An official scientific study of WRCC began in the late 1980's when the Xinjiang Water Resources Research Group met to discuss WRCC (XWRSSRG (Xinjiang Water Resources Soft Science Research Group), 1989). In 1990s, the concept of WRCC was clearly put forward by Shi Yafeng, an Academician of the Chinese Academy of Sciences (Shi and Qu, 1992). WRCC is about the relationship between the carrying "subjects" and the 'objects' in the "water resources-ecological environment-social economy" system, and whether the load generated by the objects exceeds the supporting capacity of the subjects.

After nearly 30 years of exploration and development, a large number of scientific research results have been discovered in the research of WRCC which has increasingly become a hot issue in regional water resources management. Early researches on WRCC mostly focused on cities (Yue et al., 2015; Dai et al., 2019; Yang et al., 2019), provinces (Huang et al., 2014; Yang and Ding, 2018; Deng et al., 2019; Zhu et al., 2019) and river basins (Yang et al., 2010; Wu et al., 2018a; Meng et al., 2018; Wang et al., 2018; Kang et al., 2019). With the continuous deepening of research on WRCC, especially in recent years, its research objects have also changed. More and more researches have begun to focus on the study of WRCC of some typical regions including arid and semi-arid areas (Wang et al., 2010; Xie et al., 2014; Li and Zhang, 2016; Qi et al., 2016; Xiao et al., 2017), urbanized regions (Gao, 2017), lake basins (Lei et al., 2013), water-deficient regions (Wang et al., 2014), karst regions (Bo et al., 2016; Yang et al., 2016; Li et al., 2018), mining areas (Chi et al., 2019), industrial park (Kang and Xu, 2012), islands (Cao et al., 2014; Kuspilić et al., 2018) and wetlands (Wang et al., 2017). While other studies have shown interest in WRCC research for certain specific periods, for example, some studies concentrate on WRCC of arid rangelands during the droughts (Accatino et al., 2017).

Calculation methods of WRCC have evolved over the study period. New methods including back propagation model (Yang

and Han, 2011), matter element analysis (Gao et al., 2013), grey clustering (Gao and Sun, 2018), state-space method (Tang et al., 2016), support vector machines (Zhang et al., 2008), analytic hierarchy process (Zhang et al., 2014; Chi et al., 2019), set pair analysis (Fu et al., 2008; Liu et al., 2018), multi-objective programming model (Wang and Zeng, 2013), metabolic theory (Ren et al., 2016), ecological footprint (Zhang and Li, 2012; Wang et al., 2017; Li et al., 2018; Dai et al., 2019; Yang et al., 2019), system dynamic model (Wang et al., 2014; Yang et al., 2015; Song, 2016; Fang, 2018; Sun and Yang, 2019), catastrophe theory (Chen et al., 2010; Song et al., 2020), cloud model (Cheng et al., 2018) and neural network (Lu et al., 2009; Wang, 2015) have been discovered. Some methods are a combination of two or three, such as, neural network and projection pursuit (Zhao, 2012); inexact fuzzy and multi-objective programming model (Wang and Zeng, 2013); analytic hierarchy process and fuzzy discrimination method (Chi et al., 2019); set pair analysis and entropy weight method (Cui et al., 2018); maximum entropy and entropy weight (Li et al., 2019); fuzzy set pair analysis model (Liu et al., 2018); combination weights and entropy principles (Zhou et al., 2017) and grey neural network model (Zheng et al., 2016).

The development and expansion of WRCC also witnessed the evolution of another concept of WRCC known as Water Resources Carrying State (WRCS) (Jiao and Liang, 2006; Ye et al., 2018). WRCC and WRCS are similar but differ slightly. Although the research on WRCC and WRCS both focus on the supply and demand of water resources within a certain area, WRCC tends to pay more attention on the larger economy and population that water resources in a certain area can support, making WRCC a threshold concept, while WRCS focuses on the balance between water supply and demand in a region.

1.3 The main work and innovations

Although the research on WRCC has increasingly become a hot topic in regional water resources management, bibliometric analysis of literature on it are still very limited (Zhang and Wang, 2012; Jin et al., 2019). Bibliometric analysis of the research on WRCC can clarify the development context and knowledge base, understand the development process, clarify the research progress, define research trends and provide scientific reference of WRCC studies.

To do a philosophical and scientific review of literature, we adopted René Descartes's (1596. 3. 31–1650. 2. 11) method of philosophical thinking expressed in his book, *"Discourse on the Method of Rightly Conducting One's Reason and of Seeking Truth in the Sciences"* (*Discourse on the Method*, in French: *Discours de la méthode pour bien conduire sa raison, et chercher la vérité dans les sciences*) (80). Based on his philosophical concept, René Descartes proposed a four-staged method of researching a problem which he categorized into the following: 1) The doubt stage, 2) The partition of problem stage, 3) Sequencing of thoughts and problem-solving stage, and 4) The comprehensive inspection and review stage (Wikiquote contributors, 2020b). These four stages have important guiding significance for both scientific research and social practice, and thus have been widely researched and used in other studies, however, to our knowledge, no study has yet applied this thinking in bibliometric analysis. The basis of theoretical analysis is lacking in most bibliometric studies.

While conducting studies on bibliometric analysis, researchers often have to deal with thousands of records, some, not closely related with the topic under study. Some researchers perform manual screening of records directly (Tao et al., 2020), which consumes large quantities of time. And some of the studies even lack the process of screening (Huang et al., 2020; Mallawaarachchi et al., 2020; Secinaro et al., 2020), which will lead to less credibility of the results. Since finding out the subject-related records can be very time consuming, an efficient method that can quickly and precisely sort-out topic-related records within a short period of time is necessary. Consequently, we proposed a refined literature screening process to effectively and efficiently sort out relevant from irrelevant literature.

This article aims to sort out and summarize the research on WRCC through bibliometric analysis. The remaining parts of the article are structured as follows: the second part introduces the retrieval process, the records screening method and the analysis process; the third part analyzes and discusses the results of the bibliometric analysis and statistical analysis of WRCC; the fourth part summarizes the full text, and prospects for future development of research on WRCC.

2 A four-staged bibliometric analysis for WRCC

René Descartes's *Discourse on the Method* has been used as a general guideline, by which we build the framework of this research. Section 2.1 shows how we applied Descartes's four-staged methodology. Due to the macroscopic nature of Descartes's methodology, it is difficult to guide the specific steps (Wikiquote contributors, 2020b). According to the specific process of bibliometric analysis, and based on Descartes's methodology, we also divided the concrete steps of bibliometric analysis into four stages in this research (Section 2.2).

2.1 René descartes's *Discourse on the Method* and application

In Descartes's book *Discourse on the Method*, he proposed the true method by which to arrive at the knowledge of whatever lay within the compass of his powers, and he summarized this

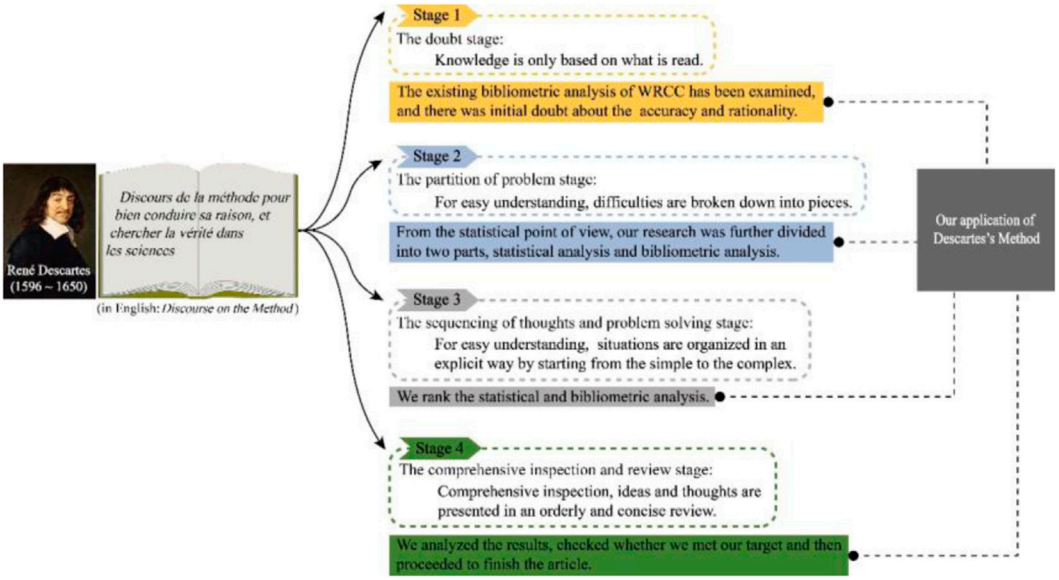

FIGURE 1
Framework and application of René Descartes's *Discourse on the Method*. Source of René Descartes's portrait: image.baidu.com.

method into four stages (Figure 1). These include: 1) The doubt stage in which ideas are scattered and uncoordinated, and knowledge is based only on what is read; 2) The partition of problem stage, where difficulties are broken down to pieces for easy understanding; 3) The sequencing of thoughts and problem solving stage, where by starting from the simple to the complex, difficult situations are organized in an explicit way for easy understanding and problem-solving; 4) The comprehensive inspection and review stage where enumerations are completed while ideas and thoughts are presented in an orderly and concise review (Wikiquote contributors, 2020b).

Putting René Descartes's study into perspective, in the first stage (Figure 1.) of this study where we examined the existing bibliometric analysis of WRCC, there was initial doubt about the rationality and accuracy of existing bibliometric research on WRCC. We found that the existing bibliometric analysis of WRCC were not systematic, lacked coherency and were not comprehensive. This confirmed our earlier assertion that bibliometric research on WRCC is limited. Only two studies by Zhang and Wang (2012) and Jin et al. (2019) have done a bibliometric analysis of WRCC. Zhang and Wang (2012) only conducted a bibliometric analysis of Chinese literature, and ignored the bibliometric analysis of English literature. Their paper is archaic ((Zhang and Wang, 2012), was published 8 years ago), and does not reflect the bibliometric analysis of current WRCC research. Even though Jin et al. (2019) was published recently, their work lacks a detailed screening process of the records (data) and also lacks rationality and accuracy of the results. The above two scenarios are part of the foundations of this research.

In the second stage of applying René Descartes's philosophy, we broke the WRCC bibliometric analysis into several units consisting literature retrieval, records screening and analysis. From the statistical point of view, our research was further divided into two parts, statistical analysis and bibliometric analysis.

In the third stage, though we needed to rank the steps, since literature retrieval, records screen and records analysis cannot be re-ranked as literature retrieval should always come first followed by records screening and then analysis records, we chose rather to rank the statistical and bibliometric analysis. We found that statistical analysis was easier compared to bibliometric, so we finished the statistical analysis and then conducted a bibliometric analysis.

In the fourth stage, we analyzed the results, checked whether we met our target and then proceeded to finish the article.

2.2 Four stages of bibliometric analysis of WRCC

Because it can be better understood and thus can be widely used, staged method has attracted more researchers' attention in recent years (Wu et al., 2018b2018; Bian et al., 2022b). René Descartes's method can be concluded into four stages, therefore, we divide our research process also into four stages. Since each of

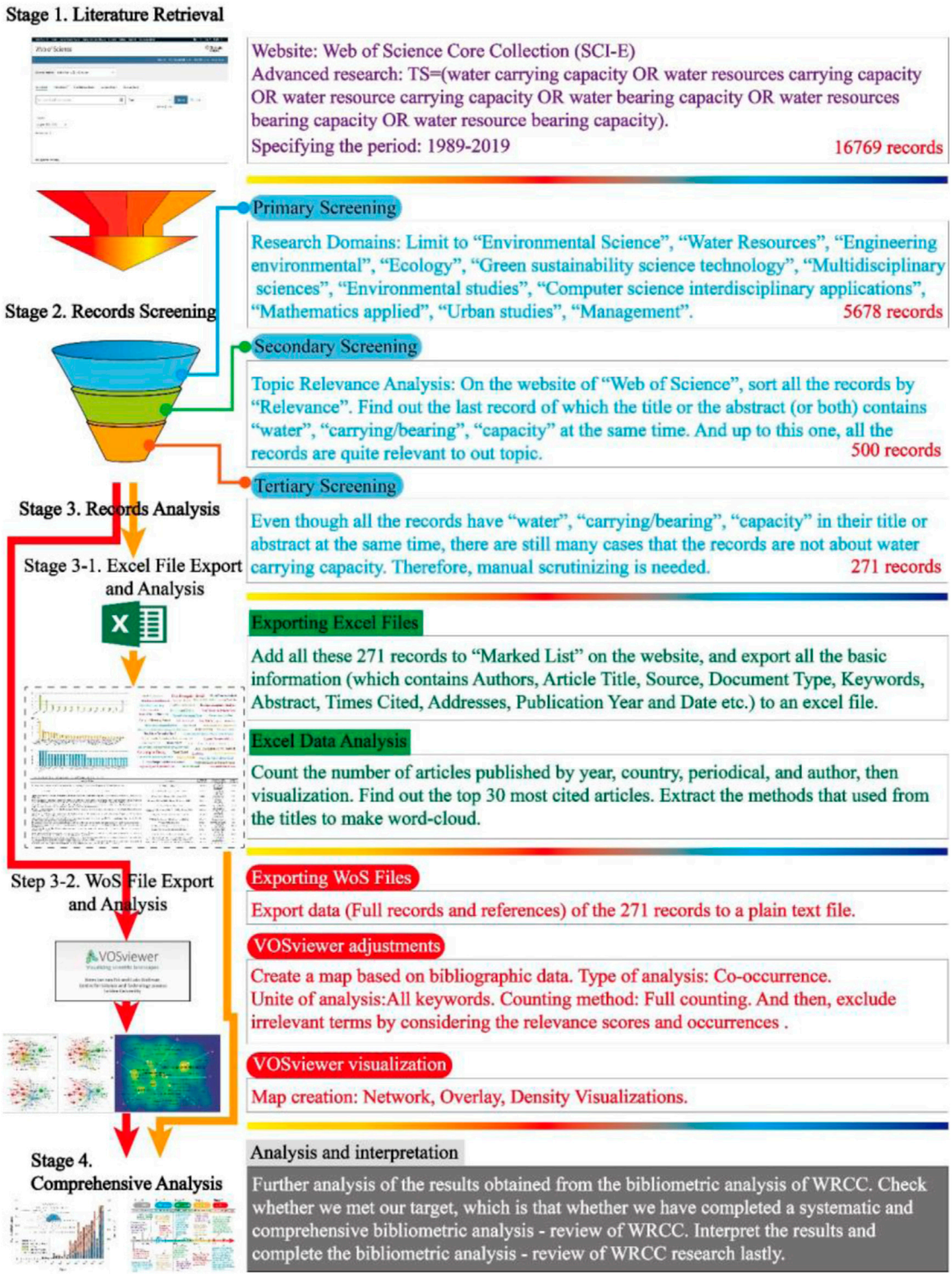

FIGURE 2
Details of application process of four-stage bibliometric analysis method.

literature retrieval, records screening and records analysis stages are very complicated and contain several steps, we treated them separately. We further divide the concrete steps of bibliometric analysis of WRCC into four stages. And the details of our four-staged bibliometric analysis proposed in this research is shown in Figure 2.

The four stages of bibliometric analysis are elaborated as follows:

Stage 1: The choice of search terms and search strategies is very important, and directly determines whether the search results are comprehensive. Many terms can be used to express the meaning of WRCC, therefore, using a single term will not present comprehensive results. In order to acquire more comprehensive search results, in the first stage, multiple search terms should be selected.

Stage 2: In the search process, files with poor relevance to the topic will inevitably be retrieved. The search results need to be accurately and carefully screened. In order to obtain more accurate topic-related results, this study proposed a refined literature screening process, which is a three-stepped screening method (Figure 2. Stage 2: The screening methods are done through records category, relevance, and manual. By adopting this three-stepped screening method, we can extract the topic-related records from even tens of thousands of records in a short period of time.

Stage 3: We analyzed all the topic-related records by using both statistical analysis and bibliometric analysis at the same time.

Stage 4: We analyzed all the results comprehensively, we checked whether we meet our target and finished this article.

2.2.1 Literature retrieval

In this study, the Web of Science Core Collection Database was explored in advanced search page, using Boolean Logic to search TS = (water carrying capacity OR water resources carrying capacity OR water bearing capacity OR water resources bearing capacity OR water resource bearing capacity) in which the subject contains "water carrying capacity", "water resources/ resource carrying capacity", "water bearing capacity" or "water resources/resource bearing capacity". The retrieval year ranges from 1989 to 2019 (in 1989, WRCC was discussed for the first time, but the concept of WRCC was not yet proposed). A total of 16769 records were obtained. The retrieval time is August 15, 2020.

2.2.2 Records screening

During the search process, some files irrelevant to the topic will inevitably be retrieved. Therefore, the search results need to be accurately and carefully screened. In order to obtain more accurate search results, this study adopted a three-stepped screening method. The specific screening steps were applied as follows: 1) The first screening explored 16769 results through Web of Science and selected the category that is related and similar to WRCC, For example, in this research, we click "Result Analysis" on the search results interface of Web of Science, and selected "Environmental Science", "Water Resources", "Engineering environmental", "Ecology", "Green sustainability science" in the "Web of Science category on the result analysis interface technologyv", "Multidisciplinary sciences", "Environmental studies", "Computer science interdisciplinary applications", "Mathematics applied", "Urban studies", "Management", 5678 records were obtained. 2) The second step is to screen 5678 search results through the relevance function of the Web of Science webpage. The 5678 search records obtained after screening were sorted in order of relevance, and it was found that the top 500 records all contained "water", "carrying", "capacity" or "water", "bearing", "capacity" in their topics. After the first 500, the records no longer contained, in relevant application, usage of the words "water", "carrying", "capacity" or "water", "bearing", "capacity". Therefore, we concluded that the content after first 500 files does not contain relevant literature related to WRCC. 3) The third step of screening was to manually check the contents of the first 500 records one after the other. During the search, the fact that "water", "carrying", "capacity" or "water", "bearing", "capacity", appears in the title of an article doesn't necessarily mean its research content belongs to the research category of WRCC, therefore the 500 records need to be manually checked, For example, "tourism water resources carrying capacity", "groundwater carrying capacity", "water resources and water environment carrying capacity", and "agricultural water resources carrying capacity " all belong to the research category of WRCC. However, though "soil water carrying capacity", "sediment carrying capacity of river flow", "carrying capacity of fishpond", "stock carrying capacity", "recreation carrying capacity", "mineral resources carrying capacity", all include the words "water", "carrying", "capacity" or "water", "bearing", "capacity" in their topics, they do not belong to the research of WRCC. We can see that due to the similarity of some research content, in order to obtain more accurate data in bibliometric research, it is very necessary to finely screen results. After the three-stepped screening process, a total of 271 records were obtained (Appendix A).

2.2.3 Records analysis

The data export of this study is divided into two parts: 1) In the first part, we added the 271 records to the Marked List on the Web of Science website, and then exported important information such as "title", "author", "source publication", "cited frequency", "document type" and "keywords" to an excel file. 2) In the second part, we directly exported the "full records and cited references" of 271 records on the Web of Science website to plain text files.

In processing of excel file data, we first sorted out the information in the exported excel file starting with the year, country, journal and number of author's publications. We then sorted out the top 30 highly cited articles, extracted the methods

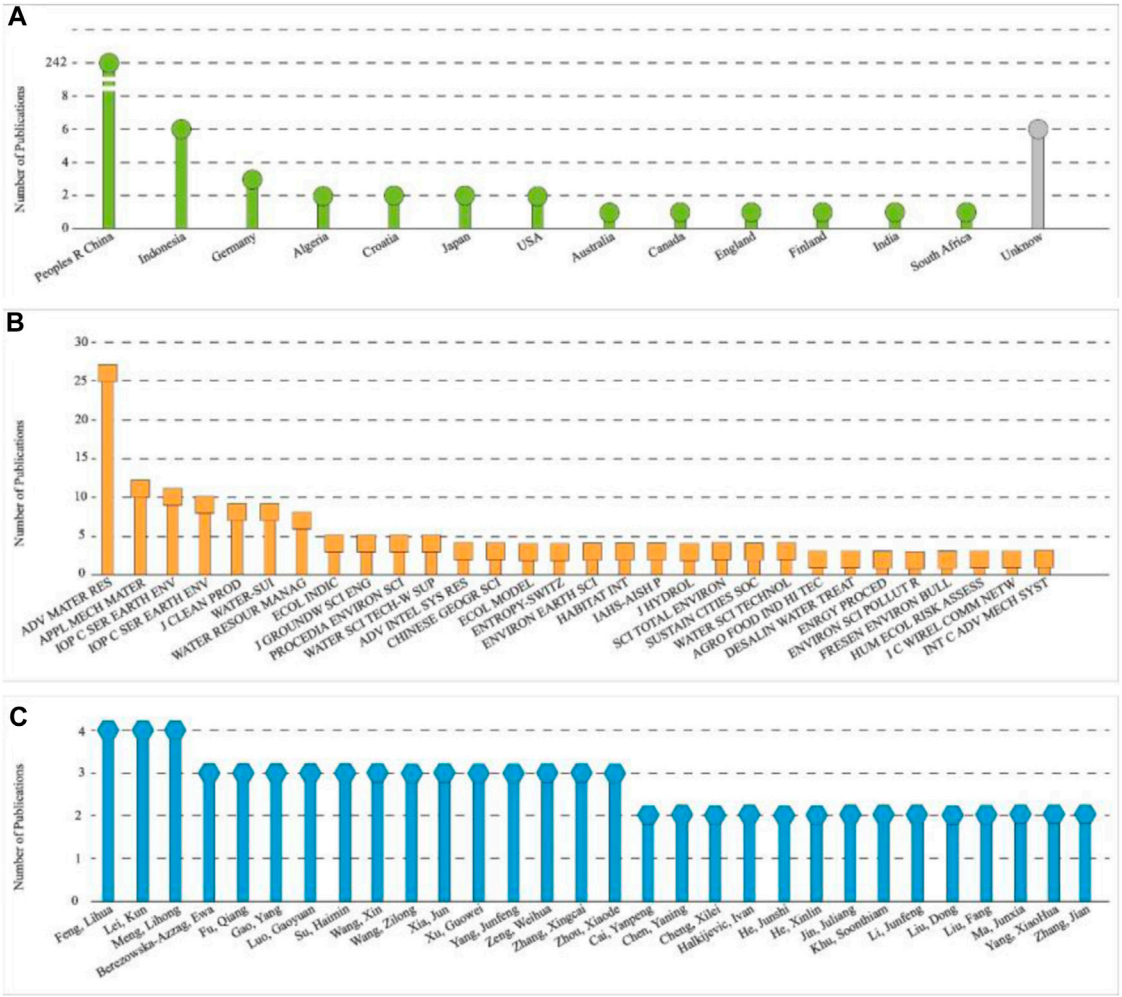

FIGURE 3
Number of articles published by countries, periodicals, and authors.

used in the articles and finally marked the time these methods were first used.

In dealing with the plain text files, we first analyzed the exported text file through the VOSviewer software. The results of keywords co-occurrence analysis, inter-year changes of keywords and heat maps were obtained. VOSviewer is a software tool for constructing and visualizing bibliometric networks, which has been developed by Nees Jan van Eck and Ludo Waltman at Leiden University's Centre for Science and Technology Studies (CWTS) (http://www.vosviewer.com/).

2.2.4 Comprehensive analysis

In order to have a more comprehensive understanding of the nature of research progress and current research state of WRCC, we adopted the comprehensive analysis method to further analyze the results obtained from the bibliometric analysis of WRCC in this stage. We also checked whether we met our target, which means that whether we have completed a systematic and comprehensive bibliometric analysis-review of WRCC in this stage. The volume of published literature and research progress have been analyzed, and stages of the development process of WRCC divided.

3 Results and discussion

In this section, both statistical and bibliometric results have been fully analyzed and discussed, and a comprehensive analysis has also been conducted lastly. 3.1 presented the number of articles published by country, periods and authors, and statistical analysis of methods; Section 3.2 analyzed the highly cited papers; 3.3 analyzed the keywords co-occurrence and research hotspots dynamics; and Section 3.4 analyzed WRCC development comprehensively.

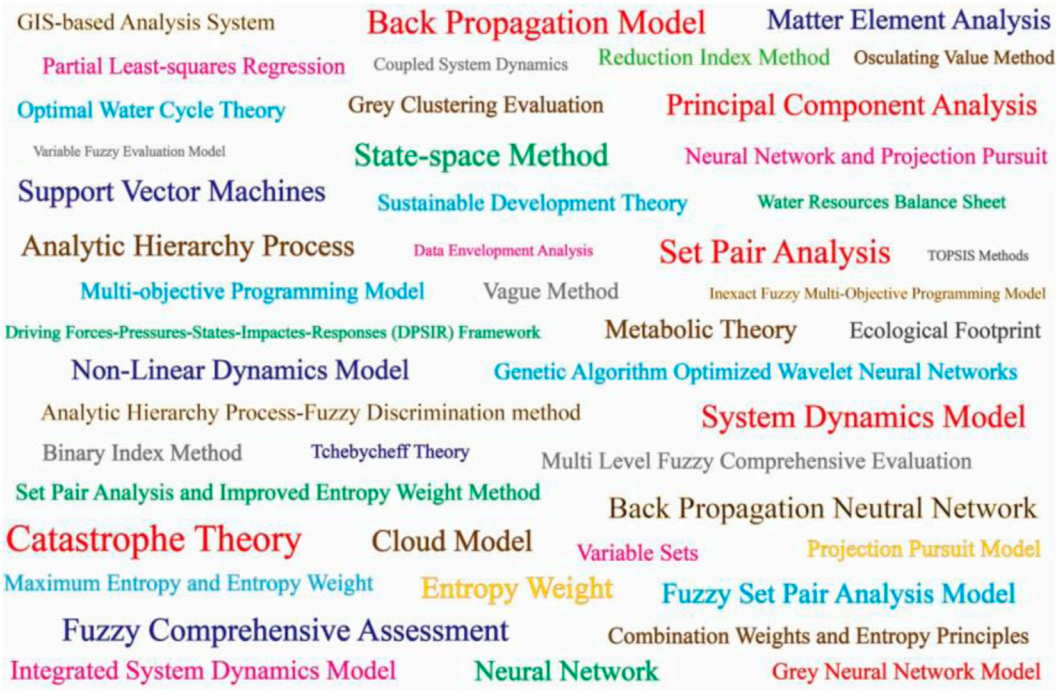

FIGURE 4
Summary of WRCC methods.

3.1 Statistical analysis of articles and methods

Number of articles by country, periods and authors are shown in Figure 3.

Number of publications by country indicates that China published the highest number of papers followed by Indonesia, Germany, Algeria and other (Figure 3A) in that order. China has the largest number of publications for two reasons: firstly, WRCC was put forward by the Chinese, and Chinese scholars have shown more research interest in this area. Secondly, due to rapid infrastructural and economic expansion witnessed by China in the last 30 years, demand for water resources has tripled and placed a huge deficit on water need. To avert this situation, the Chinese government attached great importance on WRCC research by setting up a number of National Natural Science Foundation Projects including "Innovative Research On Water Resources Carrying Capacity Based On Water Scarcity Risk Model" (approval number: 40771044), "Research On the Dynamic Mechanism And Sustainability Of the Evolution Of Water Resources Carrying Capacity Under the Framework Of Quality-Energy" (approval number: 41061053), "Risk Analysis Of Economic Development Planning Based On Water Resources Carrying Capacity Under Uncertain Conditions" (approval number: 41271536). The establishment of these National Natural Science Foundation Projects directly and vigorously promoted the research and development of WRCC.

Results of number of papers published by journals indicated that, the top 30 journals with the most papers on WRCC research are in the order shown in (Figure 3B). They include ADV MATER RES, APPL MECH MATER, IOP C SER EARTH ENV, AER ADV ENG RES, J CLEAN PROD, WATER-SUI, WATER RESOUR MANAG, ECOL INDIC, J GROUNDW SCI ENG and PROCEDIA ENVIRON SCI. The number of articles published in the order in which the journals are listed above are: 26, 11, 10, 9, 8, 8, 7, 4, 4, and 4 respectively.

From number of articles published by authors perspective, the top 30 authors with the most articles and the number of articles published are shown in (Figure 3C). The top 10 authors with the most articles include Feng, Lihua, Lei, Kun, Meng, Lihong, Berezowska-Azzag, Ewa, Fu, Qiang, Gao, Yang, Luo, Gaoyuan, Su, Haimin, Wang, Xin, Wang, Zilong. Among them, Feng, Lihua, Lei, Kun, Meng, Lihong published 4 articles each while the remaining 7 authors published 3 articles each.

By analyzing the excel files exported from the Web of Science website, we discovered 47 methods from 271 articles used in WRCC calculation and evaluation (Figure 4).

In Figure 4, the methods include TOPSIS, system dynamics model, support vector machines, state-space, set pair analysis, neural network, ecological footprint, cloud model, analytic hierarchy process-fuzzy discrimination,

TABLE 1 TOP 30 highly cited papers (as of August 14, 2020).

Article title	Authors	Publication year	Source title abbreviation	Times cited
Fuzzy comprehensive evaluation for carrying capacity of regional water resources	Gong, L; Jin, CL	2009	WATER RESOUR MANAG	109
Assessment of water resources carrying capacity in tianjin city of China	Song, XM; Kong, FZ; Zhan, CS	2011	WATER RESOUR MANAG	91
Application of system dynamics in analyzing the carrying capacity of water resources in Yiwu City, China	Feng, LH; Zhang, XC; Luo, GY	2008	MATH COMPUT SIMULAT	76
Development tendency analysis and evaluation of the water ecological carrying capacity in the Siping area of Jilin Province in China based on system dynamics and analytic hierarchy process	Zhang, Z; Lu, WX; Zhao, Y; Song, WB	2014	ECOL MODEL	73
A risk assessment model of water shortage based on information diffusion technology and its application in analyzing carrying capacity of water resources	Feng, LH; Huang, CF	2008	WATER RESOUR MANAG	70
Fuzzy comprehensive evaluation model for water resources carrying capacity in Tarim River Basin, Xinjiang, China	Meng, LH; Chen, YN; Li, WH; Zhao, RF	2009	CHINESE GEOGR SCI	61
Analysis of temporal and spatial differences in eco-environmental carrying capacity related to water in the Haihe River Basins, China	Zhu, YH; Drake, S; Lu, HS; Xia, J	2010	WATER RESOUR MANAG	56
Assessment of water ecological carrying capacity under the two policies in Tieling City on the basis of the integrated system dynamics model	Wang, S; Xu, L; Yang, FL; Wang, H	2014	SCI TOTAL ENVIRON	49
Dynamic successive assessment method of water environment carrying capacity and its application	Wang, TX; Xu, SG	2015	ECOL INDIC	48
Multi-scale analysis of the water resources carrying capacity of the Liaohe Basin based on ecological footprints	Wang, S; Yang, FL; Xu, L; Du, J	2013	J CLEAN PROD	46
An innovative method for water resources carrying capacity research-Metabolic theory of regional water resources	Ren, CF; Guo, P; Li, M; Li, RH	2016	J ENVIRON MANAGE	43
Assessment of Water Resources Carrying Capacity for Sustainable Development Based on a System Dynamics Model: A Case Study of Tieling City, China	Yang, JF; Lei, K; Khu, S; Meng, W	2015	WATER RESOUR MANAG	42
Optimization of industry structure based on water environmental carrying capacity under uncertainty of the Huai River Basin within Shandong Province, China	Li, N; Yang, H; Wang, LC; Huang, XJ; Zeng, CF; Wu, H; Ma, XX; Song, XT; Wei, YN	2016	J CLEAN PROD	39
Assessment of water environmental carrying capacity for sustainable development using a coupled system dynamics approach applied to the Tieling of the Liao River Basin, China	Yang, JF; Lei, K; Khu, S; Meng, W; Qiao, F	2015	ENVIRON EARTH SCI	36
Water resources carrying capacity of wetlands in Beijing: Analysis of policy optimization for urban wetland water resources management	Wang, CH; Hou, YL; Xue, YJ	2017	J CLEAN PROD	34
Water Resources Carrying Capacity Evaluation and Diagnosis Based on Set Pair Analysis and Improved the Entropy Weight Method	Cui, Y; Feng, P; Jin, JL; Liu, L	2018	ENTROPY-SWITZ	33
Carrying capacities and standards as bases towards urban infrastructure planning in India: A case of urban water supply and sanitation	Joardar, SD	1998	HABITAT INT	33
Water ecological carrying capacity of urban lakes in the context of rapid urbanization: A case study of East Lake in Wuhan	Ding, L; Chen, KL; Cheng, SG; Wang, X	2015	PHYS CHEM EARTH	31
Comprehensive evaluation and scenario simulation for the water resources carrying capacity in Xi'an city, China	Yang, ZY; Song, JX; Cheng, DD; Xia, J; Li, Q; Ahamad, MI	2019	J ENVIRON MANAGE	26
Evaluating Beijing's human carrying capacity from the perspective of water resource constraints	Zhang, YX; Chen, M; Zhou, WH; Zhuang, CW; Ouyang, ZY	2010	J ENVIRON SCI	26
Water resources carrying capacity assessment: The case of Algeria's capital city	Ait-Aoudia, MN; Berezowska-Azzag, E	2016	HABITAT INT	25
Regionalization of water environmental carrying capacity for supporting the sustainable water resources management and development in China	Jia, ZM; Cai, YP; Chen, Y; Zeng, WH	2018	RESOUR CONSERV RECY	20

(Continued on following page)

TABLE 1 (*Continued*) TOP 30 highly cited papers (as of August 14, 2020).

Article title	Authors	Publication year	Source title abbreviation	Times cited
Advances in Study on Water Resources Carrying Capacity in China	Mei, H; Liuyuan; Duhuan; Yangxiaoyan	2010	PROCEDIA ENVIRON SCI	20
Water environment carrying capacity in Bosten Lake basin	Wang, YM; Zhou, XD; Engel, B	2018	J CLEAN PROD	17
Water Environmental Carrying Capacity Assessment of an Industrial Park	Kang, P; Xu, LY	2012	PROCEDIA ENVIRON SCI	17
Algiers carrying capacity with respect to per capita domestic water use	Naimi-Ait-Aoudia, M; Berezowska-Azzag, E	2014	SUSTAIN CITIES SOC	14
Integrated modeling framework for evaluating and predicting the water resources carrying capacity in a continental river basin of Northwest China	Wu, L; Su, XL; Ma, XY; Kang, Y; Jiang, YA	2018	J CLEAN PROD	13
Comprehensive Evaluation of Water Resources Carrying Capacity of Jining City	Du, M; Xu, ZH; Peng, LM; Zhu, YH; Xu, XF	2011	ENRGY PROCED	13
Research on the Risk of Water Shortages and the Carrying Capacity of Water Resources in Yiwu, China	Feng, LHH; Zhang, XC; Luo, GY	2009	HUM ECOL RISK ASSESS	13
Quantitative evaluation and optimized utilization of water resources-water environment carrying capacity based on nature-based solutions	Zhang, J; Zhang, CL; Shi, WL; Fu, YC	2019	J HYDROL	12

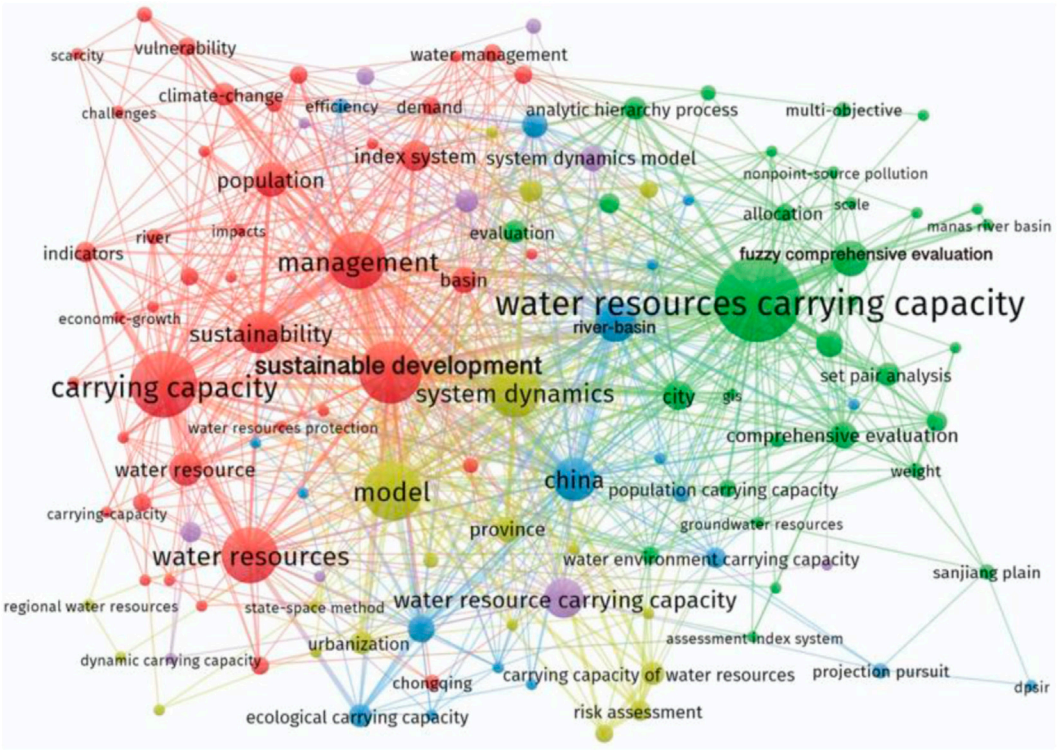

FIGURE 5
Keywords co-occurrence.

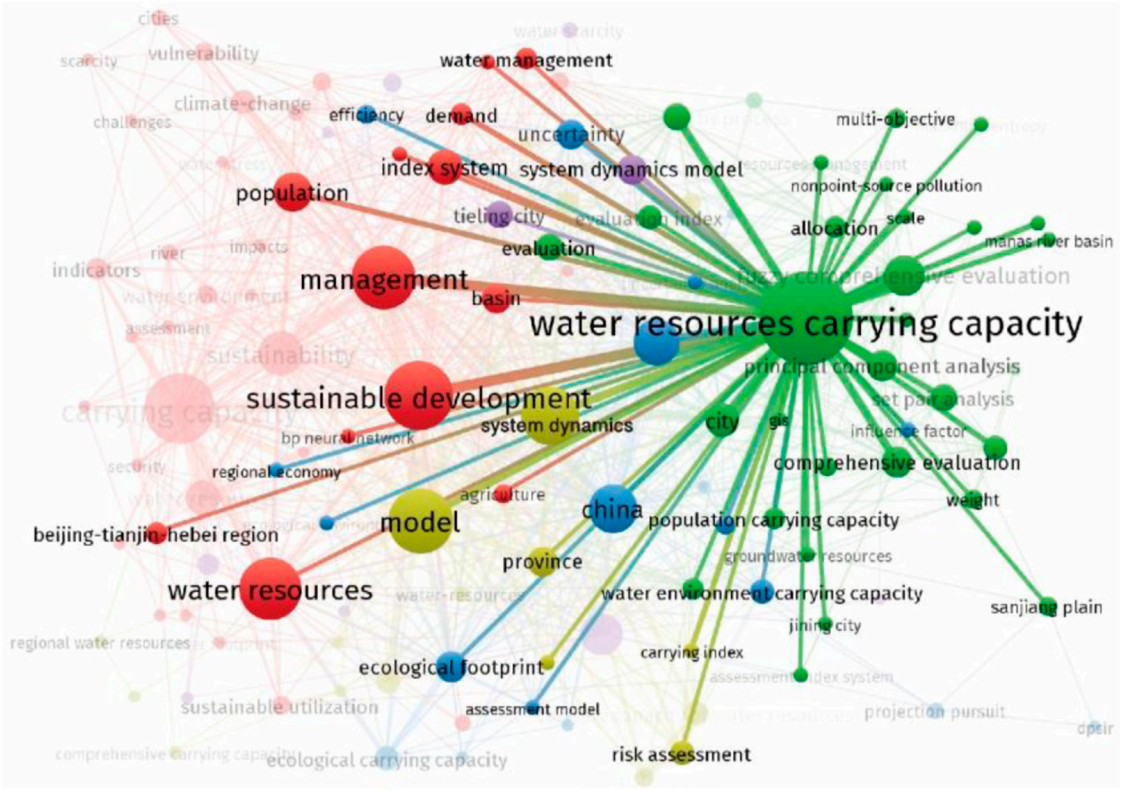

FIGURE 6
Nodes connected to water resources carrying capacity Node.

inexact fuzzy multi-objective programming model, etc. have been used in WRCC research.

3.2 Analysis of highly cited papers

In sorting citations of the 271 articles retrieved, we first checked the title of the article, author, publication year, journal source, and number of citations of the top 30 articles with the most citations (as of August 14, 2020) Table 1.

From Table 1, the top 5 documents were all within the period from 2008 to 2014. This period belongs to the research and development stage of WRCC study. Two of the five articles were published in 2008, and one each in 2009, 2011 and 2014. The number of citations of the 5 articles are in the order 109, 91, 76, 73, 70. Among the 5 articles, 3 are from WATER RESOUR MANAG, MATH COMPUT SIMULAT and ECOL MODEL, indicating that the journal WATER RESOUR MANAG plays an important role in publishing WRCC papers, and papers published in this journal have a greater impact. It can be seen intuitively from the titles that three of the articles are studied in cities in China including Tianjin, Yiwu, and Siping and the other two articles equally studied in China (Feng and Huang, 2008; Gong and Jin, 2009) in Lanzhou and Jinhua Cities. This confirms results of earlier analysis that China was the country with the highest number of research work on WRCC.

3.3 Keywords co-occurrence and hotspots dynamics analysis

Keywords can reflect the main content of the article, and the analysis of keywords can understand the general status of the research field. When using VOSviewer software to analyze the co-occurrence of keywords, the larger the node means the more frequently the keyword appeared (Figure 5). The width of the connection between nodes can reflect the frequency of two connected keywords. The wider the connection indicates that the two keywords appear more frequently.

The results shown in Figure 5 indicate that the most frequently occurring keywords are “water resources carrying capacity”, “carrying capacity”, “management”, “water resources”, “system dynamics”, “model”, and “sustainable development”, “Sustainability”, “china”, “river-basin” etc. From the perspective of the width of the connection between

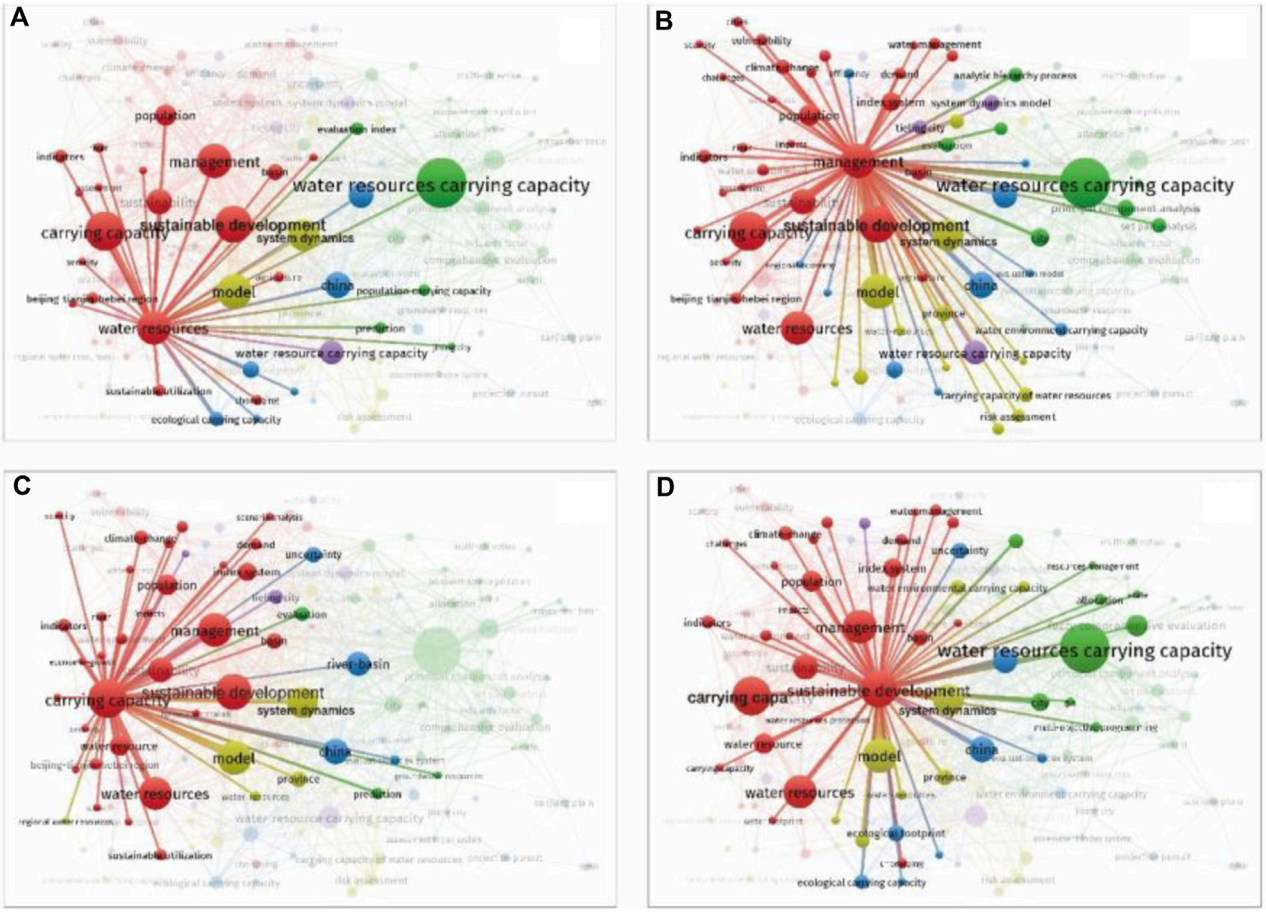

FIGURE 7
Connection of key nodes.

nodes, the connection between water resources carrying capacity and management and sustainable development is wider, and the connection between China and river-basin is wider. It shows that these two groups of keywords appear more frequently at the same time.

From the clustering results, the water resources carrying capacity node is the largest among all, which is shown in green. The yellow node emphasizes the methods, the main two yellow nodes are model and system dynamics. The blue node focuses on the research objects, and the two main blue nodes are China and river-basin. The red nodes focus on management, and the main red nodes are management, sustainability, sustainable development, carrying capacity and water resources.

In the analysis of keywords co-occurrence in papers related to water resources carrying capacity, the most frequently occurred keyword is "water resources carrying capacity". Many nodes are directly connected to "water resources carrying capacity", and other nodes are connected to this node through intermediate nodes. The nodes that are most closely connected to the water resources carrying capacity node are the management node and the sustainable development node (Figure 6.). The carrying capacity of water resources is an important means for water resources management and an important measure for achieving sustainable development of water resources.

From the results of cluster analysis, the red nodes emphasize water resources management. The number of nodes connected to the management node and the sustainable development node is greater than the number of nodes connected to the water resources node and the carrying capacity node (Figures 7A–D). This is because more nodes are connected to the water resources carrying capacity node, the number of nodes connected to the water resources node and the carrying capacity node is relatively reduced. It is worth noting that the largest node connected to the management node and the sustainable development node is the water resources carrying capacity node, and the width of the

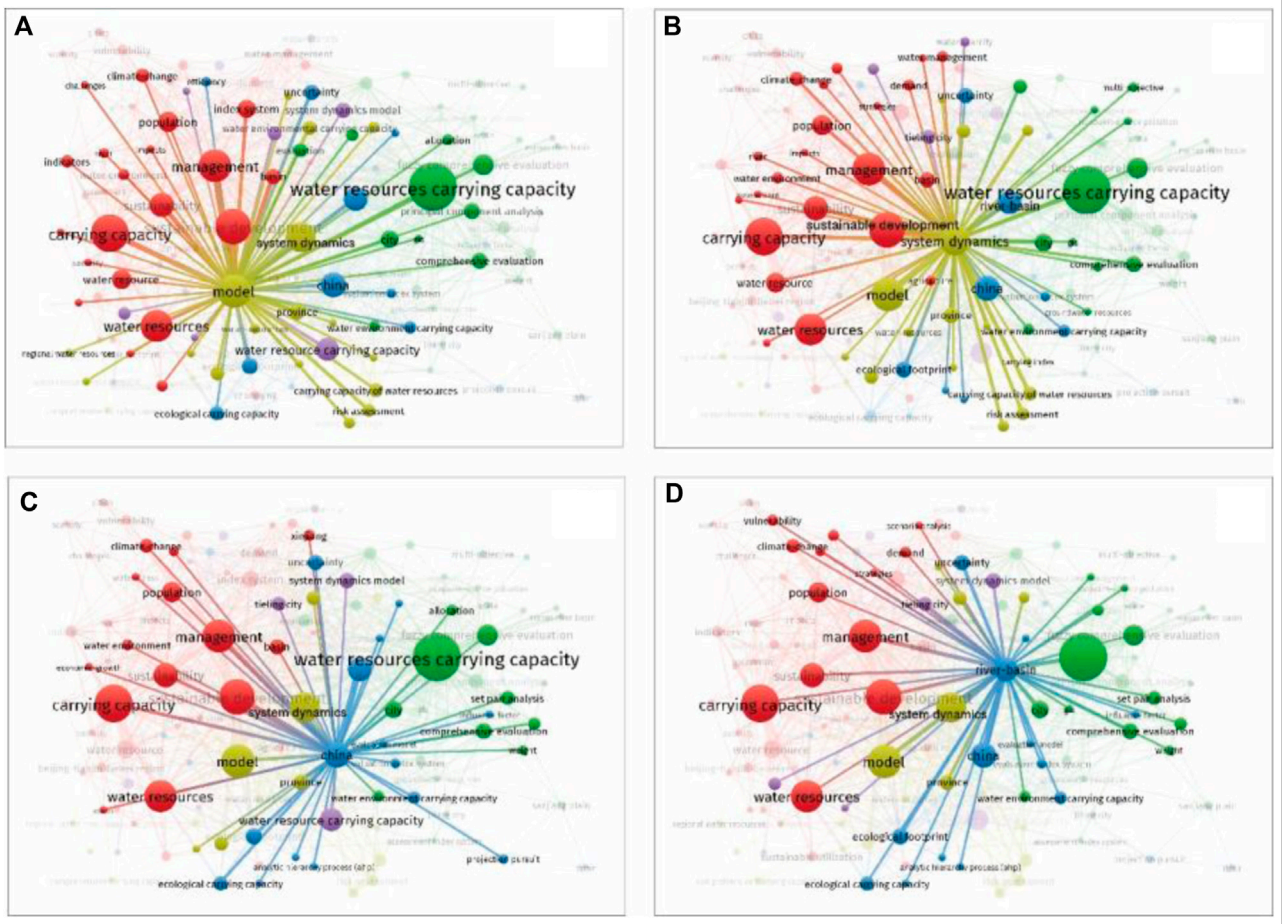

FIGURE 8
Method and object node analysis.

connection with this node is the widest, indicating that they have the largest frequency of co-occurrence.

Analysis results of research methods indicates that the most frequently occurring research methods in the keyword co-occurrence graph are model and systems dynamics. This means that building various models and adopting system dynamics in the research process of WRCC are mainstream. Many nodes are closely connected to these two nodes (Figures 8A,B). Water resources carrying capacity, carrying capacity, and management are the nodes that are most closely connected to the model node and the system dynamics node. At the same time, the model node and the system dynamics node are also the most closely connected nodes to each other. This shows that these nodes appear more frequently at the same time. In the analysis of keywords co-occurrence, China is the only country that appeared. River basin is the only node closely connected to China (Figure 8C). Furthermore, China is the only node closely connected to the river-basin node (Figure 8D). It can be seen that the number of nodes connected to the China node and the river-basin node is significantly less than the number of nodes connected to the model node and the system dynamics node, indicating that more research on WRCC tends to be methodological innovation and application, while research on WRCC in some specific areas is relatively lacking.

From the keywords co-occurrence density map, we can clearly find research hotspots in the field. The density map of WRCC keywords co-occurrence in this study is shown in Figure 9.

In Figure 9, apart from water resources carrying capacity, there is also carrying capacity, water resources, management, sustainable development, model, China, system dynamics, and other hot spots in the field of WRCC research. WRCC is an important method to realize the sustainable use of water resources and an important means to realize the effective management of water resources. Therefore, these three words, sustainable development, management, and water resources often appear in the keywords of research papers on WRCC.

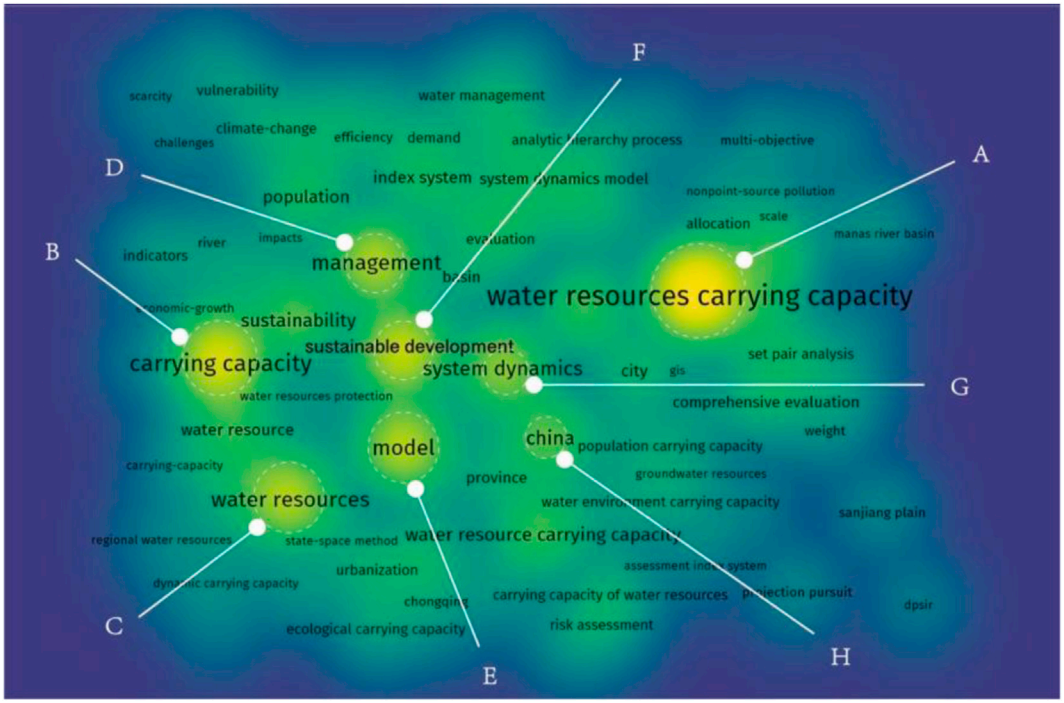

FIGURE 9
Hotspot analysis.

These three words are hot topics in the research of WRCC. WRCC and land resources carrying capacity belong to the research category of resources carrying capacity, therefore carrying capacity is also a hot vocabulary in the research scope of WRCC. China was the only count name of a country that appeared in Figure 9, which again confirms the assertion that China is the main country in the study of WRCC. It can also be seen from Figure 9 that model and system dynamics are the commonest vocabularies, meaning that a lot of research is carried out by building models or using system dynamics methods to study WRCC.

The time sequence analysis of keywords can reflect the changes of researchers' interest in some aspects to a large extent. Therefore, time sequence analysis of keywords helps to clarify the development context and knowledge base of the concept. This study conducted a time series analysis on the keywords of WRCC. The analysis results are shown in Figure 10. The darker the color of the node, the longer the research time in this area. The lighter the color of the node means that the research in that area is the current hotspot.

From the perspective of time series analysis of the keywords of WRCC, WRCC is gradually generated and developed from scholars' attention to population carrying capacity, groundwater resources, urbanization, water shortage, risk assessment, etc, (Figure 10 regions A, B). From the perspective of the spatial scale of WRCC research, the evaluation of WRCC initially focused on the study of cities and provinces. As the research continued to deepen, scholars began to pay more attention to the impact of WRCC on regional water resources. The guiding significance of the deployment, is that the research scale of WRCC has begun to gradually shift to the basin scale (regions C and D in Figure 10).

3.4 Comprehensive analysis of WRCC development

The overall situation of the number of papers retrieved in the core database of Web of Science is shown in Figure 11.

From Figure 11, we can see that although the search period is set from 1989 to 2019, the search results indicated that the earliest literature on WRCC from Web of Science Core Database was published between 1997 and 1998. Within this period Joardar and other scholars comprehensively considered natural resources and social resources, established a set of index system for calculating water supply capacity, and used it for the calculation of urban carrying capacity to provide help for the formulation of urban development plans (Joardar, 1998). As

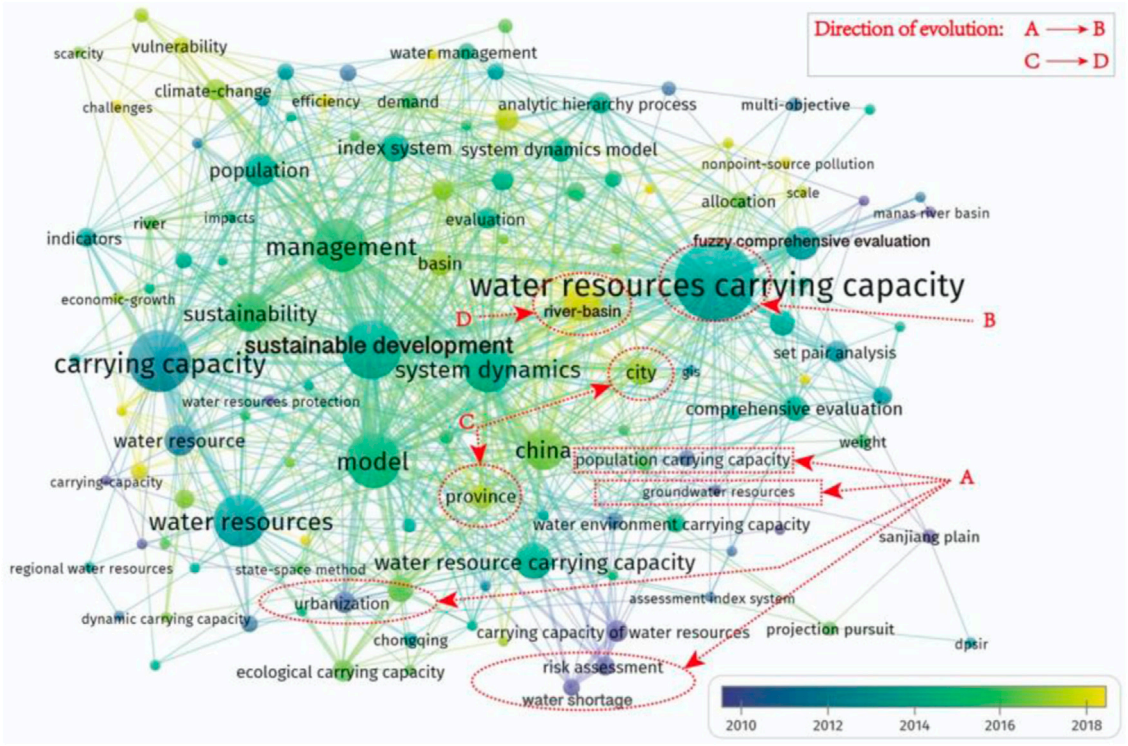

FIGURE 10
Keyword evolution process.

research advanced, the number of published papers increased by the year. At the concept proposition stage as well as the early exploration stage, the number of articles published was relatively few and almost all were written in Chinese. Therefore, no articles were retrieved in the Web of Science Core Database for this time. From 2000 to 2010, the number of articles published increased. This however decreased slightly in 2011 compared with 2010, and maintained a steady upward trend from 2011 to 2016. In 2017, both the number of articles and the number of proceeding papers decreased significantly. From 2018 to 2019, the number of papers increased significantly and the types of articles became more diverse. Articles on editorial materials and review papers appeared at this stage. In general, the number of articles published on WRCC has been increasing meaning that studies on WRCC has received attention over the past 3 decades. From the WoS (Web of Science) Categories analysis result shown in Figure 11, we can see that most of the WRCC research belong to two categories, Environmental Sciences and Water Resources.

Results on types of papers published indicates that 41.7% are articles while editorial materials and reviews account for 1.5%. Conference and other meetings proceedings papers account for a large proportion of papers published on WRCC research. The period from 2007 to 2016 recorded the most numerous proceeding papers published per year, indicating that a large number of proceeding papers published have played an important role in the development of WRCC.

Based on research progress, the volume of published literature, period at which calculation methods were proposed, and our knowledge in WRCC research, this paper divides the research progress of WRCC into five stages (Figure 12).

These five stages have been further elaborated as follows:

- The concept formation stage (-1990). Park and Burgess (1921) took the lead in 1921 and proposed the idea to calculate the maximum population that a region can carry based on regional endowments. Later, other scholars and institutions have successively proposed concepts that are closely related to the WRCC, such as resources carrying capacity, environmental carrying capacity. In 1989, the Xinjiang Water Resources Research Group (XWRSSRG (Xinjiang Water Resources Soft Science Research Group), 1989) completed the first discussion on the issue of WRCC which laid a solid foundation for the concept of WRCC.

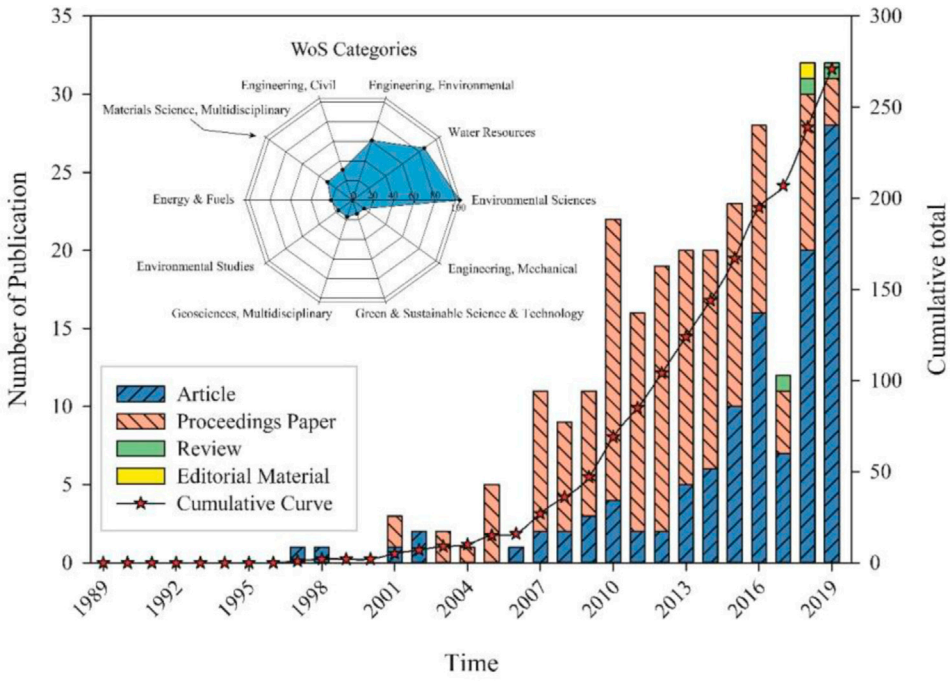

FIGURE 11
Analysis of publication on WRCC studies.

- The second stage is the qualitative analysis period (1990s decade). Most of the research in this period focused on the qualitative description stage, while the number of papers on quantitative research is relatively limited. Qualitative research mostly elaborates its theoretical basis and important significance. In 1992, Academician Shi Yafeng clearly put forward the concept of WRCC for the first time (Shi and Qu, 1992). Wang et al. (1999) conducted an in-depth discussion on the concept and theory of WRCC. Cai (1994) elaborated on the issues that needed attention in the study of WRCC in Xinjiang.
- At the methods exploration stage (2000s decade), many quantitative analysis methods have been proposed and applied, For example, Qu and Fan (2000) analyzed and calculated the WRCC in the middle reaches of the Heihe River Basin based on available water resources as well as social and economic water requirements. Li et al. (2009) used an improved fuzzy matter-element model to evaluate water resources carrying capacity. However, in the 10-year exploration stage of the method, only 9 of the 47 methods (47 methods extracted in Section 3.1) were proposed and applied at this stage.
- During the method development period (2011–2016), a large number of research methods have been introduced into the evaluation and research process of WRCC, For example, Zhang et al. (2012) used the ecological footprint method to study the WRCC of the Shule River Basin; Xing et al. (2013) used the principal component analysis method to evaluate ground WRCC of Xi'an from 7 indicators. At this stage, which extends 6 years, 20 methods out of 47 methods have been proposed and applied. The speed of progress at this stage was much faster than the method exploration stage. This study defines this stage as the method development stage.
- The fifth stage is referred as the all-round development stage (2016-). On one hand theoretical system of WRCC has been further enriched and improved, For example, Wang et al. (2017) first constructed an evaluation index system for WRCC from the four aspects of "quantity, quality, region and flow". At the other hand, application of the methods has also been expanded to a greater extent. Among the 47 methods, 18 methods have been proposed and applied at this stage, and the time limit from this stage to the study of this review is only 3 years. This explains that more methods were applied at this stage. At the same time, most of the subtle changes (Introduction paragraph 6) that occurred in the evaluation objects of WRCC all occurred at this stage. Based on this precept, this stage is defined as the all-round development stage of WRCC.

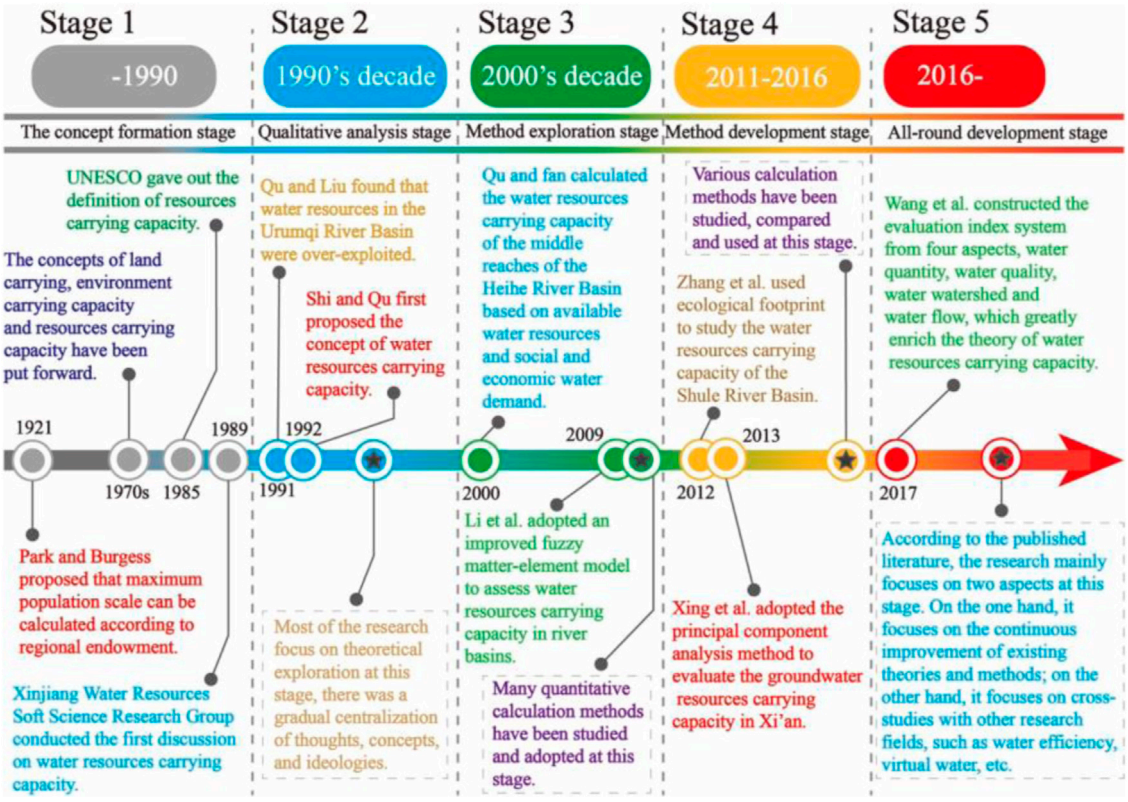

FIGURE 12
Development stages division of WRCC.

4 Conclusions and prospects

In this review, a four-staged bibliometric analysis method was used based on the René Descartes's *Discourse on the Method*. This makes the bibliometric research process more systematic and efficient compared to previous studies. The four-staged bibliometric analysis method proposed in this research is equipped with a records screening stage, in which we proposed a three-stepped screening method, that solved the problem of large file sorting. Through the three-stepped screening method proposed in this research, it was possible to finally determine the document records highly related to the research topic from tens of thousands of records within a short period of time.

The bibliometric analysis - review results show that a total of 47 methods including system dynamics, cloud model, set pair analysis, neural network and ecological footprint have been introduced into the evaluation process of WRCC. Through keyword co-occurrence analysis, we found that building various kinds of models and adopting system dynamics methods are the mainstream methods in the research of WRCC. We also found that China is the only country that appears in the keywords co-occurrence analysis chart, which shows that China is the main country in the study of WRCC. Through time series analysis of keywords, we found that the research on WRCC originated from scholars'attention to population carrying capacity, groundwater resources, urbanization, water shortage and risk assessment. From the perspective of research objects, previous studies have focused more on some provinces and cities. In recent years, more and more scholars have begun to study the WRCC of some typical regions, such as arid and semi-arid regions, urbanized areas and water-deficient regions. Based on the research status, the amount of published literature over time, the analysis of the time when the method was first adopted, and our knowledge in this area, this study divided the development process of WRCC into the concept formation stage, qualitative analysis stage, method exploration stage, method development stage and all-round development stage.

Author contributions

XY contributed to conception and design of the study. FL organized the database. YQ performed the statistical analysis. BS, XY wrote the first draft of the manuscript. All authors contributed to manuscript revision, read, and approved the submitted version.

Acknowledgments

Thanks to the National Key Research And Development Program funded project 2021YFC3000203, and the Ministry of Water Resources' flood and drought disaster prevention strategy research talent innovation team project WH0145B042021.We also would like to extend special thanks to the editor and the reviewers for their insightful comments and constructive suggestions.

Conflict of interest

The authors declare that the research was conducted in the absence of any commercial or financial relationships that could be construed as a potential conflict of interest.

Supplementary material

The Supplementary Material for this article can be found online at: https://www.frontiersin.org/articles/10.3389/feart.2022.970582/full#supplementary-material

References

Accatino, F., Ward, D., Wiegand, K., and De Michele, C. (2017). Carrying capacity in arid rangelands during droughts: The role of temporal and spatial thresholds. *Animal* 11 (2), 309–317. doi:10.1017/S1751731116001531

Arrow, K., BolinCostanza, R., Dasgupta, P., Folke, C., and Holling, C. S. (1995). Economic growth, carrying capacity, and the environment. *Science* 268, 520–521. doi:10.1126/science.268.5210.520

Bian, D., Yang, X., Wu, F., Babuna, P., Luo, Y., Wang, B., et al. (2022). A three-stage hybrid model investigating regional evaluation, pattern analysis and obstruction factor analysis for water resource spatial equilibrium in China. *J. Clean. Prod.* 331, 129940. doi:10.1016/j.jclepro.2021.129940

Bian, D., Yang, X., Xiang, W., Sun, B., Chen, Y., Babuna, P., et al. (2022). A new model to evaluate water resource spatial equilibrium based on the game theory coupling weight method and the coupling coordination degree. *J. Clean. Prod.* 366, 132907. doi:10.1016/j.jclepro.2022.132907

Bo, L., Qiang, W., and Li-xia, C. (2016). An analytical method of regional water resources carrying capacity in karst area – A case study in guizhou province, China. Water pract. *Tech* 11 (4), 796–805. doi:10.2166/wpt.2016.085

Bolis, I., Morioka, S. N., and Sznelwar, L. I. (2017). Are we making decisions in a sustainable way? A comprehensive literature review about rationalities for sustainable development. *J. Clean. Prod.* 145, 310–322. doi:10.1016/j.jclepro.2017.01.025

Cai, A. (1994). A Brief Talk on Water Resources Carrying Capacity—A few issues that should be paid attention to in the study of appropriate water resources carrying capacity in Xinjiang. *Environ. Prot. Xinjiang* 04, 190.

Cao, J. K., Zhang, J., and Ma, S. Q. (2014). "The analysis of water resource ecological carrying capacity of Hainan international island," in *Ecosystem Assessment and fuzzy systems management* (Cham: Springer), 63–71. doi:10.1007/978-3-319-03449-2_7

Chen, N. X., Qu, J. H., Xu, J. X., Li, Z. P., and Yang, L. (2010). "Evaluation of Groundwater Environment Carrying Capacity Based on Catastrophe Theory." in 2010 4th International Conference on Bioinformatics and Biomedical Engineering, Chengdu, 18-20 June 2010, 1–4.

Cheng, K., Fu, Q., Meng, J., Li, T. X., and Pei, W. (2018). Analysis of the spatial variation and identification of factors affecting the water resources carrying capacity based on the cloud model. *Water Resour. manage.* 32 (8), 2767–2781. doi:10.1007/s11269-018-1957-x

Chi, M., Zhang, D., Fan, G., Zhang, W., and Liu, H. (2019). Prediction of water resource carrying capacity by the analytic hierarchy process-fuzzy discrimination method in a mining area. *Ecol. Indic.* 96, 647–655. doi:10.1016/j.ecolind.2018.09.021

Cui, Y., Feng, P., Jin, J., and Liu, L. (2018). Water resources carrying capacity evaluation and diagnosis based on set pair analysis and improved the entropy weight method. *Entropy* 20 (5), 359. doi:10.3390/e20050359

Dai, D., Sun, M., Xu, X., and Lei, K. (2019). Assessment of the water resource carrying capacity based on the ecological footprint: A case study in zhangjiakou city, North China. *Environ. Sci. Pollut. Res.* 26 (11), 11000–11011. doi:10.1007/s11356-019-04414-9

Deng, W., Yan, L., Wang, Y., Jin, X., and Hu, Y. (2019). A study on water resources carrying capacity based on water usage intensity in hainan province IOP conference series: Earth and environmental science. *IOP Conf. Ser. Earth Environ. Sci.* 237 (3), 032090. doi:10.1088/1755-1315/237/3/032090

Dhondt, A. A. (1988). Carrying capacity: A confusing concept. *Acta Oecol* 9 (4), 337–346.

Falkemark, M., and Lundqvist, J. (1998). Towards water security: Political determination and human adaptation crucial. *Nat. Resour. Forum* 21 (1), 37–51. doi:10.1111/j.1477-8947.1998.tb00708.x

Fang, H. (2018). "Application of system dynamics and WCCI in water resources evaluation: Taking Pakistan as an example," in 2018 International Conference on Mechanical, Electronic, Control and Automation Engineering (MECAE 2018), Qingdao, March 30–31, 2018.

Feng, L. H., and Huang, C. F. (2008). A risk assessment model of water shortage based on information diffusion technology and its application in analyzing carrying capacity of water resources. *Water Resour. manage.* 22 (5), 621–633. doi:10.1007/s11269-007-9182-z

Fu, Q., Liu, D., and Wang, Z. (2008). "Evaluation of region water resources carrying capacity based on set pair analysis technology," in 2008 4th International Conference on Wireless Communications, Networking and Mobile Computing, South Korea, 12-14 Oct. 2008, 1–4.

Gao, H., and Sun, L. (2018). Grey clustering evaluation of water resources carrying capacity based on triangle whitening weight function. *IOP Conf. Ser. Earth Environ. Sci.* 208, 012101. doi:10.1088/1755-1315/208/1/012101

Gao, S. (2017). Study on the bearing capacity of water resources in urbanized area. *Agro Food Ind. Hi-Tech* 28 (1), 3026–3029.

Gao, Y., Zhang, H. M., Xu, G. W., Su, H. M., and Zhang, Y. (2013). "Sustainable utilization evaluation on water resources base on matter element analysis in Huaibei City," in *Advanced materials research* (Switzerland: Trans. Tech. Publications Ltd), 610, 2671–2674. doi:10.4028/www.scientific.net/AMR.610-613.2671

Gleick, P. H., and Palaniappan, M. (2010). Peak water limits to freshwater withdrawal and use. *Proc. Natl. Acad. Sci. U. S. A.* 107, 11155–11162. doi:10.1073/pnas.1004812107

Gong, L., and Jin, C. (2009). Fuzzy comprehensive evaluation for carrying capacity of regional water resources. *Water Resour. manage.* 23 (12), 2505–2513. doi:10.1007/s11269-008-9393-y

Huang, L., Zhou, M., Lv, J., and Chen, K. (2020). Trends in global research in forest carbon sequestration: A bibliometric analysis. *J. Clean. Prod.* 252, 119908. doi:10.1016/j.jclepro.2019.119908

Huang, Q., Wang, W. P., and Deng, H. Y. (2014). "Agricultural restructuring based on the water resources carrying capacity in shandong province, China," in *Applied mechanics and materials* (Switzerland: Trans Tech Publications Ltd), 675, 783–786. doi:10.4028/www.scientific.net/AMM.675-677.783

Jiao, S., and Liang, H. (2006). *A research on spatio-temporal characteristics of the water resource carrying status in Guiyang City*. Guiyang: J. Guizhou Norm. Univ., 21–26. (in Chinese).04.

Jin, J., Chen, P., Chen, M., Li, J., Xu, C., and Chang, T. (2019). Bibliometric analysis of research progress on water resources carrying capacity based on knowledge map. *Water Resour. Prot.* 35, 14.

Joardar, S. D. (1998). Carrying capacities and standards as bases towards urban infrastructure planning in India: A case of urban water supply and sanitation. *Habitat Int.* 22 (3), 327–337. doi:10.1016/S0197-3975(98)00002-2

Jonathan, H. M. (1999). Carrying capacity in agriculture: Globe and regional issue. *Ecol. Econ.* 29 (3), 443–461. doi:10.1016/S0921-8009(98)00089-5

Kang, J., Zi, X., Wang, S., and He, L. (2019). Evaluation and optimization of agricultural water resources carrying capacity in haihe river basin, China. *Water* 11 (5), 999. doi:10.3390/w11050999

Kang, P., and Xu, L. (2012). Water environmental carrying capacity assessment of an industrial park. *Procedia Environ. Sci.* 13, 879–890. doi:10.1016/j.proenv.2012.01.082

Kessler, J. J. (1994). Usefulness of the human carrying capacity concept in assessing ecological sustainability of land-use in semi-arid regions. *Agric. Ecosyst. Environ.* 48 (3), 273–284. doi:10.1016/0167-8809(94)90109-0

Kuspilić, M., Vuković, Ž., and Halkijević, I. (2018). Assessment of water resources carrying capacity for the Island of Cres. *Gradevinar* 70 (04), 305–313. doi:10.14256/JCE.2167.2017

Lei, H. J., Yin, L., and Xi, B. D. (2013). "Scenario analysis on the water environment carrying capacity of wuliangsuhai lake basin," in *Advanced materials research* (Switzerland: Trans Tech Publications Ltd), 616, 1388–1393. doi:10.4028/www.scientific.net/AMR.616-618.1388

Li, B., Wang, X., Wei, T., Zeng, Y., and Zhang, B. (2018). Analysis of sustainable utilization of water resources in karst region based on the ecological footprint model–Liupanshui city case. *J. Water Supply Res. Trans.* 67 (6), 566–575. doi:10.2166/aqua.2018.016

Li, C., Li, H. J., Feng, S. D., Liu, X. Y., and Guo, S. (2019). A study on the spatiotemporal characteristics and change trend of the atmospheric environmental carrying capacity in the Jing-Jin-Ji region, China. *J. Clean. Prod.* 211, 27–35. doi:10.1016/j.jclepro.2018.11.045

Li, J., Yang, X., and Lu, G. (2009). Fuzzy matter-element model based on improved membership degree for comprehensive assessment of water resources carrying capacity in river basins. *J. Hydroelectr. Eng.* 28, 78–83.

Li, W. M., and Zhang, K. (2016). "Evaluation and analysis of water resources carrying capacity in arid zone—a case of manas basin," in Water Resources and Environment Proceedings of the 2015 International Conference on Water Resources and Environment, Beijing, 25–28 July 2015 (Leiden, Netherlands: CRC Press/Balkema), 103–108.

Liu, T., Yang, X., and Song, F. (2018). "Comprehensive evaluation for water resources carrying capacity in jilin province based on fuzzy set pair analysis model," in International Conference on Environmental and Water Resources Engineering (EWRE), South Korea, Oct 12-14, 2018.

Lu, F., Xu, J., and Wang, Z. (2009). "Application of GA optimized wavelet neural networks for carrying capacity of water resources prediction," in 2009 international conference on environmental science and information application technology, Wuhan, China, July 4 2009 to July 5 2009, 308–311. doi:10.1109/ESIAT.2009.591

Mallawaarachchi, H., Sandanayake, Y., Karunasena, G., and Liu, C. (2020). Unveiling the conceptual development of industrial symbiosis: Bibliometric analysis. *J. Clean. Prod.* 258, 120618. doi:10.1016/j.jclepro.2020.120618

Malthus, T. R. (1798). *An essay on the principle of population*. Ann Arbor, Michigan, United States: University of Michigan Press.

Mcnaughton, S. J., and Wolf, L. L. (1970). Dominance and the niche in ecological systems. *Science* 167 (39), 131–139. doi:10.1126/science.167.3915.131

Meng, C., Wang, X., and Li, Y. (2018). An optimization model for water management based on water resources and environmental carrying capacities: A case study of the yinma river basin, northeast China. *Water* 10 (5), 565. doi:10.3390/w10050565

Park, R. E., and Burgess, E. W. (1921). *Introduction to the science of sociology*. Chicago: University of Chicago Press.

Qi, H., Jiang, J. Y., Ying, L. I., Shi, Z. G., and Yin, P. H. (2016). Current research status and perspective of water resources carrying capacity in the arid and semi-arid regions of northwest China. *DEStech Trans. Soc. Sci. Educ. Hum. Sci.* 2016, 383–390 doi:10.12783/dtssehs/icssd2016/4756

Qu, G., and Fan, S. (2000). Water resources capacity and developing strategies in Heihe River Basin. *Chin. Desert* 20, 1–8.

Ren, C., Guo, P., Li, M., and Li, R. (2016). An innovative method for water resources carrying capacity research–metabolic theory of regional water resources. *J. Environ. Manage.* 167, 139–146. doi:10.1016/j.jenvman.2015.11.033

Rijisberman, M. A., and Frans, H. (2000). Different approaches to assessment of design and management of sustainable urban water system. *Environ. Impact Assess. Rev.* 129 (3), 333–345. doi:10.1016/S0195-9255(00)00045-7

Secinaro, S., Brescia, V., Calandra, D., and Biancone, P. (2020). Employing bibliometric analysis to identify suitable business models for electric cars. *J. Clean. Prod.* 264, 121503. doi:10.1016/j.jclepro.2020.121503

Shi, Y., and Qu, G. (1992). *Water resources carrying capacity and reasonable utilization of urumqi river basin*. Beijing: Science Press.

Shi, Y. S., Wang, H. F., and Yin, C. Y. (2013). Evaluation method of urban land population carrying capacity based on gis—a case of shanghai, China. *Comput. Environ. Urban Syst.* 39, 27–38. doi:10.1016/j.compenvurbsys.2013.02.002

Song, F., Yang, X., and Wu, F. (2020). Catastrophe progression method based on M-K test and correlation analysis for assessing water resources carrying capacity in Hubei province. *J. Water Clim. Chang.* 11 (2), 556–567. doi:10.2166/wcc.2018.114

Song, X. (2016). "Evaluation of water resources carrying capacity based on system dynamics model," in 3rd International Conference on Economic, Business Management and Education Innovation (EBMEI), Prague, Czech Republic, May 10-11, 2016.

Sun, B., and Yang, X. (2019). Simulation of water resources carrying capacity in Xiong'an New Area based on system dynamics model. *Water* 11 (5), 1085. doi:10.3390/w11051085

Tang, B., Hu, Y., Li, H., Yang, D., and Liu, J. (2016). Research on comprehensive carrying capacity of Beijing–Tianjin–Hebei region based on state-space method. *Nat. Hazards (Dordr).* 84 (1), 113–128. doi:10.1007/s11069-015-1891-7

Tao, J., Qiu, D., Yang, F., and Duan, Z. (2020). A bibliometric analysis of human reliability research. *J. Clean. Prod.* 260, 121041. doi:10.1016/j.jclepro.2020.121041

UNESCO&FAO (1985). *Carrying capacity assessment with a pilot study of Kenya: A resource accounting methodology for sustainable development*. Paris and Roma: FAO.

Wang, C., Hou, Y., and Xue, Y. (2017). Water resources carrying capacity of wetlands in Beijing: Analysis of policy optimization for urban wetland water resources management. *J. Clean. Prod.* 161, 1180–1191. doi:10.1016/j.jclepro.2017.03.204

Wang, D. L., Shi, Y. H., and Wan, K. D. (2020). Integrated evaluation of the carrying capacities of mineral resource-based cities considering synergy between subsystems. *Ecol. Indic.* 108, 105701. doi:10.1016/j.ecolind.2019.105701

Wang, J. (2015). "Comprehensive evaluation and analysis method for carrying capacity of water resource based on Neural Network," in 8th International Conference on Intelligent Computation Technology and Automation (ICICTA), Nanchang, China, Jun 14-15, 2015. doi:10.1109/ICICTA.2015.84

Wang, J., Jiang, D., Gu, Q., Qi, W., and Tang, Q. (1999). The concept and theory of the carrying capacity of regional water resources. *J. Gansu. Sci.* (02), 3–5. (in Chinese).

Wang, S., Xu, L., Yang, F., and Wang, H. (2014). Assessment of water ecological carrying capacity under the two policies in Tieling City on the basis of the integrated system dynamics model. *Sci. Total Environ.* 472, 1070–1081. doi:10.1016/j.scitotenv.2013.11.115

Wang, W., and Zeng, W. (2013). Optimizing the regional industrial structure based on the environmental carrying capacity: An inexact fuzzy multi-objective programming model. *Sustainability* 5 (12), 5391–5415. doi:10.3390/su5125391

Wang, Y. J., Yang, G., and Xu, H. L. (2010). "Evaluation of water resources carrying capacity based on fuzzy comprehensive evaluation on river basin in Arid Zone," in *Advanced materials research* (Switzerland: Trans Tech Publications Ltd), 113, 488–494. doi:10.4028/www.scientific.net/AMR.113-116.488

Wang, Y., Zhou, X., and Engel, B. (2018). Water environment carrying capacity in Bosten Lake basin. *J. Clean. Prod.* 199, 574–583. doi:10.1016/j.jclepro.2018.07.202

Wikiquote contributors, 2020b. Discourse on the method. Available at: https://en.wikiquote.org/w/index.php?title=Discourse_on_the_Method&oldid=2843135 (accessed Sep 18 2020).

Wikiquote contributors, 2020a. René Descartes. Available at: https://en.wikiquote.org/w/index.php?title=Ren%C3%A9_Descartes&oldid=2825315 (accessed Sep 18 2020).

Wu, C., Zhou, L., Jin, J., Ning, S., and Bai, L. (2020). Regional water resource carrying capacity evaluation based on multidimensional precondition cloud and risk matrix coupling model. *Sci. Total Environ136324* 710. doi:10.1016/j.scitotenv.2019.136324

Wu, F., Yang, X., and Shen, Z. (2018b2018). A three-stage hybrid model for regionalization, trends and sensitivity analyses of temperature anomalies in China from 1966 to 2015. *Atmos. Res.* 205, 80–92. doi:10.1016/j.atmosres.2018.02.008

Wu, L., Su, X., Ma, X., Kang, Y., and Jiang, Y. (2018a). Integrated modeling framework for evaluating and predicting the water resources carrying capacity in a

continental river basin of Northwest China. *J. Clean. Prod.* 204, 366–379. doi:10.1016/j.jclepro.2018.08.319

Xiao, H., Zhang, L., and Chai, Z. (2017). *IOP Conference Series: Earth and Environmental Science*, 74, 012003. doi:10.1088/1755-1315/74/1/012003Development of urbanization in arid and semi-arid regions based on the water resource carrying capacity–a case study of Changji, Xinjiang

Xie, Y., Li, X., Yang, C., and Yu, Y. (2014). Assessing water resources carrying capacity based on integrated system dynamics modeling in a semiarid river basin of northern China. *Water Sci. Tech-W sup.* 14 (6), 1057–1066. doi:10.2166/ws.2014.066

Xing, X., Shi, W., Zhang, Y., and Xie, J. (2013). Assessment of groundwater resources carrying capacity in Xi'an City based on principal component analysis. *J. Chin. Hydrol.* 33, 35–38.

XWRSSRG (Xinjiang Water Resources Soft Science Research Group) (1989). Xinjiang water resources and carrying capacity and development strategies. *Water Resour. Hydropower Tech.* (06), 2–9.

Yang, G., Wang, Y. J., He, X. L., and Li, J. F. (2010)., 113. Switzerland: Trans Tech Publications Ltd, 442–449. doi:10.4028/www.scientific.net/AMR.113-116.442The study of three evaluation models of water resources carrying capacity in Manas river basin*Adv. Mater. Res.*

Yang, J., and Ding, H. (2018). A quantitative assessment of sustainable development based on relative resource carrying capacity in Jiangsu Province of China. *Int. J. Environ. Res. Public Health* 15 (12), 2786. doi:10.3390/ijerph15122786

Yang, J., Lei, K., Khu, S., Meng, W., and Qiao, F. (2015). Assessment of water environmental carrying capacity for sustainable development using a coupled system dynamics approach applied to the Tieling of the Liao River Basin, China. *Environ. Earth Sci.* 73 (9), 5173–5183. doi:10.1007/s12665-015-4230-0

Yang, Q., Wang, H., Mu, H., Luo, J., Bao, X., Bian, J., et al. (2019). Risk assessment of water resources and environmental carrying capacity in Yinchuan city. *Hum. Ecol. Risk Assess. Int. J.* 25 (1-2), 120–131. doi:10.1080/10807039.2019.1573134

Yang, Q., Zhang, F., Jiang, Z., Yuan, D., and Jiang, Y. (2016). Assessment of water resource carrying capacity in karst area of Southwest China. *Environ. Earth Sci.* 75 (1), 37. doi:10.1007/s12665-015-4816-6

Yang, X., and Han, C. (2011). "Evaluation on water resource carrying capacity based on BP model-A case study," in Guanzhong District. International Conference on Ecological Protection of Lakes-Wetlands-Watershed and Application of 3S Technology (EPLWW3S 2011), Nanchang, China, Jun 25-26, 2011.

Ye, H., Dong, Z., Hang, Q., Liu, M., and Lu, X. (2018). Early warning of carrying status of water resources in Yancheng City. *J. Econ. Water Resour.* 36 (05), 31.

Young, C. C. (1998). Defining the range: The development of carrying capacity in management practice. *J. Hist. Biol.* 31, 61–83. doi:10.1023/A:1004205522191

Yu, M., Wang, C., Liu, Y., Olsson, G., and Wang, C. (2017). Sustainability of mega water diversion projects: Experience and lessons from China. *Sci. Total Environ.* 619-620, 721–731. doi:10.1016/j.scitotenv.2017.11.006

Yue, Q., Hou, L., Wang, T., Wang, L., Zhu, Y., Wang, X., et al. (2015). Optimization of industrial structure based on water environmental carrying capacity in Tieling City. *Water Sci. Technol.* 71 (8), 1255–1262. doi:10.2166/wst.2015.099

Zhang, J., Wang, C., Wang, X., and Yang, L. (2008). "The study of water resources carrying capacity in kaifeng city based on support vector machines," in International Conference on Informational Technology and Environmental System Science, Jiaozuo, China, May 15-17, 2008.

Zhang, J., Zhang, R., and Zhou, D. (2012). A study on water resource carrying capacityin the Shule river basin based on ecological footprints. *Acta Prataculturae Sin.* 21, 267–274.

Zhang, L., and Wang, J. (2012). Research progress and evaluation for water resources carrying capacity based on the Bibliometric method. *J. Water. Resour. Water Eng.* 23, 56–60.

Zhang, Y., and Li, S. S. (2012)., 518. Switzerland: Trans Tech Publications Ltd, 4362–4370. doi:10.4028/www.scientific.net/AMR.518-523.4362The time-series study of xiangjiang river water carrying capacity based on the ecological footprint of water resource—The ChangZhuTan region, for example*Adv. Mater. Res.*

Zhang, Z., Lu, W. X., Zhao, Y., and Song, W. B. (2014). Development tendency analysis and evaluation of the water ecological carrying capacity in the Siping area of Jilin Province in China based on system dynamics and analytic hierarchy process. *Ecol. Modell.* 275, 9–21. doi:10.1016/j.ecolmodel.2013.11.031

Zhao, X. Y., 2012. Application of coupling model with neural network and projection pursuit based on partial least-squares regression to water resources carrying capacity forecasting. In 2012 Fifth International Symposium on Computational Intelligence and Design (Vol. 2, pp. 446–449). NW Washington, DCUnited States: October 28 - 29, 2012. doi:10.1109/ISCID.2012.261

Zheng, Z., Wang, S., and Xing, J. (2016). "The complex index system of water scarcity based on the grey neural network model," in 2016 International Conference on Civil, Structure and Environmental Engineering, Guangzhou, China, March 12-13, 2016.

Zhou, R., Pan, Z., Jin, J., Li, C., and Ning, S. (2017). Forewarning model of regional water resources carrying capacity based on combination weights and entropy principles. *Entropy* 19 (11), 574. doi:10.3390/e19110574

Zhu, L., Li, X., Bai, Y., Yi, T., and Yao, L. (2019). Evaluation of water resources carrying capacity and its obstruction factor Analysis: A case study of hubei province, China. *Water* 11 (12), 2573. doi:10.3390/w11122573

Zhu, Y., Peng, L., Du, M., and Xu, X. (2010). On the evaluation of regional water resources carrying capacity. *Sci. Manage* 3, 21–24.

frontiers | Frontiers in Earth Science

TYPE Original Research
PUBLISHED 05 September 2022
DOI 10.3389/feart.2022.961871

OPEN ACCESS

EDITED BY
Celso Santos,
Federal University of Paraíba, Brazil

REVIEWED BY
Shengzhi Huang,
Xi'an University of Technology, China
Xiaoyan Song,
Northwest A & F University, China

*CORRESPONDENCE
Huiliang Wang,
wanghuiliang@zzu.edu.cn

SPECIALTY SECTION
This article was submitted to Hydrosphere, a section of the journal Frontiers in Earth Science

RECEIVED 07 June 2022
ACCEPTED 28 July 2022
PUBLISHED 05 September 2022

CITATION
Wang H, Zhu Y, Qin T and Zhang X (2022), Study on the propagation probability characteristics and prediction model of meteorological drought to hydrological drought in basin based on copula function.
Front. Earth Sci. 10:961871.
doi: 10.3389/feart.2022.961871

Study on the propagation probability characteristics and prediction model of meteorological drought to hydrological drought in basin based on copula function

Huiliang Wang[1]*, Yujia Zhu[1], Tianling Qin[2] and Xiangyang Zhang[1]

[1]School of Hydraulic Engineering and Science, Zhengzhou University, Zhengzhou, China, [2]Institute of Water Resources, China Academy of Water Resources and Hydropower Research, Beijing, China

Studying the probability characteristics of meteorological drought transmission to hydrological drought can help alleviate drought and optimize the allocation of water resources. This study takes the Yiluo River as the research object, and Standardized Precipitation Index (SPI) and Standardized Streamflow Index (SSI) were used to represent meteorological and hydrological drought, respectively. First, the stability of the precipitation and stream flow sequence is tested by using the heuristic segmentation algorithm. The correlation between meteorological and hydrological watershed was analyzed using cross wavelet transform and lag correlation to study the transmission time of meteorological drought to hydrological drought. Second, the characteristics of drought such as drought duration, drought intensity, and drought intensity are discussed by using the run theory. Finally, the joint distribution of the SPI and SSI sequence is constructed using Copula function. From the perspective of conditional probability, the propagation probability and propagation threshold from different levels of meteorological drought to hydrological drought are calculated. A hydrological drought prediction model based on the SPI—P(SSI|SPI) relation curve is proposed. The model is also validated based on the historical data. The results show that the model is suitable for light and middle hydrological drought prediction.

KEYWORDS

hydrological drought, meteorological drought, Copula function, conditional probability model, drought propagation

1 Introduction

Drought is one of the most widespread natural disasters that may cause persistent and adverse consequences for sustainable development (Lesk et al., 2016). It seriously endangers the development of economy and society and the stability of ecological environment. Large-scale droughts occur worldwide (Mishra and Singh, 2010). Also, the frequency of occurrence has increased significantly in recent years. Drought is usually defined as long-term no or little rain and water not being enough to meet the climatic phenomena of human survival and economic and social development (Sadeghipour and Dracup, 1985). In a certain river basin or area, evaporation demand is large and less precipitation, that is, water expenditure is greater than income; this state of long-term persistence will lead to the occurrence of drought. At present, the international drought types are generally divided into four categories, namely, meteorological drought, hydrological drought, agricultural drought, and social and economic drought. Meteorological drought refers to the long-term less precipitation phenomenon, and hydrological drought refers to the decrease of surface water, groundwater, or river stream flow (Zhu et al., 2019). From the perspective of water cycle, meteorological drought with precipitation as the main factor will occur first, and the occurrence of meteorological drought will propagate the water deficit signal to stream flow, groundwater, soil water, and other factors, thus leading to hydrological drought (Yuan et al., 2017). Therefore, the risk of meteorological drought is propagated to hydrological drought with water cycle after a certain lag time (Zhu et al., 2019). As an important link in water circulation, the propagation process of meteorological elements to hydrological elements is of great significance to study the propagation of meteorological drought to hydrological drought for the management of water resources and the forecast and early warning of drought (Van Loon et al., 2016).

Risk propagation between different types of drought mainly includes the propagation mechanism and process, propagation time, propagation threshold, and influencing factors. Previous studies have shown that the propagation threshold from meteorological to hydrological drought is a key feature of drought propagation and is important for drought prevention and mitigation (Lorenzo-Lacruz et al., 2013). At present, a large number of scholars have studied the propagation of meteorological drought to hydrological drought, most of which study the propagation time, threshold, and its influencing factors. At the time of drought propagation, there are many mature research results, including three characterization methods: run theory (Zhao et al., 2014), correlational analysis method (Barker et al., 2016), and nonlinear corresponding method (Lorenzo-Lacruz et al., 2013). In terms of propagation threshold, Guo et al. (2020) used Bayesian theory to study the duration and severity of meteorological drought in the three sub-basins from the meteorological basin of the Weihe River. Wu et al. applied the logarithm function to establish the response relationship model of hydrological drought to meteorological drought characteristics and obtained the critical conditions of meteorological drought evolution into hydrological drought. Gao et al. (2014)proposed the concept of climate threshold caused by drought and flood based on the study of precipitation disaster factors and crop disaster bearing body damage degree. Leasor, Quiring, and Svoboda (Lesk et al., 2016) used objective drought severity definition thresholds for improving drought monitoring (Leasor et al., 2020). Peters et al. (2003)used linear reservoir theory to study the spread of drought in groundwater. Sattar et al. (2019)analyzed the probability characteristics of the propagation of meteorological drought to hydrological drought in Korea using the Copula function and Bayesian theory. In terms of propagation influencing factors, Pandey and Ramasastri, (2001) believe that the corresponding propagation time depends on the local landscape conditions. Huang et al. (2017)used the Fu's equation in the budyko hypothesis to study the relationship between propagation time and the actual evapotranspiration and El Niño-Southern Oscillation (ENSO) and the Atlantic Oscillation (AO). Hudgins research found that the Arctic Oscillation activity is closely related to the climate in the middle and high latitudes (Hudgins and Huang, 1996). Talaee et al. (2014)found that meteorological, agricultural, and hydrological droughts are closely related to climate indices such as El Southern Nino (ENSO) and Atlantic Oscillation (AO).

However, in the previous studies on drought transmission and prediction, more quantitative characteristics of drought events such as drought duration, intensity, and severity were adopted as variables, but the calculation of these features is often based on a complete drought event. That is to say, only after the end of a complete meteorological drought can the duration, intensity, and severity of the meteorological drought be obtained. But in actual circumstances, the process of a meteorological drought not yet being ended may have led to the occurrence of hydrological drought. In this case, it is difficult to describe the hydrological drought according to the characteristic amount of meteorological drought in a timely manner. As a result, it is unable to carry out hydrological drought caused by meteorological drought in a timely manner. Therefore, this study used the month-by-month SPI and SSI values as variables, which are relative in a timelier manner, such as the SPI value obtained in this month and the SSI value of the next month can be predicted. Also, as far as known, most of the scholars will focus on some aspect of drought transmission process or drought prediction, and this study is to combine the two on the basis of a drought prediction model so as to form a complete system to provide a new idea and inspiration for later research. At present, how to predict the occurrence of hydrological drought according to real-time monitored meteorological drought index value? This is an unclear

problem in the spread of meteorological drought to hydrological drought. Therefore, the Standardized Precipitation Index (SPI) and the Standardized Streamflow Index (SSI) were used to characterize meteorological and hydrological droughts, respectively (Shukla and Wood, 2008). Directly using the drought index as the calculation condition and using the Copula function (Kolesarova et al., 2015), the conditional probability of different levels of hydrological drought under certain meteorological conditions is calculated, the propagation threshold of meteorological drought to hydrological drought is solved, and a theoretical basis for water resources management and early warning and control of drought is provided.

The main objectives of this study are ① to reveal the probability of hydrological drought of different levels after different levels of meteorological drought. ② Under certain probability conditions, the SPI-P(SSI|SPI) relationship curve is used to solve the propagation threshold of meteorological drought to different levels of hydrological drought. ③The hydrological drought early warning and forecast model based on the SPI-P(SSI|SPI) relationship curve is proposed and verified.

2 Methods and material

2.1 Methods

2.1.1 The precipitation and stream flow stability analysis method

In the current environment of rapidly changing climate conditions and increasing human activities, meteorological and hydrological conditions may change. Bernaola-Galvan et al. (2001)proposed a heuristic segmentation algorithm (BG algorithm) in 2001, which can test the stationary status of the sequence, detect the mutation point, and divide the non-stationary sequence into several stationary sequences. The main ideas are as follows:

For the time series $X = \{x_1, x_2, ..., x_n\}$, there are corresponding point sequences $K = \{k_1, k_2, ..., k_m\}$, and for any $k_i\,(i = 1, 2, ..., m)$, the means: $\mu_l\,(i), \mu_r\,(i)$ and standard deviations: s_l, s_r of the left and right sequence of the ki are calculated and then the combined deviation SD at point k_i:

$$S_D = \left(\frac{(n_l - 1) \times s_l^2 + (n_r - 1) \times s_r^2}{n_l + n_r - 2}\right)^{\frac{1}{2}} \times \left(\frac{1}{n_l} + \frac{1}{n_r}\right), \quad (1)$$

where n_l and n_r are the number of sequence points on the left and right side of the points k_i, respectively. The statistical value T(i) of the t-test is then used to quantify the difference between the mean on the left and right sides of the point k_i:

$$T\,(i) = \left|\frac{\mu_l\,(i) - \mu_r\,(i)}{S_D\,(i)}\right|. \quad (2)$$

TABLE 1 Division of the different drought grades.

Drought grade	SPI	SSI
Light drought	−1.0 < SPI < −0.5	−1.0 < SSI < −0.5
Middle drought	−1.5 < SPI < −1.0	−1.5 < SSI < −1.0
Severe drought	−2<SPI < −1.5	−2<SSI < −1.5
Extreme drought	SPI < −2	SSI < −2

The T sequence one-to-one corresponding to k_i is obtained by computing all points in K. The larger the T value, the greater the difference between the mean of the left and right parts of the current point. Statistical significance was then calculated for the maximum value of T_{max} in T:

$$P(T_{\max}) \approx \left(1 - I_{[v/(v+T_{\max}^2)]}(\delta v, \delta)\right)^{\eta}, \quad (3)$$

where obtained from Monte Carlo simulations: $\eta = 4.19 \ln N - 11.54$, $\delta = 0.4$. N is the length of the time series X, $v = N - 2$, and $I_x\,(a, b)$ is an incomplete β function.

Set the critical value P_0:

If: $P\,(T_{\max}) \geq P_0$:

At this point, the X sequence is divided into two subsequences with certain differences in the mean, and then the abovementioned process is repeated for the newly obtained subsequence so that the cycle until the abovementioned conditions is no longer met. In addition, to ensure its validity, when the subsequence length is less than or equal to l_0, no more segmentation will be conducted.

2.1.2 Standardized precipitation index

The SPI was first proposed to describe the drought conditions in Colorado by McKee et al., in 1993. The SPI can be applied to monitor long-series precipitation and is widely used in drought-related research due to its advantages of multi-time scale calculation, simple computational methods, and easy access to required data (Kao and Govindaraju, 2010). The SPI was used to characterize meteorological drought. The general calculation method can be divided into two steps: calculating the Gamma distribution probability of precipitation in a certain period and normally standardizing the Gamma distribution probability. Considering the regional characteristics of precipitation, Gamma distribution, Generalized Extreme Value distribution, and Log-logistic distribution were used to fit the stream flow data, and the tests were selected according to the Akaike information criterion (AIC) and Bayesian information criterion (BIC) (Zhang et al., 2014). The division of the different drought grades is shown in Table 1 (Vicente-Serrano et al., 2012).

2.1.3 Standardized stream flow index

The standardized streamflow drought index (SSDI) is a drought index constructed by the calculation procedure of the

analogy SPI (Niu et al., 2015). The variables calculated by the SPI were replaced by precipitation with stream flow, which includes all the advantages of SPI. In this study, the SSI was used to characterize hydrological drought. However, the distribution characteristics of stream flow sequence do not necessarily follow Gamma distribution well. Therefore, the Gamma distribution, Generalized Extreme Value distribution, and Log-logistic distribution were used to fit the stream flow data, and the test is performed according to the AIC and BIC. The calculation method is similar to that of the SPI, which is not repeated here.

2.1.4 Run theory

Run theory was proposed by Yevjevivich in 1967 and has been widely used in the identification of drought events, which can identify the characteristics of drought events, such as drought onset time, end time, drought duration, and drought intensity. Specific theory and calculation methods can be used as reference (Wu et al., 2021).

2.1.5 Cross-wavelet transform

Cross-wavelet transform (Paz and Mahler, 1993) was proposed by Hudgins et al. It is a new signal analysis technology based on continuous wavelet analysis technology and combining wavelet transform and cross-spectrum analysis, which can show the correlation of two time series in the time domain and frequency domain from the perspective of multiple time scales (Li et al., 2020). $W_n^X(s)$ and $W_n^Y(s)$ are assumed as the continuous wavelet transformations of two time series, $X = \{x_1, x_2, ..., x_n\}$ and $Y = \{y_1, y_2, ..., y_n\}$, respectively. The cross-wavelet transform between them is $W_n^{XY}(s) = W_n^X(s)W_n^{Y*}(s)$, where $W_n^{Y*}(s)$ represents the complex conjugation of $W_n^Y(s)$ and s is a time delay. The cross-over-wavelet power spectrum can be defined as $|W_n^{XY}(s)|$. It contains time–frequency–amplitude information. The larger the value, the higher the correlation between the two time series. For two stationary random processes, the standardized form of cross-wavelet transform can be written as wavelet cross-correlation coefficient (Sun and Cheng, 2008).

$$r(X,Y) = \frac{\sum_{i=1}^{n}\left(W_i^X(s) - \overline{W_i^X(s)}\right)\left(W_i^Y(s) - \overline{W_i^Y(s)}\right)}{\sqrt{\sum_{i=1}^{n}\left(W_i^X(s) - \overline{W_i^X(s)}\right)^2}\sqrt{\sum_{i=1}^{n}\left(W_i^Y(s) - \overline{W_i^Y(s)}\right)^2}}. \tag{4}$$

Cross-wavelet transform can reflect the common high-energy region of two time series and the bit-phase relationship, which is used to analyze the correlation between the SPI and SSI.

2.1.6 Cross-wavelet condensation spectrum

The wavelet condensation spectrum can measure the close degree of local correlation between two time series in the time domain and frequency domain, revealing the dependence between two time series relative to frequency, and its changing characteristics in the time domain indicates the degree of linear correlation at different frequency scales and the change of coupled period signal over time, which reflect the main information of the mutual correlation structure in the time and frequency domain (Wang et al., 2020). It is defined as

$$R_n^2(s,\tau) = \frac{\left|S\left(s^{-1}W_n^{XY}(s,\tau)\right)\right|^2}{S\left(s^{-1}\left|W_n^X(s,\tau)\right|^2\right) \times S\left(s^{-1}\left|W_n^Y(s,\tau)\right|^2\right)}, \tag{5}$$

where s is the scaling parameter, τ is the time translation parameter, and S is the smoothing function.

2.1.7 Solving conditional probability by copula function

The concept of Copula was first introduced by Sklar in 1959 when he answered M. Frechet's question about the relationship between multidimensional distribution functions and low-dimensional edges. It is currently widely used in non-parametric measures to determine the dependence between random variables. Nelsen (2005)introduced and described the Copula function concretely. . Mishra and Singh (2011) (Sadeghipour and Dracup, 1985) introduced the application of Copula in drought. The edge distribution of the Copula function is very flexible. For the same Copula function, its edge distribution can be of different types, so the Copula function can construct various types of multivariate distribution, and its connection form is not limited by edge distribution, which is the main reason for choosing the Copula function to build the joint distribution of the SPI and SSI (Hao and Singh, 2015). The main ideas of solving the conditional probability by using Copula are as follows:

$$P(X|Y) = \frac{P(X,Y)}{P(Y)}. \tag{6}$$

The abovementioned formula is a simple conditional probability calculation formula; X and Y are two random variables. When X and Y are not independent of each other, it will bring difficulties to calculate P (X,Y), but this problem can be solved by the Copula function.

$$F(X|Y) = \frac{F(X,Y)}{F(Y)} = \frac{C(F(X),F(Y))}{F(Y)}. \tag{7}$$

The calculation problem of the joint distribution function F (X,Y) can be skipped by the abovementioned equation, but the abovementioned equation can only solve the conditional probability for a fixed value of X and Y. When X and Y are in a certain interval, the calculation method is as follows:

$$F(x_1 \le X \le x_2 | y_1 \le Y \le y_2),$$
$$= \frac{C(F(x_2),F(y_2)) - C(F(x_1),F(y_2)) - C(F(x_2),F(y_1)) + C(F(x_1),F(y_1))}{F(y_2) - F(y_1)} \tag{8}$$

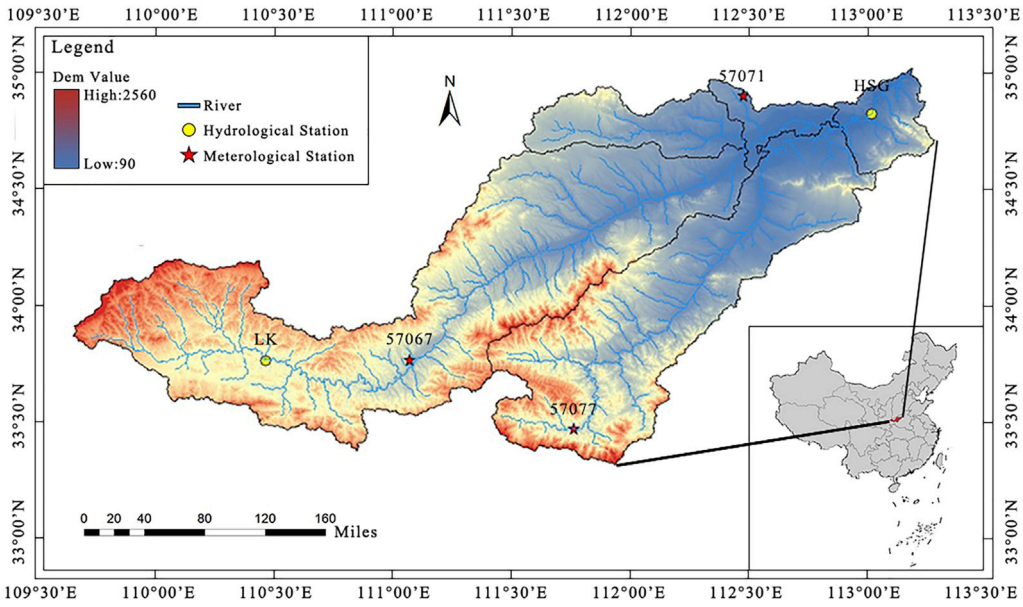

FIGURE 1
General situation of the Yiluo river basin and location of hydrological and meteorological stations.

where C represents the Copula function and F(x) and F(y) are the distribution functions of random variables X and Y, respectively.

2.2 Material

2.2.1 Study area

The Yiluo River is the largest tributary of the Yellow River below San menxia in China. There are two sources, namely, the Yi River and the Luo River. The main stream is 446.9 km in length, spanning Shanxi and Henan provinces. The basin covers about 18,900 square kilometers, and the control area of the export hydrological station is 18,563 square kilometers, accounting for about 98% of the whole basin, with an average annual stream flow of 3.2 billion cubic meters (Yue and Li, 2013).

The upper reach of the Yiluo River is a mountainous area with good vegetation and abundant water production; the middle and lower reaches are low hills and flat valleys, respectively, which are the main agricultural area.

The whole basin has a temperate monsoon climate, and the annual distribution of precipitation is uneven within the year. There are 60% of the precipitation concentrated in the flood season from July to October, which often causes large floods (Liu et al., 2013). But other seasons are often dry. Therefore, it is of great significance to study the drought characteristics and propagation process in this river basin. The basin overview is shown in Figure 1, in which HSG and LK are Heishiguan hydrological station and Lingkou hydrological station, respectively, and 57071, 57067, and 57077 are the three meteorological stations in the basin .

2.2.2 Data

Stream flow data used in this study: the monthly scale stream flow data of 1960–2020 are obtained from the Hydrologic Yearbook of China (Hydrologic data of the Yellow River Basin). Meteorological data: monthly scale precipitation data of three meteorological stations in 1960–2020, from China Meteorological Data Network: http://data.cma.cn/. The average precipitation in the river basin was calculated by the Tyson polygon method.

3 Results

3.1 Identification of mutation points

In this study, the BG segmentation algorithm was used to identify the rainfall and stream flow sequence, and L_0 is the minimum segmentation scale, ensuring the validity of the statistics, generally not less than 25, P_0 is the statistical significance critical value, if the maximum statistical significance value of a certain segment is greater than or equal to the value, then one can continue the segmentation; otherwise, the segmentation will not continue. The value of P0 generally ranges from 0.5 to 0.95, so the P_0 and L_0 were 0.95 and 25, respectively, to ensure statistical validity (Peng et al., 2017). The segmentation results are shown in Figure 2. For the precipitation

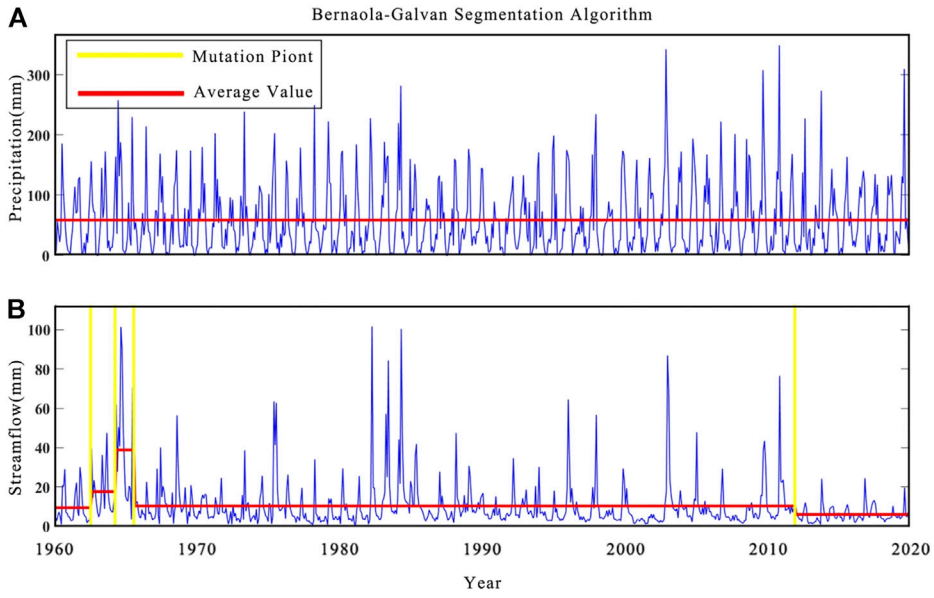

FIGURE 2
Identification results of mutation points in precipitation and streamflow sequences. **(A)** shows the mutation point of precipitation sequence. **(B)** shows the mutation point of streamflow sequence.

sequence, as shown in Figure 2A, in the period of 732 months from January 1960 to December 2020, the mean value was maintained in a stable state, which shows that in the long series from 1960 to 2020, it remained in a stable range and can be used for the study of stationary conditions. For stream flow sequence, as shown in Figure 2B, several streams flow far beyond the mean value, but according to the segmentation results, they just exist as little mutation points, and almost all of them are near in April 1964. This is due to meteorological conditions in the Yiluo River basin. The annual precipitation is concentrated in the summer, resulting in high stream flow, but it was not segmented due to its short duration and does not reach the minimum segmentation scale criterion. The mutation in April 1964 lasted for a long time, so it was identified, which is also consistent with the diachronic data of the Yiluo River basin, which had the largest surface water resources in 1964. Considering that this mutation situation is relatively short compared to that of the long series and the mean stream flow value returns to normal after that, this mutation situation is not considered in this study and is studied according to the stationary state.

3.2 Calculation of the drought index

According to the multi-time scale characteristics of the SPI and SSI, this study calculated the SPI and SSI of 1, 2 ... 12-month scales,. According to the calculation method, the distribution function of precipitation and stream flow is fitted first. Gamma distribution, Generalized Extreme Value distribution, and Log-logic distribution are fitted to precipitation and stream flow . The AIC and BIC are used to evaluate the fitting effect, and the distribution function is optimized according to the evaluation results. The distribution fitting results are shown in Table 2:

TABLE 2 Distribution function fitting effect evaluation.

		Gamma	Generalized Extreme Value	Log-logistic
P	AIC	643.10	643.30	654.97
	BIC	643.99	644.63	655.86
R	AIC	436.98	419.59	420.69
	BIC	437.88	420.93	421.58

According to the evaluation results of distribution fitting, the Gamma distribution is used for fitting the precipitation sequence, and the Generalized Extreme Value distribution is used for fitting the stream flow sequence. Then, the inverse operation of the normal distribution is performed to obtain the SPI and SSI sequences. The SPI on 1-, 3-, 6-, and 12-month scale and the SSI on 1-, 3-, 6-, and 12-month scale are as shown in Figure 3.

As can be seen from the figure, the SPI and the SSI have different temporal oscillation frequencies on different time scales, and the number of drought events identified is

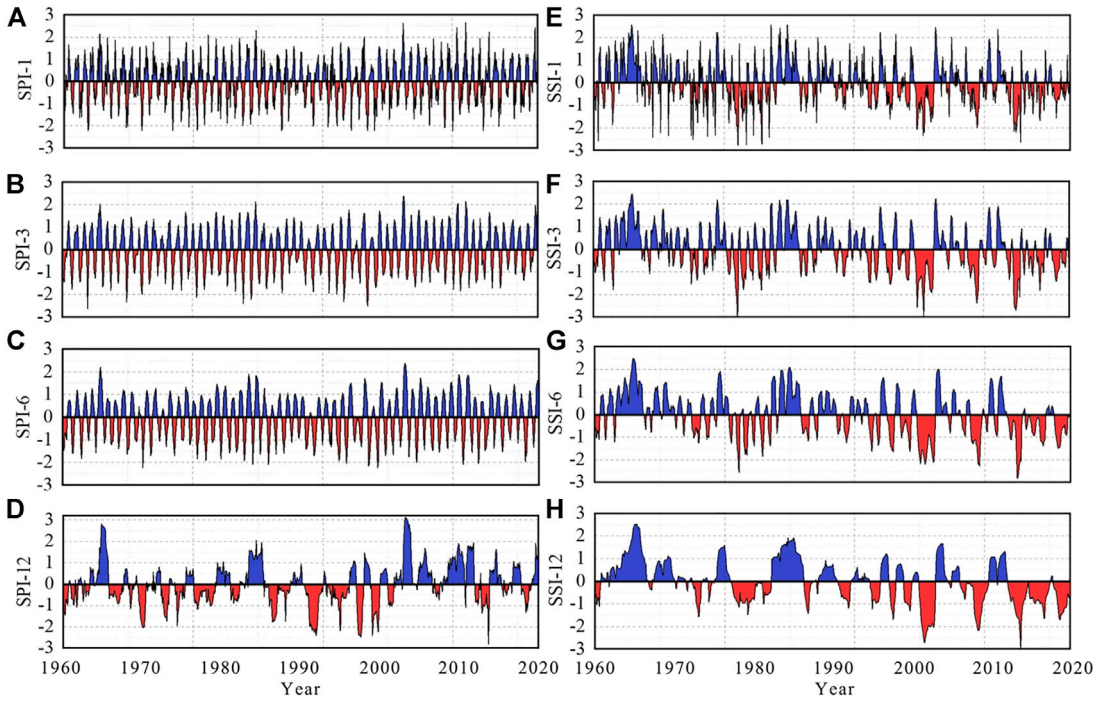

FIGURE 3
SPI and SSI values on different time scales **(A), (B), (C),** and **(D)** are the SPI on time scale of 1, 3, 6, and 12 months, respectively **(E), (F), (G),** and **(H)** are the SSI on time scale of 1, 3, 6, and 12 months, respectively.

different, and the drought duration is also different, showing different dynamic characteristics. Taking SPI as an example, specifically the SPI identified the most drought events on a short time scale of 1 month. The main drought events lasted for 1–2 months, showing frequent wet and dry alternations. The SPI on 3-month and 6-month medium time scales showed a certain seasonality to a certain extent, reflecting the cyclical variation characteristics of the climate in the Yiluo River Basin and the alternating cycles of dry and wet changes with the seasons. The SPI of the 12-month long time scales can reflect the long-term meteorological characteristics of the watershed and can clearly show the long-term drought or wet conditions of the watershed. The SSI sequence shows a similar situation to the SPI sequence.

3.3 The connection between meteorological and hydrological drought

In order to further reveal the link between meteorological drought and hydrological drought and to explore the validity of the SPI and SSI sequences, cross-wavelet analysis was used in this study. The results are shown in Figure 4. Figure 4A is the cross-wavelet power spectrum of the SPI and SSI, and Figure 4B is the cross-wavelet condensed spectrum of the SPI and SSI.

The thick solid line area in the figure represents the test of the red noise standard spectrum under the condition of significance level $\alpha = 0.05$, the arrow represents the phase relationship between the two, → represents the same phase between the impact factor and the stream flow, indicating that the two are positively correlated, ← indicates antiphase, indicating that the two are negatively correlated, ↓ indicates that the change of the impact factor precedes the change of stream flow by 90° (corresponding time is 3 months), and ↑ indicates that the change of the impact factor lags behind the change of stream flow by 90°. In order to avoid boundary effects and high-frequency wavelet false information, the area within the wavelet-influenced cone (thin arc in the figure) is the effective spectrum value (Sang, 2013). It can be seen from the figure that there is a high positive correlation between the SPI and SSI sequences on different time scales. The significance test basically runs through the entire area. The impact of the SPI on the SSI is mainly on the 8–16 month scale. The change of SPI ahead SSI stream flow varies with time, but it is basically between 30° and 90°, corresponding to 1–3 months. It reflects the propagation link between meteorological drought and hydrological drought, showing a good positive correlation, and more clearly reflects the detailed characteristics and resonance phase differences of the correlation between the two series in the time domain and frequency domain.

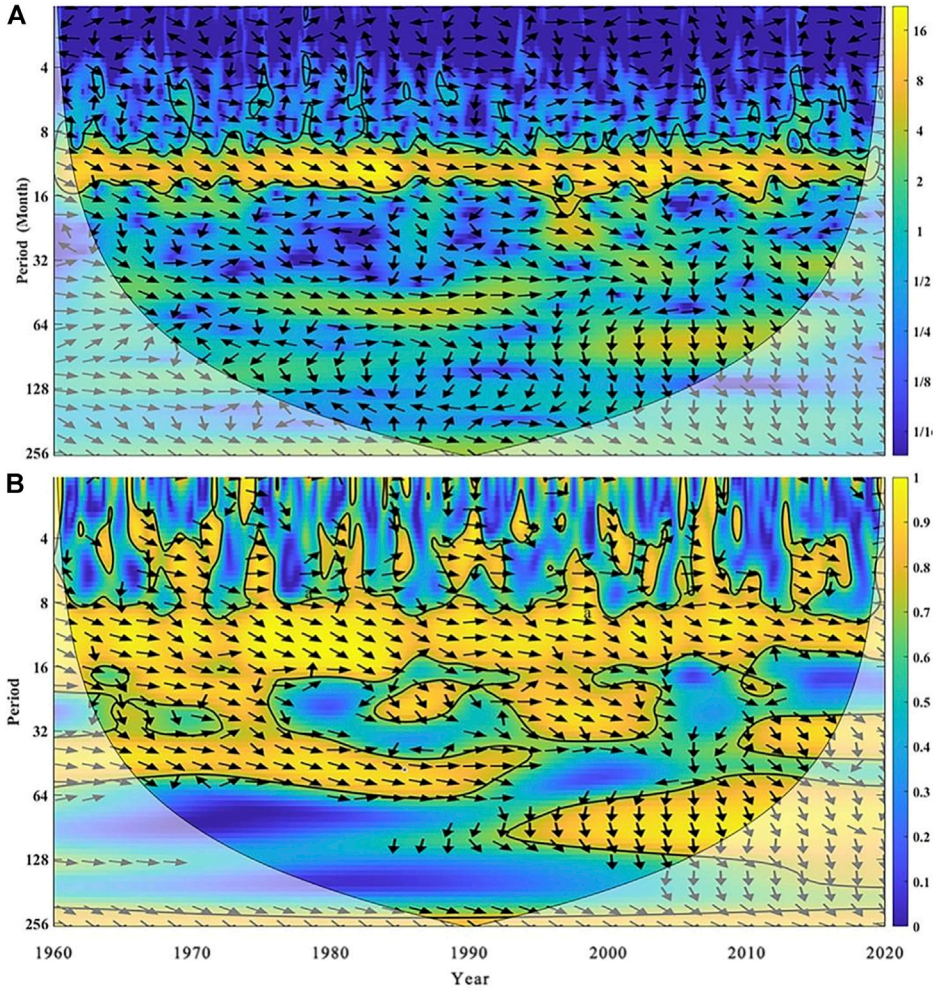

FIGURE 4
Cross-wavelet transform result **(A)** is Cross Wavelet Power Spectrum **(B)** is Cross Wavelet Condensed Spectrum.

3.4 Identification of drought events and characteristics

In this study, the run-length theory proposed by Yevjevich in 1967 was used to identify drought events and calculate related drought characteristics, including drought frequency, drought duration D, drought severity S, and drought intensity I (Montaseri et al., 2018). Among them, drought severity S is the accumulation of the drought index value within the drought duration D, and the drought intensity I is the ratio of S to D. In the process of drought identification, in order to prevent the interference of drought events with short duration and light severity, this study eliminated the drought events, that is, when the duration of a drought event is less than 1 month or its severity is greater than the threshold of drought index -0.5, the drought event was eliminated. At the same time, according to the times of meteorological drought and hydrological drought, this study calculates the propagation ratio R from meteorological drought to hydrological drought, which can measure the drought resistance of the basin (Guo et al., 2020).

TABLE 3 Frequency and propagation ratio of meteorological and hydrological droughts in different grades.

	MD	HD	Propagation ratio
Light	23	27	1.17
Middle	22	9	0.41
Severe	8	4	0.50
Extreme	2	3	1.50
ALL	55	43	0.78

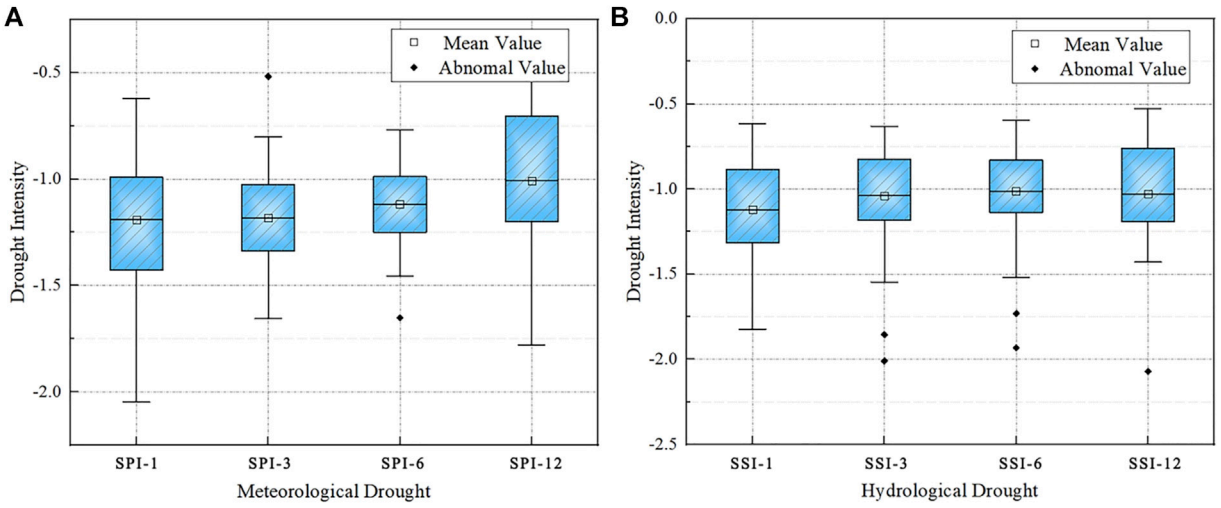

FIGURE 5
Intensity characteristic of **(A)** meteorological drought and **(B)** hydrological drought at different scales.

$$r = \frac{HD}{MD} \times 100\%, \tag{9}$$

where HD is the number of hydrological droughts and MD is the number of meteorological droughts.

The identification of meteorological and hydrological drought events at various levels is shown in Table 3. From the total number of drought events, the number of meteorological droughts is greater than that of hydrological droughts, indicating that meteorological droughts do not necessarily lead to hydrological droughts. Hydrological drought is a slow accumulation process, which is often caused by several meteorological droughts. The propagation ratio of meteorological drought to hydrological drought in the Yiluo River basin is 0.78, so the drought resistance is poor.

Among the three drought characteristics: D, S, and I, any two of them can describe drought. Compared with drought duration and drought severity, the value of drought intensity can more comprehensively represent drought characteristics, and it is easier to produce abnormal values in the sequence of drought duration and drought severity. Therefore, this study selects drought intensity as the characteristic quantity to describe drought. In this study, the SPI and SSI on the scale of 1, 3, 6, and 12 months were used to identify drought events and calculate their characteristics. The statistical calculation results of drought intensity are shown in Figure 5. It can be seen from the figure that the intensity of meteorological drought is slightly stronger than that of hydrological drought, but drought intensity identified by the two time scales is roughly the same, basically between-1.0 and-1.25.

Drought often shows certain seasonal characteristics, as shown in Figure 6. Meteorological drought is concentrated in the winter, and almost no meteorological drought occurs in summer. Hydrological drought is relatively evenly distributed in spring and winter. Hydrological drought in spring may be caused by the delayed spread of meteorological drought in the winter of the previous year. The flood season in the Yiluo River basin is summer, and the stream flow is large, so hydrological drought occurs less.

3.5 Determination of drought propagation t time

3.5.1 Correlation between multi-scale SPI and multi-scale SSI

At present, for the concept of drought propagation time, the method of calculating the correlation coefficient between the SPI of multiple time scales and the SSI of 1-month time scale is adopted, and the SPI time scale corresponding to the maximum correlation coefficient is defined as drought propagation time (Ding et al., 2021). This study revealed the correlation between the SPI of 1–12 month scale and the SSI of 1–12 month scale as shown in Figure 7A. The results showed that the SPI in 2–4 months had the highest correlation with the SSI in 3 months, and the correlation coefficient was greater than 0.6.

3.5.2 Correlation between lagging SSI and multi-scale SPI

We repeated the SSI sequence of 1 month for 1, 2, ... 12 months and obtained the correlation between SSI delayed for a certain time and SPI of 1–12 months, as shown in Figure 7B.

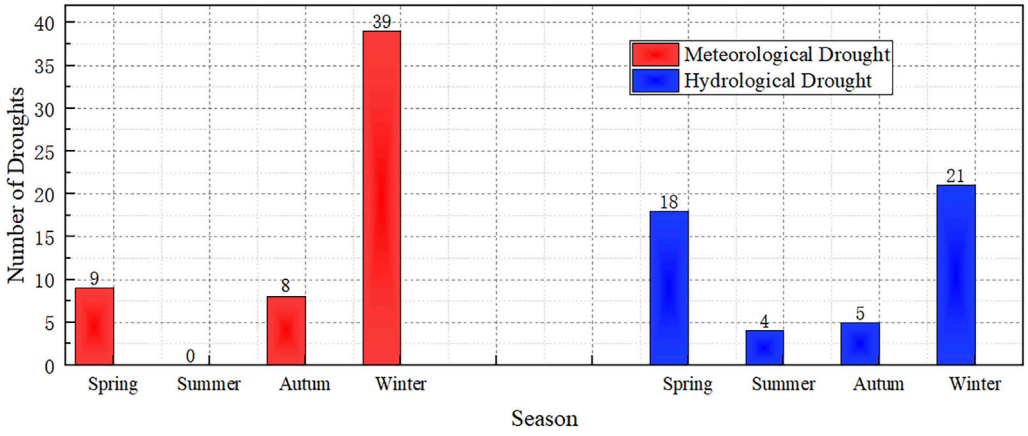

FIGURE 6
Meteorological and hydrological drought events in different seasons.

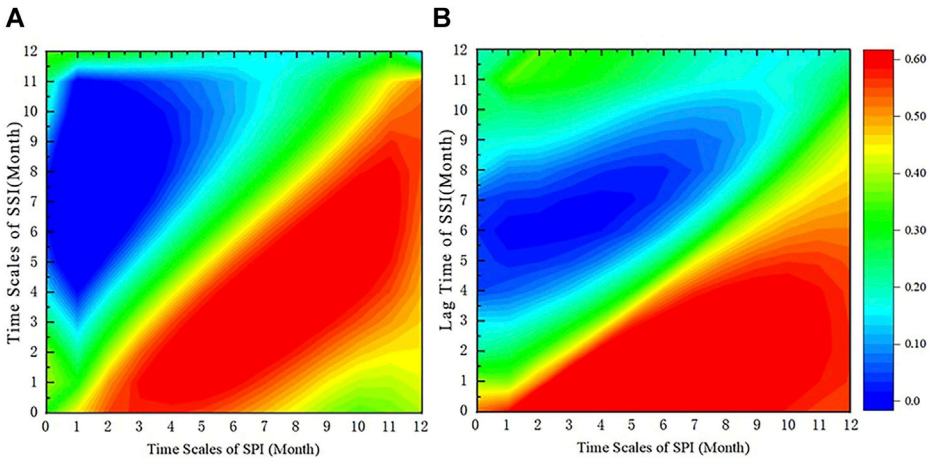

FIGURE 7
Correlation coefficient heatmap. **(A)** is the correlation between 1–12 month time scale SPI and 1–12 month time scale SSI. **(B)** is the correlation between 1–12 month time scale SPI and SSI with a lag time of 1–12 months.

When the delay time is 2–4 months, the SPI corresponding to different time scales shows good correlation, with the correlation coefficient greater than 0.6. When the SPI calculation time scale is 3 months, the correlation coefficient with SSI delayed for 3 months is the highest.

3.6 Probabilistic model between meteorological and hydrological drought

In recent years, droughts have occurred and its effects are exacerbated by increased water demand and changes in hydrometeorological variables due to climate change. Various concepts have been applied to simulate drought, from simple methods to more complex models (Mishra and Singh, 2011). Therefore, it is very important to construct the drought model to study the drought transmission process and for drought prediction. Scholars at home and abroad have also studied this from different perspectives, and Schwarz et al. (2020)have constructed drought disaster, vulnerability, and risk models in different land-use situations. The model was also cross-validated using the US Drought Monitoring (USDM) (Schwarz et al., 2020). Shin et al. (2019) developed a probabilistic hydrological drought prediction method using a Bayesian network combining

TABLE 4 Evaluation of fitting effect of different Copula functions.

Copula Function	Gauss	t	Gumbel	Clayton	Frank
SED	0.155	1.2162	0.0444	0.7641	0.1356

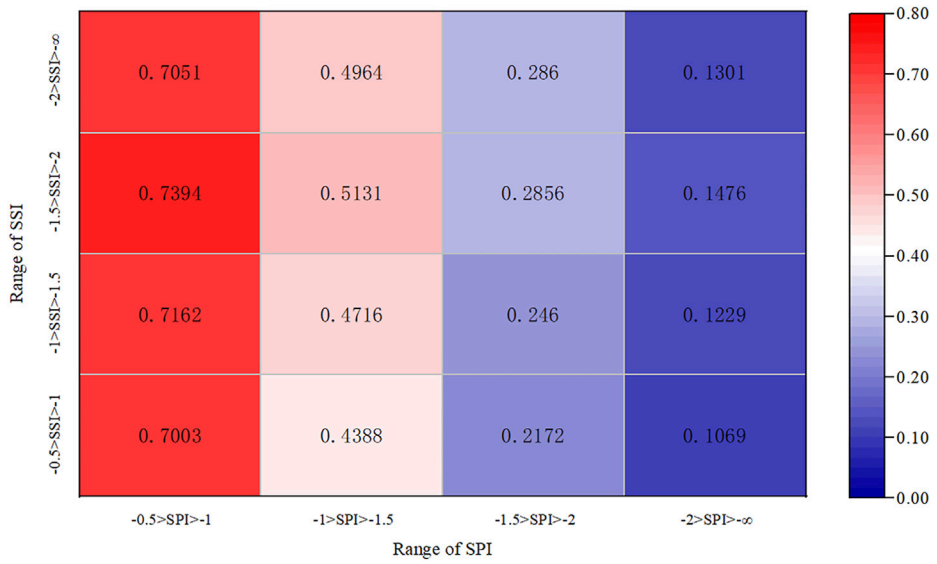

FIGURE 8
Propagation probability of meteorological drought of different grades to hydrological drought.

dynamic model prediction and drought transmission relationship to build a Bayesian network-based drought transmission drought prediction model, which is suitable for long-term hydrological drought prediction. Park et al. (2020) used the drought index based on satellite remote sensing data to build a short-term drought prediction model by convolving long and short-term memory and random forest method. Van Loon et al. (2012)studied the simulation effect of the large-scale hydrological model on the drought transmission process, and the results showed that there is still much room for improvement in the simulation of the semi-arid watershed model. This study is based on the conditional probability relationship between meteorological drought and hydrological drought and constructs the prediction model of hydrological drought based on the Standardized Precipitation Index (SPI) and the Standardized Runoff Index (SRI), which has low data requirements, simple model construction ideas, and is easy to understand and use. According to the foregoing study, the propagation time from meteorological drought to hydrological drought is 3 months, and considering that the correlation between the SPI and SSI in 3 months is the highest, this study uses the SPI and SSI sequences in 3 months as variables to construct edge distribution function, uses the Copula function to construct joint distribution, and calculates the propagation probability among meteorological and hydrological droughts of different grades based on conditional probability. In this study, Gauss, T, Gumbel, Clayton, Frank, and five Copula functions are selected to fit the edge distribution functions of the SPI and SSI. Also, the Euclidean distance (He et al., 2011) is calculated to evaluate the fitting effect. The optimizing Copula function according to evaluation results is shown in Table 4. The Cumbel–Copula function is selected as the joint distribution of the SPI and SSI.

After constructing joint distribution, the interval conditional probability (Eq. (2)) is solved by using the Copula function with the SPI value as the known condition. The calculation results are shown in Figure 8, which reveals the probability of different grades of hydrological drought. For example, when light meteorological drought occurs, the probability of light hydrological drought is about 70%. These probability characteristics can provide theoretical basis for water resource managers to apply relevant measures to deal with hydrological drought when meteorological drought is monitored by the SPI.

When the SPI value is known, how to predict hydrological drought? In this study, the values of SSI as −0.5, −1.0, −1.5, and −2.0 are given, then the points in the range of -30–10 at

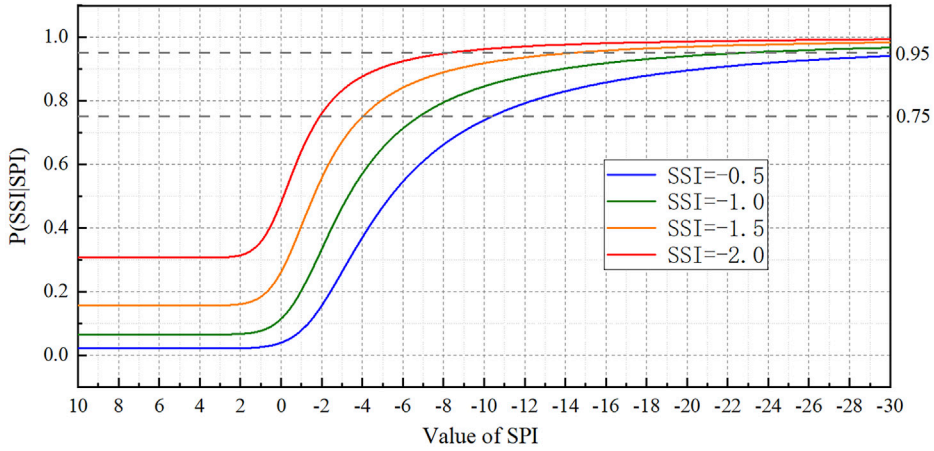

FIGURE 9
Probabilistic model of the relationship between meteorological and hydrological drought.

equal intervals as SPI values are selected, and the Copula function is used to calculate the conditional probability (Eq. 1) to obtain the relationship curve between the SPI and P(SSI|SPI), as shown in Figure 9. It can be inferred from this relationship curve that when the conditional probability value is 95%, the SPI threshold values of the propagation from meteorological drought to light, middle, severe, and extreme hydrological drought are, −7.7, −13.3, −20.8, and −29.7, respectively. According to the relationship curve between the SPI and P(SSI|SPI), combined with the monitored SPI value, we can obtain the probability of each grade of hydrological drought and further reveal the probability relationship between meteorological drought and hydrological drought. When the SPI value is abnormal, for example, if the SPI value of this month is low, the probability of occurrence of corresponding hydrological drought can be directly obtained. Combined with the propagation time from meteorological drought to hydrological drought, it provides a basis for timely decision-making on whether to take drought response measures.

3.7 Model validation and analysis

For the constructed model, the actual SPI sequence of 1, 3, 6, and 12 months is represented into the model formula for operation, and the SSI prediction sequence of 1, 3, 6, and 12 months is obtained. The calculation method is as follows:

On the basis of

$$P(SSI|SPI) = \frac{C(F_{SSI}, F_{SPI})}{F_{SPI}}, \tag{10}$$

where the Gumbel–Copula function is in the form of

$$C(F_{SSI}, F_{SPI}) = \exp\left\{ -\left[(-\ln F_{SPI})^{\theta} + (-\ln F_{SSI})^{\theta} \right]^{\frac{1}{\theta}} \right\}, \tag{11}$$

where θ = 1.6902 is the parameter of the Copula function and F_{SSI} and F_{SPI} are the fitting distribution function of SSI and SPI, respectively.

$$F_{SPI} = F(x|a,b) = \frac{1}{b^a \Gamma(a)} \int_0^x x^{a-1} e^{\frac{-t}{b}} dx, \tag{12}$$

where a and b are the parameters of the Gamma distribution function and x is the value of the SPI.

$$f_{SSI} = f(x|k,\mu,\sigma) = \left(\frac{1}{\sigma}\right) \exp\left(-\left(1 + k\frac{(x-\mu)}{\sigma}\right)^{-\frac{1}{k}} \right) \left(1 + k\frac{(x-\mu)}{\sigma}\right)^{-1-\frac{1}{k}}, \tag{13}$$

$$F_{SSI} = \int f_{SSI} dx, \tag{14}$$

where μ, σ, and k are the location parameter, scale parameter, and shape parameter of the Generalized Extreme Value probability density function, respectively; x is the value of SSI.

Then, according to the known SPI sequence, the SSI can be solved back out by substituting the SPI in the formula, that is, the predicted value of the SSI sequence. The series of SSI-predicted values of different time scales were compared with the actual values as shown in Figure 10. As can be seen from the figure, the predicted SSI sequence is relatively stable, and the hydrological extreme value phenomenon is not obvious, but between-1–1, it is more consistent with the actual SSI sequence, and the overall trend of the predicted SSI and the actual SSI sequence is roughly the same, reflecting water deficit and surplus. These

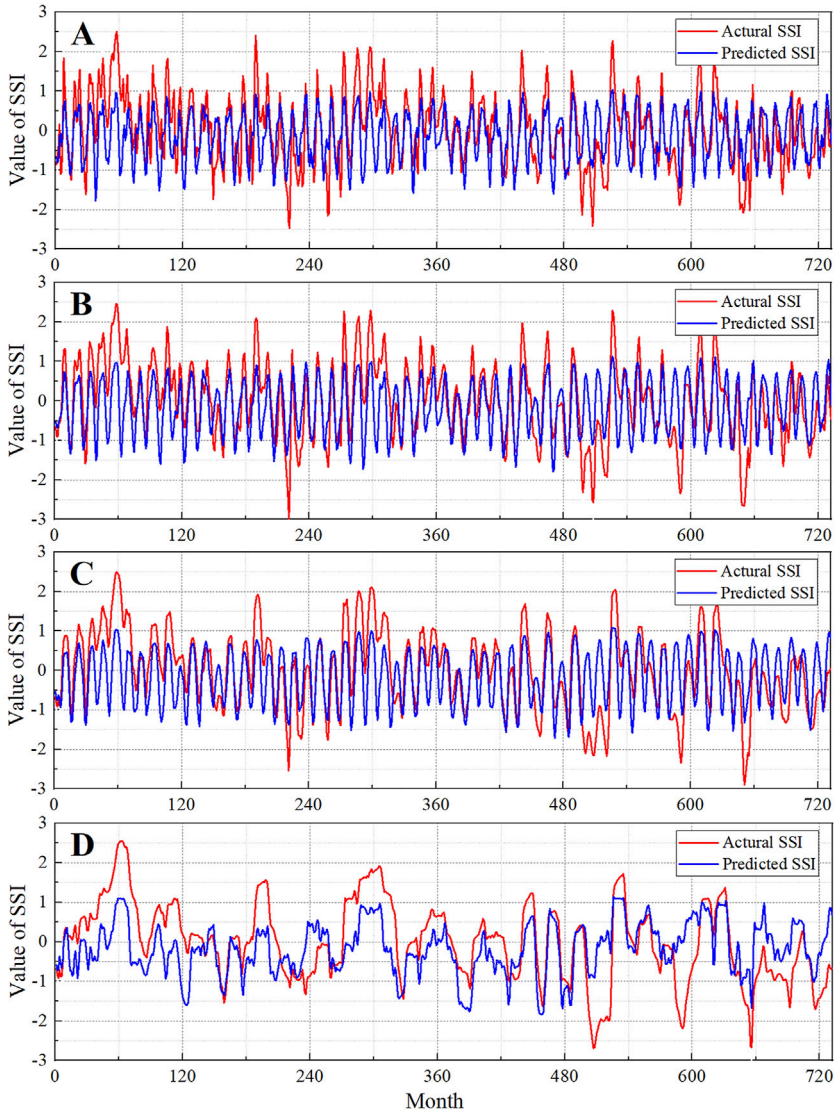

FIGURE 10
SSI sequence predicted values versus actual values**(A), (B), (C), and (D)** are calculated at a scale of 1, 3, 6, and12 months, respectively.

characteristics can be displayed more clearly at the calculated scale of 12 months.

After obtaining the predicted SSI sequence, this study also tested the detection effect of the model for the specific drought events. The combination of observations and predictions can be divided into hit, drought observed and also predicted; false, drought predicted but not observed; and miss, drought observed but not predicted. The POD indicates the probability of observed droughts that are also correctly predicted: POD = H/(H + M); FAR represents the proportion of drought predicted but not confirmed observed: FAR = F/(H + F). The CSI combining POD and FAR shows the comprehensive capability of drought detection: CSI = H/(H + M + F) (Ma et al., 2015). The results given in Table 5 showed that they are consistent with the characteristics expressed by the SSI sequence, with better effect for detecting light drought events and relatively poor effect for predicting severe drought. Meanwhile, the detection rate of this model is still very high, but there is a certain false positive rate.

4 Discussion

The stream flow data used in this study are the reduced stream flow data, so the influences of human activities such as reservoir construction, soil and water conservation measures,

TABLE 5 Detection effect on specific drought events.

Time scale of drought identification	Drought Grade	Hit	False	Miss	POD (%)	FAR (%)	CSI (%)
One Month	Light Drought	17	3	2	89	15	77
	Other Drought	15	8	3	83	35	58
Three Month	Light Drought	21	4	2	91	16	78
	Other Drought	18	9	1	95	33	64
Six Month	Light Drought	15	6	0	100	29	71
	Other Drought	20	4	2	91	17	77
Twelve Month	Light Drought	8	2	0	100	20	80
	Other Drought	6	1	3	67	14	60

and irrigation water and industrial water are excluded in the research process. At present, due to the influence of a large number of human activities, climate change has intensified, and the meteorological conditions and the underlying surface conditions of the basin have changed greatly (Hao and Singh, 2015). Therefore, this study adopted the heuristic segmentation method (BG algorithm) to check the obtained precipitation and reduced stream flow series and found that the stability of the series is relatively good, so the basin can be regarded as a relatively natural basin for research. For the selection of drought index, due to the limitation of data conditions, the SPI is selected as the meteorological drought index, ignoring the influence of evapotranspiration, which can be improved in the following research; for example, the SPEI, a standardized precipitation evapotranspiration index considering potential evapotranspiration, is selected to characterize the meteorological drought characteristics. The cross-wavelet analysis used in this research is a new technology combining cross-spectrum analysis with wavelet transform, which can better reveal the relationship between two time series in time and frequency. In the process of studying drought characteristics, according to the calculation results of propagation ratios of different grades of drought, it is found that the propagation ratios of light drought and extreme drought are all greater than 1, which indicates that in the process of drought propagation, due to the characteristics of slow development and long duration of hydrological drought, it is not only affected by meteorological conditions but also seriously affected by human activities. In fact, the response of hydrological drought to meteorological drought is dependent on large-scale atmospheric circulation and the local underlying surface (Vicente-Serrano and López-Moreno, 2005). In fact, precipitation has the greatest influence on drought, but it is often a rapid and short-term process, and it has to go through a complicated process from precipitation to stream flow production, which should take into account the influence of the underlying surface factors of the basin. In addition, the seasonal characteristics of drought are very obvious, which is closely related to the climatic characteristics of the basin and the spatial and temporal distribution of precipitation. Meanwhile, the influence of evapotranspiration should also be considered. In previous studies, some scholars analyzed the influence of climatic phenomena such as El Nino Southern Oscillation and Arctic Oscillation on drought propagation, which is strongly related to the seasonal characteristics of drought, and this climatic phenomenon is closely related to evapotranspiration, which reveals the influence of basin evapotranspiration on drought propagation (Liu et al., 2020). For the study of drought propagation time, based on the correlation analysis of the multi-scale SPI and SSI sequences in the past, this study also analyzes the correlation between multi-scale SPI and lagging SSI sequences and determines the drought propagation time by comparing the two results. In addition, the correlation coefficient diagram shows certain linear characteristics. In this study, the best Copula function was selected to construct the joint distribution function between the SPI and SSI sequences, and based on conditional probability and interval conditional probability, the propagation probability and propagation threshold between meteorological and hydrological droughts of different grades were obtained. The idea of guiding water resource management and drought response according to the SPI-P(SSI|SPI) relation curve is put forward, and the probabilistic prediction model of hydrological drought is constructed, and it is verified by historical data. The model construction in this study adopts an innovative idea to construct the drought prediction model, directly starting from the drought index and combined with the quantitative drought transmission process. It is enlightening to the construction of a drought model based on the drought transmission process and provides a new idea. According to the results, this model has good timeliness for drought prediction, which is of great significance for drought control work. The validation results showed that the model is suitable for predicting mild and moderate hydrological drought and poor, severe, and extreme hydrological drought. There are three main reasons for this: First, in terms of influencing factors, the stream flow of hydrological drought has other influencing factors besides precipitation, such as the underlying surface

conditions, human water intake, and drainage activities, and evaporation also promotes the occurrence of hydrological drought. These factors were not considered due to the limitation of data in this study; second, the drought transmission time, in this study, used more research before the correlation coefficient method, and the drought transmission time is a fixed value, but in fact, the drought transmission time cannot be fixed, such as in previous studies show temperature has a great influence on transmission time, in the later study, can be considered; third, in terms of specific drought events, in the long series of hydrological data research, the results show that drought events are mild and moderate, and severe and extreme drought events are relatively few, only a few times in 1960–2020, which led to the sample size of severe and extreme drought events, resulting in the fitting process of the model with poor accuracy, eventually leading to poor applicability of a severe and extreme drought model. However, the construction idea of this model can provide new direction and ideas for drought prediction research. For application in different watersheds, the calculation scale of the SPI can be adjusted according to the characteristics of watersheds. For example, the watershed with short drought propagation time can further refine the SPI sequence, taking weeks as the calculation time scale, while the watershed with long propagation time can appropriately expand the calculation scale of the SPI.

5 Conclusion

In this study, based on the calculation of conditional probability and interval conditional probability, the Copula function is used to put forward a probability model of meteorological drought spreading to hydrological drought, namely, the SPI-P (SSI | SPI) relationship curve. The probability of occurrence of hydrological drought at all levels can be obtained directly according to the real-time monitored SPI value, which improves the timeliness of drought forecasting and early warning. The main conclusions of this study are as follows:

1) Combining drought transmission and drought prediction, the construction of a new idea of drought prediction model is proposed.
2) Using the SPI-P(SSI|SPI) relationship curve, a drought prediction probability model based on the drought index is developed. After verification, it was found that the model has good ability to predict mild and moderate hydrological drought and still has room for improvement in predicting severe and extreme hydrological drought effect.

The drought prediction model constructed in this study can directly use the meteorological drought index to predict hydrological drought, which is easier to understand and apply. The model construction idea can provide new ideas and inspiration for relevant research and also has practical significance for the drought control work.

Data availability statement

The datasets presented in this study can be found in online repositories. The names of the repository/repositories and accession number(s) can be found below: and http://data.cma.cn/ &.

Author contributions

HW: put forward provision and suggestions and modifications to the manuscript; YZ: data analysis, writing original draft, and discussion; QT: data collection and investigation; XZ: made drawings and tables.

Funding

This research was funded by the Key Research and Development Projects of China during the 14th Five Year Plan Period (2021YFC3000204), and the Major Scientific and Technological Projects of Henan Province, China (201300311400).

Conflict of interest

The authors declare that the research was conducted in the absence of any commercial or financial relationships that could be construed as a potential conflict of interest.

Publisher's note

References

Barker, L. J., Hannaford, J., Chiverton, A., and Svensson, C. (20162016). From meteorological to hydrological drought using standardised indicators. *Hydrol. Earth Syst. Sci.* 20 (6), 2483–2505. doi:10.5194/hess-20-2483-2016

Bernaola-Galvan, P., Ivanov, P. C., Nunes Amaral, L. A., and Stanley, H. E. (2001). Scale invariance in the nonstationarity of human heart rate. *Phys. Rev. Lett.* 87 (16), 168105. doi:10.1103/physrevlett.87.168105

Ding, Y., Xu, J., Wang, X., Cai, H., Zhou, Z., Sun, Y., et al. (2021). Propagation of meteorological to hydrological drought for different climate regions in China. *J. Environ. Manag.*, 111980. doi:10.1016/j.jenvman.2021.111980

Gao, C., Chen, S., Zhai, J., Zhang, Z., and Liu, Q. (20142014). On threshold of drought and flood disasters in Huaihe River basin [淮河流域旱涝灾害致灾气候阈值]. *Adv. Water Sci.* 25 (1), 36–44.

Guo, Y., Huang, S., Huang, Q., Leng, G., Fang, W., Wang, L., et al. (2020). Propagation thresholds of meteorological drought for triggering hydrological drought at various levels. *Sci. Total Environ.*, 136502. doi:10.1016/j.scitotenv.2020.136502

Hao, Z., and Singh, V. P. (2015). Drought characterization from a multivariate perspective: A review. *J. Hydrology* 527, 668–678. doi:10.1016/j.jhydrol.2015.05.031

He, Y., Bardossy, A., and Zehe, E. (2011). A catchment classification scheme using local variance reduction method. *J. Hydrology* 411 (1-2), 140–154. doi:10.1016/j.jhydrol.2011.09.042

Huang, S., Li, P., Huang, Q., Leng, G., Hou, B., and Ma, L. (2017). The propagation from meteorological to hydrological drought and its potential influence factors. *J. Hydrology* 547, 184–195. doi:10.1016/j.jhydrol.2017.01.041

Hudgins, H., and Huang, J. (19961996). Bivariate wavelet analysis of Asia monsoon and ENSO. *Adv. Atmos. Sci.* 13 (3), 299–312. doi:10.1007/bf02656848

Kao, S-C., and Govindaraju, R. S. (2010). A copula-based joint deficit index for droughts. *J. Hydrology* 380 (1-2), 121–134. doi:10.1016/j.jhydrol.2009.10.029

Kolesarova, A., Mayor, G., and Mesiar, R. (2015). Quadratic constructions of copulas. *Inf. Sci.* 310, 69–76. doi:10.1016/j.ins.2015.03.016

Leasor, Z. T., Quiring, S. M., and Svoboda, M. D. (2020). Utilizing objective drought severity thresholds to improve drought monitoring. *J. Appl. Meteorol. Climatol.* 59 (3), 455–475. doi:10.1175/jamc-d-19-0217.1

Lesk, C., Rowhani, P., and Ramankutty, N. (2016). Influence of extreme weather disasters on global crop production. *Nature* 529 (7584), 84–87. +. English. doi:10.1038/nature16467

Li, Q., He, P., He, Y., Han, X., Zeng, T., Lu, G., et al. (2020). Investigation to the relation between meteorological drought and hydrological drought in the upper Shaying River Basin using wavelet analysis. *Atmos. Res.*, 104743. doi:10.1016/j.atmosres.2019.104743

Liu, S., Shi, H., Niu, J., Chen, J., and Kuang, X. (2020). Assessing future socioeconomic drought events under a changing climate over the Pearl River basin in South China. *J. Hydrology Regional Stud.* 30, 100700. doi:10.1016/j.ejrh.2020.100700

Liu, X., Dai, X., Zhong, Y., Li, J., and Wang, P. (2013). Analysis of changes in the relationship between precipitation and streamflow in the Yiluo River, China. *Theor. Appl. Climatol.* 114 (1-2), 183–191. doi:10.1007/s00704-013-0833-0

Lorenzo-Lacruz, J., Vicente-Serrano, S. M., Gonzalez-Hidalgo, J. C., Lopez-Moreno, J. I., and Cortesi, N. (20132013). Hydrological drought response to meteorological drought in the Iberian Peninsula. *Clim. Res.* 58 (2), 117–131. doi:10.3354/cr01177

Ma, M., Ren, L., Singh, V. P., Tu, X., Jiang, S., and Liu, Y. (2015). Evaluation and application of the SPDI-JDI for droughts in Texas, USA. *J. Hydrology* 521, 34–45. doi:10.1016/j.jhydrol.2014.11.074

Mishra, A. K., and Singh, V. P. (2010). A review of drought concepts. *J. Hydrology* 391 (1-2), 202–216. doi:10.1016/j.jhydrol.2010.07.012

Mishra, A. K., and Singh, V. P. (2011). Drought modeling - a review. *J. Hydrology* 403 (1-2), 157–175. doi:10.1016/j.jhydrol.2011.03.049

Montaseri, M., Amirataee, B., and Rezaie, H. (2018). New approach in bivariate drought duration and severity analysis. *J. Hydrology* 559, 166–181. doi:10.1016/j.jhydrol.2018.02.018

Nelsen, R. B. (2005). "Copulas and quasi-copulas: An introduction to their properties and applications. 24th linz seminar on fuzzy set theory," in *Logical, algebraic, analytic, and probabilistic aspects of triangular norms* (Linz, AUSTRIA, 391–413. Linzer Hochschulfonds SCCHESFL, Technol. Available from: <Go to ISI>://WOS:000230172000014.

Niu, J., Chen, J., and Sun, L. (2015). Exploration of drought evolution using numerical simulations over the Xijiang (West River) basin in South China. *J. Hydrology* 526, 68–77. doi:10.1016/j.jhydrol.2014.11.029

Pandey, R. P., and Ramasastri, K. S. (2001). Relationship between the common climatic parameters and average drought frequency. *Hydrol. Process.* 15 (6), 1019–1032. doi:10.1002/hyp.187

Park, S., Im, J., Han, D., and Rhee, J. (2020). Short-term forecasting of satellite-based drought indices using their temporal patterns and numerical model output. *Remote Sens.* 12 (21), 3499. doi:10.3390/rs12213499

Paz, J. P., and Mahler, G. (1993). Proposed test for temporal Bell inequalities. *Phys. Rev. Lett.* 71 (20), 3235–3239. doi:10.1103/physrevlett.71.3235

Peng, X., Zheng, W., Zhang, D., Liu, Y., Lu, D., and Lin, L. (2017). A novel probabilistic wind speed forecasting based on combination of the adaptive ensemble of on-line sequential ORELM (Outlier Robust Extreme Learning Machine) and TVMCF (time-varying mixture copula function). *Energy Convers. Manag.* 138, 587–602. doi:10.1016/j.enconman.2017.02.004

Peters, E., Torfs, P., van Lanen, H. A. J., and Bier, G. (2003). Propagation of drought through groundwater - a new approach using linear reservoir theory. *Hydrol. Process.* 17 (15), 3023–3040. doi:10.1002/hyp.1274

Sadeghipour, J., and Dracup, J. A. (19851985). Regional frequency-analysis of hydrologic multiyear droughts. *J. Am. Water Resour. Assoc.* 21 (3), 481–487. doi:10.1111/j.1752-1688.1985.tb00160.x

Sang, Y-F. (2013). A review on the applications of wavelet transform in hydrology time series analysis. *Atmos. Res.* 122, 8–15. doi:10.1016/j.atmosres.2012.11.003

Sattar, M. N., Lee, J-Y., Shin, J-Y., and Kim, T-W. (2019). Probabilistic characteristics of drought propagation from meteorological to hydrological drought in South Korea. *Water Resour. manage.* 33 (7), 2439–2452. doi:10.1007/s11269-019-02278-9

Schwarz, M., Landmann, T., Cornish, N., Wetzel, K-F., Siebert, S., and Franke, J. (2020). A spatially transferable drought hazard and drought risk modeling approach based on remote sensing data. *Remote Sens.* 12 (2), 237. doi:10.3390/rs12020237

Shin, J. Y., Kwon, H. H., Lee, J. H., and Kim, T. W. (2019). Probabilistic long-term hydrological drought forecast using Bayesian networks and drought propagation. *Meteorol. Appl.* 27 (1). doi:10.1002/met.1827

Shukla, S., and Wood, A. W. (2008). Use of a standardized runoff index for characterizing hydrologic drought. *Geophys. Res. Lett.* (2), L02405. doi:10.1029/2007gl032487

Sun, W., and Cheng, B. (2008). Application of cross wavelet transformation to analysis on regional climate variations [交叉小波变换在区域气候分析中的应用]. *J. Appl. Meteorolgical Sci.* 19 (4), 479–487.

Talaee, P. H., Tabari, H., and Ardakani, S. S. (2014). Hydrological drought in the west of Iran and possible association with large-scale atmospheric circulation patterns. *Hydrol. Process.* 28 (3), 764–773. doi:10.1002/hyp.9586

Van Loon, A. F., Gleeson, T., Clark, J., Van Dijk, A. I. J. M., Stahl, K., Hannaford, J., et al. (2016). Drought in the anthropocene. *Nat. Geosci.* 9 (2), 89–91. doi:10.1038/ngeo2646

Van Loon, A. F., Van Huijgevoort, M. H. J., and Van Lanen, H. A. J. (2012). Evaluation of drought propagation in an ensemble mean of large-scale hydrological models. *Hydrol. Earth Syst. Sci.* 16 (11), 4057–4078. doi:10.5194/hess-16-4057-2012

Vicente-Serrano, S. M., Begueria, S., Lorenzo-Lacruz, J., Camarero, J. J., Lopez-Moreno, J. I., Azorin-Molina, C., et al. (2012). Performance of drought indices for ecological, agricultural, and hydrological applications. *Earth Interact.* 16, 1–27. doi:10.1175/2012ei000434.1

Vicente-Serrano, S. M., and López-Moreno, J. I. (2005). Hydrological response to different time scales of climatological drought: An evaluation of the standardized precipitation index in a mountainous mediterranean basin. *Hydrol. Earth Syst. Sci.* 9 (5), 523–533. doi:10.5194/hess-9-523-2005

Wang, F., Wang, Z., Yang, H., Di, D., Zhao, Y., Liang, Q., et al. (2020). Comprehensive evaluation of hydrological drought and its relationships with meteorological drought in the Yellow River basin, China. *J. Hydrology* 584, 124751. doi:10.1016/j.jhydrol.2020.124751

Wu, J., Chen, X., Yao, H., and Zhang, D. (2021). Multi-timescale assessment of propagation thresholds from meteorological to hydrological drought. *Sci. Total Environ.* 765, 144232. Declaration of competing interest The authors declare that they have no known competing financial interests or personal relationships that

could have appeared to influence the work reported in this paper. doi:10.1016/j.scitotenv.2020.144232

Yuan, X., Zhang, M., Wang, L. Y., and Zhou, T. (2017). Understanding and seasonal forecasting of hydrological drought in the Anthropocene. *Hydrol. Earth Syst. Sci.* 21 (11), 5477–5492. doi:10.5194/hess-21-5477-2017

Yue, Y., and Li, Z. (2013). "Study on applications of neural network to flood forecasting in Yiluo River," in Hydraulic engineering, 2012 sree conference) Sree Conference on Hydraulic Engineering and 2nd Sree Workshop on Environment and Safety Engineering, 2012 2013, Dec 21-22;Hong Kong, (PEOPLES R CHINA, 49–53. Soc Resources E, Engn.

Zhang, Y., Liu, K., Chen, Q., and Hu, X. (20142014). Bivariate probability distribution of meteorological drought characteristics in the aksu basin using copula [区域气象干旱特征多变量Copula分析以阿克苏河流域为例]. *Sci. Geogr. Sin.* 34 (12), 1480–1487.

Zhao, L., Lyu, A., Wu, J., Hayes, M., Tang, Z., He, B., et al. (2014). Impact of meteorological drought on streamflow drought in Jinghe River Basin of China. *Chin. Geogr. Sci.* 24 (6), 694–705. doi:10.1007/s11769-014-0726-x

Zhu, Y., Liu, Y., Wang, W., Singh, V. P., Ma, X., and Yu, Z. (2019). Three dimensional characterization of meteorological and hydrological droughts and their probabilistic links. *J. Hydrology* 578, 124016. doi:10.1016/j.jhydrol.2019.124016

frontiers | Frontiers in Earth Science

TYPE Original Research
PUBLISHED 06 September 2022
DOI 10.3389/feart.2022.953318

OPEN ACCESS

EDITED BY
Celso Santos,
Federal University of Paraíba, Brazil

REVIEWED BY
Xueyan Jiang,
Ocean University of China, China
Bai Tao,
Xi'an University of Technology, China

*CORRESPONDENCE
Dengming Yan,
18519500795@163.com

SPECIALTY SECTION
This article was submitted to Hydrosphere, a section of the journal Frontiers in Earth Science

RECEIVED 26 May 2022
ACCEPTED 13 July 2022
PUBLISHED 06 September 2022

CITATION
Shang W, Yan D, Peng S, Wang Y, Ge L and Shang Y (2022), Analysis on the ecological impact of the Xiaolangdi Reservoir on the Yellow River Delta wetland and coastal areas.
Front. Earth Sci. 10:953318.
doi: 10.3389/feart.2022.953318

Analysis on the ecological impact of the Xiaolangdi Reservoir on the Yellow River Delta wetland and coastal areas

Wenxiu Shang[1,2], Dengming Yan[1,2]*, Shaoming Peng[1,2], Yu Wang[1,2], Lei Ge[3] and Yi Shang[4]

[1]Yellow River Engineering Consulting Co., Ltd., Zhengzhou, China, [2]Key Laboratory of Water Management and Water Security for Yellow River Basin, Ministry of Water Resources, Zhengzhou, China, [3]Yellow River Institute of Water Protection Research, Zhengzhou, China, [4]College of Geoscience and Engineering, North China University of Water Resources and Electric Power, Zhengzhou, China

An environmental water supplement through reservoir regulation is an important way to restore the deltaic coastal wetland. In order to quantify the impact of the reservoir on the deltaic coastal wetland ecosystem, this article proposes a quantitative analysis method for the ecological impact and contribution rate of the reservoir, which compares the ecological status in two scenarios with the presence or absence of the reservoir during the assessment period, and reveals the reservoir's impact on and contribution rate to the ecological status and environmental water supplement conditions. The results show that during 2000–2019, through the regulation of the Xiaolangdi Reservoir, the average annual drying up days at the Lijin section reduced by 81.15 days, the average annual assurance rate of ecological base flow at the Lijin section increased by 20.60%, and the volume of water flowing into the sea from April to June increased by 2.37 billion m^3. During 2008–2015, the Xiaolangdi Reservoir increased the environmental water supplement of the Yellow River Delta by 19.95 million m^3. Compared with the flow and water withdrawal during 1980–1999, the natural flow of the Yellow River decreased by 10.59% and the measured flow in the lower reaches decreased by 22.15%, and the water withdrawal in the lower reaches increased by 0.32 billion m^3 during 2000–2019, which is detrimental to provide environmental water to the Yellow River Delta wetland and coastal areas. The Xiaolangdi Reservoir reversed the adverse effects of flow and water withdrawal and ensured the continuous ecological improvement in the Yellow River Delta and coastal areas, providing the respective contribution rate of 187.85%, 137.24%, and 125.83% to the prevention of drying up at the Lijin section, the increase in the assurance rate of ecological base flow at the Lijin section, and the increase in the volume of water flowing into the sea in the critical period.

KEYWORDS

deltaic coastal wetland, reservoir regulation, contribution rate, ecological base flow, environmental water supplement, Yellow River, Xiaolangdi Reservoir

Introduction

The coastal wetland is one of the most productive ecosystems (Osland et al., 2018; Zhao et al., 2018). Coastal wetlands can provide biological habitats, purify water quality, facilitate carbon sequestration, resist coastal floods, and protect food security (Narayan et al., 2017; Wang et al., 2020; Zhu et al., 2020), and the value of ecological services is up to US$1,94,000/(ha•yr) (Liu et al., 2021). Coastal wetlands are at the junction of land and sea and are significantly affected by climate change, particularly, the sea level rise (Gabler et al., 2017; Mehvar et al., 2019; Yu et al., 2019). In addition, factors such as land use change, decrease of sediment transport, and decrease of freshwater recharge also lead to the shrinkage of coastal wetland areas and decline in ecological service function (Pascual-Aguilar et al., 2015; Ma et al., 2017; Lin and Yu, 2018). It is estimated that the world's coastal wetland area decreased by more than 50% in the 20th century (Li et al., 2018). China's coastal wetland area has declined by up to 58% from 1950 to 2014, with a shrinking area of 8.01 million ha (Sun et al., 2015). The restoration of coastal wetlands is gaining more and more attention, and many achievements have been made in relevant studies on management strategies, risk identification, hydrological and ecological action mechanisms, and the intrinsic role and optimization of wetland biological community (Stagg et al., 2016; Rodríguez et al., 2017; Borchert et al., 2018; Manuel et al., 2018; Renzi et al., 2019).

The deltaic coastal wetland is an important part of coastal wetland. It is the transition zone between rivers and the sea. An estuarine delta is generally the region where agriculture, trade, and fisheries are well developed and strongly disturbed by human activities. In addition, the estuarine delta is also affected by the water and sediment regulation process of the upstream reservoir and water intake along the river. Thus, striking changes have taken place in many deltaic ecological environments (Day et al., 2016). The decrease in freshwater recharge from the river to the delta is one of the main causes of the shrinkage and degradation of the deltaic coastal wetlands. Reservoir construction and operation is an important way of river development. There are more than 15,000 dams that were completed or under construction in the world with a dam height of more than 30 m (Duarte et al., 2016), and about two-thirds of the rivers longer than 1,000 km are not free-flowing (Grill et al., 2019). In recent years, more and more attention has been paid to the ecological protection function of the reservoir. Measures to improve the ecological environment such as discharging environmental flow and creating artificial floods have been studied and applied in many reservoirs (Poff and Schmidt, 2016; Adams et al., 2017; Leroy and Olden, 2018; Qiu et al., 2020). The protected area of the reservoir ecological regulation also gradually extends from the river to the estuary and coastal waters (Yang et al., 2019). The reservoir realizes the environmental water supplement by changing the flow process through storage and discharge regulation. But the flow change is also affected by other factors, such as climate change, water withdrawal, and utilization. Therefore, quantitative analysis of the impact and contribution rate of the reservoir itself on the flow change is a difficult point in the current studies.

The Yellow River Delta is the most complete wetland ecosystem in the warm temperate zone in China, and it is the core habitat that provides a transfer station, overwintering, and breeding place for migrating birds in the inland of Northeast Asia and the Western Pacific Rim (Cui et al., 2009; Changming et al., 2018). There is a severe contradiction between water demand and supply in the Yellow River Basin where the water resource per capita is only 473 m^3, the utilization rate of water resources has reached 80%, and the problem of insufficient environmental water has been existing for a long time (Hua and Cui, 2017; Yin et al., 2017). In the 1980s–1990s, there have been drying up days in the lower Yellow River for 15 years. In 1997, the drying up days at the Lijin section of the lower Yellow River reached 227 days, and there was no water flowing into the sea for 330 days (Liu and Zhang, 2002). Insufficient environmental water, reduced sediment transport, farmland reclamation, urbanization, and other factors have led to serious degradation of the Yellow River Delta wetland. The area of reed marsh has dropped from 16.65 thousand ha in 1986 to 11.61 thousand ha in 2006, and coastline erosion, reduction of biological species, and other problems have arisen (Kong et al., 2015; Wang et al., 2016; Zhang et al., 2017; Wang et al., 2019). In order to protect the wetland ecosystem, the Yellow River Conservancy Commission has carried out environmental water supplement for the Yellow River Delta since 2008. As of 2019, the accumulated environmental water supplement reached 461.45 million m^3, and the wetland vegetation has been restored to a certain extent. The environmental water supplement in the Yellow River Delta is mainly achieved by the large flow process created by the Xiaolangdi Reservoir. The current relevant studies mainly focus on the effect of ecological restoration in the Yellow River Delta, and the role of reservoir regulation is mainly determined by qualitative analysis.

This article aims to quantify the impact of the reservoir on the deltaic coastal wetland and coastal ecosystem. This article proposes a quantitative analysis method for the ecological impact and contribution rate of the reservoir and quantifies the contribution of the Xiaolangdi Reservoir to the prevention of drying up of the Yellow River channel, the provision of river ecological base flow, and the provision of environmental water to the Yellow River Delta wetland and coastal areas.

Materials and methods

Study area

The study area is from the Xiaolangdi Reservoir to the estuary of the Yellow River (Figure 1). The Yellow River Delta, located at the estuary of the Yellow River, faces the Bohai Sea in the north

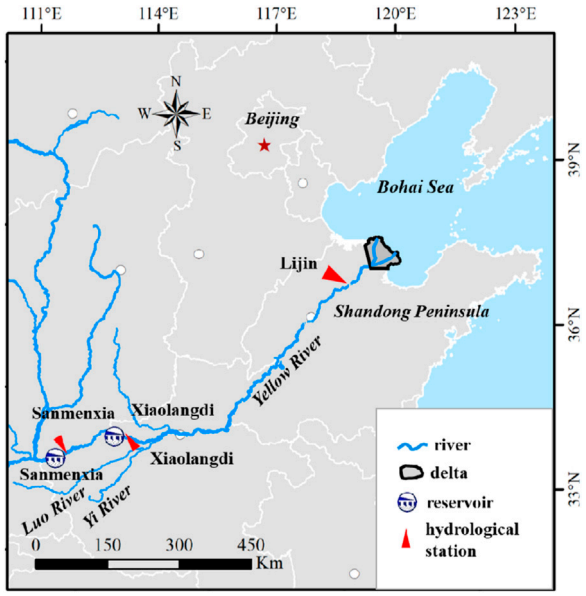

FIGURE 1
Study area.

and has an area of about 2,400 km^2. The Xiaolangdi Reservoir is 899 km away from the estuary and has a total storage capacity of 12.65 billion m^3. It was put into operation in 2000, and it controls the flow in the lower Yellow River. Since the Yellow River is a sediment-laden river, in order to reduce sedimentation, water and sediment regulation (WSR) has been conducted in the Xiaolangdi Reservoir from June to July. During WSR, large flows were artificially made to scour the reservoir and the lower Yellow River channel (Xu et al., 2016; Lu et al., 2020). The large flow during WSR also provides suitable flow conditions for the environmental water supplement to the Yellow River Delta.

Evaluation indicators

The ecological impact of the Xiaolangdi Reservoir on the Yellow River Delta and coastal areas are evaluated by four ecological indicators, namely, the drying up days at the Lijin section, the assurance rate of ecological base flow at the Lijin section, the volume of water flowing into the sea from April to June, and the environmental water supplement in the Yellow River Delta. The Lijin section is close to the estuary of the Yellow River, and its drying up days represent the duration of an extreme low flow period, which is extremely harmful to the ecology of the Yellow River Delta and coastal ecosystem. Ecological base flow is the bottom limit of flow to maintain the ecological function of the river. This article adopts ecological base flow at the Lijin section (50 m^3/s) issued by the Ministry of Water Resources of China in 2020. According to the policies of the Ministry of Water Resources of China, the assurance rate of ecological base flow should be no less than 90%. April to June is a critical period for fish reproduction in the coastal areas of the Yellow River estuary, so it is important to ensure the volume of water flowing into the sea during this period to create low-salinity areas suitable for reproduction. The Lijin section controls the environmental water supplement in the Yellow River Delta. The flow at the Lijin section over the years when the conditions for the environmental water supplement in the Yellow River Delta have been met is shown in Table 1. Therefore, the Lijin section is taken as the evaluation section, and all four ecological indicators are calculated based on the daily flow of the Lijin section.

TABLE 1 Threshold flow (Lijin section) of the environmental water supplement in the Yellow River Delta (m^3/s).

Year	Flow	Year	Flow	Year	Flow	Year	Flow
2008	3,387	2010	3,560	2012	2,763	2014	2,600
2009	3,366	2011	2,689	2013	3,300	2015	2,430

Scenario setting

This article changes the reservoir conditions in different scenarios and quantifies the ecological impact of the reservoir by comparing ecological indicator values in different scenarios. The evaluation period is set at 2000–2019. Two scenarios are set (Table 2). Scenario 1 represents the flow status at the Lijin section with the regulation of the Xiaolangdi Reservoir, whereas Scenario 2 represents the flow status at the Lijin section without the regulation of the Xiaolangdi Reservoir. The inflow into the Xiaolangdi Reservoir and the water withdrawal under the Xiaolangdi Reservoir are the same in the two scenarios.

In Scenario 2, the regulation of the Xiaolangdi Reservoir needs to be eliminated, i.e., flow restoration needs to be performed. The inflow of the Xiaolangdi Reservoir represents the flow status before the regulation of this reservoir, thus replacing the outflow of the Xiaolangdi Reservoir with the inflow to eliminate the regulation impact. Based on the water balance principle, daily flow at the Lijin section without the regulation of the Xiaolangdi Reservoir can be obtained using the following formula:

$$r_{S,t} = r_{I,t-t1} + r_{B,t-t2} - r_{w,t-t3} - r_L, \quad (1)$$

where $r_{S,t}$ is the average daily flow of the Lijin section on day t without the regulation of the Xiaolangdi Reservoir, m^3/s; $r_{I,t-t1}$ is the measured inflow of the Xiaolangdi Reservoir on day (t-t_1), m^3/s; $r_{B,t-t2}$ is the tributary inflow into the river in the region between the Xiaolangdi Reservoir and Lijin section on day (t-t_2), m^3/s; $r_{W,t-t3}$ is the water withdrawal in the region between the

TABLE 2 Scenario setting.

Scenario classification	Project condition	Evaluation period[a]	Flow type
Scenario 1	With the Xiaolangdi Reservoir regulation	2000–2019	Measured daily flow
Scenario 2	Without the Xiaolangdi Reservoir regulation	2000–2019	Simulated daily flow

[a]Since environmental water supplement was carried out in the Yellow River Delta in 2008, there was no water supplement in 2016, and there was no threshold flow data at the Lijin section after 2017, so the evaluation period of the environmental water supplement of the Yellow River Delta was from 2008 to 2015.

Xiaolangdi Reservoir and Lijin section on day (t-t_3), m^3/s; r_L is the daily average loss of flow due to evaporation and leakage in the region between the Xiaolangdi Reservoir and Lijin section, m^3/s; and t_1, t_2, and t_3 are the time for water flowing from the Xiaolangdi Reservoir, the location of the tributary flowing into the trunk stream, and the water-withdrawing location to the Lijin section, respectively, d.

Quantitative analysis method for the ecological impact of the reservoir

The ecological status of the Yellow River Delta wetland and coastal areas in the two scenarios is expressed as F_A and F_S, respectively, as follows:

$$F_A = \{f_{A,1}, f_{A,2}, \ldots, f_{A,n}\}, \quad (2)$$

$$F_S = \{f_{s,1}, f_{s,2}, \ldots, f_{s,n}\}, \quad (3)$$

where $f_{A,i}$ and $f_{S,i}$ are the ith ecological indicator in Scenario 1 and Scenario 2, respectively, and i =1,2,. . .,n; and n is the number of ecological indicators, n=4.

The ecological impact of the Xiaolangdi Reservoir on the Yellow River Delta wetland and coastal areas (E) is expressed as:

$$E = \{e_1, e_2, \ldots, e_n\}, \quad (4)$$

$$e_i = f_{A,i} - f_{S,i}, \quad (5)$$

where e_i is the impact of the Xiaolangdi Reservoir on the ith ecological indicator.

Quantitative analysis method for the contribution rate of the reservoir

The ecological status of the Yellow River Delta wetland and coastal areas is affected by reservoir regulation, climate change, land use change, and other factors. Changes in the ecological status between 1980–1999 and 2000–2019, under the influence of multiple factors, can be figured out by comparing the ecological indicator values in Scenario 1 and the ecological indicator values quantified by measured data from 1980 to 1999. The measured ecological status of the Yellow River Delta wetland and coastal areas from 1980 to 1999 (F_C) is expressed as:

$$F_C = \{f_{C,1}, f_{C,2}, \ldots, f_{C,n}\}, \quad (6)$$

where $f_{C,i}$ is the ith ecological indicator quantified by measured daily flow at the Lijin section during 1980–1999.

Compared with 1980–1999, the change (V) of ecological status in 2000–2019 is expressed as:

$$V = \{v_1, v_2, \ldots, v_n\}, \quad (7)$$

$$v_i = f_{A,i} - f_{C,i}, \quad (8)$$

where v_i is the change of the value of the ith ecological indicator between 1980–1999 and 2000–2019.

The contribution rate P of the Xiaolangdi Reservoir to the ecological status change V is expressed as:

$$P = \{p_1, p_2, \ldots, p_n\}, \quad (9)$$

$$p_i = \left(1 - \frac{f_{S,i} - f_{C,i}}{f_{A,i} - f_{C,i}}\right) \times 100\% = \frac{f_{A,i} - f_{S,i}}{f_{A,i} - f_{C,i}} \times 100\% = \frac{e_i}{v_i} \times 100\%, \quad (10)$$

where p_i is the contribution rate of the Xiaolangdi Reservoir to the change (v_i) of the value of the ith ecological indicator. The change of the ith ecological indicator value between 1980–1999 and 2000–2019 under the impact of other factors except the Xiaolangdi reservoir can be quantified by ($f_{S,i}$—$f_{C,i}$). Thus, ($f_{S,i}$—$f_{C,i}$)/($f_{A,i}$—$f_{C,i}$) shows the contribution rate of other factors except the Xiaolangdi Reservoir to the change of the ith ecological indicator value between 1980–1999 and 2000–2019.

Data

The data of water withdrawal and utilization are derived from the Yellow River Water Resources Bulletin (http://www.yrcc.gov.cn/other/hhgb/). The flow data measured at the Sanmenxia hydrological station are used as the inflow data of the Xiaolangdi Reservoir. The flow data measured at the Xiaolangdi hydrological station are used as the outflow data of the Xiaolangdi Reservoir. The daily flow data measured at the Sanmenxia, Xiaolangdi, and Lijin hydrological stations are provided by the Hydrological Bureau of the Yellow River Conservancy Commission.

Due to the lack of flow monitoring data of the Yellow River Delta before 2008, this article only evaluates the contribution rates of the Xiaolangdi Reservoir regulation to the drying up days at the Lijin

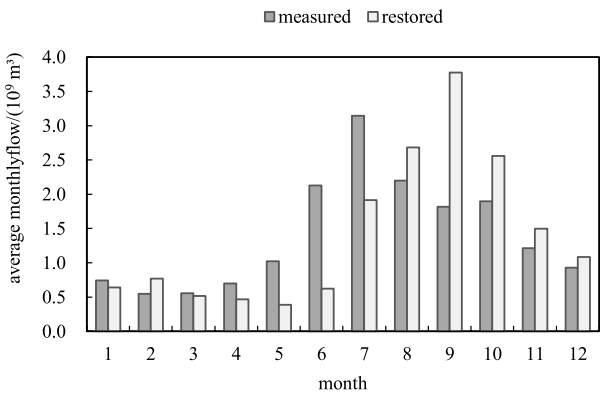

FIGURE 2
Measured and restored average monthly flow at the Lijin section in 2000–2019.

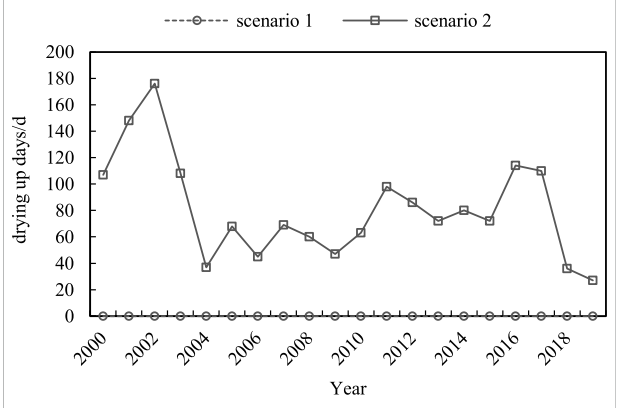

FIGURE 3
Drying up days at the Lijin section in two scenarios.

section, the assurance rate of ecological base flow at the Lijin section, and the volume of water flowing into the sea from April to June.

Results

Flow restoration results

The regulation of the Xiaolangdi Reservoir did not impose an obvious impact on the long-series flow. The measured average annual flow at the Lijin section during 2000–2019 was 16.89 billion m^3, and the average annual flow after restoration was 16.91 billion m^3. The downstream water withdrawing conditions were poor in some time periods in Scenario 2; therefore, the average annual flow after restoration was slightly higher than the measured average annual flow. As the Xiaolangdi Reservoir is an incomplete annual regulating reservoir, it mainly changes the distribution of the flow process throughout the year (Figure 2): the measured average monthly flow from April to July at the Lijin section during 2000–2019 was higher than the restored value, while the measured average monthly flow from August to November was lower than the restored value, and the change of average monthly flow from December to next March (before and after restoration) was not obvious.

Impact on the drying up days and assurance rate of ecological base flow at the Lijin section

In Scenario 1, the average annual drying up days at the Lijin section were 0 days during 2000–2019; in Scenario 2, the flow simulation results showed that the average annual drying up days at the Lijin section were 81.15 days during 2000–2019, and the annual longest drying up days were 176 days (Figure 3; Table 3).

The substandard days and assurance rate of ecological base flow at the Lijin section in two scenarios are shown in Figures 4, 5, and Table 3. In Scenario 1, on average, there were 21.30 days per year in which the flow was lower than the ecological base flow, and the average annual assurance rate of ecological base flow was 94.16%. There had been barely any substandard days of ecological base flow since 2004. In Scenario 2, the average annual substandard days of ecological base flow were 96.55 days. The average annual assurance rate of ecological base flow was 73.55% in Scenario 2, which was far below the target set by the Ministry of Water Resources of China (90%). The Xiaolangdi Reservoir decreased the average annual substandard days of ecological base flow by 75.25 days and increased the average annual assurance rate of ecological base flow by 20.60%.

Impact on the volume of water flowing into the sea from April to June

The volume of water flowing into the sea from April to June in scenarios 1 and 2 and the proportion of the annual volume of water flowing into the sea are shown in Figures 6, 7, and Table 3. In Scenario 1, the annual average volume of water flowing into the sea from April to June was 3.85 billion m^3, accounting for 22.78% of the annual volume of water flowing into the sea, and the years with the volume of water flowing into the sea from April to June exceeding 3 billion m^3 accounted for 65%. In Scenario 2, the annual average volume of water flowing into the sea from April to June reduced to 1.48 billion m^3, accounting for 8.74% of the annual volume of water flowing into the sea, and the years with the volume of water flowing into the sea from April to June exceeding 3 billion m^3 only accounted for 10%. The Xiaolangdi Reservoir increased the annual average volume of water flowing into the sea from April to June by 2.37 billion m^3.

TABLE 3 Ecological index values and their changes in two scenarios.

Indicator	F_A	F_S	F_C	E	V
Drying up days at the Lijin section (d)	0.00	81.15	43.20	−81.15	−43.20
Assurance rate of ecological base flow at the Lijin section (%)	94.17	73.57	79.16	20.60	15.01
Water volume flowing into the sea from April to June (10^9 m^3)	3.85	1.48	1.96	2.37	1.88

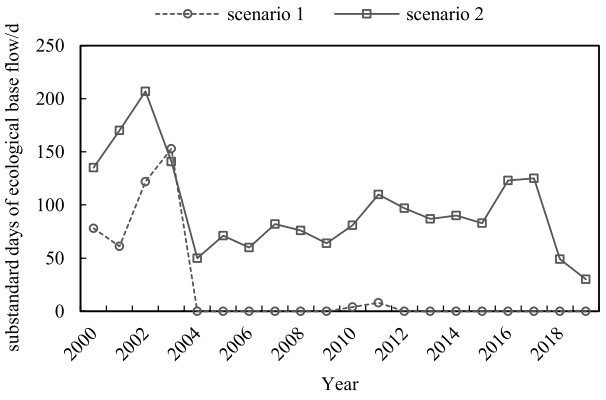

FIGURE 4
Substandard days of ecological base flow at the Lijin section in two scenarios.

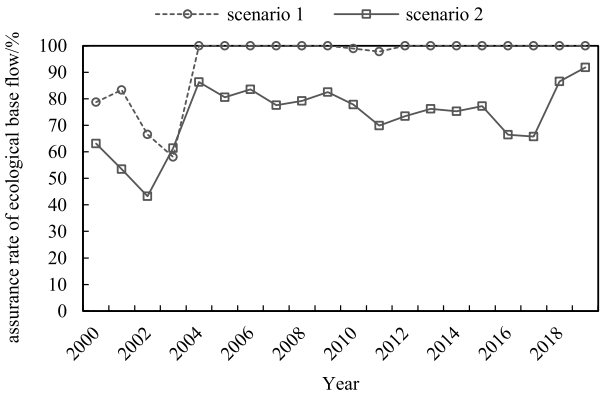

FIGURE 5
Assurance rate of ecological base flow at the Lijin section in two scenarios.

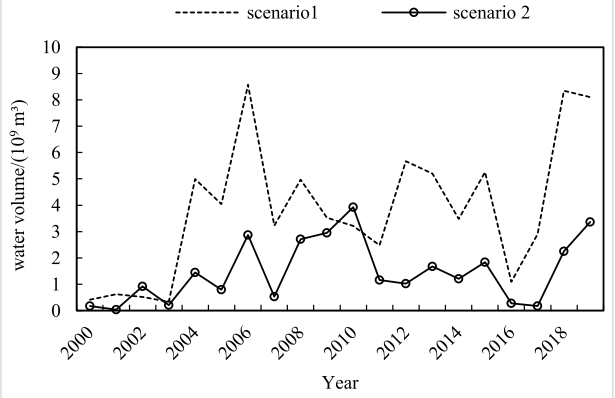

FIGURE 6
Water volume flowing into the sea from April to June in two scenarios.

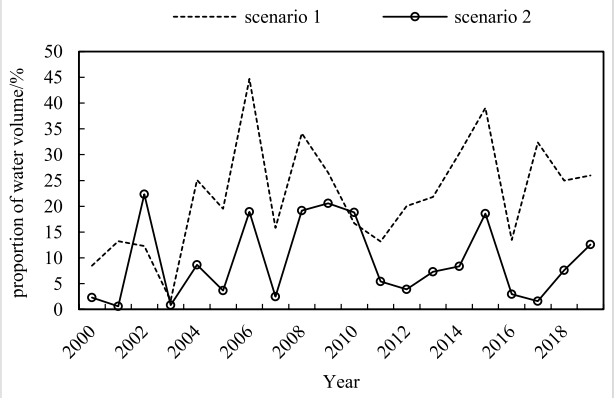

FIGURE 7
Proportion of water volume flowing into the sea from April to June in that of the whole year in two scenarios.

Impact on the environmental water supplement in the Yellow River Delta

The environmental water supplements in the Yellow River Delta in scenarios 1 and 2 are shown in Figure 8. In Scenario 1, the accumulated environmental water supplement in the Yellow River Delta from 2008 to 2015 was 303.31 million m^3, and the annual average environmental water supplement was 37.91 million m^3. In Scenario 2, the accumulated environmental water supplement in the Yellow River Delta during 2008–2015 was 143.71 million m^3, which was only 47.38% of that in Scenario 1, and the annual average environmental water supplement was 17.96 million m^3. The

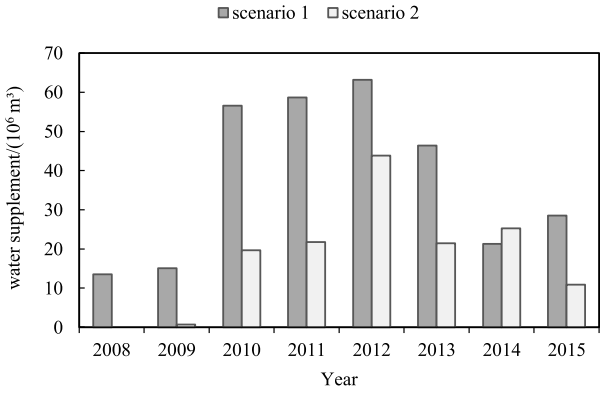

FIGURE 8
Environmental water supplement in the Yellow River Delta in two scenarios.

Xiaolangdi Reservoir has increased the environmental water supplement volume in the Yellow River Delta by 19.95 million m^3 annually.

For the environmental water supplement volume in the Yellow River Delta of each year, in Scenario 2, the flow at the Lijin section in 2008 was lower than the threshold value; therefore, the conditions for the environmental water supplement were not met. In 2009, only 1 day's flow was qualified for the environmental water supplement. The environmental water supplement volume in 2010, 2011, 2013, and 2015 was 34.71%–46.26% of that in Scenario 1. In 2012, the environmental water supplement volume reached 69.42% of that in Scenario 1. It was special in 2014 that in Scenario 2, the environmental water supplement volume in the Yellow River Delta was 25.24 million m^3, which was 3.96 million m^3 higher than that in Scenario 1. This was because during the WSR period (June 29–July 8), there was a flood under which the measured maximum flow at the Sanmenxia section was 4,020 m^3/s. Without the regulation of the Xiaolangdi Reservoir, the maximum flow at the Lijin section would reach 5,080 m^3/s, while the minimum bank full discharge of the lower reaches of the Yellow River in 2014 was only 4,250 m^3/s, which posed the overbank risk. In Scenario 1, the maximum outflow of the Xiaolangdi Reservoir was 2,630 m^3/s, and the maximum flow at the Lijin section was 3,250 m^3/s, balancing the downstream flood control and environmental water supplement in the Yellow River Delta.

Discussion

Contribution rate of the Xiaolangdi Reservoir

The values of ecological indicators in different scenarios and different periods are shown in Table 3. Compared with those in 1980–1999, the annual average drying up days at the Lijin section decreased by 43.20 days, the assurance rate of ecological base flow at the Lijin section increased by 15.00%, and the volume of water flowing into the sea from April to June increased by 1.88 billion m^3 in 2000–2019. The ecological conditions in the lower Yellow River and the coastal areas had changed to a favorable direction. The contribution rate of the Xiaolangdi Reservoir to the reduction of drying up days at the Lijin section was 187.85%, the contribution rate to the assurance rate of ecological base flow at the Lijin section was 137.24%, and the contribution rate to the increase of water volume flowing into the sea from April to June was 125.83%.

Contribution analysis of water inflow and water withdrawal

The contribution rates of the Xiaolangdi Reservoir to the reduction of drying up days at the Lijin section, the increase of the assurance rate of ecological base flow at the Lijin section, and the increase of water volume flowing into the sea from April to June all exceeded 100%, indicating that the total contribution rate of other factors was negative, that is, the combined impact of other factors was detrimental to the environmental water supply to the Yellow River Delta and coastal areas.

The analyses of water inflow and water withdrawal are shown in Table 4. The natural average annual flow of the Yellow River during 2000–2019 was 5.63 billion m^3 less than that during 1980–1999, with a degradation of 10.59%. The measured average annual flow at the Sanmenxia section during 2000–2019 was 6.66 billion m^3 less than that during 1980–1999, with a decrease of 22.15%, indicating that the volume of water flowing into the lower Yellow River was greatly reduced. The decrease in water inflow from April to June was more prominent. The measured flow at the Sanmenxia section in the period of April to June during 2000–2019 was 29.70% lower than that during 1980–1999. At the same time, the average annual water withdrawal from the lower Yellow River (downstream of the Sanmenxia section) during 2000–2019 was 0.32 billion m^3 higher than that during 1980–1999. The natural flow of the Yellow River, the measured water inflow into the lower Yellow River, and the volume of water withdrawal from the Lower Yellow River all developed in a direction that was detrimental to the Yellow River Delta and coastal areas. However, the measured ecological indicator values showed that the Xiaolangdi Reservoir eliminated the adverse impact of water inflow and water withdrawal and ensured the continuous improvement of ecology in the river, delta, and coastal areas.

Analysis of the impact on Yellow River Delta wetland and coastal organisms

The change process of the natural wetland area in the Yellow River Delta during 1986–2018 is shown in Figure 9. The natural

TABLE 4 Change in water inflow and water withdrawal of the Yellow River (billion m^3).

Period	Natural annual flow of the Yellow River	Measured annual flow at the Sanmenxia section	Measured flow from April to June at the Sanmenxia section	Water withdrawal from the Yellow River downstream of the Sanmenxia section
1980–1999 (①)	53.21	30.06	6.13	12.39
2000–2019 (②)	47.58	23.40	4.37	12.71
Change (②-①)	−5.63	−6.66	−1.76	0.32

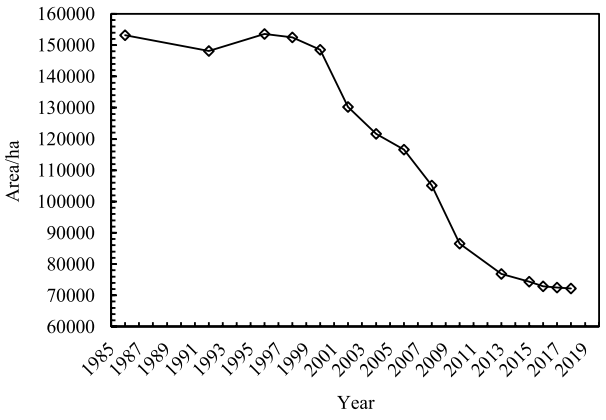

FIGURE 9
Variation of natural wetland area in the Yellow River Delta.

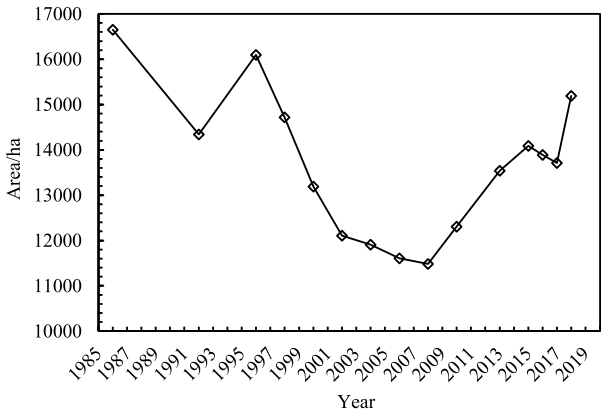

FIGURE 10
Variation of reed marsh area in the Yellow River Delta.

wetland area had continued to decline since the 21st century. To be specific, the natural wetland area had decreased by 29.20% during 2000–2007, with an annual average reduction of 5421.25 ha. There was only a small volume of environmental water supplement during 2008–2009, which did not slow down the shrinking rate of the natural wetland area. During 2010–2013, the shrinking rate of the natural wetland area had dropped to 3225.67 ha/yr; during 2014–2018, the natural wetland area tended to be stable, and the shrinking rate had dropped to 932.00 ha/yr.

Reed marsh is a representative wetland of the Yellow River Delta, and its area change process is shown in Figure 10. From 1996 to the implementation of the environmental water supplement in the Yellow River Delta, the area of reed marsh in the Yellow River Delta decreased by 28.68%. The reed marsh area showed an increasing trend after 2008, with an average annual increase of 371.40 ha during 2008–2018. In 2018, the reed marsh area had recovered to 91.26% of its area in 1986.

With the implementation of wetland restoration and other wetland protection measures, bird diversity in the Yellow River Delta National Natural Reserve has increased. In 2019, the number of bird species in the natural reserve increased by 85 species compared to that in 1992. The Yellow River Delta wetland is the largest breeding place for Oriental stork in China. The Oriental stork started nesting and breeding in the natural reserve in 2003, and the number has been increasing year by year. In 2020, there were 115 nests and a total of 315 young birds.

During 2015–2019, the Yellow River Institute of Water Protection Research conducted trawl surveys on the nektons at 66 monitoring points in the coastal areas in the Yellow River estuary, and the results showed that the biological diversity and quantity had been increasing continuously. To be specific, in 2015, the average number of species at one monitoring station was 7.89, and the average weight density of catches was 1.10 kg/h, while in 2019, the average number of species at one monitoring station was 14.90, and the average weight density of catches was 3.70 kg/h.

Conclusion

This article proposes a quantitative analysis method for the ecological impact and contribution rate of the reservoir and studies the impact of the Xiaolangdi Reservoir on the Yellow River Delta wetland and coastal areas, and the following conclusions are drawn: 1) the Xiaolangdi Reservoir played an

important role in improving the habitat of the organisms in the Yellow River Delta and coastal areas and increasing the number and diversity of organisms. The regulation of this reservoir guaranteed the continuous flow at the Lijin section for 20 years, increased the assurance rate of ecological base flow at the Lijin section by 20.60%, and increased the average annual volume of water flowing into the sea from April to June by 2.37 billion m^3 during 2000–2019 and increased the environmental water supplement in the Yellow River Delta by 19.95 million m^3 during 2008–2015. 2) The Xiaolangdi Reservoir has reversed the adverse effects of the decrease in the natural flow and the increase in water withdrawal in the past 20 years, ensuring that the flow process changed in the direction that was conducive to the ecological improvement of the Yellow River Delta wetland and the coastal areas. In ensuring the continuous flow at the Lijin section, the increase in ecological base flow at the Lijin section and the increase in water volume flowing into the sea from April to June and the contribution rates of the Xiaolangdi Reservoir all exceeded 100%.

River flow is affected by multiple factors such as climate change, water withdrawal, and reservoir operation. The method proposed in this article can quantify the ecological impact and contribution rate of the reservoir itself, which is of great value for the scientific analysis on and the improvement of ecological effect of reservoir regulation.

Data availability statement

The original contributions presented in the study are included in the article/supplementary material; further inquiries can be directed to the corresponding author.

Author contributions

WS: methodology, formal analysis, resources, writing—original draft, and data curation. DY: conceptualization. SP: visualization and supervision. YW: funding acquisition. LG: writing—review and editing. YS: data curation.

Funding

This article was supported by the National Key R&D Projects of China (2021YFC3200203) and Major Science and Technology Projects in Henan Province (201300311400).

Acknowledgments

The authors greatly appreciate the Yellow River Institute of Water Protection Research for providing remote sensing interpretation data of the Yellow River Delta wetland area from 1986 to 2018 and monitoring data of nekton in coastal waters from 2015 to 2019.

Conflict of interest

Authors WS, DY, SP, and YW were employed by Yellow River Engineering Consulting Company Limited.

The remaining authors declare that the research was conducted in the absence of any commercial or financial relationships that could be construed as a potential conflict of interest.

Publisher's note

References

Adams, L. E., Lund, J. R., Moyle, P. B., Quinones, R. M., Herman, J. D., and O'Rear, T. A. (2017). Environmental Hedging: A Theory and Method for Reconciling Reservoir Operations for Downstream Ecology and Water Supply. *Water Resour. Res.* 53, 7816–7831. doi:10.1002/2016wr020128

Borchert, M. S., Osland, M. J., Enwright, M., Griffithand Nicholas, M. (2018). Coastal Wetland Adaptation to Sea Level Rise: Quantifying Potential for Landward Migration and Coastal Squeeze. *J. Appl. Ecol.* 55, 2876–2887. doi:10.1111/1365-2664.13169

Changming, Z., Xin, Z., and Qiaohua, H. (2018). Four Decades of Estuarine Wetland Changes in the Yellow River Delta Based on Landsat Observations between 1973 and 2013. *Water* 10, 933. doi:10.3390/w10070933

Cui, B., Yang, Q., Yang, Z., and Zhang, K. (2009). Evaluating the Ecological Performance of Wetland Restoration in the Yellow River Delta, China. *Ecol. Eng.* 35, 1090–1103. doi:10.1016/j.ecoleng.2009.03.022

Day, J. W., Agboola, J., Chen, Z., 'Elia, C. D., Forbes, D. L., Giosan, L., et al. (2016). Approaches to Defining Deltaic Sustainability in the 21st Century. *Estuar. Coast. Shelf Sci.* 183, 275–291. doi:10.1016/j.ecss.2016.06.018

Duarte, R., Pinheiro, A., and Schleiss, A. J. (2016). A Technical Review of Hydro-Project Development in China. *Engineering* 2, 302–312. doi:10.1016/j.eng.2016.03.008

Gabler, C. A., Osland, M. J., Grace, J. B., Stagg, C. L., Da, Y. R. H., Hartley, S. B., et al. (2017). Macroclimatic Change Expected to Transform Coastal Wetland Ecosystems This Century. *Nat. Clim. Chang.* 7, 142–147. doi:10.1038/nclimate3203

Grill, G., Lehner, B., Thieme, M., Geenen, B., Tickner, D., Antonelli, F., et al. (2019). Mapping the World's Free-Flowing Rivers. *Nature* 569, 215–221. doi:10.1038/s41586-019-1111-9

Hua, Y., and Cui, B. (2017). Environmental Flows and its Satisfaction Degree Forecasting in the Yellow River. *Ecol. Indic.* 92, 207–220. doi:10.1016/j.ecolind.2017.02.017

Kong, D., Miao, C., Borthwick, A., Duan, Q., Liu, H., Sun, Q., et al. (2015). Evolution of the Yellow River Delta and its Relationship with Runoff and Sediment Load from 1983 to 2011. *J. Hydrol. X.* 520, 157–167. doi:10.1016/j.jhydrol.2014.09.038

Leroy, P. N., and Olden, J. D. (2018). Can Dams Be Designed for Sustainability? *Science* 358, 1252–1253. doi:10.1126/science.aaq1422

Li, X., Bellerby, R., Craft, C., and Widney, S. E. (2018). Coastal Wetland Loss, Consequences, and Challenges for Restoration. *Anthr. Coasts* 1, 1–15. doi:10.1139/anc-2017-0001

Lin, Q., and Yu, S. (2018). Losses of Natural Coastal Wetlands by Land Conversion and Ecological Degradation in the Urbanizing Chinese Coast. *Sci. Rep-Uk* 8, 15046. doi:10.1038/s41598-018-33406-x

Liu, C., and Zhang, S. (2002). Drying up of the Yellow River: its Impacts and Counter-measures. *Mitig. Adapt Strat. Gl.* 7, 203–214.

Liu, Z., Fagherazzi, S., and Cui, B. (2021). Success of Coastal Wetlands Restoration Is Driven by Sediment Availability. *Commun. Earth Environ.* 2 (44). doi:10.1038/s43247-021-00117-7

Lu, Q., Bai, J., Yan, D., Cui, B., and Wu, J. (2020). Sulfur Forms in Wetland Soils with Different Flooding Periods before and after Flow-Sediment Regulation in the Yellow River Delta, China. *J. Clean. Prod.* 276, 122969. doi:10.1016/j.jclepro.2020.122969

Ma, Z., Zhang, M., Xiao, R., Cui, Y., and Yu, F. (2017). Changes in Soil Microbial Biomass and Community Composition in Coastal Wetlands Affected by Restoration Projects in a Chinese Delta. *Geoderma* 289, 124–134. doi:10.1016/j.geoderma.2016.11.037

Manuel, M., Sara, B. G., and Alejandro, E. T. (2018). Policies in Coastal Wetlands: Key Challenges. *Environ. Sci. Policy* 88, 72–82. doi:10.1016/j.envsci.2018.06.016

Mehvar, S., Filatova, T., Sarker, M., Dastgheib, A., and Ranasinghe, R. (2019). Climate Change-Driven Losses in Ecosystem Services of Coastal Wetlands: A Case Study in the West Coast of Bangladesh. *Ocean. Coast. Manag.* 169, 273–283. doi:10.1016/j.ocecoaman.2018.12.009

Narayan, S., Beck, M. W., Wilson, P., Thomas, C. J., Guerrero, A., Shepard, C. C., et al. (2017). The Value of Coastal Wetlands for Flood Damage Reduction in the Northeastern USA. *Sci. Rep.* 7, 9463. doi:10.1038/s41598-017-09269-z

Osland, M. J., Gabler, C. A., Grace, J. B., Day, R. H., Hartley, S. B., McLeod, J. L., et al. (2018). Climate and Plant Controls on Soil Organic Matter in Coastal Wetlands. *Glob. Chang. Biol.* 24, 5361–5379. doi:10.1111/gcb.14376

Pascual-Aguilar, J., Andreu, V., Gimeno-Garcia, E., and Pico, Y. (2015). Current Anthropogenic Pressures on Agro-Ecological Protected Coastal Wetlands. *Sci. Total Environ.* 503-504, 190–199. doi:10.1016/j.scitotenv.2014.07.007

Poff, N., L., and Schmidt, J., C. (2016). How Dams Can Go with the Flow. *Science* 353, 1099–1100. doi:10.1126/science.aah4926

Qiu, H., Chen, L., Zhou, J., He, Z., and Zhang, H. (2020). Risk Analysis of Water Supply-Hydropower Generation-Environment Nexus in the Cascade Reservoir Operation. *J. Clean. Prod.* 283, 124239. doi:10.1016/j.jclepro.2020.124239

Renzi, J. J., He, Q., and Silliman, B. R. (2019). Harnessing Positive Species Interactions to Enhance Coastal Wetland Restoration. *Front. Ecol. Evol.* 7, 131. doi:10.3389/fevo.2019.00131

Rodríguez, J., Saco, P. M., Sandi, S., Saintilan, N., and Riccardi, G. (2017). Potential Increase in Coastal Wetland Vulnerability to Sea-Level Rise Suggested by Considering Hydrodynamic Attenuation Effects. *Nat. Commun.* 8, 16094. doi:10.1038/ncomms16094

Stagg, C. L., Krauss, K. W., Cahoon, D. R., Cormier, N., Conner, W. H., and Swarzenski, C. M. (2016). Processes Contributing to Resilience of Coastal Wetlands to Sea-Level Rise. *Ecosystems* 19, 1445–1459. doi:10.1007/s10021-016-0015-x

Sun, Z., Sun, W., Tong, C., Zeng, C., Yu, X., and Mou, X. (2015). China's Coastal Wetlands: Conservation History, Implementation Efforts, Existing Issues and Strategies for Future Improvement. *Environ. Int.* 79, 25–41. doi:10.1016/j.envint.2015.02.017

Wang, C., Li, X., Yu, H., and Wang, Y. (2019). Tracing the Spatial Variation and Value Change of Ecosystem Services in Yellow River Delta, China. *Ecol. Indic.* 96, 270–277. doi:10.1016/j.ecolind.2018.09.015

Wang, C., Wang, G., Dai, L., Liu, H., Zhao, Y., Zhou, Y., et al. (2020). Diverse Usage of Waterbird Habitats and Spatial Management in Yancheng Coastal Wetlands. *Ecol. Indic.* 117, 106583. doi:10.1016/j.ecolind.2020.106583

Wang, Y., Geng, Y., Wang, R., and Zhang, J. (2016). Measuring Regional Sustainability with an Integrated Social-Economic-Natural Approach: a Case Study of the Yellow River Delta Region of China. *J. Clean. Prod.* 114, 189–198. doi:10.1016/j.jclepro.2015.05.121

Xu, B., Yang, D., Burnett, W. C., Ran, X., Yu, Z., Gao, M., et al. (2016). Artificial Water Sediment Regulation Scheme Influences Morphology, Hydrodynamics and Nutrient Behavior in the Yellow River Estuary. *J. Hydrol. X.* 539, 102–112. doi:10.1016/j.jhydrol.2016.05.024

Yang, M., Lu, K., Batzer, D. P., and Wu, H. (2019). Freshwater Release into Estuarine Wetlands Changes the Structure of Benthic Invertebrate Assemblages: A Case Study from the Yellow River Delta. *Sci. Total Environ.* 687, 752–758. doi:10.1016/j.scitotenv.2019.06.154

Yin, Y., Tang, Q., Liu, X., and Zhang, X. (2017). Water Scarcity under Various Socio-Economic Pathways and its Potential Effects on Food Production in the Yellow River Basin. *Hydrol. Earth Syst. Sci.* 21, 791–804. doi:10.5194/hess-21-791-2017

Yu, Z. A., Wang, A., Ge, S. B., and Jsk, C. (2019). Coastal Wetland Resilience to Climate Variability: A Hydrologic Perspective - ScienceDirect. *J. Hydrol.* 568, 275–284.

Zhang, X., Wang, L., Fu, X., Li, H., and Xu, C. (2017). Ecological Vulnerability Assessment Based on PSSR in Yellow River Delta. *J. Clean. Prod.* 167, 1106–1111. doi:10.1016/j.jclepro.2017.04.106

Zhao, Q., Bai, J., Zhang, G., Jia, W., Wei, X. I. N., and Wang, X. (2018). Effects of Water and Salinity Regulation Measures on Soil Carbon Sequestration in Coastal Wetlands of the Yellow River Delta. *Geoderma* 319, 219–229. doi:10.1016/j.geoderma.2017.10.058

Zhu, Z., Vuik, V., Visser, P. J., Soens, T., Bouma, T. J., van de Koppel, J., et al. (2020). Historic Storms and the Hidden Value of Coastal Wetlands for Nature-Based Flood Defence. *Nat. Sustain.* 3, 853–862. doi:10.1038/s41893-020-0556-z

frontiers | Frontiers in Environmental Science

TYPE Original Research
PUBLISHED 09 September 2022
DOI 10.3389/fenvs.2022.987600

OPEN ACCESS

EDITED BY
Celso Santos,
Federal University of Paraíba, Brazil

REVIEWED BY
Naoto F. Ishikawa,
Japan Agency for Marine-Earth Science and Technology (JAMSTEC), Japan
Diego Frau,
National Institute of Limnology (INALI), Argentina

*CORRESPONDENCE
Wei Yang,
yangwei@bnu.edu.cn

SPECIALTY SECTION
This article was submitted to Conservation and Restoration Ecology, a section of the journal Frontiers in Environmental Science

RECEIVED 06 July 2022
ACCEPTED 15 August 2022
PUBLISHED 09 September 2022

CITATION
Yang W, Fu X, Li X and Yang Y (2022), Temporal changes of the food web structure and function driven by changes in hydrological regimes and water quality in a large shallow lake. *Front. Environ. Sci.* 10:987600. doi: 10.3389/fenvs.2022.987600

Temporal changes of the food web structure and function driven by changes in hydrological regimes and water quality in a large shallow lake

Wei Yang[1]*, Xianting Fu[1], Xiaoxiao Li[2] and Ying Yang[3]

[1]State Key Laboratory of Water Environment Simulation, School of Environment, Beijing Normal University, Beijing, China, [2]Guangdong Provincial Key Laboratory of Water Quality Improvement and Ecological Restoration for Watersheds, School of Ecology, Environment and Resources, Guangdong University of Technology, Guangzhou, China, [3]Research Center for Eco-environmental Engineering, Dongguan University of Technology, Dongguan, China

Assessing food web structural properties and energy fluxes under changing hydrological regimes and water quality reveals the temporal patterns of ecosystem dynamics in shallow lakes. Here, we studied northern China's largest shallow lake (Lake Baiyangdian) using quantitative food web models for five representative years (1958, 1980, 1993, 2009, and 2019). We analyzed the temporal patterns of food web structure and function by combining a Bayesian isotope mixing model with a food web energetics model. We further examined the temporal changes of unweighted and weighted food web topological attributes. Lake Baiyangdian changed from a detritus-based into a phytoplankton-based food web based on the relative contributions of basal food sources and energy flux distributions. The trophic position of fingerlings, large omnivorous fish, and carnivorous fish decreased with increasing eutrophication. The highest energy fluxes were from detritus to zooplankton and mollusks in 1958, from detritus and phytoplankton to zooplankton in 1980, 1993, and 2009, and from phytoplankton to zooplankton and detritus to mollusks in 2019. The highest total energy flux was in 1993, followed by 2019, with the lowest value in 1958. Unweighted food web metrics showed similar patterns. We observed more pronounced temporal variability in the node- and link-weighted food web metrics than in the unweighted metrics. In addition, hydrological factors (threshold, duration, reversals between high, and low water levels), eutrophication, and some water quality factors (chemical oxygen demand, dissolved oxygen, and pH) played important roles in the temporal changes of food web dynamics in Lake Baiyangdian. Our findings demonstrate the importance of integrating unweighted and weighted indicators to holistically comprehend how highly aggregated food webs respond to changing hydrological regimes and water quality, thereby improving management and restoration of shallow lake ecosystems.

KEYWORDS

food web structure, ecosystem functioning, energy fluxes, temporal dynamics, hydrological regimes, eutrophication

1 Introduction

Food webs describe the trophic interactions among species or trophic groups in an ecosystem (Lynam et al., 2017; Bartley et al., 2019). Their structures reflect the effects of external disturbance, community history, and resource availability and types, thereby offering insights that can guide ecosystem management and conservation (Thompson et al., 2012; Harvey et al., 2017). However, most temporal food web studies have focused on the differences in before and after scenarios (Yletyinen et al., 2016; Ibarra-García et al., 2020) or on changes in the historical food web structure without accounting for the current state (Kong et al., 2016; Xu et al., 2016). If the management objective is to alter the food web structure to promote the ecosystem's recovery from degradation, it is necessary to study the current food web and how it reached its current state before it is possible to identify effective restoration measures (Ushio et al., 2018; Griffith et al., 2019; Olivier et al., 2019).

In fact, the food web structure is intimately related to ecosystem functioning (Thompson et al., 2012; Hines et al., 2015). Clarifying the relationship between food web structure and ecosystem functioning is a key to understanding and predicting how an ecosystem responds to environmental change (Duffy et al., 2007; Ives et al., 2019). There is a growing interest in analyzing the temporal patterns of food web dynamics as well as linking changes in food web structure to changes in ecosystem functioning (Olivier et al., 2019; Ibarra-García et al., 2020; Kortsch et al., 2021). The energy fluxes can be regarded as a universal currency for ecosystem functioning because they describe the rate of energy flow among species or trophic groups (Barnes et al., 2018; Jochum and Eisenhauer, 2022). The food web energetics approach (Barnes et al., 2018; Gauzens et al., 2019; Jochum and Eisenhauer, 2022) combines food-web theory (Paine, 1980) with metabolic theory (Brown et al., 2004), and thereby provides a powerful tool for assessing energy fluxes. What's more, it permits quantification of critical ecosystem processes by summing all energy fluxes from animals, autotrophs, and detritus to their respective consumers (Kortsch et al., 2021; Li et al., 2021; Jochum and Eisenhauer, 2022).

Topological analyses are useful for summarizing the structural properties of food webs by extracting ecologically meaningful information (Xu et al., 2016). For instance, Dunne et al. (2002) showed that a food web with higher complexity, defined as higher connectance (the proportion of potential links in a food web that are realized), is more robust against species loss. However, most studies of structural properties were based on unweighted food webs (also known as binary- or topology-based food webs), which only contain information about the presence and absence of trophic links between species or trophic groups (Mor et al., 2018; Kortsch et al., 2019; Ru et al., 2020). This approach assumes a static food web, and ignores the temporal variability in trophic interactions, as well as the asymmetry of energy flux distributions, and may therefore overestimate some structural properties (Banašek-Richter et al., 2009; Poisot et al., 2015). Furthermore, most research on unweighted food webs suggests that food web metrics are essentially invariant over long time scales (Olesen et al., 2011; Trøjelsgaard and Olesen, 2016; Olivier et al., 2019). In contrast, weighted food webs offer an opportunity to capture subtle temporal fluctuations in the food web structure and function through changes in species dominance or energy fluxes rather than through changes in species richness and numbers of trophic links (Boit and Gaedke, 2014; Olivier et al., 2019; Kortsch et al., 2021; Jochum and Eisenhauer, 2022). Previous studies demonstrated this difference between food web metrics calculated from unweighted and weighted food web approaches, and although the binary food web structure may appear unchanged, the weighted food web structure and function may have changed considerably, or vice versa (Bersier et al., 2002; Banašek-Richter et al., 2009). In addition, multiple aspects of food web metrics may highlight complementary patterns of temporal variability in food web dynamics associated with different ecosystem processes (Boit and Gaedke, 2014; Olivier et al., 2019; Kortsch et al., 2021). Therefore, to understand how food web structure and function change over time, unweighted metrics (topology-based) and weighted metrics (node-weighted by biomass and link-weighted by energy fluxes) should be combined in food web research because each group of metrics provides different insights.

Understanding the underlying environmental drivers that govern the temporal variability of food web structures and functions is vital to guiding the management and conservation of shallow lake ecosystems (Trøjelsgaard and Olesen, 2016; Danet et al., 2021). Driven by anthropogenic or natural changes such as dam construction and climate change, the hydrological regimes and water quality of shallow lakes are profoundly modified from their natural condition (Marino et al., 2017; Li et al., 2019; Yan et al., 2020). As a consequence, community dynamics and various ecosystem processes have been significantly degraded (Evtimova and Donohue, 2014). In addition to adversely affecting the food web structure and ecosystem functioning, these changes can damage the associated ecosystem services that support humanity (Yang and Yang, 2014a; Evtimova and Donohue, 2016; Jackson et al., 2016; Gu et al., 2019; Zhao et al., 2019; Zhang et al., 2020). For example, Marino et al. (2017) found that the degree of hydrological stability (i.e., the magnitude of the water fluctuations) affects food web structure indirectly through changes in predator–prey interactions. Lake Chaohu has suffered from gradual eutrophication since the 1950s, and the food web has evolved progressively towards a simplified structure (Gu et al., 2011; Kong et al., 2016). Moreover, a given environmental factor may elicit different responses in different metrics of the food web structure and different ecosystem functions. In particular, eutrophication may increase an ecosystem's productivity and energy by stimulating the rapid growth of some basal organisms, such as phytoplankton, but may simultaneously decrease the trophic

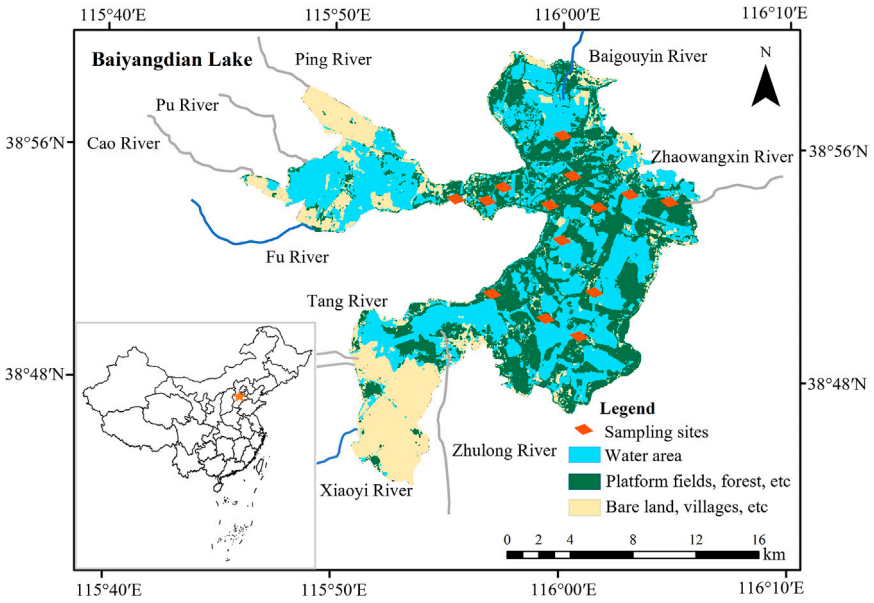

FIGURE 1
The locations of the study area, adjacent rivers, and sampling sites.

position of top predators and the food chain length (Post, 2002a; Xu et al., 2016). Hence, it is necessary to more fully understand how changes in hydrological regimes and water quality could influence food web structure and function (Ives et al., 2019).

In the present research, we selected Lake Baiyangdian, the largest shallow lake in northern China, as a case study. We aimed to 1) describe food web structure and energy fluxes in Lake Baiyangdian between 1958 and 2019 through analyzing some representative years and several sources (historical and novel data); 2) compare unweighted and weighted food web approaches to describe the food web's temporal dynamics using data obtained in Lake Baiyangdian in five representative years; and 3) determine whether the hydrological regimes and some water quality factors can explain the temporal trends of food web dynamics in Lake Baiyangdian. We hypothesized that the weighted food web approach could reveal valuable insights that are not revealed by the traditional unweighted food web approach, and that temporal variation in food web structure and function are related to changes in above mentioned environmental factors.

2 Materials and methods

2.1 Study area

Lake Baiyangdian (38°44′N to 38°59′N, 115°45′E to 116°07′E) is located near the center of Hebei Province. It is the largest freshwater lake in northern China, covering an area of around 366 km^2 at the mean surface level (Figure 1). Moreover, it is the main surface water source for the Xiong'an New Area and plays an important role in maintaining ecosystem functioning and constructing a more ecologically sustainable society. The lake lies in relatively flat terrain, with an elevation range of about 5.2–6.0 m for the lake's bottom. The macrophytes in the lake consist mainly of reeds (*Phragmites australis*). The lake plays a vital role in providing habitat for plant and bird species, protection against floods, water purification, and providing amenities and recreational opportunities for the residents of northern China. The dominant water source is surface runoff from precipitation, which averages 560 mm per year, of which 80% falls between June and September. However, the potential evaporation of 1,369 mm is much higher than precipitation.

Before 1960, Lake Baiyangdian was dominated by natural flows, but since then, dams and reservoirs have been constructed upstream for flood prevention, crop irrigation, and human consumption (Yang and Tian, 2009; Yang and Yang, 2014b; Wang et al., 2021). The resulting hydrological alterations have decreased natural flows into the lake to almost zero, which vastly reduced the water area and water level of the lake (Yang et al., 2006). Moreover, Lake Baiyangdian's watershed experienced severe drought, leading to further shrinkage of the lake, which nearly dried up from 1984 to 1988 (Song et al., 2018). Subsequently, heavy rainfall during a short period contributed to the filling of Lake Baiyangdian in July 1988. To mitigate the stress created by a shortage of water resources, the local government has intervened. From 1997 onwards, water from other sources (e.g., discharges of treated domestic wastewater, transfers from reservoirs in other watersheds) has been used to

TABLE 1 Trophic groups used to construct the food web models of Lake Baiyangdian.

Trophic groups	Taxon code	Species composition
Detritus	Detr	Particles and dissolved organic matter
Submerged macrophytes	SubM	*Ceratophyllum* L., *Charophyceae, Hydrilla verticillata*, *Myriophyllum verticillatum* L., *Najas marina* L., *Potamogeton crispus* L., *Vallisneria natans* (Lour.) Hara
Phytoplankton	Phyt	Chlorophyta, Chrysophyta, Cryptophyta, Cyanobacteria, Diatoms, Dinoflagellates, *Euglena*
Zooplankton	Zoop	Cladocera, Copepods, Protozoa, Rotifers
Meiofauna	MicZ	Chironomids, Oligochaetes
Mollusks	Moll	*Anodonta*, *Bellamya*, *Cipangopaludina*, *Planorbis*, *Radix*, *Semisulcospira*
Herbivorous fish	HerF	*Ctenopharyngodon idella*, *Parabramis pekinensis*
Filter-feeding fish	FilF	*Hypophthalmichthys molitrix*, *Hypophthalmichthys nobilis*
Fingerlings	Fing	*Abbottina rivularis*, *Hemiculter leucisculus*, *Pseudorasbora parva*
Small omnivorous fish	SomF	*Botia xanthi*, *Carassius auratus*, *Pelteobagrus fulvidraco*
Large omnivorous fish	LomF	*Cyprinus carpio*
Carnivorous fish	CarF	*Channa argus*, *Erythroculter ilishaeformis*, *Siniperca chuatsi*

sustain the lake's environmental flows, with more than 50 releases (Yang and Yang, 2014b). Due to the construction of the Xiong'an New Area in 2017 (Yuan et al., 2017), multiple sufficient artificial ecological water replenishments have promoted water level recovery in Lake Baiyangdian. Despite these inflows, the lake has become a semi-closed water body. Currently, the Fu River, Baigouyin River, and Xiaoyi River are the only three rivers that still flow into the lake. The variable frequency, quantity, and quality of the inflows have profoundly altered the hydrological regimes and water quality of Lake Baiyangdian. Consequently, changes have occurred in Lake Baiyangdian's ecosystem. We have built five quantitative food webs for Lake Baiyangdian, representative of 1958, 1980, 1993, 2009, and 2019. The reasons we focus on these 5 years in the present study are that they represent five distinct stages in the development of the lake ecosystem mentioned above, and the historical years correspond to the times when intensive investigations were conducted in Lake Baiyangdian, with relatively abundant data available in the literature.

2.2 Historical data collection

Trophic groups are defined as groups of taxa that share the same or similar predators and prey in a food web. It is widely accepted in food web studies, where it reduces the methodological biases associated with uneven resolution of taxa within and among food webs (Williams Richard and Martinez, 2000; Dunne et al., 2002; Li et al., 2021). Based on previous studies of the lake's food web structure (Yang, 2011; Zhang et al., 2022), the food web comprises 12 trophic groups (Table 1). We obtained historical biomass data for living trophic groups from the unpublished investigation reports of the Institute of Zoology of the Chinese Academy of Sciences (1958), the Department of Biology of Hebei University (1975), the Hebei Fisheries School (1980), and the Environmental Science Research Institute of Baoding (1993). We also referred to the research literature to supplement the historical biomass data in 1958, 1980, and 1993 (Jin, 1995; Yang et al., 2010; Zhang et al., 2022). We obtained biomass data for 2009 from four field surveys carried out from August 2009 to July 2010 by our research group and the published articles (Yang, 2011; Yang et al., 2014). Supplementary Table S1 shows the biomass of each trophic group in the first four representative historical years. We defined the theoretically possible feeding links among the 12 trophic groups from published information, qualitative records, and stable isotope analysis performed for consumers (Xu et al., 2016; Laigle et al., 2018; Olivier et al., 2019). The dietary preferences of consumer trophic groups in historical representative years (i.e., 1958, 1980, 1993, and 2009) were gathered from the gut content analysis in published reports and studies (Yang, 2011; Yang et al., 2014) of Lake Baiyangdian by our research group, and also referred to other relevant studies on Lake Baiyangdian (Ma et al., 2011; Zhang et al., 2022). In addition, daily water level data from 1958 to 2019 were derived by the Water Conservancy Office of Baoding City, Hebei Province. Water quality data for four historical years (i.e., 1958, 1980, 1993, and 2009) were provided by the Baoding Environmental Monitoring Center and Municipal Environmental Protection Bureau. Seasonal variations (i.e., spring, summer, and autumn) were considered, and we collected 6 samples of water quality data for each study year.

2.3 Sample collection

We performed field investigations in July and November 2018 and April 2019 (hereafter, "2019"). To improve the

comparability of the measured data and the historical dataset, we chose the same sampling sites used in the historical reports (Figure 1). We obtained 6 water samples to quantify the water quality in 2019. Each sample consisted of 14 subsamples that were collected within 14 sampling sites. We also sampled the detritus, phytoplankton, submerged macrophytes, zooplankton, meiofauna, mollusks, and fish in each sampling site during the surveys.

2.3.1 Water sampling

We measured the water temperature (*Tw*), dissolved oxygen content (*DO*), and pH in the field using a multiparameter handheld probe (YSI Professional Plus; YSI, Yellow Springs, OH, United States). In addition, we collected 2-L water samples from the surface to a depth of 0.5 m below the surface on each sampling date, and stored the samples on ice until analysis. We measured other parameters including total phosphorus (*TP*), soluble reactive phosphorus (SRP), ammonium (NH_4^+), total nitrogen (*TN*), nitrite-nitrate (NO^{2-}+NO^{3-}), and chemical oxygen demand (*COD*) according to standard protocols (CBEP, 2002).

2.3.2 Biological sampling

We collected samples of detritus, phytoplankton, submerged macrophytes, zooplankton, meiofauna, mollusks, and fish on the same dates and locations used for the water sampling. Water samples of detritus (1 L), phytoplankton (5 L), and zooplankton (10 L) were collected from the surface water (to a depth of 0.5 m) with a Plexiglass water collector. Subsequently, we pre-filtered the phytoplankton and zooplankton samples by passing the samples through 200-mesh and 125-mesh plankton nets, respectively, and then concentrated them into 50 ml. To obtain samples for stable isotope analysis of the detritus, phytoplankton, and zooplankton, we passed the concentrated samples through pre-combusted (450°C for 6 h) and pre-weighed Whatman GF/F filters (glass microfiber filters; 0.45-μm pore size) under a moderate vacuum using a standard filtration system.

We collected green leaves of the submerged macrophytes by hand and washed them with distilled water to remove epiphytes. For the meiofauna and mollusk samples, we used a Van Veen grab with a mouth area of 1/16 m^2, whose contents we washed through a 35-mesh filter to extract the meiofauna and mollusks and preserved the organisms in 75% ethanol. We used the whole body of the meiofauna and the muscle tissue of the mollusks for the stable isotope determination.

For the fish community, we used a multi-mesh gillnet with mesh sizes ranging from 5 to 55 mm and an overall size of 1.5 × 30 m (Mao et al., 2014), which we installed beside a ground cage. The ground cage had a mesh size of 5 mm and was 25 m long, and was partitioned into 20 sections with 10-cm openings at the front and at the back for fish to enter the trap. All fish sampling started in the late afternoon (approx. 18:00 h) and ended the following morning (approx. 06:00 h), for a total of 12 h. The duration was chosen to limit the number of fish caught per net (Prchalová et al., 2011). For each species, we chose three representative specimens, and used their muscle tissue for the stable isotope analysis. All samples were oven-dried at 60°C to a constant weight and then stored individually in a dry and ventilated place. The biomasses of trophic groups in 2019 are shown in Supplementary Table S1.

2.4 Stable isotope analysis and bayesian isotope mixing model

The stable isotope samples were crushed to a fine homogeneous powder using a ball mill. Subsamples were then pressed into ultra-pure tin capsules and analyzed using an Elementar Vario Micro-Cube elemental analyzer (Flash EA1112; Thermo Scientific, Monza, Italy) coupled with a continuous-flow isotope-ratio mass spectrometer (Delta V Advantage, Thermo Scientific, Dreieich, Germany) (Careddu et al., 2015; Hansen et al., 2018). The elemental analyzer and spectrometer were recalibrated after every 10 measurements following the manufacturer's directions. The obtained carbon (C) and nitrogen (N) stable isotope ratios (^{13}C:^{12}C and ^{15}N:^{14}N) were expressed in δ units (deviations in ‰ from Vienna Pee Dee Belemnite (VPDB) for C and atmospheric N_2 for N) according to the following equations:

$$\delta^{15}N = \left(\frac{\left({}^{15}N / {}^{14}N_{sample} \right)}{\left({}^{15}N / {}^{14}N_{atmosphere} \right)} - 1 \right) \times 1000 \quad (1)$$

$$\delta^{13}C = \left(\frac{\left({}^{13}C / {}^{12}C_{sample} \right)}{\left({}^{13}C / {}^{12}C_{VPDB} \right)} - 1 \right) \times 1000 \quad (2)$$

All samples were analyzed twice. Measurement errors were typically smaller than ±0.1‰ for both $\delta^{13}C$ and $\delta^{15}N$. The values (mean ± SD) of $\delta^{13}C$ and $\delta^{15}N$ of the 2019 samples are listed in Supplementary Table S2.

To elucidate the contributions of the different potential food sources to consumer trophic groups in Lake Baiyangdian in 2019, we used the Stable Isotope Analysis in R (SIAR) model (Parnell et al., 2008) with version 4.1.2 of the R software (www.r-project.org). The SIAR model is based on a Bayesian method and is fitted using a standard Markov-chain Monte Carlo method with Metropolis–Hastings steps, and we used it to generate plausible simulations and estimate the source proportions using a Dirichlet prior distribution (Parnell et al., 2010). All the potential sources for each consumer trophic group were included in the Bayesian mixing model calculations. We applied trophic enrichment factors of 0.4 ± 1.3‰ (mean ± SD) for carbon and 3.4 ± 1.0‰ for nitrogen in our model (Post, 2002b). The SIAR model performed a total of 500 000 iterations, with the first 50 000 used as the burn-in period. The output of the model was a density distribution function for plausible values of the dietary

composition in terms of the proportion of the total diet accounted for by each diet item (Parnell et al., 2010). We considered a feeding link to be effective only if the lower limit of the 50% confidence interval for the contribution of each food source to a given consumer diet exceeded 5% (Careddu et al., 2015; Bentivoglio et al., 2016). On this basis, we compared the relative contribution of food sources to the food web in 2019 and the other four representative historical years.

We calculated the trophic position of the consumer trophic groups based on their dietary preferences. Producers and detritus were defined as trophic position 1, and the consumer trophic position was weighted based on the dietary preference:

$$TP_j = 1 + \sum_{i=1}^{s} TP_{ij} P_{ij} \quad (3)$$

where TP_j is the trophic position of trophic group j; TP_{ij} is the trophic position of the food source i of trophic group j; and P_{ij} is the relative proportion of food source i in the diet of trophic group j.

2.5 Energy fluxes among trophic groups

We calculated the energy fluxes among the trophic groups in Lake Baiyangdian's food web for each study year, with the trophic links assigned using the food web energetics approach (Barnes et al., 2018; Gauzens et al., 2019). This approach estimates how much energy flux is needed to maintain the survival of the present community. Assuming a steady-state for the ecosystem, the model calculates energy fluxes in a top-down manner; that is, all energetic losses of each trophic group (estimated based on consumption of a resource by organisms at higher trophic levels and metabolic losses) are balanced by energetic gains after accounting for the assimilation efficiency. In other words, this means first calculating the energy flux at the top trophic level, where predation losses equal zero, then calculating the energy flux at lower trophic levels based on the losses to consumers at higher trophic levels, and iterating this process until the lowest trophic level is reached.

We defined food source preferences based on the collected quantitative diet data for the historical representative years (i.e., 1958, 1980, 1993, and 2009) and the outputs of the SIAR model for 2019. To account for differences in food source quality, we defined the assimilation efficiencies for each food source type: 0.906 for animals, 0.545 for plants, and 0.158 for detritus (Lang et al., 2017; Gauzens et al., 2019). Body mass estimates for each trophic group are specific to Lake Baiyangdian and derived from local biomonitoring data in 2019. The output is a metric of the total energy fluxes through the food web, as well as a matrix of energy fluxes for the trophic links among trophic groups (Kortsch et al., 2021). Energy flux calculations were performed using version 0.2.0 of the *fluxweb* package (https://cran.r-project.org/web/packages/fluxweb/index.html) for the R software.

2.6 Food web metrics

To characterize the temporal patterns of Lake Baiyangdian's food web structure, we selected three common unweighted, topology-based metrics: connectance (*C*), generality (*G*), and vulnerability (*V*). We also selected six weighted metrics: the node-weighted connectance (*nwC*), generality (*nwG*), and vulnerability (*nwV*), and the link-weighted connectance (*lwC*), generality (*lwG*), and vulnerability (*lwV*). These metrics describe the complexity and horizontal dimensions of the food webs. The calculation of unweighted metrics only considered species occurrences. Connectance ($C = L/S^2$, with L and S being the number of links and nodes, respectively) represents the number of links that exist divided by the total number of possible trophic links (Dunne et al., 2002). The generality and vulnerability properties represent the mean number of food sources per consumer and the mean number of consumers per food source, respectively (Schoener, 1989; Kortsch et al., 2015). As in the unweighted food web metrics, the node- and link-weighted metrics capture changes in the biomass and energy flux distribution among the trophic groups (Bersier et al., 2002; Olivier et al., 2019; Kortsch et al., 2021).

We also used the energy fluxes among the trophic groups to quantify ecosystem functioning. We considered six ecosystem functioning metrics (i.e., detritivory, phytoplanktivory, herbivory, zooplanktivory, benthivory, and piscivory) that were calculated as the sum of energy fluxes from detritus, phytoplankton, submerged macrophytes, zooplankton, benthos, and fish for their consumers. Here, we present each ecosystem functioning metric as a percentage of the total energy flux to the food web in each study year.

2.7 Statistical analysis

We conducted statistical analyses using version 26.0 of the SPSS software (https://www.ibm.com/analytics/spss-statistics-software). We used one-way ANOVA to identify significant temporal differences if the water quality variables satisfied the assumption of homogeneity of variance; if the result was significant at $p < 0.05$, we used least-significant difference (*LSD*) tests for pairwise comparison of variables between study years. We used Kruskal–Wallis tests to test for temporal differences if the water quality variables did not meet the assumption of homogeneity of variance; if the result was significant at $p < 0.05$, indicating significant differences among variables, we used the Mann–Whitney *U* test with Bonferroni's correction to adjust the *p* values for multiple comparisons.

We used the indicators of hydrologic alteration (IHA) method (Richter et al., 1996) to calculate the values of hydrological regime factors in each study year. Then, we performed a principal component analysis (PCA) on the hydrological indicators and water quality factors to investigate

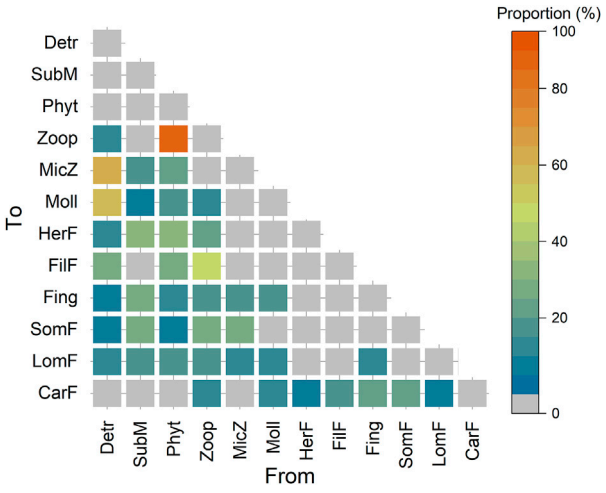

FIGURE 2
The relative contributions of the food sources to consumers in 2019. Data for the other four representative historical years are presented in Supplementary Figure S1. Abbreviations of trophic groups: CarF, carnivorous fish; Detr, detritus; FilF, filter-feeding fish; Fing, fingerlings; HerF, herbivorous fish; LomF, large omnivorous fish; MicZ, meiofauna; Moll, mollusks; Phyt, phytoplankton; SomF, small omnivorous fish; SubM, submerged macrophytes; Zoop, zooplankton.

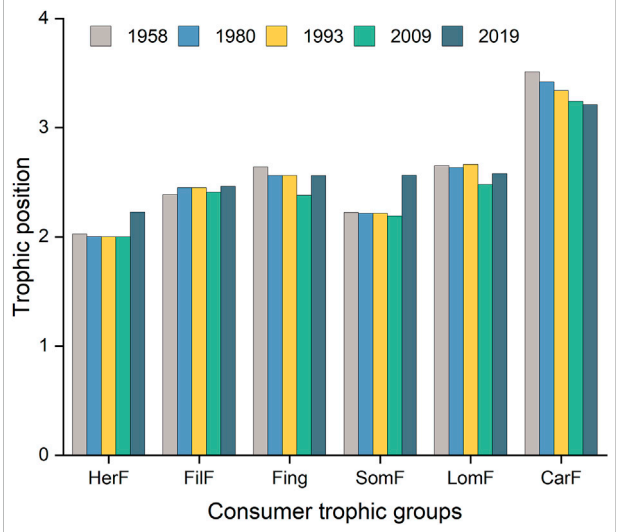

FIGURE 3
Temporal changes in the trophic positions of the six fish consumer trophic groups: CarF, carnivorous fish; FilF, filter-feeding fish; Fing, fingerlings; HerF, herbivorous fish; LomF, large omnivorous fish; SomF, small omnivorous fish.

their temporal dynamics using SPSS. We performed partial least-squares regression (PLSR) with SPSS and the *pls* package for the R software (https://cran.r-project.org/web/packages/pls/index.html) to determine the relationship between environmental factors and food web metrics. In addition, we used the variable importance in projection (*VIP*) and regression coefficient (*RC*) values from PLSR to finely screen the most important environmental factors according to their explanatory power. In our study, we considered hydrological and water quality factors with $VIP \geq 1$ to be important to the food web structure, whereas those with $VIP < 1$ were of minor importance (Wold, 1995; Onderka et al., 2012; Zhao et al., 2020).

3 Results

3.1 Quantitative food webs in lake baiyangdian

Figure 2 illustrates the relative contributions of the various potential food sources to the diets of consumers in 2019, which we estimated using the SIAR model. We found that the zooplankton diet was composed of detritus and phytoplankton in all study years (Figure 2, Supplementary Figure S1), but phytoplankton replaced detritus as the dominant food source in 2019 (Figure 2). Meiofauna and mollusks both functioned primarily as detritivores (75.7% ± 7.7% and 63.8% ± 3.0%, respectively) in all study years. The contribution of submerged macrophytes to the diet of herbivorous fish was greater than 95% until 2019, when ingested phytoplankton (32.3%) and zooplankton (22.8%) also became significant components. Filter-feeding fish mostly consumed phytoplankton and zooplankton in all study years. Fingerlings showed a dietary preference for zooplankton (39.2% ± 1.1%) in 1958, 1980, and 1993, but shifted to a phytoplankton preference (30.7%) in 2009 and a submerged macrophytes preference (27.9%) in 2019. Small omnivorous fish initially fed mainly on submerged macrophytes, but the proportion decreased from 57.4% in 1958 to 28.5% in 2019. Large omnivorous fish had a dietary preference for mollusks in the first four historical representative years but changed to a more even preference for diverse food sources in 2019. Fingerlings and small omnivorous fish comprised a major contribution to the diet of carnivorous fish during the first 4 years, accounting for 36.1% ± 1.9% and 25.6% ± 7.08% of the total, respectively; however, in 2019, the proportions of fingerlings, small omnivorous fish, and filter-feeding fish were 21.4, 20.6, and 18.6%, respectively.

We observed large interannual variations in the relative contributions of basal food sources to the food web (Supplementary Figure S2). For the first 4 years, detritus and submerged macrophytes were the main food sources in the food webs, accounting for averages of 30.1 and 22.1% of the total, respectively. However, the contributions of detritus and submerged macrophytes decreased to 21.4 and 15.2% in 2019, respectively. Furthermore, the contribution of phytoplankton increased from an average of 15.7% in the first three study

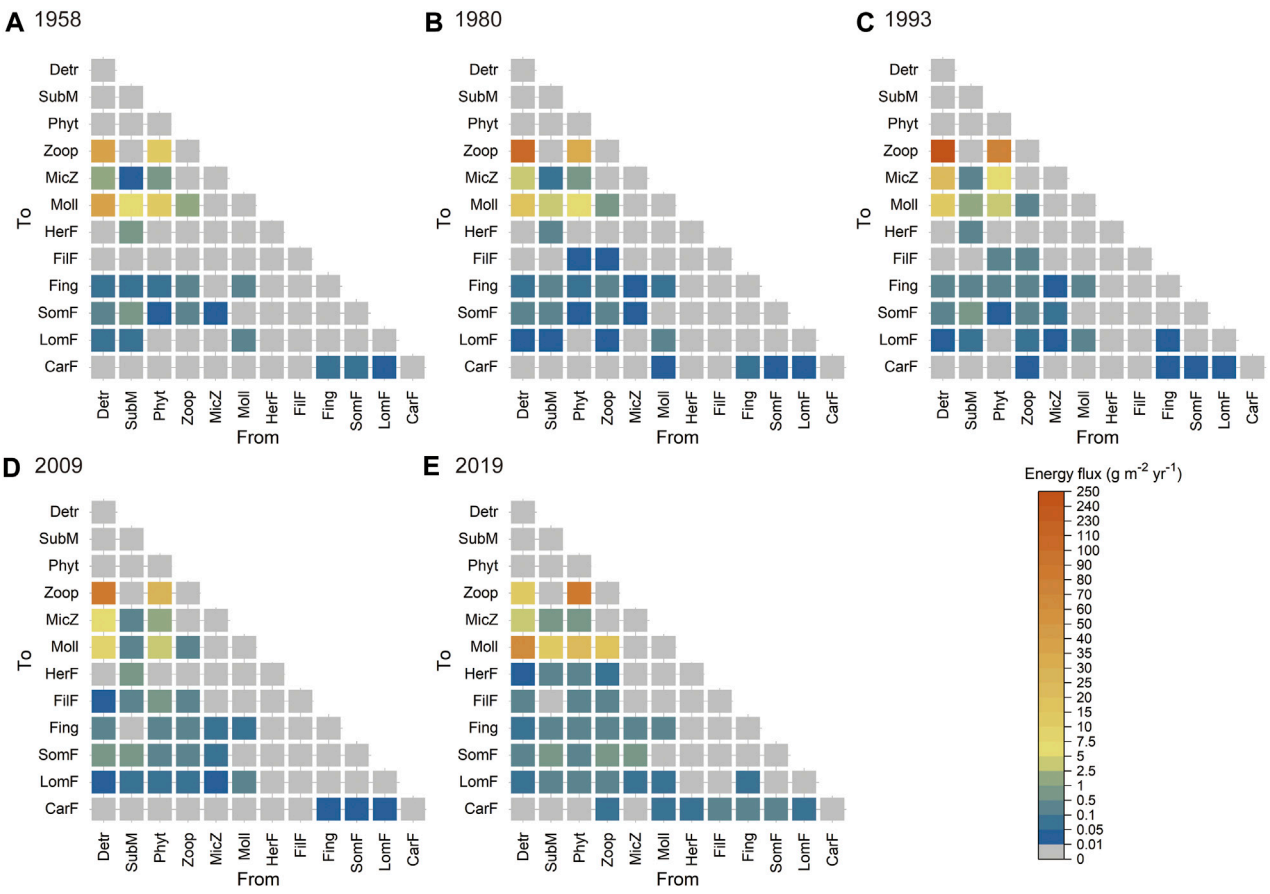

FIGURE 4
Distribution of energy fluxes from food sources to their consumers in the food webs for five representative years: **(A)** 1958, **(B)** 1980, **(C)** 1993, **(D)** 2009, and **(E)** 2019, represented as heat maps. Colour intensity represents the energy flux from the trophic groups in the column to the trophic groups in the row. Abbreviations of trophic groups: CarF, carnivorous fish; Detr, detritus; FilF, filter-feeding fish; Fing, fingerlings; HerF, herbivorous fish; LomF, large omnivorous fish; MicZ, meiofauna; Moll, mollusks; Phyt, phytoplankton; SomF, small omnivorous fish; SubM, submerged macrophytes; Zoop, zooplankton.

years to 23.7% in 2009 and then became the main food source in 2019, with a contribution of 25.3%. Together, these results demonstrate a shift of the food web from detritus-based to phytoplankton-based from 1958 to 2019.

The trophic position of the trophic groups ranged from 1 (detritus, submerged macrophytes, and phytoplankton) to an average of 3.34 ± 0.13 (carnivorous fish) (Figure 3). The trophic positions of zooplankton, meiofauna, and mollusks were relatively stable, with an average value of 2.02 ± 0.03. The carnivorous fish occupied the top trophic position, but their trophic position decreased from 3.51 in 1958 to 3.21 in 2019. This was followed by large omnivorous fish (2.60 ± 0.07) and fingerlings (2.54 ± 0.10). The highest trophic positions for small omnivorous, filter-feeding, and herbivorous fish in 2019 were 2.56, 2.46, and 2.23, respectively. The lowest trophic positions for herbivorous fish, fingerlings, and small and large omnivorous fish occurred in 2009, but these values recovered slightly in 2019.

Figure 4 illustrates the temporal changes in energy fluxes from food sources to their consumers in the food webs in the five study years. A low proportion (25.6–28.6%) of these energy fluxes was ingested by the consumer trophic groups, and a higher proportion (71.4–75.4%) of these energy fluxes entered the detritus pool. The highest total energy fluxes in the food webs were observed in 1993 (376.06 g m^{-2} yr^{-1}), followed by in 2019 (227.34 g m^{-2} yr^{-1}), with the lowest value in 1958 (107.18 g m^{-2} yr^{-1}). The ingestion by primary consumers (zooplankton, meiofauna, and mollusks) accounted for more than 90% of the total ingestion of consumers in all study years. Among the energy fluxes along specific trophic links, the energy fluxes from detritus to zooplankton (35.70 g m^{-2} yr^{-1}) and mollusks (35.24 g m^{-2} yr^{-1}) were highest in 1958. The highest values characterized energy fluxes of trophic links from detritus to

TABLE 2 Temporal changes in the unweighted and weighted (including biomass-based and flux-based) food web structure metrics. Values are the unweighted, link-weighted (*lw*), and node-weighted (*nw*) connectance (*C*), generality (*G*), and vulnerability (*V*).

Food web metrics	1958	1980	1993	2009	2019
C	0.303	0.311	0.303	0.303	0.311
nwC	0.276	0.274	0.275	0.278	0.280
lwC	0.204	0.165	0.156	0.172	0.190
G	4.444	4.556	4.444	4.444	4.556
nwG	4.402	4.321	4.139	4.291	4.322
lwG	2.157	1.877	1.796	1.856	2.381
V	3.636	3.727	3.636	3.636	3.727
nwV	5.745	5.928	5.886	5.701	5.424
lwV	2.333	1.756	1.642	1.921	1.807

zooplankton, followed by values from phytoplankton to zooplankton, in three study years (1980, 1993, and 2009). Energy fluxes from phytoplankton to zooplankton (88.55 g m^{-2} yr^{-1}) and from detritus to mollusks (67.98 g m^{-2} yr^{-1}) were higher than those of other trophic links in 2019. Supplementary Figure S3 shows the temporal variability in flux-based ecosystem functioning metrics. The proportion of detritivorous flows increased first and then decreased over time, with the highest and lowest values observed in 1993 (75.2%) and 2019 (36.5%), respectively. The percentage of planktivorous flows showed an increasing trend, from 22.0% in 1958 to 24.7% in 2009, and became the main energy flow (49.5%) in 2019. In addition, the proportions of herbivorous, zooplanktivorous, benthivorous, and piscivorous flows in food webs showed a trend of first decreasing and then increasing over time, which were relatively higher in 2019 and 1958 than in the other three study years.

The different types of food web metrics (i.e., unweighted, node-, and link-weighted) displayed temporal variability and complementary dynamics from 1958 to 2019 (Table 2). Three unweighted food web metrics (*C*, *G*, and *V*) showed similar trends, with the highest values in 1980 and 2019. The highest and lowest node-weighted connectance (*nwC*) values were observed in 2019 and 1980, respectively. Link-weighted connectance (*lwC*) was highest in 1958, after which it decreased to its lowest value in 1993. Node-weighted generality (*nwG*) and link-weighted generality (*lwG*) both decreased initially and then increased, with the highest values observed in 1958 and 2019, respectively. In contrast, node-weighted vulnerability (*nwV*) first increased and then decreased, with the highest and lowest values in 1980 and 2019, respectively. Link-weighted vulnerability (*lwV*) was highest in 1958, with all other values much lower.

3.2 Relationships between water environmental factors and metrics of food web structure and function

The extreme maximum and minimum water levels were highest in 1958, followed by 2019 and 1980, respectively (Supplementary Table S3). The amplitudes of the water level fluctuation represent the difference between the maximum and minimum water levels for a given period, and they were highest in 1958 and lowest in 2019. The highest pulse duration was reported in 2009, whereas the lowest frequency of hydrologic reversals was observed in 2019. The threshold of water level pulses decreased gradually from 1958 to 2009, and then partially recovered in 2019. Since hydrological indicators of the 1-day, 3-days, 7-days, 30-days, and 90-days scale water level were significantly positively correlated with each other (Supplementary Figure S4), we have focused on the 7-days scale in our descriptions, since this period is broadly representative of the other periods. Supplementary Figure S5 and Supplementary Table S4 show the PCA results for the hydrological indicators. The first two principal component axes (i.e., PC1 and PC2) account for 81.2% of the variation in hydrological regime indicators of five representative years, 56.9% and 24.3% respectively. PC1 was strongly positively associated with *HPT* (factor loading: 0.986), *WLMaxd7* (0.981), *LPT* (0.910), *WLMind7* (0.886), and *WLAmpd7* (0.758). PC2 was strongly positively associated with *HPD* (0.935) and *LPD* (0.851).

Table 3 shows the values (mean ± SD) of the water quality variables for the five study years. All variables except for *DO* differed significantly among the five study years ($p < 0.05$). Lake Baiyangdian generally showed slightly alkaline water, with the mean pH value ranging from 7.96 to 8.72 in the five representative years, but with increasing acidity over time. T_w was highest in 2009, when it was significantly higher than in 1958 and 1980. Serious eutrophication occurred in Lake Baiyangdian, with average *TN* and *TP* concentrations ranging from 0.70 mg/L to 3.75 mg/L and from 0.03 mg/L to 0.34 mg/L, respectively, with both values increasing from 1958 to 2009, then decreasing. In addition, NO_2^-+NO_3^- was much higher in 2019 and 2009 than in the other 3 years, and this difference was significant; except for a decrease in 1993, NO_2^-+NO_3^- increased significantly from 1958 to 2019. The highest concentrations of *SRP*, *TN*, *TP*, and NH_4^+ were all observed in 2009. The average *COD* ranged from 12.0 mg/L to 59.2 mg/L, and increased to a maximum in 1993, and although it decreased thereafter, it remained much higher than in 1958. The PCA captures the relationship and associations in the dynamics among water quality factors in the five study years (Figure 5, Supplementary Table S5). The first two principal components (i.e., PC1 and PC2) together explained 62.8% of the variance, 43.0% and 19.8% respectively. PC1 was positively correlated with *SRP* (0.889), NH_4^+ (0.867), *TN* (0.827), *TP* (0.802), and T_w

TABLE 3 Mean and standard deviation (mean ± SD) for the water quality variables in the five study years. Values of a variable followed by different letters (a, b, c) differed significantly between study years (one-way ANOVA followed by *LSD* test or Kruskal–Wallis test followed by Mann-Whitney *U* test, $p < 0.05$).

Water quality factors	1958	1980	1993	2009	2019
Water temperature (T_w, °C)	17.3 ± 5.03^{b}	18.0 ± 1.42^{b}	18.90 ± 2.33^{ab}	26.65 ± 1.43^{a}	22.21 ± 4.45^{ab}
pH	8.72 ± 0.18^{a}	8.35 ± 0.26^{ab}	8.60 ± 0.39^{ab}	8.19 ± 0.14^{b}	7.96 ± 0.29^{b}
Dissolved oxygen (*DO*, mg/L)	7.25 ± 1.19^{a}	8.72 ± 0.71^{a}	7.64 ± 0.61^{a}	7.71 ± 1.03^{a}	6.45 ± 2.60^{a}
Nitrite-nitrate (NO_2^-+NO_3^-, mg/L)	0.32 ± 0.05^{bc}	0.44 ± 0.05^{b}	0.08 ± 0.02^{c}	1.98 ± 0.77^{ab}	2.61 ± 0.45^{a}
Soluble reactive phosphorus (*SRP*, mg/L)	0.01 ± 0.004^{c}	0.01 ± 0.003^{c}	0.13 ± 0.007^{b}	0.26 ± 0.04^{a}	0.02 ± 0.005^{c}
Chemical oxygen demand (*COD*, mg/L)	12.0 ± 2.66^{b}	25.29 ± 7.9^{b}	59.15 ± 11.9^{a}	21.99 ± 9.97^{b}	25.76 ± 5.62^{b}
Total nitrogen (*TN*, mg/L)	1.53 ± 0.16^{b}	0.70 ± 0.23^{b}	2.49 ± 0.34^{ab}	3.75 ± 1.11^{a}	2.55 ± 1.53^{ab}
Total phosphorus (*TP*, mg/L)	0.03 ± 0.004^{b}	0.04 ± 0.02^{b}	0.27 ± 0.08^{a}	0.34 ± 0.17^{a}	0.08 ± 0.05^{ab}
Ammonium (NH_4^+, mg/L)	0.92 ± 0.48^{bc}	0.17 ± 0.06^{c}	1.47 ± 0.38^{b}	3.45 ± 0.58^{a}	0.63 ± 0.22^{c}

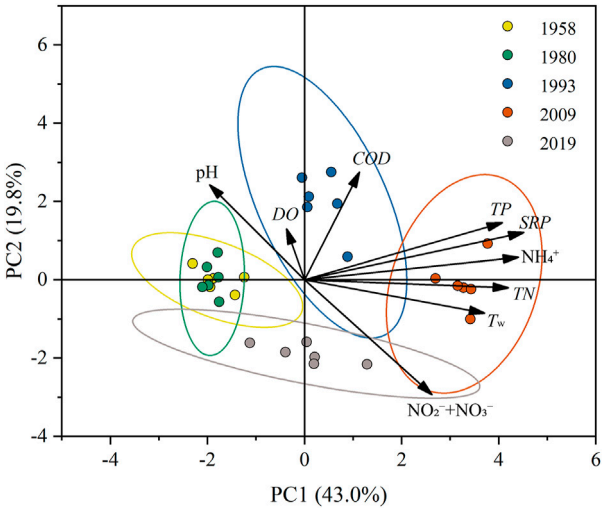

FIGURE 5
Biplot of principal component analysis (PCA) summarizing the variations in water quality factors of five representative years.

(0.730). NO_2^-+NO_3^- (−0.735) showed a negative loading on PC2, while *COD* (0.688) and pH (0.607) were positively correlated with this dimension. Furthermore, PCA arranged the five representative years into three groups according to the gradient of nutrient concentrations (i.e., *SRP*, NH_4^+, *TN*, *TP*, and NO_2^-+NO_3^-): 1958 and 1980 with low nutrients, 1993 and 2019 with relatively high nutrients, and 2009 with high nutrients.

We detected minor variations (i.e., most of them are similar) in values of the unweighted food web metrics over time. Therefore, these unweighted metrics were not appropriate for further analyses. We used the *VIP* (Table 4) and *RC* (Supplementary Table S6) values from the PLSR to select the most important environmental factors that affected the food web structure and function. *nwC* and *nwV* were mainly affected by NO_2^-+NO_3^-, *NumOfRev*, and *DO*, whereas the *RC* values showed correlations with opposite signs for these two weighted metrics. For node-weighted generality (*nwG*), the highest *VIP* was for *COD* (1.936), followed by *HPD* and *HPT* (1.684 and 1.252, respectively). Link-weighted connectance (*lwC*) and vulnerability (*lwV*) were both negatively correlated with *COD* (*VIP* = 1.486 and 1.613, respectively), and positively correlated with the threshold (*LPT* and *HPT*) and duration (*LPD* and *HPD*) of the water level pulse, respectively. Link-weighted generality (*lwG*) was negatively correlated with *DO*, and positively associated with NO_2^-+NO_3^-, *LPT*, and *WLMind7*. In addition, detritivory, phytoplanktivory, and zooplanktivory were mainly affected by NO_2^-+NO_3^-, *DO*, pH, and *NumOfRev*, whereas the RC values showed correlations with opposite signs for detritivory and the other two metrics. Herbivory was positively correlated with the threshold (*LPT* and *HPT*) of the water level pulse and *WLMind7*, and negatively correlated with *DO*. Moreover, benthivory and piscivory were both negatively correlated with *DO* (*VIP* = 1.821 and 1.551, respectively), and positively correlated with *LPT* and NO_2^-+NO_3^-.

4 Discussion

4.1 Temporal dynamics of the food web structure and function

In recent decades, Lake Baiyangdian has faced severe eutrophication (Zhao et al., 2010; Zeng et al., 2021). Nutrient over-enrichment associated with anthropogenic activities has accelerated eutrophication since the 1980s, leading to a high abundance of phytoplankton (Bumpers et al., 2017; Yang et al., 2021). Rogers et al. (2020) reported that grazing might have a negligible impact on phytoplankton dynamics at high

TABLE 4 Mean values of the variable importance in the projection (*VIP*) obtained via partial least-squares regression. Metrics are the node-weighted (nw) and link-weighted (lw) connectance (C), generality (G), and vulnerability (V), and six flow-based ecosystem functioning metrics.

Environmental factors	Food web metrics											
	nwc	***lwc***	***nwG***	***lwG***	***nwV***	***lwV***	**Detritivory**	**Herbivory**	**Phytoplanktivory**	**Zooplanktivory**	**Benthivory**	**Piscivory**
7-days minimum water level (*WLMind7*)	0.569	1.264	0.828	1.467	0.810	0.801	1.186	1.461	0.888	1.223	1.271	1.427
7-days maximum water level (*WLMaxd7*)	0.556	1.319	1.164	0.915	0.282	1.416	0.221	1.329	0.291	0.266	0.614	0.929
7-days amplitude water level (*WLAmpd7*)	0.896	0.946	1.159	0.326	0.803	1.627	0.953	0.779	1.309	0.922	0.340	0.344
Low-water pulse duration (*LPD*)	0.797	0.928	0.905	0.194	0.622	1.462	0.299	0.475	0.451	0.306	0.330	0.205
High-water pulse duration (*HPD*)	0.476	1.007	1.684	0.356	0.459	1.364	0.128	0.539	0.225	0.122	0.546	0.478
Low-water pulse threshold (*LPT*)	0.592	1.447	1.010	1.495	0.829	1.058	1.111	1.567	0.765	1.148	1.316	1.466
High-water pulse threshold (*HPT*)	0.507	1.309	1.252	1.125	0.356	1.188	0.545	1.373	0.225	0.589	0.856	1.149
Number of reversals (*NumOfRev*)	1.693	0.634	0.353	1.019	1.693	0.371	1.413	0.604	1.532	1.384	1.298	0.947
Water temperature (T_w)	1.213	0.451	0.491	0.364	1.010	0.491	0.467	0.620	0.707	0.429	0.472	0.377
pH	1.347	0.217	0.393	0.902	1.413	0.864	1.558	0.274	1.774	1.525	1.180	0.940
Dissolved oxygen (*DO*)	1.626	1.289	0.304	1.658	1.838	0.590	1.799	1.324	1.668	1.797	1.821	1.551
Nitrite-nitrate (NO_2^-+NO_3^-)	1.722	0.694	0.649	1.230	1.800	0.273	1.695	0.612	1.801	1.663	1.563	1.241
Soluble reactive phosphorus (*SRP*)	0.510	0.879	0.891	1.122	0.391	0.617	0.883	1.102	0.692	0.919	0.847	1.140
Chemical oxygen demand (*COD*)	0.614	1.486	1.936	0.950	0.732	1.613	0.506	1.107	0.216	0.508	1.061	1.055
Total nitrogen (*TN*)	1.156	0.502	0.663	0.389	0.937	0.543	0.333	0.630	0.559	0.303	0.369	0.405
Total phosphorus (*TP*)	0.486	1.027	1.203	1.117	0.368	0.773	0.766	1.161	0.538	0.801	0.872	1.165
Ammonium (NH_4^+)	0.603	0.552	0.560	0.810	0.315	0.628	0.719	0.778	0.652	0.751	0.488	0.822

10.3389/fenvs.2022.987600

phytoplankton concentrations. In addition, nutrient enrichment often alters the elemental composition of phytoplankton (Sterner and Elser, 2002; Burson et al., 2016), and often improves its nutritional quality for potential consumers. The higher nutritional enrichment of phytoplankton relative to detritus (Guo et al., 2016; Thorp and Bowes, 2017), and the associated increase in phytoplankton production, can turn detritus-based into phytoplankton-based food webs (Power et al., 2013; Mor et al., 2018), which is what happened in our study. It is acknowledged that eutrophication promotes changes in primary productivity that could potentially affect trophic interactions and alter the dietary preferences of consumers (Bumpers et al., 2017; Zhang et al., 2018; van der Lee et al., 2021). In addition, temporal changes in dietary preferences of consumers among five representative years may also be attributed to the difference in methodologies between the gut content analysis and the stable isotope analysis. For example, in a review paper on diet tracing methods in ecology, it was concluded that these two approaches measure the diet at various stages during ingestion and assimilation, and the relative dietary contribution can vary substantially (Nielsen et al., 2018). Furthermore, the contributions of detritus were the highest with averages of 30.1% in the first four study years. This may be due to the fact that the taxonomic impediment of identifying partially digested material by the gut content analysis can render some components unknown and classify them as detritus (Nielsen et al., 2018). Recently, stable carbon isotopes values of subfossils have been successfully tracked the food sources of consumers over a long-time scale (Cheng et al., 2020), which may provide an opportunity for temporal studies of highly resolved food webs.

Consumers may change their dietary preferences to take advantage of multiple food sources based on the relative availability or nutritional quality of the resources (de Carvalho et al., 2019), and this may cause changes in their trophic positions and hence in the food web structure (Rooney and McCann, 2012; McMeans et al., 2019). In the present study, three fish trophic groups (i.e., fingerlings, large omnivorous fish, and carnivorous fish) shifted their dietary preferences toward food resources with higher nutritional quality until 2009 (fingerlings and large omnivorous fish) and until 2019 (carnivorous fish), and their trophic position decreased accordingly. Similarly, some previous studies concluded that omnivorous consumers might lower their trophic position by adjusting their diet from consumption of animal resources to increased consumption of plant resources with high nutritional quality when both resources are offered simultaneously (Zhang et al., 2018; van der Lee et al., 2021). In addition, lower trophic positions of omnivorous and carnivorous fish have been reported during the wet season in tropical floodplains, leading to increased consumption of plants or invertebrates (Blanchette et al., 2014; McMeans et al., 2019). The trophic position of the top predator or the maximum trophic position of species in a food web is conceptually similar to food chain length (Briand and Cohen, 1987). Carnivorous fish consistently occupied the highest trophic position in all five representative years, and the decrease in its trophic position over time implies a shortening of the food chain length between the top and bottom of Lake Baiyangdian's food webs, which may be caused by increased trophic omnivory and reduced dietary specialization at any or all trophic levels (Post et al., 2000; Post and Takimoto, 2007). Furthermore, the dietary preferences of consumers can shape biomass ratios between different trophic levels (McCauley et al., 2018; Burian et al., 2020). Our results showed that the biomass of trophic groups was unequally distributed across the food webs, and decreased with increasing trophic level, which is consistent with previous studies (Trebilco et al., 2013; Hatton et al., 2015).

Any changes in dietary preferences can affect energy fluxes because different food sources have different concentrations of carbon and nutrients, which leads to different assimilation efficiencies (Sterner and Elser, 2002; Jochum and Eisenhauer, 2022). The highest total energy flux in the food web was observed in 1993, followed by 2019, with the lowest in 1958. This is related to the biomass pools of phytoplankton, submerged macrophytes, and detritus, as well as the biomass flow from these pools to primary consumers. The efficiency of the energy fluxes ingested by the consumers was low, and a considerable proportion of the energy fluxes directly entered the detritus pool, where the biomass and its contained energy served as fuel for ecosystem recycling in Lake Baiyangdian's food webs, which agrees with Zeng et al. (2021). According to Barnes et al. (2018), trophic complementarity can be an important mechanism for promoting ecosystem functioning in food webs, where greater consumer diversity reduces competition for food sources, thereby increasing the total energy fluxes to consumers (Poisot et al., 2013; Peralta et al., 2014).

In addition, the distribution of energy flux is important for determining food web stability. The ingestion by primary consumers (zooplankton, meiofauna, and mollusks) accounted for more than 90% of the total ingestion of consumers in our study. The bottom-heavy food web energetics structure (i.e., larger energy fluxes at lower trophic levels) may confer greater food web stability (Rip and McCan, 2011; Barnes et al., 2018). Zooplankton and mollusks, which dominated the total energy fluxes in Lake Baiyangdian, were strongly connected to the phytoplankton and detritus energy pathways. Both energy channels can convey significant energy fluxes from basal food sources to consumers at higher trophic levels, thereby potentially stabilizing food webs (Ward et al., 2015; Mougi, 2020). However, the primary consumers that feed on more nutritious phytoplankton can use less energetically costly mechanisms to meet their nutrient uptake, assimilation, and retention needs (Sardans et al., 2012; Teurlincx et al., 2017).

4.2 Changes in unweighted and weighted food web metrics

Although the food webs displayed large differences in the underlying dietary preferences and energy flux distribution in 1980 and 2019, or in 1958, 1993, and 2009, they showed similar values for the unweighted food web metrics. This suggests that unweighted food web metrics are inadequate predictors of highly aggregated food web structures and functions, since they are

limited to a static view, and are more sensitive to changes in species and link richness (Kortsch et al., 2021). However, some studies indicated that changes in community composition did not always trigger changes in the food web structure (Yletyinen et al., 2016; Griffith et al., 2019; Frelat et al., 2022). Moreover, previous studies concluded that macroscopic unweighted food web descriptors may be invariant at a broader temporal scale (spanning years to millennia), whereas strong dynamics were observed at finer temporal scales (from hours to months) (Fründ et al., 2011; Trøjelsgaard and Olesen, 2016; CaraDonna et al., 2021). We observed more pronounced temporal variability in the weighted (node- and link-weighted) food web metrics than in the unweighted food web metrics in all study years, which can be related to the fact that unweighted and weighted food web metrics likely reflect different underlying ecosystem processes (Olivier et al., 2019; Kortsch et al., 2021; Frelat et al., 2022). Previous studies show that weighted food web metrics can capture the associated consequences of energy flux distribution and thus predict ecosystem functioning (Kortsch et al., 2021). In our study, three weighted metrics (i.e., *lwC*, *lwG*, and *nwG*) showed the same trend of decreasing first and then increasing over time as most metrics of ecosystem functioning (i.e., herbivory, zooplanktivory, benthivory, and piscivory), while the detritivory showed the opposite trend. Some studies of temporal changes of node-weighted food web metrics suggest that food web structure was influenced by changes in species dominance (Olivier et al., 2019). Node-weighted connectance (*nwC*) was highest in 2019, which can be explained by the high biomass of highly connected nodes, such as mollusks and omnivorous fish, that reflect dominance of the food web by particular trophic groups in 2019.

Node-weighted vulnerability (*nwV*) was always much higher than unweighted vulnerability (*V*) in our study, which was consistent with previous studies (Olivier et al., 2019; Kortsch et al., 2021). We also found that link-weighted metrics had lower values than the corresponding unweighted metrics in Lake Baiyangdian's food webs. Similar results were observed in a previous study (Kortsch et al., 2021), which indicates that energy fluxes are not equally distributed in food webs, but rather are skewed towards a few strong fluxes and many weak fluxes. Link-weighted connectance (*lwC*) showed higher values in 1958 and 2019, which was related to the fact that several trophic groups with many interactions also had relatively high and even inflows and outflows, and this increases link-weighted food web complexity. Together these results indicate that an approach that considers the dominant species, their dietary preferences, and the energy flux distribution will challenge the conclusion about temporal changes in food web structures based only on unweighted metrics (Scotti et al., 2009; Kortsch et al., 2021; López-López et al., 2022). However, in other studies, weighted metrics were similar (Frelat et al., 2022) or complementary (Kortsch et al., 2021) to unweighted metrics in their ability to describe temporal changes in the food web structure. Therefore, it is necessary to integrate unweighted, node-weighted, and link-weighted metrics to identify the complementary temporal patterns of food web dynamics, since this provides better support for management decisions.

4.3 Effect of environmental factors on food web dynamics

The changing hydrological regimes and water quality factors that we observed can explain the temporal trends of food web dynamics. Disentangling their relationships is crucial for guiding conservation and restoration strategies in shallow lakes. Studies of ecosystem processes in shallow lakes have generally shown that water level fluctuations are a dominant force and that many other environmental factors vary concurrently with these fluctuations (Kolding and van Zwieten, 2012; Jeppesen et al., 2015). In our study, the low- and high-water level pulse thresholds (i.e., *LPT* and *HPT*) were (after *COD*) the hydrological regime indicators that most strongly affected the link-weighted connectance (*lwC*). They were positively associated with link-weighted food web complexity. Values of *LPT* and *HPT* represent variable conditions that provide a broader range of hydrologic niches that can provide conditions suitable for organisms at different trophic positions (Yan et al., 2020; Zheng et al., 2020). The number of water level reversals (*NumOfRev*) was negatively associated with node-weighted connectance (*nwC*). Frequent water level fluctuations may prevent the establishment and development of organisms, thereby decreasing biodiversity and food web complexity.

Eutrophication due to excessive nutrient loading is a common stressor for changes in food web structure and function in shallow lakes (Paerl et al., 2011). It affects the relative availability of basal resources, which further affects consumers at higher trophic positions (Bumpers et al., 2017). Eutrophication also can homogenize the composition of lake benthic assemblages (Olden et al., 2004; Donohue et al., 2009). Moreover, lakes exposed to prolonged eutrophication are prone to hypoxia, and subsequent fish kills (Bullerjahn et al., 2016). Our results showed that the biomass of phytoplankton increased from 1958 to 2009, which coincided with the intensive eutrophication in Lake Baiyangdian. As a result, most of the consumer trophic groups shifted in the direction of phytoplankton, and the food web then became more dependent on algae-based energy channels. Meanwhile, the food chain length declined from 1958 to 2009, which mean the food web structure of Lake Baiyangdian was simplified even though eutrophication brought sufficient nutrient into the ecosystem. Similar results have been reported in Lake Taihu with long-term eutrophication (Xu et al., 2016). The overall water quality of Lake Baiyangdian was better in 2019 than in 2009 and 1993, which is likely to be related to a series of governance policies and restoration projects, including a prohibition of fish breeding, water diversion projects,

wastewater treatment in villages, and dredging key channels (Zhu et al., 2019; Wang et al., 2021). The highest *lwC* value was in 1958, followed by 2019, whereas *nwC* was highest in 2019, followed by 2009. Taken together, the restoration of hydrological regimes and water quality improvements contributed to improving the lake's food web complexity by increasing the node- and link-weighted connectance in 2019. In addition, previous studies showed that most biological communities might be suppressed when a lake became eutrophication, leading to a decline in the total energy fluxes of the ecosystem (Kong et al., 2016; Wang et al., 2020). This finding is not evident in our study, as we observe the highest total energy fluxes in 1993, followed by in 2019, and the lowest value in 1958.

5 Conclusion

We confirmed our research hypotheses that the food web structure and function would vary over time in response to changes in hydrological regimes, eutrophication, and some related water quality factors. Our results revealed temporal variability of the food web structure and function in a shallow lake in northern China using both unweighted and weighted approaches and food web energetics approach. The lake changed from a detritus-based food web into a phytoplankton-based web based on the relative contributions of the basal food sources and the energy flux distribution. Fingerlings, large omnivorous fish, and carnivorous fish shifted their dietary preferences towards food sources with higher nutritional quality in the latter three study years, and their trophic position decreased accordingly. The link-weighted metrics had lower values than the corresponding unweighted topology-based metrics, which indicates that energy fluxes were not equally distributed, but rather were skewed towards a few strong fluxes and many weak fluxes. We observed more pronounced temporal variability in the weighted (node- and link-weighted) food web metrics than the unweighted food web metrics, and this may be related to the fact that unweighted and weighted food web metrics reflect different underlying ecosystem processes. Furthermore, our study demonstrated that restoring the lake's hydrological regimes and improving the water quality contributed to improving the food web complexity and function, with increased node- and link-weighted connectance and most of the flow-based ecosystem functioning metrics values in 2019. Overall, our results suggested that studies of weighted food web metrics will complement the information provided by classical topology-based (unweighted) metrics. Our approach can therefore provide useful data to support the management and restoration of the structure and functions of shallow lake ecosystems. In future research, it will be necessary to find ways to integrate the effects of additional hydrologic and water quality metrics (e.g., the differences between long- and short-term indicators, heavy metal concentrations in the water and sediments) and to expand our analysis to spatiotemporally highly resolved food webs to improve lake ecosystem management.

Data availability statement

The original contributions presented in the study are included in the article/Supplementary Material, further inquiries can be directed to the corresponding author.

Author contributions

WY: Conceptualization, Resources, Supervision, Data analysis—original draft, Writing—review and editing. XF: Investigation, Methodology, Visualization, Data analysis—original draft, Writing—original draft. XL: Data analysis—original draft, Writing—review and editing. YY: Data analysis—original draft, Writing—review and editing.

Funding

This study was financially supported by the National Natural Science Foundation of China (No. 52079006), the National Key R&D Program of China (No. 2017YFC0404505), and the Beijing Advanced Innovation Program for Land Surface Science.

Acknowledgments

We thank Geoffrey Hart for providing language help during the writing of this paper.

Conflict of interest

The authors declare that the research was conducted in the absence of any commercial or financial relationships that could be construed as a potential conflict of interest.

Publisher's note

its manufacturer, is not guaranteed or endorsed by the publisher.

Supplementary material

The Supplementary Material for this article can be found online at: https://www.frontiersin.org/articles/10.3389/fenvs.2022.987600/full#supplementary-material.

References

Banašek-Richter, C., Bersier, L. F., Cattin, M. F., Baltensperger, R., Gabriel, J. P., Merz, Y., et al. (2009). Complexity in quantitative food webs. *Ecology* 90, 1470–1477. doi:10.1890/08-2207.1

Barnes, A. D., Jochum, M., Lefcheck, J. S., Eisenhauer, N., Scherber, C., O'Connor, M. I., et al. (2018). Energy flux: The link between multitrophic biodiversity and ecosystem functioning. *Trends Ecol. Evol.* 33, 186–197. doi:10.1016/j.tree.2017.12.007

Bartley, T. J., McCann, K. S., Bieg, C., Cazelles, K., Granados, M., Guzzo, M. M., et al. (2019). Food web rewiring in a changing world. *Nat. Ecol. Evol.* 3, 345–354. doi:10.1038/s41559-018-0772-3

Bentivoglio, F., Calizza, E., Rossi, D., Carlino, P., Careddu, G., Rossi, L., et al. (2016). Site-scale isotopic variations along a river course help localize drainage basin influence on river food webs. *Hydrobiologia* 770, 257–272. doi:10.1007/s10750-015-2597-2

Bersier, L. F., Banašek-Richter, C., and Cattin, M. F. (2002). Quantitative descriptors of food-web matrices. *Ecology* 83, 2394–2407. doi:10.1890/0012-9658(2002)083[2394:QDOFWM]2.0.CO;2

Blanchette, M. L., Davis, A. M., Jardine, T. D., and Pearson, R. G. (2014). Omnivory and opportunism characterize food webs in a large dry-tropics river system. *Freshw. Sci.* 33, 142–158. doi:10.1086/674632

Boit, A., and Gaedke, U. (2014). Benchmarking successional progress in a quantitative food web. *PloS One* 9, e90404. doi:10.1371/journal.pone.0090404

Briand, F., and Cohen, J. E. (1987). Environmental correlates of food chain length. *Science* 238, 956–960. doi:10.1126/science.3672136

Brown, J. H., Gillooly, J. F., Allen, A. P., Savage, V. M., and West, G. B. (2004). Toward a metabolic theory of ecology. *Ecology* 85, 1771–1789. doi:10.1890/03-9000

Bullerjahn, G. S., McKay, R. M., Davis, T. W., Baker, D. B., Boyer, G. L., D'Anglada, L. V., et al. (2016). Global solutions to regional problems: Collecting global expertise to address the problem of harmful cyanobacterial blooms. A Lake Erie case study. *Harmful Algae* 54, 223–238. doi:10.1016/j.hal.2016.01.003

Bumpers, P. M., Rosemond, A. D., Maerz, J. C., and Benstead, J. P. (2017). Experimental nutrient enrichment of forest streams increases energy flow to predators along greener food-web pathways. *Freshw. Biol.* 62, 1794–1805. doi:10.1111/fwb.12992

Burian, A., Nielsen, J. M., and Winder, M. (2020). Food quantity–quality interactions and their impact on consumer behavior and trophic transfer. *Ecol. Monogr.* 90, 1–19. doi:10.1002/ecm.1395

Burson, A., Stomp, M., Akil, L., Brussaard, C. P. D., and Huisman, J. (2016). Unbalanced reduction of nutrient loads has created an offshore gradient from phosphorus to nitrogen limitation in the North Sea. *Limnol. Oceanogr.* 61, 869–888. doi:10.1002/lno.10257

CaraDonna, P. J., Burkle, L. A., Schwarz, B., Resasco, J., Knight, T. M., Benadi, G., et al. (2021). Seeing through the static: The temporal dimension of plant–animal mutualistic interactions. *Ecol. Lett.* 24, 149–161. doi:10.1111/ele.13623

Careddu, G., Costantini, M. L., Calizza, E., Carlino, P., Bentivoglio, F., Orlandi, L., et al. (2015). Effects of terrestrial input on macrobenthic food webs of coastal sea are detected by stable isotope analysis in Gaeta Gulf. *Estuar. Coast. Shelf Sci.* 154, 158–168. doi:10.1016/j.ecss.2015.01.013

Cheng, L., Kattel, G., Xue, B., Yao, S., Li, L., and Liu, J. (2020). Application of subfossil Bosmina and its $\delta^{13}C$ values in tracing the long-term food web dynamics of shallow eutrophic lakes: A case in Taihu lake, southeast China. *Sci. Total Environ.* 730, 138909. doi:10.1016/j.scitotenv.2020.138909

China Bureau of Environmental Protection (Cbep) (2002). *Methods for monitoring and analysis of 616 water and wastewater*. fourth ed. Beijing: China Environmental Science Press. (in Chinese).

Danet, A., Mouchet, M., Bonnaffé, W., Thébault, E., and Fontaine, C. (2021). Species richness and food-web structure jointly drive community biomass and its temporal stability in fish communities. *Ecol. Lett.* 24, 2364–2377. doi:10.1111/ele.13857

de Carvalho, D. R., de Castro, D. M. P., Callisto, M., Chaves, A. J. de M., Moreira, M. Z., and Pompeu, P. S. (2019). Stable isotopes and stomach content analyses indicate omnivorous habits and opportunistic feeding behavior of an invasive fish. *Aquat. Ecol.* 53, 365–381. doi:10.1007/s10452-019-09695-3

Donohue, I., Jackson, A. L., Pusch, M. T., and Irvine, K. (2009). Nutrient enrichment homo- genizes lake benthic assemblages at local and regional scales. *Ecology* 90, 3470–3477. doi:10.1890/09-0415.1

Duffy, J. E., Cardinale, B. J., France, K. E., McIntyre, P. B., Thébault, E., and Loreau, M. (2007). The functional role of biodiversity in ecosystems: Incorporating trophic complexity. *Ecol. Lett.* 10, 522–538. doi:10.1111/j.1461-0248.2007.01037.x

Dunne, J. A., Williams, R. J., and Martinez, N. D. (2002). Network structure and biodiversity loss in food webs: Robustness increases with connectance. *Ecol. Lett.* 5, 558–567. doi:10.1046/j.1461-0248.2002.00354.x

Evtimova, V. V., and Donohue, I. (2014). Quantifying ecological responses to amplified water level fluctuations in standing waters: An experimental approach. *J. Appl. Ecol.* 51, 1282–1291. doi:10.1111/1365-2664.12297

Evtimova, V. V., and Donohue, I. (2016). Water-level fluctuations regulate the structure and functioning of natural lakes. *Freshw. Biol.* 61, 251–264. doi:10.1111/fwb.12699

Frelat, R., Kortsch, S., Kröncke, I., Neumann, H., Nordström, M. C., Olivier, P. E. N., et al. (2022). Food web structure and community composition: A comparison across space and time in the north sea. *Ecography* 2022 (2). doi:10.1111/ecog.05945

Fründ, J., Dormann, C. F., and Tscharntke, T. (2011). Linné's floral clock is slow without pollinators—Flower closure and plant-pollinator interaction webs. *Ecol. Lett.* 14, 896–904. doi:10.1111/j.1461-0248.2011.01654.x

Gauzens, B., Barnes, A., Giling, D. P., Hines, J., Jochum, M., Lefcheck, J. S., et al. (2019). fluxweb: an R package to easily estimate energy fluxes in food webs. *Methods Ecol. Evol.* 10, 270–279. doi:10.1111/2041-210X.13109

Griffith, G. P., Hop, H., Vihtakari, M., Wold, A., Kalhagen, K., and Gabrielsen, G. W. (2019). Ecological resilience of Arctic marine food webs to climate change. *Nat. Clim. Chang.* 9, 868–872. doi:10.1038/s41558-019-0601-y

Gu, B., Schelske, C. L., and Waters, M. N. (2011). Patterns and controls of seasonal variability of carbon stable isotopes of particulate organic matter in lakes. *Oecologia* 165, 1083–1094. doi:10.1007/s00442-010-1888-6

Gu, X. D., Li, N., Liu, W. L., and Xia, B. (2019). Soil moisture in relation to Lake fluctuations in a river-lake-basin system: A case study of the poyang lake region, China. *Ecol. Indic.* 104, 306–312. doi:10.1016/j.ecolind.2019.05.018

Guo, F., Kainz, M. J., Sheldon, F., and Bunn, S. E. (2016). The importance of high-quality algal food sources in stream food webs - current status and future perspectives. *Freshw. Biol.* 61, 815–831. doi:10.1111/fwb.12755

Hansen, A. G., Gardner, J. R., Connelly, K. A., Polacek, M., and Beauchamp, D. A. (2018). Trophic compression of lake food webs under hydrologic disturbance. *Ecosphere* 9 (6), e02304. doi:10.1002/ecs2.2304

Harvey, E., Gounand, I., Ward, C. L., and Altermatt, F. (2017). Bridging ecology and conservation: From ecological networks to ecosystem function. *J. Appl. Ecol.* 54, 371–379. doi:10.1111/1365-2664.12769

Hatton, I. A., McCann, K. S., Fryxell, J. M., Davies, T. J., Smerlak, M., Sinclair, A. R. E., et al. (2015). The predator-prey power law: Biomass scaling across terrestrial and aquatic biomes. *Science* 349 (6252), aac6284. doi:10.1126/science.aac6284

Hines, J., van der Putten, W. H., De Deyn, G. B., Wagg, C., Voigt, W., Mulder, C., et al. (2015). Towards an integration of biodiversity–ecosystem functioning and food web theory to evaluate relationships between multiple ecosystem services. *Adv. Ecol. Res.* 53, 161–199. doi:10.1016/bs.aecr.2015.09.001

Ibarra-García, E. C., Abarca-Arenas, L. G., Ortiz, M., and Rodríguez-Zaragoza, F. A. (2020). Impact of hurricane dean on chinchorro bank coral reef (western caribbean): Temporal variation in the food web structure. *Ecol. Indic.* 118, 106712. doi:10.1016/j.ecolind.2020.106712

Ives, J. T., McMeans, B. C., McCann, K. S., Fisk, A. T., Johnson, T. B., Bunnell, D. B., et al. (2019). Food-web structure and ecosystem function in the laurentian great lakes—Toward a conceptual model. *Freshw. Biol.* 64, 1–23. doi:10.1111/fwb.13203

Jackson, M. C., Loewen, C. J. G., Vinebrooke, R. D., and Chimimba, C. T. (2016). Net effects of multiple stressors in freshwater ecosystems: A meta-analysis. *Glob. Change Biol.* 22, 180–189. doi:10.1111/gcb.13028

Jeppesen, E., Brucet, S., Naselli-Flores, L., Papastergiadou, E., Stefanidis, K., Nõges, T., et al. (2015). Ecological impacts of global warming and water abstraction on lakes and reservoirs due to changes in water level and related changes in salinity. *Hydrobiologia* 750, 201–227. doi:10.1007/s10750-014-2169-x

Jin, X. C. (1995). *Lake environment in China*, Vol. 2. Beijing, China: Ocean Press. (in Chinese).

Jochum, M., and Eisenhauer, N. (2022). Out of the dark: Using energy flux to connect above- and belowground communities and ecosystem functioning. *Eur. J. Soil Sci.* 73, 1–11. doi:10.1111/ejss.13154

Kolding, J., and van Zwieten, P. A. M. (2012). Relative lake level fluctuations and their influence on productivity and resilience in tropical lakes and reservoirs. *Fish. Res.* 116, 99–109. doi:10.1016/j.fishres.2011.11.008

Kong, X. Z., He, W., Liu, W. X., Yang, B., Xu, F. L., Jørgensen, S. E., et al. (2016). Changes in food web structure and ecosystem functioning of a large, shallow Chinese lake during the 1950s, 1980s and 2000s. *Ecol. Modell.* 319, 31–41. doi:10.1016/j.ecolmodel.2015.06.045

Kortsch, S., Frelat, R., Pecuchet, L., Olivier, P., Putnis, I., Bonsdorff, E., et al. (2021). Disentangling temporal food web dynamics facilitates understanding of ecosystem functioning. *J. Anim. Ecol.* 90, 1205–1216. doi:10.1111/1365-2656.13447

Kortsch, S., Primicerio, R., Aschan, M., Lind, S., Dolgov, A. V., and Planque, B. (2019). Food-web structure varies along environmental gradients in a high-latitude marine ecosystem. *Ecography* 42, 295–308. doi:10.1111/ecog.03443

Kortsch, S., Primicerio, R., Fossheim, M., Dolgov, A. V., and Aschan, M. (2015). Climate change alters the structure of arctic marine food webs due to poleward shifts of boreal generalists. *Proc. R. Soc. B* 282, 20151546. doi:10.1098/rspb.2015.1546

Laigle, I., Aubin, I., Digel, C., Brose, U., Boulangeat, I., and Gravel, D. (2018). Species traits as drivers of food web structure. *Oikos* 127, 316–326. doi:10.1111/oik.04712

Lang, B., Ehnes, R. B., Brose, U., and Rall, B. C. (2017). Temperature and consumer type dependencies of energy flows in natural communities. *Oikos* 126, 1717–1725. doi:10.1111/oik.04419

Li, X. X., Yang, W., Sun, T., and Gaedke, U. (2021). Quantitative food web structure and ecosystem functions in a warm-temperate seagrass bed. *Mar. Biol.* 168, 74–17. doi:10.1007/s00227-021-03878-z

Li, Y. K., Qian, F. W., Silbernagel, J., and Larson, H. (2019). Community structure, abundance variation and population trends of waterbirds in relation to water level fluctuation in Poyang Lake. *J. Gt. Lakes. Res.* 45, 976–985. doi:10.1016/j.jglr.2019.08.002

López-López, L., Genner, M. J., Tarling, G. A., Saunders, R. A., and O'Gorman, E. J. (2022). Ecological networks in the scotia sea: Structural changes across latitude and depth. *Ecosystems* 25, 457–470. doi:10.1007/s10021-021-00665-1

Lynam, C. P., Llope, M., Möllmann, C., Helaouët, P., Bayliss-Brown, G. A., and Stenseth, N. C. (2017). Interaction between top-down and bottom-up control in marine food webs. *Proc. Natl. Acad. Sci. U. S. A.* 114, 1952–1957. doi:10.1073/pnas.1621037114

Ma, X., Liu, C., Liu, L., Wang, Y., Wang, J., and Zhang, Y. (2011). Study on the food web of fish in baiyangdian lake based diet analysis. *J. Hydroecology* 32, 85–90. (In Chinese).

Mao, Z. G., Gu, X. H., Zeng, Q. F., and Pan, G. (2014). Seasonal and spatial variations of the food web structure in a shallow eutrophic lake assessed by stable isotope analysis. *Fish. Sci.* 80, 1045–1056. doi:10.1007/s12562-014-0771-5

Marino, N. A. C., Srivastava, D. S., MacDonald, A. A. M., Leal, J. S., Campos, A. B. A., and Farjalla, V. F. (2017). Rainfall and hydrological stability alter the impact of top predators on food web structure and function. *Glob. Change Biol.* 23, 673–685. doi:10.1111/gcb.13399

McCauley, D. J., Gellner, G., Martinez, N. D., Williams, R. J., Sandin, S. A., Micheli, F., et al. (2018). On the prevalence and dynamics of inverted trophic pyramids and otherwise top-heavy communities. *Ecol. Lett.* 21, 439–454. doi:10.1111/ele.12900

McMeans, B. C., Kadoya, T., Pool, T. K., Holtgrieve, G. W., Lek, S., Kong, H., et al. (2019). Consumer trophic positions respond variably to seasonally fluctuating environments. *Ecology* 100 (2), e02570. doi:10.1002/ecy.2570

Mor, J. R., Ruhí, A., Tornés, E., Valcárcel, H., Muñoz, I., and Sabater, S. (2018). Dam regulation and riverine food-web structure in a Mediterranean river. *Sci. Total Environ.* 625, 301–310. doi:10.1016/j.scitotenv.2017.12.296

Mougi, A. (2020). Coupling of green and Brown food webs and ecosystem stability. *Ecol. Evol.* 10, 9192–9199. doi:10.1002/ece3.6586

Nielsen, J. M., Clare, E. L., Hayden, B., Brett, M. T., and Kratina, P. (2018). Diet tracing in ecology: Method comparison and selection. *Methods Ecol. Evol.* 9, 278–291. doi:10.1111/2041-210X.12869

Olden, J. D., Poff, N. L. R., Douglas, M. R., Douglas, M. E., and Fausch, K. D. (2004). Ecological and evolutionary consequences of biotic homogenization. *Trends Ecol. Evol.* 19, 18–24. doi:10.1016/j.tree.2003.09.010

Olesen, J. M., Stefanescu, C., and Traveset, A. (2011). Strong, long-term temporal dynamics of an ecological network. *PLoS One* 6, e26455–6. doi:10.1371/journal.pone.0026455

Olivier, P., Frelat, R., Bonsdorff, E., Kortsch, S., Kröncke, I., Möllmann, C., et al. (2019). Exploring the temporal variability of a food web using long-term biomonitoring data. *Ecography* 42, 2107–2121. doi:10.1111/ecog.04461

Onderka, M., Wrede, S., Rodný, M., Pfister, L., Hoffmann, L., and Krein, A. (2012). Hydrogeologic and landscape controls of dissolved inorganic nitrogen (DIN) and dissolved silica (DSi) fluxes in heterogeneous catchments. *J. Hydrol. X.* 450–451, 36–47. doi:10.1016/j.jhydrol.2012.05.035

Paerl, H. W., Xu, H., McCarthy, M. J., Zhu, G., Qin, B., Li, Y., et al. (2011). Controlling harmful cyanobacterial blooms in a hyper-eutrophic lake (Lake Taihu, China): The need for a dual nutrient (N & P) management strategy. *Water Res.* 45, 1973–1983. doi:10.1016/j.watres.2010.09.018

Paine, R. T. (1980). Food webs: Linkage, interaction strength and community infrastructure. *J. Anim. Ecol.* 49, 666–685. doi:10.2307/4220

Parnell, A. C., Haslett, J., Allen, J. R. M., Buck, C. E., and Huntley, B. (2008). A flexible approach to assessing synchroneity of past events using Bayesian reconstructions of sedimentation history. *Quat. Sci. Rev.* 27, 1872–1885. doi:10.1016/j.quascirev.2008.07.009

Parnell, A. C., Inger, R., Bearhop, S., and Jackson, A. L. (2010). Source partitioning using stable isotopes: Coping with too much variation. *PLoS One* 5, e9672–5. doi:10.1371/journal.pone.0009672

Peralta, G., Frost, C. M., Rand, T. A., Didham, R. K., and Tylianakis, J. M. (2014). Complementarity and redundancy of interactions enhance attack rates and spatial stability in host–parasitoid food webs. *Ecology* 95, 1888–1896. doi:10.1890/13-1569.1

Poisot, T., Mouquet, N., and Gravel, D. (2013). Trophic complementarity drives the biodiversity–ecosystem functioning relationship in food webs. *Ecol. Lett.* 16, 853–861. doi:10.1111/ele.12118

Poisot, T., Stouffer, D. B., and Gravel, D. (2015). Beyond species: Why ecological interaction networks vary through space and time. *Oikos* 124, 243–251. doi:10.1111/oik.01719

Post, D. M., Pace, M. L., and Halrston, N. G. (2000). Ecosystem size determines food-chain length in lakes. *Nature* 405, 1047–1049. doi:10.1038/35016565

Post, D. M., and Takimoto, G. (2007). Proximate structural mechanisms for variation in food-chain length. *Oikos* 116, 775–782. doi:10.1111/j.0030-1299.2007.15552.x

Post, D. M. (2002a). The long and short of food-chain length. *Trends Ecol. Evol.* 17, 269–277. doi:10.1016/S0169-5347(02)02455-2

Post, D. M. (2002b). Using stable isotopes to estimate trophic position: Models, methods, and assumptions. *Ecology* 83, 703–718. doi:10.1890/0012-9658(2002)083[0703:USITET]2.0.CO;2

Power, M. E., Holomuzki, J. R., and Lowe, R. L. (2013). Food webs in Mediterranean rivers. *Hydrobiologia* 719, 119–136. doi:10.1007/s10750-013-1510-0

Prchalová, M., Mrkvička, T., Peterka, J., Čech, M., Berec, L., and Kubečka, J. (2011). A model of gillnet catch in relation to the catchable biomass, saturation, soak time and sampling period. *Fish. Res.* 107, 201–209. doi:10.1016/j.fishres.2010.10.021

Richter, B. D., Baumgartner, J. V., Powell, J., and Braun, D. P. (1996). A method for assessing hydrologic alteration within ecosystems. *Conserv. Biol.* 10, 1163–1174. doi:10.1046/j.1523-1739.1996.10041163.x

Rip, J. M. K., and McCann, K. S. (2011). Cross-ecosystem differences in stability and the principle of energy flux. *Ecol. Lett.* 14, 733–740. doi:10.1111/j.1461-0248.2011.01636.x

Rogers, T. L., Munch, S. B., Stewart, S. D., Palkovacs, E. P., Giron-Nava, A., Matsuzaki, S. S., et al. (2020). Trophic control changes with season and nutrient loading in lakes. *Ecol. Lett.* 23, 1287–1297. doi:10.1111/ele.13532

Rooney, N., and McCann, K. S. (2012). Integrating food web diversity, structure and stability. *Trends Ecol. Evol.* 27, 40–46. doi:10.1016/j.tree.2011.09.001

Ru, H. J., Li, Y. F., Sheng, Q., Zhong, L. Q., and Ni, Z. H. (2020). River damming affects energy flow and food web structure: A case study from a subtropical large river. *Hydrobiologia* 847, 679–695. doi:10.1007/s10750-019-04130-y

Sardans, J., Rivas-Ubach, A., and Peñuelas, J. (2012). The elemental stoichiometry of aquatic and terrestrial ecosystems and its relationships with organismic lifestyle and ecosystem structure and function: A review and perspectives. *Biogeochemistry* 111, 1–39. doi:10.1007/s10533-011-9640-9

Schoener, T. W. (1989). Food webs from the small to the large: The robert H. MacArthur award lecture. *Ecology* 70, 1559–1589. doi:10.2307/1938088

Scotti, M., Bondavalli, C., Bodini, A., and Allesina, S. (2009). Using trophic hierarchy to understand food web structure. *Oikos* 118, 1695–1702. doi:10.1111/j.1600-0706.2009.17073.x

Song, C. Q., Ke, L. H., Pan, H., Zhan, S. G., Liu, K., and Ma, R. H. (2018). Long-term surface water changes and driving cause in xiong'an, China: From dense landsat time series images and synthetic analysis. *Sci. Bull. (Beijing).* 63, 708–716. doi:10.1016/j.scib.2018.05.002

Sterner, R. W., and Elser, J. J. (2002). *Ecological stoichiometry*. Princeton, New Jersey, USA: Princeton University Press.

Teurlincx, S., Velthuis, M., Seroka, D., Govaert, L., van Donk, E., Van de Waal, D. B., et al. (2017). Species sorting and stoichiometric plasticity control community C:P ratio of first-order aquatic consumers. *Ecol. Lett.* 20, 751–760. doi:10.1111/ele.12773

Thompson, R. M., Brose, U., Dunne, J. A., Hall, R. O., Hladyz, S., Kitching, R. L., et al. (2012). Food webs: Reconciling the structure and function of biodiversity. *Trends Ecol. Evol.* 27, 689–697. doi:10.1016/j.tree.2012.08.005

Thorp, J. H., and Bowes, R. E. (2017). Carbon sources in riverine food webs: New evidence from amino acid isotope techniques. *Ecosystems* 20, 1029–1041. doi:10.1007/s10021-016-0091-y

Trebilco, R., Baum, J. K., Salomon, A. K., and Dulvy, N. K. (2013). Ecosystem ecology: Size-based constraints on the pyramids of life. *Trends Ecol. Evol.* 28, 423–431. doi:10.1016/j.tree.2013.03.008

Trøjelsgaard, K., and Olesen, J. M. (2016). Ecological networks in motion: Micro- and macroscopic variability across scales. *Funct. Ecol.* 30, 1926–1935. doi:10.1111/1365-2435.12710

Ushio, M., Hsieh, C. H., Masuda, R., Deyle, E. R., Ye, H., Chang, C. W., et al. (2018). Fluctuating interaction network and time-varying stability of a natural fish community. *Nature* 554, 360–363. doi:10.1038/nature25504

van der Lee, G. H., Vonk, J. A., Verdonschot, R. C. M., Kraak, M. H. S., Verdonschot, P. F. M., and Huisman, J. (2021). Eutrophication induces shifts in the trophic position of invertebrates in aquatic food webs. *Ecology* 102, e03275–13. doi:10.1002/ecy.3275

Wang, M. X., Yao, Y., Shen, Q., Gao, H. J., Li, J. S., Zhang, F. F., et al. (2021). Time-series analysis of surface-water quality in xiong'an new area, 2016–2019. *J. Indian Soc. Remote Sens.* 49, 857–872. doi:10.1007/s12524-020-01264-8

Wang, S. C., Liu, X., Liu, Y., and Wang, H. (2020). Benthic-pelagic coupling in lake energetic food webs. *Ecol. Modell.* 417, 108928. doi:10.1016/j.ecolmodel.2019.108928

Ward, C. L., McCann, K. S., and Rooney, N. (2015). HSS revisited: Multi-channel processes mediate trophic control across a productivity gradient. *Ecol. Lett.* 18, 1190–1197. doi:10.1111/ele.12498

Williams Richard, J., and Martinez, N. D. (2000). Simple rules yield complex food webs. *Nature* 404, 180–183. doi:10.1038/35004572

Wold, S. 1995. "Chemometric methods in molecular design methods and principles in medicinal chemistry," in *PLS for multivariate linear modeling*, H. van deWaterbeemd, Ed., pp.195–218. Verlag-Chemie,Weinheim, Germany.

Xu, D. L., Cai, Y., Jiang, H., Wu, X. Q., Leng, X., and An, S. Q. (2016). Variations of food web structure and energy availability of shallow lake with long-term eutrophication: A case study from Lake Taihu, China. *Clean. Soil Air Water* 44, 1306–1314. doi:10.1002/clen.201300837

Yang, Y., Chen, H., and Yang, Z. F. (2010). *Assessing changes of trophic interactions during once anthropogenic water supplement in Baiyangdian Lake. International Conference on Ecological Informatics and Ecosystem Conservation (ISEIS)*, 2. Beijing: Procedia Environmental Sciences, 1169–1179.

Yan, S. J., Wang, X., Zhang, Y. L., Liu, D., Yi, Y. J., Li, C. H., et al. (2020). A hybrid PCA–GAM model for investigating the spatiotemporal impacts of water level fluctuations on the diversity of benthic macroinvertebrates in Baiyangdian Lake, North China. *Ecol. Indic.* 116, 106459. doi:10.1016/j.ecolind.2020.106459

Yang, J., Strokal, M., Kroeze, C., Chen, X. J., Bai, Z. H., Li, H. B., et al. (2021). Seasonal river export of nitrogen to guanting and baiyangdian lakes in the hai He basin. *J. Geophys. Res. Biogeosci.* 126, 1–20. doi:10.1029/2020JG005689

Yang, W., and Yang, Z. F. (2014b). Effects of long-term environmental flow releases on the restoration and preservation of Baiyangdian Lake, a regulated Chinese freshwater lake. *Hydrobiologia* 730, 79–91. doi:10.1007/s10750-014-1823-7

Yang, W., and Yang, Z. F. (2014a). Integrating ecosystem-service tradeoffs into environmental flows decisions for Baiyangdian Lake. *Ecol. Eng.* 71, 539–550. doi:10.1016/j.ecoleng.2014.07.065

Yang, Y. H., and Tian, F. (2009). Abrupt change of runoff and its major driving factors in Haihe River Catchment, China. *J. Hydrol. X.* 374, 373–383. doi:10.1016/j.jhydrol.2009.06.040

Yang, Y. (2011). *Study on ecological water demand based on the dynamics of food web structure and function in the Baiyangdian wetland*. China: Beijing Normal University.

Yang, Y., Yin, X. A., Chen, H., and Yang, Z. F. (2014). Determining water level management strategies for lake protection at the ecosystem level. *Hydrobiologia* 738, 111–127. doi:10.1007/s10750-014-1923-4

Yang, Y., Yin, X. A., and Yang, Z. F. (2016). Environmental flow management strategies based on the integration of water quantity and quality, a case study of the Baiyangdian Wetland, China. *Ecol. Eng.* 96, 150–161. doi:10.1016/j.ecoleng.2015.12.018

Yletyinen, J., Bodin, Ö., Weigel, B., Nordström, M. C., Bonsdorff, E., and Blenckner, T. (2016). Regime shifts in marine communities: A complex systems perspective on food web dynamics. *Proc. R. Soc. B* 283 (1825), 20152569. doi:10.1098/rspb.2015.2569

Yuan, R. Q., Wang, S. Q., Wang, P., Song, X. F., and Tang, C. Y. (2017). Changes in flow and chemistry of groundwater heavily affected by human impacts in the Baiyangdian catchment of the North China Plain. *Environ. Earth Sci.* 76, 571. doi:10.1007/s12665-017-6918-9

Zeng, Y., Zhao, Y. W., and Qi, Z. F. (2021). Evaluating the ecological state of Chinese Lake Baiyangdian (BYD) based on ecological network analysis. *Ecol. Indic.* 127, 107788. doi:10.1016/j.ecolind.2021.107788

Zhang, J. H., Huang, T., Chen, L., Zhu, D. Z., Zhu, L. L., Feng, L. J., et al. (2020). Impact of the three gorges reservoir on the hydrologic regime of the river-lake system in the middle yangtze river. *J. Clean. Prod.* 258, 121004. doi:10.1016/j.jclepro.2020.121004

Zhang, P., Van Den Berg, R. F., Van Leeuwen, C. H. A., Blonk, B. A., and Bakker, E. S. (2018). Aquatic omnivores shift their trophic position towards increased plant consumption as plant stoichiometry becomes more similar to their body stoichiometry. *PLoS One* 13, e0204116–13. doi:10.1371/journal.pone.0204116

Zhang, X. X., Yi, Y. J., and Yang, Z. F. (2022). The long-term changes in food web structure and ecosystem functioning of a shallow lake: Implications for the lake management. *J. Environ. Manage.* 301, 113804. doi:10.1016/j.jenvman.2021.113804

Zhao, C. S., Yang, Y., Yang, S. T., Xiang, H., Ge, Y. R., Zhang, Z. S., et al. (2020). Effects of spatial variation in water quality and hydrological factors on environmental flows. *Sci. Total Environ.* 728, 138695. doi:10.1016/j.scitotenv.2020.138695

Zhao, C. S., Yang, Y., Yang, S. T., Xiang, H., Wang, F., Chen, X., et al. (2019). Impact of spatial variations in water quality and hydrological factors on the food-web structure in urban aquatic environments. *Water Res.* 153, 121–133. doi:10.1016/j.watres.2019.01.015

Zhao, Y., Yang, Z. F., and Li, Y. X. (2010). Investigation of water pollution in baiyangdian lake, China. *Procedia Environ. Sci.* 2, 737–748. doi:10.1016/j.proenv.2010.10.085

Zheng, L. I., Zhan, P. F., Xu, J. Y., Xu, L. G., Tan, Z. Q., and Wang, X. L. (2020). Aquatic vegetation dynamics in two pit lakes related to interannual water level fluctuation. *Hydrol. Process.* 34, 2645–2659. doi:10.1002/hyp.13757

Zhu, Y. Y., Jin, X., Tang, W. Z., Meng, X., and Shan, B. Q. (2019). Comprehensive analysis of nitrogen distributions and ammonia nitrogen release fluxes in the sediments of Baiyangdian Lake, China. *J. Environ. Sci.* 76, 319–328. doi:10.1016/j.jes.2018.05.024

frontiers | Frontiers in Environmental Science

TYPE Original Research
PUBLISHED 25 October 2022
DOI 10.3389/fenvs.2022.1017605

OPEN ACCESS

EDITED BY
Chunhui Li,
School of Environment, Beijing Normal University, China

REVIEWED BY
Leilei Bai,
Nanjing Institute of Geography and Limnology (CAS), Nanjing, China
Wei Guo,
Beijing University of Technology, China

*CORRESPONDENCE
Lulu Zhang,
zhanglulu@scu.edu.cn
Xueqin Gao,
gaoxueqin@scu.edu.cn

SPECIALTY SECTION
This article was submitted to Conservation and Restoration Ecology, a section of the journal Frontiers in Environmental Science

RECEIVED 12 August 2022
ACCEPTED 13 October 2022
PUBLISHED 25 October 2022

CITATION
Zhang Y, Gao X, Zhang L and He S (2022), Study on coal ash loaded nano iron filler to improve the efficient phosphorus removal of biological detention facility.
Front. Environ. Sci. 10:1017605.
doi: 10.3389/fenvs.2022.1017605

Study on coal ash loaded nano iron filler to improve the efficient phosphorus removal of biological detention facility

Yuxuan Zhang[1,2], Xueqin Gao[2]*, Lulu Zhang[3]* and Shunde He[4]

[1]West China School of Medicine, West China Hospital, Sichuan University, Chengdu, Sichuan, China, [2]College of Polymer Science and Engineering, Sichuan University, Chengdu, Sichuan, China, [3]College of Foreign Languages, Sichuan University, Chengdu, Sichuan, China, [4]College of Water Resource and Hydropower, Sichuan University, Chengdu, Sichuan, China

Bioretention cells are an important facility to solve the hydrological and non-point pollution problems in urban areas, especially phosphorus. In this paper, ceramsite composite was made from coal ash and modified by nano-iron through coprecipitation and reduction, which was used to remove the phosphorus in the water. The results of the characteristics of the ceramsite composite using scanning electron microscope showed that the surface of the ceramsite loaded with nano-iron became rougher and the iron nanoparticles were uniformly distributed on the surface, and there was no obvious agglomeration of nano-iron particles. The loading effect was good and the activity of the ceramsite was greatly improved. The results from the static and dynamic continuous experiments indicated that the modified ceramsite with nano-iron had a good removal effect on phosphorus, and the removal rate reached over 99%. The results of this study can provide a new way for the resource utilization of coal ash, and also inspires a new idea for the improvement of filler in bioretention facilities.

KEYWORDS

bioretention cells, coal ash, modified ceramsite, nano-iron particles, phosphorus removal

1 Introduction

The increases in impervious underlying surface in the process of urbanization have resulted in frequent urban waterlogging and a rapid increase in surface rainwater runoff (Solpuker et al., 2014; Xu et al., 2015). There are a large number of nutrients such as nitrogen (N) and phosphorus (P) from municipal garbage, waste water and atmospheric deposition in rainwater runoff, which aggravate the surface rainwater runoff pollution (Djukic et al., 2016; Chen et al., 2022). When these N and P pollutants entered the natural water body with rainwater runoff, they can cause eutrophication of water body (Kabenge et al., 2016; L. Li et al., 2021a; Wu et al., 2020). At the same time, surface runoff pollutants are characterized by strong randomness, wide sources, complex components and a wide range of pollution, making the pollution problem difficult to deal with. How to control the

runoff pollutants effectively in the urban area has become a hot research pot for protecting the water environment.

In recent years, the investigation of urban surface runoff pollution in China shows that phosphorus pollution in urban surface runoff is becoming increasingly serious (Luo et al., 2012). A series of low-impact development measures in the sponge city construction, such as the permeable pavement, constructed wetland, filtration system and bioretention cells, integrate flood peak flow regulation and runoff reduction as a whole, which can not only purify water quality and regulate rainwater runoff but also serve as urban landscape facilities to beautify the urban environment. Such measures are mainly based on the absorption and filtration of phosphorus from wastewater through plants, soil and filler. The composition and properties of fillers are the key factors in determining the phosphorus removal efficiency of surface runoff treatment facilities. However, the widely used filler is mainly sand and soil with low carbon content, and the filler layer's water purification effect is insignificant. Therefore, the optimization study of the filler layer is of great significance for the purification of surface runoff pollution (M. Zheng et al., 2022; Y. Zheng and Zhang, 2020).

Coal ash is a waste produced by coal-fired power generation in thermal power plants, which has a low recycling rate and will have an impact on the environment if no measures are taken to treat it (Z. Li et al., 2021b). However, research in recent years has found that coal ash has good phosphorus removal properties. Therefore, ceramsite sintered by coal ash to form a strong, non-clogging, easily recyclable, large particle material to remove phosphorus from wastewater has become a new method to use waste coal ash to remove P from surface runoff pollution. Compared with common phosphorus removal materials, nano-iron have the advantages of better phosphorus removal performance, high reaction efficiency and low-cost effectiveness, so the phosphorus removal effect of ceramsite made by coal ash can be further improved by loading nano-iron (Maamoun et al., 2018). However, the existence of large magnetic and van der Waals forces between the nano-iron makes it easy to agglomerate, and the small particle size of the nano-iron particles makes the material easy to be lost and difficult to be recovered in liquid, these problems and defects make it difficult to promote nano-iron in practical environmental engineering (Phenrat et al., 2007).

This work intends to further study the loading of nano-iron on the surface or well-developed pore structure of the ceramsite made by coal ash to avoid the agglomeration of nano-iron while increasing the contact area between nano-iron and pollutants, to improve the reactivity. And then, this paper intends to determine the phosphorus removal performance of modified coal ash ceramsite loaded with nano-iron and the effect of different laying thicknesses on the phosphorus removal effect through static and dynamic continuous experiments. On this basis, it is also investigated the mechanism of phosphorus removal by modified ceramsite.

This work proposes a new way for the utilization of coal ash and provides a new idea for the improvement of fillers in the treatment of surface rainwater runoff in sponge city construction.

2 Materials and methods

2.1 Materials

2.1.1 Preparation of coal ash sintered ceramsite

Coal ash sintered ceramsite is made of coal ash as the main raw material, bentonite as binder and pulverized coal as pore-making agent sintered at high temperature. It is a large particle material with high strength, not easy to block, easy to recover, and can be recycled. In this study, the reasonable dosage ranges of coal ash, bentonite and pulverized coal are 140–180 g, 120–160 g, and 30–50 g, respectively. On this basis, orthogonal experimental design was used to optimize the ratio scheme of coal ash, bentonite and pulverized coal. Finally, the ratio of the three materials was determined as 50% of coal ash, 37.5% of bentonite and 12.5% of pulverized coal respectively. According to the proportioning scheme, coal ash, bentonite and

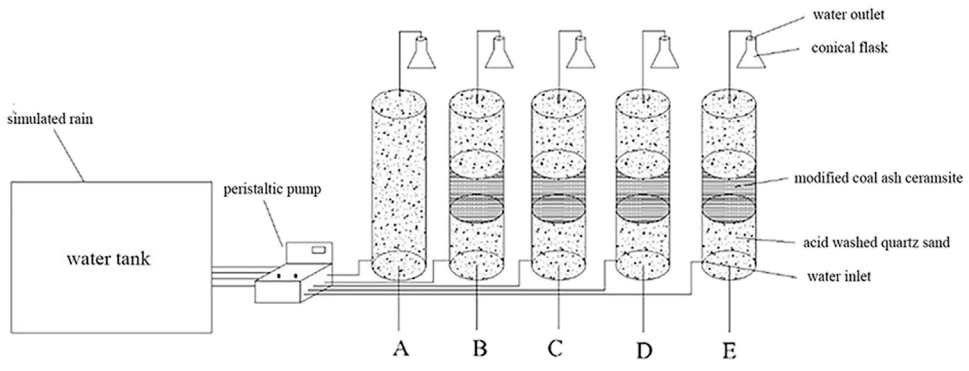

FIGURE 1
Diagram of the cylindrical experimental setup.

TABLE 1 Results of isothermal adsorption experiment.

C_0 (mg/L)	1.95	4.04	6.04	7.8	9.87	12.1
C_e (mg/L)	0.501	1.64	3.63	5.42	7.54	9.68
q_e (mg/kg)	108.675	180	180.75	178.5	174.75	181.5

pulverized coal are mixed evenly, and then a certain amount of water is added according to the solid-water ratio of 3:1 to stir into a uniform liquid shape, which is then put into a small granulator to form particles with a diameter of 2–3 mm and a length of about 5–10 mm. The formed ceramite was air dried in natural state for 2 h and then put into Muffle furnace for preheating at 400°C for 15 min and sintering at 1,000°C for 45 min. After natural cooling in the furnace, the pulverized coal ash ceramite needed in this study was obtained.

2.1.2 Modification of ceramsite

The coal ash ceramsite was modified by hydrochloric acid, sodium hydroxide, ferric chloride, sulfuric acid and loaded nano iron. It was found that the adsorption and phosphorus removal effect of the ceramic particles modified by sodium hydroxide was not good, and the effect of the ceramic particles modified by loaded nano iron was the best. The main methods for the preparation of loaded iron nanoparticles are gas-phase reduction, liquid-phase reduction, sol-gel method and thermal decomposition carbonyl iron method. Among them, the liquid-phase reduction method and the pyrolysis carbonyl iron method are the most widely used. In addition, the liquid phase reduction method has the advantages of lower cost, higher yield, good loading effect and easy application. Therefore, this experiment used the liquid-phase reduction method to modify the coal ash ceramic pellets with loaded iron nanoparticles. The liquid-phase reduction method is to reduce the low-valent iron salts by strong reducing agents and reduce the iron ions to iron monomers loaded on the solid particles.

The experimental loaded iron nanomodified ceramic pellets were prepared as follows: $FeSO_4 \bullet 7H_2O$ with concentrations of 0.04 mol/L, 0.05 mol/L, 0.06 mol/L, 0.07 mol/L, 0.08 mol/L, 0.09 mol/L, and 0.1 mol/L (seven concentration gradients) and 1 g of ascorbic acid as a stabilizer were added to seven beakers filled with 100 ml distilled water. Then, $NaBH_4$ solution was dropped into the beaker through a constant pressure funnel to reduce iron ions, the dropping rate was controlled at about 2 drops/sec, the boron/iron (B/Fe) mass ratio was required to be 3:1, and the glass rod was used for continuous stirring during the reaction. After the dropwise addition of the $NaBH_4$ solution is completed, continue to stir the mixed solution for 5 min to complete the reaction. Then, the product was washed 3 times with anhydrous ethanol, and the resultant product was ceramsite loaded with nano-iron.

The modified ceramsite was used to remove phosphorus from simulated wastewater, and the adsorption capacity of modified coal ash ceramsite for phosphorus was compared to determine the optimum modification concentration of the modifier. A conical flask was filled with 150 ml of simulated wastewater containing phosphorus with 1 mg/L, and 5 g of coal ash ceramsite modified by different concentrations. 7 conical flasks were placed in a constant temperature oscillator and allowed to oscillate at a constant temperature of 25°C and an oscillation speed of 250 r/min for 4 h. After the reaction was completed, the solution containing phosphorus was aspirated with a syringe. The phosphorus concentration in the solution was measured after the solution containing phosphorus was filtered through a filter membrane, and the phosphorus removal rate was calculated by Eq. 1.

$$R = \frac{C_0 - C}{C_0} \times 100\% \quad (1)$$

where R represents each of the characteristics of pollutants' removal rates, C_0 represents initial heavy metal ion concentration, and C represents sampling point concentration.

The results showed that when the ceramic pellets were modified with iron nanoparticles loaded with ascorbic acid as a stabilizer, the removal rates were all stable above 99%.

2.2 Cylindrical experiment method of modified coal ash ceramsite

In this study, a cylindrical experimental device was used to explore the phosphorus removal effect of loaded nano-iron ceramsite as medium filler. The experimental device consisted of four parts: digital peristaltic pump, water tank, experimental column and rubber tube. The experimental column was a glass column with 30 cm height, 5 cm inner diameter and 0.5 cm wall thickness. The

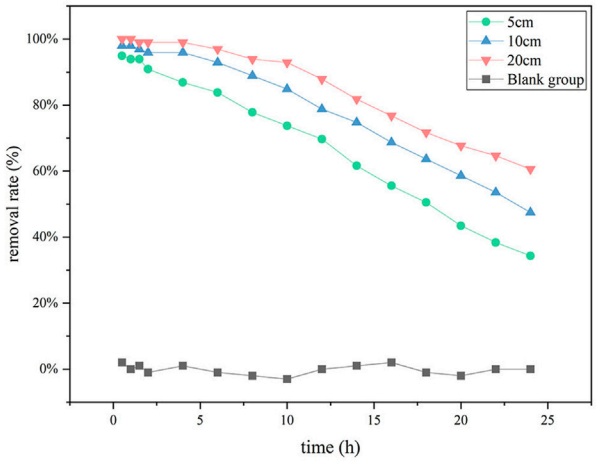

FIGURE 2
Dynamic phosphorus removal effect of ceramsite loaded with nano-iron of different thickness.

bottom of the experimental column is provided with a water inlet, and the top is provided with a water outlet. The water tank, peristaltic pump and experimental column are connected by rubber tubing. The experimental setup is shown in Figure 1.

To study the phosphorus removal effect of nano-iron ceramsite loaded with different thicknesses, nano-iron ceramsite loaded with different thicknesses was added to the experimental columns numbered A, B, C, and D, respectively. The test column A was set as the blank control group, in which only three layers of acid-washed quartz sand were added, 300 g for each layer. Test column B was successively added with 375 g pickling quartz sand, 83 g loaded nano-iron ceramsite and 375 g pickling quartz sand, in which the thickness of the loaded nano-iron ceramsite was 5 cm. Test column C was successively added with 300 g pickling quartz sand, 167 g loaded with nano-iron ceramsite and 300 g pickling quartz sand, in which the thickness of the loaded nano-iron ceramsite was 10 cm. Test column D was successively supplemented with 150 g pickling quartz sand, 334 g nano-iron ceramsite and 150 g pickling quartz sand, in which the thickness of nano-iron ceramsite loaded was 20 cm. A peristaltic pump was used to feed self-prepared simulated wastewater with phosphorus concentration of 1 mg/L into the lower part of the cylindrical tube at the speed of 10 ml/min. The experimental solution was obtained from the upper outlet at 0.5, 1, 1.5, 2, 4, 6, 8, 10, 12, 14, 16, 18, 20, 22, and 24 h elapsed time. The phosphorus ion concentration in the solution was measured, and the phosphorus removal rate was calculated by Eq. 1, to explore the changing trend of phosphorus removal rate with time of nano-iron ceramsite loaded with different thicknesses.

2.3 Method of the mechanism of phosphorus removal from water by modified coal ash ceramsite

The adsorption isotherm model and adsorption kinetics model were used to fit the adsorption process of phosphorus on the ceramsite loaded with nano-iron and judge the adsorption type and the maximum adsorption capacity. Field emission scanning electron microscope (SEM) (JEOL, Japan) was used and the energy spectrum analysis was performed, to further analyze and explain the loading effect of coal ash ceramsite and the main reaction mechanism of phosphorus removal of coal ash ceramsite loaded with nano-iron.

2.3.1 Adsorption isotherm research method

Six conical bottles were taken out, and 150 ml phosphorus-containing wastewater with concentrations of 2 mg/L, 4 mg/L, 6 mg/L, 8 mg/L, 10 mg/L, and 12 mg/L was added to each conical bottle, then 2 g ceramsite loaded with nano-iron were added respectively. The six conical bottles were put into a thermostatic shaking chamber, and the conical bottles were kept at a constant temperature of 25°C. The oscillation speed was 250r/min for 24 h. After the reaction, the concentration of residual phosphorus in the solution was determined, and the adsorption capacity of phosphorus on the ceramsite loaded with nano-iron was calculated. After the reaction, the equilibrium concentration of phosphorus (C_e) in each solution was determined, and the equilibrium adsorption capacity (q_e) was calculated according to Eq. 2.

$$q_e = \frac{V(C_0 - C_e)}{m} \tag{2}$$

Where q_e represents the adsorption at equilibrium, mg/g; V represents the volume of adsorbent solution, L; C_0 represents the initial mass concentration of adsorbent in solution, mg/L; C_e represents the concentration of solution at equilibrium, mg/L; m represents the mass of loaded iron nanoparticles injected, kg.

The Langmuir isothermal adsorption model and Freundlich isothermal adsorption model were used to fit the equilibrium concentration (C_e) and equilibrium adsorption quantity (q_e) (Li et al., 2020), and the determination coefficient (R^2) was calculated. The higher the determination coefficient, the more suitable the model was to describe the adsorption equilibrium process. The Langmuir isothermal adsorption model and Freundlich isothermal adsorption model are shown in Eq. 3 and Eq. 4.

$$\frac{C_e}{q_e} = \frac{1}{(bQ_m)} + \frac{C_e}{Q_m} \tag{3}$$

$$ln\, q_e = ln\, K + \frac{ln\, C_e}{n} \tag{4}$$

Where Q_m is the maximum saturated adsorption at equilibrium, mg/g; b is the Langmuir equation adsorption equilibrium

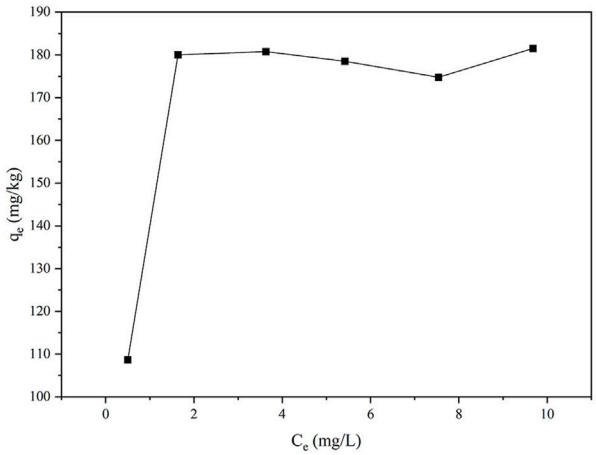

FIGURE 3
Adsorption isotherms of phosphorus on ceramsite loaded with nano-iron.

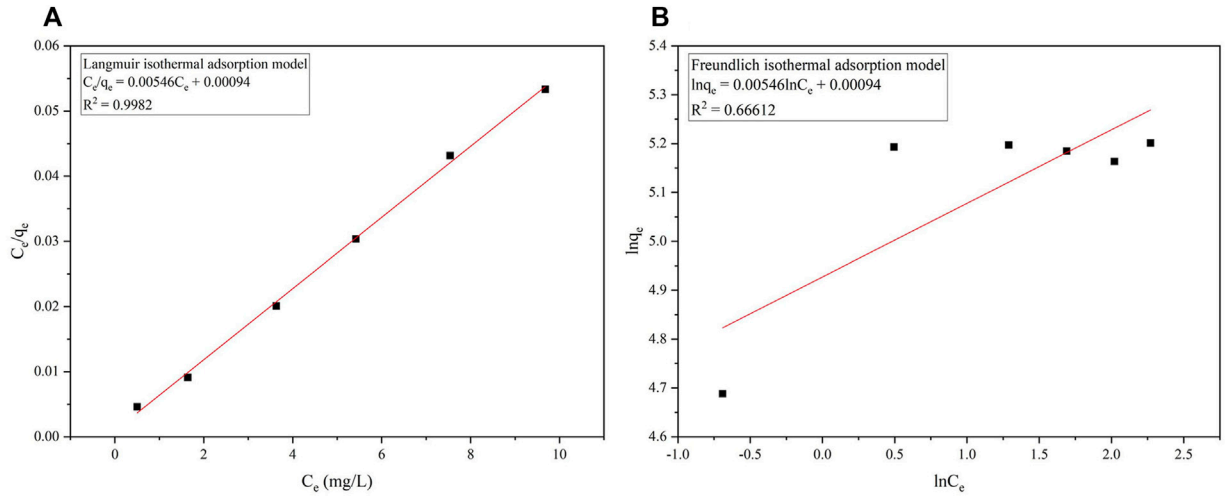

FIGURE 4
Fitting of the isothermal adsorption models. **(A)** the Langmuir isothermal adsorption model; **(B)** the Freundlich isothermal adsorption model.

constant, L/mg; K is the Freundlich isothermal adsorption equation constant; n is the adsorption intensity parameter.

2.3.2 Adsorption kinetics research method

In the experiment, ceramsite loaded with nano-iron was used as adsorbent. Nine conical bottles were taken out, and 150 ml phosphorus-containing wastewater with a concentration of 2 mg/L was added to each conical bottle, and then 2 g ceramsite loaded with nano-iron were added respectively. The 9 conical bottles were put into a constant temperature oscillation chamber, and the conical bottles were allowed to oscillate at a constant temperature of 25°C and an oscillation speed of 250r/min. The conical flask was removed at the oscillation adsorption time of 10 min, 30 min, 1, 1.5, 2, 4, 6, 8 , and 24 h, respectively, and the phosphorus-containing solution was aspirated with a syringe and filtered through a filter membrane to determine the phosphorus concentration C_t in the solution, and the adsorption amount q_t of phosphorus by the loaded iron nanoparticles at different adsorption times was calculated by Eq. 5.

$$q_t = \frac{V(C_0 - C_t)}{m} \tag{5}$$

Where q_t is the adsorption capacity at time t, mg/g; C_t is the concentration of solution at time t, mg/L; m is the mass of loaded iron nanoparticles injected, kg.

The pseudo-first-order kinetic model, pseudo-second-order kinetic model, and Elovich kinetic model were used to fit the data according to the adsorption quantity q_t and equilibrium adsorption quantity q_e of loaded nano-iron ceramsite at different times (Largitte and Pasquier, 2016; Li et al., 2020). By comparing the determination coefficient (R^2), it can be concluded which model can fully reflect the kinetic mechanism of phosphorus adsorption on nano-sized iron ceramsite supported by adsorbent. The pseudo-first-order kinetic model, pseudo-second-order kinetic model, and Elovich kinetic model are shown in Eq. 6, Eq. 7, and Eq. 8.

$$ln(q_e - q_t) = ln\, q_e - k_1 t \tag{6}$$

$$\frac{t}{q_t} = \frac{1}{(k_2 q_e^2)} + \frac{t}{q_e} \tag{7}$$

$$q_t = \frac{1}{\beta} ln(\alpha\beta) + \frac{1}{\beta} ln\, t \tag{8}$$

Where k_1 is the quasi-first-order adsorption rate constant, g·mg^{-1}·min^{-1}; k_2 is the quasi-second-order adsorption rate constant, g·mg^{-1}·min^{-1}; α is the initial adsorption rate constant of the Elovich kinetic model, g·mg^{-1}·min^{-1}; β is the desorption constant related to the surface coverage and adsorption activation energy, g/mg; t is the adsorption time, min.

2.3.3 Material characterization and energy spectrum analysis method

After confirming the feasibility of ceramsite loaded with nano-iron as filler, a field emission scanning electron microscope was used to obtain the scanning electron

TABLE 2 Fitting results of adsorption isotherm model.

Adsorption isotherm model	Fitting parameters		R^2
Langmuir isothermal adsorption model	Q_m	183.15	0.9982
	b	5.81	
Freundlich isothermal adsorption model	k	138.1	0.663
	n	6.653	

TABLE 3 The adsorption capacity of phosphorus on ceramsite loaded with nano-iron by different adsorption time.

t (min)	10	30	60	90	120	240	360	480	1,440
C_0 (mg/L)	1.95	1.95	1.95	1.95	1.95	1.95	1.95	1.95	1.95
C_t (mg/L)	1.669	1.553	1.409	1.263	1.141	1.04	0.817	0.608	0.501
q_t (mg/g)	21.08	29.78	40.58	51.53	60.68	68.25	84.98	100.7	108.7

microscope images of the coal ash ceramsite unloaded with nano-iron and the coal ash ceramsite loaded with nano-iron before and after the adsorption of phosphorus, and the energy spectrum analysis was performed, to further analyze and explain the loading effect of coal ash ceramsite and the main reaction mechanism of phosphorus removal of coal ash ceramsite loaded with nano-iron.

3 Results and discussion

3.1 Cylindrical experiment of modified coal ash sintered ceramsite

Based on the phosphorus concentration C_t detected at different times and the phosphorus concentration C_0 at the

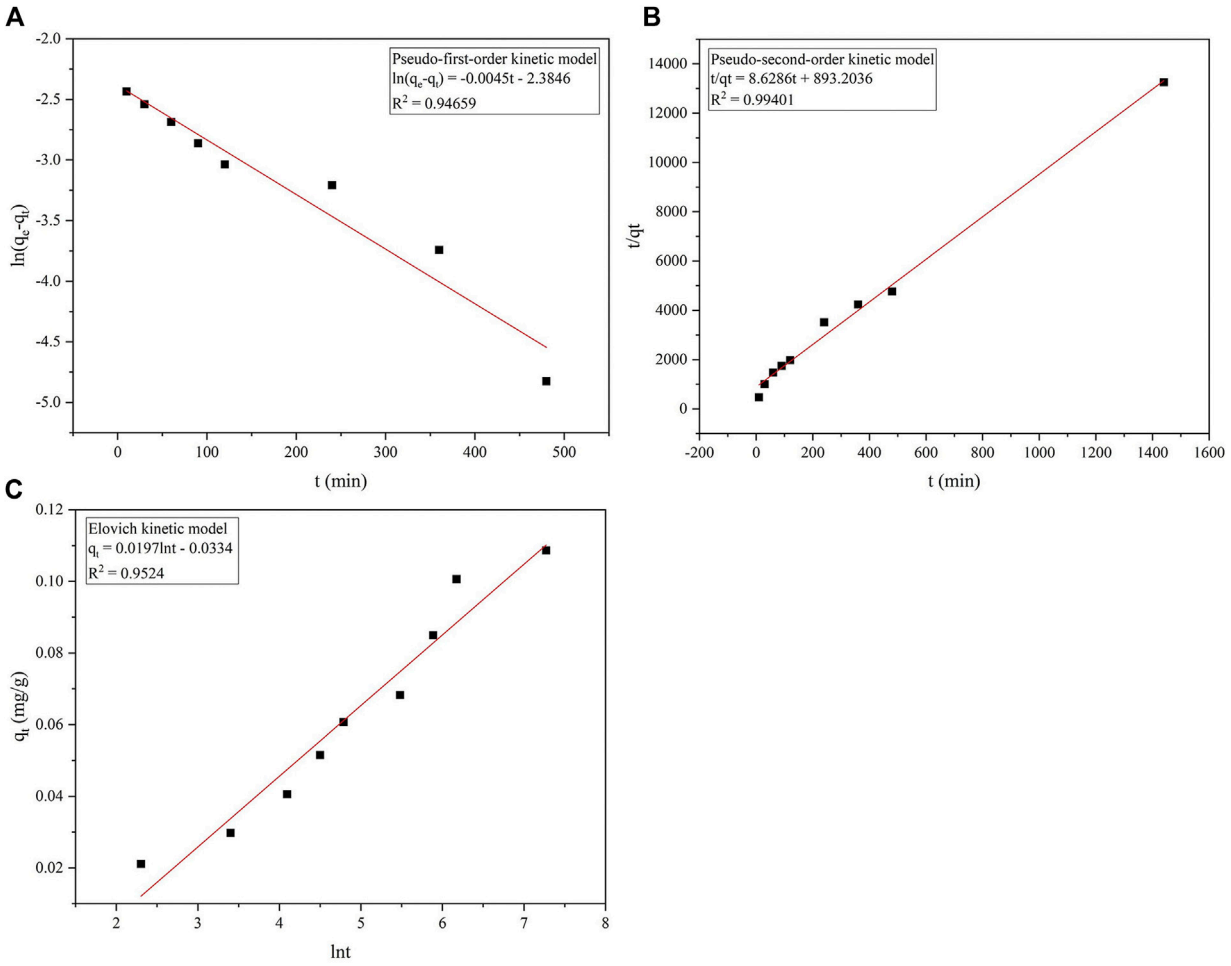

FIGURE 5
Fitting of the adsorption kinetic model of phosphorus on the ceramsite loaded with nano-iron. **(A)** the pseudo-first-order kinetic model; **(B)** the pseudo-second-order kinetic model; **(C)** the Elovich kinetic model.

initial time, the phosphorus removal rate of nano-ferric coal ash ceramsite loaded with different thicknesses varied with time. As shown in Figure 2, with the increase in thickness of coal ash ceramsite loaded with nano-sized iron, the phosphorus removal rate is increased. This is mainly because with the increase of the thickness of the loaded nano-iron ceramsite, the content of iron ions in the solution also increases, so that the active site increases (Tan et al., 2015), which makes the contact space between phosphate ions and nano-iron increase, leading to the increase of phosphorus removal efficiency in the solution. At the same time, it can be seen from Figure 2 that the phosphorus removal rate of coal ash ceramsite loaded with nano-iron with different thicknesses gradually decreases over time, and the decreasing slope of the phosphorus removal rate decreases with the increase of thickness. The reason is that at the initial moment, there are many adsorption sites on the loaded nano-iron ceramsite, and the phosphorus adsorption rate is high. With the continuous occupation of the adsorption sites, the phosphorus removal effect of the loaded nano-iron ceramsite is gradually weakened.

3.2 Study on the mechanism of phosphorus removal from water by modified coal ash ceramsite

3.2.1 Study on adsorption isotherms

According to the concentration of residual phosphorus in the solution measured after the reaction of wastewater containing phosphorus of different concentrations, the adsorption capacity of ceramsite loaded with nano-iron on phosphorus was calculated as shown in Table 1 and Figure 3 was drawn according to Table 1.

As can be seen from Figure 3, with the progress of adsorption, the active sites in the adsorbent are occupied, the active sites in the adsorbent are occupied and it becomes more difficult for the adsorbent molecules to contact the active sites on the surface, and the adsorption thus gradually tends to equilibrium. Langmuir isothermal adsorption model and Freundlich isothermal adsorption model were used to fit the adsorption isotherms respectively, and the fitting results were shown in Figure 4 and Table 2.

It can be seen from Figure 4 that the determination coefficient of 0.99 fitted by the Langmuir isothermal adsorption model is much higher than that fitted by the Freundlich isothermal adsorption model of 0.66, indicating that the Langmuir isothermal adsorption model can better describe the process of phosphorus adsorption by ceramsite loaded with nano-iron and that the adsorption of phosphorus on the surface of ceramsite loaded with nano-iron is single-layer adsorption. Surface adsorption plays a leading role in the adsorption process.

3.2.2 Study on adsorption kinetics

According to the concentration of phosphorus in the solution measured at different time points in the oscillating adsorption process, the adsorption capacity of phosphorus on the ceramsite loaded with nano-iron at different adsorption times was calculated as shown in Table 3.

The experimental results were fitted with the quasi-first-order kinetic model, quasi-second-order kinetic model and Elovich model respectively, and the fitting results were shown in Figure 5 and Table 4.

According to Figure 5A, the determination coefficient R^2 of quasi-first-order kinetic model fitting is 0.947. The equilibrium adsorption capacity calculated from the equation intercept is 92.13 mg/kg, while the experimentally measured equilibrium adsorption capacity is 108.68 mg/kg, there is a certain gap between the two. Therefore, the quasi-first-order kinetic model is not applicable to fit the adsorption of phosphorus by ceramsite loaded with nano-iron in this experiment. Figure 5B shows that the determination coefficient of the quasi-second-order kinetic model is as high as 0.994. The equilibrium adsorption capacity of ceramsite loaded with nano-iron simulated by the quasi-second-order dynamics model is 115.89 mg/kg, which has a small difference from the experimental equilibrium adsorption capacity of 108.86 mg/kg, indicating that the quasi-second-order kinetic model can be used to estimate the equilibrium adsorption capacity of ceramsite loaded with nano-iron to phosphorus. The model shows that the adsorption process of phosphorus on the ceramsite loaded with nano-iron is monolayer chemisorption. It can be seen from Figure 5C that the determination coefficient of the Elovich model is 0.952, and the correlation is between the quasi-second-order kinetic model and the quasi-first-order kinetic model.

In summary, it is concluded that the quasi-second-order kinetic model has the best correlation, and the equilibrium adsorption calculated according to the fitted straight line is the closest to the measured value in the experiment, indicating that the adsorption

TABLE 4 Fitting results of adsorption kinetic model.

Adsorption kinetic model	Fitting parameters		R^2
pseudo-first-order kinetic model	q_e	92.13	0.9466
	k_1	−0.0045	
pseudo-second-order kinetic model	q_e	115.89	0.9941
	k_2	0.0834	
Elovich kinetic model	α	0.0036	0.9524
	β	50.76	

process of the ceramsite loaded with nano-iron for phosphorus is the most suitable for use. According to the quasi-second-order kinetic model, the adsorption rate of phosphorus on the ceramsite loaded with nano-iron is proportional to the square of the unoccupied active sites on its surface.

3.2.3 Material characterization and energy spectrum analysis

The comparison of scanning electron microscope before and after phosphorus adsorption is illustrated in the following image.

As can be seen from Figure 6, the surface of the coal ash ceramsite was flat, smooth and dense when they were not loaded with nano-iron. After the coal ash ceramsite was loaded with nano-iron, the surface of the ceramsite became rough, and the nano-iron particles were uniformly loaded on the surface of the ceramsite with a particle size of about 20–50 nm. There was no obvious agglomeration phenomenon of nano-iron, and the loading effect is good, which improved the material activity. The comparison shows the changes in the ceramsite loaded with nano-iron after the adsorption of phosphorus. With the adsorption of phosphorus by ceramsite loaded with nano-iron, the morphology of nano-iron changed greatly, some nano-iron particles disappeared and many amorphous precipitates appeared, which are supposed to be $Fe(OH)_2$ and $Fe(OH)_3$ produced by zero-valent iron during the reaction process.

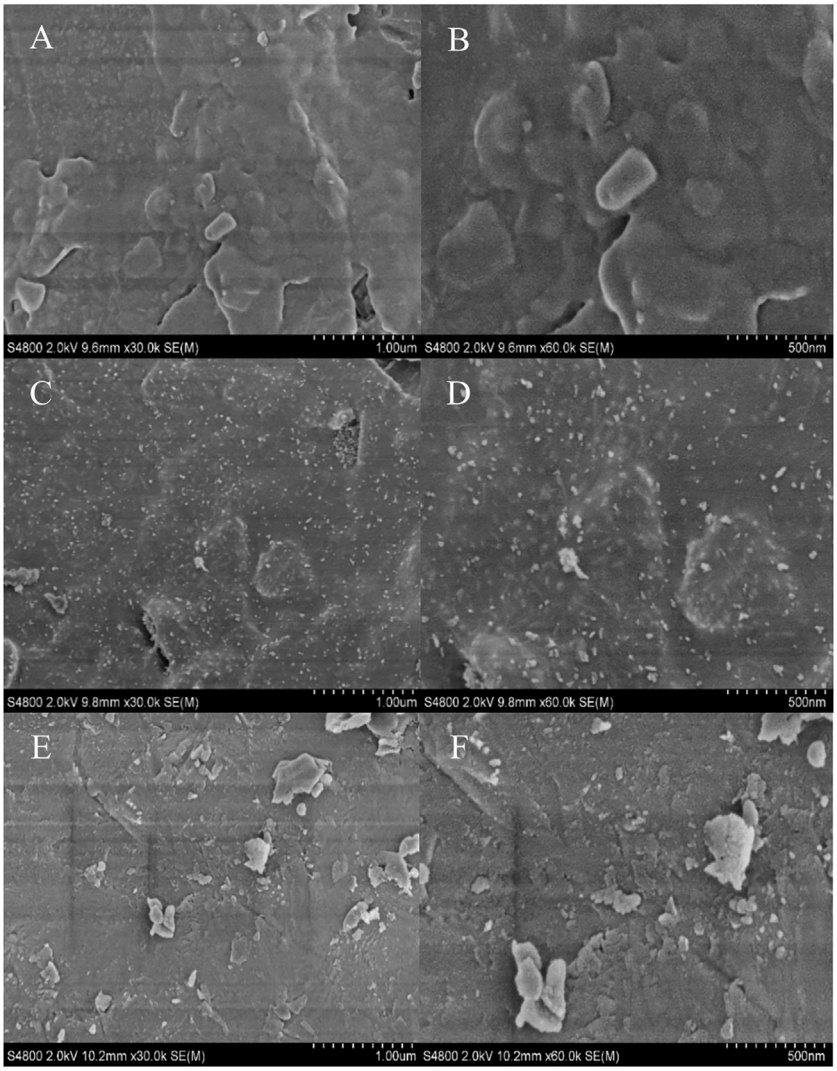

FIGURE 6
Comparison of scanning electron microscope before and after phosphorus adsorption **(A)** coal ash ceramsite unloaded with nano-iron (1 μm); **(B)** coal ash ceramsite unloaded with nano-iron (500 nm); **(C)** coal ash ceramsite loaded with nano-iron before the adsorption of phosphorus (1 μm); **(D)** coal ash ceramsite loaded with nano-iron before the adsorption of phosphorus (500 nm); **(E)** coal ash ceramsite loaded with nano-iron after the adsorption of phosphorus (1 μm); **(F)** coal ash ceramsite loaded with nano-iron after the adsorption of phosphorus (500 nm).

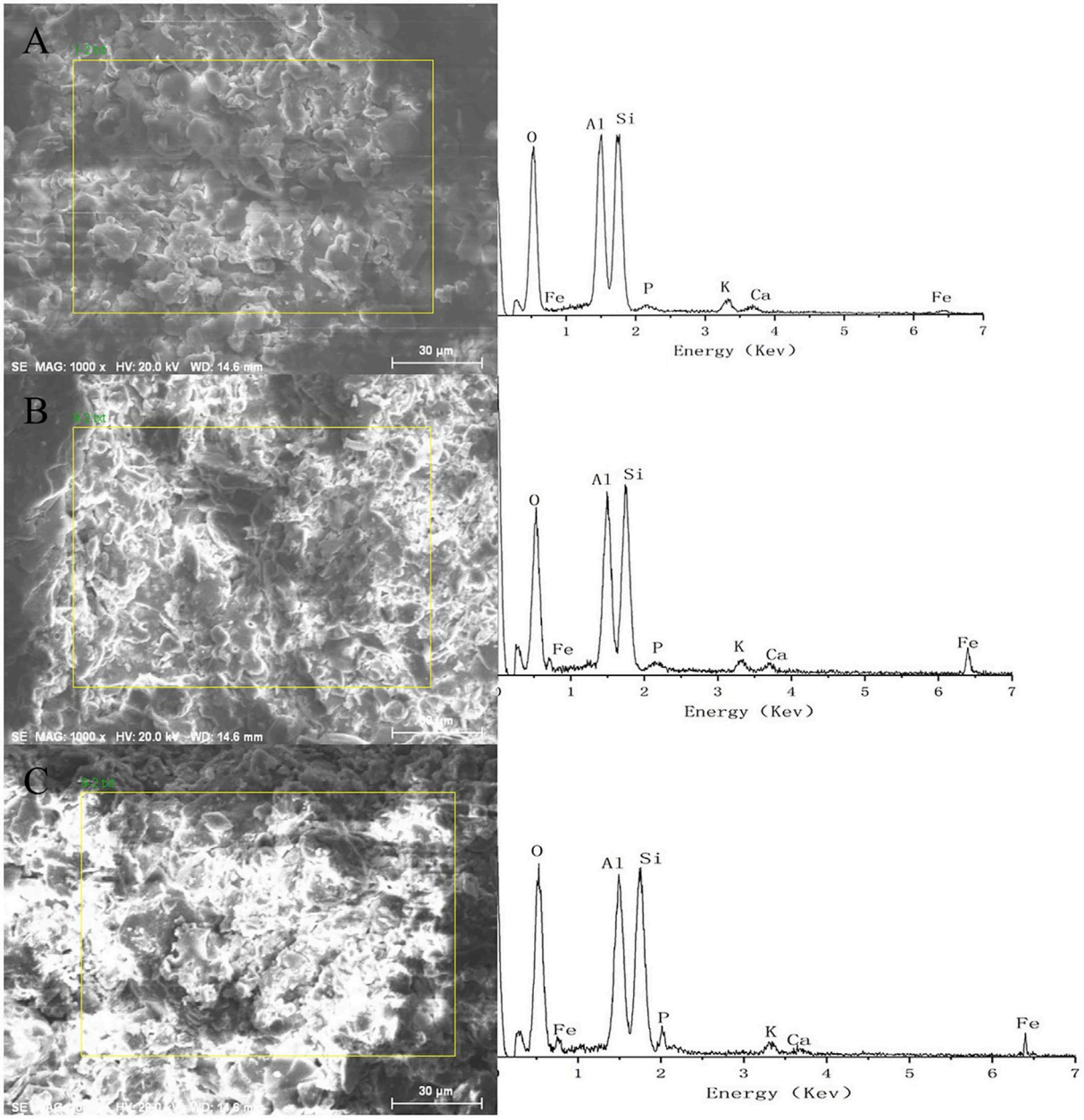

FIGURE 7
Comparison of energy spectrum analysis diagram before and after phosphorus adsorption **(A)** coal ash ceramsite unloaded with nano-iron; **(B)** coal ash ceramsite loaded with nano-iron before the adsorption of phosphorus; **(C)** coal ash ceramsite loaded with nano-iron after the adsorption of phosphorus.

It can be seen from Figure 7 that the main elements in the coal ash ceramsite are oxygen (O), aluminum (Al) and silicon (Si). The iron element in the ceramsite increased after the loading of nano-iron, indicating that nano-iron was loaded on the ceramsite. By comparison, it can be seen that the O and P elements in the ceramsite loaded with nano-iron increased after the adsorption of phosphorus, indicating that the ceramsite loaded with nano-iron has an obvious adsorption effect on phosphorus.

The elemental fractions of iron in the complete spectrum were amplified by X-viewer software to obtain the spectrum of iron in ceramsite loaded with nano-iron before and after the adsorption of phosphorus, as shown in Figures 8, 9.

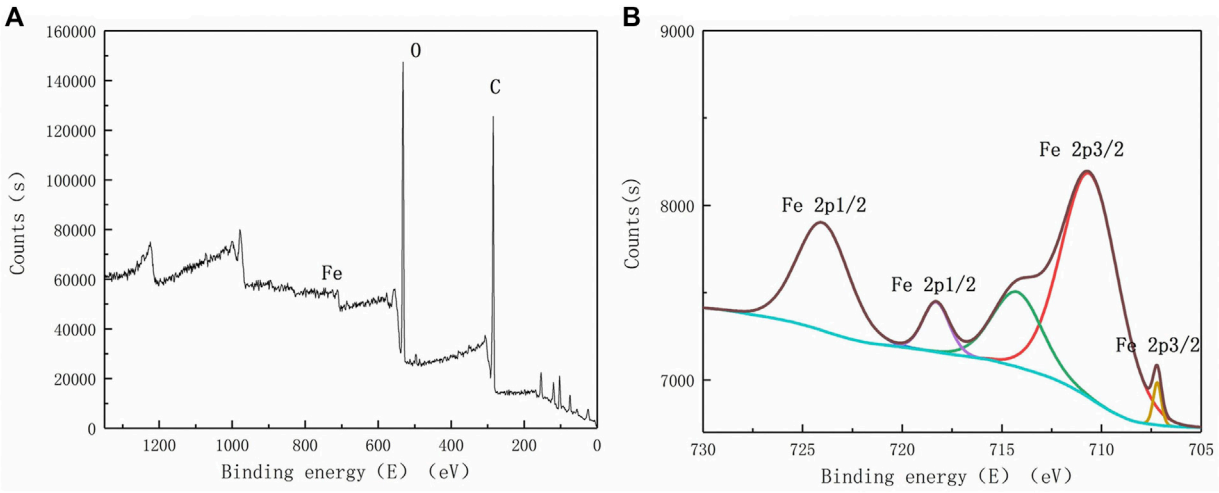

FIGURE 8
X-ray photoelectron spectroscopy before phosphorus adsorption **(A)** complete spectrum; **(B)** enlarged spectrum of Fe.

As can be seen from Figure 8, the main elements contained in the coal ash ceramsite loaded with nano-iron are carbon (C) and oxygen (O). In addition, the iron element is also observed, which is not prominent in the complete spectrum. The iron element mainly contains five peaks, among which the characteristic peaks of 707.20eV and 718.30eV correspond to electron binding energy of Fe2p3/2 and Fe2p1/2, characteristic peaks of 710.60eV correspond to the electron binding energy of Fe_3O_4, and characteristic peaks of 714.23eV and 724.00eV correspond to electron binding energy of Fe(III) Fe2p3/2 and Fe2p1/2, inferring that there are iron oxides in the coal ash ceramsite loaded with nano-iron.

By comparing Figures 8, 9, it can be found that the photoelectronic characteristic peak near 707.20eV disappears, and the position of the binding energy of other peaks changes, indicating that nano-iron reacted to produce other substances. X-ray photoelectron spectroscopy scanning of ceramsite loaded with nano-iron showed that it was partially oxidized to produce iron oxide, and the nano-iron loaded on the ceramsite adsorbed phosphorus to produce FeOOH, $FePO_4$, $Fe(OH)_3$ and so on. It can be inferred that the main reactions that occurred in the removal of phosphorus by ceramsite loaded with nano-iron were chemical precipitation, adsorption and co-precipitation.

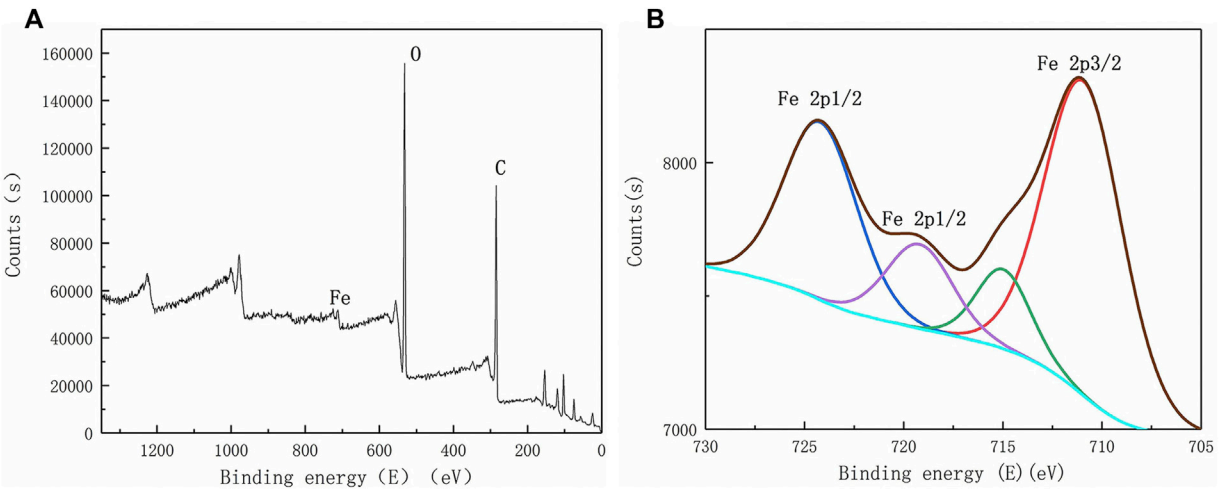

FIGURE 9
X-ray photoelectron spectroscopy after phosphorus adsorption **(A)** complete spectrum; **(B)** enlarged spectrum of Fe.

4 Conclusion

In this paper, different modifiers were used to modify the coal ash ceramsite at different concentrations to compare their static adsorption capacity of phosphorus and to determine the optimum modification concentration of the modifiers. Then the dynamic removal effect of coal ash ceramsite modified by different modifiers and ceramsite loaded with nano-iron of different thicknesses was studied by dynamic cylinder experiments. Scanning electron microscope (SEM) and X-ray photoelectron spectroscopy (XPS) were used to characterize and analyze the material, so as to analyze the phosphorus removal mechanism of ceramsite loaded with nano-iron. The main conclusions of this paper are as follows:

(1) The most effective modification method for coal ash ceramsite is the loading of nano-iron for modification, and the removal rates of phosphorus were all stable at over 99% when ascorbic acid was used as the stabilizer.
(2) The maximum removal rate of phosphorus by ceramsite loaded with nano-iron was 98.0% after 0.5 h from the beginning of the dynamic continuous experiment. As time increased, phosphorus's removal effect decreased, and the removal rate decreased to 47.5% after 24 h of the experiment. Under the condition of ceramsite loaded with different thicknesses of nano-iron, the phosphorus removal rates decreased gradually with time, and the decreasing slope of removal rate decreased with the increase of thickness.
(3) The adsorption process of the ceramsite loaded with nano-iron to phosphorus belongs to the uniform monomolecular layer of chemical adsorption on the surface. And the adsorption rate of the ceramsite loaded with nano-iron to phosphorus is proportional to the square of the unoccupied adsorption sites on the iron powder. The nano-iron particles were uniformly loaded on the surface of the coal ash ceramsite and no obvious agglomeration phenomenon was observed. With the adsorption of phosphorus by ceramsite loaded with nano-iron, some nano-iron particles disappeared and many amorphous precipitates appeared. At the same time, iron-nanoparticles were partially oxidized before adsorption to generate iron oxides, which produced $FePO_4$, FeOOH, $Fe(OH)_3$ and so on after adsorption of phosphorus. It can be inferred that the main reactions that occurred in the removal of phosphorus by ceramsite loaded with nano-iron were chemical precipitation, adsorption and co-precipitation.

If the loaded nano-iron ceramsite is applied to practical applications, we still need to consider some problems, such as further improving the load rate and load strength of nano-iron, expanding the study of material laying, material recovery, material recycling and reducing secondary pollution.

Data availability statement

The original contributions presented in the study are included in the article/Supplementary Material, further inquiries can be directed to the corresponding authors.

Author contributions

XG contributed to the conception of the study and provided financial support. YZ and SH performed the experiment and the data analyses. YZ and LZ contributed significantly to the analysis and manuscript preparation. YZ wrote the manuscript. All authors approved the final draft.

Funding

This study was funded by the Major Scientific and Technological Special Program of Sichuan Province, China (2018SZDZX0027 and 2019-YF09-00081-SN).

Conflict of interest

The authors declare that the research was conducted in the absence of any commercial or financial relationships that could be construed as a potential conflict of interest.

Publisher's note

All claims expressed in this article are solely those of the authors and do not necessarily represent those of their affiliated organizations, or those of the publisher, the editors and the reviewers. Any product that may be evaluated in this article, or claim that may be made by its manufacturer, is not guaranteed or endorsed by the publisher.

References

Chen, X., Wang, Y., Bai, Z., Ma, L., Strokal, M., Kroeze, C., et al. (2022). Mitigating phosphorus pollution from detergents in the surface waters of China. *Sci. Total Environ.* 804, 150125. doi:10.1016/j.scitotenv.2021.150125

Djukic, A., Lekic, B., Rajakovic-Ognjanovic, V., Veljovic, D., Vulic, T., Djolic, M., et al. (2016). Further insight into the mechanism of heavy metals partitioning in stormwater runoff. *J. Environ. Manage.* 168, 104–110. doi:10.1016/j.jenvman.2015.11.035

Kabenge, M., Wang, H., and Li, F. (2016). Urban eutrophication and its spurring conditions in the murchison bay of Lake victoria. *Environ. Sci. Pollut. Res.* 23, 234–241. doi:10.1007/s11356-015-5675-0

Largitte, L., and Pasquier, R. (2016). A review of the kinetics adsorption models and their application to the adsorption of lead by an activated carbon. *Chem. Eng. Res. Des.* 109, 495–504. doi:10.1016/j.cherd.2016.02.006

Li, L., Wu, L., Yang, L., Liu, C., Li, J., and Li, N. (2021a). Combined impact of organic matter, phosphorus, nitrate, and ammonia nitrogen on the process of blackwater. *Environ. Sci. Pollut. Res.* 28, 32831–32843. doi:10.1007/s11356-021-13050-1

Li, W., Luo, S., Ma, H., Yi, F., Li, Z., Guo, W., et al. (2020). Adsorption kinetics and isothermal adsorption model of crystal violet on modified red mud. *IOP Conf. Ser. Earth Environ. Sci.* 508, 012151. doi:10.1088/1755-1315/508/1/012151

Li, Z., Qian, W., Chen, Y., Xu, P., Li, J., and Yang, J. (2021b). A new treasure in industrial solid waste—Coal fly ash for effective oil/water separation. *J. Taiwan Inst. Chem. Eng.* 118, 196–203. doi:10.1016/j.jtice.2020.12.026

Luo, Z., Wang, T., Gao, M., Tang, J., and Zhu, B. (2012). Stormwater runoff pollution in a rural township in the hilly area of the central Sichuan Basin, China. *J. Mt. Sci.* 9, 16–26. doi:10.1007/s11629-012-2189-9

Maamoun, I., Eljamal, O., Khalil, A. M. E., Sugihara, Y., and Matsunaga, N. (2018). Phosphate removal through nano-zero-valent iron permeable reactive barrier; column experiment and reactive solute transport modeling. *Transp. Porous Media* 125, 395–412. doi:10.1007/s11242-018-1124-0

Phenrat, T., Saleh, N., Sirk, K., Tilton, R. D., and Lowry, G. V. (2007). Aggregation and sedimentation of aqueous nanoscale zerovalent iron dispersions. *Environ. Sci. Technol.* 41, 284–290. doi:10.1021/es061349a

Solpuker, U., Sheets, J., Kim, Y., and Schwartz, F. W. (2014). Leaching potential of pervious concrete and immobilization of Cu, Pb and Zn using pervious concrete. *J. Contam. Hydrol.* 161, 35–48. doi:10.1016/j.jconhyd.2014.03.002

Tan, K. B., Vakili, M., Horri, B. A., Poh, P. E., Abdullah, A. Z., and Salamatinia, B. (2015). Adsorption of dyes by nanomaterials: Recent developments and adsorption mechanisms. *Sep. Purif. Technol.* 150, 229–242. doi:10.1016/j.seppur.2015.07.009

Wu, L., Liu, C., Hu, Y., Tan, B., He, Y., and Li, N. (2020). Dephosphorization using ceramsites modified by coprecipitation with FeSo4 and KMnO4 and high-temperature combustion. *J. Water Process Eng.* 34, 101162. doi:10.1016/j.jwpe.2020.101162

Xu, H., Chen, L., Zhao, B., Zhang, Q., and Cai, Y. (2015). Green stormwater infrastructure eco-planning and development on the regional scale: A case study of shanghai lingang new city, east China. *Front. Earth Sci.* 10, 366–377. doi:10.1007/s11707-015-0516-5

Zheng, M., Chen, W., Gao, Q., Liu, S., Deng, C., Ma, Y., et al. (2022). Research on the reduction performance of surface runoff pollution through permeable pavement with different structures. *Water Air Soil Pollut.* 233, 147. doi:10.1007/s11270-022-05619-4

Zheng, Y., and Zhang, J. (2020). Experimental study on the adsorption of dissolved heavy metals by nano-hydroxyapatite. *Water Sci. Technol.* 82, 1825–1832. doi:10.2166/wst.2020.465

frontiers | Frontiers in Earth Science

TYPE Original Research
PUBLISHED 14 December 2022
DOI 10.3389/feart.2022.1033673

OPEN ACCESS

EDITED BY
Celso Santos,
Federal University of Paraíba, Brazil

REVIEWED BY
Didier G. Leibovici,
The University of Sheffield,
United Kingdom
Aznarul Islam,
Aliah University, India

*CORRESPONDENCE
Nelly Moulin,
nelly.moulin@institut-agro.fr
Zahra Thomas,
zahra.thomas@institut-agro.fr

SPECIALTY SECTION
This article was submitted to Hydrosphere, a section of the journal Frontiers in Earth Science

RECEIVED 31 August 2022
ACCEPTED 24 November 2022
PUBLISHED 14 December 2022

CITATION
Moulin N, Gresselin F, Dardaillon B and Thomas Z (2022), River temperature analysis with a new way of using Independant Component Analysis. *Front. Earth Sci.* 10:1033673. doi: 10.3389/feart.2022.1033673

River temperature analysis with a new way of using Independant Component Analysis

Nelly Moulin[1]*, Frederic Gresselin[2], Bruno Dardaillon[3] and Zahra Thomas[1]*

[1]Intitut Agro, UMR 1069 SAS, Rennes, France, [2]DREAL Normandie, Caen, France, [3]Université de Caen-Normandie, LMNO, UMR 6139, Rennes, France

In the context of global warming, river management is essential to maintain favourable water temperature ranges for aquatic species. Therefore, understanding the main factors influencing the water temperature becomes a key part in the management process. In this paper, we used Independent Component Analysis (ICA) to identify these main factors and improve water temperature forecasting. The study is caried out on two rivers in Normandy (France) with quite different characteristics. Each river was equipped with several temperature sensors which series range from 2011 to 2021. The ICA analysis of the data series reveals that the thermal regime of these two rivers is mainly controlled by seasonal and daily climatic factors. The *Sélune* regime also turns out to be influenced by the presence of a dam, dismantled during the monitoring of the river. The temperature of the *Odon* appears to be clearly controlled by seasonal lightening conditions in connection with the presence of the riparian vegetation. Complementary, an innovative approach called "successive ICA" is used to reconstruct the natural thermal regime of the *Sélune* without the presence of the dam. Emphasis is therefore placed here on the interest of ICA in hydrology as en elementary method for extracting the main influencing factors and quantifying their importance on the thermal regime of a river. It also allows to remove the influence of a particular factor and reconstruct time series better suited for temperature forecasting. The method used here is not specific to temperature time series and can be applied to any region even with different hydrological characteristics.

KEYWORDS

river temperature, time series analysis, ICA, river management, water temperature prediction, dam removal influence, riparian vegetation

1 Introduction

Temperature is a key parameter in river ecology as it influences the environment and several species life cycles (Magnuson et al., 1979; Ebersole et al., 2001; Daufresne and Boët, 2007; Caissie, 2006; Comte et al., 2013; Souchon and Tissot, 2012). Thermal regimes are mainly influenced by atmospheric factors at the site scale, at the catchment scale or at larger ones (Webb and Walling, 1993; Poole and Berman, 2001; Webb et al., 2008; Ryan et al., 2013; Hannah and Garner, 2015; Jones and Schmidt, 2018). Atmosphere-water heat

TABLE 1 Characteristics for each monitored location (in C). Orientation N-E-S-W stand respectively for North-East-South-West.

Sensors	Od1	Od2	Od3	Se1	Se2	Se3
Height IGN 69 (m)	202	110	45	60	30	13
Distance from the source (km)	3.8	13.6	33.9	41.8	57.5	64.7
Vegetation	++++	++++	+++++	+	++	+++
Orientation	SE/NW	SW/NE	SSW/NNE	NW/SE	SSE/NNW	NNE/SSW
Width (m)	1.5	3	5	20	19*	22
Downriver from the dam (km)	N/A	N/A	N/A	N/A	0.4* (V)	3.6 (RQB)
Time depth	30/03/2011 07/06/2021	30/03/2011 29/10/2021	27/05/2011 07/06/2021	30/03/2011 14/06/2021	30/03/2011 14/06/2021	30/03/2011 14/06/2021

* = Before dam's removal in 2019 (V) = *Vezins*, (RQB)= *la Roche-Qui-Boit*.

transfers, and to a lesser extent water-aquifer transfers, control the major part of thermal variation in large rivers (Sinokrot and Stefan, 1994; Evans et al., 1998; Lalot et al., 2015). These transfers vary with the residence time of the water in the environment and the river's width. Also, water temperature increases from upriver to downriver, with a mean gradient of 0.1°C/km for large plain rivers (Torgersen et al., 2001), until reaching an equilibrium temperature. Thermal regimes are also influenced by the river flow, the geo-morphology, the riparian vegetation or hydraulic constructions (Kelleher et al., 2012; Arismendi et al., 2013; Ryan et al., 2013; Johnson et al., 2013; Jackson et al., 2017; Garner et al., 2017; Dugdale et al., 2018; Beaufort et al., 2020).

In France, most big rivers are monitored in temperature since the 70 s or 80 s (in accordance with the electricity production) (Moatar and Gailhard, 2006; Poirel et al., 2008; Larnier et al., 2010). Environmental monitoring developed from 2008 thanks to a national network created by the French Office for Biodiversity in order to better understand river ecology. In Normandy, the Regional Directorate for Planning and Housing (DREAL) equipped about one-third of the 18.000 km Normand rivers.

A particular focus is held on dams' effects. Dams and reservoirs usually have a significant impact on rivers temperature (Webb and Walling, 1993; Poirel et al., 2010; Seyedhashemi et al., 2021). Large dams tend to decrease rivers temperature in summer and to modify annual cycles whereas ponds and shallow reservoirs (less than 15 m) tend to increase the temperature (Seyedhashemi et al., 2021). This is because the solar radiation heats the surface layers faster than deeper layers. Even smaller dams (water drops less than 2 m) can strongly influence rivers' thermal regime by increasing the temperature (Chandesris et al., 2019). Dams' impact depends on the surface, the depth and the residency time in the structure. Thus, rivers with dams present a different thermal signature than natural rivers. In the Loire catchment (North-West of France), dam-equipped rivers can have a mean temperature higher than the air temperature (T_a) all year long (Seyedhashemi et al., 2021).

In this paper, the thermal regime of two rivers in Normandy were analysed: the *Sélune*, influenced by 2 dams and the *Odon*, considered as natural. Each river was equipped with three temperature sensors to analyse the temperature along the river and identify the main influencing factors and quantify their importance on a river's thermal regime (Table 1). Data was analysed using Independent Component Analysis (ICA), a statistical method not often used in hydrology but already tested on two other rivers in Normandy (Gresselin et al., 2021) and in several studies across the world (Hannachi et al., 2009; Aires et al., 2000; Moradkhani and Meier, 2010; Westra et al., 2008; Middleton et al., 2015; Gong et al., 2014). In addition, a new way of using ICA is proposed in order to remove some components from a signal and improve the results of a linear regression prediction model.

2 Studied catchments

2.1 The *Odon* catchment

The *Odon* catchment area extends over 217 km^2. The river travels 49 km before ending in the *Orne* in Caen (Figure 1). The *Odon* flows on the Armorican massif for the most part and the Parisian massif close to the confluence with the *Orne*. It drains successive hills mainly composed of schist and sandstone. Three temperature sensors are installed on this river.

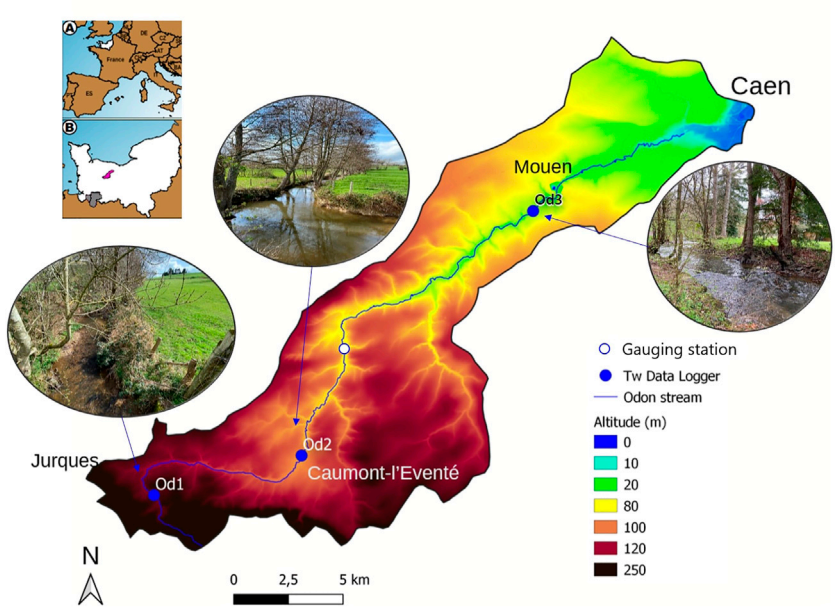

FIGURE 1
Odon catchment Digital Elevation Model (DEM) showing the water temperature (Tw) sensors' locations from upriver to downriver: Od1, Od2 and Od3. The empty blue circle indicates the location of the gauging station providing the discharge time series. Pictures were taken in a leafless period (April 2022).

The *Odon* starts in a Variscan syncline where bar sandstones form high points in the Normandy region. The river then flows along a narrow valley in a SE/NW orientation. In Od1, the corridor is around 40 m with a main channel around 1.5 m and quite shallow. The rivers flows between sills and pools in a sinuous way. Riverbanks are densely vegetated. The watertable is relatively low, varying from a few centimeters to a few decimeters at the end of winter. The riverbed is mainly composed of rough sediments. After the Variscan syncline, the *Odon* follows a meander from West to East then continues along a N/S orientation in Brioverian lands (hills and open valleys made of shale and sandstone).

In Od2, the corridor is 100 m wide and the main channel is an artificial 2.5 m wide section bordered with high trees. The river flows between pools and high waters with a mix of mud and stone riverbed. The watertable varies quickly up to several decimetres. Finally, near the city of Caen, the *Odon* drops in a chalk plateau at the west of the Parisian basin. The river takes a SW/NE orientation until its confluence with the *Orne*. Slopes are gentle except at the bottom of the valley where they can reach 30% (Supplementary Figure S1).

In Od3, the site is shaded from the direct influence of the Sun (especially in winter). The south side is densely forested with conifers which limits the sunlight all year long. However, the main river channel reaches 5 m wide so the middle of the river is exposed to direct sunlight in summer.

2.2 The *Sélune* catchment

The *Sélune* is one of the three coastal rivers ending in the Mont-St-Michel bay in the North-West of France (Figure 2). The catchment area is close to 1100 km^2. It drains several hills on the schist-sandstone and granite Armorican massif. The *Sélune* travels around 76 km in total along its longitudinal profile. In the first half of the XXst century, two hydroelectric dams were built at a few kilometers from the mouth of the river: the *Vezins* dam and *la Roche-Qui-Boit* dam, respectively 36 and 16 m high. To reestablish a natural flow regime and provide ecological benefits, the French government decided to remove some facilities which did not allow certain fish species, such as European eels, to cross them. The *Vezins* dam was removed in 2019 and the destruction of *la Roche-Qui-Boit* dam is scheduled for 2022.

The river water temperature monitoring was performed using three temperature sensors installed along the river and respectively named: Se1, Se2 and Se3. Se1 is located upriver the *Vezins* dam and its lake (Figure 2). At this location, the river is an open site (Supplementary Figure S2), about 20 m wide and strongly influenced by atmospheric factors. Se2 is located about a hundred meters downriver the dam. At this place, the vegetation is denser and the riverbed is 19 m wide (before the dam's removal). Se3 is located a few kilometers below *la Roche-Qui-Boit* dam. At this location, the river is 22 m wide and densely vegetated on the banks.

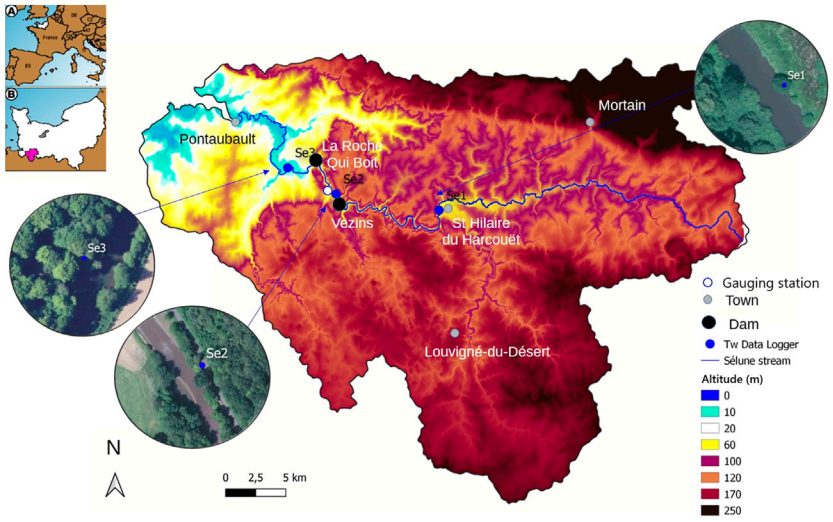

FIGURE 2
Sélune catchment DEM showing the temperature sensors' locations. The empty blue circle indicates the location of the gauging station providing the discharge time series. Pictures were taken from the IGN database.

3 Times series collection and pre-processing

3.1 Temperature data

The *Sélune* and the *Odon* were equipped by the DREAL of Normandy with temperature sensors HOBO water Temp Pro v2 (U22-001) with an accuracy of ±0.2°C. The sensors were fixed on riparian trees' roots, mostly in shaded areas and at depths which ensure a continuous immersion (except for Se2). Temperature is measured every 2 h, interpolated to a hourly basis in order to get a homogeneous time frame with other measurements (T_a, streamflow etc). In this study, for each river, a dataset of 10 years was analysed. A common time series was chosen between the 27 May 2011 and the 7 June 2021 (Table 1). Each dataset is composed of 89,490 time steps.

The temperature on both rivers evolves according to a seasonal cycle (Figure 3). Colder in winter (November to February) and warmer in summer (June to September). Minimal temperatures get close to 0°C for the *Odon* and the *Sélune* upriver and around 3°C for the *Sélune* downriver. The mean temperature of both rivers tends to increase downriver. This rise reaches 1°C in the *Odon* and 0.7°C in the *Sélune*. Measured maxima are higher for the *Sélune* which is a wider river and less shaded than the *Odon*. Stations on the *Sélune* are further from the source than stations on the *Odon*. The distance has an impact on the sensibility of the thermal regime to climatic factors (Le Lay et al., 2019).

Concerning Se2, as the temperature sensor was located at the foot of the *Vezins* dam, it was regularly emerged during reservoir fillings to produce electricity. Therefore, the temperature at this station could reach thermal minima way below 0°C when it was emerged because then, it measured the air temperature. After the destruction of the dam in 2019, Se2 was covered by a thick sediment layer and its thermal amplitude was reduced (Figure 3).

3.2 Pre-processing

Due to occasional sensor failures and/or maintenance operations, river temperature time series are not perfectly continuous. In total, less than 0.2% of the time steps was filtered as outliers or filled with the methods described below.

- Missing data: it can affect a very specific period (a few hours only) due to maintenance operation or longer periods (several days, weeks or months) due to sensor failure. To address this defect, several strategies were considered. If the number of missing points remained low enough (less than 20 h), linear interpolation was used to fill the gap without compromising the physical evolution of the series. If more points were missing, three options were chosen depending on the needs: 1) averaging over upriver and downriver stations (if possible and if coherent); 2) simply removing this part of data from all series to perform ICA or 3) replace with the mean value of the series (in order to avoid missed raw data presented as NaN; acronym for Not a Number).
- Outliers: some points displayed extreme values which were not consistent with the physics involved (such as negative water temperatures for immersed sensors). In this case, a common

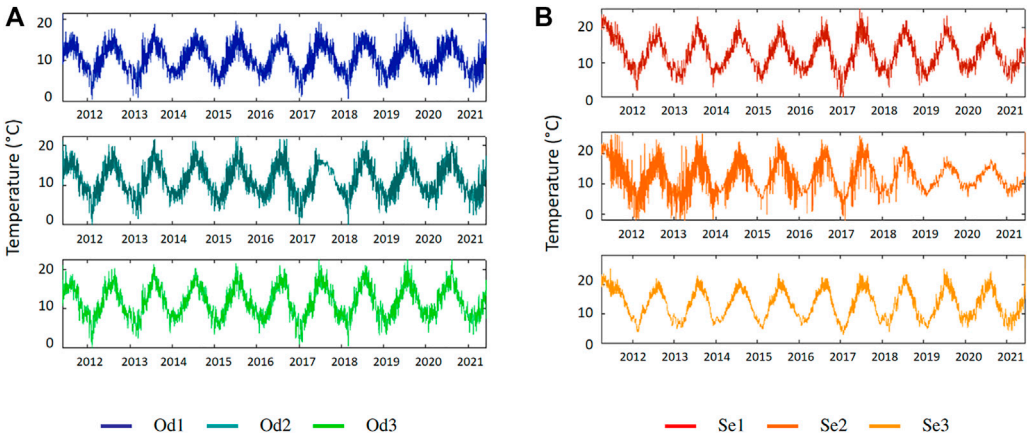

FIGURE 3
Stream temperature time series at the three location on **(A)** the *Odon* in Od1-Od2-Od3 and **(B)** the *Sélune* in Se1-Se2-Se3. Upriver stations at the top and downriver stations at the bottom.

method was to remove data points which were further than x times the series mean value.

- Homogeneous frequency: all the stations had different time depth and not all of them use the same measurement settings. This created heterogeneous time series that were difficult to compare and much less to use in ICA. To use the data, stations with a wide common time range were chosen (i.e. from the 27th May 2011 to the 7th June 2021). Also, the data frequency was set to a hourly basis. It is to be noted that the lowest measuring frequency was one point/2 h, so a temporal down scaling from 2 to 1 h did not affect the interpretation of the data.

In the following sections, all data presented were pre-processed with the methods mentioned above for the period 2011–2021.

4 The analysis methods

4.1 Independant component analysis method

ICA can identify hidden factors which influence the observed data without knowing mixing mechanisms. It can decompose one or several random non Gaussian signals $X \in R^m$ in a linear combination of independent signals such as:

$$X = A \cdot S \tag{1}$$

with $X = [x_1, x_2, \ldots, x_m]^T$ gathering all the signals, S an independent factor matrix $S = [s_1, s_2, \ldots, s_m]^T$ gathering all the sources with a standard distribution and A, a coefficient matrix or mixing matrix.

Decomposing observations in several independent sources can estimate A and S with two main hypothesis. On the one hand, the sources are statistically independent. On the other hand, not more than one independent component can have a Gaussian distribution.

Each independent component S is represented by a graph and a weight matrix A. The graph shows the variation of S with time whereas the matrix shows the variation of S with the stations.

ICA analysis was performed using the Fast-ICA package from the R software (Hyvärinen and Oja, 2000; Marchini et al., 2021). This algorithm is suited to estimate the mixing matrix A and the source matrix S. Data are centered so the initial observations X can be obtained by adding $A \cdot S$ to the mean of the X series.

$$X_i = \sum A_{ij} \cdot S_j + \bar{x}_i \tag{2}$$

with $\bar{x}$ the mean value of the initial X_ith serie. The main limit of this method is the number of sources than can be extracted. In our case, three temperature sensors limit the number of sources to three for each river.

4.2 The successive ICA method

In order to overcome the limit of the available datasets, we applied a successive ICA method to extract more information. This method uses the following steps.

1) From initial temperature datasets, run an ICA.
2) Sort the ICA source components and remove some of them according to the criteria listed below.
3) Build new temperature datasets by applying the corresponding matrix coefficients on the remaining

components and by adding the mean value of the datasets used in 1.
4) Repeat steps 1 to 3.

This successive ICA method allows to extract further information from the first ICA components. By removing an obvious contribution after the first ICA, one can get to more complex phenomena. Choosing which ICA component to remove relies on several criteria.

- When a physical signal is clearly identified (for example a seasonal variation correlated with the air temperature).
- To isolate a specific component and identify several factors included in this specific component.
- When a signal is specific to one location and reflects a particular condition.
- When a signal is identified as a noise or as a residual signal (amplitude less than the measurement's accuracy).

In all cases, the new dataset's distribution should be non-Gaussian. Ultimately, the decomposition process ends when the remaining ICA components are reduced to white noise or when there is only one exploitable signal left. Therefore, after each ICA, Box-Pierce tests were performed to remove useless white noise signals in the process. In this study, signals were considered exploitable when their amplitude was larger than the sensor's accuracy (±0.2°C). Signals with smaller amplitudes were either considered as residual signals or identified as white noise with Box-Pierce tests.

The example below shows how after extracting ICA components, a non-Gaussian component can be refined by subtracting noise signals. The main calculation steps are described below.

1) Run a first ICA with the measured time series. Identify a component to work on (here the seasonal component).
2) Recompose time series using only the chosen component multiplied by the matrix coefficient for each station and adding the measured time series mean value.
3) Run a second ICA with the three new times series.
4) Identify the seasonal component and run a Box-Pierce noise test on the two residual components.

The Box-Pierce test indicates if a signal is characteristic of a white noise with a p-value > 0.05 (diamond boxes in Figure 4). This p-value measures the probability of auto-correlation in the signal. The higher the p-value, the higher the probability for the signal to be a white noise.

The diagram below (Figure 4) shows the process of the successive ICA method applied to a measured time series. All ICA components in this figure were multiplied by the mean of their matrix coefficients on the three stations. From the first ICA, only the component $X1$ is kept (black frame). The second time series (black frame middle left) are composed from $X1$ only. The second ICA (red and blue frames middle) displays a seasonal component ($X1$') and two other signals with very low amplitudes (< 0.04°C). In the 1) red-framed path, only the seasonal component is kept and the third datasets 1) are formed (red bottom middle). The third ICA (red frame bottom right) shows a seasonal component and two residual signals $X2a$ and $X3a$ with amplitudes at the limit of the sensor's accuracy. In the 2) blue-framed path, the seasonal component is removed and the third time series 2) are composed with the residual ICA components $X2$' and $X3$'. The third ICA (blue frame upper right) displays three components among which $X2b$ and $X3b$ are tested as white noises (p-values respectively 0.08 and 0.274). $X1b$ is negative to the Box-Pierce test but its amplitude remains much lower than the sensor's accuracy.

In the end, the last seasonal component $X1a$ can be considered "cleaner" as its predecessors $X1$ and $X1$'. In this case, the residual signals show very low amplitudes so the differences between the different stages of the seasonal components remains subtle.

4.3 The successive ICA method in water temperature prediction

This study takes advantage of the successive ICA method to generate a hypothetical temperature time series on the *Sélune*. This new signal is a proposition of what the temperature time series in Se2 would have been if the *Vezins* dam had not been constructed. On a long time scale, the dam operation can be considered as temporary. For example, when confronting the river thermal regime with climate change, it could be useful to remove the effect of the dam. To do this, the following steps were applied.

1) Run a first ICA with the original temperature time series. Identify the dam component.
2) Recompose temperature time series with only the two other components (seasonal and daily) by multiplying the ICA component with the correspond matrix coefficients for each station and adding the mean value of the original time series.
3) For further information, run a second ICA with the new time series.

The chart below (Figure 5) shows in 1) the new time series on the three stations (solid black) compared with the original time series. We see that for stations Se1 and Se3, there is almost no difference as they are little affected by the dam component. The new signal is shifted by −2 °C in average. However, in Se2, we can see that the signal is more regular in the new time series. Irregular peaks and variations originating

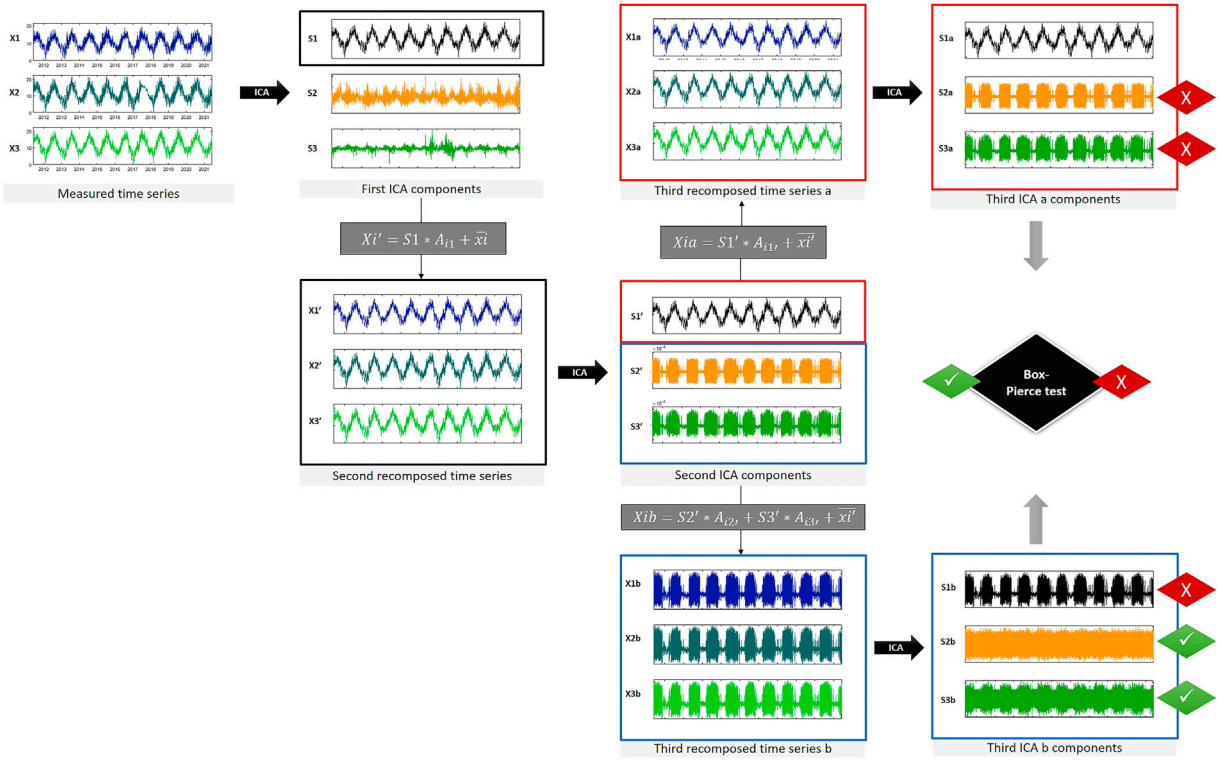

FIGURE 4
Schematic view of the successive ICA process applied on a time series. $\bar{x}$ as the mean value of the time series X. Diamond boxes show the results of the Pierce-box test for ICA components.

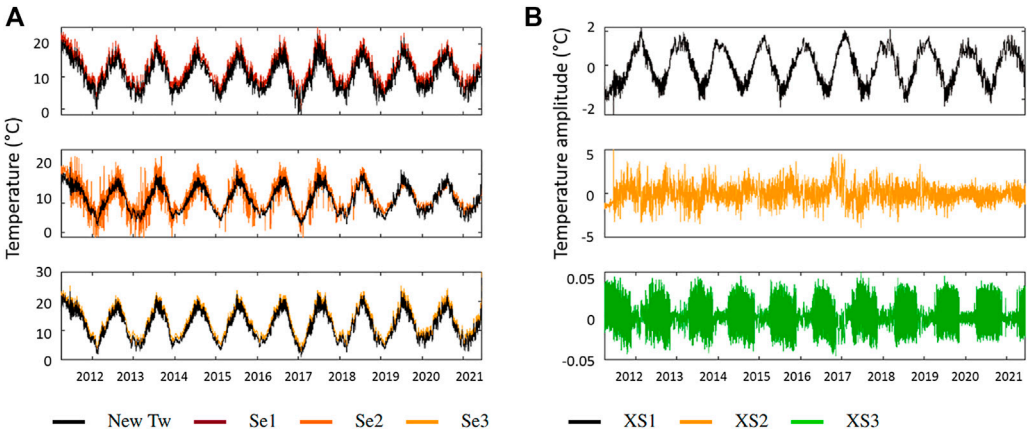

FIGURE 5
(A) Recomposed temperature time series without the dam's ICA component in black superimposed on the measured temperature time series. **(B)** Second ICA with the new temperature time series from **(A)**.

from the dam have disappeared. After 2019 and the dam's removal, the two signals are closer and there is less difference between them.

In (b), the chart shows the ICA components obtained with the new temperature datasets (black curves in Figure 5). We can recognise the seasonal component ($XS1$ in black) as well as

TABLE 2 Improvement in water temperature prediction on Se2 by removing the dam component.

Data type	Test 1	Test 2	Difference
Train R2	0.59	0.59	+0%
Test R2	0.32	0.43	+34.37%
Train RMSE	3.11	2.74	−11.90%
Test RMSE	2.88	2.63	−8.87%

TABLE 3 Mixing matrix coefficients for the ICA components for 1) the *Odon* and 2) the *Sélune*.

Name\Sensors	Od1	Od2	Od3	Characteristics
XOdA	3.12	3.71	3.90	Seasonal
XOdB	0.66	0.45	-0.08	Daily
XOdC	0.09	-0.55	-6.68e-4	Effect in Od2

Name\Sensors	Se1	Se2	Se3	Characteristics
XSeA	4.09	4.24	4.73	Seasonal
XSeB	1.55	0.21	0.44	Daily
XSeC	0.20	1.43	-0.18	Effect of the dam

the daily component (*XS*2 in orange). The third one (*XS*3 in green) is negative to the Box-Pierce noise test but shows an amplitude under the accuracy of the measuring sensor. Therefore, it is likely coming from the sensor itself and considered as a residual signal.

The interest of the successive method was tested in water temperature prediction using a regression linear model. In this test, two runs were made. First, the model was applied on original T_W time series with a separation of 70–30% between the train and test data. Then, the model was applied on corrected data for the train part, which means without the dam component. The test data was kept identical to the first test. Among the three stations, the difference between the two runs was most visible on station Se2 where the dam component is the most important. Removing the dam component from the time series improved the fit between predicted and measured test data by 34.4% and contributed to reduce the RMSE by 8.9% (Table 2).

Although this test used a simple regression model, it shows the interest of removing a particular signal which affects a temporary period. In this case, the dam itself is not supposed to affect the river thermal regime several years after its removal. By using the successive ICA method, it is easier to choose the influence of environmental factors for future thermal regimes.

5 Results and discussions

5.1 About the mixing matrix

From the temperature time series, at least three components were extracted for each river to take advantage of the number of stations in the range 2011–2021. Corresponding ICA components will herein be referred with their code names in the tables below (Table 3). For each ICA component, the mixing coefficients make the link with each station. Signs indicate the relative relationships between the components and the station. For example, *XOdA* shows the same kind of relationship for all stations as all the coefficients have the same sign. Then, the absolute value of the coefficients shows the impact of each component on the different stations. A high absolute value indicates a strong influence of this component on the thermal regime of the station. On the contrary, a value close to 0 means that the component has little effect on the thermal regime at this station. For example, *XOdC* has a strong influence in Od2 whereas it has a negligible effect in Od3.

From the matrix coefficients, we can see that the first components (*XOdA* for the *Odon* and *XSeA* for the *Sélune*) clearly have a dominant effect on the thermal regimes and affect all stations quite equally. On the contrary, looking at the coefficients values, *XOdC* affects mainly Od2 and *XOdB* seems correlated to the upriver stations Od1 and Od2. On the *Sélune*, *XSeB* affects the upriver station Se1 more and *XSeC* is clearly correlated to Se2.

At this stage, we can separate the first components which are regular and affect all stations with the same magnitude (including an increasing effect downriver) on the one hand, and other components which affect some stations in particular on the other hand. Complementary to the mixing coefficients, graphic representations of the ICA components (Figure 6) show their impacts on the stations. The graphs represent the time variation of each ICA component for each station weighted with the corresponding matrix coefficient.5b

On the *Odon*, the maximum amplitude is obtained with the first component *XOdA* (±10 °C). *XOdB* and *XOdC* represent secondary components of the signal with smaller amplitudes than *XOdA* (±2°C). Finally, Od3 displays a behaviour quite different from Od1 and Od2 based on the three ICA components. In Od3, *XOdA*'s matrix coefficient is the strongest of all stations whereas *XOdC* is almost nil and *XOdB* takes an opposite sign compared to Od1 and Od2.

On the *Sélune* however, the three components take high amplitudes depending on the stations. The maximum amplitude is observed for *XSeA* for all stations. Then, *XSeB* shows a signal half the amplitude of *XSeA* for station Se1 and *XSeC* shows an amplitude almost as high as *XSeA* in the period 2011–2013 for station Se3.

In the following subsections, physical factors are attributed to the different components. As the number of ICA components is limited to 3, all components can contain several factors'

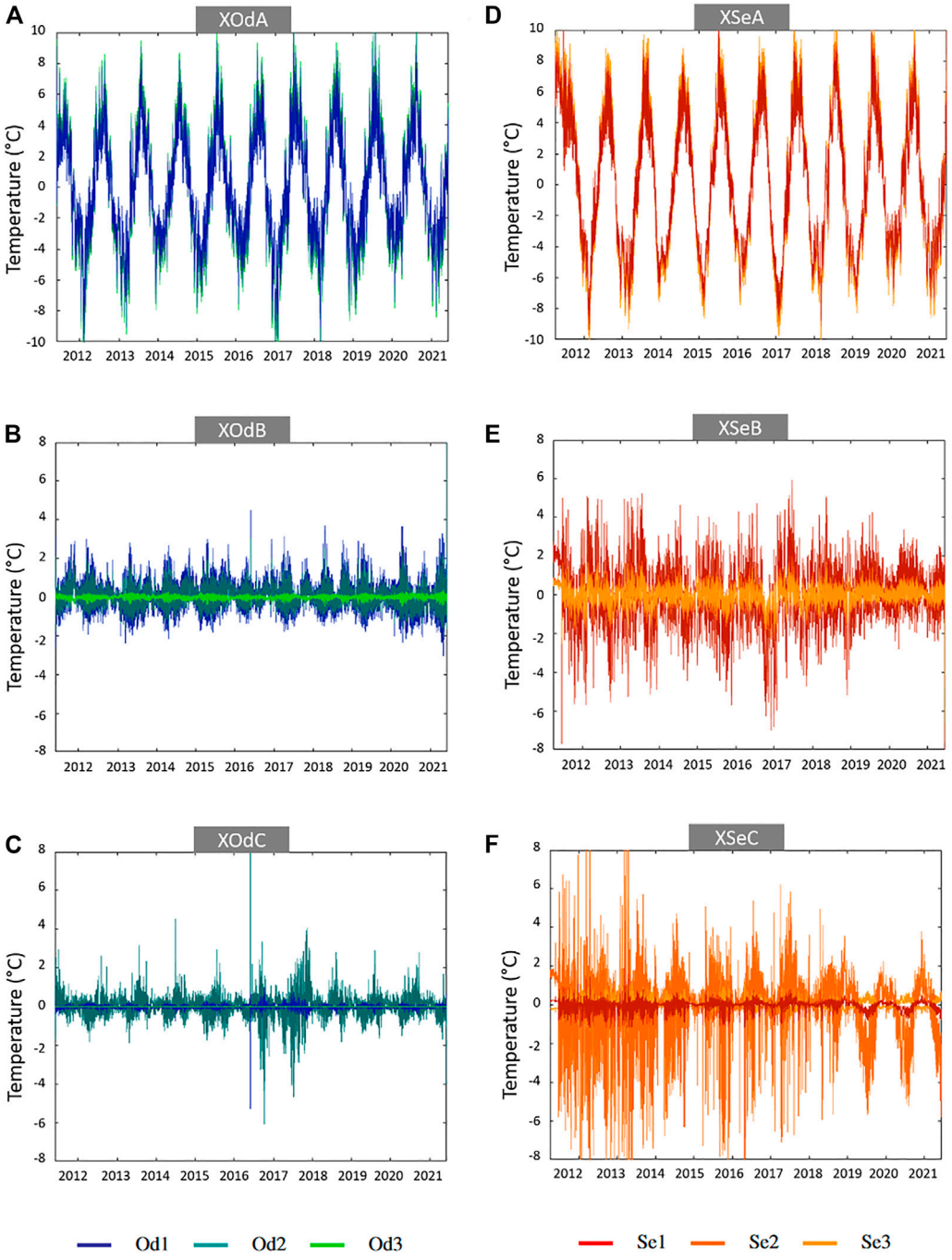

FIGURE 6
Temperature ICA components for the *Odon* in **(A–C)** and the *Sélune* in **(D–F)**. **(A–D)** Seasonal components. **(B–E)** Daily components. **(C)** Component specific to Od1 and Od2. **(F)** Component linked to the *Vezins* dam.

signatures. Therefore, the physical factor attributed to the ICA component will concern the most visible ones. Physical factors can be separated between climatic factors at the catchment or regional scale and environmental factor at the measuring site scale.

5.2 Climatic factors

5.2.1 Seasonal variations

On both rivers, the first ICA components to come out, *XOdA* and *XSeA*, show a clear seasonal variation (Figures 6A,D). These

signals have their maxima in summer and minima in winter. Due to heat reservoirs (sea and soils), maxima are shifted by half a month from the winter and summer solstices. These variations are quite similar every year. The seasonal components show the strongest matrix coefficients (Supplementary Table S3) and increase downriver for both rivers as the water-atmosphere heat exchanges increase with the surface, the distance from the source and the width of the river. On the *Odon*, for example, *XOdA* accounts for 80.6% of the three contributions in Od1 whereas it accounts for 98% in Od3. This confirms that the seasonal variation is the main physical phenomenon governing water temperature in Normandy (Gresselin et al., 2021) and in general (Caissie, 2006). Comparing the rivers, the seasonal component is stronger for the *Sélune* (coefficients around 4) than for the *Odon* (coefficients around 3). The amplitude difference can be explained by geometric factors. The *Odon* is a narrower river than the *Sélune* on the measuring sites, and thus less influenced by atmospheric factors. Also, measuring sites on the *Sélune* are further downriver than the ones on the *Odon*. Correlation factors between the seasonal components and the air temperature (T_a) rise up to 81,89% for *XOdA* and 76.65% for *XSeA* (whole time range).

The high frequency signal superimposed on the seasonal signal is mostly due to strong thermal variations caused by cyclonic and anticyclonic events (frequent in Normandy). This secondary source generates an extra signal common to all stations. On the *Sélune*, we can notice that the ICA component *XSeA* is much smoother, before 2017, than the corresponding component on the *Odon*. The ICA extraction attributes the high frequency variations to other factors before 2019 than a regular variation. After 2019 and the dam's removal, the *Sélune* seasonal variation seems closer to a "natural" river such as the *Odon* and the high frequency signal appears more clearly in *XSeA*.

This first components *XOdA* and *XSeA* are seasonal variations strongly correlated with the air temperature. These seasonal components are not necessarily exclusive to the air temperature effect but can gather several atmospheric factors with similar behaviours.

5.2.2 Daily variations (*XOdB*, *XSeB*)

After the seasonal variations, the most important factors are daily variations (Figures 6B,E). Daily variations record day/night temperature differences over the year but without the seasonal variation. That is why *XOdB* and *XSeB* do not exhibit a "saw-tooth" type signal as for *XOdA* and *XSeA*. The ICA components *XOdB* and *XSeB* show smaller amplitudes over the year than the seasonal components *XOdA* and *XSeA*. Amplitudes vary around ±3 °C for the *Odon* and ±4 °C for the *Sélune*.

In order to highlight the different influences over the stations, typical years were selected in temperature time series for the *Sélune* (Figure 7) and the *Odon* (Figure 8). Figure 7 shows the component *XSeB* in 2 years: before the dam's removal (2014) and after (2020). Figure 8 shows the component *XOdB* for the *Odon* on a typical year (2013).

On the *Sélune*, *XSeB* is more steady throughout the year. However, we can distinguish two phases before and after the dam's removal (Figures 7A,B). The amplitude of the variations is more important before 2019 (±5°C) than after (±2 C). Before 2019, *XSeB* is marked by a temperature drop in August and irregular fluctuations especially in Se1. These fluctuations remain important until mid-December where the mean temperature increases again. For this period (2011–2019), it is difficult to consider a "typical" year as the variations in *XSeB* are quite irregular and strong. But in average, the strongest variations occur in early summer before a drop in early autumn. *XSeB* in Se2 and Se3 appear steadier and vary less throughout the year whereas in Se1, it varies above and under the signal of the downriver stations. This effect in a river equipped with a dam was also observed in the Loire basin (France) (Seyedhashemi et al., 2021). After 2019, the daily variations are lower over the year and display seasonal variations as on the *Odon*. We can notice a higher day/night amplitude from April to October but in a relatively small range (±2°C).

On the *Odon*, *XOdB* can be described by the amplitude of the day/night variations (Figure 8). Thus, from March, the day/night amplitude increases until its maximum in May. After that, the amplitude decreases and stabilises throughout the summer. It starts to increase again in September and decreases in November to stabilise in winter. This behaviour does not follow the seasonal variation seen in *XOdA* but is caused by a combination of climatic factors: length of the day, day/night thermal variations as well as environmental factors described later. This component affects mainly Od1 and Od2 because the thermal variations in Od3 are almost exclusively explained by the seasonal component *XOdA*. As it will be described later, daily variations in Od1 and Od2 reflect a group of factors repeatable every year.

The second components *XOdB* and *XSeB* express daily variations. It contains a seasonal cycle for the *Odon* stations and a strong contrast before and after 2019 for the *Sélune* stations. Contrary to the first component it shows very different aspects on the two rivers and on the two different periods for the *Sélune*. Unlike *XOdA* and *XSeA* which are mainly explained by atmospheric factors, daily components *XOdB* and *XSeB* also contain environmental factors' signatures which will be described in the following sections.

5.3 Environmental factors

In addition to climatic daily variations, ICA can also highlight a more general influence of environmental factors. This section focuses on the temperature ICA components containing environmental factors' signatures such as the X_B

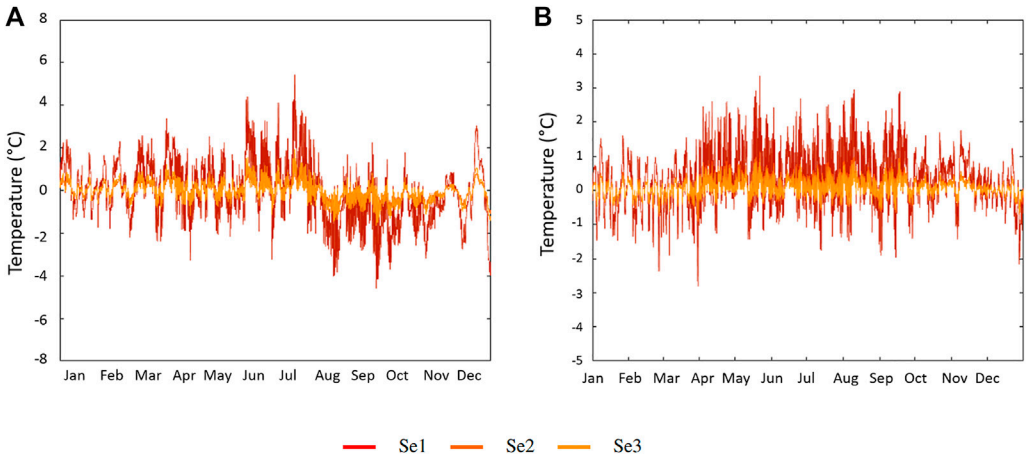

FIGURE 7
Temperature ICA component *XSeB* for the *Sélune* on typical years **(A)** before the dam's removal (2014) and **(B)** after the dam's removal (2020).

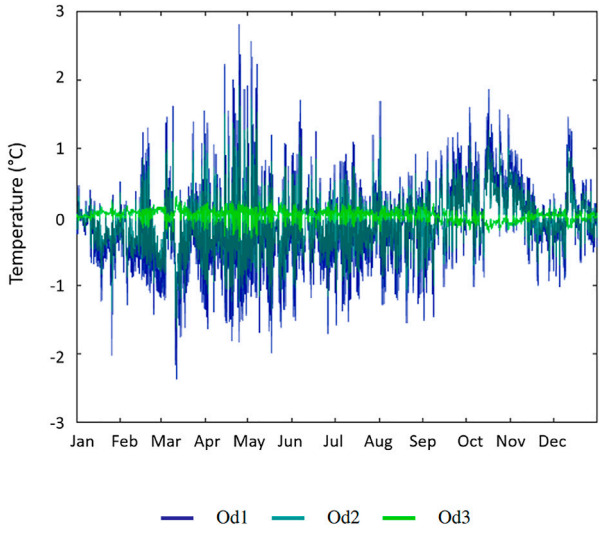

FIGURE 8
ICA component *XOdB* for each *Odon* station in 2013.

and X_C components for each river. The most visible factors are attributed to ICA components. Complementary analysis with PCA will refine the determination of the factors.

5.3.1 Soils and riparian Vegetation's influence (*XOdB*)

Source component *XOdB* (Figure 8) shows that the circadian temperature signal of the river is not only influenced by climatic factors but also by environmental ones especially in Od1 and Od2.

In *XOdB*, the amplitude increases from January to May. At the beginning of the spring, soils have not yet warmed up. The air temperature rises during the day but keeps dropping during the night. In addition, anticyclonic conditions in March and April create cloudless nights which do not limit nocturnal heat losses in the atmosphere. This creates strong variations between cold nights and warm days.

Between mid-March and May, the riparian vegetation's foliage progressively grows over the water, thus protecting the river from the influence of the Sun during the day and also limiting energy losses during the night (Dugdale et al., 2018). At the same time, heat accumulation in soils starts. This combination of factors decreases the amplitude of the signal at the end of June where it should be at its maximum according to the local climate.

After that, *XOdB* rises again from August until almost November. The upriver part of the *Odon* (Od1 and Od2) lays on the Armorican massif in which aquifers are filled quite early at the end of summer. Their recharge can transfer heat from the soil to the river during autumn through runoff with the first effective rains.

Finally, the decline of the signal's amplitude from mid-November is explained by climatic factors but also by the riparian vegetation which loses its foliage on the river. This contributes to decrease the temperature by several degrees at the beginning of winter.

The ICA source component *XOdB* highlights several factors, and in particular the role of the riparian vegetation and the soil as a heat reservoir. Od3 highlights less of this effect because its banks are more protected from the direct sunlight. Thus, the exposition conditions are very different from Od1 and Od2 (Supplementary Figure S1).

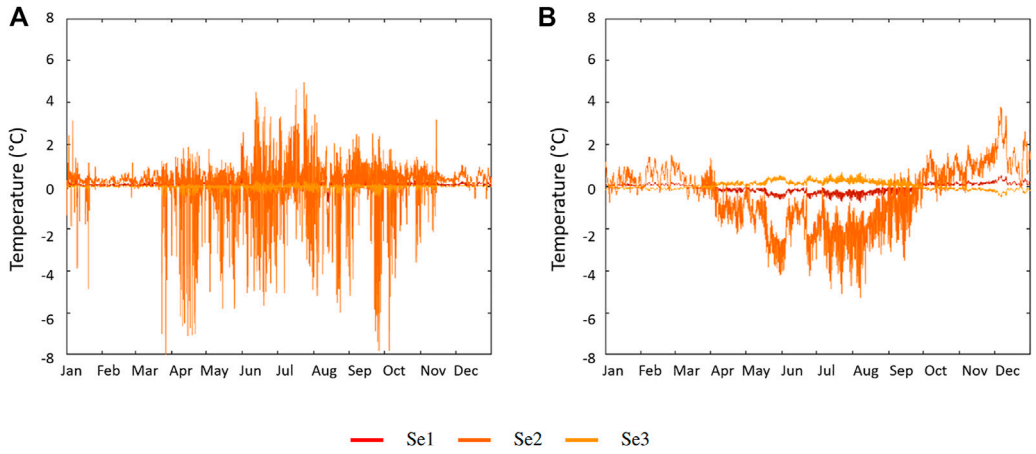

FIGURE 9
Temperature ICA component *XSeC* for the *Sélune* for typical years **(A)** before the dam's removal (2014) and **(B)** after the dam's removal (2020). The signal before 2019 is highly disturbed by the dam's activity. After 2019, the signal is smoother and shows an opposite seasonal variation as the sensor was covered by sediments.

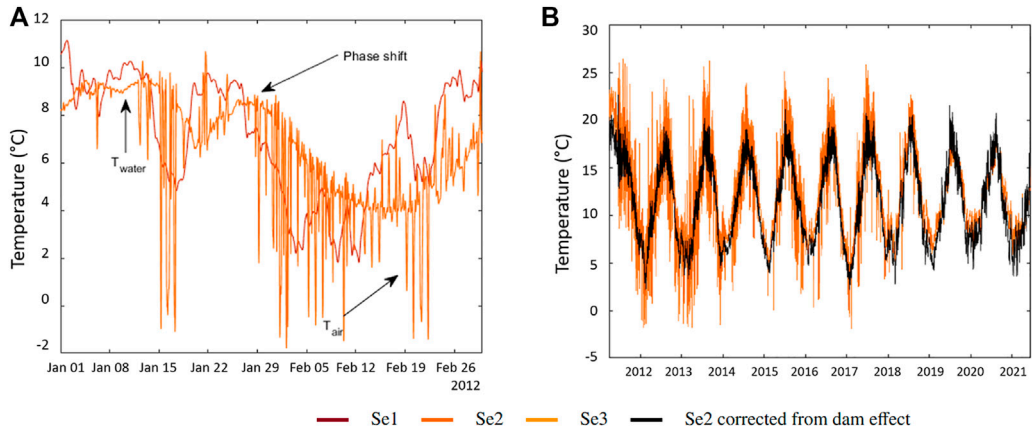

FIGURE 10
(A) Influence of hydraulic peaks on the temperature in Se2. The dam buffers the temperature amplitude and creates phase shifts. When the sensor is emerged, it measures the air temperature. **(B)** Temperature time series on the *Sélune* after removing the influence of the dam.

5.3.2 *Vezins* Dam's influence (*XSeC*)

On the *Sélune*, the component *XSeC* (Figure 6F) consists of a seasonal signal with superimposed high frequency variations. This signal seems linked with the presence of the *Vezins* dam and its destruction in 2019. Indeed, it is irregular until 2019 but structured after that year. When discriminating by station on a specific year (Figure 9A), in 2014 for example, *XSeC* affects mainly station Se2 which is located at the foot of the dam.

XSeC also contains a seasonal signal which stops at the dam's removal. Such signal may be linked to the upriver lake (around 200 ha). It has a large surface exposed to atmospheric factors which can gather heat from spring to autumn and contribute to warm the *Sélune*. This warming is around 1.5°C in July (Figure 9A). In winter, the presence of the dam seemed to have a less significant impact even though the lake contributed to smooth and shift the phase of thermal events (Figure 10A).

The main hypothesis here is that ICA gathered most of the dam's effects in *XSeC*. It was confirmed by another ICA run with only *XSeA* and *XSeB* (excluding the dam's effect in *XSeC*). In this second run (Figure 5), the new temperature datasets were very

similar for stations Se1 and Se3 as on Figure 7, thus confirming that it was not affected by the presence or absence of the dam.

During the dam's operation period, the production of electricity through hydraulic peaks affected the immersion of the sensor. When it was emerged, it measured T_a (Figure 10A). Indeed, if the river flow upriver the dam was low, the hydraulic head took time to come back to its original value. At these times, the electricity company EDF had to release part of the water but it was not enough to keep Se2 immersed. On the contrary, during floods (mostly in winter), the river flow could be sufficient, so EDF did not need to use hydraulic peaks. During these times, most of the upcoming river flow was released and the sensor remained immersed. Such events occurred from 2012 to 2016 (Supplementary Figure S3). In 2018, although the dam was not operating anymore, water movements previous to the dam's removal were expressed by irregular peaks in *XSeC*.

After the dam's removal (Figure 9B), *XSeC* shows a seasonal signal in Se3 but opposite to *XSeA*. This is explained by the fact that the sensor was covered by sediments after the dam's removal and thus, the seasonal signal is strongly shifted from the atmospheric variation. Even though, it is not possible to state that the river is not affected by other dams (such as *la Roche-Qui-Boit* dam located between Se2 and Se3), it seems that the remaining structures do not affect the thermal regime as strongly as the *Vezins* dam. Using the successive ICA method described above, a reconstruction of the temperature time series without the influence of the dam (Figure 10B) was made. It shows a regular seasonal signal similar to a "natural" stream's signal such as the *Odon*.

ICA extraction highlights the impact of a dam on a river and its effects on a seasonal level as well as on a daily level. In this case, the operations of the dam led to peak temperatures and a very irregular thermal regime compared to a natural river. It also led to two very different thermal regimes between the upriver station Se1 and downriver stations Se2 and Se3.

5.4 About using ICA

When analysing time series, most commonly methods such as Fourier or Morlet wavelets are frequency dependent. The initial signal is separated into several contributions based on the frequency of the phenomenon. This first approach can separate different physical phenomena which operate on very different time scale (seasonal, daily etc. . .). ICA, however, does not discriminate frequency scaled phenomena. Therefore, it can separate signals with similar frequency signatures. Therefore, these methods are complementary: frequency based methods are sensitive to the sampling frequency whereas ICA is sensitive to the homogeneity of the time series. The main limit of ICA lies in the separation of signals. On the two rivers, ICA could extract only three mathematically independent components on the one hand and residual signals and white noise on the other hand. Physical factors influencing the temperature are never completely independent and therefore, ICA alone can not fully separate all the contributions, unless the number of sensors is important.

However, as a first analysis step, ICA provides useful information and draws a first study frame for the physical phenomenon to look into. Also, it can be used in a backwards methodology where a factor is known to have an impact on the thermal regime but the way it impacts remains to be determined. ICA can highlight a specific signal which can be identified as the specific factor. In this study, the *Vezins* dam was known to influence the thermal regime of the *Sélune* and ICA could extract a specific signal to remove its temporary effect.

5.4.1 Contributions of ICA components

Figure 11 shows all the ICA contributions weighted by the matrix coefficients for each station. To sum up, the ICA analysis highlighted the following points:

- *XOdA* and *XSeA* (black), attributed to seasonal components, explain the majority of the rivers' thermal signal.
- *XOdB* and *XSeB* (yellow), attributed to daily variations are regular over the years and generally stronger for upriver stations. *XOdB* variations correspond to a combined effect of four factors: the day/night variations, the sunlight exposition throughout the year (duration and intensity) and on top of that the vegetation's growth and soils' heat storage.
- *XOdC* and *XSeC* (green) contain the remainder of the temperature signal. Therefore it contains most of the particular events and local conditions affecting one station in particular. On the *Odon*, *XOdC* concerns mostly Od2 and a particularly open environment (Supplementary Figure S2). On the *Sélune*, *XSeC* concerns mostly Se2 and the effects of the *Vezins* dam.

With this first analysis, several physical factors (climate, vegetation, soils, dam . . .) could be linked with ICA components and their impact evaluated according to the local context based on geology, remote sensing data, topography, land use and riparian vegetation density. However, some of known factors such as the river flow did not appear in this analysis.

5.4.2 Importance of the measuring network

ICA allowed to highlight several factors (natural or artificial) that influence the thermal regime on two rivers in Normandy. It also showed the downriver evolution of several of them.

This performance comes from the method itself but also from the measuring network which focused on less rivers but with a greater density of sensors. Ideally, five measuring sites on the *Odon* would have allowed to highlight the groundwater's influence (Le Lay et al., 2019) and the impact of the distance

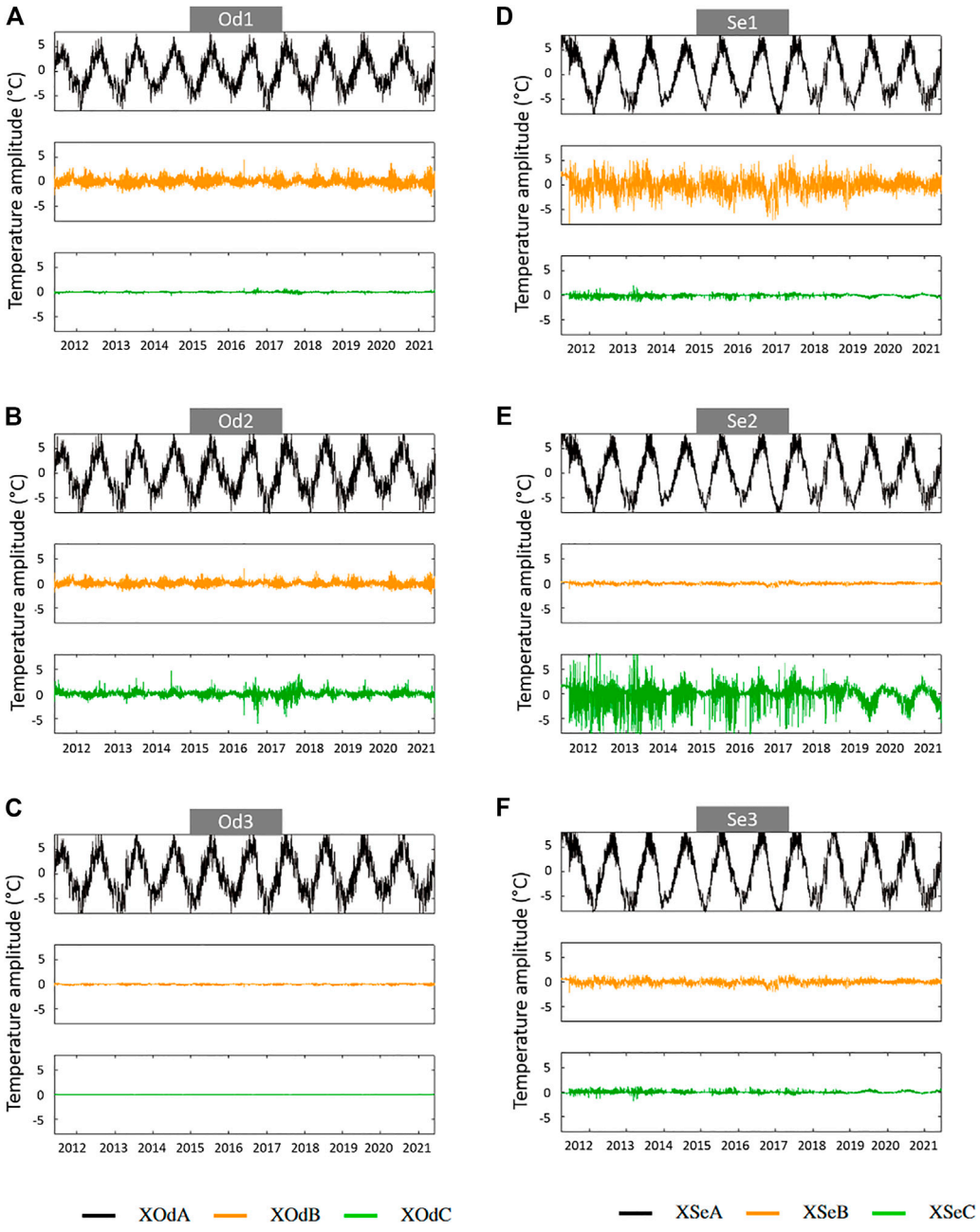

FIGURE 11
ICA components for each station of the *Odon* in **(A–C)** and the *Sélune* in **(D–F)**. Seasonal components in black, daily components in yellow, specific components in green.

from the sea. For the *Sélune*, three more stations would be necessary to study the mouth environment (1 station), the upriver basin (2 stations) which contains two main types of aquifer. Among all the measuring stations, ICA allowed to isolate the ones with specific environments. But this is only possible if the river is equipped with enough stations.

However, with a successive ICA method, more components than the number of sensors would initially allow can be extracted. ICA also gives information about the variation of the components in space (measuring stations along the river) and time. This information is useful to determine the physical factors involved.

6 Conclusion

ICA linearly decomposes the signal with the hypothesis of noise cancellation. The quality of the decomposition and the separation can be affected in the case of a strong noise. Source density under ICA is often either fixed or selected among a limited family of densities, which can cause a loss of flexibility. To counter those aspects, it could be interesting to use Independent Factors Analysis (IFA) which proposes a generative model with noise (Attias, 1999). In this model, densities are modelled with a Gaussian mix that is closer to arbitrary densities. In our case, an IFA model with time structured sources would provide further information.

In a previous paper (Gresselin et al., 2021), ICA was combined to PCA with a multiple linear regression model to characterize the respective role of groundwater and runoff in the thermal regime of a Normandy river (the *Touques*, France). The method has also made it possible to identify the increasing role from upstream to downstream of two climatic factors: the air temperature and the solar irradiance.

In this paper, ICA was used to characterise the influence of a hydrolelectric dam and its dismantling on the thermal regime of the *Sélune* (Normandy, France). ICA also identified particular periods where the sensor was covered by sediments and when it was emerged. In addition, with a new protocol called "Successive ICA", the natural thermal regime of the river was reconstructed and testes in water temperature prediction.

On the *Odon*, considered as a natural river, the ICA characterized the role of the riparian vegetation and the soil on the thermal regime. The intensity of each environmental factor identified with the ICA was studied from upstream to downstream and over 10 years time.

ICA has proved the extent of its performance in classifying a wide range of control factors from a set of pre-processed time series on the one hand. On the other hand, the successive method developed here has shown its ability to remove a temporary effect, which can be useful when dealing with long-term processes. In hydrology, ICA can address at least three situations: what is the importance of other factors than the atmosphere on a river's thermal regime? what is the evolution of a particular known factor on a river's thermal regime? are there influencing factors that are related to one station in particular?

In Normandy for example, results produced by this study led the DREAL to create a regional map of the riparian vegetation density on the rivers' banks (about 10 m wide on each side of the river). This map is used to determine on which stretches of watercourse the trees' shade can be used as a limiting factor to the increasing water temperature. Such information is essential to guide decisions on river management to limit the impact of climate change (Whitehead et al., 2009; Dugdale et al., 2017).

Data availability statement

Publicly available datasets were analyzed in this study. This data can be found here: https://www.normandie.developpement-durable.gouv.fr/temperature-des-cours-d-eau-a4364.html.

Author contributions

BD and FG conceived of the presented idea. NM developed the theory and performed the computations. ZT and FG verified the analytical methods and supervised the findings of this work. All authors discussed the results and contributed to the final manuscript.

Funding

Support for this study was provided by the Agence de l'Eau Seine Normandie (Grant OPE-2020–0382).

Acknowledgments

The authors thank the Direction Régionale de l'Environnement, de l'Aménagement et du Logement (DREAL) de Normandie as well as the Office Français de la Biodiversité for the availability of the measurement data.

Conflict of interest

The authors declare that the research was conducted in the absence of any commercial or financial relationships that could be construed as a potential conflict of interest.

Publisher's note

Supplementary material

The Supplementary Material for this article can be found online at: https://www.frontiersin.org/articles/10.3389/feart.2022.1033673/full#supplementary-material

References

Aires, F., Chédin, A., and Nadal, J.-P. (2000). Independent component analysis of multivariate time series: Application to the tropical SST variability. *J. Geophys. Res.* 105, 17437–17455. doi:10.1029/2000JD900152

Arismendi, I., Safeeq, M., Johnson, S. L., Dunham, J. B., and Haggerty, R. (2013). Increasing synchrony of high temperature and low flow in Western north American streams: Double trouble for coldwater biota? *Hydrobiologia* 712, 61–70. doi:10.1007/s10750-012-1327-2

Attias, H. (1999). Independent factor analysis. *Neural Comput.* 11, 803–851. doi:10.1162/089976699300016458

Beaufort, A., Moatar, F., Sauquet, E., Loicq, P., and Hannah, D. M. (2020). Influence of landscape and hydrological factors on stream–air temperature relationships at regional scale. *Hydrol. Process.* 34, 583–597. doi:10.1002/hyp.13608

Caissie, D. (2006). The thermal regime of rivers: A review. *Freshw. Biol.* 51, 1389–1406. doi:10.1111/j.1365-2427.2006.01597.x

Chandesris, A., Van Looy, K., Diamond, J. S., and Souchon, Y. (2019). Small dams alter thermal regimes of downstream water. *Hydrol. Earth Syst. Sci.* 23, 4509–4525. doi:10.5194/hess-23-4509-2019

Comte, L., Buisson, L., Daufresne, M., and Grenouillet, G. (2013). Climate-induced changes in the distribution of freshwater fish: Observed and predicted trends. *Freshw. Biol.* 58, 625–639. doi:10.1111/fwb.12081

Daufresne, M., and Boët, P. (2007). Climate change impacts on structure and diversity of fish communities in rivers. *Global Change Biology, Wiley* 12 (13), 2467–2478.

Dugdale, S. J., Hannah, D. M., and Malcolm, I. A. (2017). river temperature modelling: A review of process-based approaches and future directions. *Earth. Sci. Rev.* 175, 97–113. doi:10.1016/j.earscirev.2017.10.009

Dugdale, S. J., Malcolm, I. A., Kantola, K., and Hannah, D. M. (2018). Stream temperature under contrasting riparian forest cover: Understanding thermal dynamics and heat exchange processes. *Sci. Total Environ.* 610-611, 1375–1389. doi:10.1016/j.scitotenv.2017.08.198

Ebersole, J. L., Liss, W. J., and Frissell, C. A. (2001). Relationship between stream temperature, thermal refugia and rainbow trout *Oncorhynchus mykiss* abundance in arid-land streams in the northwestern United States. *Ecol. Freshw. Fish.* 10, 1–10. doi:10.1034/j.1600-0633.2001.100101.x

Evans, E. C., McGregor, G. R., and Petts, G. E. (1998). River energy budgets with special reference to river bed processes. *Hydrol. Process.* 12, 575–595. doi:10.1002/(SICI)1099-1085(19980330)12:4⟨575:AID-HYP595⟩3.0.CO;2-Y

Garner, G., Malcolm, I. A., Sadler, J. P., and Hannah, D. M. (2017). The role of riparian vegetation density, channel orientation and water velocity in determining river temperature dynamics. *J. Hydrol. X.* 553, 471–485. doi:10.1016/j.jhydrol.2017.03.024

Gong, W., Yang, D., Gupta, H. V., and Nearing, G. (2014). Estimating information entropy for hydrological data: One-dimensional case. *Water Resour. Res.* 50, 5003–5018. doi:10.1002/2014WR015874

Gresselin, F., Dardaillon, B., Bordier, C., Parais, F., and Kauffmann, F. (2021). Use of statistical methods to characterize the influence of groundwater on the thermal regime of rivers in normandy, France: Comparison between the highly permeable, chalk catchment of the touques river and the low permeability, crystalline rock catchment of the orne river. *Geol. Soc. Lond. Spec. Publ.* 517 (1), SP517-2020-117. doi:10.1144/SP517-2020-117

Hannachi, A., Unkel, S., Trendafilov, N. T., and Jolliffe, I. T. (2009). Independent component analysis of climate data: A new look at eof rotation. *J. Clim.* 22, 2797–2812. doi:10.1175/2008JCLI2571.1

Hannah, D. M., and Garner, G. (2015). River water temperature in the United Kingdom: Changes over the 20th century and possible changes over the 21st century. *Prog. Phys. Geogr. Earth Environ.* 39, 68–92. doi:10.1177/0309133314550669

Hyvärinen, A., and Oja, E. (2000). Independent component analysis: Algorithms and applications. *Neural Netw.* 13, 411–430. doi:10.1016/S0893-6080(00)00026-5

Jackson, F., Hannah, D. M., Fryer, R., Millar, C., and Malcolm, I. (2017). Development of spatial regression models for predicting summer river temperatures from landscape characteristics: Implications for land and fisheries management. *Hydrol. Process.* 31, 1225–1238. doi:10.1002/hyp.11087

Johnson, M. F., Wilby, R. L., and Toone, J. A. (2013). Inferring air-water temperature relationships from river and catchment properties: AIR-WATER temperature relationships in rivers. *Hydrol. Process.* 28 (6). doi:10.1002/hyp.9842

Jones, N. E., and Schmidt, B. J. (2018). Thermal regime metrics and quantifying their uncertainty for north American streams. *River Res. Appl.* 34, 382–393. doi:10.1002/rra.3257

Kelleher, C., Wagener, T., Gooseff, M., McGlynn, B., McGuire, K., and Marshall, L. (2012). Investigating controls on the thermal sensitivity of Pennsylvania streams. *Hydrol. Process.* 26, 771–785. doi:10.1002/hyp.8186

Lalot, E., Curie, F., Wawrzyniak, V., Baratelli, F., Schomburgk, S., Flipo, N., et al. (2015). Quantification of the contribution of the beauce groundwater aquifer to the discharge of the loire river using thermal infrared satellite imaging. *Hydrol. Earth Syst. Sci.* 19, 4479–4492. doi:10.5194/hess-19-4479-2015

Larnier, K., Roux, H., Dartus, D., and Croze, O. (2010). Water temperature modeling in the garonne river (France). *Knowl. Manag. Aquat. Ecosyst.* 04, 04. doi:10.1051/kmae/2010031

Le Lay, H., Thomas, Z., Rouault, F., Pichelin, P., and Moatar, F. (2019). Characterization of diffuse groundwater inflows into stream water (Part II: Quantifying groundwater inflows by coupling FO-dts and vertical flow velocities). *Water* 11, 2430. doi:10.3390/w11122430

Magnuson, J. J., Crowder, L. B., and Medvick, P. A. (1979). Temperature as an ecological resource. *Am. Zool.* 19, 331–343. doi:10.1093/icb/19.1.331

Marchini, J. L., Heaton, C., and Ripley, B. D. (2001). Maintainer and Algorithm, Fastica. *The fastICA Package*.

Middleton, M. A., Whitfield, P. H., and Allen, D. M. (2015). Independent component analysis of local-scale temporal variability in sediment-water interface temperature: Ica to examine sediment-water. *Water Resour. Res.* 51, 9679–9695. doi:10.1002/2015WR017302

Moatar, F., and Gailhard, J. (2006). Water temperature behaviour in the river loire since 1976 and 1881. *Comptes Rendus Geosci.* 338, 319–328. doi:10.1016/j.crte.2006.02.011

Moradkhani, H., and Meier, M. (2010). Long-lead water supply forecast using large-scale climate predictors and independent component analysis. *J. Hydrol. Eng.* 15, 744–762. doi:10.1061/(ASCE)HE.1943-5584.0000246

Poirel, A., Lauters, F., and Desaint, B. (2008). 1977-2006: Trente années de mesures des températures de l'eau dans le bassin du rhône. *Hydroecol. Appl.* 16, 191–213. doi:10.1051/hydro/2009002

Poirel, J., Gailhard, J., and Capra, H. (2010). Influence des barrages-réservoirs sur la température de l'eau : Exemple d'application au bassin versant de l'ain. *La Houille Blanche* 4, 7279–79. doi:10.1051/lhb/2010044

Poole, G. C., and Berman, C. H. (2001). An ecological perspective on in-stream temperature: Natural heat dynamics and mechanisms of human-CausedThermal degradation. *Environ. Manage.* 27, 787–802. doi:10.1007/s002670010188

Ryan, D. K., Yearsley, J. M., and Kelly-Quinn, M. (2013). Quantifying the effect of semi-natural riparian cover on stream temperatures: Implications for salmonid. *habitat Manag.* 20, 494–507. doi:10.1111/fme.12038

Seyedhashemi, H., Moatar, F., Vidal, J.-P., Diamond, J. S., Beaufort, A., Chandesris, A., et al. (2021). Thermal signatures identify the influence of dams and ponds on stream temperature at the regional scale. *Sci. Total Environ.* 766, 142667. doi:10.1016/j.scitotenv.2020.142667

Sinokrot, B. A., and Stefan, H. G. (1994). Stream water?temperature sensitivity to weather and bed parameters. *J. Hydraul. Eng.* 120, 722–736. doi:10.1061/(asce)0733-9429(1994)120:6(722)

Souchon, Y., and Tissot, L. (2012). Synthesis of thermal tolerances of the common freshwater fish species in large Western Europe rivers. *Knowl. Manag. Aquatic Ecosyst.* 405 (405). doi:10.1051/kmae/2012008

Torgersen, C. E., Faux, R. N., McIntosh, B. A., Poage, N. J., and Norton, D. J. (2001). Airborne thermal remote sensing for water temperature assessment in rivers and streams. *Remote Sens. Environ.* 76, 386–398. doi:10.1016/S0034-4257(01)00186-9

Webb, B., and Walling, D. (1993). Temporal variability in the impact of river regulation on thermal regime and some biological implications. *Freshw. Biol.* 29, 167–182. doi:10.1111/j.1365-2427.1993.tb00752.x

Webb, B. W., Hannah, D. M., Moore, R. D., Brown, L. E., and Nobilis, F. (2008). Recent advances in stream and river temperature research. *Hydrol. Process.* 22, 902–918. doi:10.1002/hyp.6994

Westra, S., Sharma, A., Brown, C., and Lall, U. (2008). Multivariate streamflow forecasting using independent component analysis. *Water Resour. Res.* 44. doi:10.1029/2007WR006104

Whitehead, P. G., Wilby, R. L., Battarbee, R. W., Kernan, M., and Wade, A. J. (2009). A review of the potential impacts of climate change on surface water quality. *Hydrological Sci. J.* 54, 101–123. doi:10.1623/hysj.54.1.101

frontiers | Frontiers in Earth Science

TYPE Original Research
PUBLISHED 12 January 2023
DOI 10.3389/feart.2022.929613

OPEN ACCESS

EDITED BY
Xander Wang,
University of Prince Edward Island, Canada

REVIEWED BY
Md Shahid Latif,
University of Western Ontario, Canada
Yong Zeng,
China University of Petroleum, Beijing, China

*CORRESPONDENCE
Xuan Wang,
wangx@bnu.edu.cn

SPECIALTY SECTION
This article was submitted to Hydrosphere, a section of the journal Frontiers in Earth Science

RECEIVED 27 April 2022
ACCEPTED 31 October 2022
PUBLISHED 12 January 2023

CITATION
Wei C, Wang X, Fang J, Wang Z, Li C, Liu Q and Yu J (2023), A new method for estimating multi-source water supply considering joint probability distributions under uncertainty. *Front. Earth Sci.* 10:929613. doi: 10.3389/feart.2022.929613

A new method for estimating multi-source water supply considering joint probability distributions under uncertainty

Chenxi Wei[1,2], Xuan Wang[1,2]*, Jiajia Fang[1,2], Zhijing Wang[3], Chunhui Li[1,2], Qiang Liu[1,2] and Jingzhi Yu[1,2]

[1]State Key Laboratory of Water Environment Simulation, School of Environment, Beijing Normal University, Beijing, China, [2]Key Laboratory for Water and Sediment Sciences of Ministry of Education, School of Environment, Beijing Normal University, Beijing, China, [3]School of Statistics, Beijing Normal University, Beijing, China

A new method integrating techniques of copula and interval estimation to estimate multi-source water supply was proposed. Using the copula theory, joint probability distributions of multiple water sources were constructed for the estimation of water supply. In addition, the interval estimation was used to obtain the interval of water supply under uncertainty for the formulation of water-diversion strategies and the efficient allocation of water resources. This method can give an in-depth investigation on correlations and synchronous–asynchronous characteristics of runoff variations for multiple water sources, thus solving the uncertainty problem of water supply. To demonstrate its applicability, the method was applied to a case study in the Xiong'an New Area, a future metropolis in North China. The results showed that log-normal distributions for the marginal distributions of source 2 (i.e., the Water Diversion Project from the Yellow River to Baiyangdian Lake) and source 3 (i.e., the South-to-North Water Diversion Project) were feasible. The combined channel source, composed of source 2 and source 3, provided [5.20, 12.10] × 10^8 m^3, and reservoir source provided [0.76, 3.60] × 10^8 m^3 of water resources to the Xiong'an New Area per year. Furthermore, without the implementation of multi-source combined water supply pattern in the Xiong'an New Area, there would be a large water supply deficit. This research can provide effective practical suggestions and guidance on water-resource planning and management.

KEYWORDS

joint probabilities, multi-source combined water supply, uncertainty, copula, interval estimation

1 Introduction

Due to the boom of population and the acceleration of urbanization progress worldwide, the contradiction between water supply and demand has become increasingly prominent (Song et al., 2020), especially in arid and semi-arid areas. Accordingly, many inter-basin water diversion projects have been constructed as the main means to alleviate water shortage (Yu et al., 2017; Zhang et al., 2019; Song et al., 2020), and examples include but are not limited to the South-to-North Water Diversion Project (Zhang et al., 2021). The required amount of water relocated through the water diversion projects can be calculated with two constraints, i.e., the amount of water demand of receiving regions and economic benefits from water relocation. Therefore, the estimation of water supply is of great significance for optimal allocations of regional water resources and improvements of water-use efficiency (Huang et al., 2021).

According to different estimation principles, water-supply estimation models fall into two categories: process-simulation models based on runoff generation and data-driven phenomenological models (Fleming et al., 2021). Using the two types of models, point estimation can be obtained; that is, the estimated water supply amount is a fixed value for a certain time and space. However, most hydrological runoff series are usually non-stationary with seasonal fluctuations (Ghasempour et al., 2021) leading to corresponding fluctuations in the water supply within a certain range when river runoff is used as a water source. In addition, urban areas are always in a dynamic state of development, so the point estimation of water supply is neither operable nor practical for water management in the real world. By contrast, interval estimation can not only effectively cover the range of water supply (Mykhailovych and Fryz 2020; Shimakawa and Murakami 2003), but also bring convenience to decision-makers of water resource management. With regard to the uncertainty of water supply and practical water planning and management, the interval estimation is desired.

In recent years, water supply systems have rapidly developed from a single water source to multiple water sources due to their obvious advantage of ensuring the reliability of urban water supply (Puleo et al., 2014; Zhang et al., 2019; An et al., 2021). This multi-source water supply faces new challenges in water resource management (Gao et al., 2018; Yu et al., 2017). On the one hand, available water supply along with spatial and temporal distributions of multiple water resources are different (Zhang et al., 2018; Song et al., 2020), resulting in the increased complexity of water supply management. On the other hand, the indefinite competition and complementarity of multiple water sources, as well as special water supply rules may cause conflicts in water supply calculations (Song et al., 2020). Therefore, it is necessary to conduct the multivariate joint probability analysis of multiple water sources, which is of great significance for reducing the water shortage risk through maintaining the water supply safety.

Copula is a powerful tool for constructing multivariate joint probability distributions and exploring dependency structures between random variables (Hao and Singh, 2016; Wang et al., 2017). As copula can analyze the interactions and interconnections between multiple variables quantitatively, it has been widely used to construct joint probability distributions of multiple variables. One of the main characteristics of copula is that the construction of joint probability distributions and marginal distributions is separated (Hao and Singh, 2016). To date, besides numerous investigations of multivariate flood frequency (Han et al., 2018; Naz et al., 2020), the frequency of rainfall (Zhang and Singh, 2007b; Kuhn et al., 2007), and multivariate drought events (Ayantobo et al., 2019; Li et al., 2020), some studies have reported successful applications of copula in the field of water resource allocation, e.g., the confirmation of compensative operating feasibility of the South-to-North Water Diversion Project (Huang and Niu, 2015). It has been proved that copula can offer technical and decision-making support for the smooth implementation of multi-source water supply.

Taking the Xiong'an New Area, a future metropolis in North China, as an example, this study attempted to propose a water supply estimation method based on joint probability distributions of multiple water sources. The specific objectives were: 1) to generate appropriate marginal distributions of single water source and further construct joint probability distributions of multiple water sources with copula; 2) to determine the interval estimation of water supply according to joint probability distributions of multiple water sources; and 3) to calculate the interval of water supply and guarantee the rate of water use, laying a necessary basis for water resource allocation. The proposed method considering joint probability distributions of multiple water sources for water supply estimation proved to be a reliable and reasonable method, which can provide scientific support for ensuring water supply safety through the optimal allocation of water resources.

2 Materials and methods

2.1 Study area

The Xiong'an New Area (115°37′E–116°20′E, 38°41′N–39°10′N) sits at the heart of the triangular area formed by the cities of Beijing, Tianjin, and Baoding. It is an important area of China's strategic planning of the Coordinated Development of the Beijing–Tianjin–Hebei Region (Figure 1). It covers Xiong County, Rongcheng County, Anxin County, and other surrounding areas with an initial development zone covering 100 km^2. Currently, its economic development level

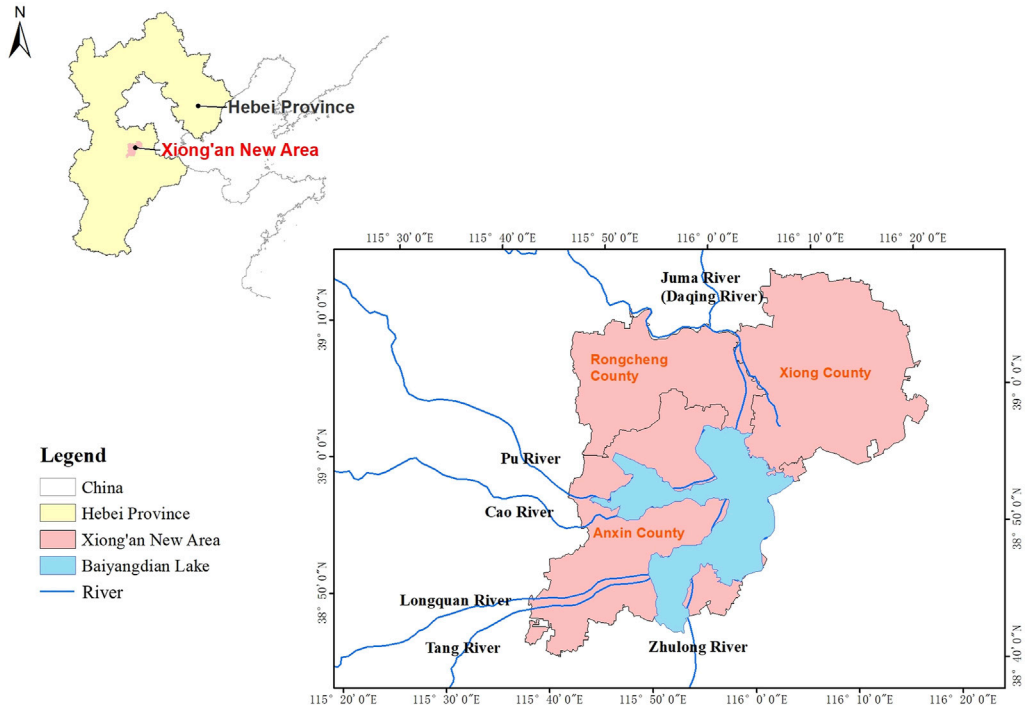

FIGURE 1
The location of the Xiong'an New Area, North China.

and urbanization rate are far lower than the average level of the Hebei Province and China, still having much room for improvement. Consequently, the rapid development of the Xiong'an New Area has great demand for water resources.

Located in the mid-latitude zone, the Xiong'an New Area has a semi-arid temperate monsoon continental climate with four distinct seasons. The annual average precipitation and evaporation are 551.5 mm and 1,369 mm, respectively (Li et al., 2021; Yang et al., 2021). Eighty percent of the precipitation occurs from June to September during the flood season (Liu et al., 2020b). The average annual temperature is 11.7°C and the lowest average monthly temperature is −4.9°C (Yang et al., 2021). The study area used to be rich in wetland resources, including the Baiyangdian Lake and several rivers (Yang et al., 2021). However, in the past five decades, due to the dual effects of climate change and human activity interference, the input water from upstream rivers and reservoirs to the Baiyangdian Lake has gradually decreased with only a few rivers running all year round at present. Water shortage has become a major problem in the region (Zhao et al., 2021).

In general, the water resource conditions in the Xiong'an New Area are poor at this stage. The development of this area is limited due to the grim water resource situation and the contradiction between water supply and demand. In view of the current situation of water resources in the Xiong'an New Area, a large number of water diversion projects, mainly including the Water Diversion Project from Xidayang Reservoir and Wangkuai Reservoir, the Water Diversion Project from the Yellow River to Baiyangdian Lake and the South-to-North Water Diversion Project, have been implemented with joint water supply patterns to alleviate regional water shortage (Zhang et al., 2019; Song et al., 2020; An et al., 2021).

2.2 Data collection

The runoff data of the Water Diversion Project from Xidayang Reservoir and Wangkuai Reservoir (1956–2000), the Water Diversion Project from the Yellow River to Baiyangdian Lake (1919–2013) and the South-to-North Water Diversion Project (1980–2005) were obtained from the Hydrological Yearbook of the People's Republic of China. The economic and social data of the Xiong'an New Area were obtained from the Baoding City Economic Statistics Yearbook, Hebei Province Economic Statistical Yearbook, Hebei Province National Economic and Social Development Statistical Bulletin, Anxin County Chronicles, and relevant data released by the local statistical bureau.

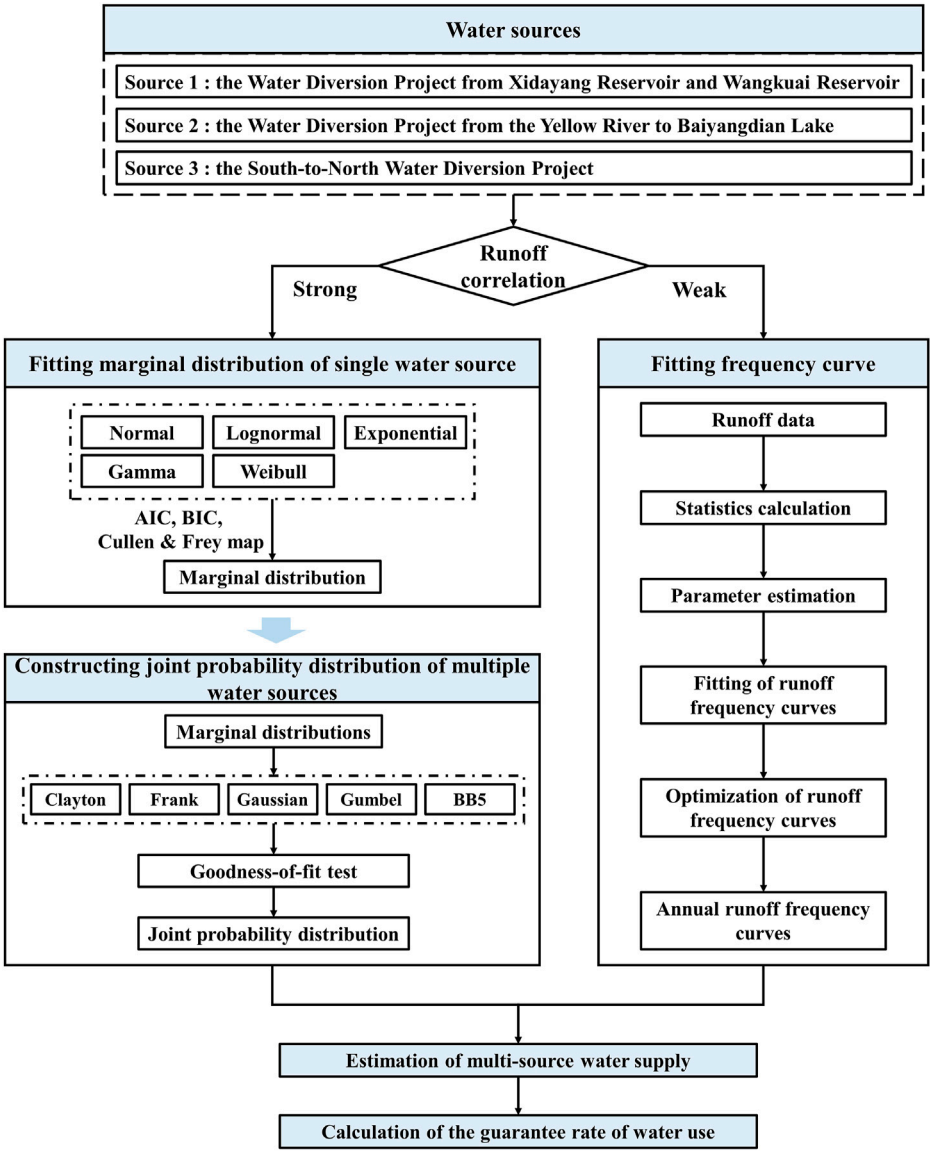

FIGURE 2
Framework for estimating the water supply for multiple water sources.

2.3 Methods

2.3.1 Framework for water-supply estimation based on joint probability distributions of multiple water sources

A new method considering the joint probability distributions of multiple water sources was proposed for water supply estimation. The amount of water supply was calculated under different scenarios by setting various frequency combinations of multiple water sources, so as to provide a quantitative basis for the optimal deployment of regional water resources. The technical roadmap of the study is shown in Figure 2. The main steps are as follows: 1) calculate the correlation coefficients of the runoff series for paired water sources; 2) generate and identify the optimal marginal distribution type of single water sources; 3) construct joint probability distributions of water sources with strong correlation by copula and plot the annual runoff frequency curves of water sources with weak correlation by using the Pearson-III distribution curve; 4) determine the amount of water supply of multiple water sources; and 5) calculate the guarantee rate of water use in sixteen schemes.

2.3.2 Measurement of runoff correlations between paired water sources

The Pearson, Spearman, and Kendall correlation coefficients have been widely used to measure the correlation of variables (Wang et al., 2017). Among them, the Pearson correlation coefficient is often used to measure the correlation between two variables that are linearly related (Hao and Singh, 2016; Wang et al., 2017). In cases where the normal assumption is not true or non-linear correlation exists between variables, the Pearson correlation coefficient is not applicable while the Spearman correlation coefficient and Kendall correlation coefficient can be used instead (Hao and Singh, 2016). More details can be found in the published literature by Wang et al. (2017). We used the Pearson, Spearman, and Kendall correlation coefficients to measure the correlation of random variables.

2.3.3 Construction of marginal distributions and evaluation of fitting degree

The kernel density estimation (KDE) was used for obtaining the probability density function to define univariate marginals. Five distributions including normal distribution, log-normal distribution, Gamma distribution, Weibull distribution, and exponential distribution were selected as candidates to fit the marginal distributions of multiple water sources, with their parameters being estimated by the maximum likelihood method (MLE). According to the Akaike information criterion (AIC), Bayesian information criterion (BIC), and Kolmogorov–Smirnov test (K–S test), appropriate marginal distributions and parameters were determined (Tu et al., 2016). In addition, the fitting of theoretical frequency and empirical frequency was compared. The empirical frequency was calculated by using Gringorten formula (Gringorten, 1963; Zhang and Singh, 2007a).

2.3.4 Construction of joint probability distributions of multiple water sources

Copula can be used to construct multivariate joint probability distributions by linking univariate marginal distributions which can characterize dependence structures among variables (Yu and Zhang, 2021). The main advantage of copula is that it can connect any form of marginal distribution. Moreover, the construction of joint probability distributions is independent of the marginal distributions (Hao and Singh, 2016; Wang et al., 2017). Copula has great flexibility to characterize the dependency between variables (Yu and Zhang, 2021), and thus has become a powerful tool for constructing multivariate joint probability distributions and exploring the correlation among random variables (Wang et al., 2017). Based on Sklar's theorem (Nelsen, 2006), $H(x_1, x_2, \cdots, x_n)$ is the joint distribution with marginal distributions of $H_1(x_1), H_2(x_2) \ldots H_n(x_n)$. For any $x \in R_n$, the distribution function is shown in Eq. 1. If $H_1(x_1), H_2(x_2) \ldots H_n(x_n)$ are all continuous, then C_θ serving as a connection operator is unique.

$$H(x_1, x_2, \cdots, x_n) = C_\theta((H_1(x_1), H_2(x_2), \cdots, H_n(x_n)) \quad (1)$$

where θ is the parameter of copula; C_θ is a copula function; and $H_i(x_i)$ is the marginal distribution for the i-th random variable x_i.

There are many types of copulas with different dependency characteristics (Yu and Zhang, 2021). A variety of copulas can be used for the construction of multivariate joint probability distributions, e.g., Archimedean copulas and Elliptical copulas. Archimedean copulas contain only one parameter and are easy to generate (Salvadori and Michele, 2010; Serinaldi and Grimaldi, 2007), thus having a high utilization frequency in hydrology (Song and Singh, 2010). In this study, Clayton copula, Frank copula, Gaussian copula, Gumbel copula, and BB5 copula were selected as the candidate copulas to construct joint probability distributions of multiple water sources. Frank copula and Gaussian copula exhibited symmetric dependence behavior. Both Clayton copula and Gumbel copula permitted asymmetric dependence (Hao and Singh, 2016); however, in contrast to Gumbel copula, which exhibits strong right tail dependence, Clayton copula exhibits strong left tail dependence. Joe's BB5 copula belongs to extreme-value copulas (Genest and Favre, 2007; Joe, 1997; Sadegh et al., 2017) which can be used to model the dependence structure of rare events or extreme values (Hao and Singh, 2016). The maximum likelihood estimation (MLE) method was used to obtain the parameters of these five candidate copulas. The goodness-of-fit test was performed by using the square Euclidean distance to test the fitting degree to select an optimal copula.

The three-dimensional and contour figures of joint cumulative distributions of multiple water sources were used to calculate the amount of water supply in the multi-source combined water supply system. Each curve in the contour figures represented a joint probability value. The projection of the points on this curve on *x*-axis and *y*-axis represented the water supply from each of the two water sources. The joint water supply at a certain joint probability was equal to the sum of projections of this point on the *x*-axis and *y*-axis. Since there were an infinite number of points on this curve, the amount of water supply fluctuated within a certain range.

2.3.5 Guarantee rate of water use for multiple water sources

With the implementation of water diversion projects including the Water Diversion Project from Xidayang Reservoir and Wangkuai Reservoir, the Water Diversion Project from the Yellow River to Biayangdian Lake, and the South-to-North Water Diversion Project, a multi-source

TABLE 1 The results of runoff correlation measurements for multiple water sources by various correlation coefficients.

	Pearson correlation coefficient	Spearman correlation coefficient	Kendall correlation coefficient
Source 1- Source 2	0.03	0.07	0.03
Source 1- Source 3	−0.04	0.04	0
Source 2- Source 3	0.82**	0.73**	0.60**

Note: * represents 95% confidence level; ** represents 99% confidence level.

combined water supply pattern was formed in the Xiong'an New Area. The guarantee rate of water use under various encounter situations can be calculated based on the different occurrence frequency combinations for the aforementioned three projects which reflect the synchronous–asynchronous characteristics of runoff for these water sources. Based on the runoff correlation results shown in Table 1, water sources can be divided into two groups, which were, a combined channel source with strong correlation and a reservoir source with weak correlation. Among them, the combined channel source here contained the Water Diversion Project from the Yellow River to Baiyangdian Lake and the South-to-North Water Diversion Project; the reservoir source was the Water Diversion Project from Xidayang Reservoir and Wangkuai Reservoir. Since the combined channel source and reservoir source were independent of each other, the concept of mutually independent events from the probability theory was used (Michael Steele, 2015; Zhang et al., 2018; Zhang et al., 2019). Assuming that the combined channel source was event A and the reservoir source was event B, the probability that the combined channel source and reservoir source would occur simultaneously at different encounter probabilities was:

$$P\left(A_iB_j\right) = P\left(A_i\right) \times P\left(B_j\right) \quad (2)$$

where $P(A_i)$ is the joint probability i of combined channel source A; $P(B_j)$ is the runoff frequency j of reservoir source B; and $P(A_iB_j)$ is the encounter probability of the combined channel source A with the joint probability i and reservoir source B with the runoff frequency j.

The water shortages are usually derived from the contradiction between water supply and water demand. The guarantee rate of water use, defined as the degree to which water demand is met, was mainly based on the comparison between the actual water supply and water demand of the water resource system (Zhang et al., 2019). The guarantee rate of water use ranges from 0 to 1; in the case that the actual water supply was greater than water demand, the guarantee rate of water use was 1.

$$G = Q_s/Q_d \quad (3)$$

where G is the guarantee rate of water use; Q_s is the amount of water supply (10^8 m^3); and Q_d is the amount of water demand (10^8 m^3).

3 Results

3.1 Measurement of runoff correlations between multiple water sources

The Xiong'an New Area has three external water sources, namely, the Water Diversion Project from Xidayang Reservoir and Wangkuai Reservoir (source 1), the Water Diversion Project from the Yellow River to Baiyangdian Lake (source 2), and the South-to-North Water Diversion Project (source 3). The results of runoff correlation measurements for the three water sources by various correlation coefficients are shown in Table 1. It can be seen that, three correlation coefficients between source 2 and source 3 were high (specifically, the Pearson correlation coefficient was 0.82, the Spearman correlation coefficient was 0.73, and the Kendall correlation coefficient was 0.60), indicating a strong correlation between source 2 and source 3. Therefore, copula can be used to construct joint probability distributions of source 2 and source 3. The values of the aforementioned three correlation coefficients of source 1 and source 2 were small, indicating a weak correlation between them. Correlation coefficients of source 1 and source 3 were also small. Therefore, copulas were not suitable for constructing joint probability distributions of source 1 and source 2/source 3 due to their weak correlations. The Pearson type III (P-III) distribution was used to fit the distribution of source 1 for hydrological frequency analysis.

3.2 Water supply estimation based on joint probability distributions of multiple water sources

3.2.1 Marginal distribution analysis of water sources

The Cullen and Frey map is a good summary of the properties of marginal distributions. Two Cullen and Frey maps were plotted to preliminarily identify the marginal distribution types of source 2 and source 3 (Figure 3). As Figure 3 shows, compared to other types of marginal distributions, log-normal distribution was more suitable for marginal distributions of both source 2 and source 3. The results of the fitting degree evaluation for source 2 and source

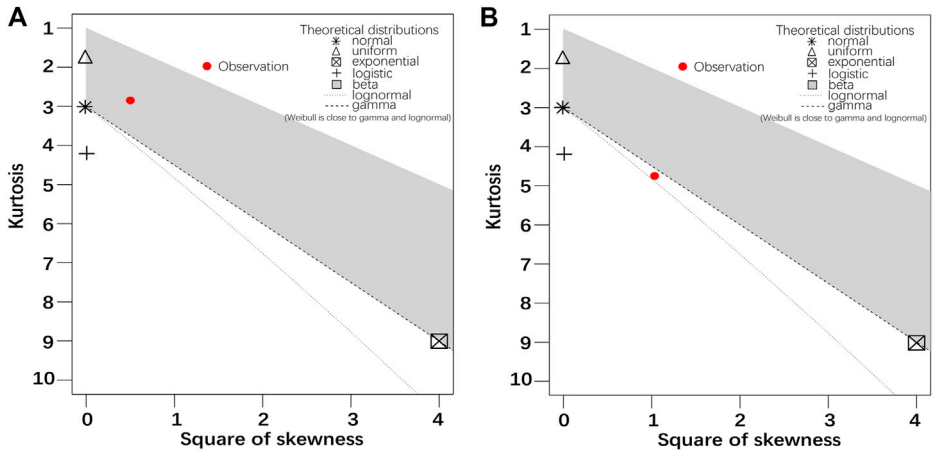

FIGURE 3
Cullen and Frey maps of **(A)** source 2 and **(B)** source 3.

TABLE 2 AIC and BIC results of five candidate marginal distributions.

Distributions	Source 2		Source 3	
	AIC	BIC	AIC	BIC
Normal distribution	245.61	247.53	270.91	273.00
Log-normal distribution	**243.28**	**245.30**	**267.87**	**269.96**
Exponential distribution	264.85	285.72	291.39	292.44
Weibull distribution	244.98	247.16	269.95	272.04
Gamma distribution	243.75	245.63	267.90	269.99

3 with candidate marginal distributions are summarized in Table 2. The smaller the values of AIC and BIC, the better the fitting effects of candidate marginal distributions (Zang et al., 2022). For source 2, log-normal distribution presented the lowest AIC and BIC (243.28 and 245.30, respectively) among the five candidate marginal distributions and passed the K–S test. For source 3, log-normal distribution also presented the lowest AIC and BIC (267.87 and 269.96, respectively) among the five candidate marginal distributions and passed the K–S test. In addition, the results of fitting degree between theoretical frequency and empirical frequency show that the log-normal distribution presented low values of SSE and RMSE, indicating a good performance in fitting the marginal distributions of source 2 and source 3 (Supplementary Table S1). Therefore, log-normal distribution was employed to describe the marginal distributions of source 2 and source 3. Parameter estimation results of the marginal distribution for runoff volume of source 2 and source 3 can be found in Supplementary Table S2. Figure 4 shows the fitting distribution results of source 2 with log-normal distribution. Figure 5 shows the fitting distribution results of source 3 with log-normal distribution. The results further confirmed that it was satisfactory to fit marginal distributions with log-normal distribution for source 2 and source 3.

3.2.2 Joint probability distribution analysis of water sources

Among the five candidate copulas (i.e., Clayton copula, Frank copula, Gaussian copula, Gumbel copula, and BB5 copula), Clayton copula exhibited the smallest square Euclidean distance, suggesting the highest fitting effect. Therefore, Clayton copula was selected to construct joint probability distributions of source 2 and source 3. Figure 6 shows the three-dimensional contour figures of joint probability density distributions of the runoff volume for source 2 and source 3. According to Figure 6, joint probability distributions and dependency characteristics of the runoff volume for various combinations of water sources at specific probability levels were estimated. On the whole, joint probability density distributions of the runoff volume fitted by Clayton copula were bell-shaped with no symmetry on both sides. The overall upper-left trend indicated that variations of joint probability densities of the runoff volume were greatly affected by source 3. Therefore, it was inferred that the high joint probability of the runoff volume would not easily occur in the low-value interval of source 3 (less than 400 million m^3). As shown in Figure 6B, runoff volume contours were dense in the low-value interval (less than 400 million m^3) and sparse in the high-value interval, indicating that the variation of joint probability was much significant in the low-value interval.

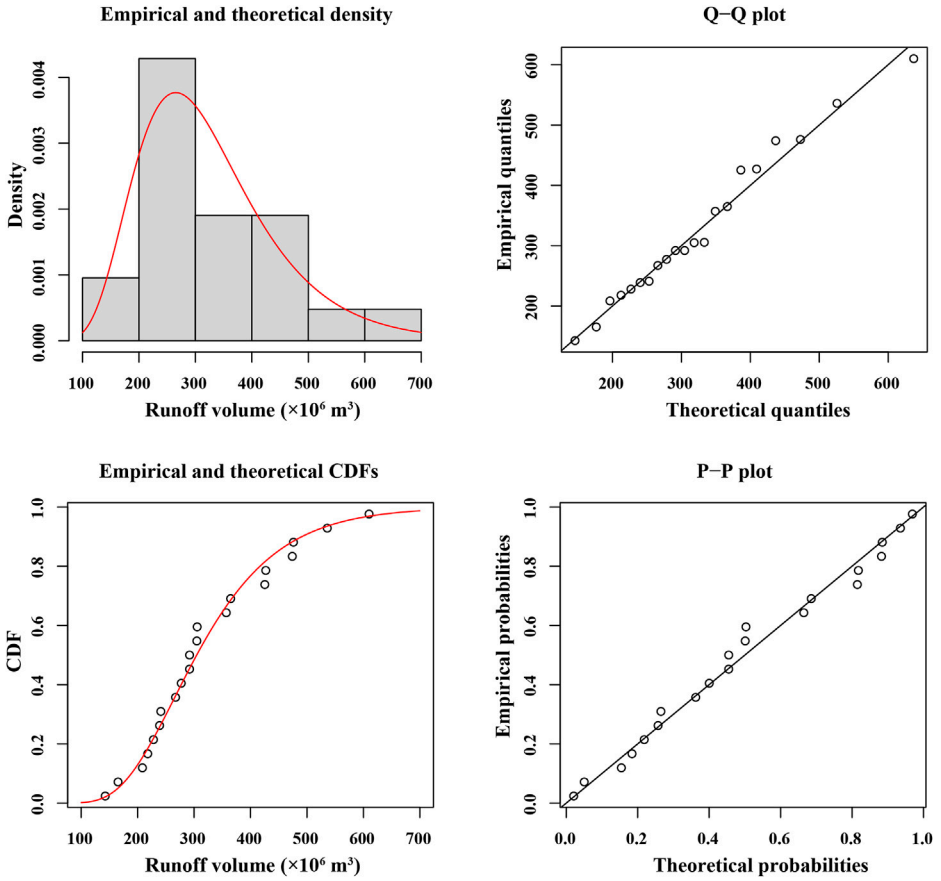

FIGURE 4
Fitting distribution results of source 2 with log-normal distribution.

Figure 7 shows the three-dimensional joint cumulative distributions and their contour figures of runoff volume for source 2 and source 3. As can be seen, the joint cumulative probability increased with the increase of runoff volume of a single water source. When the joint cumulative probability was larger than 0.6, the contour spacing became sparse and the isosurface spacing became larger. In other words, variations of joint cumulative probabilities became less significant in high-value intervals (greater than 0.6) when compared to low-value interval. Through an in-depth analysis of joint cumulative distributions in Figure 7, the encounter situations when the joint probability was equal to or less than a certain probability were obtained. Then, the interval estimations of water supply under different encounter situations were obtained. Figure 7 also shows that when joint cumulative probabilities were 12.5%, 37.5%, 62.5%, and 87.5%, the corresponding interval estimations of water supply were [5.20, 8.90] × 10^8 m^3, [6.80, 9.70] × 10^8 m^3, [8.30,10.40] × 10^8 m^3, [11.40, 12.10] × 10^8 m^3, respectively. Therefore, source 2 and source 3 provided [5.20, 12.10] × 10^8 m^3 of water resources to the Xiong'an New Area per year.

3.3 Water supply estimation based on the runoff frequency analysis of reservoirs

The Pearson-III distribution was used to fit the marginal distribution of the runoff volume of the Xidayang Reservoir and the Wangkuai Reservoir. The Pearson-III distribution is asymmetrically unimodal with a finite boundary on one side but infinite on the other. It is one of the most popular distributions for hydrological frequency analysis (Liu et al., 2015; Wang et al., 2017). The parameters of Pearson-III distribution were determined by using the curve-fitting method and the results of the statistical parameters are shown in Table 3. The runoff frequency curves were drawn by using MATLAB software and the fitting lines were optimized by the non-linear least-square method (Figures 8, 9). According to Figure 8, when the frequencies were 12.5%, 37.5%, 62.5%, and 87.5%, the runoff volume of the Wangkuai Reservoir were 11.80 × 10^8 m^3, 5.60 × 10^8 m^3, 3.90 × 10^8 m^3, and 2.40 × 10^8 m^3, respectively. According to Figure 9, when the frequencies were 12.5%, 37.5%, 62.5%, and 87.5%,

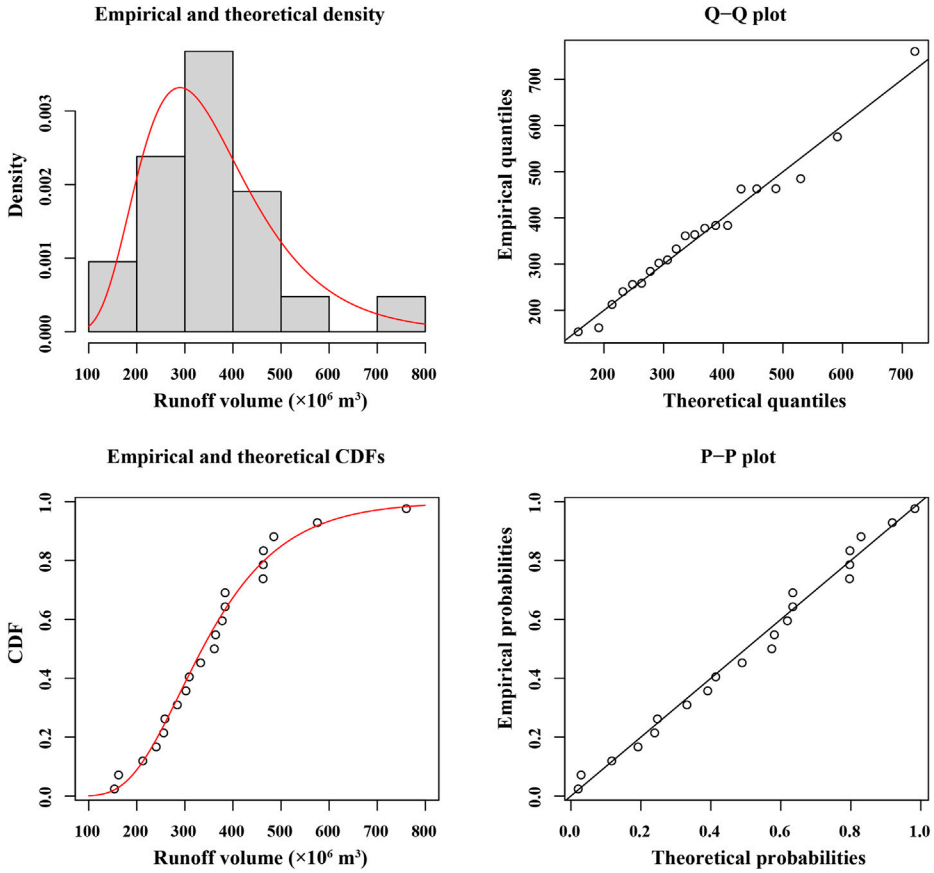

FIGURE 5
Fitting distribution results of source 3 with log-normal distribution.

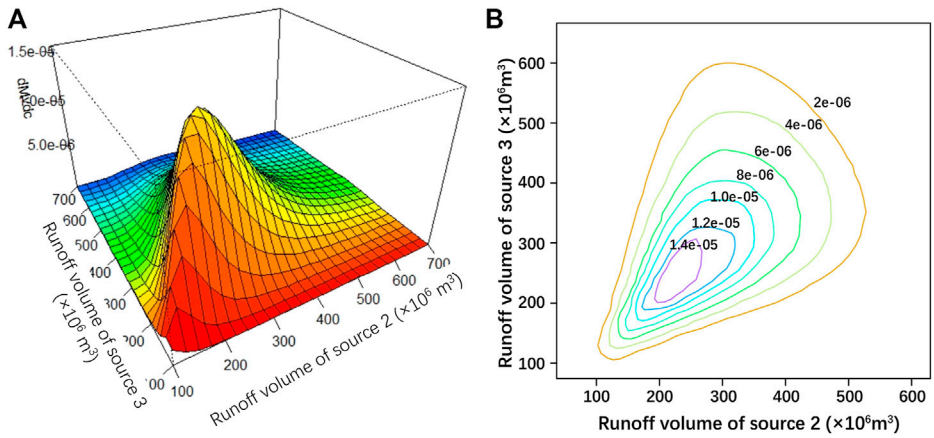

FIGURE 6
(A) Three-dimensional and **(B)** contour figures of joint probability density distributions of source 2 and source 3.

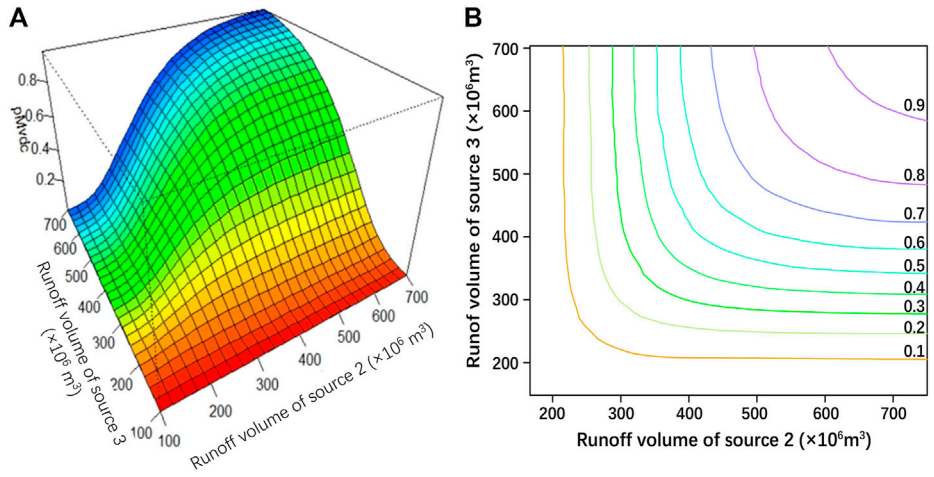

FIGURE 7
(A) Three-dimensional and **(B)** contour figures of joint cumulative distributions of source 2 and source 3.

TABLE 3 The statistical parameters of the runoff frequency curves for the Xidayang Reservoir and the Wangkuai Reservoir (Unit: 10^8 m^3).

Reservoir	Parameters			
	N	Mean	C_V	C_S/C_V
Xidayang Reservoir	45	4.66	0.67	2.00
Wangkuai Reservoir	45	6.24	0.74	

Note: N is the sample size; C_v is variation coefficient; and C_s is deviation coefficient.

the runoff volume of the Xidayang Reservoir were 8.70 × 10^8 m^3, 4.70 × 10^8 m^3, 2.60 × 10^8 m^3, and 2.10 × 10^8 m^3, respectively. Considering water storage requirements as well as basic ecological base flow requirements of the Wangkuai Reservoir and the Xidayang Reservoir, 3.60 × 10^8 m^3, 2.25 × 10^8 m^3, 1.22 × 10^8 m^3, and 0.76 × 10^8 m^3 of water resources were provided to the Xiong'an New Area when the frequencies were 12.5%, 37.5%, 62.5%, and 87.5%, respectively.

3.4 Calculation of the guarantee rate of water use

Figure 10 shows the variations of the guarantee rate of water use in the Xiong'an New Area when combined channel source or reservoir source was used as the only water source. As seen from Figure 10A, when a reservoir source was the only water source, the guarantee rate of water use for the four schemes (i.e., frequencies = 12.5%, 37.5%, 62.5%, and 87.5%, respectively) was generally low (less than 0.1), indicating a large water supply deficit in the region. As can be seen in Figure 10B, when a combined channel source was the only water source, the guarantee rate of water use increased with the increase of joint probabilities ranging from 0.07 to 1 for the four schemes (i.e., joint probabilities = 12.5%, 37.5%, 62.5%, and 87.5%, respectively). It was worth noting that the guarantee rate of water use reached 1 when the joint probability increased to 87.5%. Therefore, the combined channel source was an indispensable water source for the Xiong'an New Area. By comparing Figures 10A, B, it can be found that only the multi-source combined water supply system (namely, both combined channel source and reservoir source) can ensure a high guarantee rate of water use for improving water supply safety.

To analyze variations of the guarantee rate of water use under different encounter situations, sixteen schemes were set up (Table 4), and the results are shown in Figure 11. It can be seen that the Xiong'an New Area had a low guarantee rate of water use (less than 0.6) in most cases, showing that there existed a certain risk of water shortages. With the increase of water supply (from 1.10 × 10^8 m^3 to 10.82 × 10^8 m^3), the guarantee rate of water use gradually increased (from 0.11 to 1), which was consistent with the trend shown in Figure 10. In addition, under the same frequency, the guarantee rate of water use increased significantly with the increase of the joint probability. Without the combined channel source, there would be a large gap between water supply and demand. These illustrated that the combined channel source had a great impact on the mitigation of the water shortage risk. Therefore, the implementation of multi-source combined water supply pattern was a necessary way to improve regional water security.

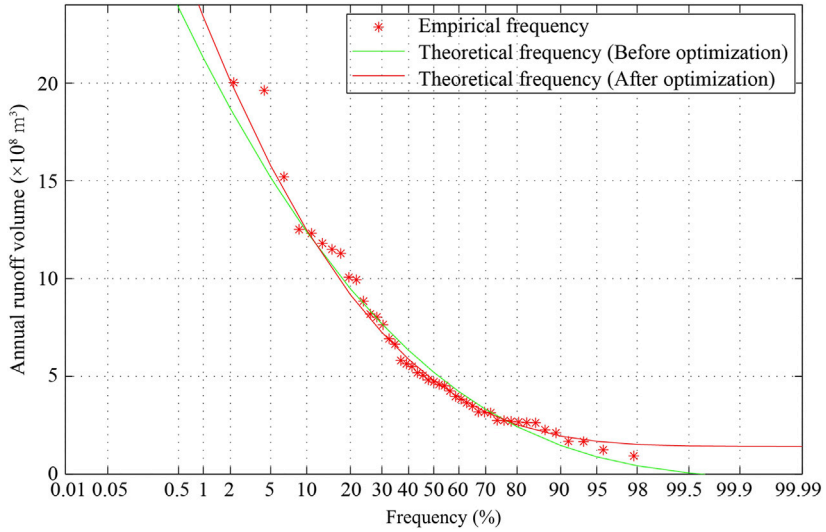

FIGURE 8
Annual runoff frequency curve of Wangkuai Reservoir.

4 Discussion

4.1 Analysis of correlations and variation pace differences of runoff in multi-source system using copula

The estimation of water supply of the multi-source combined water supply system is essentially a stochastic sequential decision-making process with uncertainty (Song et al., 2020). Water sources located in different hydrological zones usually have complex correlations and synchronous–asynchronous characteristics of runoff variations in the multi-source system. However, the commonly used methods have limitations in characterizing the correlation and dependence structure between water sources. The proposed copula-based method conducted a joint probability analysis of three water sources and comprehensively assessed the overall characteristics of water diversion events, overcoming the shortcomings of conventional methods. Hou et al. (2022) predicted that the water supply from upstream reservoirs in 2025 were 0.29×10^8–3.71×10^8 m³, which were basically consistent with our results of interval estimations of water supply. However, their results about the total available water supply were based on the simple linear composition for multiple water sources, without considering their correlations and synchronous–asynchronous characteristics of runoff variations in actual situations. The proposed method made up this deficit by using copulas to take account of various encounter probabilities in a multi-source water supply system, improving the reliability of the estimation results. The results demonstrated the feasibility of the copula-based method considering joint probability distributions of water sources for estimating the water supply in a multi-source combined water supply system. Successful applications of this method have also been reported in the research on the Yellow River Basin, Yangtze River Basin, Yalong River Basin, and Indus River Basin (Huang and Niu, 2015; Gao et al., 2018; Lei et al., 2018; Nazir et al., 2020; Wu et al., 2020; An et al., 2021), demonstrating that the copula-based method is both reliable and generalizable in different regions or basins.

4.2 Treatment of interrelationship between hydrological variables considering their distribution characteristics using copula

In a previous analysis of multivariate hydrological events, some models were built based on the assumption of linear correlation between variables, but this was not in accordance with the fact of complex dependencies usually existing among variables (Hao and Singh, 2016). Another frequently used assumption was that random variables conformed to the same marginal distribution. However, the marginal distributions of different random variables in hydrological events tend to be inconsistent. As a result, these assumptions reduce the accuracy and reliability of the models. As an important connection tool, copula has the following two prominent advantages. First, it can completely describe the correlation structure between random variables with arbitrary marginal distributions by analyzing their joint probability distributions (Cai et al., 2021; Hao and Singh, 2016; Wang et al., 2017). Second, unlike other multivariate parametric distribution models, copula-based methods allow us to separate the univariate margins from the dependence structure for

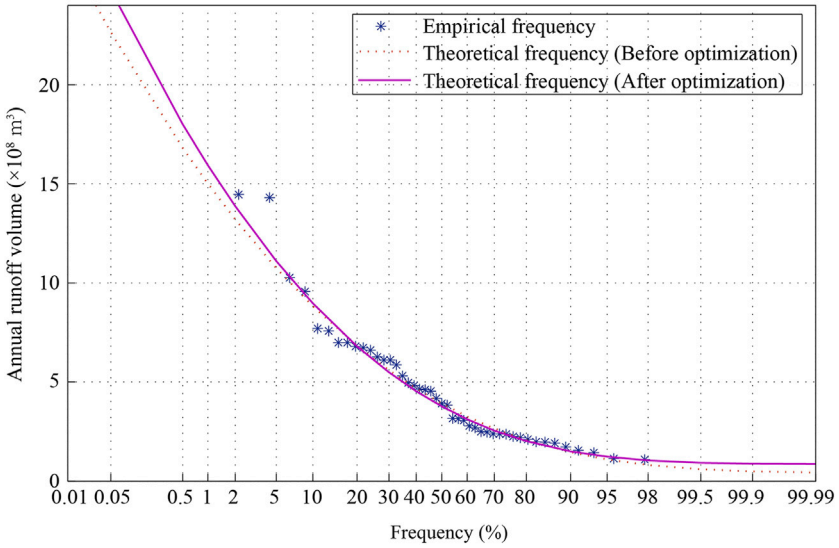

FIGURE 9
Annual runoff frequency curve of Xidayang Reservoir.

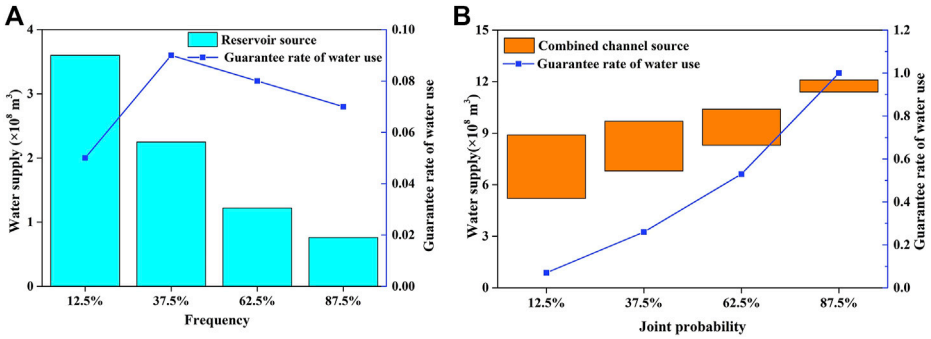

FIGURE 10
The amount of water supply and guarantee rate of water use for four schemes when **(A)** the reservoir source; and **(B)** the combined channel source was the only water source.

the construction of joint probability distributions with the characteristics of flexibility and diversity (Czado and Nagler, 2022; Hao and Singh, 2016). Based on this advantage, the selection of the copula function becomes more flexible; for example, the tail dependency can be captured and expressed using certain copula functions which is essential in assessing risks such as water scarcity in hydrological process analysis (Ayantobo et al., 2019; Hao and Singh, 2016; Liu X. et al., 2020). Interestingly, we found that different copulas were used for solving the same hydrological-related problem. The reason is that copulas lack a physical basis in hydrology; thus, they cannot determine the theoretical joint distribution models of each random variable in a physical sense (Hou et al., 2021). Therefore, the selection of a suitable copula instead of a complex one is particularly critical (Zhang et al., 2021).

4.3 Applicability of interval estimations using copula in water supply management

From Figure 7, the water supply from source 2 and source 3 to the Xiong'an New Area per year was obtained in the form of intervals using copulas. According to Zhang (2017), the corresponding amount of water supply by these two sources were 2×10^8 m^3 and 4×10^8 m^3; that is, a total of approximately 6×10^8 m^3, which was consistent with our interval estimations of water supply. According to Lv et al. (2021),

TABLE 4 Water supply scheme settings under different encounter situations.

Schemes	Joint probability/frequency of water source		Water supply (10^8 m^3)
	Combined channel source ($P(A_i)$)	Reservoir source ($P(B_j)$)	
1	12.5%	12.5%	(5.20 | 3.60)
2		37.5%	(5.20 | 2.25)
3		62.5%	(5.20 | 1.22)
4		87.5%	(5.20 | 0.76)
5	37.5%	12.5%	(6.80 | 3.60)
6		37.5%	(6.80 | 2.25)
7		62.5%	(6.80 | 1.22)
8		87.5%	(6.80 | 0.76)
9	62.5%	12.5%	(8.30 | 3.60)
10		37.5%	(8.30 | 2.25)
11		62.5%	(8.30 | 1.22)
12		87.5%	(8.30 | 0.76)
13	87.5%	12.5%	(11.40 | 3.60)
14		37.5%	(11.40 | 2.25)
15		62.5%	(11.40 | 1.22)
16		87.5%	(11.40 | 0.76)

Note: The two columns for the item of water supply represent the amount of water supply at the joint probability i of combined channel source and the frequency j of reservoir source, respectively.

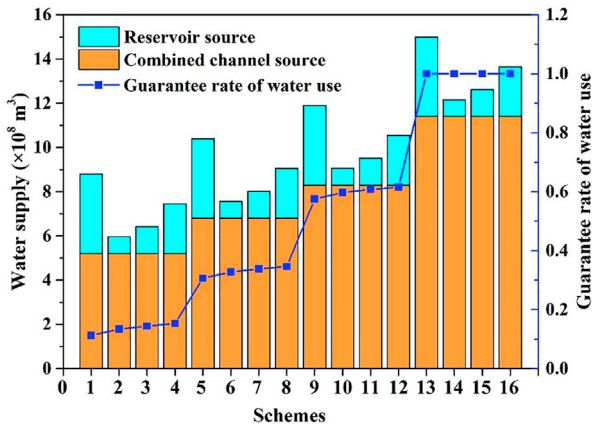

FIGURE 11
Sixteen schemes when both the combined channel source and reservoir source were used.

the water consumption should be controlled at 9.8×10^8 m^3 per year in the context of focusing on the socioeconomic development and eco-environmental protection, and was generally consistent with our interval estimation results of water supply. In addition, the interval estimation of water supply of source 2 and source 3 was almost the same as the amount of water supply of the actual planning and management (Zhang, 2017). These results confirmed the reliability of our relationship analysis between water supply and water consumption when compared with deterministic results.

Actually, as the results from copula-based methods are displayed correspondingly in the form of intervals under some certain probabilities, it overcomes the defect of point estimation results that cannot take advantage of error estimations when conventional deterministic models are applied (Mykhailovych and Fryz, 2020; Shimakawa and Murakami, 2003). Obviously, interval estimations are more reasonable than point estimations and thus more appropriate for real-world decision-making. For example, as the water supply is determined by the water demand of the receiving area for water diversion projects (Zhang et al., 2021), the water supply amount fluctuates over time without keeping a deterministic value. Considering that the joint probability reflects the occurrence of stochastic events, the multi-source water supply under uncertainty can be modeled by bivariate joint probability distribution functions using copula-based methods (Gao et al., 2018). For bivariate joint probability distributions of variables A and B, there are infinite combinations satisfying the solution conditions under a given occurrence probability characterizing their coexistence status (Dodangeh et al., 2020). For example, the joint probabilities of water supply were set based on the local situations, acquiring various combinations of water supply scenarios. These combinations can be selected for formulating alternative schemes of water resource planning and management with a comprehensive consideration of actual situations, e.g., water supply objectives, social and economic benefits, and so on. In

summary, owing to its flexibility and adaptability, copula-based methods can be used to solve joint probability distribution problems of water sources for estimating the water supply in multi-source combined water supply system, expanding its application scopes in the field of water resource research.

5 Conclusions

Taking the Xiong'an New Area in northern China as a typical area, we proposed a new method for the estimation of water supply that considered the joint probability distributions of multiple water sources under uncertainty. Considering runoff correlations between water sources and synchronous–asynchronous characteristics of the water supply capacity related to runoff variations for water sources in different hydrological regions, the copula was used to construct joint probability distributions for describing the dependence structure of a multi-source water supply system and estimating water supply under different encounter situations. It was an innovative application of copulas into the field of water supply estimation. Interval estimation was used in this research to represent the estimation results, which can effectively predict the fluctuation ranges of water supply amount for the convenience of the practical operation of optimal regional water resource allocation. Considering different encounter probabilities of runoff variations, the Water Diversion Project from the Yellow River to Baiyangdian Lake and the South-to-North Water Diversion Project can provide [5.20, 12.10] $\times$ 10^8 m^3 of water resources, and the Water Diversion Project from Xidayang Reservoir and Wangkuai Reservoir can provide [0.76, 3.60] $\times$ 10^8 m^3 of water resources to the Xiong'an New Area per year with the multi-source water supply pattern. The water demand of the Xiong'an New Area can be met through the joint operation of these three water sources.

Due to the limitation of the data availability, this research did not take water quality into consideration. Water quality and water quantity are equally important properties for the water supply. If there was not enough water that met the water quality requirements of regional production and domestic water, a risk of available water shortage would occur (Song et al., 2020). Therefore, the influence of water quality constraints should be highlighted in the estimation of water supply. In addition, besides surface water that accounted for a large proportion of regional water supply, groundwater and reclaimed water should also be considered in subsequent studies.

Data availability statement

The original contributions presented in the study are included in the article/Supplementary Material; further inquiries can be directed to the corresponding author.

Author contributions

CW: conceptualization, methodology, validation and writing—original draft preparation. XW: writing—review and editing, supervision. JF: software, resources, and visualization. ZW: software, data curation, and visualization. CL: supervision. QL: supervision. JY: editing. All authors have read and agreed to the published version of the manuscript.

Funding

This research was financially supported by the National Natural Science Foundation of China (Grant Nos. 52070024, 52270194 and 51679008).

Acknowledgments

The authors would like to extend their special thanks to the editor from the AJE team for editing the English text of a draft of this manuscript. The authors would also like to extend their special thanks to the editor and the reviewers for their valuable comments and suggestions in greatly improving the quality of this manuscript.

Conflict of interest

The authors declare that the research was conducted in the absence of any commercial or financial relationships that could be construed as a potential conflict of interest.

Publisher's note

Supplementary material

The Supplementary Material for this article can be found online at: https://www.frontiersin.org/articles/10.3389/feart.2022.929613/full#supplementary-material

References

An, C., Dou, M., Zhang, J., and Li, G. (2021). Method for analyzing copula-based water shortage risk in multisource water supply cities. *Water Resour. manage.* 35 (14), 4877–4894. doi:10.1007/s11269-021-02975-4

Ayantobo, O. O., Li, Y., and Song, S. (2019). Copula-based trivariate drought frequency analysis approach in seven climatic sub-regions of mainland China over 1961-2013. *Theor. Appl. Climatol.* 137 (3-4), 2217–2237. doi:10.1007/s00704-018-2724-x

Cai, Y., Cai, J., Chen, D., Xie, Y., and Feng, J. (2021). Development of an integrated prediction-optimization modeling approach for coupled risk management of water and energy nexus systems. *Sci. Total Environ.* 781, 146744. doi:10.1016/j.scitotenv.2021.146744

Czado, C., and Nagler, T. (2022). Vine copula based modeling. *Annu. Rev. Stat. Appl.* 9 (1), 453–477. doi:10.1146/annurev-statistics-040220-101153

Dodangeh, E., Singh, V. P., Binh Thai, P., Yin, J., Yang, G., and Mosavi, A. (2020). Flood frequency analysis of interconnected rivers by copulas. *Water Resour. manage.* 34 (11), 3533–3549. doi:10.1007/s11269-020-02634-0

Fleming, S. W., Vesselinov, V. V., and Goodbody, A. G. (2021). Augmenting geophysical interpretation of data-driven operational water supply forecast modeling for a Western US river using a hybrid machine learning approach. *J. Hydrology* 597, 126327. doi:10.1016/j.jhydrol.2021.126327

Gao, X., Liu, Y., and Sun, B. (2018). Water shortage risk assessment considering large-scale regional transfers: A copula-based uncertainty case study in lunan, China. *Environ. Sci. Pollut. Res.* 25 (23), 23328–23341. doi:10.1007/s11356-018-2408-1

Genest, C., and Favre, A. C. (2007). Everything you always wanted to know about copula modeling but were afraid to ask. *J. Hydrol. Eng.* 12, 347–368. doi:10.1061/(ASCE)1084-0699(2007)12:4(347)

Ghasempour, R., Azamathulla, H. M., and Roushangar, K. (2021). EEMD and VMD based hybrid GPR models for river streamflow point and interval predictions. *Water Supply* 21 (7), 3960–3975. doi:10.2166/ws.2021.151

Gringorten, I. I. (1963). A plotting rule for extreme probability paper. *J. Geophys. Res.* 68, 813–814. doi:10.1029/JZ068i003p00813

Han, C., Liu, S., Guo, Y., Lin, H., Liang, Y., and Zhang, H. (2018). Copula-based analysis of flood peak level and duration: Two case studies in taihu basin, China. *J. Hydrol. Eng.* 23 (6), 05018009. doi:10.1061/(ASCE)HE.1943-5584.0001661

Hao, Z., and Singh, V. P. (2016). Review of dependence modeling in hydrology and water resources. *Prog. Phys. Geogr. Earth Environ.* 40 (4), 549–578. doi:10.1177/0309133316632460

Hou, E., Zhang, S., Wang, R., Zhang, C., Yang, H., Duan, J., et al. (2021). Change in water quality and its relationship to water quantity in tai'an section of the dawen River Basin. *J. Irrigation Drainage* 40, 137–144. in Chinese with English abstract. doi:10.13522/j.cnki.ggps.2021141

Hou, X., Yang, R., Hou, B., Lu, F., Zhao, Y., Zhou, Y. Y., et al. (2022). Joint allocation of multiple water sources in Xiongan New Area under complex and uncertain environment. *Water Resour. Hydropower Eng.* 53 (1), 45–54. in Chinese with English abstract. doi:10.13928/j.cnki.wrahe.2022.01.005

Huang, H., and Niu, J. (2015). Compensative operating feasibility analysis of the west route of South-to-North Water transfer project dased on M-copula function. *Water Resour. manage.* 29 (11), 3919–3927. doi:10.1007/s11269-015-1036-5

Huang, H., Zhang, Z., and Song, F. (2021). An Ensemble-Learning-Based method for short-term water demand forecasting. *Water Resour. manage.* 35 (6), 1757–1773. doi:10.1007/s11269-021-02808-4

Joe, H. (1997). "Multivariate models and dependence concepts," in *Monographs in Statistics and probability* (London: Chapman & Hall).

Kuhn, G., Khan, S., Ganguly, A., and Branstetter, M. (2007). Geospatial–temporal dependence among weekly precipitation extremes with applications to observations and climate model simulations in South America. *Adv. Water Resour.* 30, 2401–2423. doi:10.1016/j.advwatres.2007.05.006

Lei, X., Tan, Q., Wang, X., Wang, H., Wen, X., Wang, C., et al. (2018). Stochastic optimal operation of reservoirs based on copula functions. *J. Hydrology* 557, 265–275. doi:10.1016/j.jhydrol.2017.12.038

Li, Z., Shao, Q., Tian, Q., and Zhang, L. (2020). Copula-based drought severity-area-frequency curve and its uncertainty, a case study of Heihe River basin, China. *Hydrology Res.* 51 (5), 867–881. doi:10.2166/nh.2020.173

Li, Z., Sun, W., Chen, H., Xue, B., Yu, J., and Tian, Z. (2021). Interannual and seasonal variations of hydrological connectivity in a large shallow wetland of north China estimated from Landsat 8 Images. *Remote Sens.* 13 (6), 1214. doi:10.3390/rs13061214

Liu, D., Guo, S., Lian, Y., Xiong, L., and Chen, X. (2015). Climate-informed low-flow frequency analysis using nonstationary modelling. *Hydrol. Process.* 29 (9), 2112–2124. doi:10.1002/hyp.10360

Liu, X., Pan, F., Cai, W., and Peng, R. (2020a). Correlation and risk measurement modeling: A markov-switching mixed Clayton copula approach. *Reliab. Eng. Syst. Saf.* 197, 106808. doi:10.1016/j.ress.2020.106808

Liu, Y., Cui, B., Du, J., Wang, Q., Yu, S., and Yang, W. (2020b). A method for evaluating the longitudinal functional connectivity of a river-lake-marsh system and its application in China. *Hydrol. Process.* 34 (26), 5278–5297. doi:10.1002/hyp.13946

Lv, L., Jiang, B., Geng, L., Zhang, H., and Yu, X. (2021). Water use intensity and water demand prediction of Xiongan New Area under different development scenarios. *Hydro-science Eng.* 1, 18–25. in Chinese with English abstract. doi:10.12170/2020040100

Michael Steele, J. (2015). *Probability theory: Formal international encyclopedia of the social & behavioral sciences*. UK: Cambridge University Press.

Mykhailovych, T., and Fryz, M. (2020). "Model and information technology for hourly water consumption interval forecasting," in Proceedings of the 2020 IEEE 15th International Conference on Advanced Trends in Radioelectronics, Telecommunications and Computer Engineering (TCSET), Lviv-Slavske, Ukraine, 25-29 Feb. 2020, 341–345.

Naz, S., Jamil, S. S., and Iqbal, M. J. (2020). Archimedean copula-based bivariate flood-frequency analysis on Sukkur, Pakistan. *Arab. J. Geosci.* 13 (7), 282. doi:10.1007/s12517-020-5223-1

Nazir, H. M., Hussain, I., Faisal, M., Shoukry, A. M., Sharkawy, M. A. W., Al-Deek, F. F., et al. (2020). Dependence structure analysis of multisite river inflow data using vine copula-CEEMDAN based hybrid model. *Peerj* 8, e10285. doi:10.7717/peerj.10285

Nelsen, R. B. (2006). *An introduction to copulas*. New York: Springer.

Puleo, V., Fontanazza, C. M., Notaro, V., and Freni, G. (2014). Multi sources water supply system optimal control: A case study. *Procedia Eng.* 89, 247–254. doi:10.1016/j.proeng.2014.11.184

Sadegh, M., Ragno, E., and Aghakouchak, A. (2017). Multivariate copula analysis toolbox (MvCAT): Describing dependence and underlying uncertainty using a bayesian framework. *Water Resour. Res.* 53, 5166–5183. doi:10.1002/2016WR020242

Salvadori, G., and Michele, C. D. (2010). Multivariate multiparameter extreme value models and return periods: A copula approach. *Water Resour. Res.* 46, 2009WR009040. doi:10.1029/2009WR009040

Serinaldi, F., and Grimaldi, S. (2007). Fully nested 3-copula: Procedure and application on hydrological data. *J. Hydrol. Eng.* 12 (4), 420–430. doi:10.1061/(asce)1084-0699(2007)12:4(420)(2007)12:4(420)

Shimakawa, M., and Murakami, S. (2003). Fuzzy prediction model for water demand prediction using an interpolative fuzzy reasoning method. *Int. J. Syst. Sci.* 34 (14-15), 775–785. doi:10.1080/00207720310001640250

Song, P., Wang, C., Zhang, W., Liu, W., Sun, J., Wang, X., et al. (2020). Urban multi-source water supply in China: Variation tendency, modeling methods and challenges. *Water* 12 (4), 1199. doi:10.3390/w12041199

Song, S., and Singh, V. P. (2010). Meta-elliptical copulas for drought frequency analysis of periodic hydrologic data. *Stoch. Environ. Res. Risk Assess.* 24 (3), 425–444. doi:10.1007/s00477-009-0331-1

Tu, X., Singh, V. P., Chen, X., Ma, M., Zhang, Q., and Zhao, Y. (2016). Uncertainty and variability in bivariate modeling of hydrological droughts. *Stoch. Environ. Res. Risk Assess.* 30 (5), 1317–1334. doi:10.1007/s00477-015-1185-3

Wang, X., Zang, N., Liang, P., Cai, Y., Li, C., and Yang, Z. (2017). Identifying priority management intervals of discharge and TN/TP concentration with copula analysis for Miyun Reservoir inflows, North China. *Sci. Total Environ.* 609, 1258–1269. doi:10.1016/j.scitotenv.2017.07.135

Wu, Z., Chentao, H., Wang, H., and Zhang, Q. (2020). Reservoir inflow synchronization analysis for four reservoirs on a mainstream and its tributaries in flood season based on a multivariate copula model. *Water Resour. manage.* 34 (9), 2753–2770. doi:10.1007/s11269-020-02572-x

Yang, M., Gong, J., Zhao, Y., Wang, H., Zhao, C., Yang, Q., et al. (2021). Landscape pattern evolution processes of wetlands and their driving factors in the xiong'an new area of China. *Int. J. Environ. Res. Public Health* 18 (9), 4403. doi:10.3390/ijerph18094403

Yu, B., Zhang, C., Jiang, Y., Li, Y., and Zhou, H. (2017). Conjunctive use of inter-basin transferred and desalinated Water in a multi-source water supply system

based on cost-benefit analysis. *Water Resour. manage.* 31 (11), 3313–3328. doi:10.1007/s11269-017-1669-7

Yu, R., and Zhang, C. (2021). Early warning of water quality degradation: A copula-based bayesian network model for highly efficient water quality risk assessment. *J. Environ. Manag.* 292, 112749. doi:10.1016/j.jenvman.2021.112749

Zang, N., Zhu, J., Wang, X., Liao, Y., Cao, G., Li, C., et al. (2022). Eutrophication risk assessment considering joint effects of water quality and water quantity for a receiving reservoir in the South-to-North Water Transfer Project, China. *J. Clean. Prod.* 331, 129966. doi:10.1016/j.jclepro.2021.129966

Zhang, C., Nong, X., Shao, D., Zhong, H., Shang, Y., and Liang, J. (2021). Multivariate water environmental risk analysis in long-distance water supply project: A case study in China. *Ecol. Indic.* 125, 107577–107582. doi:10.1016/j.ecolind.2021.107577

Zhang, L., and Singh, V. P. (2007a). Bivariate rainfall frequency distributions using Archimedean copulas. *J. Hydrology* 332 (1), 93–109. doi:10.1016/j.jhydrol.2006.06.033

Zhang, L., and Singh, V. P. (2007b). Gumbel-Hougaard copula for trivariate rainfall frequency analysis. *J. Hydrol. Eng.* 12 (4), 409–419. doi:10.1061/(asce)1084-0699(2007)12:4(409)(200712:4(409)

Zhang, S., Yang, J., Wan, Z., and Yi, Y. (2018). Multi-water source joint scheduling model using a refined water supply network: Case study of Tianjin. *Water* 10 (11), 1580. doi:10.3390/w10111580

Zhang, S., Yang, J., Xu, Z., and Zhang, C. (2019). Effect of frequency of multi-source water supply on regional guarantee rate of water use. *Water* 11 (7), 1356. doi:10.3390/w11071356

Zhang, Y. (2017). Yellow River water diversion to ensure the supply of water resources in Xiong'an New Area. *Water Resour. Plan. Des.* 10, 5–9. in Chinese with English abstract. doi:10.3969/j.issn.1672-2469.2017.10.002

Zhao, Y., Wang, S., Zhang, F., Shen, Q., Li, J., and Yang, F. (2021). Remote sensing-based analysis of spatial and temporal water colour variations in Baiyangdian Lake after the establishment of the Xiong'an New Area. *Remote Sens.* 13 (9), 1729. doi:10.3390/rs13091729

frontiers | Frontiers in Earth Science

TYPE Original Research
PUBLISHED 12 January 2023
DOI 10.3389/feart.2022.961299

OPEN ACCESS

EDITED BY
Wouter Buytaert,
Imperial College London,
United Kingdom

REVIEWED BY
Shuhong Wang,
Shandong University of Finance and Economics, China
Corrado Lo Storto,
University of Naples Federico II, Italy
Yong Zeng,
China University of Petroleum, Beijing, China

*CORRESPONDENCE
Chunhui Li,
Chunhuili@bnu.edu.cn

SPECIALTY SECTION
This article was submitted to Hydrosphere, a section of the journal Frontiers in Earth Science

RECEIVED 06 June 2022
ACCEPTED 31 October 2022
PUBLISHED 12 January 2023

CITATION
Bu J, Zhang S, Wang X, Li C, Wang X, Liu Q, Xu X and Wang X (2023), Study on the influence of industrial structure optimization on water environment and economy: A case study of Changzhou city.
Front. Earth Sci. 10:961299.
doi: 10.3389/feart.2022.961299

Study on the influence of industrial structure optimization on water environment and economy: A case study of Changzhou city

Jiuhe Bu[1,2], Shuiling Zhang[2], Xuesong Wang[3], Chunhui Li[2]*, Xuan Wang[2], Qiang Liu[2], Xiangen Xu[4] and Xia Wang[1]

[1]School of Environmental Engineering, Wuxi University, Wuxi, Jiangsu, China, [2]Key Lab of Water and Sediment Science of Ministry of Education, School of Environment, Beijing Normal University, Beijing, China, [3]Changzhou Branch of Jiangsu Province Hydrology and Water Resources Investigation Bureau, Changzhou, Jiangsu, China, [4]Changzhou Environmental Science Research Institute, Changzhou, Jiangsu, China

Economic development and large amounts of industrial production have led to environmental deterioration. The assessment and prediction of water environment capacity (WEC) are crucial supports for water quality target management. Therefore, this study aims to improve WEC *via* changes in the industrial structure and to analyze the economic changes. For this purpose, the economic efficiency (EE), water use efficiency (WUE), and water treatment efficiency (WTE) are estimated by the EE–SBM (slack-based measure)–DEA (data envelopment analysis) model. Based on the proposed model, the industry is divided into three types: green enterprises, yellow enterprises, and red enterprises. Yellow enterprises and red enterprises are the major supervision subjects, and the spatial distribution of different environmental risks is identified. The WECs of the main canals are analyzed based on dynamic changes in the industrial structure by integrating the 0-D and MIKE11 models. The results showed that after adjusting the industrial structure, the maximum added values of the WEC of chemical oxygen demand (COD), total nitrogen (TN), ammonia nitrogen (NH_3–N), and total phosphorus (TP) are 1,744.66 t/a, 536.14 t/a, 24.81 t/a, and 4.16 t/a, respectively. The results show that the canals (R40, R41, R20, R19, and R17) are overloaded with pollutants and indicate that TN is included as a water environment quality assessment target. Furthermore, after the optimization of the industrial structure, the loss of industrial output value is 174.44 million yuan, and the added value of the environmental economy is 232.12 million yuan. The findings provide important technical support for achieving industrial upgrading and sustainable development.

KEYWORDS

water environment capacity, MIKE11, EE–SBM–DEA, industrial structure, sustainable development

1 Introduction

Since the 21st century, rapid population growth, economic development, and urbanization have led to the deterioration of the water environment of the Taihu Lake, which is associated with a dense canal network (Zhang et al., 2018; Wang J. et al., 2019; 2021b; Ni et al., 2019). Changzhou city is located in the northwestern Taihu Lake, which is an important part of the Taihu Basin. Meanwhile, Changzhou city has been experiencing a poor-quality water environment crisis from non-point and point pollution sources (Li et al., 2018),where point source pollution presents significant challenges (Schmidt et al., 2020).

The water environmental capacity (WEC) has been widely used to control water pollution (Kim et al., 2012; Fakhraei et al., 2014; Yang et al., 2015; Wang Q. et al., 2019), and the key factors that affect the WEC are the amount of pollutant discharge and spatial emissions of pollutants (Guan et al., 2016; Huang and Tong, 2019). Previous studies have shown that point sources were the key influencing factor for the WEC in Changzhou city. Therefore, the actual WEC was improved considering the industrial pollutant problem. The issue of how to harmonize the industrial economy, water use, and environment must be resolved. To address this issue, many studies had focused on the assessment of industrial water use efficiency and water treatment efficiency (Frija et al., 2009; Carvalho et al., 2012; Asghar et al., 2018; Rahman et al., 2019). For instance, Liu et al. (2020) estimated industrial water use and wastewater efficiency to adjust industrial structures by a data envelopment analysis (DEA) model. Wang et al. (2015) presented an approach to assess water use efficiency (WUE) and pollutant reduction potential based on the DEA model. An et al. (2019) investigated the environmental efficiency in the Xiangjiang River Basin based on a slack-based measure (SBM) model. Yang et al. (2020) calculated the environmental treatment, sewage treatment, and water supply efficiency to improve the water quality with the SBM–DEA model in the eastern area of China.

Based on the aforementioned analysis, the DEA model became popular in the water environment. Additionally, the DEA and SBM models have been used to assess water use and water treatment efficiency (WTE). As a type of black box model, the DEA method had an advantage in that it ignored the mechanism relationship between input and output parameters, and its disadvantage was that the solving difficulty and calculation time of the model increased sharply with the expansion of the sample size (Wang et al., 2021c). Therefore, the SBM–DEA model was adopted to simulate multiple inputs and outputs of WUE and WTE stages to correct DEA deviations.

It should be noted that few studies had considered the economic efficiency (EE), water use, and water treatment efficiency with pollutants. As a result, EE, WUE, and WTE were considered simultaneously to optimize the industrial structure and improve the WEC in the article. Meanwhile, the construction of the EE model (output value efficiency) was based on the scale of medium-sized enterprises. The results of the efficiency of all enterprises in the study area were applied to improve the industrial structure, thereby increasing the actual WEC.

In general, the calculation models of WEC were divided into three types: 0-D, 1-D, and 2-D models (Liu et al., 2012; Yan et al., 2019a). However, the three models were used as calculation methods of WEC rather than prediction methods. Therefore, the 0-D model should be coupled with the water quality simulation model to calculate and predict the WEC based on limited observed data in the paper. The MIKE11 model was widely applied to river quality simulation (Keupers and Willems, 2017; Bu et al., 2020). In this article, MIKE11 was selected as the water quality simulation model. Meanwhile, to calculate EE, researchers usually applied the alternative engineering method of pollutants to estimate their abatement costs. Consequently, an alternative engineering method was used to analyze the impact of industrial structure optimization on the economy in the study area.

By reason of the foregoing, the objectives of this study were to evaluate the WUE, WTE, and EE of industries based on coupling the EE and SBM–DEA models to optimize the industrial structure and to analyze the impact on the water environment and economy. In addition, (1) the efficiency evaluation approach was introduced to the coupled EE and SBM–DEA models, (2) the dynamic prediction model of the WEC was established by integrating the 0-D and MIKE11 models, and (3) the economic value was analyzed based on optimization of the industrial structure in Changzhou city.

2 Methodology

In this article, we presented the EE–SBM–DEA model for measuring the output value efficiency (OVE), WUE, and WTE of regional industrial systems. Then, the industry was divided into three types: red industry, yellow industry, and green industry. Management measures were implemented based on different types of industries. Furthermore, we integrated the MIKE11 and 0-D models to create a dynamic assessment and prediction model for the WEC. The calculation results of the EE–SBM–DEA model were input into the MIKE11 and 0-D models. Finally, the WEC of the canal caused by the change in the industrial type was evaluated and simulated in Changzhou city. Meanwhile, the economic benefits after the optimization of the industrial structure were evaluated. The flow is depicted in Figure 1.

2.1 Study area

This study area is Changzhou city (31.15°–32.07°N and 119.13°–120.20°E), which is located in the southern Jiangsu Province of China (Figure 2). The city is situated in the

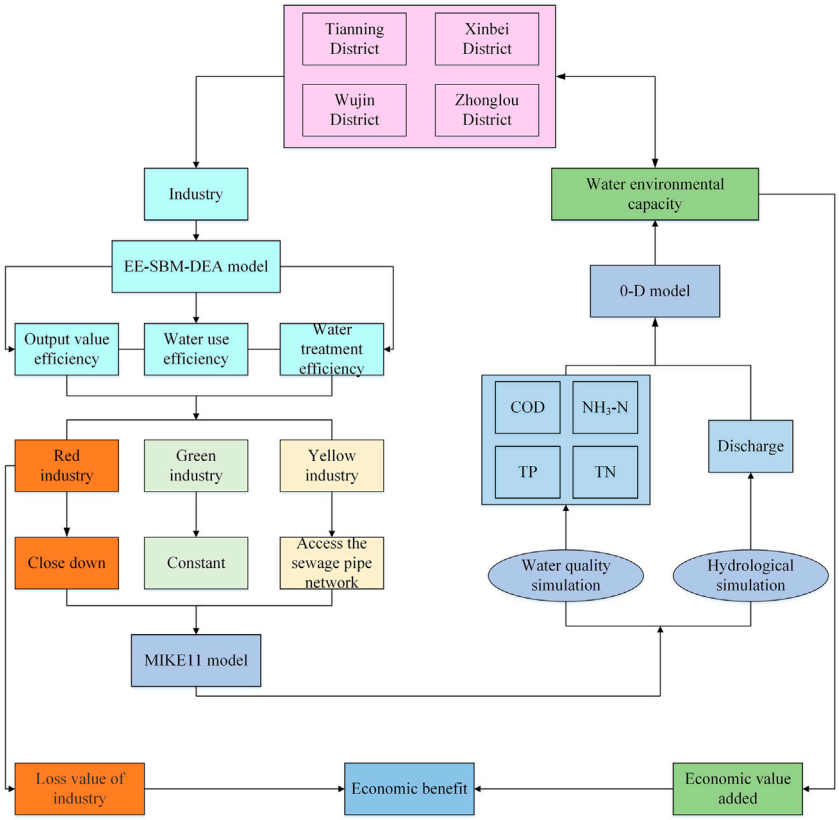

FIGURE 1
Flow chart of water environmental capacity optimization and economic benefit. The EE–SBM–DEA model is used to classify firms into three types, after different industrial types are treated with different methods, the water environmental capacity of the canal are calculated by the MIKE11 and 0-D model, then the economic benefits are obtained by water environmental capacity and industrial types.

Yangtze Delta region, with a total area of 4,375 km^2, and it contains Liyang and Jintan counties and urban districts, including the Wujin, Xinbei, Tianning, and Zhonglou urban districts. This study takes the urban area as the research area (Figure 2). Changzhou city belongs to the northern subtropical monsoon area and has a mild climate and an average annual temperature of 17.4°C. The annual precipitation in wet years reaches 1,243.8 mm. The rainy season is from May to September. The precipitation in the flood season reaches 870.3 mm. The spatial distribution of precipitation does not present considerable variations. The terrain is slightly higher in the southwest and lower in the northeast. The topography is a plain with many rivers, most of which are plain river network areas, and these rivers are canals in cities and are heavily influenced by humans.

2.2 Industrial classification method

The EE, SBM, and DEA methods were used to construct an industrial classification model that identifies industries with a greater impact on the economy and the environment through the analysis of OVE, WUE, and WTE.

2.2.1 Industrial classification model

The DEA model was applied to evaluate the relative effectiveness of different departments (Bian et al., 2014; Wang M. et al., 2021). The traditional DEA model did not consider the intermediate process from input to output, while the network DEA model examined the impact of input to output on efficiency (Gidion et al., 2019). Therefore, the network DEA model was used to measure the efficiency of each link in the industry. The utilization rate of water resources in the industrial production stage was the basis for measuring pollutant emissions. Therefore, the evaluation of industrial WUE was a prerequisite for analyzing the impact of the industry on the water environment (Hu et al., 2018). In summary, the impact of industrial water and sewage treatment on the water environment of the canal network was taken into consideration, and the efficiency calculation of the network DEA model was divided into two stages (Figure 3). The first stage was the industrial water use, and the second stage was

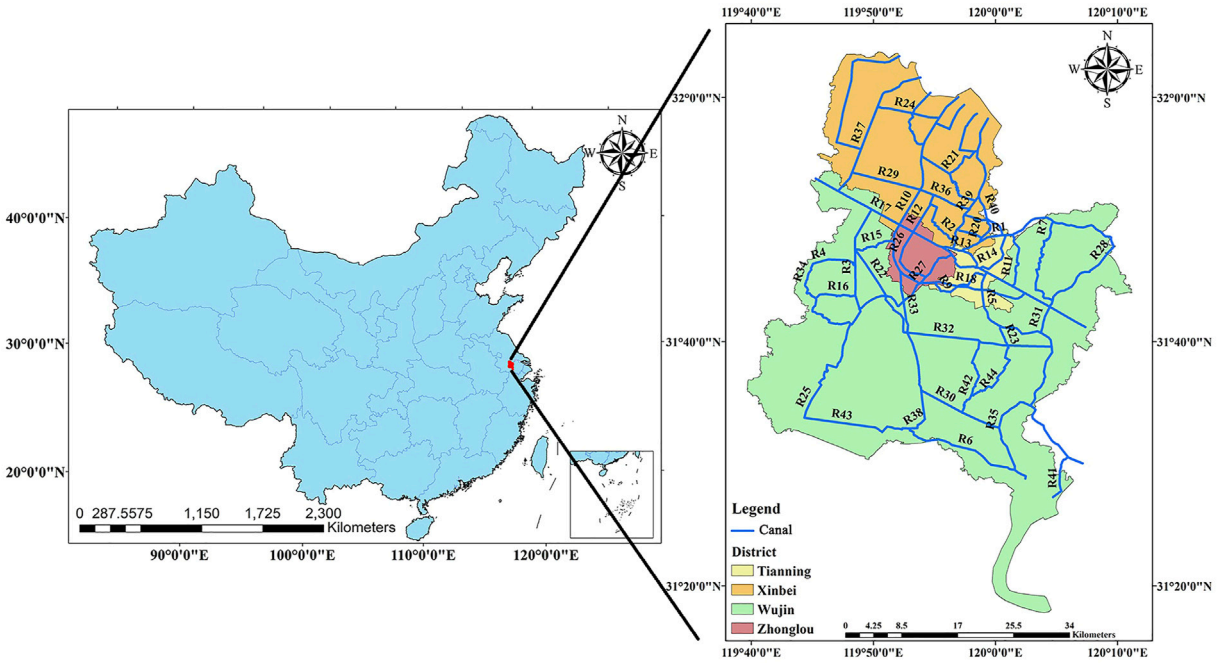

FIGURE 2
Location of geographic space of canals in Changzhou city.

the sewage treatment. Among them, the amount of industrial wastewater discharge was the connecting variable of the two stages because it was the output of the first stage and the input of the second stage (Table 1).

In addition, the conventional network DEA model had radial and slack problems, and the radial network DEA model would overestimate the efficiency of each stage with redundant inputs or insufficient output. Therefore, to overcome the shortcomings of the traditional DEA model, the slack variable SBM was introduced (Tone and Tsutsui, 2014).

It should be noted that for enterprises, some indicators were expected to be improved, and some indicators were needed to be reduced. For these reduced indicators, Koopmans (1951) first proposed the concept of undesired output. In data envelopment analysis, pollutants (wastewater) were usually called undesired outputs, while the outputs that can bring competitive advantages to enterprises were called desired outputs (industrial output value, profit, etc.). In addition, there were three kinds of methods to deal with undesired output problems, which were data conversion function, curve measure evaluation method, and distance function method (Chung et al., 1997; Chen et al., 2021). In this article, the directional distance function method was adopted in the SBM–DEA model, and both radial and relaxation problems were solved. The DEA model was selected using MaxDEA8.0 software, and then input, desired output, and undesired output parameters were set using MaxDEA8.0 software.

In the SBM–DEA model, the water resource utilization efficiency of n decision-making units DMU$_j$ (j=1...,n) and k nodes (k=1...,k) was considered. If m_k and r_k are the number of input and output variables at node k, respectively, then the relationship between node k and the node h is (k, h) and the number of connection variables is L. If the input variable, output variable, and connection variable arex_j^k, y_j^k, and $z_j^{(k,h)}$, respectively, then the production possible set is defined as follows:

$$x^k \geq \sum_{j=1}^{n} x_j^k \lambda_j^k \quad (k = 1, \ldots, K), \tag{1}$$

$$y^k \geq \sum_{j=1}^{n} y_j^k \lambda_j^k \quad (k = 1, \ldots, K), \tag{2}$$

$$Z^{(k,h)} = \sum_{j=1}^{n} z_j^{(k,h)} \lambda_{j,}^k \tag{3}$$

$$Z^{(k,h)} = \sum_{j=1}^{n} z_j^{(k,h)} \lambda_{j,}^h \tag{4}$$

$$\lambda_j^k \geq 0 (\forall j, k), \tag{5}$$

where λ_j^k is the weight vector of the k stage, stage k is the output, and stage h is the input. In addition, the constraint condition is that the sum of unauthorized weights is equal to 1, indicating that the DEA model is constant in return to scale.

The SBM model is introduced, and DMUo (o=1... n) can be written as follows:

$$x_o^k = X^k \lambda^k + s^{k-}, y_o^k = Y^k \lambda^k - s^{k+}, \lambda^k \geq 0, s^{k+} \geq 0, \forall k, \tag{6}$$

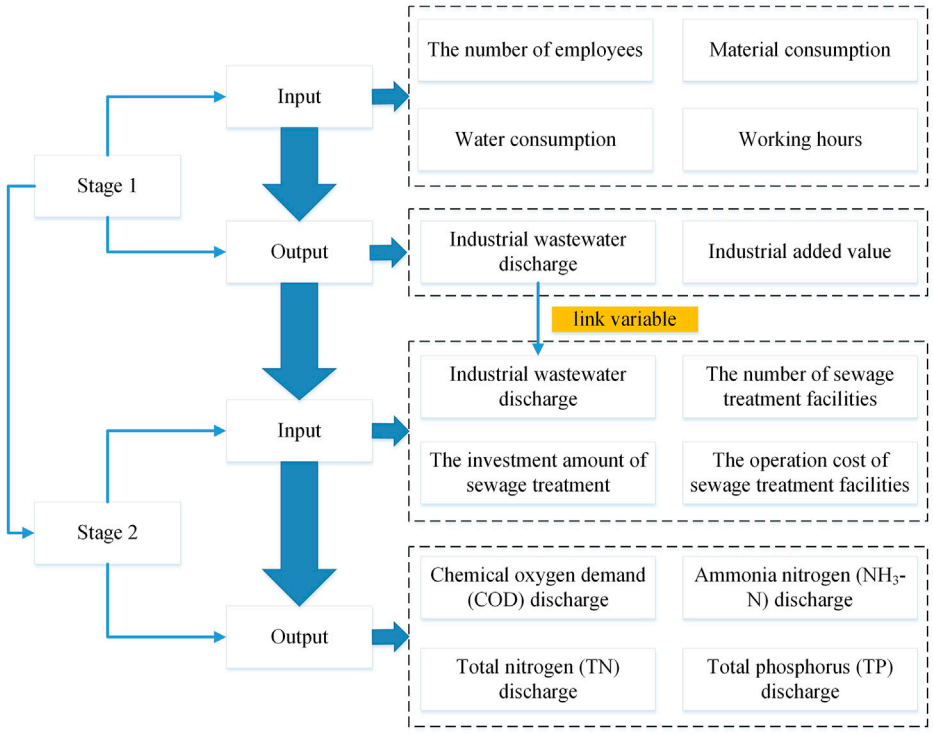

FIGURE 3
Diagram of the SBM–DEA model process.

TABLE 1 Input and output indicators of the SBM–DEA model.

Stage	Type	Indicator	Unit
Water use efficiency (stage 1)	Inputs	Number of employees	Person
		Water consumption	Ton
		Material consumption	Pcs
		Working hours	h
	Desired output	Industrial added value	10 thousand yuan
	Undesired output	Industrial wastewater discharge	Ton
Water treatment efficiency (stage 2)	Inputs	Industrial wastewater discharge	Ton
		Number of sewage treatment facilities	Pcs
		Operation cost of sewage treatment facilities	10 thousand yuan
		Investment amount of sewage treatment	10 thousand yuan
	Undesired output	Chemical oxygen demand (COD) discharge	Ton
		Ammonia nitrogen (NH_3–N) discharge	Ton
		Total nitrogen (TN) discharge	Ton
		Total phosphorus (TP) discharge	Ton

TABLE 2 Industrial type and regulatory measures.

Type	OVE	WUE	WTE	Code	Measure
Green industry	H	H	H	HHH	Constant
	L	H	H	LHH	Constant
Yellow industry	H	L	H	HLH	Access the sewage pipe network or improve the effluent quality
	H	H	L	HHL	Access the sewage pipe network or improve the effluent quality
	L	L	H	LLH	Access the sewage pipe network or improve the effluent quality
	L	H	L	LHL	Access the sewage pipe network or improve the effluent quality
	H	L	L	HLL	Access the sewage pipe network or improve the effluent quality
Red industry	L	L	L	LLL	Close down

TABLE 3 Unit treatment cost of different pollutants in Changzhou city.

Type	COD (CNY/T)	TN (CNY/T)	NH_3–N (CNY/T)	TP (CNY/T)
Treatment cost	4,923.29	63,558.38	87,356.49	1,057,846.11

where $X^k = (x^1, \ldots, x^k)$, $Y^k = (y^1, \ldots, y^k)$, s^{k-} is the input redundancy, and s^{k+} is the output shortage.

At the same time, a free link was chosen as the constraint condition of the connection variable, and it was believed that link activities were freely determined while maintaining the continuity between input and output.

$$Z^{(k,h)}\lambda^h = Z^{(k,h)}\lambda^k, \forall k, h, \tag{7}$$

where $Z^{(k,h)} = Z_1^{(k,h)}, \ldots, Z_n^{(k,h)}$.

2.2.2 Industrial classification

Based on the calculation of the EE–SBM–DEA model, enterprises were divided into three types (as shown in Table 2). Among them, HHH and LHH were green enterprises and did not need to be improved; HLH, HHL, LLH, LHL, and HLL were yellow enterprises and needed to be rectified; and LLL was a red enterprise and it was recommended to shut down.

Note: When the evaluation efficiency is 1, then the index is H; when the evaluation efficiency is less than 1, then the index is L.

2.3 Dynamic simulation of water environment capacity

By classifying industries and implementing corresponding measures for different types of enterprises (Table 2), the impact of industrial adjustment on the WEC of the canal network in the study area could be analyzed. The MIKE11 and EE–SBM–DEA models were used to simulate changes in canal water quality and hydrodynamics before and after industrial adjustment, and the impact of enterprise classification on the water environment capacity of the canal network was evaluated. The MIKE11 model can be used to obtain the future variation values of flow and pollutant concentration in different sections of the canal. The 0-D model was one of the important methods to calculate WEC. In this paper, the MIKE11 model was used to obtain the flow and pollutant concentration of the main section of the canal in the study area. Then, the flow and pollutant concentration were used as input parameters of the 0-D model to obtain the WEC of the canal. The specific description of MIKE11 and 0-D models was as follows:

2.3.1 MIKE11 model

The MIKE11 model was used to simulate changes in hydrology and water environmental capacity. Therefore, in this study, it was selected to simulate the environmental quality of canals. Meanwhile, the MIKE11 model included HD (Eq. 8) and AD modules (Eq. 9). The equation is as follows:

$$\frac{\partial Q}{\partial t} + \frac{\partial}{\partial x}\left(a\frac{Q^2}{A}\right) + g\Lambda\frac{\partial h}{\partial x} + g\frac{Q}{X^2AR} = 0, \tag{8}$$

$$\frac{\partial AC}{\partial t} + \frac{\partial QC}{\partial x} - \frac{\partial}{\partial x}\left(AD\frac{\partial C}{\partial x}\right) = -AKC + S, \tag{9}$$

where x is the distance coordinate (m), t is the time coordinate (s), A is the cross-sectional area (m^2), Q is the flow along the canal (m^3/s), Λ is the momentum correction coefficient (dimensionless), g is the

acceleration of gravity (m/s^2), h is the water level (m), and x is the Chezy coefficient. C is the pollutant concentration (mg/L), D is the longitudinal diffusion coefficient (m/s), K is the degradation coefficient (1/d), and S is the source concentration (mg/L).

A total of 44 canals (Supplementary Appendix SA) were constructed in the MIKE11 model of the urban districts of Changzhou city (Figure 2).

The attenuation coefficient reflected the effect of hydrological changes on pollutants. A reasonable attenuation coefficient was vital to guarantee the accuracy of the model. COD, NH_3–N, TP, and TN were selected as the simulated pollutants in this study, and the attenuation coefficients, K, were 0.18, 0.16, 0.02, and 0.16/d without floodgate scenarios, respectively.

2.3.2 Water environmental capacity model (0-D model)

The 0-D model was selected as the WEC calculation model. The dilution capacity E_d and self-purification capacity E_s were included in two parts.

The dilution capacity formula is as follows:

$$E_d = 86.4 \times (S - C_b) \times Q_r, \tag{10}$$

where E_d is the dilution capacity, kg/d; S is the water quality standard, mg/L; C_b is the canal background concentration, mg/L; and Q_r is the canal discharge, m^3/s.

The self-purification capacity formula is as follows:

$$E_s = 86.4 \times SQ_t\left(1 - e^{-\frac{kL}{86400v}}\right), \tag{11}$$

where E_s is the self-purification capacity, kg/d; S is the water quality standard, mg/L; Q_t is the sum of river and wastewater flows, m^3/s; L is the length of the river, m; k is the comprehensive attenuation coefficient, 1/d; and v is the river velocity, m/s.

The water environment comprehensive capacity formula is as follows:

$$E = E_d + E_s. \tag{12}$$

2.4 Economic valuation

An alternative engineering method was used to calculate economic value, and the calculation formula is as follows:

$$V_r = P_r \times E_r, \tag{13}$$

where V_r is the total cost of water purification for the r pollutant, P_r is the unit treatment cost of the r pollutant, and E_r is the water environmental capacity of the r pollutant.

Furthermore, the unit treatment costs of different pollutant types were obtained from sewage treatment plant in Changzhou city (Table 3).

2.5 Data

Industrial data were collected from the Changzhou Statistical Yearbook and Changzhou Research Academy of Environmental Sciences (2016). Historical discharge and canal level data were acquired through the Changzhou Hydrological Bureau. Water quality data were obtained from the water quality monitoring stations (2016).

3 Results

3.1 Model calibration and verification

To ensure the unity of industrial wastewater and canal flow units in the MIKE11 model, the unit of industrial wastewater discharge was switched from m^3/d to m^3/s. The calculation time duration was set as 366 days (2016) to reduce the model error, the calibration time was from May to July, and the remaining time was the verification time in 2016.

In this study, the relative error (RE) was used to evaluate the accuracy of the model (Eq. 14). According to the simulation results of the MIKE11 model, the RE was obtained. The results of the RE indicated that the model was reliable (Feng et al., 2016).

$$RE = \frac{|y_o - y_s|}{y_o} \times 100\%, \tag{14}$$

where y_o is the observed value, and y_s the is simulated value.

3.1.1 Hydrology verification

The hydrological simulation sites were Buyiqiao, Caoqiao, Jiuli, Henglin, and Wujingang stations. The average discharge and error of each site in 2016 are shown in Figure 4. In the hydrologic simulation, the relative error was smaller than 0.16.

3.1.2 Water quality verification

The water quality concentrations of major canals were simulated (COD, NH_3–N, TN, and TP). The average value and error of the canal water quality concentration in 2016 are shown in Figure 5. In the COD, NH_3–N, TN, and TP simulations, the maximum average relative errors were 0.08, 0.06, 0.11, and 0.03, respectively.

The aforementioned analysis showed the relative error between the observed and simulated values of hydrology and pollutant concentrations (COD, NH_3–N, TN, and TP), and the results indicated that the model was acceptable for further modeling work.

3.2 Classification of the industrial structure

This study takes the urban area of Changzhou as the research object. The area is divided into four administrative districts,

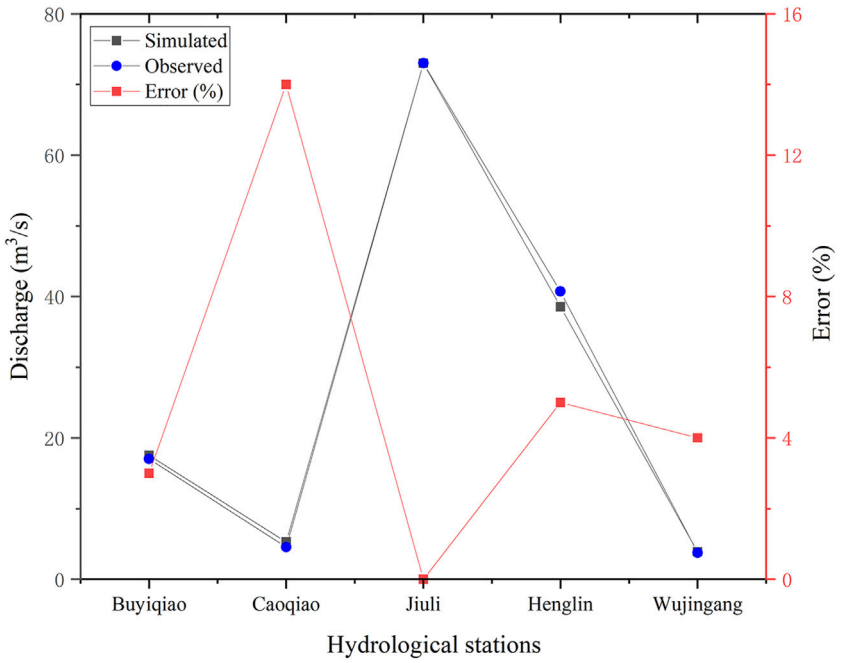

FIGURE 4
Canal discharge simulation and error analysis.

namely, Tianning, Wujin, Xinbei, and Zhonglou districts. Then, the EE–SBM–DEA model was used to classify the industries in each district to obtain the type of each enterprise. Based on the SBM–DEA model, the relevant efficiency statistics results were obtained (Supplementary Appendix SA). In this study, preliminary data had been analyzed and outliers had been removed. Furthermore, the input and output variables were analyzed by Pearson correlation. As shown in Supplementary Table SA3 (Supplementary Appendix SA), EM (the number of employees) and MC (material consumption) in the input indicators were poorly correlated with other input and output indicators, and the output index was strongly correlated with other indexes. Overall, input and output indicators can be used in DEA models, and the sample size included a total of 627 enterprises in the four districts (Tianning, Xinbei, Zhonglou, and Wujin districts); moreover, each enterprise represented a DMU, and the input and output indicators are shown in Table 1. At the same time, the enterprises were divided into six major departments, namely, paint manufacturing, other manufacturing, chemicals, textiles, metal processing, and other industries. Therefore, the DMUs were consistent with the department of the enterprise.

3.2.1 Tianning District

Figure 6A shows that the economic scale of most of the enterprises in Tianning District exceeded 20 million RMB, which was medium-sized and accounts for 60.69%. The average output value efficiency was 0.76, indicating that the enterprises below the medium scale had the potential to reach the medium scale.

The WUE results of various enterprises in Tianning District showed that most enterprises had low WUE, resulting in more wastewater. The average water efficiency (0.51) also proved that the water efficiency of enterprises was low. Among the 144 enterprises, only 25.82% met the water efficiency. Among them, enterprise serial numbers 11, 33, 37, 39, 42, 59, 61, 70, 105, 106, 109, and 118 had the lowest water efficiency and should be considered. The WTE of various enterprises in Tianning District showed that the high concentration of pollutants in wastewater had increased the pressure on the water environment. The WTE was only 0.44, and the proportion of enterprises meeting the water treatment efficiency was only 7.64%. The companies with the lowest water treatment efficiency accounted for 18.05%, and the enterprise serial numbers were 2, 54, 65, 70, 72, 73, 74, 75, 76, 77, 78, 79, 80, 81, 82, 83, 84, 86, 88, 90, 94, 96, 98, 101, 103, and 104. The environmental protection department should focus on inspection of the sewage treatment of these enterprises. Meanwhile, the low WTE indicated that Tianning District had great potential for environmental improvement.

The aforementioned results showed that most enterprises in Tianning District had adopted an extensive economic development mode with environmental destruction. In the future, industrial development should be pursued with equal emphasis on the economy and environment. Figure 7A shows that the proportion of green enterprises was 18.06%, the

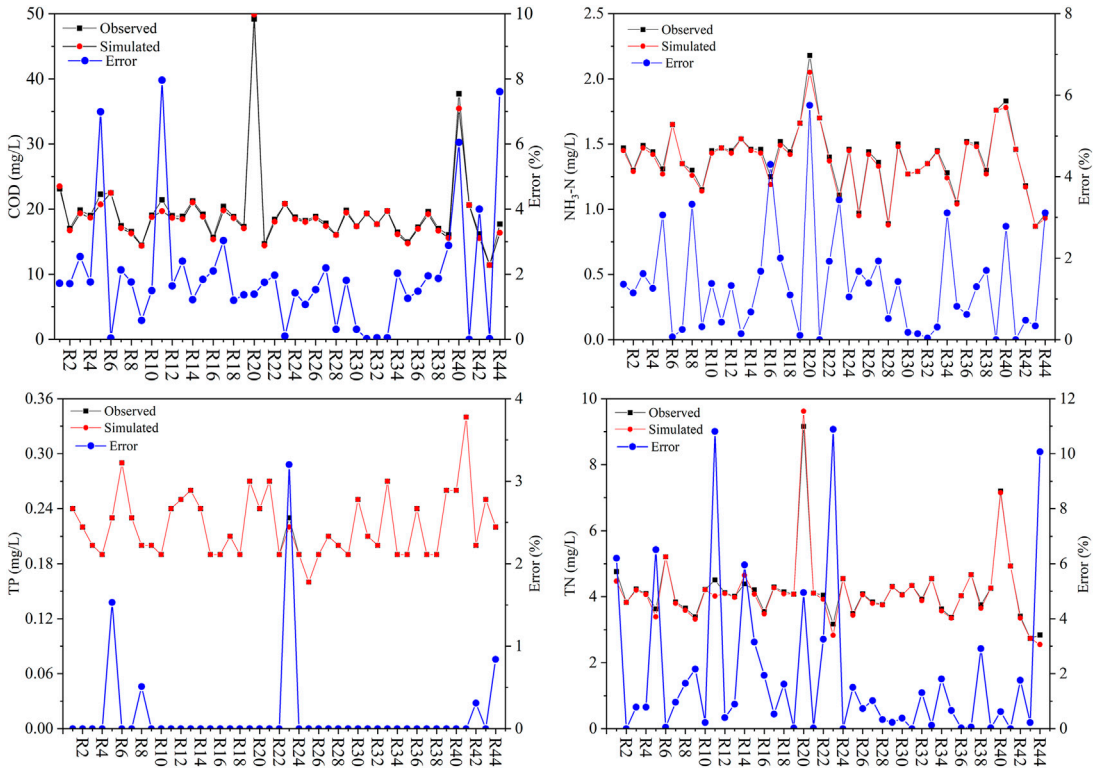

FIGURE 5
Water quality concentration simulation and error analysis of canal.

proportion of red enterprises was 15.97%, and the proportion of yellow enterprises was 65.97%, which also verified that Tianning District had a high water environment improvement potential.

3.2.2 Wujin District

Figure 6B shows that the proportion of medium-sized and above-scale output value enterprises in Wujin District was 59.54% and the average OVE was 0.78, indicating that Wujin District enterprises have better economic benefits. The average WUE of all enterprises in Wujin District was 0.54, indicating that enterprises have low water efficiency. Among them, 22.13% of enterprises met the WUE and 18.32% of enterprises had extremely low water use efficiency, indicating that enterprises in Wujin District waste more water resources, and the government should focus on enterprises with extremely low WUE. The average WTE of the enterprises was 0.58, but only 6.11% of the enterprises met the WTE, whereas 0.76% of the enterprises were extremely low WTE, indicating that the WTE of enterprises in Wujin District was concentrated in the medium level. The shape of the WUE in Figure 6B was more divergent than that of the WTE, which also proved that Wujin District had better control of the pollutant concentration in the wastewater discharge of enterprises. Figure 7B shows that green companies accounted for 16.41%, red companies accounted for 17.18%, and yellow companies accounted for 66.41%. In the process of industrial regulation, the government should focus on red enterprises and improve the efficiency of yellow enterprises to ease the pressure on the water environment in Wujin District.

3.2.3 Xinbei District

Figure 6C shows that the proportion of output value enterprises above the medium scale was 61.06%, and the average OVE was 0.78, indicating that the economic effects of enterprises in Xinbei District were better. The average water use efficiency of all enterprises was 0.42, of which the proportion of enterprises meeting the water efficiency was 20.35%. The proportion of enterprises with extremely low water efficiency was 16.81, indicating that the water efficiency level of enterprises in Xinbei District was low. The enterprise serial numbers were 18, 20, 23, 29, 33, 39, 42, 43, 44, 45, 47, 81, 90, 91, 93, 94, 99, 104, and 107. The WUE of most enterprises was below the average value (0.42), which also proved that the enterprises in Xinbei District waste serious water resources and should increase the water-saving investments. The average WTE of all enterprises in Xinbei District was 0.47, and the proportion of enterprises meeting the WTE was only 8.85%. Companies with extremely low WTE accounted for 8.85%. The specific enterprise serial numbers

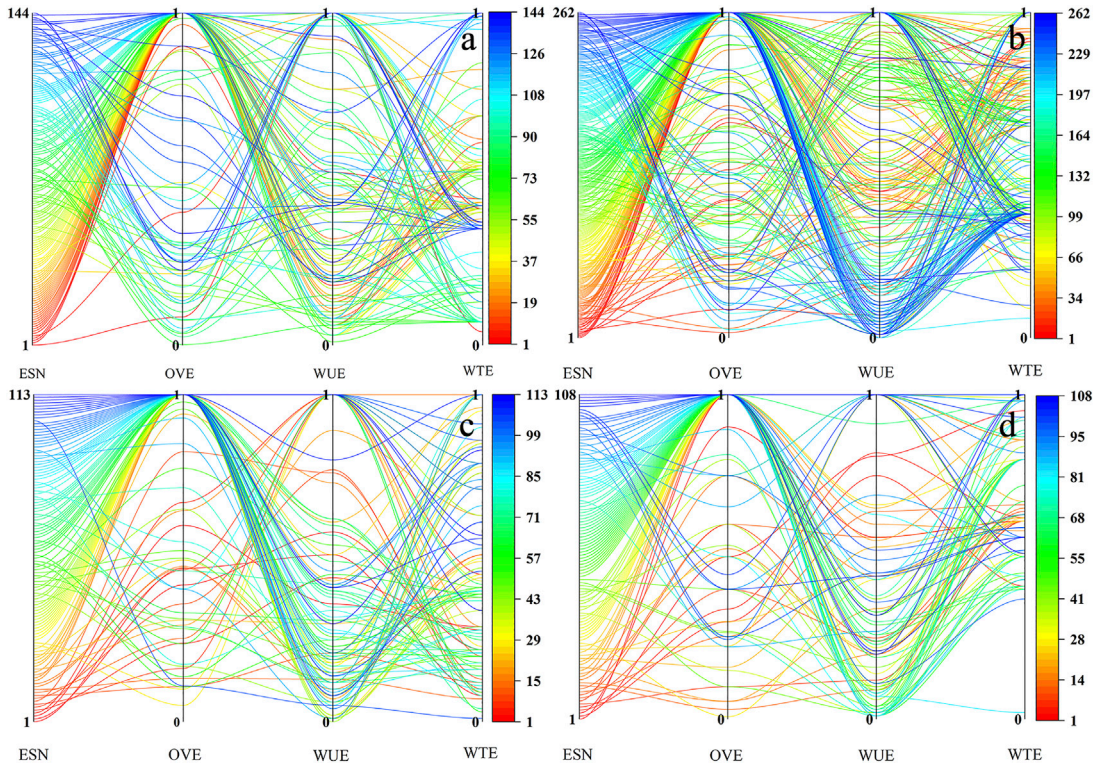

FIGURE 6
Analysis of the industrial output value efficiency, water use efficiency, and water treatment efficiency in Tianning **(A)**, Wujin **(B)**, Xinbei **(C)**, and Zhonglou districts **(D)**. It is important to note that each line represents an enterprise. ESN = enterprise serial number, OVE = output value efficiency, WUE = water use efficiency, and WTE = water treatment efficiency. The enterprise codes are shown in Supplementary Appendix SA. The ordinate of ESN is the serial numbers of all enterprises, and detailed information about the enterprise serial numbers is displayed in the Supplementary Appendix SA. The ordinate of OVE, WUE, and WTE are the display of the efficiency statistical results calculated by the EE–SBM–DEA model.

were 1, 7, 12, 15, 28, 56, 59, 71, 83, and 104, indicating that most companies in Xinbei District had medium WTE. The WTE showed that the water treatment efficiency of enterprises was concentrated between 0 and 1, but relatively scattered, indicating that the WTE of enterprises was quite varied. Figure 7C shows that green companies accounted for 17.70%, red companies accounted for 14.16%, and yellow companies accounted for 68.14%. These findings show that industrial adjustments will help ease the pressure on the water environment of Xinbei District.

3.2.4 Zhonglou District

Figure 6D shows that the proportion of enterprises with medium-sized and above-scale output value in Zhonglou District was 62.04%, and the average OVE was 0.78, indicating that enterprises in Zhonglou District had better economic benefits. The average water use efficiency of enterprises in Zhonglou District was 0.39, the proportion of enterprises meeting WUE was 18.52%, and the proportion of enterprises with extremely low water use efficiency was 26.85%, indicating that enterprises in Zhonglou District had extremely low water efficiency. In Figure 6D, the WUE of most companies was below the average, indicating that companies waste water more seriously. The average WTE in Zhonglou District was 0.71, and the proportion of enterprises meeting the WTE was 9.26%. Companies with extremely low water treatment efficiency accounted for 0.93%, and the specific company serial number was 82. These findings showed that the WTE of enterprises in Zhonglou District was higher, which effectively reduces the concentration of pollutants in discharged wastewater. Figure 6D verifies that the WTE of most companies was above average. The enterprise classification results of Figure 7D show that green companies account for 25%, red companies account for 20.37%, and yellow companies account for 54.63%. The aforementioned results showed that the lower WUE of enterprises in Zhonglou District was the main factor for more pollutant emissions. Therefore, the government should guide enterprises to enhance the efficiency of water circulation, pay attention to the pollution discharge of red enterprises, and ease the pressure on the water environment in Zhonglou District.

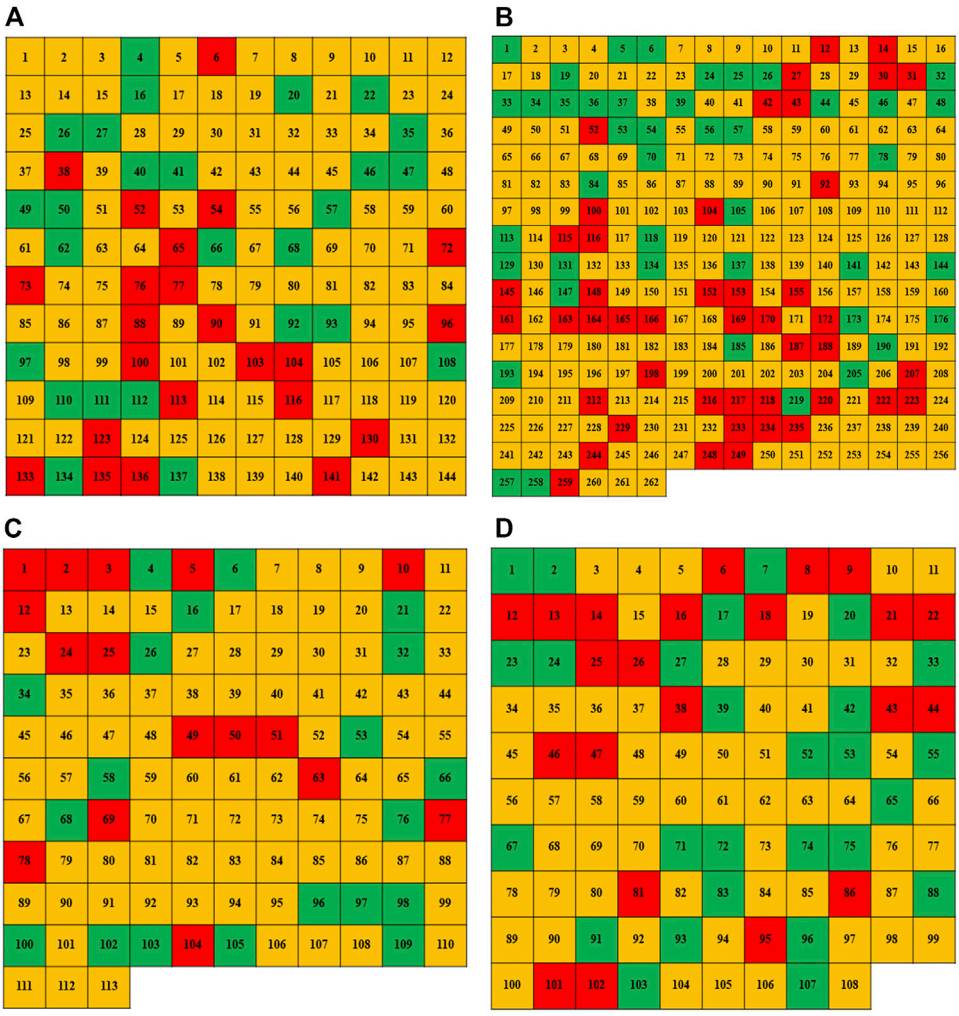

FIGURE 7
Results of enterprise classification in Tianning **(A)**, Wujin **(B)**, Xinbei **(C)**, and Zhonglou districts **(D)**. Colors in the squares represent the type of enterprise calculated by the EE–SBM–DEA model, the numbers in the squares are the serial numbers of all enterprises (Supplementary Appendix SA for the meaning of numerical serial number). Additionally, green indicates green enterprises, yellow indicates yellow enterprises, and red indicates red enterprises.

In summary, this article analyzed the OVE, WUE, and WTE of the four districts of Tianning, Wujin, Xinbei, and Zhonglou in Changzhou city, and enterprises in each district were divided into three types. The results showed that the OVE of these four study areas was high and the proportion of medium-sized enterprises was more than 60%. The WUE of enterprises in Zhonglou District was significantly lower than that of the other three research areas, although the WTE in Zhonglou District was higher, indicating that enterprises in Zhonglou District paid more attention to sewage treatment. The WUE and WTE of Tianning District and Xinbei District were relatively divergent, indicating that the administrative department may not impose strict restrictions on the enterprise's water use and pollutant concentration. The classification of enterprises showed that industrial regulation had great potential for improving the WEC of canal networks.

3.3 Water environmental capacity

This paper classified the enterprises in the study area based on the EE–SBM–DEA model. Then, MIKE11 and the 0-D models were used to calculate the WEC of the canal (COD, NH_3–N, TP, and TN). Figure 8A shows that the COD of canals R40 and R20 exceeded the carrying capacity before the regulation, while R40 could have a COD load of 397.25 t/y after regulation, which indicated that industrial regulation increased the COD capacity of R40 by 1,110.04 t/y. The COD

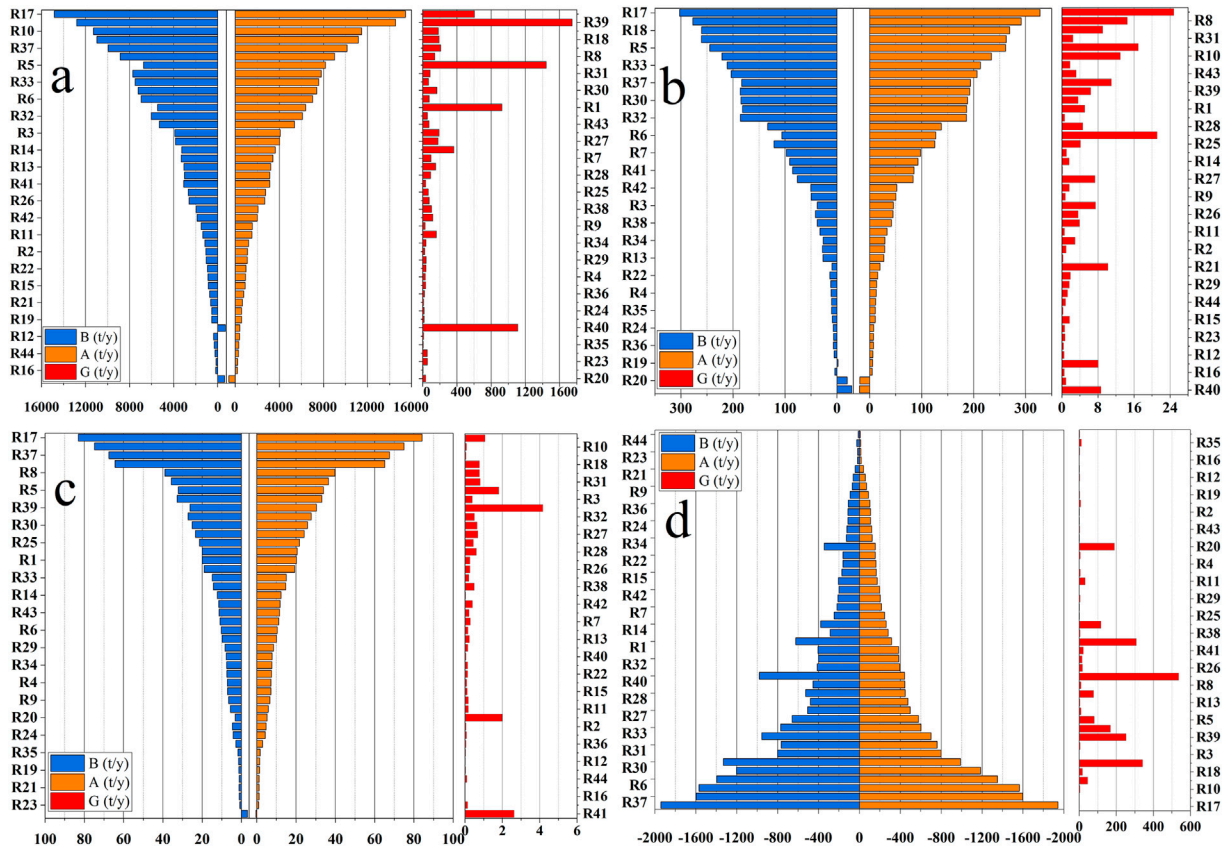

FIGURE 8
Water environmental capacity of COD **(A)**, NH_3–N **(B)**, TP **(C)**, and TN **(D)** in the canal network of the study area. B = WEC before industry adjustment, A = WEC after industry adjustment, and G = WEC growth value. The ordinate of this figure is the canal in the study area, and the horizontal axis represents the total amount of pollutants the canal can carry.

capacity of canal R17 was the largest at 14,839.97 t/y before regulation and 15,444.49 t/y after regulation. Industrial regulation presented the largest increase in the COD capacity of R39 reaching 1,744.66 t/y. However, the COD capacity of R16 only increased slightly by 4.26 t/y.

Figure 8B shows that the NH_3–N of R40, R20, and R19 exceeded the carrying capacity before regulation, while only R19 met the NH_3–N load of 6 t/y after industrial regulation. Therefore, the focus should be on R40 and R20. Among the canal network water systems, the capacity of NH_3–N in R17 was the largest, with 302.74 t/y before regulation and an increase of 24.81 t/y after regulation. Industrial regulation had led to the smallest improvement in the NH_3–N capacity of R13, which was only 0.27 t/y.

Figure 8C shows that only canal R41 exceeded the TP-carrying capacity, and the TP load of this canal still exceeded 0.49 t/y after regulation. R17 had the largest TP-carrying load at 80.07 t/y before industrial regulation and 84.14 t/y after regulation. The canal with the largest increase in TP environmental capacity after industrial regulation was R39, with an added value of 4.16 t/y.

Figure 8D shows that the TN load of the canal network in the study area was overloaded. Meanwhile, the overload capacity of R17 had reached 1,942.21 t/y, and it was increased by 0.9 t/y after industrial regulation. Thus, the TN emissions in the canal network must be addressed. After industrial regulation, the maximum increased in TN-carrying capacity of R40 was 536.14 t/y, with a growth rate of 54.73%; and the canal with the smallest increase was R17 at only 0.15 t/y.

In summary, the water environment capacity of the canal network had been improved through the classification and regulation of industries in the study area. Among them, the improvement effect of COD and TN was more evident. However, the improvement effect of NH_3–N and TP was not notable, which showed that the concentrations of COD and TN in the wastewater of the enterprise were relatively high. In addition, the carrying capacity of COD, NH_3–N, and TP of canal R17 was the largest. The main reason may be that R17 was the canal with the largest flow and length in the study area, which increased the

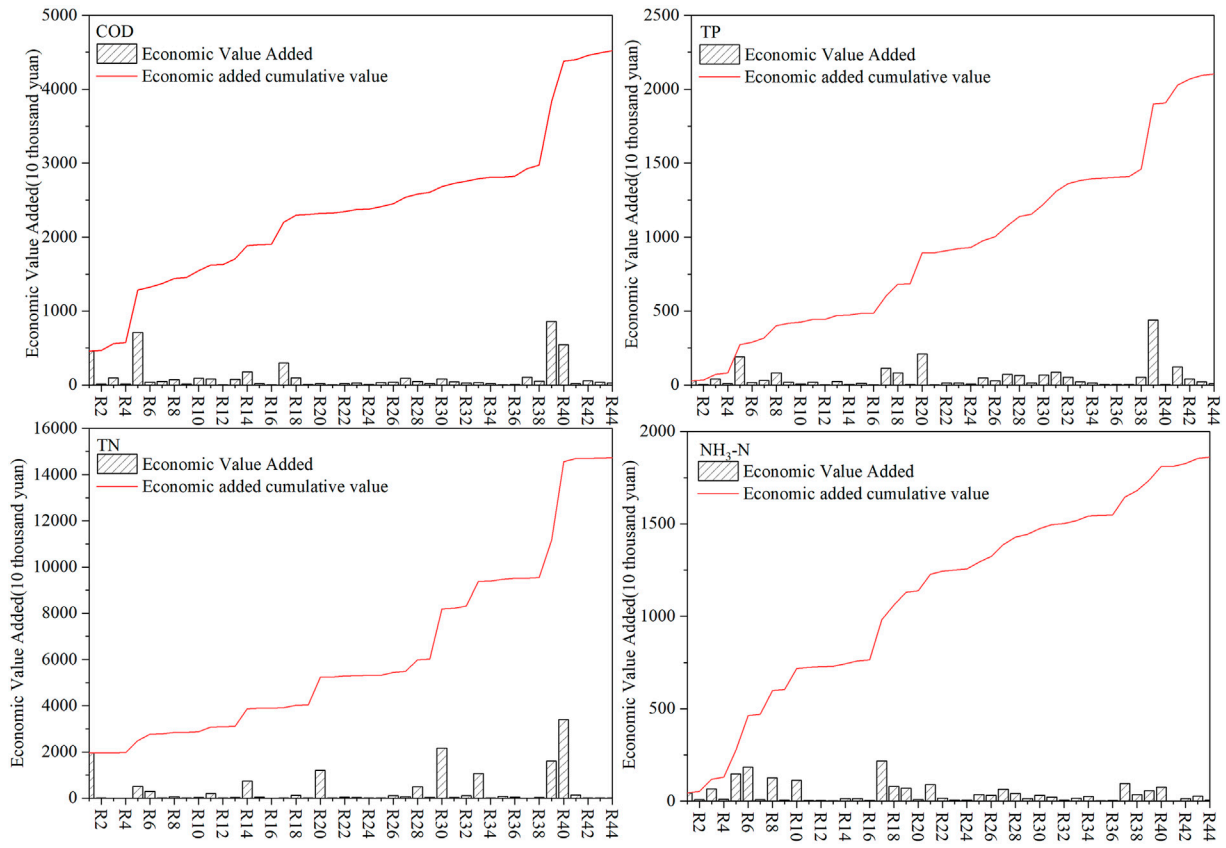

FIGURE 9
Economic value added of different canals in the study area.

water environment capacity of the canal. The carrying capacity of the water environment of canal R40 was weak, and the carrying capacity had increased greatly after industrial regulation. The main reason may be that there were more yellow and red companies around the canal, which caused greater pollution, and the improvement effect after regulation was more evident. The TN overload in the study area was more serious, the main reason may be that the TN in the study area was not set as a goal by the bureaucracy, which led to a high TN concentration in the canal network. Therefore, industrial regulation can effectively increase the water environmental capacity of canals. In addition, to improve the TN-carrying load of the canal network, TN should be included in performance assessments by the government.

3.4 Economic value added

Figure 9 shows the added economic value of different canals in the study area after the optimization of the industrial structure. According to the formula of economic value, the added economic value was positively correlated with the added value of water environmental capacity. Therefore, the growth of water environmental capacity of COD/NH_3–N/TP/TN was consistent with the growth of economic value of canals. Table 4 shows that the improvement in water environment quality increased the economic value of 232.12 million yuan. Due to the optimization of the industrial structure, red enterprises were shut down. Therefore, a certain economic loss was caused. After calculation, the economic loss value was 174.44 million yuan. Although the optimization of the industrial structure caused a certain economic loss, the improvement in environmental quality brought by it not only made up for the economic loss, but also created a certain surplus, reaching 57.68 million yuan.

4 Discussion

The spatial distribution of industrials showed that Tianning and Zhonglou districts had higher industrial density (Figure 10), and canals in areas with higher industrial density were more likely to be polluted (Dsikowitzky et al., 2017; Rodgers et al.,

TABLE 4 Economic value of optimization of the industrial structure.

Type	Economic value added	Loss value of industry	Surplus value
Value (10 thousand yuan)	23,212	17,444	5,768

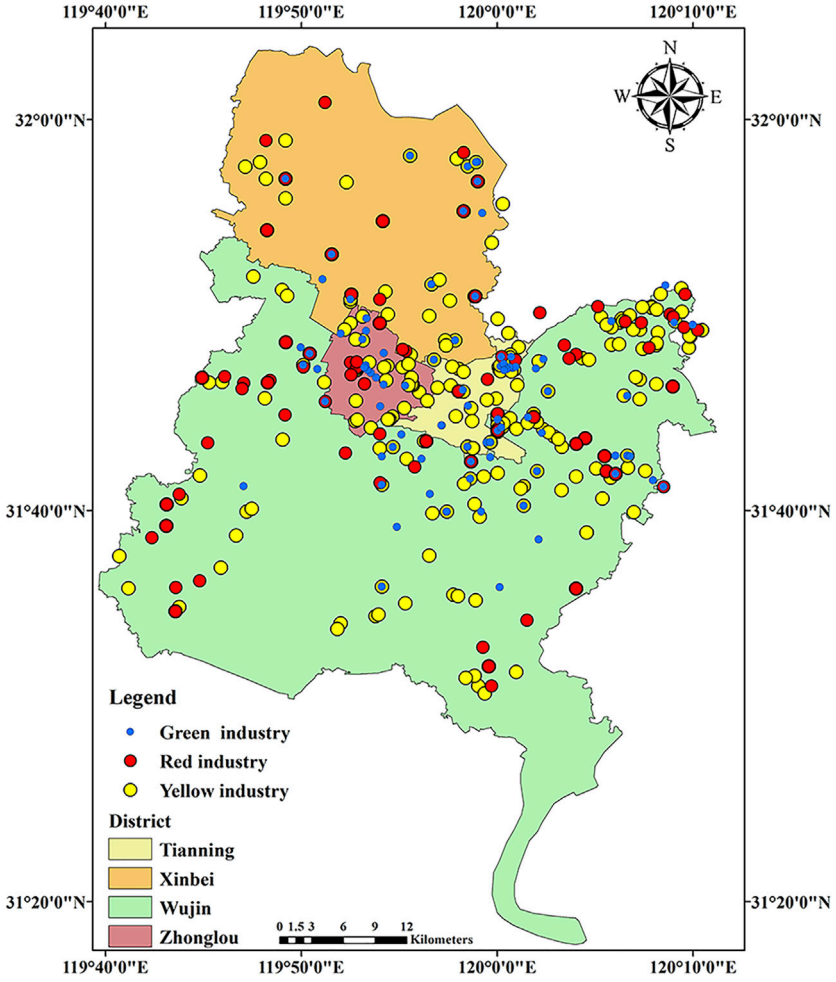

FIGURE 10
Spatial distribution of different industrial types.

2020). Meanwhile, among the all industrial types, yellow and red industries were the center of attention. We also found that canals with large fluctuations in WEC were consistent with the industrial spatial distribution (yellow and red industries) (Figures 10, 11), and the pollutant discharge types of enterprises could be identified through the analysis of canal pollution. For example, enterprises around R39 had contributed more to the concentration of COD and TP, followed by TN. The enterprises surrounding R5 had a greater contribution to the concentration of COD, NH_3–N, and TP. The type of enterprise that had the greatest impact on R6 was the yellow enterprise, and the NH_3–N emissions of the enterprise were higher. The enterprise around R33 had relatively high TN emissions, while COD, TP, and NH_3–N emissions were relatively low. Therefore, the EE–SBM–DEA model could be used to identify areas at risk of pollution. These areas could be monitored, and the water environmental capacity of each canal was analyzed to identify the major pollution types of

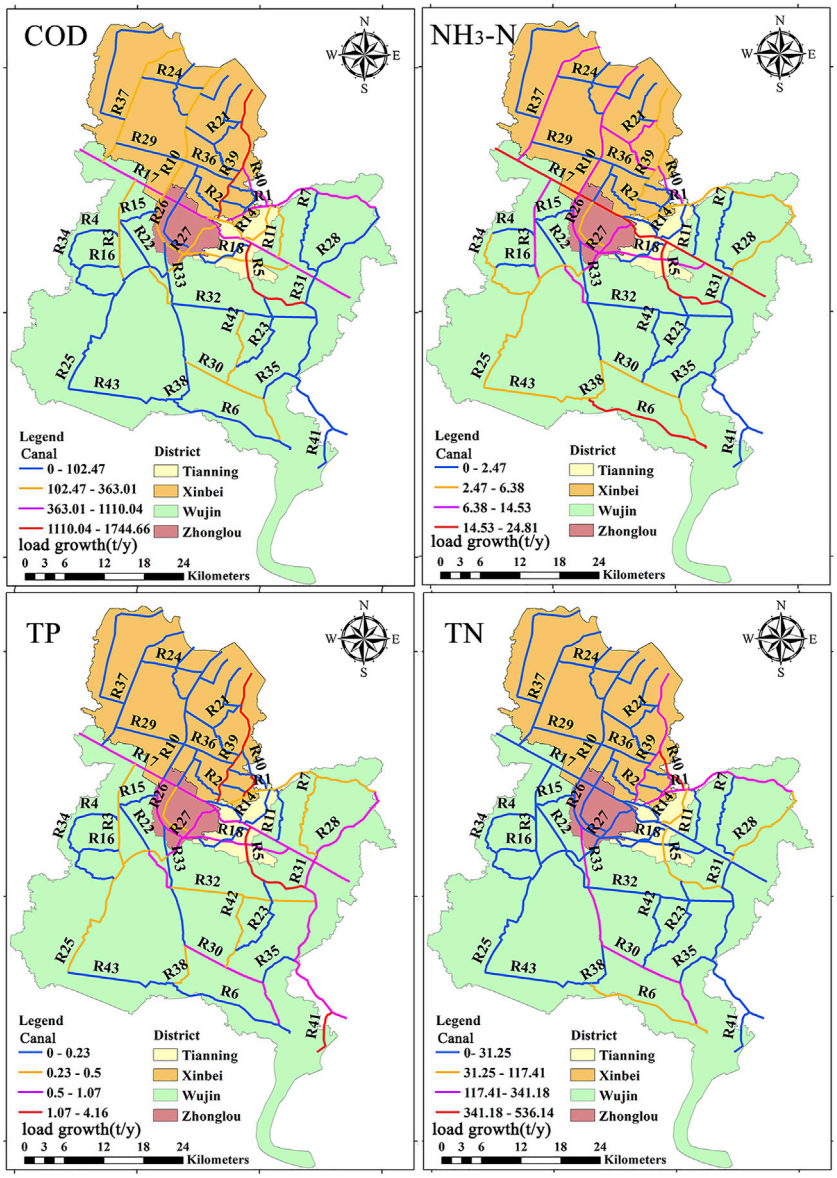

FIGURE 11
Water environmental capacity fluctuation of different canals.

different enterprises. Pollution monitoring could be carried out in the process of monitoring the pollution of enterprises, saving a lot of manpower and financial costs. In short, the model identified different risk levels of enterprises and regions, which was beneficial to improve management efficiency.

In addition, Wang et al. (2018) found that the water quality policies forced many small, heavily polluting firms to shut down, but it was non-effective in reducing the COD concentration. We also found the same problem: although the density of red enterprises around R4 was relatively high, it did not contribute much to improve canal pollution when they were closed. It may be that the contribution of point sources to the canal network was far less than that of non-point sources or internal sources. Correlational research studies showed that non-point and endogenous pollution sources had contributed more to canal network pollution in the Taihu Lake (Wang M. et al., 2019; Yan et al., 2019b; Luo et al., 2019; Xu et al., 2020). Therefore, non-point source and endogenous pollution management measures were considered to improve the canal water environment. For instance, the sediment dredging was conducted for decreasing the pollution load (Chen et al., 2020). Constructed wetland technology and low-impact development

technology were also widely applied for the malodorous canal (Pereira Souza et al., 2019; Bu et al., 2020; Lu et al., 2020; Tuttolomondo et al., 2020). Moreover, the identified high-risk areas were also key areas where non-point source and internal source control measures were considered.

5 Conclusion

The development of enterprises had brought greater pressure to the urban water environment, and enterprises were classified as green enterprises, yellow enterprises, and red enterprises by constructing the EE–SBM–DEA model in this study. Furthermore, the temporal and spatial dynamic simulation model of the WEC was constructed, changes in the WEC of canals were analyzed based on enterprise regulation, and the economic valuation model was used to evaluate the economic benefits of water environment improvement. The related conclusion was drawn as follows:

(1) The calculation results of enterprise efficiency were used to classify the enterprises in the study area and took corresponding control measures. The results of the enterprise efficiency calculation in Tianning, Wujin, Xinbei, and Zhonglou districts showed that red companies accounted for 65.97%, 66.41%, 68.14%, and 54.63%, respectively.
(2) The results showed that the loads of COD and TN increased by industrial regulation and reached their highest values of 1744.66 t/y and 536.14 t/y, respectively. However, the improvement in NH_3–N and TP loads was not evident, and the highest values reached 24.81 t/y and 4.16 t/y, respectively. In addition, canals R40, R41, R20, R19, and R17 were partially overloaded with pollutants and should be considered.
(3) The result of research showed that industrial structure optimization could effectively improve water environment quality and generate economic value. After the optimization of the industrial structure, the economic loss value was 174.44 million yuan. However, environmental improvements had brought economic benefits up to 57.68 million yuan.

In conclusion, this research provided technical support for industrial management policies and water environment improvement. It was recommended that TN should be included as a water environment quality assessment target to improve the concentration of TN in the canal network. Changzhou city must make full use of the advantages of technology, manpower, and capital to accelerate the optimization and upgrading of the industrial structure. Among them, technological progress and innovation will be an important support to reduce the emission of pollutants for economic development.

Data availability statement

The original contributions presented in the study are included in the article/Supplementary Material; further inquiries can be directed to the corresponding author.

Author contributions

JB and CL: Conceived and designed the research; Xue W and XX: Software and validation; Xua W, QL, and XiW: Supervision; JB and SZ: Analyzed the data and writing—original draft preparation, reviewing and editing. All authors have read and agreed to the published version of the manuscript.

Funding

This research was funded by the National Natural Science Foundation of China (52070023), the Foundation of Basic Science (Natural Science) research in Jiangsu Province (22KJB570008), and the Wuxi University Research Start-up Fund for Introduced Talents (550222020, 550221041).

Acknowledgments

The authors would like to extend special thanks to the editor and the reviewers for their valuable comments in greatly improving the quality of this research.

Conflict of interest

The authors declare that the research was conducted in the absence of any commercial or financial relationships that could be construed as a potential conflict of interest.

Publisher's note

Supplementary material

The Supplementary Material for this article can be found online at: https://www.frontiersin.org/articles/10.3389/feart.2022.961299/full#supplementary-material

References

An, Q., Wu, Q., Li, J., Xiong, B., and Chen, X. (2019). Environmental efficiency evaluation for Xiangjiang River basin cities based on an improved SBM model and Global Malmquist index. *Energy Econ.* 81, 95–103. doi:10.1016/j.eneco.2019.03.022

Asghar, S., Sasaki, N., Jourdain, D., and Tsusaka, T. (2018). Levels of technical, allocative, and groundwater use efficiency and the factors affecting the allocative efficiency of wheat farmers in Pakistan. *Sustainability* 10, 1619. doi:10.3390/su10051619

Bian, Y., Yan, S., and Xu, H. (2014). Efficiency evaluation for regional urban water use and wastewater decontamination systems in China: A DEA approach. *Resour. Conservation Recycl.* 83, 15–23. doi:10.1016/j.resconrec.2013.11.010

Bu, J., Peng, C., Li, C., Wang, X., Zhang, Y., Yang, Z., et al. (2020). A method for determining reasonable water area ratio based on flood risk and cost-effectiveness in Rainy City. *Environ. Earth Sci.* 79, 450. doi:10.1007/s12665-020-09201-1

Carvalho, P., Marques, R. C., and Berg, S. (2012). A meta-regression analysis of benchmarking studies on water utilities market structure. *Util. Policy* 21, 40–49. doi:10.1016/j.jup.2011.12.005

Chen, C., Kong, M., Wang, Y.-Y., Shen, Q.-S., Zhong, J.-C., and Fan, C.-X. (2020). Dredging method effects on sediment resuspension and nutrient release across the sediment-water interface in Lake Taihu, China. *Environ. Sci. Pollut. Res.* 27, 25861–25869. doi:10.1007/s11356-019-06192-w

Chen, C., Liu, H., Tang, L., and Ren, J. (2021). A range adjusted measure of super-efficiency in integer-valued data envelopment analysis with undesirable outputs. *J. Syst. Sci. Inf.* 9, 378–398. doi:10.21078/jssi-2021-378-21

Chung, Y. H., Färe, R., and Grosskopf, S. (1997). Productivity and undesirable outputs: A directional distance function approach. *J. Environ. Manag.* 51, 229–240. doi:10.1006/jema.1997.0146

Dsikowitzky, L., Hagemann, L., DwiyitnoAriyani, F., Irianto, H. E., and Schwarzbauer, J. (2017). Complex organic pollutant mixtures originating from industrial and municipal emissions in surface waters of the megacity jakarta—An example of a water pollution problem in emerging economies. *Environ. Sci. Pollut. Res.* 24, 27539–27552. doi:10.1007/s11356-017-0164-2

Fakhraei, H., Driscoll, C. T., Selvendiran, P., DePinto, J. V., Bloomfield, J., Quinn, S., et al. (2014). Development of a total maximum daily load (TMDL) for acid-impaired lakes in the Adirondack region of New York. *Atmos. Environ.* 95, 277–287. doi:10.1016/j.atmosenv.2014.06.039

Feng, L., Sun, X., and Zhu, X. (2016). Impact of floodgates operation on water environment using one-dimensional modelling system in river network of Wuxi city, China. *Ecol. Eng.* 91, 173–182. doi:10.1016/j.ecoleng.2016.02.042

Frija, A., Chebil, A., Speelman, S., Buysse, J., and Van Huylenbroeck, G. (2009). Water use and technical efficiencies in horticultural greenhouses in Tunisia. *Agric. Water Manag.* 96, 1509–1516. doi:10.1016/j.agwat.2009.05.006

Gidion, D. K., Hong, J., Adams, M. Z. A., and Khoveyni, M. (2019). Network DEA models for assessing urban water utility efficiency. *Util. Policy* 57, 48–58. doi:10.1016/j.jup.2019.02.001

Guan, X., Liu, W., and Chen, M. (2016). Study on the ecological compensation standard for river basin water environment based on total pollutants control. *Ecol. Indic.* 69, 446–452. doi:10.1016/j.ecolind.2016.05.011

Hu, Z., Yan, S., Yao, L., and Moudi, M. (2018). Efficiency evaluation with feedback for regional water use and wastewater treatment. *J. Hydrology* 562, 703–711. doi:10.1016/j.jhydrol.2018.05.032

Huang, Z., Tongand Tong, T. (2019). Water environmental capacity calculation and allocation of the Taihu lake basin in Jiangsu Province based on control unit. *Int. J. Environ. Res. Public Health* 16, 3774. doi:10.3390/ijerph16193774

Keupers, I., and Willems, P. (2017). Development and testing of a fast conceptual river water quality model. *Water Res.* 113, 62–71. doi:10.1016/j.watres.2017.01.054

Kim, J., Engel, B. A., Park, Y. S., Theller, L., Chaubey, I., Kong, D. S., et al. (2012). Development of Web-based Load Duration Curve system for analysis of total maximum daily load and water quality characteristics in a waterbody. *J. Environ. Manag.* 97, 46–55. doi:10.1016/j.jenvman.2011.11.012

Koopmans, A. (1951). Cytogenetic studies on Solanum tuberosum L. And some of its relatives: Avec un résumé en français. *Genetica* 25, 193–337. doi:10.1007/bf01784832

Li, Z., Dong, M., Wong, T., Wang, J., Kumar, A., and Singh, R. (2018). Objectives and indexes for implementation of sponge cities—a case study of Changzhou city, China. *Water* 10, 623. doi:10.3390/w10050623

Liu, K., Yang, G., and Yang, D. (2020). Investigating industrial water-use efficiency in mainland China: An improved SBM-DEA model. *J. Environ. Manag.* 270, 110859. doi:10.1016/j.jenvman.2020.110859

Liu, R. M., Sun, C. C., Han, Z. X., Chen, L., Huang, Q., Chen, Y. X., et al. (2012). Water environmental capacity calculation based on uncertainty analysis: A case study in the baixi watershed area, China. *Procedia Environ. Sci.* 13, 1728–1738. doi:10.1016/j.proenv.2012.01.166

Lu, J., Guo, Z., Kang, Y., Fan, J., and Zhang, J. (2020). Recent advances in the enhanced nitrogen removal by oxygen-increasing technology in constructed wetlands. *Ecotoxicol. Environ. Saf.* 205, 111330. doi:10.1016/j.ecoenv.2020.111330

Luo, X., Li, Y., Wu, Q., Wei, Z., Li, Q., Wei, L., et al. (2019). Characteristics of internal ammonium loading from long-term polluted sediments by rural domestic wastewater. *Int. J. Environ. Res. Public Health* 16, 4657. doi:10.3390/ijerph16234657

Ni, L., Gu, G., Rong, S., Hu, L., Wang, P., Li, S., et al. (2019). Effects of cyanobacteria decomposition on the remobilization and ecological risk of heavy metals in Taihu Lake. *Environ. Sci. Pollut. Res.* 26, 35860–35870. doi:10.1007/s11356-019-06649-y

Pereira Souza, F., Leite Costa, M. E., and Koide, S. (2019). Hydrological modelling and evaluation of detention ponds to improve urban drainage system and water quality. *Water* 11, 1547. doi:10.3390/w11081547

Rahman, M. T., Nielsen, R., Khan, M. A., and Asmild, M. (2019). Efficiency and production environmental heterogeneity in aquaculture: A meta-frontier DEA approach. *Aquaculture* 509, 140–148. doi:10.1016/j.aquaculture.2019.05.002

Rodgers, K., McLellan, I., Peshkur, T., Williams, R., Tonner, R., Knapp, C. W., et al. (2020). The legacy of industrial pollution in estuarine sediments: Spatial and temporal variability implications for ecosystem stress. *Environ. Geochem. Health* 42, 1057–1068. doi:10.1007/s10653-019-00316-4

Schmidt, C., Kumar, R., Yang, S., and Büttner, O. (2020). Microplastic particle emission from wastewater treatment plant effluents into river networks in Germany: Loads, spatial patterns of concentrations and potential toxicity. *Sci. Total Environ.* 737, 139544. doi:10.1016/j.scitotenv.2020.139544

Tone, K., and Tsutsui, M. (2014). Dynamic DEA with network structure: A slacks-based measure approach. *Omega* 42, 124–131. doi:10.1016/j.omega.2013.04.002

Tuttolomondo, T., Virga, G., Licata, M., Leto, C., and La Bella, S. (2020). Constructed wetlands as sustainable technology for the treatment and reuse of the first-flush stormwater in agriculture—a case study in sicily (Italy). *Water* 12, 2542. doi:10.3390/w12092542

Wang, C., Wu, J., and Zhang, B. (2018). Environmental regulation, emissions and productivity: Evidence from Chinese COD-emitting manufacturers. *J. Environ. Econ. Manag.* 92, 54–73. doi:10.1016/j.jeem.2018.08.004

Wang, J., Fu, Z., Qiao, H., and Liu, F. (2019a). Assessment of eutrophication and water quality in the estuarine area of Lake Wuli, Lake Taihu, China. *Sci. Total Environ.* 650, 1392–1402. doi:10.1016/j.scitotenv.2018.09.137

Wang, M., Huang, Y., and Li, D. (2021a). Assessing the performance of industrial water resource utilization systems in China based on a two-stage DEA approach with game cross efficiency. *J. Clean. Prod.* 312, 127722. doi:10.1016/j.jclepro.2021.127722

Wang, M., Xu, X., Wu, Z., Zhang, X., Sun, P., Wen, Y., et al. (2019b). Seasonal pattern of nutrient limitation in a eutrophic lake and quantitative analysis of the impacts from internal nutrient cycling. *Environ. Sci. Technol.* 53, 13675–13686. doi:10.1021/acs.est.9b04266

Wang, Q., Liu, R., Men, C., Guo, L., and Miao, Y. (2019c). Temporal-spatial analysis of water environmental capacity based on the couple of SWAT model and differential evolution algorithm. *J. Hydrology* 569, 155–166. doi:10.1016/j.jhydrol.2018.12.003

Wang, S., Chen, S., Zhang, H., and Song, M. (2021b). The model of early warning for China's marine ecology-economy symbiosis security. *Mar. Policy* 128, 104476. doi:10.1016/j.marpol.2021.104476

Wang, S., Lei, L., and Xing, L. (2021c). Urban circular economy performance evaluation: A novel fully fuzzy data envelopment analysis with large datasets. *J. Clean. Prod.* 324, 129214. doi:10.1016/j.jclepro.2021.129214

Wang, Y., Bian, Y., and Xu, H. (2015). Water use efficiency and related pollutants' abatement costs of regional industrial systems in China: A slacks-based measure approach. *J. Clean. Prod.* 101, 301–310. doi:10.1016/j.jclepro.2015.03.092

Xu, Y., Su, B., Wang, H., He, J., and Yang, Y. (2020). Analysis of the water balance and the nitrogen and phosphorus runoff pollution of a paddy field *in situ* in the

Taihu Lake basin. *Paddy Water Environ.* 18, 385–398. doi:10.1007/s10333-020-00789-5

Yan, R., Gao, Y., Li, L., and Gao, J. (2019a). Estimation of water environmental capacity and pollution load reduction for urban lakeside of Lake Taihu, eastern China. *Ecol. Eng.* 139, 105587. doi:10.1016/j.ecoleng.2019.105587

Yan, R., Li, L., and Gao, J. (2019b). Framework for quantifying rural NPS pollution of a humid lowland catchment in Taihu Basin, Eastern China. *Sci. Total Environ.* 688, 983–993. doi:10.1016/j.scitotenv.2019.06.114

Yang, J., Lei, K., Khu, S., Meng, W., and Qiao, F. (2015). Assessment of water environmental carrying capacity for sustainable development using a coupled system dynamics approach applied to the Tieling of the Liao River Basin, China. *Environ. Earth Sci.* 73, 5173–5183. doi:10.1007/s12665-015-4230-0

Yang, J., Liu, X., Ying, L., Chen, X., and Li, M. (2020). Correlation analysis of environmental treatment, sewage treatment and water supply efficiency in China. *Sci. Total Environ.* 708, 135128. doi:10.1016/j.scitotenv.2019.135128

Zhang, M., Shi, X., Yang, Z., Yu, Y., Shi, L., and Qin, B. (2018). Long-term dynamics and drivers of phytoplankton biomass in eutrophic Lake Taihu. *Sci. Total Environ.* 645, 876–886. doi:10.1016/j.scitotenv.2018.07.220

frontiers | Frontiers in Earth Science

TYPE Original Research
PUBLISHED 16 January 2023
DOI 10.3389/feart.2022.1018980

OPEN ACCESS

EDITED BY
Weili Duan,
Xinjiang Institute of Ecology and Geography (CAS), China

REVIEWED BY
Wei Sun,
School of Geography and Planning, Sun Yat-Sen University, China
Yuan Zhang,
Guangdong University of Technology, China

*CORRESPONDENCE
Chunhui Li,
chunhuili@bnu.edu.cn
Yujun Yi,
yiyujun@bnu.edu.cn

SPECIALTY SECTION
This article was submitted to Hydrosphere, a section of the journal Frontiers in Earth Science

RECEIVED 14 August 2022
ACCEPTED 31 October 2022
PUBLISHED 16 January 2023

CITATION
Zhang S, Li H, Li C, Yi Y, Wang X and Liu Q (2023), Allocation of water resources in the lower Yellow river based on ecological footprint.
Front. Earth Sci. 10:1018980.
doi: 10.3389/feart.2022.1018980

Allocation of water resources in the lower Yellow river based on ecological footprint

Shuiling Zhang, Hui Li, Chunhui Li*, Yujun Yi*, Xuan Wang and Qiang Liu

Key Lab of Water and Sediment Science of Ministry of Education, School of Environment, Beijing Normal Univ., Beijing, China

With the development of the economy, the contradiction of water resources in the lower Yellow River area is becoming increasingly serious. Economic development not only increases the socio-economic water demand, but also causes damage to the environment. In order to ensure the safety of the vast plains along the lower Yellow River, protect the environment of the lower Yellow River and estuaries, and achieve environmental sustainability of the lower Yellow River, a model was established to optimize the allocation of water resources with the goal of ecological, safety, and social benefits, combining the uncertainty of water resources, the uncertainty of the water demand during the flood season under different water and sediment conditions, and the water requirements of different water users. An improved ecological footprint method considering soil water was applied during the allocation. Thirty different scenarios were set up, and appropriate scenarios for 2025 and 2030 in wet, normal, and dry years were calculated, providing a reference for decision makers. Results show that: 1) The water supply is affected by the amount of water resources and water demand for sediment transport in the lower Yellow River. The satisfaction of sediment transport and the water supply rate during wet years can reach a high level of satisfaction. 2) When the regional water resources ecological footprint is the smallest, the allocation of water resources tends to the section or unit with a smaller ecological footprint. Therefore, the river sections with the lowest water shortage rates are Lijin-Hekou and Sunkou-Aishan, and the unit with a low water shortage is ecological and industrial water.

KEYWORDS

the lower Yellow River, water resources management, water resources allocation, ecological footprint, sustainable development

1 Introduction

The ecological footprint can comprehensively calculate the utilization of resources, and measure the relationship between the degree of human utilization of natural resources and the ability of the environment to provide services to humans (Rees 1992; Wackernagel and Rees 1996). After being proposed, the concept of ecological footprint was then introduced by some scholars and gradually applied to the calculation of water resource

utilization, the calculation of water resources carrying capacity, and the evaluation of sustainable development.

The water utilization described in the ecological footprint model did not reflect the actual integrated use of water resources, Chinese scholar Fan (2005), to reduce previous limitations in describing water resources, proposed the water resources ecological footprint model to reduce previous limitations in describing water resource by increasing the assessment of the use of water resources by human activities and the health of aquatic ecosystems (Wang et al., 2006; Dai et al., 2019). The advantage of the ecological footprint of water resources is that it considers the degree of ecological resources occupied by humans and indicates the ecological sustainability of regional development (Hoekstra 2008; Stoeglehner et al., 2011). The water resources ecological footprint method mainly evaluates the sustainable development and utilization of water resources by establishing a calculation model of the ecological footprint of water resources and the corresponding ecological carrying capacity (Huang et al., 2008). Since the introduction of the ecological footprint of water resources, its meaning has been continuously expanded and improved, scholars have taken into account the concept of ecological footprint of water resources for CNY 10,000 of GDP and the impact of water pollution on the environment (Wang et al., 2013), the regional characteristics of equalization and yield factors (Wang et al., 2020) to make the ecological footprint of water resources more accurate for the respective areas. Su et al. (2018) compared water ecological footprint in four municipalities in China to help identify the key gaps between different cities under different developing back ground. The ecological footprint of water resources considers the carrying capacity of regional water resources and can demonstrate whether the local sectors use water resources in a sustainable approach.

The allocation of water resources is concerned with how limited resources should be distributed fairly among competing activities (Wang et al., 2007). In the process of research and development in the allocation of water resources worldwide, the research objective has changed from simply optimizing the water volume to coordinating the economy and ecological environment. Linear programming, dynamic programming, nonlinear programming, multi-objective programming, multi-objective genetic algorithms, and other theoretical methods were applied to achieve the comprehensive goal (Chen et al., 2006; Song, 2008). Scholars have modified the methods to make them more suitable for their own study area by establishing agriculture and hydropower sectors and the marginal net benefit from domestic and industrial sectors (Divakar et al., 2011), developing a multi-stage fuzzy stochastic programming (MFSP) method to hybrid uncertainties with the consideration of ecological water demand (Li et al., 2018), considering hydropolitic conditions (Kazemi et al., 2020), applying the sustainability index to the optimization model (Dadmand et al., 2020), etc.

The Yellow River is China's second largest river, and water resource of the Yellow River basin is decreasing (Zhang et al., 2009). Since the middle and lower reaches of the Yellow River Basin are more economically efficient in water use and the water demand in the lower reaches of the Yellow River is higher (Guan et al., 2021). Many Chinese scholars have conducted research on the optimization of water resources in the lower Yellow River and the Yellow River Delta (Shao et al., 2009; Yang, 2011; Zhang et al., 2014; Zhang and Oki, 2021). Water resources are needed for household production, ecology, and sediment transport in the lower Yellow River. In order to coordinate the conflicts of interests of all parties in water use, and consider the coordinated and sustainable development of different elements in various regions, water resources need to be allocated according to local conditions. In this study, the water resources were allocated to meet the goals of high-quality development and ecology protection with ecological footprint of water resources. The ecological footprint calculation takes into account the soil water, which improves the comprehensiveness of this method.

2 Study area

2.1 Overview of the study area

With the development of the economy and society and the improvement of people's living standards, China's water shortage problem has become increasingly prominent. Defining the status quo of sustainable water resources is of great significance for the rational allocation of limited water resources, improving water use efficiency and achieving the sustainable development of society. Due to natural and human factors, the shortage of water resources in the lower Yellow River has become more serious.

The urban clusters in the lower Yellow River selected in this study cover 17 cities in Henan Province and Shandong Province (Figure 1). The area is 12,171,513 square kilometres with a temperate monsoon climate. The temperature from May to September is 21.5–27.3°C, December to February is −2.4–2.8°C, the rest of the months is 7.1–15.7°C. The annual average temperature is 14.1–15.1°C. The annual average precipitation is 490–720 mm, and the precipitation from June to September accounts for three-quarters of the total.

2.2 Generalization of water resources users in the lower Yellow River

Considering the regulating performance and storage capacity of Xiaolangdi Reservoir, we believe that the downstream water regulation can be achieved during the year. Therefore, the problem to be solved is how to allocate water resources in the lower Yellow River and achieve the maximum benefit among different water users.

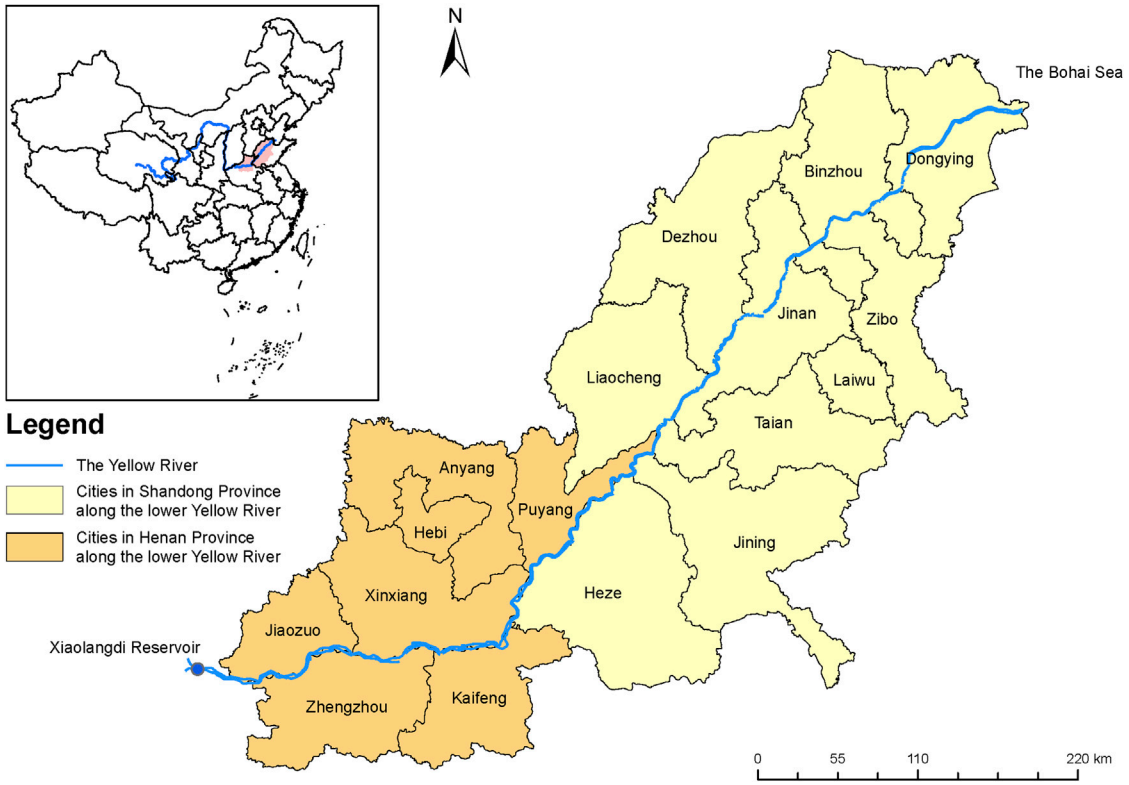

FIGURE 1
City group map along the lower Yellow River.

TABLE 1 Comparison table of generalized administrative units in the lower Yellow River.

Sections	Administrative regions (cities)
Huayuankou-Jiahetan (HJ)	Zhengzhou, Kaifeng, Jiaozuo, Xinxiang
Jiahetan-Gaocun (JG)	Anyang, Hebi, Shangqiu
Gaocun-Sunkou (GS)	Puyang, Heze
Sunkou-Aishan (SA)	Jining, Taian
Aishan- Luokou (AL)	Jinan, Liaocheng, Dezhou
Luokou-Lijin (LL)	Zibo, Binzhou, Laiwu
Liji-Hekou (LH)	Dongying

Based on the conditions in the lower Yellow River, water resources can be divided into two major aspects: the ecological water used for sediment transport in the river, and the domestic water outside the river. It is a multi-objective problem as it is necessary to consider both the spatial and temporal allocation of water resources.

To solve the problem, it is necessary to identify the water consumption of each type of water use, each river section, and each period; generalize the downstream area; and convert the problem into a mathematical problem. Based on the above requirements, a spatial generalization of the lower Yellow River area was carried out.

According to the relationship between the water supply project and the natural geographical location, the study area is generalized into 7 river sections according to the main control hydrological station downstream, namely, Huayuankou-Jiahetan (HJ), Jiahetan-Gaocun (JG), Gaocun-Sunkou (GS), Sunkou-Aishan (SA), Aishan- Luokou (AL), Luokou-Lijin (LL), and Lijin-Hekou (LH), and 8 nodes: Huayuankou, Jiahetan, Gaocun, Sunkou, Aishan, Luokou, Lijin, and Hekou. The administrative regions (cities) corresponding to each river section are shown in Table 1. The lower Yellow River is generalized as shown in Figure 2, where ecological water refers to the ecological water outside the river.

3 Construction of water allocation model

3.1 Procedure

The steps for the allocation of water resources are as follows:

TABLE 2 Water resources in the lower Yellow River/10^8 m^3.

	Wet year	Normal year	Dry year
Water resources in the lower Yellow River	460	320	260
Measured runoff at Huayuankou Hydrological Station	448	305	241

TABLE 3 Water demand by users in the lower Yellow River/10^8 m^3 (water use outside the basin is water diverted to the Huai River Basin and the Shandong Peninsula, details can be found in the cited article).

Category	2025				2030			
	Within the basin	Outside the basin	Total		Within the basin	Outside the basin	Total	
			min	max			min	max
Agricultural water	42.23	125.95	86.31	105.21	41.38	123.25	84.52	103.01
Industrial water	8.12	24.26	16.61	20.25	8.84	26.39	18.08	22.04
Domestic water	6.08	18.70	12.63	15.43	6.22	19.14	12.92	15.79
Ecological water	2.30	7.67	4.98	6.14	2.30	7.67	4.98	6.14
Total	58.73	176.58	120.54	147.02	58.74	176.45	120.50	146.97

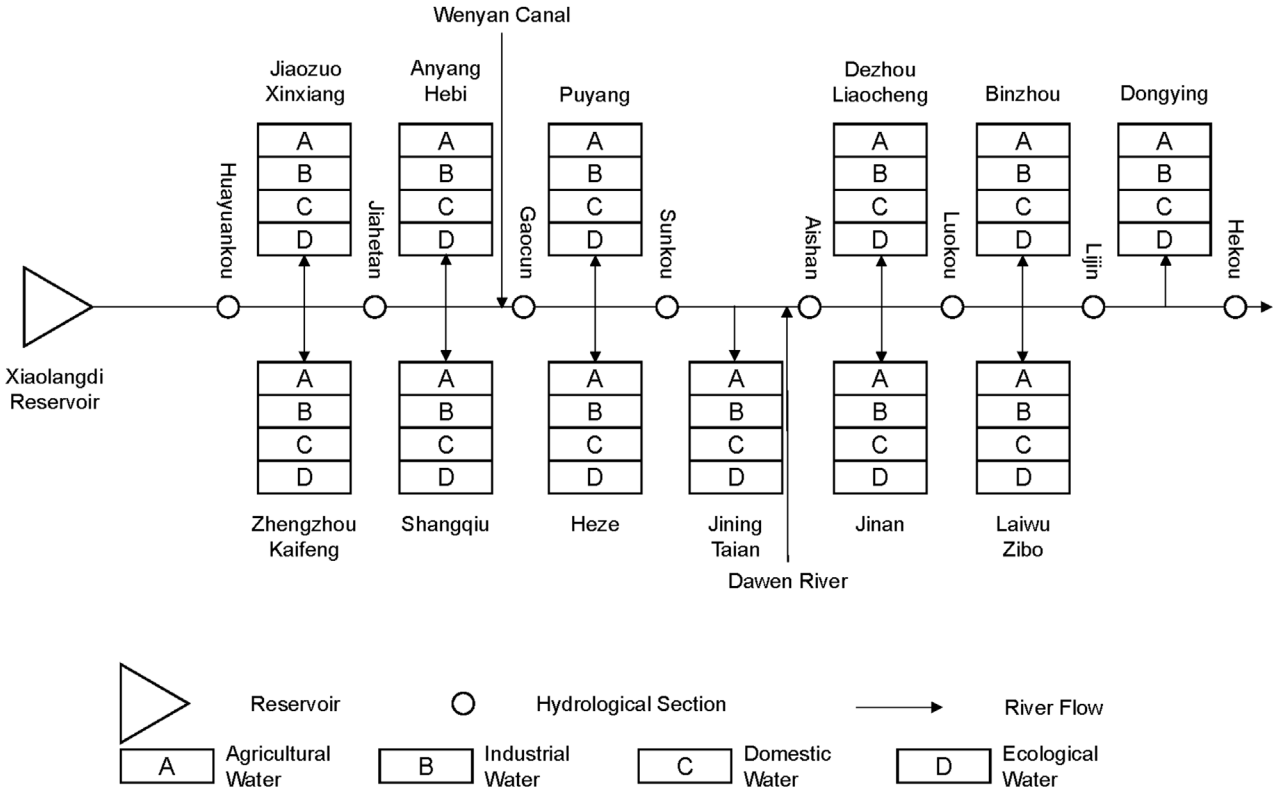

FIGURE 2
Generalized diagram of water resource users in the lower Yellow River.

TABLE 4 Water demand in the lower Yellow River/10^8 m^3.

	Wet years	Normal year	Dry year
Water demand in the lower Yellow River	180.42	234.94	305.6

TABLE 5 Water diversion and water lifting projects in the lower Yellow River.

	Water diversion project	Designed flow (m^3/s)	Actual water diversion capacity (m^3/s)	Monthly water supply capacity (10^8 m^3)	Actual irrigation area (km^2)
HJ	14	561	322	8.35	2304.8
JG	15	500	244	6.32	3839.1
GS	15	490	403	10.45	3912.8
SA	3	335	335	8.68	3946.3
AL	11	370	321	8.32	5145.6
LL	31	897	801	20.76	6606.2
LH	17	333	257	6.67	810.7

1) Determine the scope of the research: the scope of this study was the lower Yellow River.
2) Determine the objectives of the research: according to national ecological protection and high-quality development plan of the Yellow River (The State Council of the People's Republic of China Gov, 2021), ecological water use should be considered first. The management of the Yellow River, the protection of germplasm resources, and farmland agriculture should be planned as a whole.
3) Users identification and generalization: a) water sources, including the inflow of upstream rivers, the inflow of tributaries, the storage of reservoirs, the groundwater, and the externally transferred water sources; b) users, including household, industry, agriculture, and ecology; c) transmission and water supply systems, including the industrial water intake and channels in the study area. Based on the studies of Li et al. (2020) and the actual situation of the lower Yellow River, the basic data in this study are shown in Tables 2–5:
4) Target determination: coordination should be conducted to meet the goals of each department in time and space.
5) Constraint determination: various constraints were set to achieve system goals.
6) Model establishment.
7) Model solving: find a suitable algorithm and program to solve the model.
8) The generation of the system plan: optimize and coordinate the water resources to obtain the final allocation plan of water resources.

3.2 Principle

According to the natural and economic conditions of the lower Yellow River, the principles for constructing the allocation model were determined as follows:

1) Put people first and guaranteeing people's lives along the river.
2) Ensure the basic ecological water use of the river, and ensure the water requirements of the ecological environment of the estuary.
3) Ensure production safety, which means the agricultural water use should meet water demand during the growth period of crops in the lower Yellow River.
4) Ensure the safety of downstream flood control and ensure water for sediment transport during the flood season.
5) The relationship between water used within the river basins and water transferred across river basins should be handled well. Water demand of users in various sections should be considered comprehensively.
6) Promote a virtuous cycle of the ecological environment, maintain and improve the regional ecological environment.

3.3 Objective

The overall goal of the spatial allocation of water resources in the lower Yellow River was to achieve the sustainable development of the social economy through the process. The objectives of this study are mainly reflected in three aspects:

1) The safety goal was to protect the vast plains along the lower Yellow River from floods, ensure that the water supply meets the demand for planting and the demand for sediment transport in the lower Yellow River.
2) The ecological environment goal was to improve the environment of the lower Yellow River, the ecological environment of the Yellow River and estuaries, and gradually increase the amount of water used for the ecological environment.
3) The socio-economic goal was to ensure the quality and quantity of water for urban and rural residents.

According to the above objectives and requirements, the water resources of the lower Yellow River can be divided into two major aspects. One is the ecological water used for sediment transport in the river, and the other is the water used for production and domestic outside the river. Time and space are the factors that must be considered while allocating water resources, so the water requirements of each type of water use, river section, and period must be identified.

Due to the positive linear correlation between the runoff and sediment load (Kong et al., 2015) and water volume of the Yellow River Basin during wet, normal, and dry years varies greatly, water used for water and sediment regulation varies in different years. In wet years, it is necessary to ensure the basic ecological water demand in the river, and provide a longer period of time for water and sediment regulation to ensure water for sediment transport during the flood season. In normal years, the time for water and sediment regulation should be reduced due to the limitation of incoming water. In dry years, the water used for water and sediment regulation should be restricted.

3.4 Model construction

3.4.1 Construction method

According to the relevant planning and the actual situation of the river basin, agricultural water, industrial water, domestic water, ecological water (referring to ecological water outside the river), sediment transport and river ecological water (river water) were selected as five users of three objectives of the allocation. Meanwhile, the temporal and spatial distribution of water resources was taken into account.

Building a multi-objective allocation model should include the following aspects:

1) Goal: Achieve a balance among demand of ecology, sediment transport, and economy.
2) Time: Meet the water demands of different periods.
3) Space: Meet the water demands of different river sections.

The lower Yellow River is at an ecological deficit (Li et al., 2020); the ecological footprint of water resources is mainly derived from household and production, involving domestic, agricultural and industrial water consumption. Therefore, the ecological footprint can be used as the objective function to balance the relationship between agricultural, industrial, domestic water and the environment. Taking sediment transport and ecological satisfaction as the objective function reflects the goals of sediment transport and river ecological water use.

3.4.2 Objective function

Benefits will be generated when distributing water resources to various users, and there will also be costs when using water resources. The purpose of water resources optimization is to meet the needs of all users, increase benefits, and reduce costs when allocating water resources. According to the general guiding concept of taking into account the safety, ecological safety, and social development of the lower Yellow River, this article considers the ecological benefit objective, safety benefit objective, and social benefit objective as the objectives of the lower Yellow River area.

1) Ecological footprint function

The ecological footprint can reflect the sustainable development of a region. The ecological footprint of water consumption is calculated according to the definition of the improved ecological footprint (Li et al., 2020), which added the soil water as an indicator to make the assessment more comprehensive. For the lower Yellow River, the ecological footprint calculation includes four aspects, namely, agricultural, industrial, domestic and ecological water consumption.

$$f_1 = \sum_j PEF_j{}^{\star} q_j \tag{1}$$

where PEF_j is the ecological footprint of unit water resources produced by j water type outside the river. q_j is the water consumption of the j water type outside the river.

2) Satisfaction function

The satisfaction function of ecological water use for river sediment transport was selected as the objective function of safety and ecology. The objective satisfaction function (Zhao et al., 2007) is defined as:

$$p[f(x)] = \begin{cases} \dfrac{f(x) - f^-}{f^\star - f^-} \\ \dfrac{f^+ - f(x)}{f^+ - f^\star} \end{cases}, \quad x = 1, 2, \cdots, n \tag{2}$$

where $p[f(x)]$ is the goal achievement satisfaction function, f^* is the ideal value of the x goal, f^+ is the upper limit of the x goal, and f^- is the lower limit of the x goal. When the goal reaches the ideal value, the degree of satisfaction is 1.

Based on this, the ecological satisfaction function of river sediment transport is established:

$$f_2 = p(Q_r) = \begin{cases} \dfrac{f(Q_r) - f^-_{Q_r}}{f^*_{Q_r} - f^-_{Q_r}} \\ \dfrac{f^+_{Q_r} - f(Q_r)}{f^+_{Q_r} - f^*_{Q_r}} \end{cases} \tag{3}$$

where Q_r represents the total river water consumption, f^-_{Qr} represents the lower limit of the total river water consumption, f^*_{Qr}represents the lower limit of the river water consumption for sediment transport, and f^+_{Qr} represents the upper limit of the total river water consumption for sediment transport.

3) Water shortage rate function

The total water shortage rate function was selected as the social benefit objective function. Social benefit refers to the social value generated after the water source is allocated to the four water users (household, industry, agriculture, and environment). Under limited water resources conditions, the minimum total water shortage rate of the lower Yellow River is selected as the social benefit target, and the formula is as follows:

$$f_3 = \min \frac{\sum_i \sum_t \sum_j \left(qx_{i,t,j} - q_{i,t,j}\right)}{QX} \tag{4}$$

where $qx_{i,t,j}$ represents the water demand of the water type j at time t in the i section; $q_{i,t,j}$ represents the allocated water volume of the water j outside the channel at time t in the i section; QX represents the sum of the water demand of all users. t is the order of the months, with January as 1, February as 2, etc Table 2.

3.4.3 Constraint function

1) Constraints on the total amount of water resources: the amount of water taken by all users outside the river channel and the amount of water in the river channel shall not exceed the total amount of water resources.

$$\sum_j \sum_i \sum_t \left(q_{i,t,j}\right) + \sum_t q_{t,r} = Q \tag{5}$$

where Q represents the total amount of water resources in a year, and $q_{t,r}$ represents the water consumption of the river at time t.

2) Water balance restriction of diversion section: according to the principle of water balance, the inflow section is equal to the outflow section plus the water withdrawal of the river section minus the river receding water.

$$q_{i,t,r} = \sum_j q_{i,t,j} + q_{i+1,t,r} - q_{i,t,v} \tag{6}$$

where $q_{i,t,r}$ represents the water consumption of the i -th river section at time t ; that is, the inflow section, $q_{i+1,t,r}$, represents the water consumption of the $(i+1)$ -th river section at time t, and $q_{i,t,v}$ represents the returned water at time t of the i -th river section from water consumption.

3) River water restriction: in order to ensure the safety of the environment in the lower Yellow River, the river must have a certain amount of flow to transport sediment and protect the environment, which is expressed by the ecological water use constraints of sediment transport and the river ecological water:

$$q_{i,t,r} \geq \min q_{t,sand} \tag{7}$$

where $\min q_{t,sand}$ represents the lower limit of water used for sediment transport at t time when t=7, 8, 9, 10.

$$q_{i,t,r} \geq \min q_{t,eco} \tag{8}$$

where $\min q_{t,eco}$ represents the lower limit of ecological water used in rivers when t=1–6, 11, 12.

4) Water diversion restriction: the water drawn from the river channel cannot exceed its water demand.

$$\sum_i \sum_t q_{i,t,j} \leq Q_j \tag{9}$$

where Q_j represents water demand for agriculture, industry, household, and ecology.

5) Water supply capacity constraints: the water drawn from the river cannot exceed than its water supply capacity.

$$\sum_j \sum_t q_{i,t,j} \leq QG_i \tag{10}$$

where QG_i represents the water supply capacity of the i section.

6) Non-negative constraints

$$q_{i,t,j} \geq 0 \tag{11}$$

According to the prediction results of water demand in Table 3 and Table 4, the corresponding constraint values of water in the river and outside the river were obtained, and the constraints of water use in the river are as follows: the sediment transport water in the flood season was calculated according to the bankfull discharge in the flood season. The upper limit of the sediment transport water requirement in the flood season, as found in Table 3, is the ideal value of the objective function, and the lower limit of the sediment transport water requirement is the lower limit of the objective function; the nonflood season's suitable ecological water demand in Table 3 is the ideal value

of the objective function, and the lower limit ecological water demand is the lower limit of the objective function.

3.4.4 Model solving

At present, linear programming is the best way to solve multi-objective problems, and its core concept is to transform multi-objective problems into single-objective problems. This paper adopted the main objective function method, that is, a primary objective function is selected from a series of objective functions, while the remaining objectives are limited to a certain range and converted into new constraints, established the model according to the above constraints, and used the General Algebraic Modelling System (GAMS) to solve it.

The objective function is:

$$f = PEF_j * \sum_i \sum_t q_{i,t,j} \tag{12}$$

The constraint functions are:

$$\begin{aligned}
&\sum_j \sum_i \sum_t \left(q_{i,t,j}\right) + \sum_t q_{t,r} = Q \\
&q_{i,t,r} = \sum_j q_{i,t,j} + q_{i+1,t,r} - q_{i,t,v} \\
&q_{i,t,r} \geq \min q_{t,sand} \\
&q_{i,t,r} \geq \min q_{t,eco} \\
&\sum_i \sum_t q_{i,t,j} \leq Q_j \\
&\sum_j \sum_t q_{i,t,j} \leq QG_i \\
&q_{i,t,j} \geq 0 \\
&p_n \leq f_2 \leq 1 \\
&\frac{\sum_i \sum_t \sum_j \left(qx_{i,t,j} - q_{i,t,j}\right)}{QX} \leq \theta
\end{aligned} \tag{13}$$

where each symbol in the formula is the same as before.

3.4.5 Target plan setting

According to the water demand forecast results (2025 and 2030) from Table 5 and the uncertainty of incoming water and sediment (frequency of water resources and range of water used for sediment transport), this research combined high, medium, and low inflow scenarios (that is, corresponding to wet years, normal years, and dry years in Table 4) with different ecological satisfaction levels of sediment transport to form different simulation scenarios. Among them, the different types of sediment transport satisfaction were divided into A, B, C, D, and E, respectively, corresponding to the scenarios with satisfaction levels of 0, 0.25, 0.5, 0.75, and 1. A total of 30 scenarios were set up to analyze the quantitative relationship between different sediment transport requirements and water shortage rates under different water requirements and different incoming water conditions. The parameters of each simulation scenario are shown in Table 6.

4 Results and discussion

4.1 Overall water shortage rate under different scenario combinations

The overall water shortage rate trend of the 15 scenarios in the 2025 forecast year in the lower Yellow River basin is shown in Figure 3. It can be seen from the figure that when the satisfaction degree of ecological sediment transport increases, the water shortage rate of water outside the river channel increases. In the low and medium scenarios, only when the satisfaction degree is 0 and 0.25, can it be ensured that there is no shortage of water outside the river, while in the high scenario, the water demand outside the river can be fully satisfied.

The overall water shortage rate trend of the 15 scenarios in the 2030 forecast year in the lower Yellow River basin is shown in Figure 4. It can be seen from the figure that the overall trend is the same as in 2025, but compared to 2025, the water shortage rate under the same sediment transport satisfaction rate drops slightly.

4.2 Analysis of suitable plans for different scenarios

According to the model, the feasible solutions under different water shortage rates and different satisfaction levels are as follows:

When the water shortage rate for water outside the river is less than 30%, only two of the 2025 and 2030 plans cannot meet the requirements, namely, 2025-low -E and 2025-medium-E, and 2030-low-E and 2030-medium-E.

When the water shortage rate for water outside the river is less than 20%, four of the 2025 and 2030 plans cannot meet the requirements, namely, 2025-low-D, 2025-medium-D, 2025-low-E, and 2025-medium-E, and 2030-low-D, 2030-medium-D, 2030-low-E, and 2030-medium-E.

When the water shortage rate for water outside the river is less than 10%, four of the 2025 and 2030 plans cannot meet the requirements, namely, 2025-low-D, 2025-medium-D, 2025-low-E, and 2025-medium-E, and 2030-low-D, 2030-medium-D, 2030-low-E, and 2030-medium -E.

It can be seen from the above that the water resources in the lower Yellow River face a great shortage. In dry years and normal years, the average water demand for sediment transport in flood seasons cannot meet the demand for water outside the river and within the river.

TABLE 6 Proposed plans.

Scenarios		Uncertainty		Water resources, satisfaction level, water requirement (10^8 m^3, -, 10^8 m^3)	
	Satisfaction levels	Designed water resources frequency (%)	Sediment transport requirement (90%confidence level) (10^8 m^3)	2025	2030
Low	A	75	[49.40, 144.75]	(260, 0, 147.02)	(260, 0, 146.97)
	B			(260, 0.25, 147.02)	(260, 0.25, 146.97)
	C			(260, 0.5, 147.02)	(260, 0.5, 146.97)
	D			(260, 0.75, 147.02)	(260, 0.75, 146.97)
	E			(260, 1, 147.02)	(260, 1, 146.97)
Medium	A	50	[112.70, 199.27]	(320, 0, 147.02)	(320, 0, 146.97)
	B			(320, 0.25, 147.02)	(320, 0.25, 146.97)
	C			(320, 0.5, 147.02)	(320, 0.5, 146.97)
	D			(320, 0.75, 147.02)	(320, 0.75, 146.97)
	E			(320, 1, 147.02)	(320, 1, 146.97)
High	A	25	[177.87, 269.93]	(460, 0, 147.02)	(460, 0, 146.97)
	B			(460, 0.25, 147.02)	(460, 0.25, 146.97)
	C			(460, 0.5, 147.02)	(460, 0.5, 146.97)
	D			(460, 0.75, 147.02)	(460, 0.75, 146.97)
	E			(460, 1, 147.02)	(460, 1, 146.97)

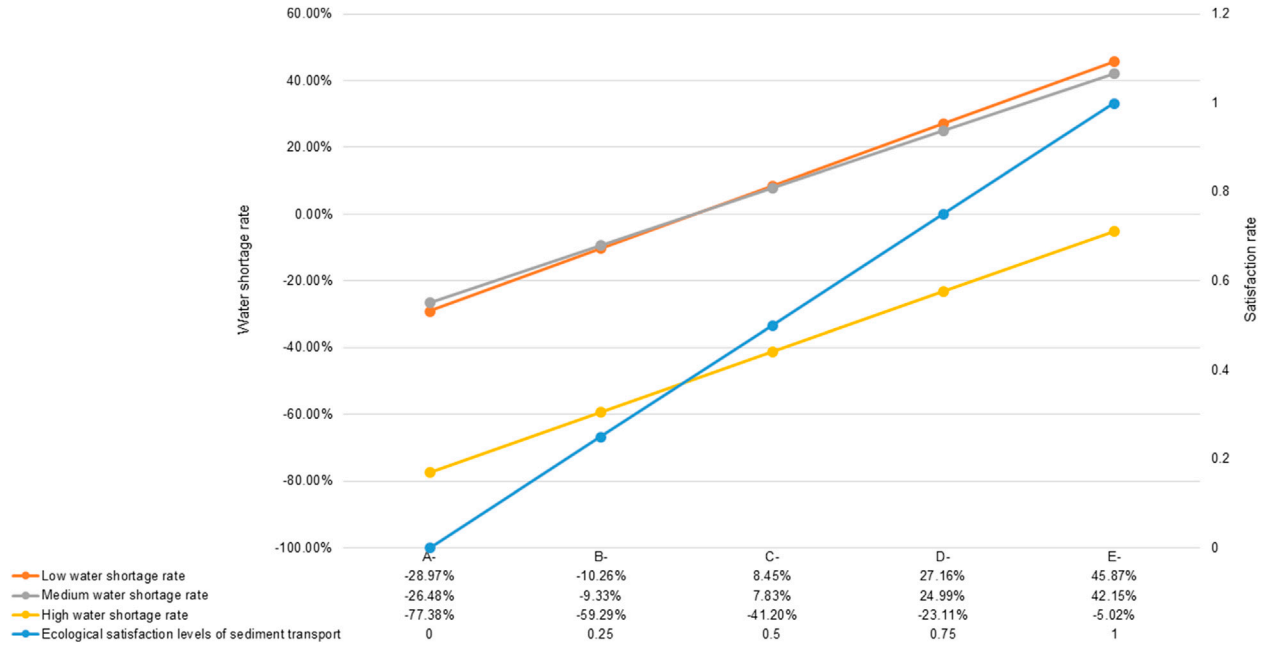

FIGURE 3
Changes in satisfaction and water shortage rate under different scenarios (2025)

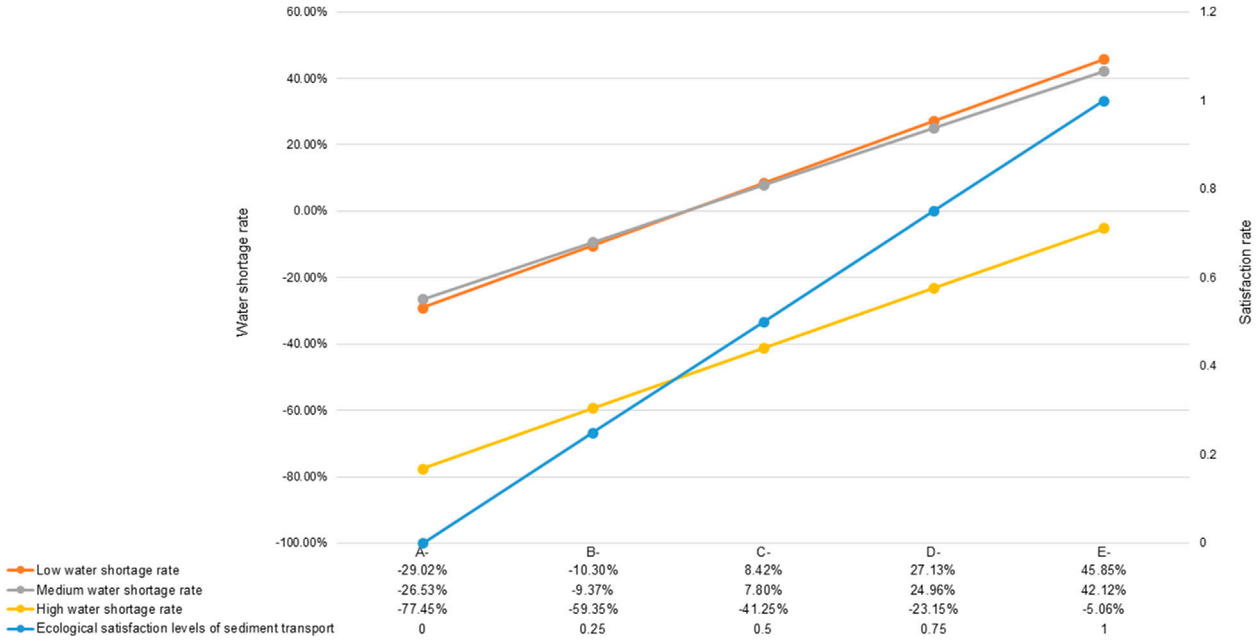

FIGURE 4
Changes in satisfaction and water shortage rate under different scenarios (2030)

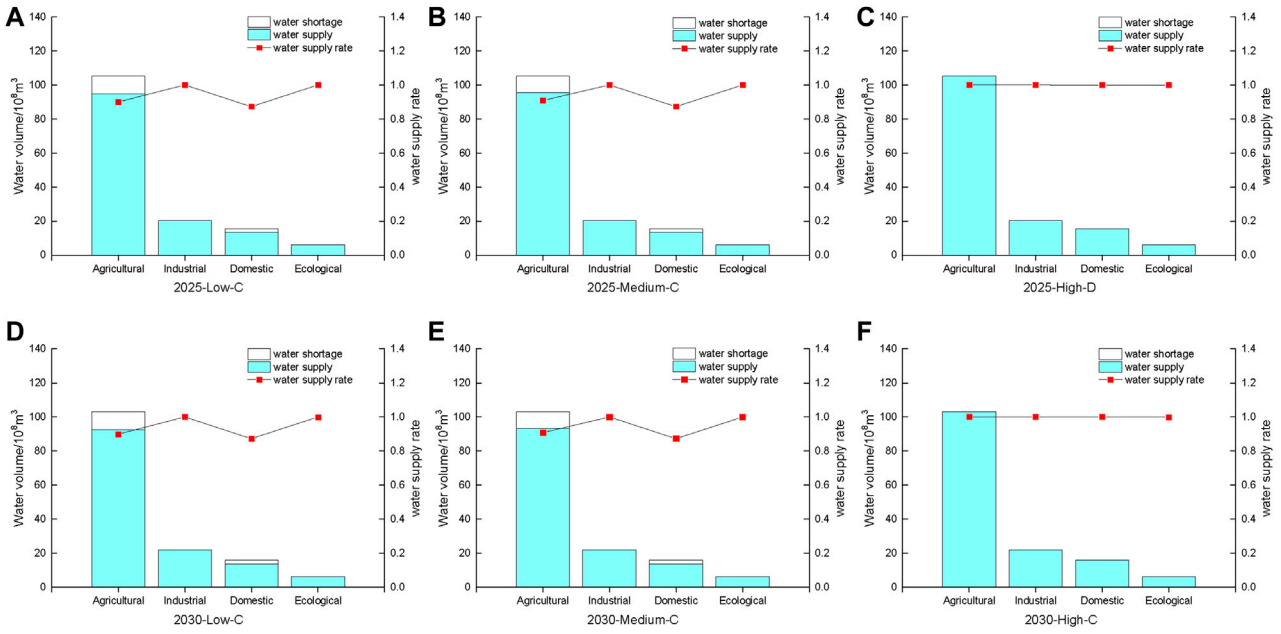

FIGURE 5
Water resource allocation of six suitable scenarios [**(A–F)** represent 6 selected scenarios respectively].

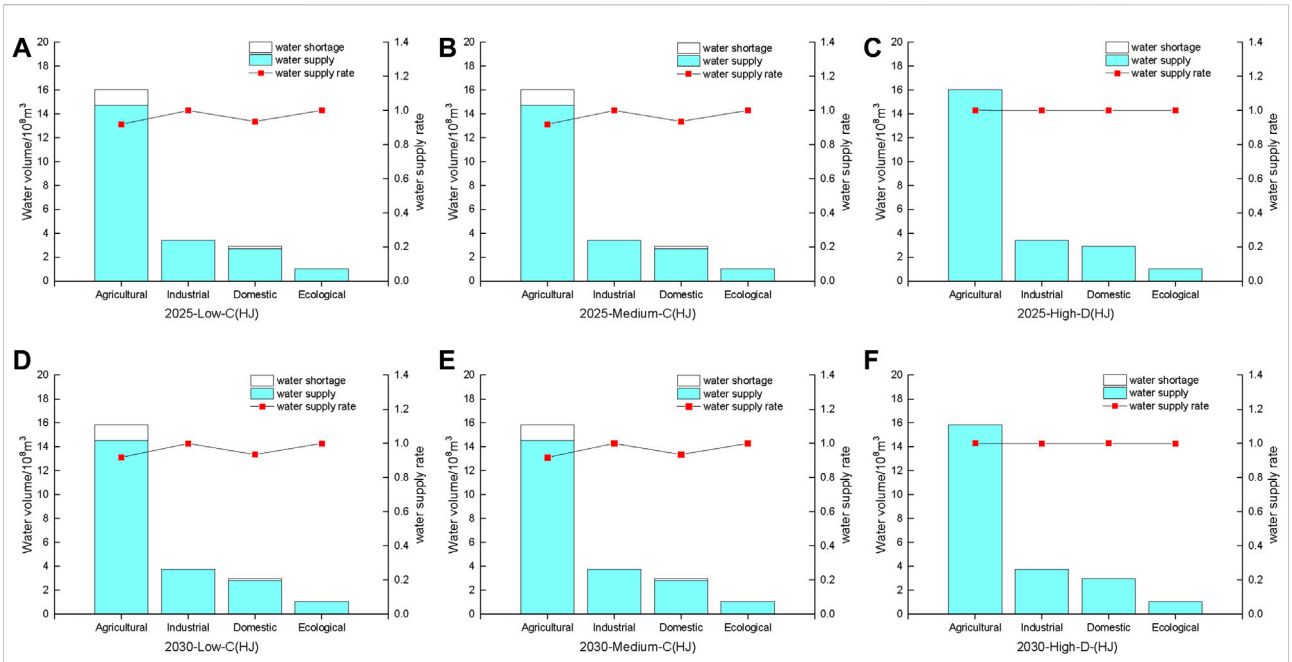

FIGURE 6
Distribution of water resources for six suitable scenarios in Huayuankou-Jiahetan section [**(A–F)** represent 6 selected scenarios respectively].

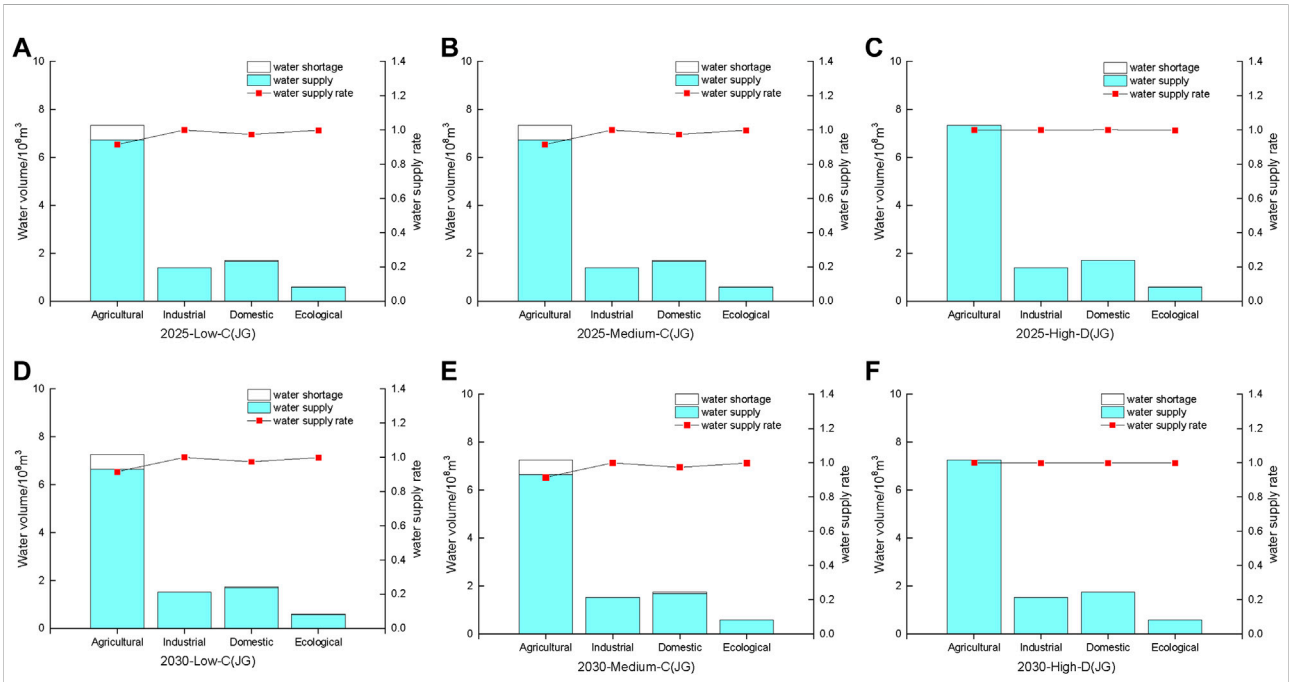

FIGURE 7
Distribution of water resources for six suitable scenarios in Jiahetan-Gaocun section [**(A–F)** represent 6 selected scenarios respectively].

TABLE 7 Water supply rate of six suitable scenarios in seven sections.

Sections	Scenarios	Water supply rate				
		Agricultural water	Industrial water	Domestic water	Ecological water	Total
HJ	2025-low-C	0.92	1.00	0.94	1.00	0.94
	2025-medium-C	0.92	1.00	0.94	1.00	0.94
	2025-high-D	1.00	1.00	1.00	1.00	1.00
	2030-low-C	0.92	1.00	0.93	1.00	0.94
	2030-medium-C	0.92	1.00	0.94	1.00	0.94
	2030-high-D	1.00	1.00	1.00	1.00	1.00
JG	2025-low-C	0.91	1.00	0.97	1.00	0.94
	2025-medium-C	0.92	1.00	0.97	1.00	0.94
	2025-high-D	1.00	1.00	1.00	1.00	1.00
	2030-low-C	0.92	1.00	0.93	1.00	0.94
	2030-medium-C	0.92	1.00	0.94	1.00	0.94
	2030-high-D	1.00	1.00	1.00	1.00	1.00
GS	2025-low-C	0.85	1.00	0.82	1.00	0.87
	2025-medium-C	0.85	1.00	0.82	1.00	0.87
	2025-high-D	1.00	1.00	1.00	1.00	1.00
	2030-low-C	0.85	1.00	0.82	1.00	0.88
	2030-medium-C	0.85	1.00	0.82	1.00	0.88
	2030-high-D	1.00	1.00	1.00	1.00	1.00
SA	2025-low-C	1.00	1.00	0.97	1.00	1.00
	2025-medium-C	1.00	1.00	0.97	1.00	1.00
	2025-high-D	1.00	1.00	1.00	1.00	1.00
	2030-low-C	1.00	1.00	0.97	1.00	1.00
	2030-medium-C	1.00	1.00	0.97	1.00	1.00
	2030-high-D	1.00	1.00	1.00	1.00	1.00
AL	2025-low-C	0.87	1.00	0.78	1.00	0.88
	2025-medium-C	0.87	1.00	0.78	1.00	0.88
	2025-high-D	1.00	1.00	1.00	1.00	1.00
	2030-low-C	0.87	1.00	0.78	1.00	0.89
	2030-medium-C	0.87	1.00	0.78	1.00	0.89
	2030-high-D	1.00	1.00	1.00	1.00	1.00
LL	2025-low-C	0.85	1.00	0.81	1.00	0.87
	2025-medium-C	0.91	1.00	0.81	1.00	0.91
	2025-high-D	1.00	1.00	1.00	1.00	1.00
	2030 -low-C	0.84	1.00	0.81	1.00	0.87
	2030-medium-C	0.90	1.00	0.81	1.00	0.91
	2030-high-D	1.00	1.00	1.00	1.00	1.00
LH	2025-low-C	1.00	1.00	1.00	1.00	1.00
	2025-medium-C	1.00	1.00	1.00	1.00	1.00
	2025-high-D	1.00	1.00	1.00	1.00	1.00
	2030-low-C	1.00	1.00	1.00	1.00	1.00
	2030-medium-C	1.00	1.00	1.00	1.00	1.00
	2030-high-D	1.00	1.00	1.00	1.00	1.00

Therefore, we selected suitable plans for different satisfaction levels of years and different water resources, according to the requirements of wet years, normal years, and dry years. In the wet year, the plans with a satisfaction degree of one were selected, that is, 2025-high-D and 2030-high-D. In the normal years, the plans with a satisfaction

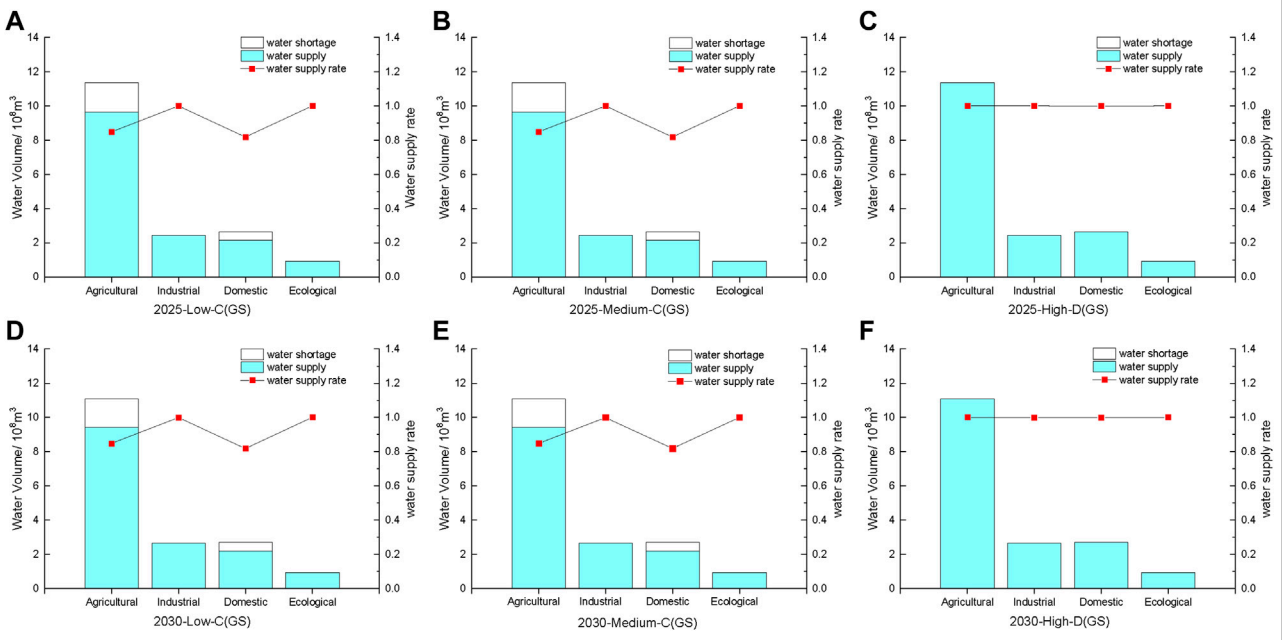

FIGURE 8
Distribution of water resources for six suitable scenarios in Gaocun-Sunkou section [**(A–F)** represent 6 selected scenarios respectively].

degree greater than or equal to 0.5 and the water shortage rate of less than 10% were selected, that is, 2025-medium-C and 2030-medium-C. In the dry years, the plans with a satisfaction degree greater than or equal to 0.5 and the water shortage rate of less than 10% were selected, that is, 2025-low-C and 2030-low-C.

4.2.1 Analysis of overall water supply in the lower Yellow River

The results of the ecological footprint-based water distribution scenarios of the above six scenarios were analyzed. The result is shown in Figure 5 with 5(a) to 5(f) represents 6 selected scenarios respectively. In 2025, the water shortage rate under the suitable scenarios of dry year, normal year, and wet year is 8.45%, 7.83%, and 0%, respectively. In 2030, the water shortage rate under the suitable scenarios of dry year, normal year, and wet year is 8.42%, 7.80%, and 0%, respectively.

Within the same year, there is a small difference in the water shortage rate of the water resources allocated outside the river in a normal year and a dry year in 2025. That is, the total amount of water resources in normal years is more than that in dry years, but the amount of water used for sediment transport in normal years also increases. This is due to the fact that with the increase in the inflow of water, the sediment load increases (Kong et al., 2015), and the amount of water required for sediment transport increases. Therefore, although the total amount of water resources in a normal year increases, under the same satisfaction degree of sediment transport, the distribution of water resources outside the river does not change significantly. In a wet year, although the water demand for sediment transport increases, the efficiency of transporting sediment may increase due to the large amount of inflow. Therefore, even if the satisfaction of water for sediment transport increases (from 0.5 to 1), the water resources allocated outside the river course will also increase significantly, which can fully meet all water demand outside the river course.

Although existing dams and reservoirs play a key role in trapping sediments in the Yellow River, the ability will decline in the future (Wang et al., 2016), slowing down the erosion of the Loess Plateau which causes larger sediment load is the source management method to control water demand for sediment transport.

4.2.2 Analysis of water supply by sections in the lower Yellow River

Table 7 and Figures 6–12 show the changes in four water users outside the river from seven sections in the lower Yellow River under the six scenarios, respectively and (a) to (f) represent 6 selected scenarios.

Figure 13 shows the overall water supply rate in every region in 6 scenarios. It can be concluded from the above that on the whole scale, cities in GS and AL sections suffer more from lower water supply rate. According to studies of Gong et al. (2020), Puyang in GS section, Dezhou and Liaocheng in AL section performed poorly in efficiency of water utilization, which may cause larger water demand. Moreover, as shown in Figure 2, GS and AL sections are in the lower reaches of the main tributaries of

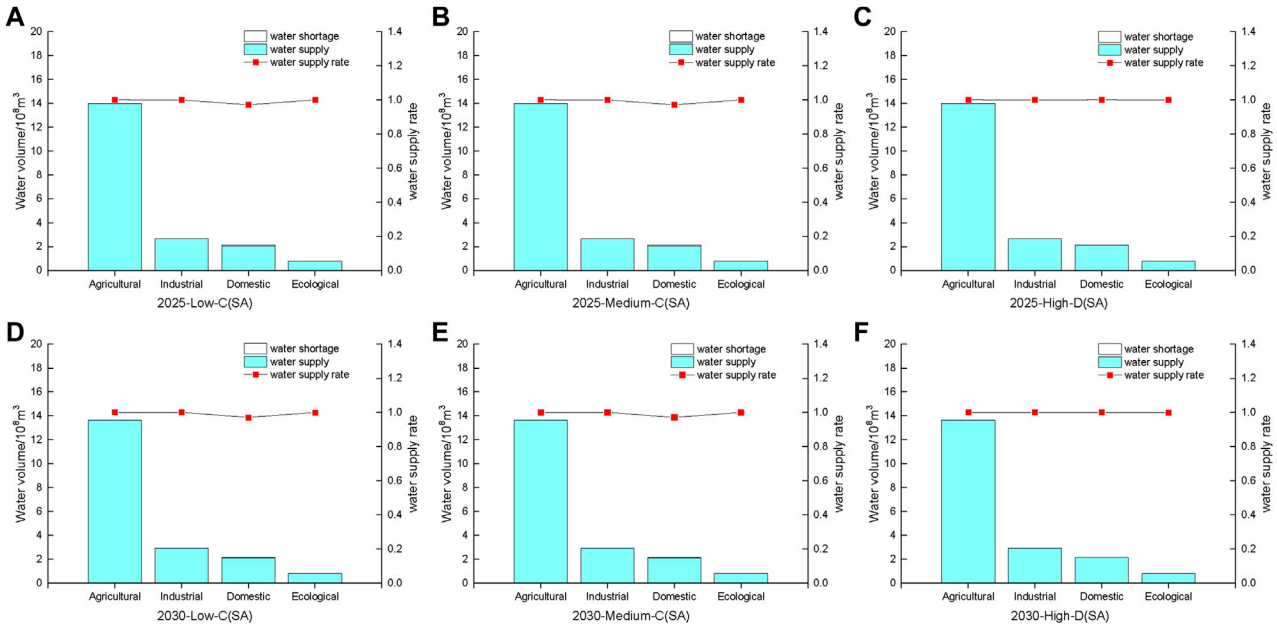

FIGURE 9
Distribution of water resources for six suitable scenarios in Sunkou-Aishan section [**(A–F)** represent 6 selected scenarios respectively].

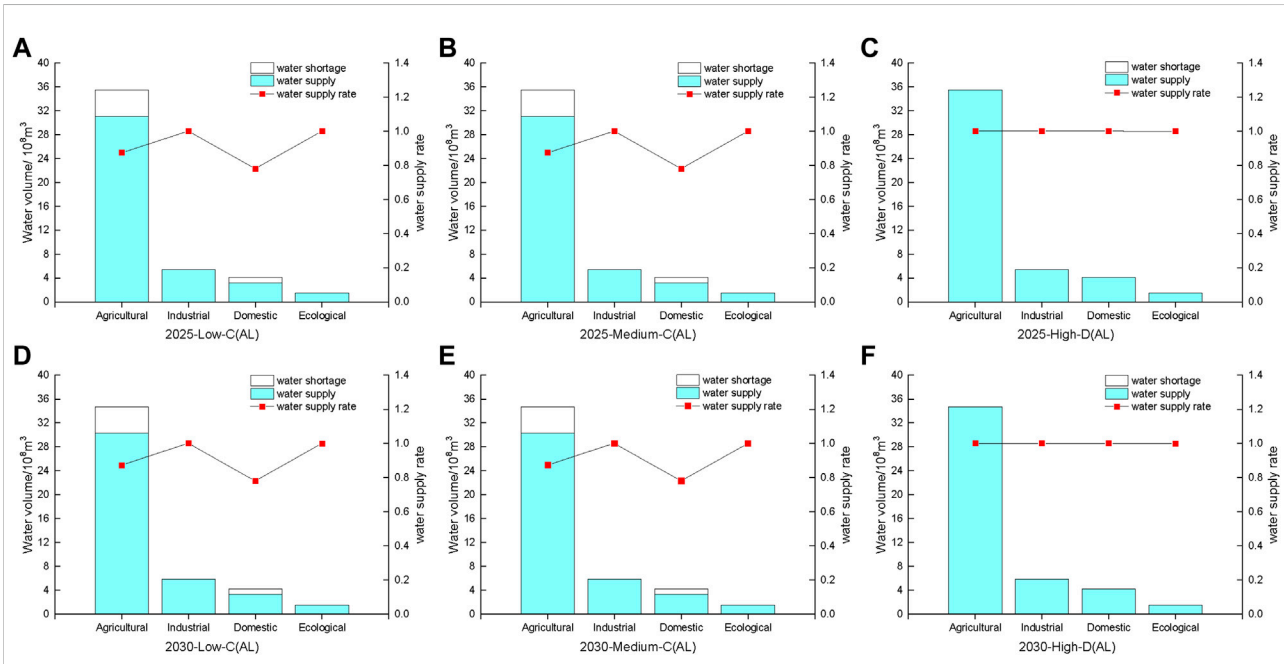

FIGURE 10
Distribution of water resources for six suitable scenarios in Aishan-Luokou section [**(A–F)** represent 6 selected scenarios respectively].

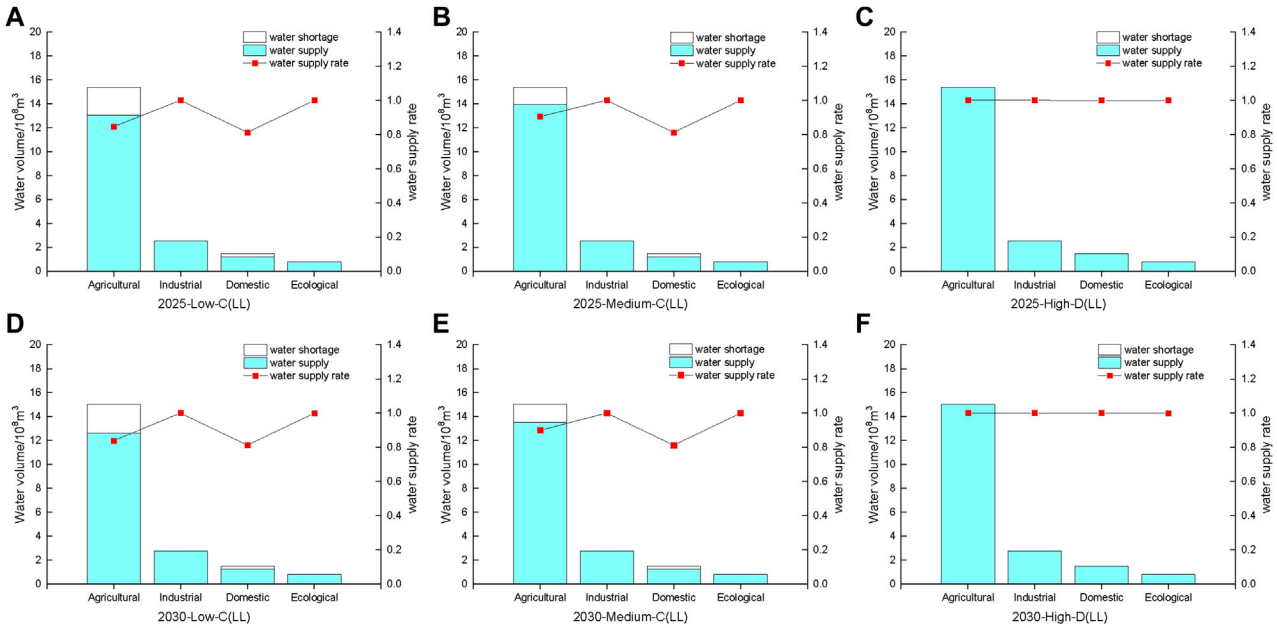

FIGURE 11
Distribution of water resources for six suitable scenarios in Luokou-Lijin section [**(A–F)** represent 6 selected scenarios respectively].

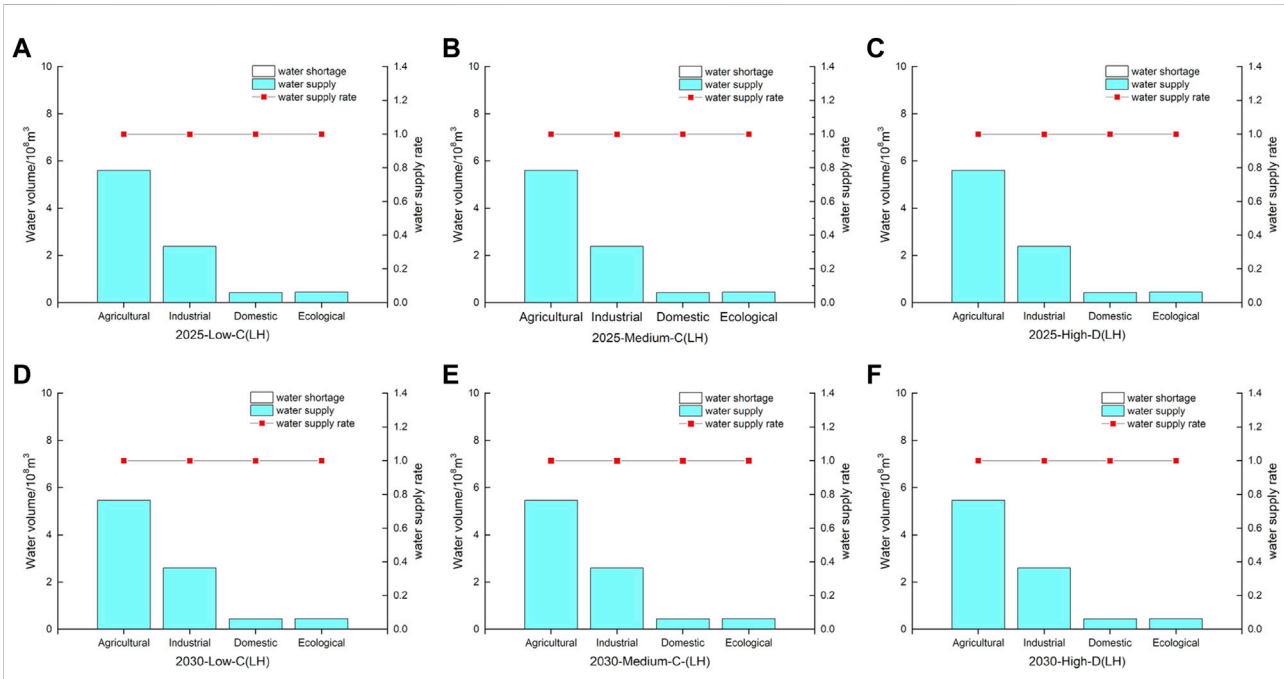

FIGURE 12
Distribution of water resources for six suitable scenarios in Lijin-Hekou section [**(A–F)** represent 6 selected scenarios respectively].

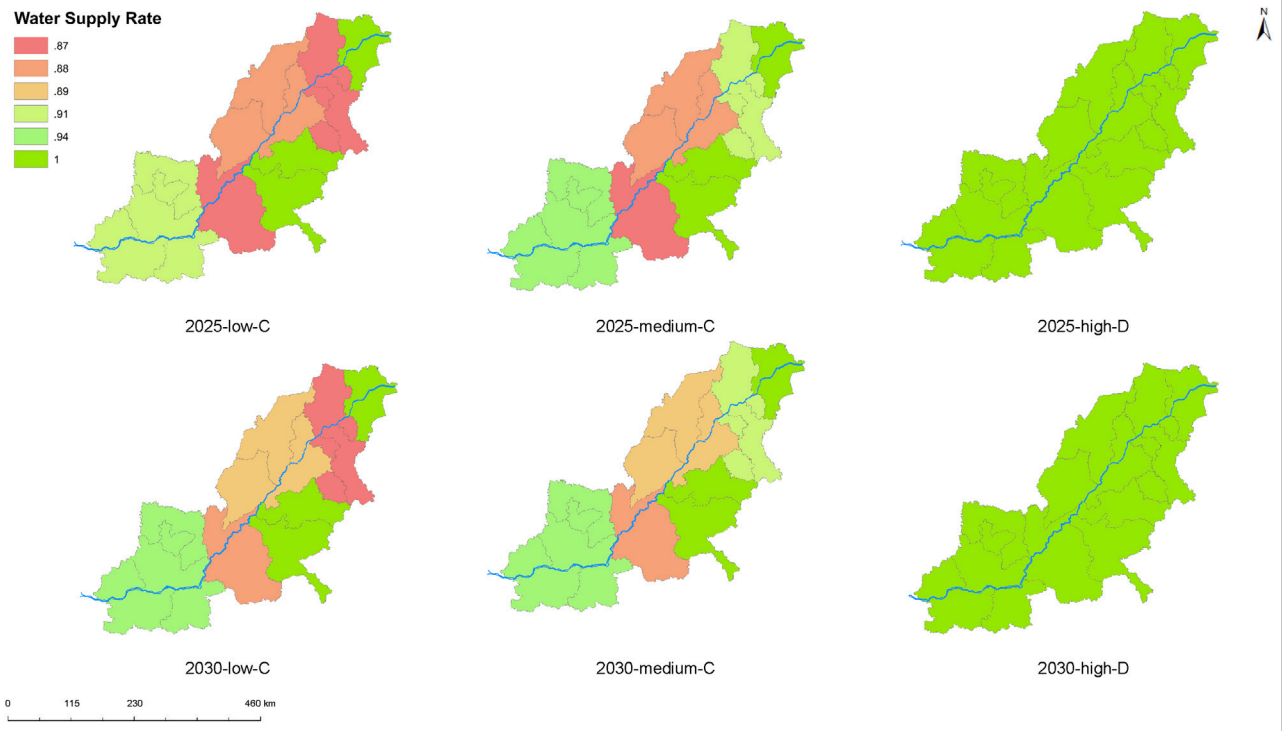

FIGURE 13
Overall water supply rate in study area in six scenarios.

the Yellow River (Wenyan Canal and Dawen River), restricting upper cities' water intake from these tributaries may supplement main stream water and improve the water supply rate.

From the perspective of different industries, ecological, and industrial water supply rates of the sections other than SA and LH are better than those of domestic and agricultural water supply rates, which indicates that the ecological footprint of domestic and agricultural water in these sections is greater than that of ecological and industrial water. Therefore, these sections should focus on improving the efficiency of domestic water and agricultural water or making industrial adjustments to reduce the production of ecological footprint. In the SA section, the water supply rate of ecology, industry, and agriculture in this area is better than that of domestic use, which reflects the larger ecological footprint generated by domestic water in the section. Therefore, this section should focus on improving the efficiency of domestic water. In the LH section, under the water demand forecast scenarios in 2025 and 2030, the water supply rate of each department in the dry year and normal year also reached 1.0.

Analyzing the above results, among the sections, the river sections with the largest water supply rate are the LH section and the SA section, which are close to 1. The river sections with the smallest water supply rate are the GS section and the LL section, which are 0.87; that is, the GS section and the LL section have a relatively large ecological footprint. Among industries, the water supply rate of agricultural and domestic water is lower than that of ecological and industrial water. This reflects that the ecological footprint generated by agricultural water and domestic water in the lower Yellow River is larger. Measures should be taken to improve the efficiency of agricultural and domestic water utilization. Among the years, there is a significant conflict between the water demand for sediment transport outside the river in normal and dry years.

Since water use priorities vary from region to region, there are some studies that also set priorities between both cities and types of water utilization (Li et al., 2021). However, when prioritizing using analytical hierarchy process (AHP) or other methods (Wang et al., 2003), there is still the problem of subjectivity and possibly insufficient rationality in the water allocation.

The result of the allocation plan is similar to Zhang and Oki (2021) based on Nash–Harsanyi bargaining game theory. Since the concept of ecological footprint of water resources applied in this paper innovatively includes soil water as one of the indicators of water resources carrying capacity (Li et al., 2020), the ecological footprint of water resources in agriculture, which is one of the main water uses in the lower reaches of the Yellow River, can be considered more objectively, and the ecological footprint of water

resources in the lower reaches of the Yellow River can be assessed more comprehensively. However, this study only focuses on the water resources allocation in the lower reaches of the Yellow River, and there may be a need for more in-depth studies in the basin as a whole in the future.

The suggestions for normal and dry years are as follows:

1) Broaden sources of income: increase the amount of water resources, including inter-annual reservoir regulation of water resources; introduce external water resources, such as the South-to-North Water Diversion and seawater desalination.
2) Reduce expenditure: since the main water demand for water outside the lower Yellow River is agricultural water, water-saving irrigation should be conducted to improve the utilization efficiency of water resources. Furthermore, the efficiency of sediment transport can be improved since the main water used in the river is for sediment transport. Water conservancy projects need to be fully utilized, such as the Xiaolangdi Reservoir for water and sediment regulation. In addition, more stringent policies and laws and regulatory regimes may be needed.

5 Conclusion

Based on the evaluation results of ecological footprint and the results of water demand prediction, a multi-objective allocation model of water resources in the lower Yellow River was constructed and solved with GAMS software. The model results are shown as follows:

1) The shortage of water resources in the lower Yellow River is related to the amount of water resources and the water demand for sediment transport in the year. When there is a wet year, the shortage of water resources is significantly reduced, but there is no significant difference between a dry year and a normal year.
2) Water shortages in different areas of the lower Yellow River are related to the ecological footprints of different users in the area. The rivers with the largest shortages are GS and AL sections, the rivers with the smallest shortages are the LH and SA sections. Restricting upper cities' water intake from tributaries of the Yellow River may supplement main stream water and improve the water supply ability.

The model explores the relationship among incoming water and sediment conditions, the ecological footprint produced by water utilizations, and the distribution of water resources, which can provide decision makers with different allocation scenarios, comprehensively considering ecological, safety, and social benefits to achieve the goal of optimal system benefits.

Data availability statement

The original contributions presented in the study are included in the article/supplementary material, further inquiries can be directed to the corresponding authors.

Author contributions

All authors contributed to the study conception and design. Material preparation, data collection and analysis were performed by SZ and HL. The first draft of the manuscript was written by SZ and HL; CL, YY, XW, and QL commented on previous versions of the manuscript. All authors read and approved the final manuscript.

Funding

This study was funded by the Joint Funds of the National Natural Science Foundation of China (U2243236) and the National Science Foundation for Distinguished Young Scholars (52025092).

Conflict of interest

The authors declare that the research was conducted in the absence of any commercial or financial relationships that could be construed as a potential conflict of interest.

Publisher's note

All claims expressed in this article are solely those of the authors and do not necessarily represent those of their affiliated organizations, or those of the publisher, the editors and the reviewers. Any product that may be evaluated in this article, or claim that may be made by its manufacturer, is not guaranteed or endorsed by the publisher.

References

Chen, N., Li, Y., and Xu, C. (2006). Optimal deployment of water resources based on multi-objective genetic algorithm. *J. Hydraulic Eng.* 9 (03), 308–313. doi:10.3321/j.issn:0559-9350.2006.03.009

Dadmand, F., Naji-Azimi, Z., Motahari Farimani, N., and Davary, K. (2020). Sustainable allocation of water resources in water-scarcity conditions using robust fuzzy stochastic programming. *J. Clean. Prod.* 276, 123812. doi:10.1016/j.jclepro.2020.123812

Dai, D., Sun, M., Xu, X., and Lei, K. (2019). Assessment of the water resource carrying capacity based on the ecological footprint: A case study in zhangjiakou city, north China. *Environ. Sci. Pollut. Res.* 26 (11), 11000–11011. doi:10.1007/s11356-019-04414-9

Divakar, L., Babel, M. S., Perret, S. R., and Gupta, A. D. (2011). Optimal allocation of bulk water supplies to competing use sectors based on economic criterion – an application to the Chao Phraya River Basin, Thailand. *J. Hydrol. X.* 401 (1), 22–35. doi:10.1016/j.jhydrol.2011.02.003

Fan, X. (2005). "Study on the principle of water resources ecological footprint and application inJiangsu province," (China: Hohai University). Master Dissertation.

Gong, C., Xu, C., and Zhang, X. (2020). Spatio-temporal evolution and influencing factors of water resources utilization efficiency of cities along the middle and lower reaches of the Yellow River. *Sci. Geogr. Sin.* 40 (11), 1930–1939. doi:10.13249/j.cnki.sgs.2020.11.018

Gov (2021). The state Council of the people's republic of China. Available at: http://www.gov.cn/zhengce/2021-10/08/content_5641438.html.

Guan, X., Dong, Z., Luo, Y., and Zhong, D. (2021). Multi-objective optimal allocation of river basin water resources under full probability scenarios considering wet–dry encounters: A case study of Yellow River basin. *Int. J. Environ. Res. Public Health* 18, 11652. doi:10.3390/ijerph182111652

Hoekstra, A. Y. (2008). Human appropriation of natural capital: A comparison of ecological footprint and water footprint analysis. *Ecol. Econ.* 68 (7), 1963–1974. doi:10.1016/j.ecolecon.2008.06.021

Huang, L., Zhang, W., Jiang, C., and Fan, X. (2008). Ecological footprint method in water resources assessment. *Acta Ecol. Sin.* 28 (03), 1279–1286. doi:10.3321/j.issn:1000-0933.2008.03.044

Kazemi, M., Bozorg-Haddad, O., Fallah-Mehdipour, E., and Loáiciga, H. A. (2020). Inter-basin hydropolitics for optimal water resources allocation. *Environ. Monit. Assess.* 192 (7), 478. doi:10.1007/s10661-020-08439-3

Kong, D., Miao, C., Borthwick, A. G. L., Duan, Q., Liu, H., Sun, Q., et al. (2015). Evolution of the Yellow River Delta and its relationship with runoff and sediment load from 1983 to 2011. *J. Hydrol. X.* 157-167, 157–167. doi:10.1016/j.jhydrol.2014.09.038

Li, C., Cai, Y., and Qian, J. (2018). A multi-stage fuzzy stochastic programming method for water resources management with the consideration of ecological water demand. *Ecol. Indic.* 95, 930–938. doi:10.1016/j.ecolind.2018.07.029

Li, H., Zhao, F., Li, C., Yi, Y., Bu, J., Wang, X., et al. (2020). An improved ecological footprint method for water resources utilization assessment in the cities. *Water (Basel)* 12 (2), 503. doi:10.3390/w12020503

Li, J., Cui, L., Dou, M., and Ali, A. (2021). Water resources allocation model based on ecological priority in the arid region. *Environ. Res.* 199, 111201. doi:10.1016/j.envres.2021.111201

Rees, W. E. (1992). Ecological footprints and appropriated carrying capacity: What urban economics leaves out. *Environ. Urban.* 4 (2), 121–130. doi:10.1177/095624789200400212

Shao, W., Yang, D., Hu, H., and Sanbongi, K. (2009). Water resources allocation considering the water use flexible limit to water shortage—a case study in the Yellow River basin of China. *Water Resour. manage.* 23 (5), 869–880. doi:10.1007/s11269-008-9304-2

Song, Y. (2008). "Study on optimal allocation of water resources based on the development benefit in the yinmahe drainage basin," (Jilin: University of Jilin). Master Dissertation.

Stoeglehner, G., Edwards, P., Daniels, P., and Narodoslawsky, M. (2011). The water supply footprint (WSF): A strategic planning tool for sustainable regional and local water supplies. *J. Clean. Prod.* 19 (15), 1677–1686. doi:10.1016/j.jclepro.2011.05.020

Su, Y., Gao, W., Guan, D., and Su, W. (2018). Dynamic assessment and forecast of urban water ecological footprint based on exponential smoothing analysis. *J. Clean. Prod.* 195, 354–364. doi:10.1016/j.jclepro.2018.05.184

Wackernagel, M., and Rees, W. (1996). *Ecological footprints for beginners: Our ecological footprint: Reducing human impact on the Earth*. Washington, DC: Island Press/Center for Resource Economics. doi:10.5822/978-1-61091-491-8_45

Wang, H., Huang, J., Zhou, H., Deng, C., and Fang, C. (2020). Analysis of sustainable utilization of water resources based on the improved water resources ecological footprint model: A case study of hubei province, China. *J. Environ. Manage.* 262, 110331. doi:10.1016/j.jenvman.2020.110331

Wang, J., Zhang, J., and Dong, Z. (2003). Harmoniousness analysis of water resources allocation. *J. Hohai Univ. Nat. Sci.* 31 (6), 702–705. doi:10.3321/j.issn:1000-1980.2003.06.025

Wang, L. H., Fang, L. P., and Hipel, K. W. (2007). On achieving fairness in the allocation of scarce resources: Measurable principles and multiple objective optimization approaches. *IEEE Syst. J.* 1 (1), 17–28. doi:10.1109/JSYST.2007.900242

Wang, S., Yang, F., Xu, L., and Du, J. (2013). Multi-scale analysis of the water resources carrying capacity of the Liaohe Basin based on ecological footprints. *J. Clean. Prod.* 53, 158–166. doi:10.1016/j.jclepro.2013.03.052

Wang, S., Fu, B., Piao, S., Lu, Y., Ciais, P., Feng, X., et al. (2016). Reduced sediment transport in the Yellow River due to anthropogenic changes. *Nat. Geosci.* 9, 38–41. doi:10.1038/ngeo2602

Wang, Y., Huang, Q., and Liu, C. (2006). Research on real-time regulation-control for river basin water resources and its model. *J. Hydraulic Eng.* 9, 1122–1128. doi:10.3321/j.issn:0559-9350.2006.09.015

Yang, W. (2011). A multi-objective optimization approach to allocate environmental flows to the artificially restored wetlands of China's Yellow River Delta. *Ecol. Modell.* 222 (2), 261–267. doi:10.1016/j.ecolmodel.2010.08.024

Zhang, C. Y., and Oki, T. (2021). Optimal multi-sectoral water resources allocation based on economic evaluation considering the environmental flow requirements: A case study of Yellow River basin. *Water* 13 (16), 2253. doi:10.3390/w13162253

Zhang, Q., Xu, C., and Yang, T. (2009). Variability of water resource in the Yellow River basin of past 50 Years, China. *Water Resour. manage.* 23, 1157–1170. doi:10.1007/s11269-008-9320-2

Zhang, Z., Ma, H., Li, Q., Wang, X., and Feng, G. (2014). Agricultural planting structure optimization and agricultural water resources optimal allocation of Yellow River Irrigation Area in Shandong Province. *Desalination Water Treat.* 52 (13-15), 2750–2756. doi:10.1080/19443994.2013.819167

Zhao, Z., Liu, L., and Chen, N. (2007). Study multi-objective decision-making method on water resources optimum distribution. *J. North China Univ. Water Resour. Electr. Power* 5, 1–3. doi:10.19760/j.ncwu.zk.2007.05.001

Frontiers in Earth Science

Investigates the processes operating within the major spheres of our planet

Advances our understanding across the earth sciences, providing a theoretical background for better use of our planet's resources and equipping us to face major environmental challenges.

Discover the latest Research Topics

See more →

Frontiers

Avenue du Tribunal-Fédéral 34
1005 Lausanne, Switzerland
frontiersin.org

Contact us

+41 (0)21 510 17 00
frontiersin.org/about/contact